UNIVERSITÀ DEGLI STUDI DI SALERNO

Dipartimento di Chimica e Biologia "Adolfo Zambelli"

Tesi di dottorato di ricerca in Chimica

XXXIV Ciclo

New metal catalysts for Ring-Opening Polymerization of cyclic esters

Candidato:

Impemba Salvatore

Matr. 8800100049

Tutor:

Prof. Milione Stefano

Coordinatore:

Prof. Pellecchia Claudio

Anno Accademico: 2021/2022

Index

Ligands reported in thesis

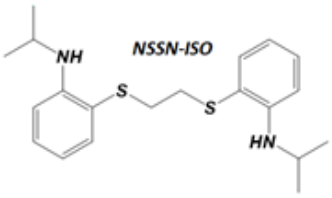

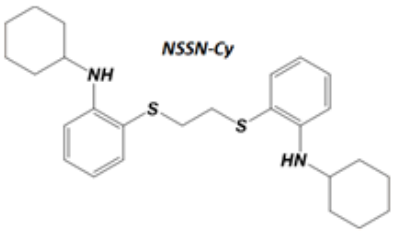

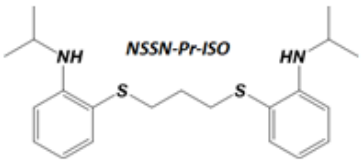

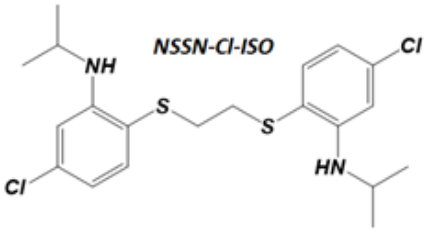

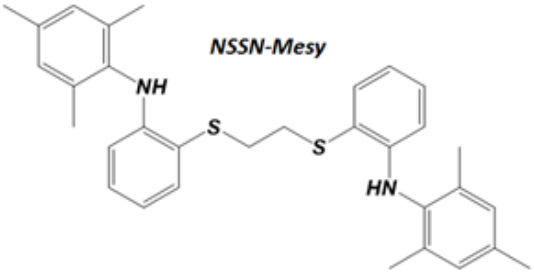

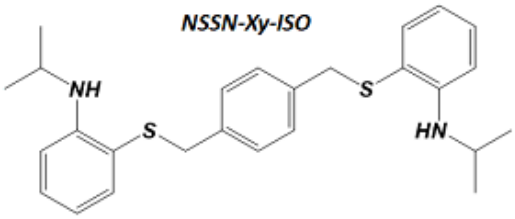

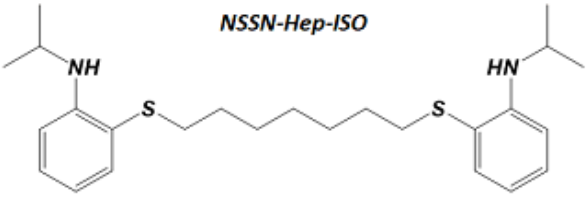

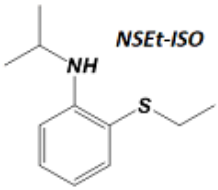

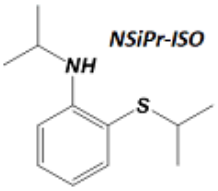

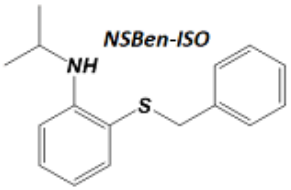

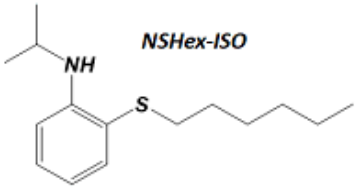

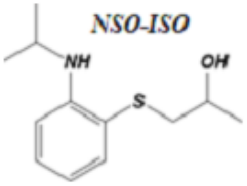

Complexes reported in thesis

Zr-NSSN-ISO

Zr-NSSN-Cy

Zr-NSSN-Mesy

Hf-NSSN-ISO

Hf-NSSN-Cy

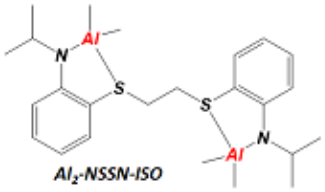

Al_2-NSSN-ISO

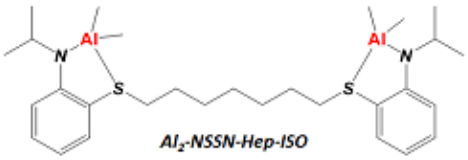

Al_2-NSSN-Hep-ISO

Al_2-NSSN-Pr-ISO

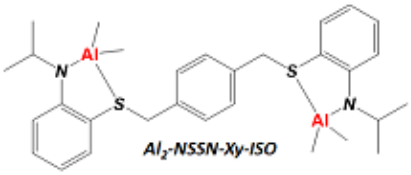

Al_2-NSSN-Xy-ISO

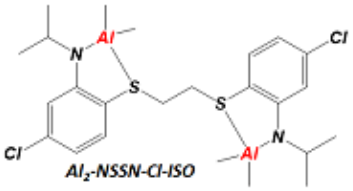

Al_2-NSSN-Cl-ISO

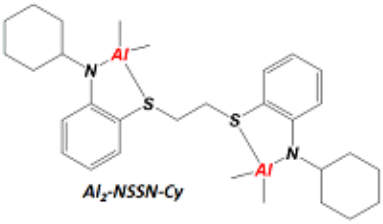

Al_2-NSSN-Cy

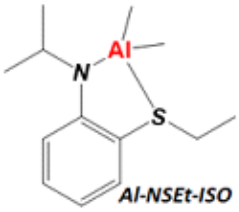

Al-NSEt-ISO

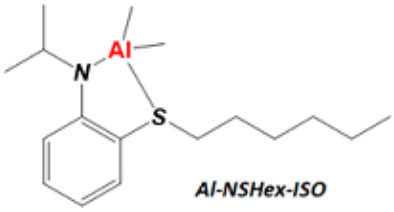

Al-NSHex-ISO

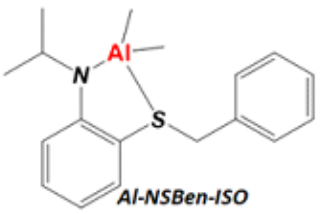

Al-NSBen-ISO

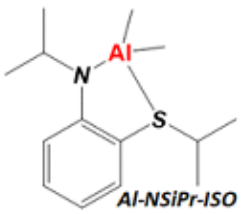

Al-NSiPr-ISO

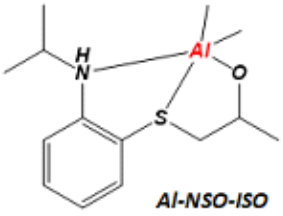

Al-NSO-ISO

LIST OF ABBREVIATIONS

Al: aluminum

APEs: aliphatic polyesters

AROP: anionic ring-opening polymerization

β-BL: butyrolactone

BnOH: butanol

BzOH: benzyl alcohol

CROP: cationic ring-opening polymerization

Đ: dispersity

DOSY: diffusion order spectroscopy

DFT: density functional theory

ε-CL: caprolactone

E_a*:* activation energy

ESI: electrospray ionization mass spectrometry

GPC: gel permeation chromatography

Hf: hafnium

^{i}*PrOH:* isopropanol

k_{app}*:* apparent propagation rate constant

L-LA: L-lactide

MALDI-TOF: matrix-assisted laser desorption ionization time-of-flight

Meso-LA: meso-lactide

NMR spectroscopy: nuclear magnetic resonance spectroscopy

NSSN: 1,2-bis(aminophenylthio)ethane

NSSN-ISO: 2,2’-(ethane-1,2-diylbis(sulfanediyl))bis(N-isopropylaniline)

NSSN-CY: 2,2’-(ethane-1,2-diylbis(sulfanediyl))bis(N-cyclohexylaniline)

NSSN-MESY: N,N’-((ethane-1,2-diylbis(sulfadeniyl))bis(2,1-phenylene))bis(2,4,6-trimethylaniline)

NSSN-Cl: 6,6’-(ethane-1,2-diylbis(sulfanediyl))bis(3-chloroaniline)

NSSN-Cl-ISO: 6,6'-(ethane-1,2-diylbis(sulfanediyl))bis(3-chloro-*N*-isopropylaniline)

NSSN-Pr: 2,2'-(propane-1,3-diylbis(sulfanediyl))dianiline

NSSN-Pr-ISO: 2,2'-(propane-1,3-diylbis(sulfanediyl))bis(*N*-isopropylaniline)

NSSN-Hep: 2,2’-(heptane-1,7-diylbis(sulfanediyl))dianiline

NSSN-Hep-ISO: 2,2'-(heptane-1,7-diylbis(sulfanediyl))bis(*N*-isopropylaniline)

NSSN-Xy: 2,2'-((1,4-phenylenebis(methylene))bis(sulfanediyl))dianiline

NSSN-Xy-ISO: 2,2’-((1,4-phenylenebis(methylene))bis(sulfanediyl))bis(*N*-isopropylaniline)

NSEt: 2-(ethylthio)aniline

NSEt-ISO: 2-(ethylthio)-*N*-isopropylaniline

NSiPr: 2-(isopropylthio)aniline

NSiPR-ISO: N-isopropyl-2-(isopropylthio)aniline

NSHex: 2-(hexylthio)aniline

NSHex-ISO: 2-(hexylthio)-*N*-isopropylaniline

NSBen: 2-(benzylthio)aniline

NSBen-ISO: 2-(benzylthio)-*N*-isopropylaniline

PBL: polybutyrolactone

PCL: polycaprolactone

PET: polyethylene terephthalate

PLA: polylactide

PS: polystyrene

PSGE: pulsed gradient spin-echo

rac-LA: rac-lactide

ROP: ring-opening polymerization

T_g*:* glass transition temperature

T_m*:* melting temperature

TOF: turnover frequency ($M_{product}/t \cdot mol_{cat}$)

V_{bur}*:* buried volume

Zr: zirconium

1 Introduction

1.1 Biodegradable polymers

Nowadays, about 350 million of tons of plastics are produced annually all over the world and most of these plastics are of petroleum origin.[1]

Figure 1: Ineos oil refinery in Grangemouth (Scotland).

The environmental and economic problems related to the current polymers from petroleum origin, have driven the academic research toward the development of green and degradable alternatives to conventional plastics.[2] The biodegradable polymers can be considered as safe for the environment and represent an interesting alternative to conventional plastics. A biodegradable polymer is defined as a polymer susceptible to degradation by microorganisms (bacteria, fungi, etc…). Biodegradation depends on

[1] M. Jamshidian, E. A. Tehrany, M. Imran, M. Jacquot, S. Desobry, *Compr. Rev. Food Sci. Food Saf.*, ***2010**, 9, 552-571;* A. J. R. Lasprilla, G. A. R. Martinez, B. H. Lunelli, A. L. Jardini , R. M. Filho, *Biotechnol. Adv.*, ***2012**, 30, 213-221.*

[2] A. –C. Albertsson, I. K. Varma, *Biomacromolecules*, ***2003**, 4, 1466-1486;* S. Mecking, *Angew. Chem.*, ***2004**, 43, 1078–1085;* C. S. Ha, J. A. Gardella, *Chem. Rev.*,***2005**, 105, 4205-4232;* A. J. Ragauskas, C. K. Williams, B. H. Davison, G. Britovsek, J. Cairney, C. A. Eckert, W. J. Jr Frederick, J. P. Hallett, D. J. Leak, C. L. Liotta, J. R. Mielenz, R. Murphy, R. Templer, T. Tschaplinski, *Science*, **2006**, 311, 484-489*;* C. Robert, F. de Montigny, C. M. Thomas, *Nat. Commun.*, ***2011**, 2, 586;* G. –Q. Chen, M. K. Patel, *Chem. Rev.*, ***2012**, 112, 2082-2099;* J. Jambeck, M. Perryman, A. Andrady, R. Narayan , K. Law, *Science*, ***2015**, 347, 768-771;* S. Kubowicz , A. M. Booth, *Environ. Sci. Technol.*, ***2017**, 51, 12058-12060***.**

polymer structure, polymer morphology and molecular weight.[3] Biodegradable polymers maybe divided into two different categories: native or synthetic origin. The first ones are the result of a synthesis developed during millions of years of evolution and includes materials such as proteins, polysaccharides, nucleic acids and lipids. The second ones can be synthesized from the polymerization of renewable monomers, obtained from natural carbohydrates (starch, cellulose, etc…).[4]

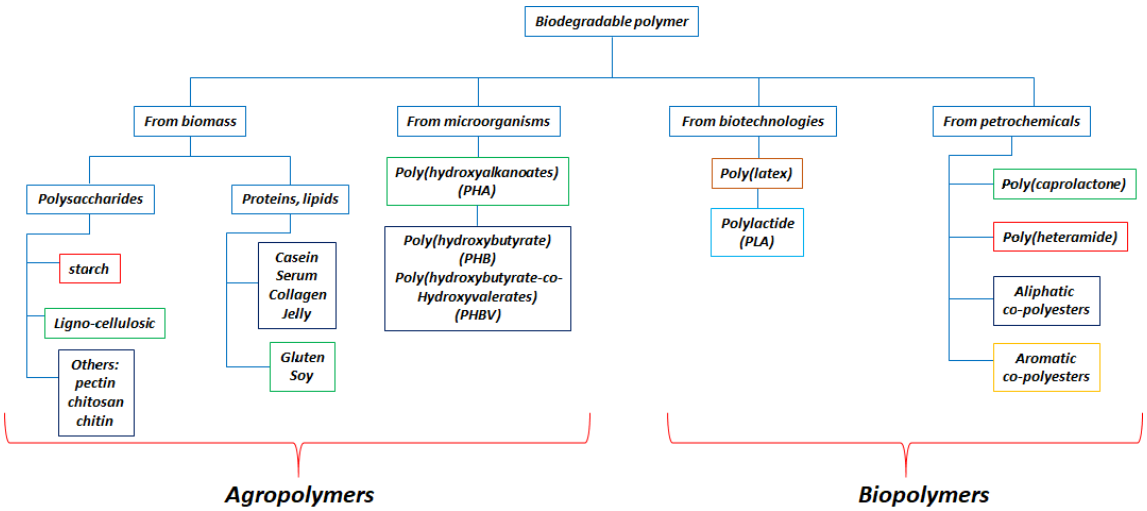

Figure 2: biodegradable polymer classification.

Aliphatic polyesters *(APEs)* are biodegradable polymer due to the potentially hydrolysable ester bonds and relative short aliphatic chains present in the macromolecules and are the most representative examples of environmentally relevant polymeric materials.[5] Several examples of *APEs* have been produced until now as possible substitutes of well-established polymeric commodities (such as

[3] M. Okada, *Prog. Polymer. Sci.*, ***2002***, *27, 87-133;* R. M. Rasal, A.V. Janorkar, D.E. Hirt, *Prog. Polym. Sci.*, ***2010***, *35,338-356.*

[4] L. Avérous, *J. of Macr.*, ***2004***, *44, 231-274;* Y. Zhu, C. Romain, C.K. Williams, *Nature*, ***2016***, *540, 354-362.*

[5] M. Vert, *Biomacromolecules*, ***2005***, *6, 538-546;* J. K. Oh, *Soft Matter*, ***2011***, *7, 5096–5108.*

polypropylene, polyethylene and polystyrene).[6] These materials have found several applications for instance in drug delivery, medical tools and food packaging.[7]

Figure 3: biopolymer as drug delivery and food packaging.

[6] P. Lecomte, C. Jérome in *Synthetic Biodegradable Polymers Advances in Polimer Science, Vol. 245* (Eds. B. Rieger, A. Kenkel, G. W. Coates, R. Reichardt, E. Dinjus, A. T. Zevaco), Springer, Berlin, Heidelberg, ***2012***, pp. 173-217.

[7] U. Edlund, A. C. Albertsson, *Adv. Polym. Sci.*, ***2000***, *157, 67-112;* V. Siracusa, P. Rocculi, S. Romani, M. D. Rosa, *Trends Food Sci. Technol.*, ***2008***, *19, 634-643;* E. S. Place, J. H. George, C. K. Williams, M. M. Stevens, *Chem. Soc. Rev.*, ***2009***, *38, 1139-1151;* Y. Li, G. A. Thouas, Q. Z. Chen, *RSC Adv.*, ***2012***, *2, 8229-8242.*

1.2 Polycondensation

This synthetic route can be explained as the formation of polymer through repeated condensation reactions of diacids with diols, with formation of water molecules. This reaction usually involves use of solvents, high temperature and vacuum conditions to remove the formed water. These reaction conditions lead to poor control on polymerization process (low molecular weights) and low yields over long reaction time. In fact, in literature are presented few examples where *APEs* with number average molecular weights greater than 30000 are obtained using this synthetic approach to avoid the use of metal catalyst.[8]

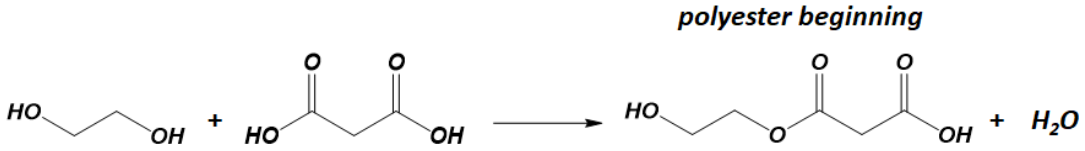

Figure 4: example of starting polycondensation.

[8] H. Shirahama, Y. Kawaguchi, M. S. Aludin, H. Yasuda, *J. Appl. Polym. Sci.*, ***2001***, *80, 340-347*; C. Y. Zhu, Z. Q. Zhang, Q. P. Liu, Z. P. Wang, J. Jin, *J. Appl. Polym. Sci.*, ***2003***, *90, 982-990;* B. Saulnier, J. Coudane, H. Garreau, M. Vert, *Polymer*, ***2006***, *47, 1921-1929;* M. Sokolsky-Papkov, R. Langer, A. J. Domb, *Polym. Adv. Technol.*, ***2011***, *22, 502-511*.

1.3 ROP of cyclic esters

The *ROP* is a form of polymerization in which an active specie attacks a cyclic monomer, causing it to open and the formation of a new reactive center to which further cyclic monomers can be added by ring-opening. Typical monomers that can be polymerized via *ROP* are cyclic amide and esters.

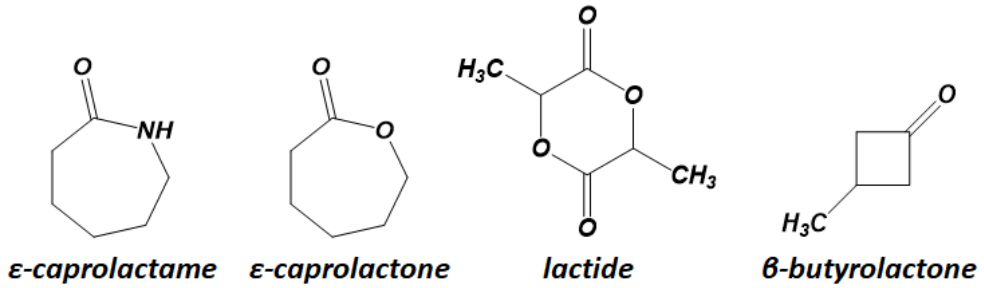

Figure 5: examples of polymerizable monomers via ROP.

Mechanism and thermodynamics of *ROP* were explained in the 1950 but it has been used in the past to synthesize polysaccharides such as dextran, xanthan, gellan gum, diutan gum from anhydro sugars and polypeptides by Leuchs.[9] Actually an industrial application is the production of Nylon-6.

ROP can proceed through anionic, cationic, radical, coordination-insertion and activated monomer mechanism, and it offers many advantages compared to polycondensation: mild reaction conditions, possibility of solvent free polymerization and to avoid the production of small molecules as by-product.[10] The mechanisms below see *LA* as monomer, but they can be extended to other cyclic esters.

Anionic ring-opening polymerization (*AROP*) is a kind of polymerization where the ring-opening of cyclic monomer is induced by an anionic initiator that attacks carbonyl group of *LA*, producing the cleavage of *C-O* bond. The derived specie promotes the propagation step of the polymerization causing the ring-opening and additional of other monomer units (*figure 6*).[11] Species able to promote *AROP* are generally

[9] H. Leuchs, *Ber. Dtsch. Chem.*, ***1906***, *39, 857-861;* A. Conix, G. Smets, *J. of Polym. Scie.*, ***1955***, *15, 221-229;* F. S. Dainton, T. R. E. Devlin, P. A. Small, *Tran. of the Far. Soc.*, ***1955***, *51, 1710-1720.*

[10] O. Nuiken, D. P. Pasken, *Polymers*, ***2013***, *5, 361-403;* R. Tong, *Ind. Eng. Chem. Res.*, ***2017***, *56, 4207-4219.*

[11] A. Bhaw-Luximon, D. Jhurry, N. Spassky, S. Pensec, *J. Polymer*, ***2001***, *42, 9651-9656.*

potassium alcoholates, organic lithium and superbases such as alkyllithium-lithium alcoxide complexes *RLi-LiOR*.[12]

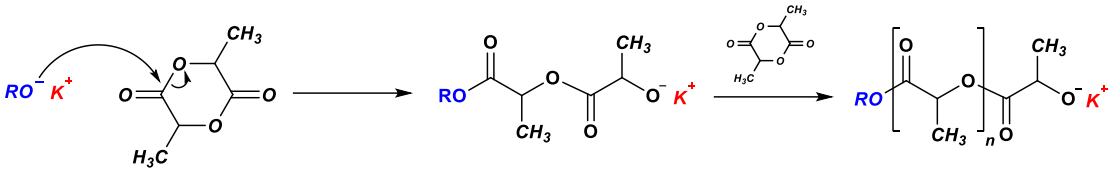

Figure 6: AROP of LA.

Unlike *AROP*, the cationic *ROP* (*CROP*) proceeds by the alkylation of a carbonyl group of *LA*, which becomes positively charged. The propagation step takes place thanks to the nucleophilic attack of another monomeric unit that breaks the *O-CH* bond, giving life a new electrophilic species (*figure 7*).[13]

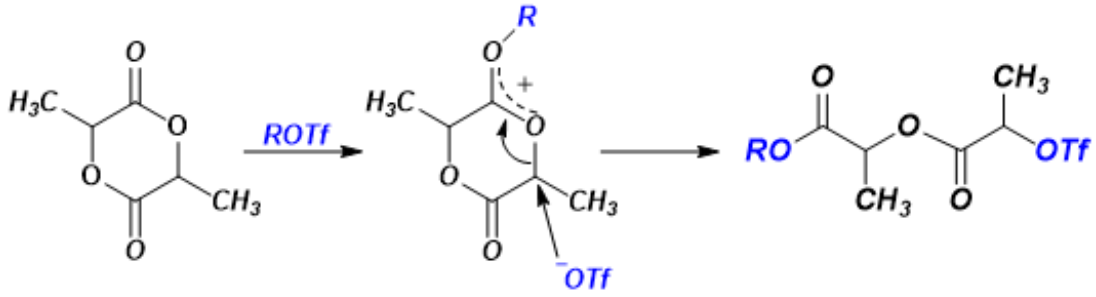

***R** = H, Me or growing polymer chain, **Tf** = CF_3SO_2*

Figure 7: CROP of LA.

Numerous agents have been tested to promote the *CROP* but only trifluoromethanesulfonic acid and methyl trifluoromethanesulfonate have proven to be efficient initiators to 50 °C in nitrobenzene.[14] Promising results were recently obtained

[12] Z. Jedlinski, W. Walach, P. Kurcok, G. Adamus, *Makromol., Chem.*, ***1991***, *192, 201-2057;* H. R. Kricheldorf, C. Boettcher, *Makromol. Chem.*, ***1993***, *194, 1665-1669;* H. R. Kricheldorf, C. Boettcher, *Makromol. Chem., Macromol. Symp.*, ***1993***, *73, 47-64;* L. Lochmann, *J. Inorg. Chem.*, ***2000***, *30, 1115-1126;* B. T. Ko, C. C. Lin, *J. Am. Chem. Soc.*, ***2001***, *123, 7973-7977;* M. H. Chisholm, C. C. Lin, J. C. Gallucci, B. T. Ko, *Dalton Trans*, ***2003***, *71, 406-412.*

[13] C. Scholz, R. A. Gross, *ACS Symp. Ser.*, ***1996***, *5, 317-343;* Z. Tang, X. Chen, Q. Liang, X. Bian, L. Yang, L. Piao, X. Jing, *J. Polym. Sci.*, ***2003***, *41, 1934-1941.*

[14] H. R. Kricheldorf, R. Dunsing, *Makromol. Chem.*, ***1986***, *187, 1611-1625;* H. R. Kricheldorf, I. Kreiser, *Makromol. Chem.* ***1987***, *188, 1861-1873.*

through a combination of acid (such as *HCl*) and a protic agent (such as water or an alcohol).[15]

The most efficient synthetic process for production of polyesters is *ROP* through a coordination-insertion mechanism. Indeed, through appropriate catalytic systems, allows obtaining polymers with controlled properties in terms of molecular weight, stereoregularity and end groups.[16] The first hypothesis for the *ROP* of cyclic esters was formulated by Dittrich and Schulz in 1971 and subsequently Kricheldorf and Teyssié which reported the first experimental proof for such a mechanism in the $Al(O^iPr)_3$-initiated polymerization of lactide.[17] The coordination-insertion mechanism can be so divided:

Coordination of the monomer to metal center;

1) Attack of the alkoxide group to the activated carbonyl carbon via nucleophilic addition, followed with formation a new metal-alkoxide bond;
2) The intermediate undergoes a ring-opening via acyl-oxygen cleavage.

The polymerization ends when the active *O-M* bond is hydrolyzed, which leads to formation of a hydroxyl-end group of the polymer chain (*figure 8)*.[18]

---

[15] Y. Shibasaki, F. Sanda, M. Yokoi, T. Endo, *Macromolecules*, ***2000***, *33, 4316-4320;* S. Penczek, *J. Polym. Sci.*, ***2000***, *38, 1919-1933;* X. Lou, C. Detrembleur, R. Jerome, *Macromolecules*, ***2002***, *35, 1190-1195.*

[16] B. J. O'Keefe, M. A. Hillmyer, W. B. Tolman, *J. Chem. Soc., Dalton Trans.*, ***2001***, *2215-2224;* M. J. Stanford, A. P. Dove, *Chem. Soc. Rev.*, ***2010***, *39, 486-494;* C. M. Thomas, *Chem. Soc. Rev.*, ***2010***, *39, 165-173.*

[17] W. Dittrich, R. C. Schulz, *Angew. Makromol. Chem.*, ***1971***, *15, 109-126;* H. R. Kricheldorf, M. Berl, N. Scharnagl, *Macromolecules*, ***1988***, *21, 286-293;* P. Dubois, C. Jacobs, R. Jerome, P. Tessyé, *Macromolecules*, ***1991***, *24, 2266-2270.*

[18] H. Von Schenk, M. Ryner, A. C. Albertsson, M. Svensson, *Macromolecules*, ***2002***, *35, 1556-1562;* C. Wang, H. Li, X. Zhao, *Biomaterials*, ***2004***, *25, 5797-5801;* R. H. Platel, L. M. Hodgson, C. K. Williams, *Polymer Reviews*, ***2008***, *48, 11-63.*

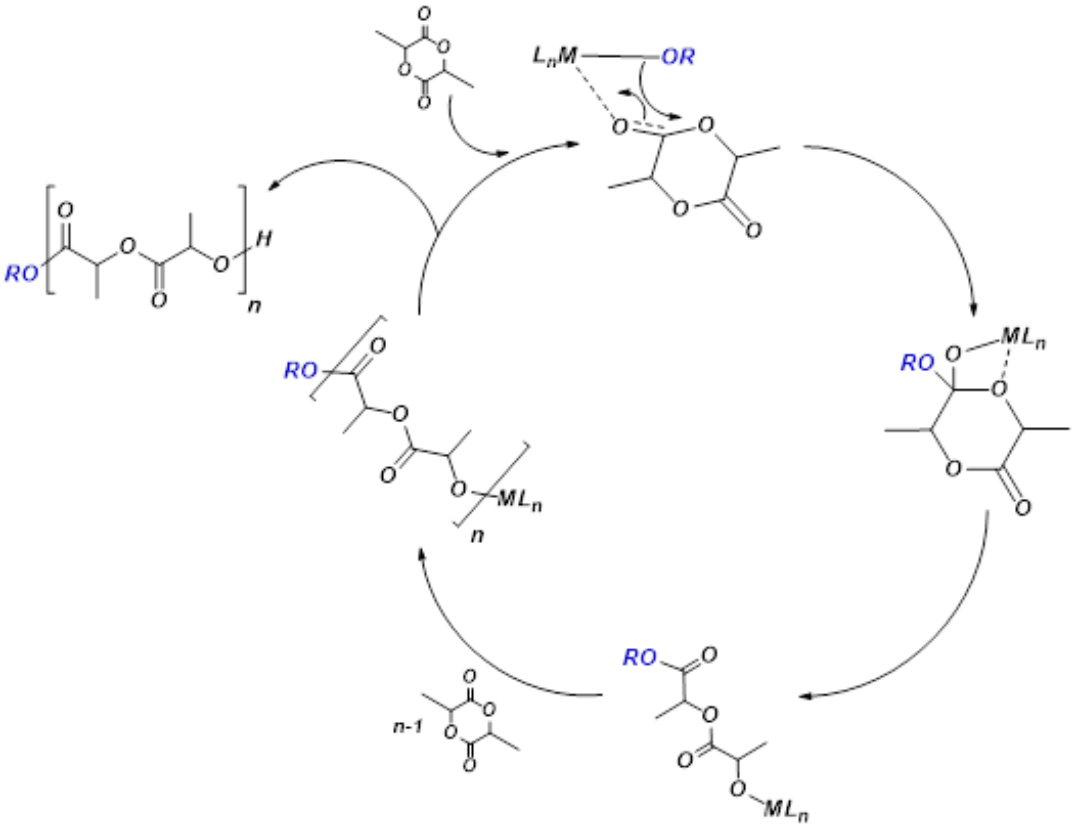

Figure 8: coordination-insertion mechanism of LA.

The coordination-insertion mechanism can be promoted using a nucleophilic agent, which attacks the carbonyl group of lactone previously activated by metal complex (*figure 9*). The activation of monomer is carried out by alcohol, phosphine, ammine, which establishes only an electrostatic interaction with the complex, but attacks the carbonyl group of the ring causing it to open.[19]

[19] F. Nederberg, E. F. Connor, M. Moller, T. Glauser, J. L. Hedrick, *Angew. Chem. Int. Ed.*, ***2001***, *40, 2712-2715;* W. A. Herrmann, *Angew. Chem., Int. Ed.*, ***2002***, *41, 1290-1309;* M. Myers, E. F. Connor, T. Glauser, A. Mock, G. Nyce, J. L. Hedrick, *Polym. Chem.*, ***2002***, *40, 844-851;* N. Ajella, J. F. Carpentier; C. Guillaume, S. M. Guillame, M. Helou, V. Poirier, Y. Sarazin, A. A. Trifonov, *Dalton Trans*, ***2010***, *39, 8363-8376*; Y. Sarazin, B. Liu, T. Roisnel, L. Maron, J. F. Carpentier, *J. Amer. Chem. Soci.*, ***2011***, *133, 9069-9087;* S. –C. Rosca, D. –A. Rosca, V. Dorcet, C. M. Kozac, F. M. Kerton, J. –F. Carpentier, Y. Sarazin, *Dalton Trans.*, ***2013***, *42, 9361-9375;* Y. Sun, Y. Cui, J. Xiong, Z. Dai, N. Tang, J. Wu, *Dalton Trans.*, ***2015***, *44, 16383-16391;* Y. Cui, C. Chen, Y. Sun, J. Wu, X. Pan, *Inorg. Chem. Front.*, ***2017***, *4, 261-269.*

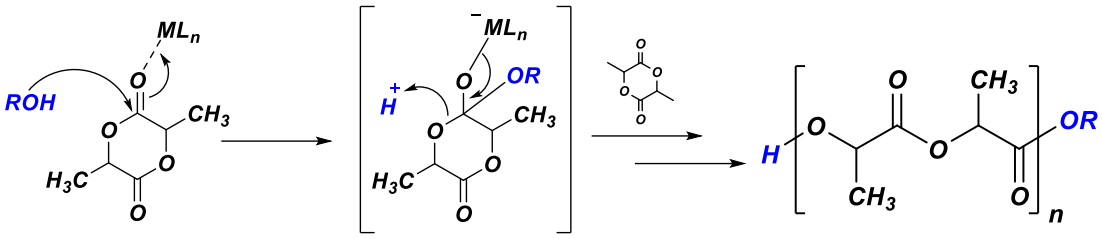

Figure 9: activation of LA.

The molecular weight of final polymer in *ROP* depends on from the ratio $k_{propagation}$ / $k_{initiation}$ and from the transesterification inter- or intra-molecularly (*figure 10*). These undesirable side reactions were found to depend strongly on the metallic center of initiator, and sometimes they are the origin of broader molecular weight distributions.[20]

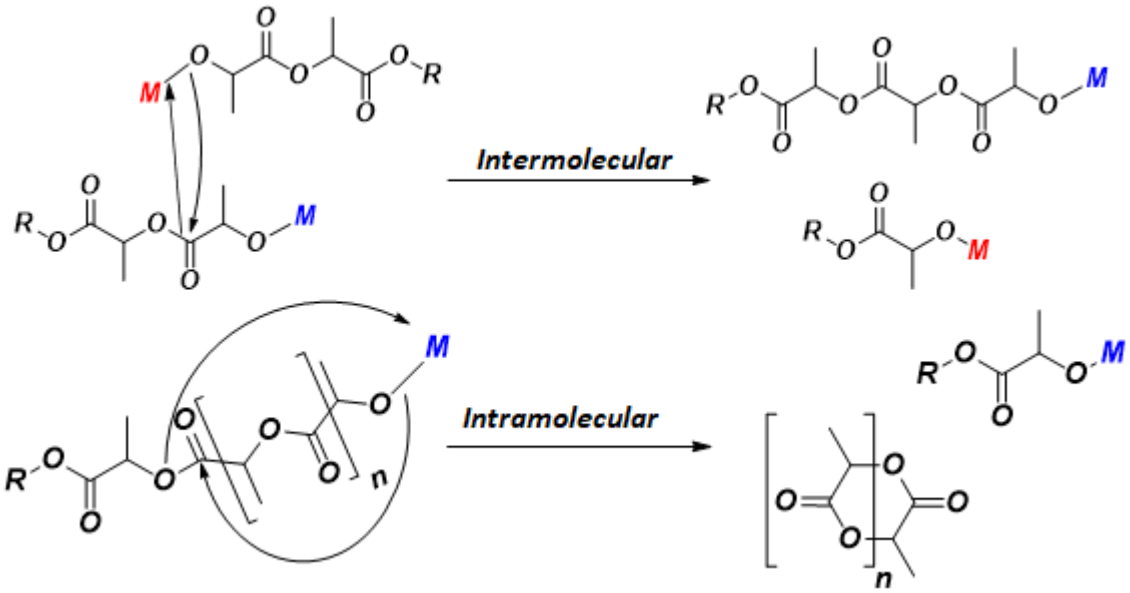

Figure 10: inter- and intra-molecular transesterification of PLA.

[20] J. Baran, A. Duda, A. Kowalski, R. Szymanski, S. Penczek, *Macromol. Symp.*, ***1997***, *123, 93-101;* S. Penczek, A. Duda, R. Szymanski, *Macromol. Symp.*, ***1998***, *132, 441-449.*

1.4 Immortal ROP

The addition of a nucleophilic agent, for example an alcohol, in combination with the catalyst has a beneficial effect on polymerization process. In absence of an alcohol, the maximum number of growing polymer chains is equal to the number of active sites or possibly to the number of metal atoms in the catalyst. Alcohol acts as a chain transfer agent, causing chain transfer between growing and dormant macromolecules. In this way, the number of growing polymer chains becomes equal to or greater than the number of metal atoms in the catalyst. This type of cyclic esters polymerization is called "immortal *ROP*". However, due to the reaction speed, transesterification reactions are more likely than in the absence of a nucleophilic agent, and for this reason it is easy to find polymers with high *Đs* and lower molecular weights than expected.[21]

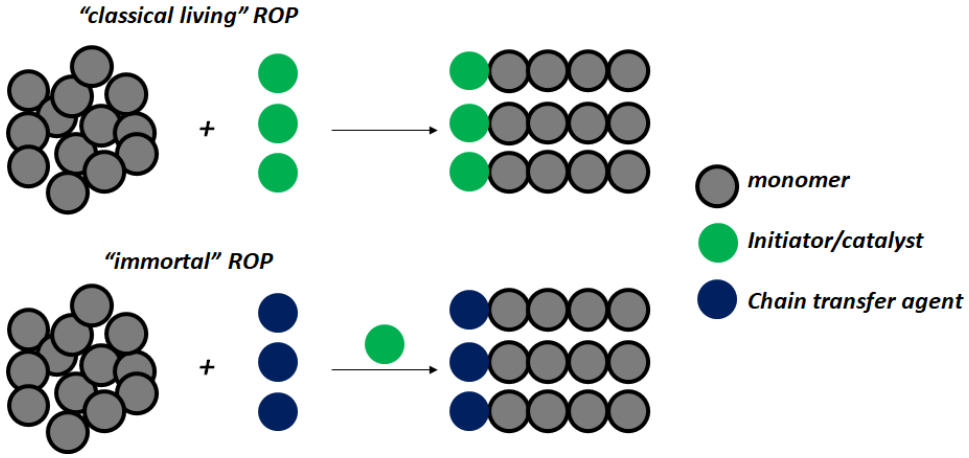

Figure 11: classical living and immortal representation of ROP.

[21] S. Asano, T. Aida, S. Inoue, *J. Chem. Soc., Chem. Commun.*, ***1985**, 1148-1149;* S. Inoue, *Makromol. Chem., Macromol. Symp.*, ***1986**, 3, 295-300;* Y. Sarazin, V. Poirier, T. Roisnel, J. –F. Carpentier, *Eur. J. Inorg, Chem.*, ***2010**, 3423-3428.*

1.5 Short summary of the active catalyst in ROP

Simple homoleptic metal complexes constituted the first generation of active initiators for *ROP* of ε-*CL* and *LA*. The complex used for industrial preparation of *PCL* and *PLA* is undoubtedly *tin(II)bis(2-ethylhexanoate)*, referred to as $Sn(Oct)_2$. It is highly active, commercially available, easy to handle, soluble in melt monomers and allows obtaining high molecular weight polymers. The problem of $Sn(Oct)_2$ is its toxicity, which is an drawback in case of biomedical applications of polymer and requires high temperature, which favors intermolecular and intramolecular transesterification reactions.[22] *Al* alkoxides [$Al(O^iPr_3)$] and zinc derivates [*ZnO*, $Zn(lactate)_2$,etc…] have also proved to be efficient catalyst for *ROP* of several cyclic esters, but less active than tin compounds because of underside aggregation phenomena and transesterification reactions, thus inhibiting the propagation of polymerization.[23] The studies on *Al* alkoxides has stimulated the investigation of researches of alkoxides of other metals, especially yttrium and lanthanum, which proved to be much more active than *Al* compounds.[24]

Then attention focalized on a second catalyst generation of heteroleptic type with formula: L_nMX_m (L = ligand; M = metal center; X = initiator group). Ligand is important for catalyst design because it can influence the catalytic activity through chelating, electronic and steric effects and reduce transesterification reaction.[25] Thanks

[22] P. Degée, P. Dubois, R. Jerome, S. Jacobsen, H. G. Fritz, *Macromol. Symp.*, ***1999**, 144, 289-302.*

[23] H. R. Kricheldorf, D. O. Damrau, *Macromol. Chem. Phys.*, ***1997**, 198, 1753-1766;* A. Kowalski, A. Duda, S. Penczek, *Macromolecules*, ***1998**, 31,2114-2122;* F. Chabot, M. Vert, S. Chapelle, P. Granger, *Polymer*, ***1983**, 24, 53-59;* G. Schwach, J. Coudane, R. Engel, M. Vert, *Polym. Int.*, ***1998**, 46, 177-182.*

[24] W. M. Stevels, M. J. K. Ankoné, P. J. Dijkstra, J. Feijen, *Macromolecules*, ***1996**, 29, 33232-3333;* W. M. Stevels, M. J. K. Ankoné, P. J. Dijkstra, J. Feijen, *Macromolecules*, ***1996**, 29, 6132-6138;* M. Save, A. Soum, *Macromol. Chem. Phys.*, ***2002**, 203, 2591-2603;* H. Li, C. Wanh, F. Bai, J. Bai, H. G. Woo, *Organometallics*, ***2004**, 23, 1411-1415.*

[25] Y. Yu, E. J. Fischer, G. Storti, M. Morbidelli, *Ind. Eng. Chem. Res.*, ***2014**, 53, 7333-7342;* S. R. Kosuru, T. H. Sun, L. F. Wang, J. K. Vandavasi, W. Y. Lu, Y. C. Lai, S. C. N. Hsu, M. Y. Chiang, H. Y. Chen, *Inorg. Chem.*, ***2017**, 56, 7998-8006;* L. Qin, Y. Zhang, J. Chao, J. Cheng, X. Chen, *Dalton Trans.*, ***2018**, 48, 12315-12325;* D. J. Marell, A. M. Luke, M. Mandal, B. D. Neisen, D. J. Marell, C. J. Cramer, W. B. Tolman, *Inorg. Chem.*, ***2018**, 57, 3451-3457;* C. –C. Chang, Y. –C. Chang, W. –Y. Lu, Y. –C. Lai, K. –H. Wu, Y. –F. Lin, H. –Y. Chen, *Eur. Polym. J.*, ***2019**, 115, 399-408.*

also to the development of numerous ligands, this second generation allows a better control on polymerization process and many metals have been tested in the *ROP* of cyclic esters.[26] Scientific research is currently focused on the development of catalytic systems based on non-toxic metals, such as Titanium, Zirconium, Hafnium, Magnesium[27], Calcium[28], Iron[29], Aluminum, etc.

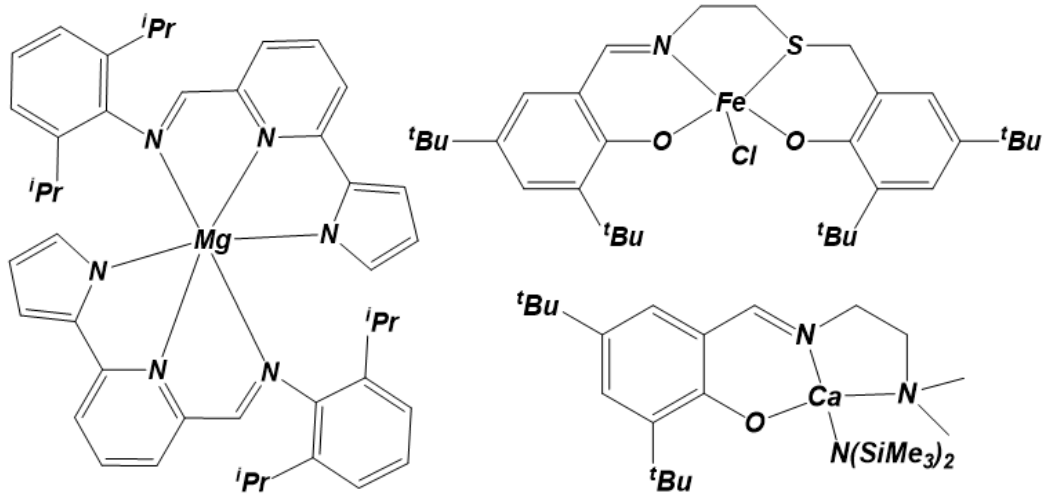

Figure 12: examples of non-toxic metal complexes reported in literature.

[26] H. Ma, T. P. Spaniol, J. Okuda, *Angew. Chem.*, ***2006***, *118, 3554-3558*; A. Amgoune, C. M. Thomas, J.F. Carpentier, *Macromol. Rapid Commun.*, ***2007***, *28, 693-697*; M. Zintl, F. Molnar, T. Urban, V. Bernhart, P. Preishuber-Pflu, B. Rieger, *Angew. Chem. Int. Ed.*, ***2008***, *47, 3458-3460.*

[27] I. D'Auria, C. Tedesco, M. Mazzeo, C. Pellecchia, *Dalton Trans*, ***2017***, *46, 12217-12225;* P. McKeown, S. N. McCormick, M. F. Mahona, M. D. Jones, *Polym. Chem.*, ***2018***, *9, 5339-5347;* W. A. Munzeiwa, V. O. Nyamori, B. Omondi, *Inorg. Chim. Acta.*, ***2019***, *487, 264-274;* R. M. Slattery, A. E. Stahl, K. R. Brereton, A. L. Rheingold, D. B. Green, J. M. Fritsch, *J. Polym. Sci. A Polym. Chem.*, ***2019***, *57, 48-59.*

[28] J. B. L. Gallaway, J. R. K. McRae, A. Decken, M. P. Shaver, *Can. J. Chem.*, ***2012***, *90, 419-426;* M. –W. Hsiao, G. –S. Wu, B. –H. Huang, C. –C. Lin, *Inorg. Chem. Commun.*, ***2013***, *36, 90-95.*

[29] E. Fazekas, G. S. Nichol, J. A. Garden, M. P. Shaver, *ACS Omega*, ***2018***, , *3, 16945-16953;* O. J. Driscoll, C. K. C. Leung, M. F. Mahon, P. McKeown, M. D. Jones, *Eur. J. Inorg. Chem.*, ***2018***, *47, 5129-5135;* M. Cozzolino, V. Leo, C. Tedesco, M. Mazzeo, M. Lamberti, *Dalton Trans.*, ***2018***, *47, 13229-13238;* Y. Liang, R. –L. Duan, C. –Y. Hu, L. –L. Li, X. Pang, W. –X. Zhang, X. –S. Chen, *Chin. J. Polym. Sci.*, ***2018***, *36, 185-189.*

1.6 Cyclic esters

As previously mentioned, cyclic esters can be polymerized to give aliphatic polyesters and are therefore considered potential substitutes for olefins. However, a certain number of these polymer precursors are obtained from fossil resources while others derive from appropriate biomass treatments. Therefore, a large number of cyclic esters are available and, since their structural diversity is not insignificant, it is advisable to select in advance the monomers on the basis of the polymer to be obtained.[30] In this work, two cyclic esters have been chosen on the basis above all of their importance from an applicative point of view. The esters selected were *LA* and *ε-CL*. The polymers synthesized starting from the selected monomers are briefly described below.

[30] G. L. Gregory, E. M. Lopez-Vidal, A. Buchard, *Chem. Commun.*, ***2017**, 53, 2198-2217;* X. Zhang, M. Fevre, G. O. Jones, R. M. Waymouth, *Chem. Rev.*, ***2018**, 118, 839-885.*

1.7 Polycaprolactone (PCL)

PCL is a biodegradable polymer composed of hexanoate repeat units and can reach a degree of crystallinity of 69%. The properties of this aliphatic polyester depend on its molecular weight and its degree of crystallinity.

Table 1: properties of PCL

Properties	Range
Number average molecular weight (g/mol)	530 - 630000
Density (g/cm^3)	1,071 - 1,200
Glass transition temperature (°C)	(-65) - (-60)
Melting Temperature (°C)	56 - 65
Tensile strength (Mpa)	4 - 78,5
Decomposition temperature (°C)	350
Tensile strength (Mpa)	4 - 78,5
Young Modulus (Gpa)	0,21 - 0,44
Elongation at break (%)	20 - 1000

It's highly soluble at room temperature in chloroform, benzene, toluene, but slightly soluble in acetone, alcohols, diethyl ether and water. It shows a very good miscibility with a large variety of polymers, such as polyvinyl chloride, poly(styrene-acrylonitrile), nitrocellulose, poly(bisphenol-A) and other polycarbonates, and is mechanically compatible with polyolefins and natural rubber.[31] The biodegradability of *PCL* depend on several factors (degree of crystallinity, molecular weight and conditions of degradation), and many microorganisms in nature are able to biodegrade

[31] V. R. Sinha, K. Bansal, R. Kaushik, R. Kumria, A. Trehan, *Int. J. Pharm.*, ***2004***, *278, 1-23.*

this polyester, but it cannot be degraded in the body by enzymatic degradation.[32] *PCL* can be used in various sectors ranging from packaging to electronics.[33]

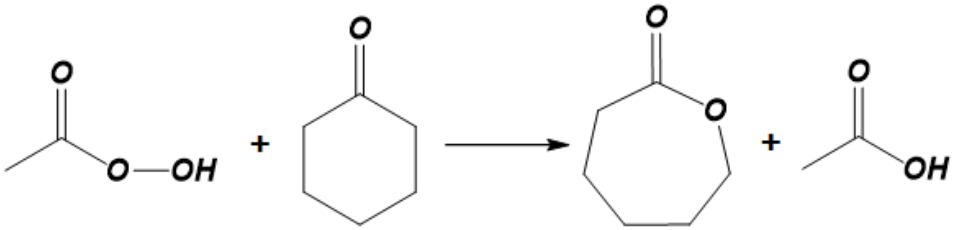

Figure 13: production of ε-caprolactone from cyclohexanone.

The *PCL* can be produced by two methods: condensation of 6-hydroxycaproic acid (6-hydroxyhexanoic acid)[34] or *ROP* of *ε-CL*. The ε-caprolactone (ε-CL) is industrially produced from the oxidation of cyclohexanone by peracetic acid (*figure 13*).[35]

The catalyst used for *ROP* of *ε-CL* is the stannous (II) ethylhexanoate (or stannous octanoate) in combination with a nucleophilic compound (generally an alcohol) and generally, the reaction temperature required is up to 175 °C. The reaction time can vary between 2/3 hours, with stirring and inert gas flow applied continuously during polymerization. The polymer will arrive in the molten state, and it can be processed (extruded or pelletized later).[36]

---

[32] D. R. Chen, J. Z. Bei, S. G. Wang, *Polym. Degrad. Stab.*, ***2000**, 67, 455-459;* Y. Ikada, H. Tsuji, *Macromol. Rapid Commun.*, ***2000**, 21, 117-132*; R. A. Gross, B. Kalra, *Science*, ***2002**, 297, 803-807;* C. X. F. Lam, S. H. Teoh, D. W. Hutmacher, *Polym. Int.*, ***2007**, 56, 718-728;* P. Joshi, G. Madras, *Polym. Degrad. Stab.*, ***2008**, 93, 1901-1908;* M. A. Woodruff, D. W. Hutmacher, *Prog. Polym. Sci.*, ***2010**, 35, 1217-1256.*

[33] J. L. Hendrick, T. Magbitang, E. F. Connor, T. Glauser, W. Volksen, C. J. Hawker, V. Y. Lee, R. D. Miller, *Chem.-Eur. J.*, ***2002**, 8, 3308-3319.*

[34] C. Braud, R. Devarieux, A. Atlan, C. Ducos, V. Michel, *J. Chromatogr., B: Biomed. Sci. Appl.*, ***1998**, 706, 73-82;* H. Dong, H. –D. Wang, S. –G. Cao, J. –C. Shen, *Biotechnol. Lett.*, ***1998**, 20, 905-908;* A. Mahapatro, A. Kumar, R. A. Gross, *Biomacromolecules*, ***2004**, 5, 62-68.*

[35] M. C. Rocca, G. Carr., A. B. Lambert, D. J. Macquerrie, J. H. Clark, *US Pat., 6, 531, 615 B2, **2003**.*

[36] A. Kowalski, A. Duda, S. Penczek, *Macromol. Rapid Commun.*, ***1998**, 19, 567-572;* A. Kowalski, A. Duda, S. Penczek, *Macromolecules*, ***2000**, 33, 689-695;* J. Libiszowski, A. Kowalski, A. Duda, S. Penczek, *Macromol. Chem. Phys.*, ***2002**, 203, 1694-1701;* M. Degirmenci, G. Hizal, Y. Yagci, *Macromolecules*, ***2002**, 35, 8265-8270;* M. Degirmenci, O. Izgin, Y. Yagci, *J. Polym. Sci., Part A: Polym. Chem.*, ***2004**, 42, 3365-3372;* B. Kiskan, Y. Yagci, *Polymer*, ***2005**, 46, 11690-11697;* A. Bhaw-Luximon, D. Jhurry, S. Motala-Timol, Y. Lochee, *Macromol. Symp.*, ***2005**, 231, 60-68.*

1.8 Polylactide (PLA)

PLA is a synthetic biocompatible, biodegradable and non-toxic polyester with similar properties to *PS* and *PET*.[37] Under appropriate conditions, it can be decomposed by enzymatic process to water and carbon dioxide (*figure 14)* or recycled through mechanical or chemical processes (*figure 15*).[38]

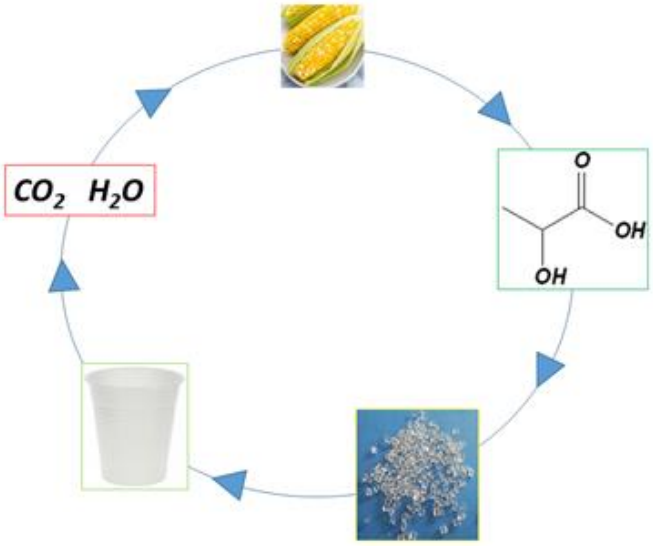

Figure 14: life cycle of PLA.

[37] T. Suyama, Y. Tokiwa, P. Quichanpagdee, T. Kanagawa, Y. Kamagata, *App. Environ. Microbiol*, ***1998***, *64, 5008-5011;* T. R. Al-Itry, K. Lamnawar, A. Maazouz, *Polym. Degrad. Stab.*, ***2012***, *97, 1898-1914;*

[38] H. Tsuji, Y. Ikada, *J. Appl. Polym. Sci.*, ***1998***, *67, 405-415;* L. I. Palade, H. J. Lehermeier, J. R. Dorgan, *Macromolecules*, ***2001***, *34, 1384-1390;* M. Buggy, *Natural Fibres, Biopolymers and Biocomposites* (Eds. A. Mohanty, M. Misra, L. Drzal,) CRC Press, Taylor & Francis Group, *New York*, ***2005***; H. Kometani, T. Matsumura, T. Suga, T. Kanai, *Int. Polym. Process.*, ***2006***, *21, 24-31;* F. Vilaplana, S. Karlsson, *Macromol. Mater. Eng.*, ***2008***, *293, 274-297;* S. M. Al-Salem, P. Lettieri, J. Baeyens, *Waste Manage*, ***2009***, *29, 2625-2643;* V. Piemonte, F. Gironi, *J. Polym. Environ.*, ***2013***, *21, 313-318;* M. F. C. de Andrade, P. M. Souza, O. Cavalett, A. R. Morales, *J. Polym. Ednviron.*, ***2016***, *24, 372-384.*

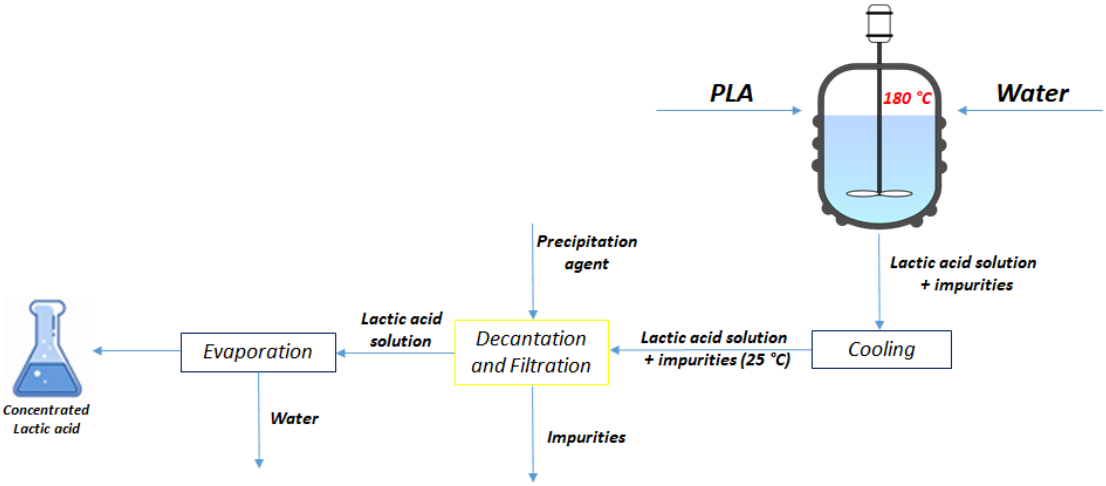

Figure 15: chemical recycle process of PLA.

In 1932, Carothers (*DuPont)* discovered that *PLA*, with a low molecular weight, maybe synthesized by heating *lactic acid* under vacuum. At the beginning, the uses of *PLA* were limited to medical application such as sutures and bioabsorbable implants due to high cost of production and low molecular weight.[39] The recent advancement that has dramatically reduced the cost to make *lactic acid*, which is the monomer of *PLA* production, allowed an increase world production of polymer, so much so that today it also used in packaging.[40]

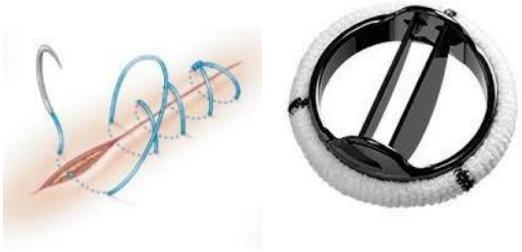

Figure 16: biocompatible implants.

Actually, it is produced on a large scale in two big plants by Total Corbion in Thailand and NatureWorks LLC in USA, but also in some smaller plants in the world: Kanebo Gohsen Ltd, Shimadzu Corp, Toray Industries, Kuraray and Mitsui Chemicals.[41]

[39] E. S. Lipinsky, R. G. Sinclair, *Chem. Eng. Prog.*, ***1986***, *82, 26-32.*

[40] R. Auras, B. Harte, S. Selke, *Macromol. Biosci.*, ***2004***, *4, 835–864.*

[41] K. Yamanda, *Chem. Fibers Int.*, ***1999***, *49, 501-503;* M. Matsui, *Chem. Fibers Int.*, ***1996***, *46, 318-319;* M. Dartee, J. Lunt, A. Shafer, *Man-Made Fiber Year Book*, **2001**, *29.*

Experts predict that there will be an increase significantly *PLA* production capacity from 2018 to 2023.[42]

Figure 17: NatureWorks plant.

The production of *PLA* starts from plants with the extraction of starch (from corn, rice, wheat) or sugar (from sugar beet, whey, molasses).[43] The starch is converted to glucose and dextrose (fermentable sugars) by enzymatic hydrolysis. Microorganisms into a smaller molecule known as *lactic acid*, through fermentation, convert these sugars.[44] Fermentation generally leads to a mixture of the two optically active stereoisomers of *lactic acid*: 99,5% (*L*) and 0,5% (*D*).[45] The polycondensation of *lactic acid* were carried out under vacuum and high temperature, for the first time, by Carothers to produce *PLA*. However, due to difficulties of removing water produced by condensation reaction, the polymer obtained tends to have low to intermediate molecular weight (10000 – 20000).[46]

A second method is the ring-opening polymerization (*ROP*) of lactide (*LA*), the cyclic dimer of *lactic acid*. The prepolymer or oligomers that are formed are depolymerized and then all are subsequently polymerized. The *ROP* uses milder conditions of reaction

[42] European Bioplastics. Bioplastics Market Data. Available online: https://www.european-bioplastics.org/market/ (accessed on *12 February* ***2019***).

[43] R. Hagen, *Chem. Fibers Int.*, ***2000**, 50, 540-542;* C. Woodings, *Nonwovens World*, ***2001**, 10, 71-78;* P. A. Koch, *Chem. Fibers Int.*, ***2003**, 53, 426-432.*

[44] D. J. Sawyer, *Macromol Symp.*, ***2003**, 201, 271-281.*

[45] O. Avinc, A. Khoddami, *Fiber Chemistry*, ***2009**, 41, 391-401.*

[46] W. Zhong, J. Ge, Z. Gu, W. Li, X. Chen, Y. Zang, *J. of Appl. Polym. Sci.*, ***1999**, 74, 2546-2551;* J. C. Bogaert, P. Coszach, *Nonwovens World*, ***2000**, 9, 83-91;* J. R. Dorgan, H. J. Lehermeier, L. Palade, J. Cicero, *Macromol. Symp.*, ***2001**, 175, 55-66.*

and leads to higher molecular weight polymer thanks to the fact that the formation of small molecules, such as water, is avoided.[47]

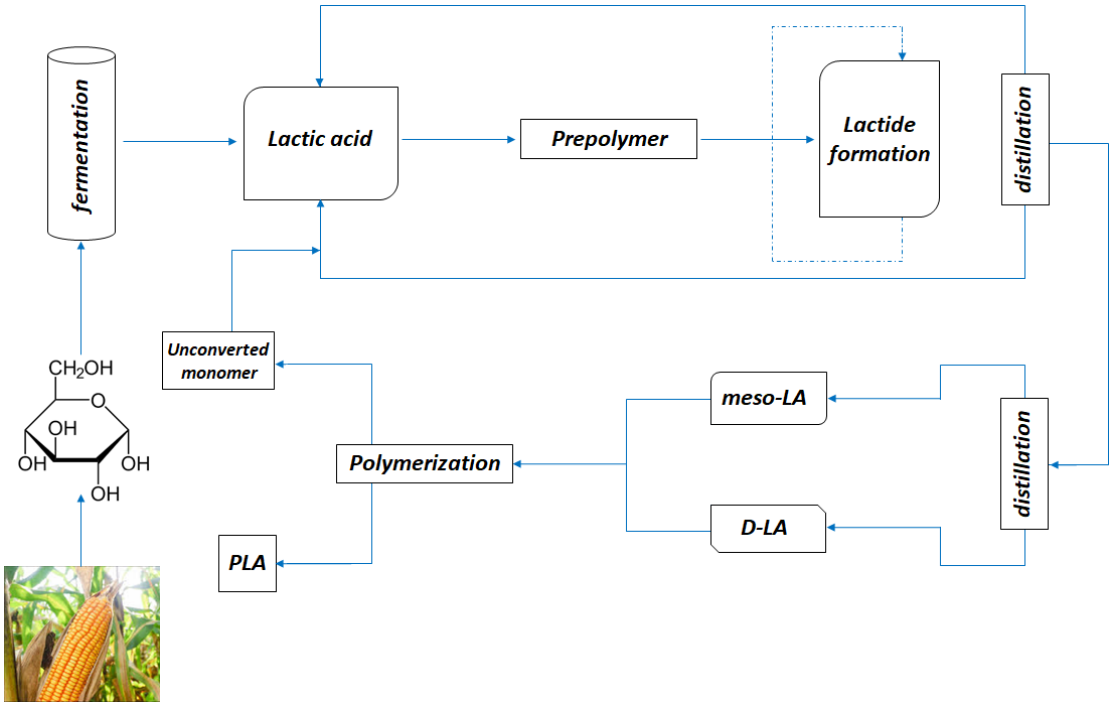

Figure 18: PLA production plant.

There are three different stereoisomeric forms of *LA*, namely: *L-lactide*, *D-lactide* and *meso-lactide*.

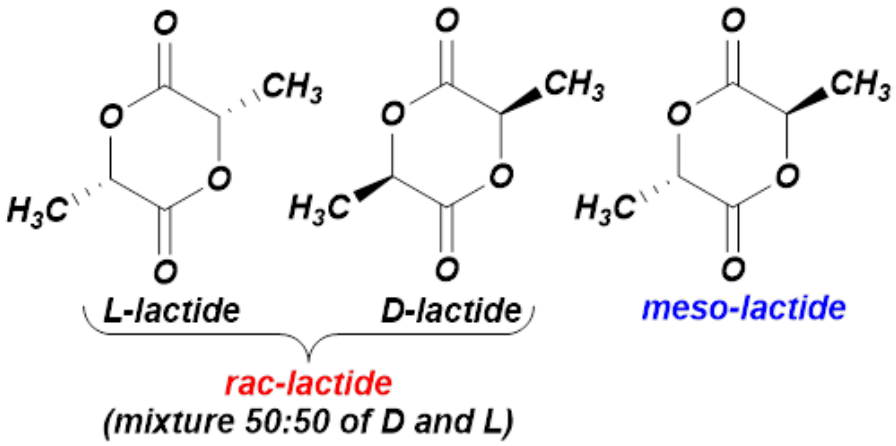

Figure 19: different forms of LA isomers.

[47] A. Yamaguchi, et al., *J Env Polym Degradation*, ***1995***, *3, 25-34;* R. E. Drumright, P. R. Gruber, D. E. Henton, *Adv. Mater.*, ***2000***, *12, 1841-1846;* O. Dechy-Cabaret, B. Martin-Vaca, D. Bourissou , *Chem. Rev.*, ***2004***, *104, 6147–6176.*

Meso-lactide is optically inactive, and it has a lower melting point than optically active *L-* and *D-LA*. *rac-LA* is a mixture 50:50 of *D* and *L* forms. *ROP* gives to different stereopolymers that depending on starting *LA*.[48] The possible microstructures of the *PLA* are shown in the *figure 21* below.

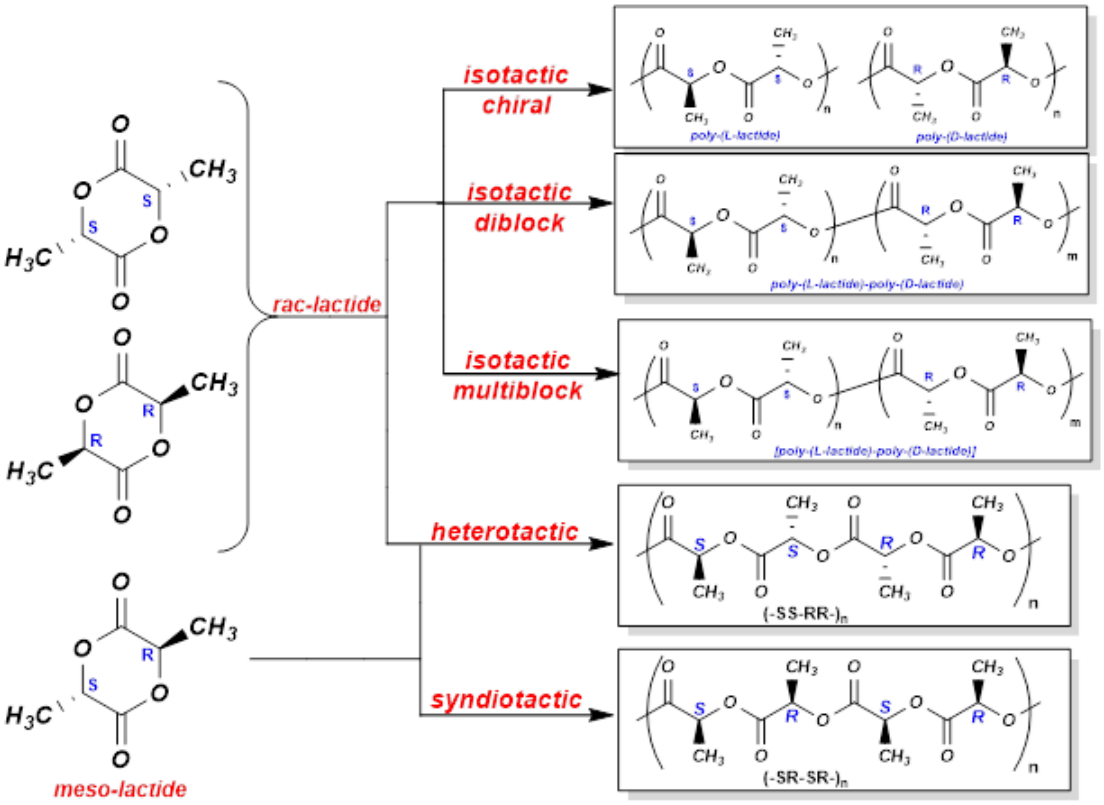

Figure 20: microstructures of PLA.

The *ROP* of *LA* allows the possibility to obtain a polymer with controlled physical properties; indeed, the tacticity influences the physical properties and different types of *PLA* could be obtained by controlling sequences of the optical isomers of the *LA* into polymer. Different melting points of *PLA* varying from 130 to 220 °C: *P(L)LA*, having only *L-lactide* units, and *P(D)LA*, having only *D-lactide* units, are semicrystalline and hard polymers with a T_g of about 60 °C and a T_m around 180 °C; the corresponding syndiotactic *PLA* has a T_m of about 150 °C. A blend of *P(L)LA* and *P(D)LA* (1:1) can lead to a final polymeric stereocomplex with a T_m higher than either *D-* or *L*-polymers, around 220 °C. Otherwise, atactic and heterotactic, having a random stereosequence, are not crystalline but they are amorphous transparent materials, with a T_g range of 50-60 °C, and soluble in common solvents as acetonitrile, chloroform

[48] S. Jacobsen, H. G. Fritz, P. Degee, P. Dubois, R. Jerome, *Ind. Crops Prod.*, ***2000***, *265-275.*

and toluene.[49] *ROP* of *L-LA* produce isotactic *PLA*, if there is no epimerization of stereogenic centers. With *meso-* and *rac-LA* it is possible to obtain different microstructures depending on the mechanisms for controlling stereochemistry: control by terminal chain (**1**) or control by active site (**2**).

(1) The last unit inserted controls the insertion of the next one. This control allows to obtain isotactic *PLA* from *rac-LA* and heterotactic *PLA* from *meso-LA* if the system prefers a homochiral insertion (**a**). Should the system prefer a heterochiral insertion, syndiotactic *PLA* is obtained from *meso*-LA and heterotactic *PLA* from *rac-LA* (**b**).

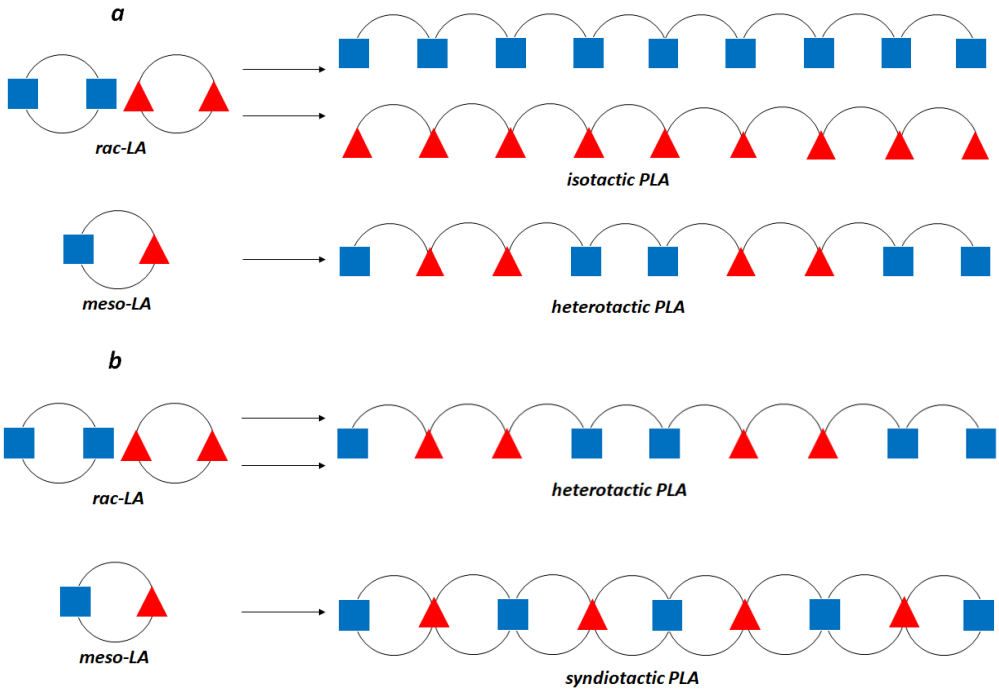

Figure 21: control by chain end. a) homochiral preference; b) heterochiral preference.

(2) The chirality of the catalytic site controls the stereochemistry of monomer insertion, obtaining syndiotactic *PLA* from *meso*-LA and isotactic *PLA* from *rac*-LA.

[49] T. Okihara, M. Tsuji, A. Kawaguchi, K. I. Katayama, *J. Macromol. Sci.-Phys.*, ***1991***, *30, 119-140;* S. Brochu, R.E. Prud'homme, I. Barakat, R. Jerome, *Macromolecules*, ***1995***, *28, 5230-5239;* H. R. Kricheldorf, *Chemosphere*, ***2001***, *43, 49-54;* B. Linnemann, M. S. Harwoko, T. Gries, *Chemical Fibers International*, ***2003***, *53, 426-433.*

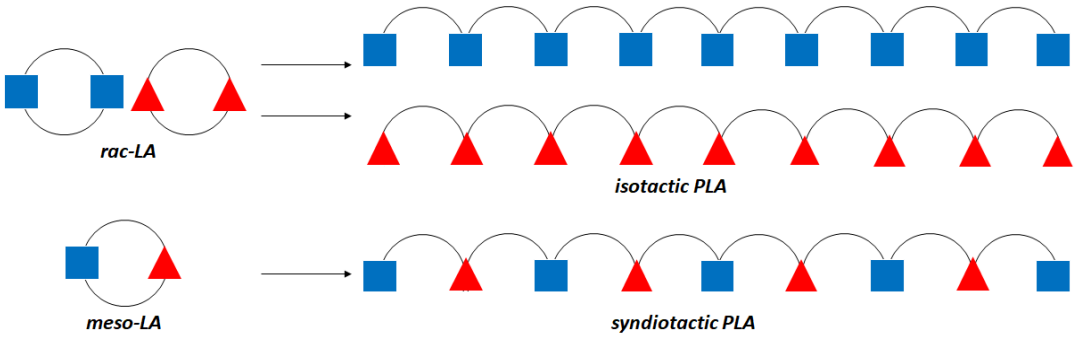

Figure 22: control by catalytic site.

1.9 Aim of PhD project

This PhD project has the aim to develop new catalytic system for the *ROP* of cyclic esters based on group *IV* or *Al* metal complexes. The chosen metals are nontoxic, biocompatible and non-expensive. These characteristics are high desirable for effective catalysts for the *ROP* of cyclic esters since trace amounts of the catalyst may be incarcerated within the polymer and this may affect the quality and the utility of the polymer product. The use of catalysts based on nontoxic and biocompatible metals is a high desirable goal both in academic and industrial field.

The aim of the project has been pursued through the synthesis and characterization of new ligands featuring amide donor groups because amide donor ligands have been proven to be well-suite ligands for early transition metals. Moreover, as the combination of hard and soft donor groups was proved to be effective in obtaining effective catalytic systems, we decided to pair the hard Lewis nitrogen donor atoms with neutral sulphur atoms. In particular in this project we developed linear bidentate, tetradentate and tridentate ligands that exhibit amide functions coupled with thioether groups (*NS*, *NSSN* and *NSO*).

It is worth to note that the efficiency of group *IV* and *Al* complexes with amide ligands in the *ROP* of cyclic esters was barely explored.[50] The most significant results with group *IV* initiators featuring amide ligands are reported by Mountford, Dagorne and Otero. Mountford et al. developed group *IV* initiators supported by tetradentate bis(sulfonamide)amine ligands (A in *figure 23*), which were fairly active (95% of 100 equivalents within 6 h in toluene at 70 °C) with good control over the polymerization process.[51] Dagorne et al. reported on *Zr* complexes with tetradentate dianionic cyclam

[50] K. –C. Hsieh, W. –Y. Lee, L. –F. Hsueh, H. M. Lee, J. –H. Huang, *Eur. J. Inorg. Chem.*, ***2006***, *11, 2306-2312;* Y. Ning, Y. Zhang, A. Rodriguez-Delgado, E. Y. –X. Chen, *Organometallics*, ***2008***, *27, 5632-5640;* F. Zhang, H. Song, G. Zi, *J. Organomet. Chem.*, ***2010***, *695, 1993-1999;* R. Lapenta, M. Mazzeo, F. Grisi, *RSC Adv.*, ***2015***, *5, 87635-87644;* H. –C. Tseng, F. –S. Chen, M. Y. Chiang, W. –Y. Lu, Y. –H. Chen, Y. –C. Laia, H. –Y. Chen, *RSC Adv.*, ***2015***, *5, 90682–90690;* C. G. Gianopoulos, N. Kumar, Y. Zhao, L. Jia, K. Kirschbauma, M. R. Mason, *Dalton Trans.*, ***2016***, *45, 13787–13797;* Y. Wei, S. Wang, S. Zhou, *Dalton Trans.*, ***2016***, *45, 4471-4485.*

[51] A. D. Schwarz, A. L. Thompson, P. Mountford, *Inorg. Chem.*, ***2009***, *48, 10442-10454;* A. D. Schwarz, K. R. Herbert, C. Paniagua, P. Mountford, *Organometallics*, ***2010***, *29, 4171-4188.*

ligands (B in *figure 23*) afforded *PLA* with narrow *Đs* and predictable molecular weights.[52] Recently, Otero et al. described a series of robust and thermally stable *Zr* complexes coordinated by *NON*-scorpionate ligands (C in *figure 23)* that resulted active in the *ROP* of unpurified *rac-LA* under industrially conditions (absence of solvent, elevated temperature and monomer not rigorously purified).[53]

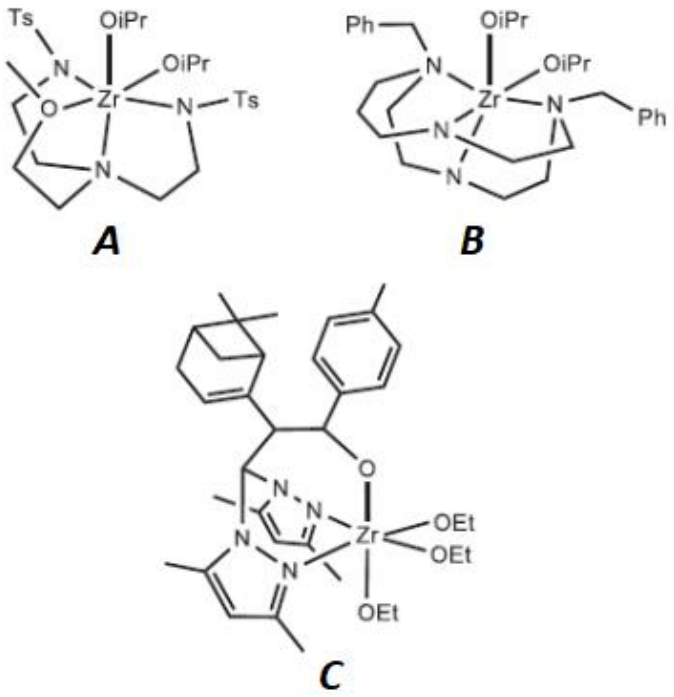

Figure 23: structure of group IV catalysts reported in literature.

As concern the *Al* complexes supported by amide ligands, the most significant examples are the following. Dagorne et al. developed a family of *Al* complexes (A in *figure 24*) of the type (*NON*)*AlX*. The complexes were active in *ROP* of *rac-LA* and *ε-CL* with a good control over the polymerization process (narrow *Đs* and molecular weights that grow linearly over time).[54] Recently, Chen et al. reported a series of *Al* complexes bearing amidate ligands and tested them in the *ROP* of *ε-CL*. The results after the optimization of the polymerization conditions revealed that an *Al* complex

[52] L. G. Alves, F. Hild, R. F. Munhá, L. F. Veiros, S. Dagorne, A. M. Martins, *Dalton Trans.*, ***2012***, *41, 14288-14298.*

[53] A. Otero, J. Fernández-Baeza, A. Garcés, L. F. Sánchez-Barba, A. Lara-Sánchez, J. Martinez-Ferrer, *Dalton Trans.*, ***2017***, *46, 6654-6662.*

[54] F. Hild, N. Neehaul, F. Bier, M. Wirsum, C. Gourlaouen, S. Dagorne, *Organometallics*, ***2013***, *32, 2, 587–598.*

bearing (4-methoxyphenyl)carbamate (B in *figure 24*) had the highest catalytic activity and allowed to obtained polymers with narrow *Đs*.[55]

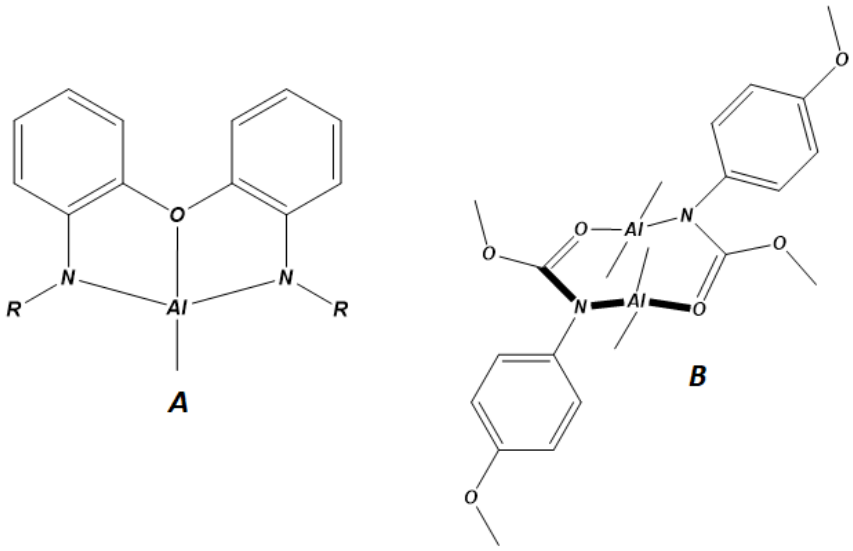

Figure 24: Al complexes reported in literature.

We hope that our study could contribute to deepen the structure−activity relationships affecting the reactivity of group *IV* and *Al* complexes and to furnish a guidance to the modifying of the supporting ligands to tune catalyst reactivity.

[55] H. –T. Tseng, F. –S. Chen, M. Y. Chiang, W. –Y. Lu, Y. –H. Chen, Y. –C. Lai, H. –Y. Chen, *RSC Adv.*, ***2015***, *5*, *90682–90690.*

2 Group *IV* metal complexes for *ROP* of cyclic esters

Thanks to their low toxicity, good activity and stability even in presence of protic impurities, group *IV* metal complexes are very promising catalysts to apply in the ring opening polymerization of cyclic esters.[56] Among the different group *IV* metal complexes, much attention has been focused on octahedral complexes featuring tetradentate *bis(phenolato)* ligands. In these ligands, the anionic oxygen atoms are usually paired with neutral imine or amino groups (*ONNO* ligands), with neutral thioether groups (*OSSO* ligands) or with a combination of these (*ONSO* ligands, *figure 25*).[57]

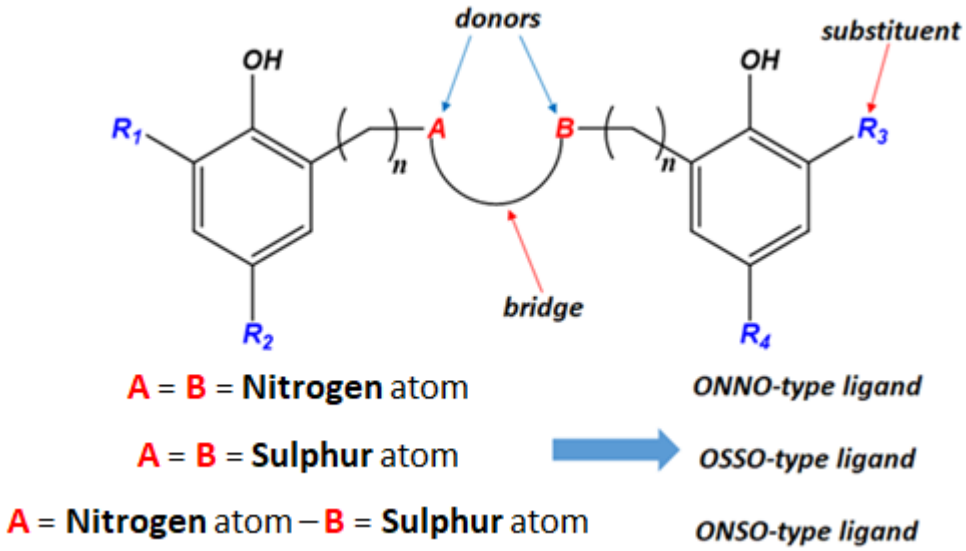

Figure 25. general structure of bis(phenolato) complex.

[56] A. J. Chimura, M. G. Davidson, M. D. Jones, M. D. Lunn, M. F. Mahon, S. L. Roberts, S. S. F. Wong, *Macromolecules* ***2006**, 39, 7250-7257;* R. Lapenta, A. Buonerba, A. De Nisi, M. Monari, A. Grassi, Stefano Milione, C. Capacchione, *Inorg. Chem.*, ***2017**, 56, 3447−3458*

[57] A. J. Chimura, M. G. Davidson, M. D. Jones, M. D. Lunn, M. F. Mahon, S. L. Roberts, S. S. F. Wong, *Macromolecules*, ***2006**, 39, 7250-7257;* A. Sauer, A. Kapelski, C. Fliedel, S. Dagorne, M. Kol, J. Okuda, *Dalton Transactions*, ***2013**, 42, 9007-9023;* R. Lapenta, A. Buonerba, A. De Nisi, M. Monari, A. Grassi, S. Milione, C. Capacchione, *Inorg. Chem.*, ***2017**, 56, 3447−3458.*

Jones et al. have reported some examples of complexes with *ONNO-type* ligands able to afford highly isotactic enriched polymers in the *ROP* of *rac-LA*. In these complexes the *Zr* or *Hf* metal is coordinated by a 2,2'-bipyrrolidine-derived salan ligand.[58]

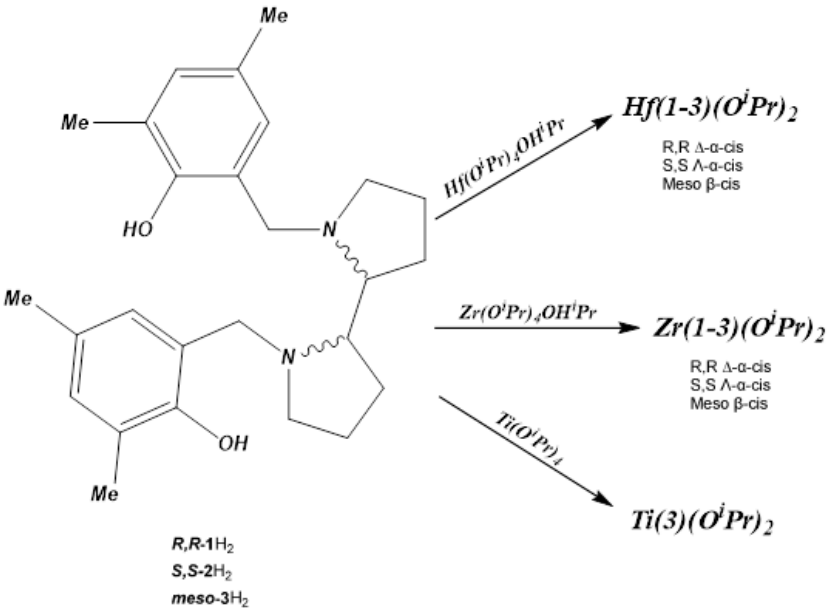

Figure 26: synthesis of ONNO-type complexes of Jones.

The *OSSO-type* complexes of *Zr* and *Hf* were studied by Buffet and Okuda. These complexes promoted the controlled *ROP* of *meso*-LA; syndiotactic or heterotactically enriched *PLA* were produced. Studies carried out on these catalysts have shown that the *ROP* of *meso*-LA is influenced by the length of the bridge between the sulphur atoms. In fact, a higher activity was observed as the length of the bridge increases, which corresponds to a greater fluxionality of the complex. The complexes with a propylene group as bridge were more active than the analogues rigid complexes in which the bridge is of an ethyl or a cyclohexyl group.[59]

[58] M. D. Jones, S. L. Hancock, P. McKeown, P. M. Schafer, A. Buchard, L. H. Thomas, M. F. Mahon, *Chem. Commun.*, ***2014***, *50, 15967-15970;* M. D. Jones, L. Brady, P. McKeown, A. Buchard, P. M. Schafer, L. H. Thomas, M. F. Mahon, T. J. Woodman, J. P. Lowe, *Chem. Sci.*, ***2015***, *6, 5034-5039.*

[59] J. C. Buffet, A. N. Martin, M. Kol, J. Okuda, *Polym. Chem.*, ***2011***, *2, 2378-2384;* J. C. Buffet, J. Okuda, *Chem. Commun.*, ***2011***, *47, 4796–4798*.

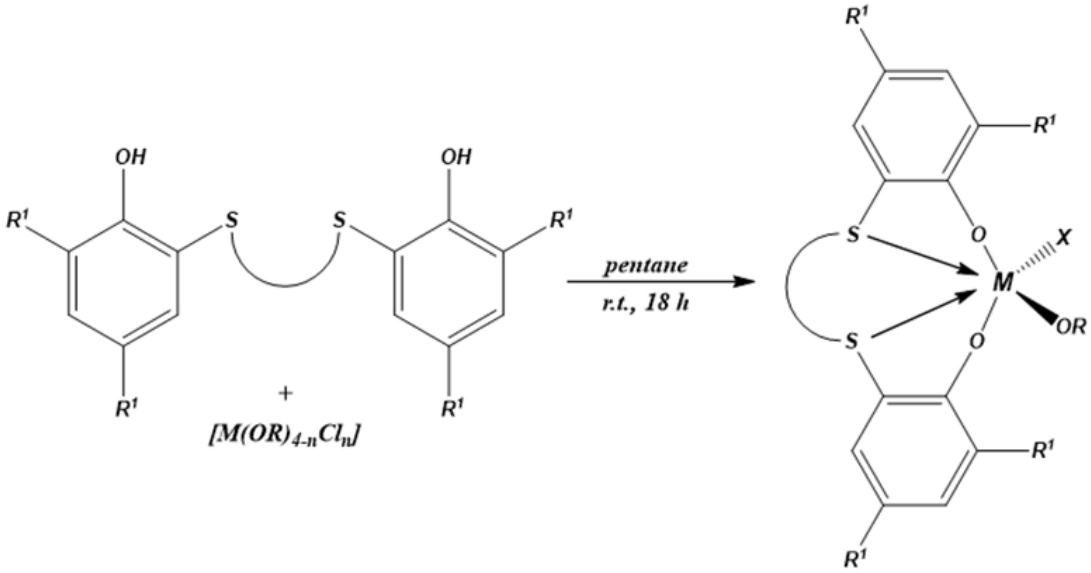

Bridge	Metal	R	X	R¹
$(CH_2)_2$	Ti	^{i}Pr	O^{i}Pr	^{t}Bu
$(CH_2)_2$	Ti	^{i}Pr	Cl	cumyl
$(CH_2)_2$	Ti	^{i}Pr	O^{i}Pr	cumyl
$(CH_2)_2$	Zr	^{t}Bu	O^{i}Pr	cumyl
c-C_6H_{10}	Ti	^{i}Pr	O^{i}Pr	^{t}Bu
$(CH_2)_3$	Ti	^{i}Pr	O^{i}Pr	^{t}Bu
$(CH_2)_3$	Ti	^{i}Pr	Cl	^{t}Bu

Figure 27: synthesis of OSSO-type complexes of Okuda.

A very interesting and important result was reported by Kol with a *Hf* tetradentate dithiodiolate ligand; this complex was able to convert 300 equivalents of *rac-LA* after 1 min and represents one of the most active group *IV* complexes reported in the literature (*figure 28*).[60]

[60] E. Sergeeva, J. Kopilov, I. Goldberg, M. Kol, *Inorg. Chem.*, ***2010***, *49, 3977-3979.*

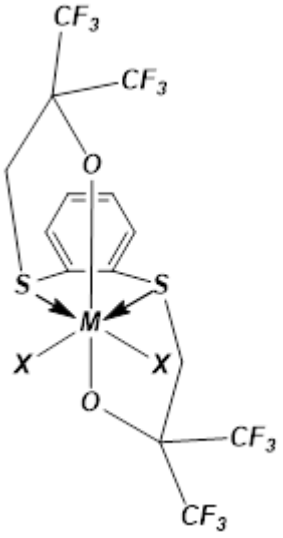

Figure 28: most active group 4 complex.

The combination of sulphur and nitrogen atoms as neutral donors in the *bis(phenolato)*ligand was explored by Kol and Okuda. They reported that *ONSO-type* complexes were able to polymerize *rac-LA* to obtain *PLA* with different tacticities depending on the nature of the substituents on the aromatic ring. Variyng the steric encumbrance of the ligand, the complex passes from rigid to fluxional complexes and the micro-structure of the produced polymers passes from predominantly isotactic to predominantly heterotactic.[61]

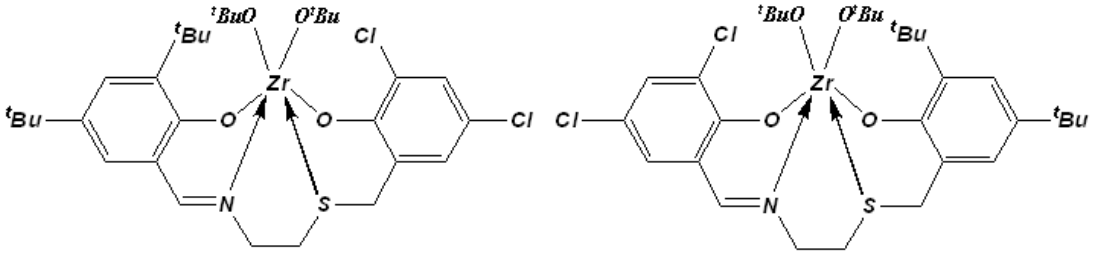

Figure 29: examples of ONSO-type complex.

With the scope of exploring new coordinative environments, we sought for alternative donor groups that could match with the hard Lewis acidity of the metal center. In this search, our attention focused on amide donor group as amide donor ligands have been proved to be well suited ligands for early transition metals. Moreover the efficiency of group *IV* complex with amide ligands in the *ROP* of cyclic ester was barely explored.

[61] A. Stopper, J. Okuda, M. Kol, *Macromolecules*, ***2012***, *45, 698-704;* A. Stopper, K. Press, J. Okuda, I. Goldberg, M. Kol, *Inorg. Chem.*, ***2014***, *53, 9140-9150.*

The most significant examples have been already report in the previous section. Moreover, we have been interested in developing ligands with a combination of hard and soft donor groups as this combination was proved to be effective in obtaining catalytic systems with good performance in the polymerization of cyclic esters. So, we decided to explore the catalytic performances of group *IV* metal complexes coordinated by a linear tetradentate ligands that exhibit two amide functions coupled with two thioether groups. In this chapter the synthesis and the characterization of a new class of complexes and the study of their activity in the *ROP* of cyclic esters is presented.

2.1 Synthesis and characterization of ligands

The linear tetradentate *NSSN* ligands described and used in this chapter feature a central flexible ethane bridge flanked by two rigid phenylene bridges. In order to introduce a steric hindrance around the metal centre, the nitrogen atoms were designed with isopropyl, cyclohexyl or mesityl substituents. The synthesis of the ligands was accomplished in two steps: first it was prepared the *NSSN* ligands without substituents on the aniline nitrogen atoms, then the aniline nitrogen atoms were properly alkylated with the desired alkyl groups. The ligand precursor was obtained through the reaction of 2-aminothiophenol in a 1:2 ratio with 1,2-dibromoethane in refluxing methanol according to a literature procedure.[62] Starting from this, the preparation of the isopropyl or cyclohexyl derivative was carried out via a reductive amination of acetone or cyclohexanone using zinc/acetic acid according to *Scheme 1*.[63] Differently the introduction of the mesityl group was achieved by reacting the ligand precursor with mesityl bromide through a palladium-catalysed cross coupling reaction (*Scheme 1*).[64]

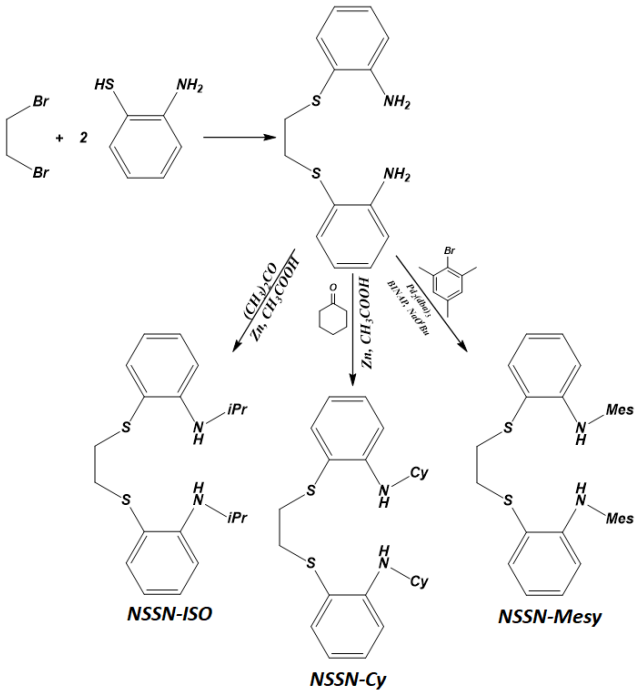

Scheme 1

[62] B. S. Chhikara, N. Kumar, V. Tandona, A. K. Mishra, *Bioorganic & Medicinal Chemistry, **2005**, 13, 4713–4720.*

[63] I. V. Micovic, M. D. Ivanovic, D. M. Piatak, V. D. Bojic, *Synthesis, **1991**, 1043-1045.*

[64] D.D. Graf, R. R. Schrock, W. M. Davis, R. Stumpf, *Organometallic, **1999**, 18, 843-852.*

All the ligands were prepared in high yields (45-98%), purified by recrystallization in hexane and full characterized by ^{1}H NMR spectroscopy. The NMR patterns of signals were consistent with the expected symmetry and the chemical shifts were observed in the typical ranges for this class of compounds.

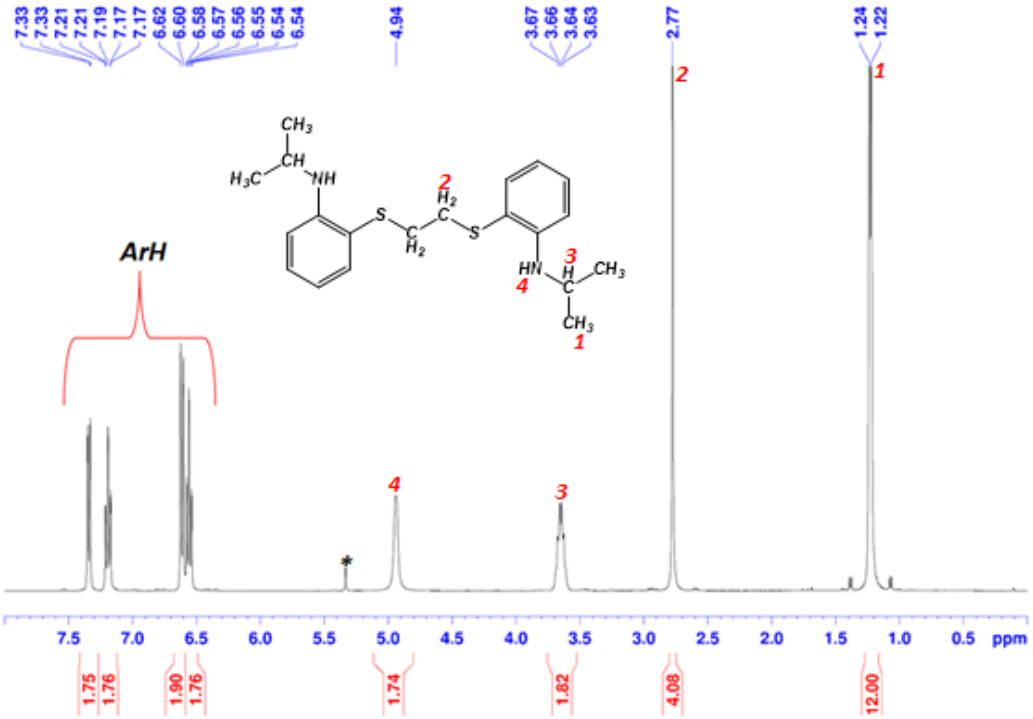

*Figure 30: ^{1}H NMR of NSSN-ISO ligand (400.13 MHz, *CD_2Cl_2, 25°C).*

X-ray quality crystals of *NSSN-ISO* and *NSSN-Cy* were grown from a saturated hexane solution upon slow evaporation of the solvent.

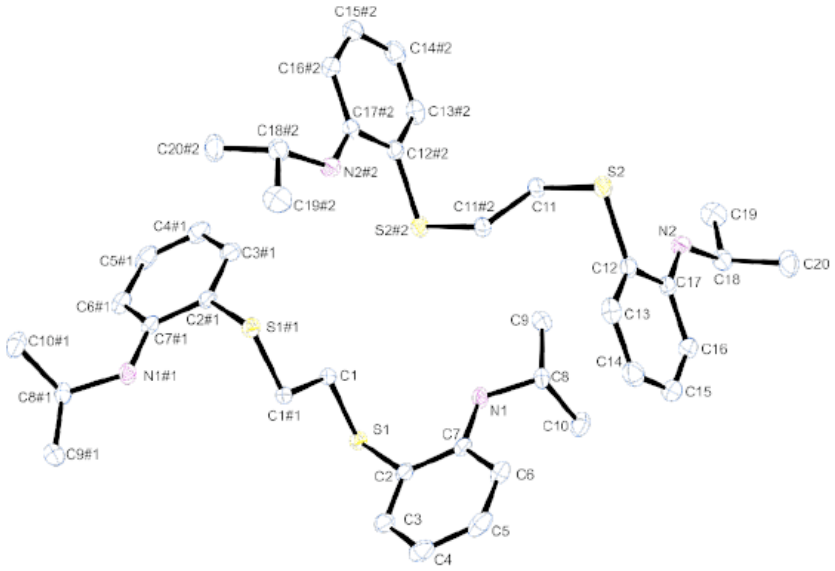

Figure 31: Ortep 3 view of NSSN-ISO ligand.

NSSN-ISO crystallizes in a triclinic unit cell according to the space group *P-1*. In the unit cell, the asymmetric unit is represented by two independent half molecules generating, by symmetry, two independent molecules characterized by a similar *trans*-planar conformation and analogous geometrical parameters. The aromatic rings of each molecule are parallel to each other.

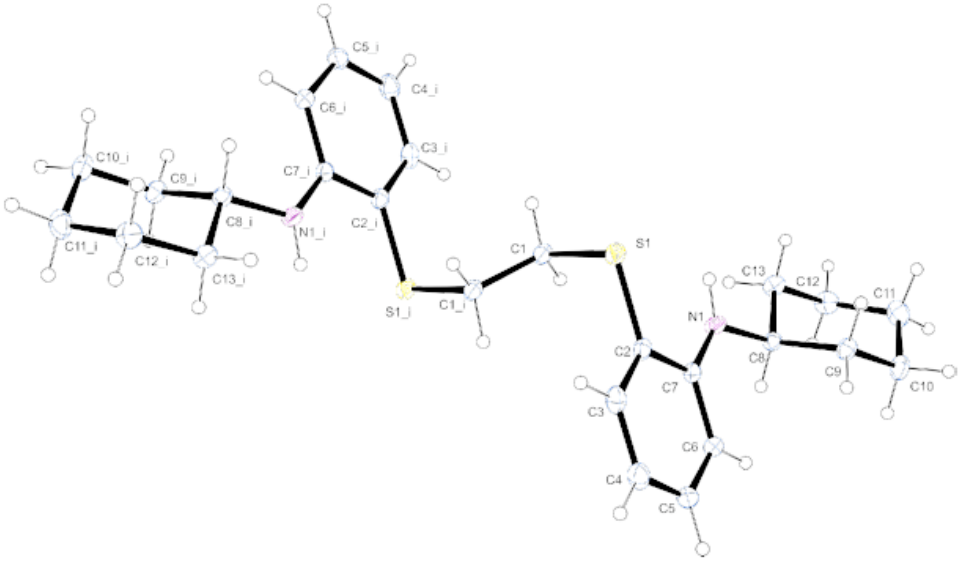

Figure 32: Ortep 3 view of NSSN-Cy ligand.

NSSN-Cy molecule (monoclinic, P21/c) sits on a crystallographic inversion center. Also in this case, due to conditions imposed by the crystallographic elements, the molecule assumes a *trans* planar conformation, with the aromatic moieties pointing to opposite sides. Phenyl rings are parallel to each other. Cyclohexyl substituents show a *chair* conformation.

2.2 *Synthesis and characterization of group IV metal complexes (1-5)*

The complexes **1-5** (*figure 33*) were synthesized by reaction of the corresponding *NSSN*-type ligand with $Zr(NMe_2)_4$ or $Hf(NMe_2)_4$ in refluxing toluene (*scheme 2*). The complexes were obtained in good yields (54-85%) and purified by recrystallization from cold hexane. With the aim of preparing the entire series of *group IV* metal complexes, the synthesis of the titanium amide derivative was attempted but the treatment of $Ti(NMe_2)_4$ with *NSSN-iPr-*H_2 resulted in no reaction, even after prolonged heating.

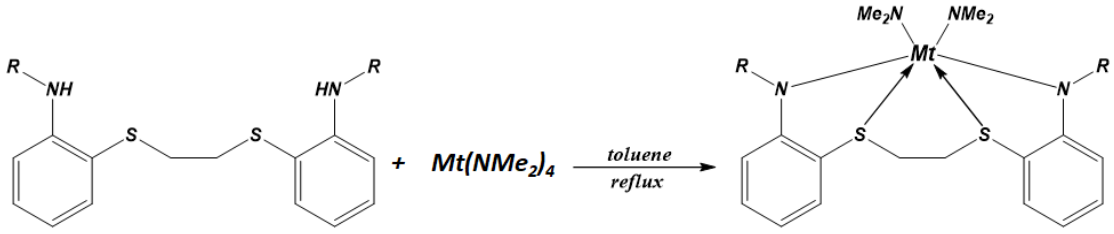

Scheme 2

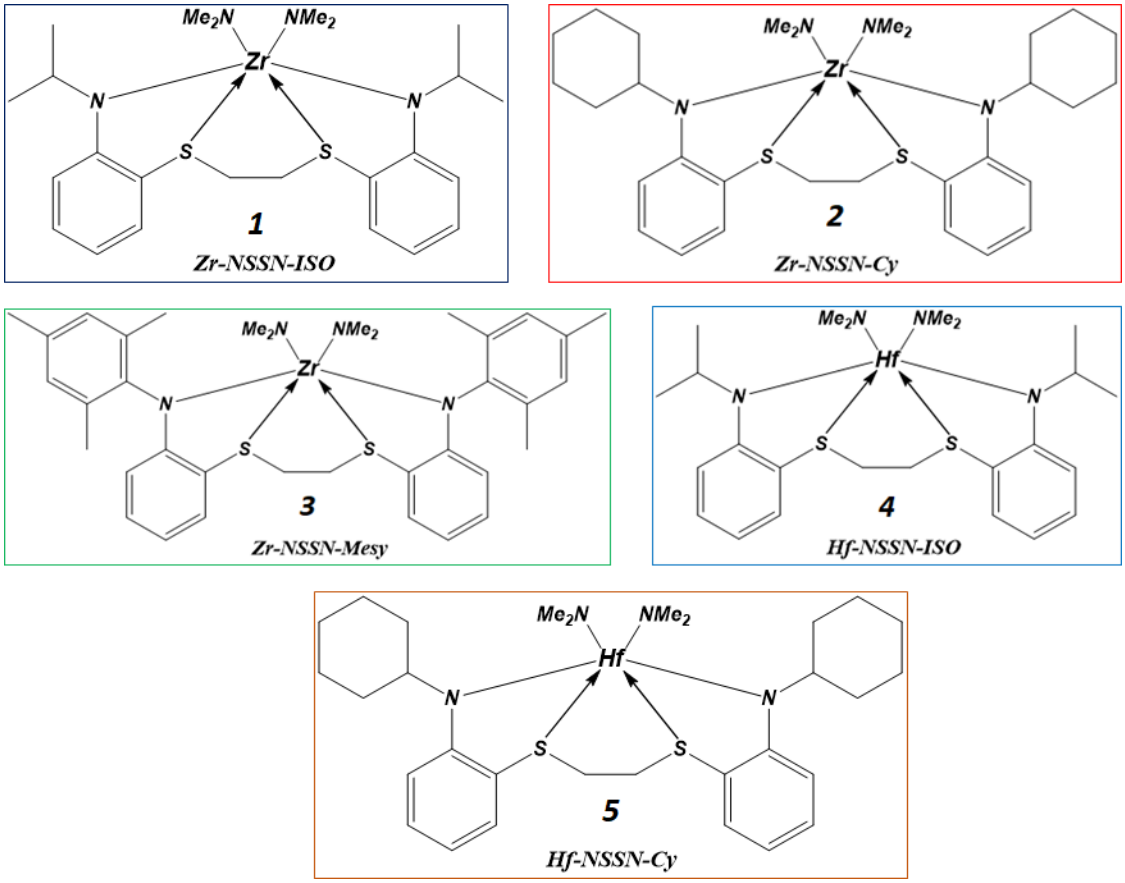

Figure 33: complexes 1-5

Each complex was characterized by ^{1}H and ^{13}C NMR spectroscopy and the attribution $^{1}H/^{13}C$ was possible thanks to HSQC experiments. The wrapping of linear tetradentate ligands around octahedral metal centers may produce three configurational isomers designated as *mer-mer* (trans), *fac-fac* (cis-α), or *fac-mer* (cis-β) showing the corresponding C_2, C_1, or C_v symmetries. The last two structures are chiral-at-metal isomers and exist as two stereoisomers (*figure 34).*

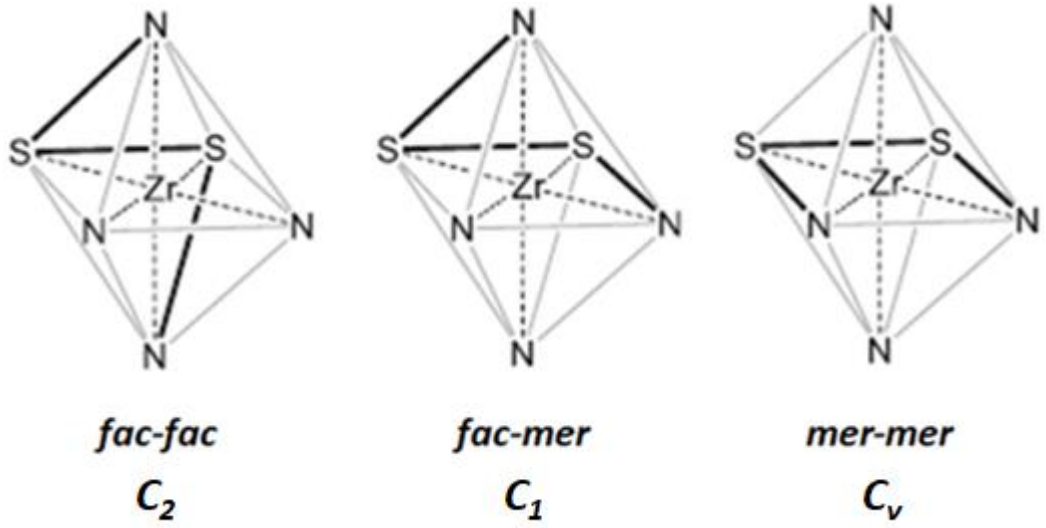

Figure 34: possible stereoisomers for NSSN-complexes.

In all cases, the ^{1}H NMR experiment showed that:

1) One set of resonance was found;
2) The methylene protons of the ethylene bridge appeared as a four-line *AB* pattern.

These indicate that the complexes, at room temperature in solution, were present as a single isomer with a C_2 symmetry and, consequently, a wrapping of the ligand in *fac-fac* coordination mode (*figure 35*).

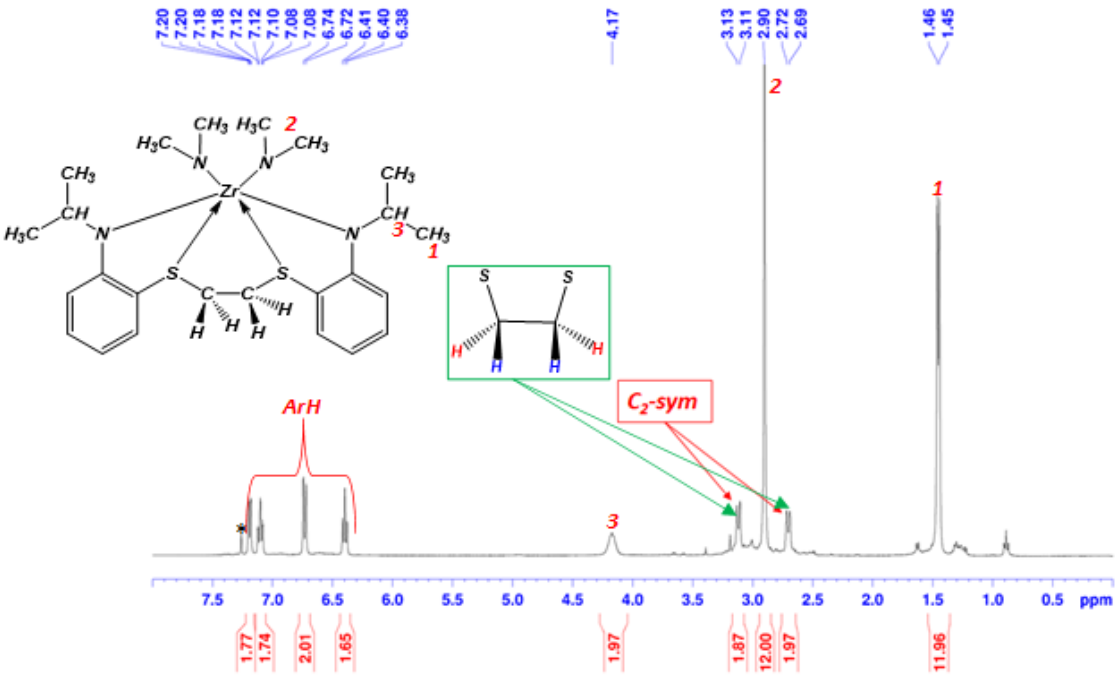

*Figure 35: ^{1}H NMR of complex 1 (400.13 MHz, *$CDCl_3$, 25°C).*

The methyl group of *–NMe_2* bound to metal center appear as singlets when the *NSSN* ligand has isopropyl or cyclohexyl substituents, while it appear as broad singlet when mesityl substituents are present on coordinate ligand. Probably in the complex **3** the rotation of the *–NMe_2* is restricted on the NMR time scale due to higher steric encumbering determined by mesityl substituent. The barrier to rotation of the methyl amide groups around the *Mt-NMe_2* bound was evaluated by theoretical calculations. The energy profile determined by plotting the total energy as a function of the torsion angle revealed an activation barrier of 3.0, 3.1 and 8.4 kcal/mol for **1**, **2** and **3** respectively. These results are in accord with the free rotation observed for **1** or **2** and a restricted rotation for **3** on the NMR time scale and can be addressed to the higher steric encumbering determined by the mesityl substituents in **3**, compared with the isopropyl or cyclohexyl substituents in **1** or **2**. To visualize the steric hindrance of the substituents around the metal center we made use of topographic steric maps in which altimetry isocontour lines circumscribes the hampering areas of the ligand. In these maps the metal atom is placed in the center, the nitrogen atoms occupy the apical positions whereas the sulphur atoms lie in the equatorial belt. The inspection of the maps reported in *figure 36* revealed that the coordination of the ligand produces a horizontal groove in which the metal and the amide ligands can be allocated. The substituents on the amide atoms of the ligand cause an encumber that is visible by the

two bulges in north and south position of the map. The size of this protuberance increases from ligand with isopropyl or cyclohexyl substituents to ligand with mesityl substituents. Anyway the coordination environment around the metal center is rather opened, the percentage of the total volume occupied by the ligand of the sphere with a radius of 4.5 Å and the metal at the core ($\%V_{bur}$) is 54.2 %, 54.4% and 62.0% for complex **1**, **2** and **3**.

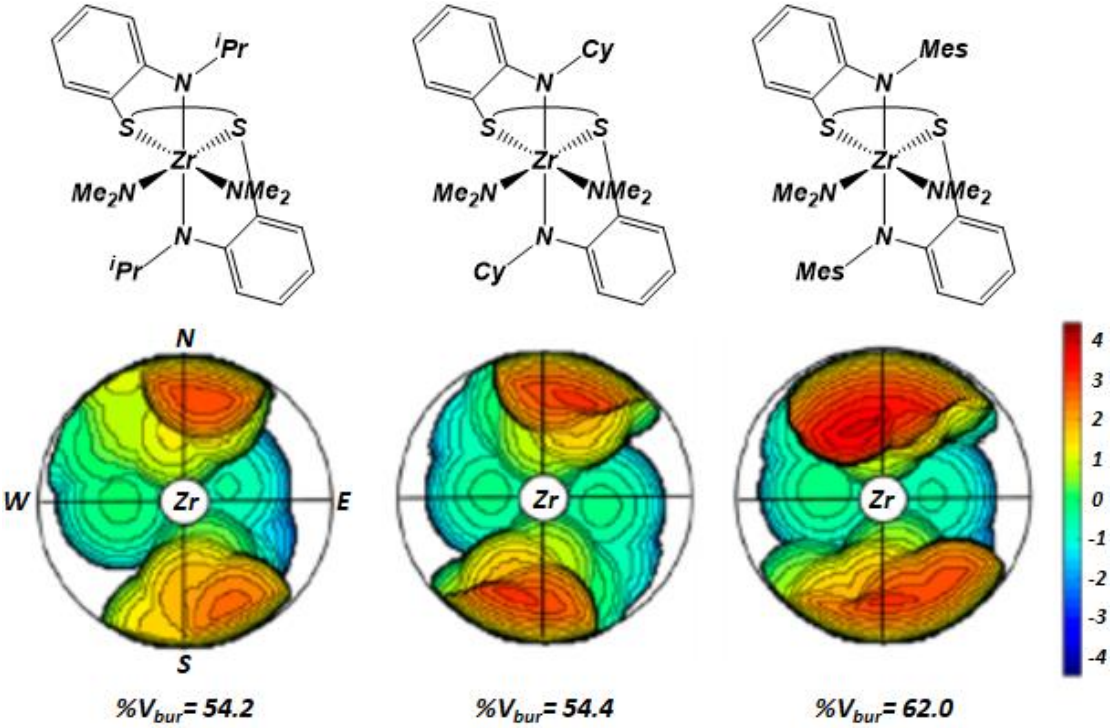

Figure 36: steric maps of Zr complexes. The isocontour curves are given in angstroms.

In order to explore the presence of other isomers in solution, the NMR analysis of complex **1** was performed in the range of temperature -60-25 °C (*figure 37*). Going down in temperature, the NMR signals broadened and split into different sets of resonances, as can be seen in the *figure 38*.

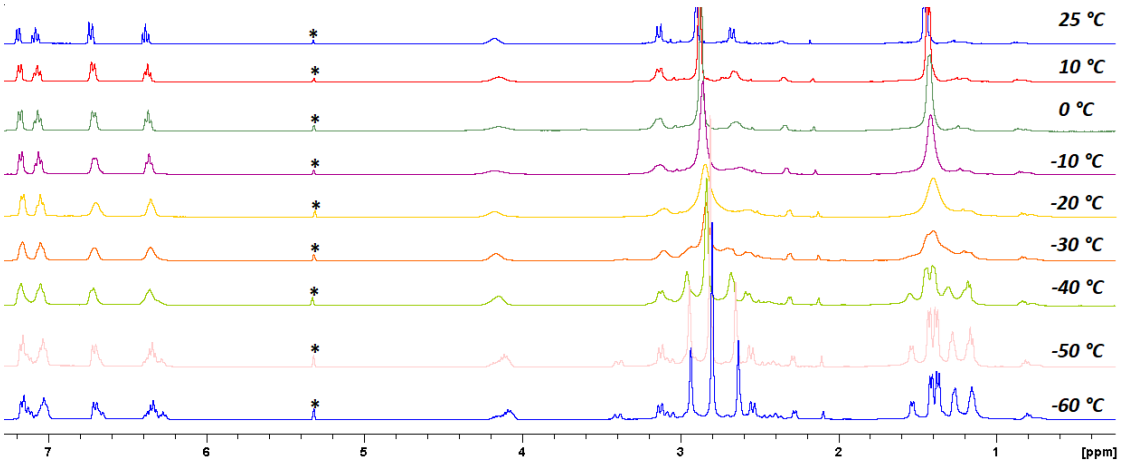

*Figure 37: variable temperature ^{1}H NMR of Zr-NSSN-ISO complex (400.13 MHz, *CD_2Cl_2).*

The methyl functions –NMe_2, which occur as a single at 2.90 ppm at room temperature, gave rise to three singlets (2.63, 2.80 and 2.93 ppm) in a 1:4:1 intensity ratio, when the experiment was carried out at -60 ° C. Also the signals for methylene protons of ethylene bridge gave rise into several signals highlighted in blue (three doublets at 2.28, 3.06 and 3.39 ppm and a multiplet at 2.40 ppm). The experiment at -60 °C confirms the presence of two distinct stereoisomers in solution in a 2:1 molar ratio, an isomer with C_2 symmetry, already observed at room temperature, and an isomer with C_1 symmetry that originated by the *fac-mer* wrapping of the *NSSN*-ligand around the metal center.

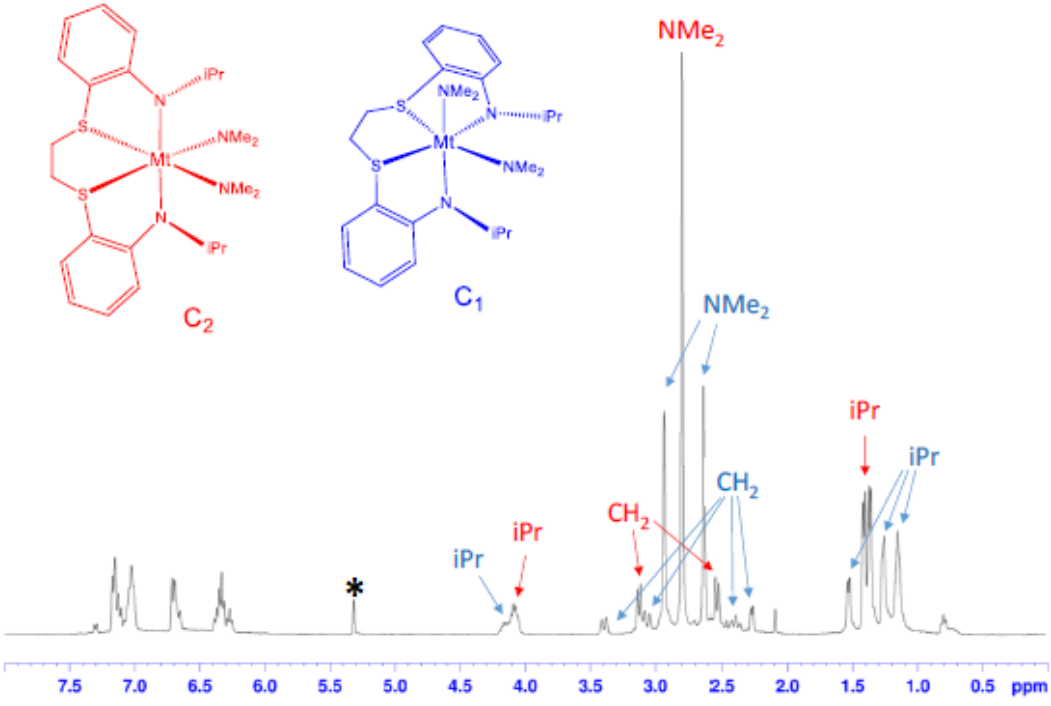

*Figure 38: ^{1}H NMR of Zr-NSSN-ISO complex (400.13 MHz, *CD_2Cl_2, -60°C).*

Density functional theory (*DFT*) calculations were carried out on complex **1** to better understand the equilibrium between different isomers in solution. The most stable stereoisomer is that with the C_2 symmetric structure, the energies of the C_1 and C_v symmetric structures are higher by 10.3 and 23.7 kcal/mol, respectively. These results justifies the non-observation of the C_v symmetric stereoisomer in solution. The differences in energies between the three isomers have a significant contribute from the energy required to the dianonic ligand to adopt the conformation necessary for the coordination to the metal center.

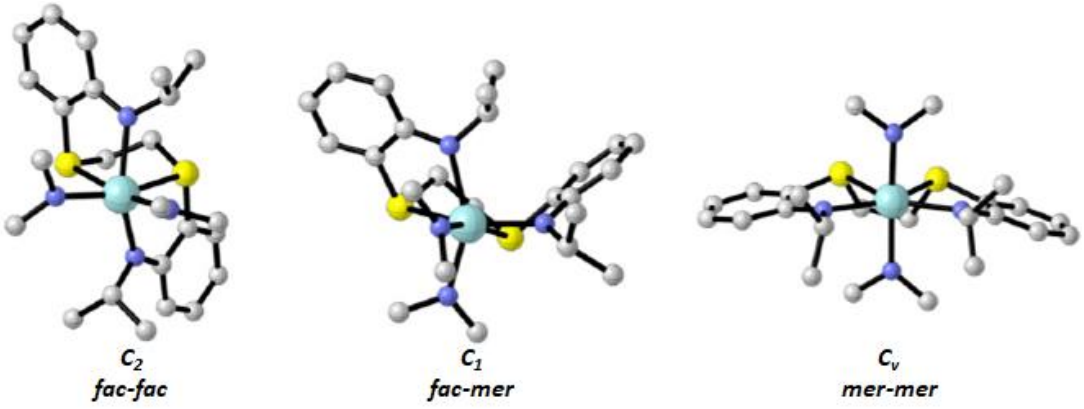

Figure 39: DFT optimized structures for the three stereoisomers of Zr-NSSN-ISO.

X-ray quality crystals of the complexes were grown from a saturated hexane solution upon slow evaporation of the solvent. The crystal structures and all information of the complexes are reported in *Crystallographic Data*. The complexes have a distorted octahedral coordination geometry around the metal center, adopting a pseudo-C_2-symmetrical configuration. The dimethylamine groups form angles with the metal center which vary according to the group present on the nitrogen atoms (*N-Mt-N* between 98.9°-103.9°).

As shown in *Crystallographic Data*, the octahedral coordination geometry is distorted due to the restrictions imposed by the tetradentate ligand. Major deviations from ideal octahedral coordination are observed in both complexes *Zr* and *Hf* containing the cyclohexyl group. Probably, the steric hindrance of cyclohexyl group induces a significant deformation in the coordination area (see table 16 in *Crystallographic Data*). In all the complexes, the two sulphur atoms of the *NSSN* ligand show a *gauche* conformation (see dihedral angle *SCCS* in table 16 in *Crystallographic Data*), that induces the *trans* coordination of the nitrogen atoms of the tetradentate ligand. As can

be seen from table 14 and 15 in *Crystallographic Data*, there are notable similarities in the geometric parameters of the coordination environment within each of the pairs **1**/**4** and **2**/**5**. *M-N* and *M-S* distances are in agreement with those reported in the literature for analogous complexes. It is worth pointing out that a slight elongation of the nitrogen-metal bond of the *NSSN* ligand in respect to that of dimethylamido group (see table 16 in *Crystallographic Data*) is observed. Finally, it is worth noting that structures of **2** and **5** are isomorphic.[65] In fact, both complexes crystallize in an orthorhombic lattice, Space Group Pbca, showing the same cell parameters (see in *Crystallographic Data*).

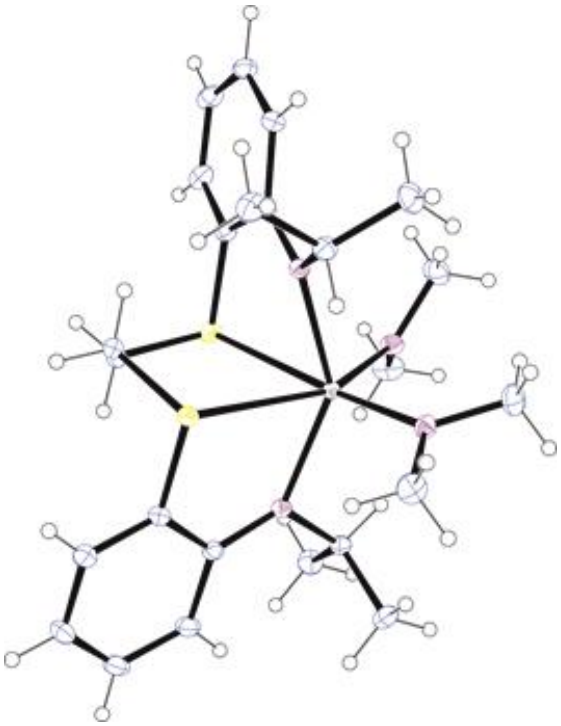

Figure 40: ORTEP 3 view of Zr-NSSN-ISO complex.

[65] V. Mdluli, P. J. Hubbard, A. Kuznicki, J. A. Golen, A. L. Rheingold, D. R. Manke Polyhedron, ***2017***, *121, 264-268;* T. N. Lenton, D. G. VanderVelde, J. E. Bercaw, *Organometallics*, ***2012***, *31, 7492−7499*; C. Capacchione, A. Proto, H. Ebeling, R. Mulhaupt, K. Moller, T. P. Spaniol, J. Okuda, *J. Am. Chem. Soc.*, ***2003***, *125, 4964-4965*; J-C. Buffet, J. Okuda, *Chem. Commun.*, ***2011***, *47, 4796-4798*; D. D. Graf, R. R. Achrock, W. M. Davis, R. Stumpf, *Organometallics*, ***1999***, *18, 843-852*; E. Bernabé-Pablo, A. Campirán-Martínez, V. Jancik, D. Martínez-Otero, M. Moya-Cabrera, *Polyhedron*, ***2016***, *110, 305–313.*

2.3 ROP of cyclic esters catalyzed by 1-5

The synthesized group *IV* complexes were tested as catalysts in the *ROP* of *L*- and *rac*-*LA* in a toluene solution at 80°C. The most representative results are reported in table 2. The complex **1** proved to be an efficient catalyst, capable of converting 69% of monomer in 1 hour, an almost quantitative conversion was obtained in 2 hours. Under these conditions, the TOF was 42 h^{-1}, which shows that this catalyst has a higher catalytic activity than *Zr* complexes featuring *OSSO* ligands, but comparable with those of the most active group *IV* complexes operating in toluene solution. To get more information on *ROP* with these catalysts, the reaction was sampled by taking aliquots of the product mixture at regular intervals and analysing them by ^{1}H NMR spectroscopy and GPC measurements.

Table 2: ROP of L- and rac-LA

Entry	Complex	Monomer	[M]/[Cat]	t (h)	Conv.[a] (%)	TOF (h^{-1})	$M_{n(theo)}$[b]	$M_{n(exp)}$[c]	$Đ$[c]
1	***1***	*L-LA*	100	1	69	69	9.9	8.7	1.20
2	***1***	*L-LA*	100	2	90	42	13.0	11.4	1.15
3	***1***	*L-LA*	1000	16	95	59	137.1	60.2	1.18
4	***1***	*L-LA*	2000	15	70	93	-	n.d.	n.d.
5	***1***	*L-LA*	3000	16	74	139	320.8	66.5	1.19
6	***1***	*rac-LA*	100	2	45	22	-	n.d.	n.d.
7	***1***	*rac-LA*	100	16	97	6	14.0	4.0	1.12
8	***2***	*L-LA*	100	1	55	55	7.9	6.5	1.12
9	***2***	*rac-LA*	100	2	15	8	-	n.d.	n.d.
10	***3***	*L-LA*	100	1	25	25	3.5	2.6	1.27
11	***3***	*rac-LA*	100	2	14	7	2.0	1.8	1.16
12	***4***	*L-LA*	100	1	47	47	6.8	5.8	1.11
13	***4***	*L-LA*	100	2	69	35	10.0	9.1	1.10
14	***5***	*L-LA*	100	1	46	46	6.7	5.8	1.19
15	***5***	*L-LA*	100	2	78	39	11.2	9.8	1.17

All reaction were carried out in 2 mL of toluene, 80°C, $[Cat]_0$= 5.0 mM, [Monomer]= 1.4 M; [a]Molecular conversion determined by ^{1}H NMR spectroscopy ($CDCl_3$, 298 K); [b]Calculated molecular weight using $M_{n(theo)}$(kg/mol)=($PM_{Monomer}$ x 100 x conversion)/1000; [c]Experimental molecular weight $M_{n(exp)}$(kg/mol) and *Đ* determined by GPC using THF polystyrene standards and corrected using the factor 0.58 for PLA.

In *figure 42* the plot $\ln([L\text{-}LA]_0/[L\text{-}LA]_t]$ versus time is reported, it resulted that the *ROP* of *L-LA* with these new complexes follows a first-order kinetic law with respect to the monomer concentration. In this plot it is also evidence that the k_{app} of complex **1** is higher than those of the other synthesized complexes (k_{app} = 1.33 ± 0.03 h^{-1}).

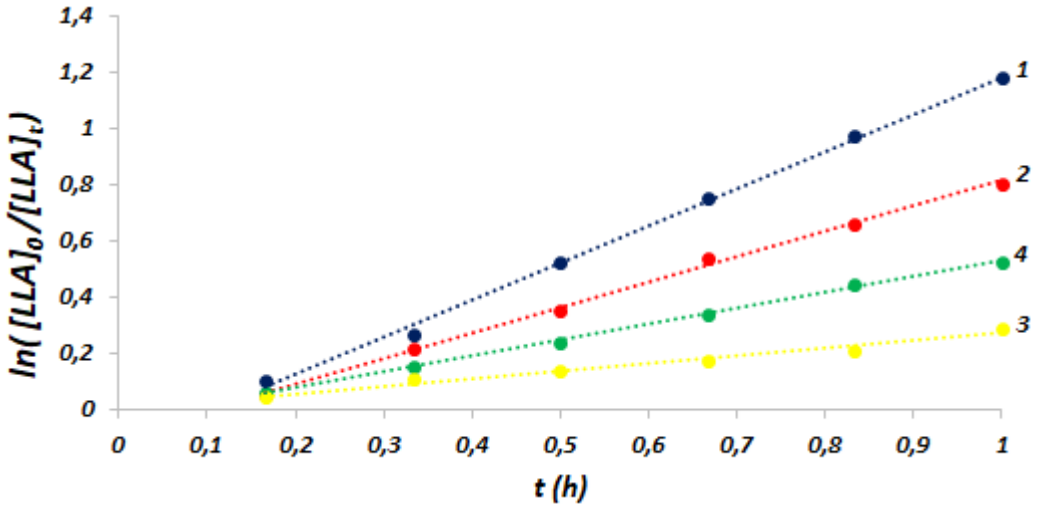

Figure 41: Pseudo-first order kinetic plots for ROP of L-LA by 1 (k_{app}= 1.33 ± 0.03 h^{-1}, R^2= 0.998, blue), 2 (k_{app}= 0.99 ± 0.02 h^{-1}, R^2= 0.998, red), 3 (k_{app}= 0.27 ± 0.01 h^{-1}, R^2= 0.981, yellow), 4 (k_{app}= 0.56 ± 0.01 h^{-1}, R^2= 0.998, green). *Conditions: $[L\text{-}LA]_0$ = 1.4 M, $[L\text{-}LA]_0/[I]_0$ = 100, T = 80 °C, and toluene as the solvent.*

In the *figure 41* it can be seen a non-zero intercepts of the kinetic plots. This is due the experimental condition used to carry out the polymerization experiments; in particular it is due to the time required to the solid lactide to dissolve. To verify this hypothesis a solution of the catalyst was added to a pre-dissolved solution of lactide (see *Experimental Part*). Following this new experimental procedure, the induction period was significantly reduced (*figure 42*) but the k_{app} remained very similar to the one obtained previously with complex **1** (k_{app} = 1.21 ± 0.02 h^{-1}, R^2= 0.998).

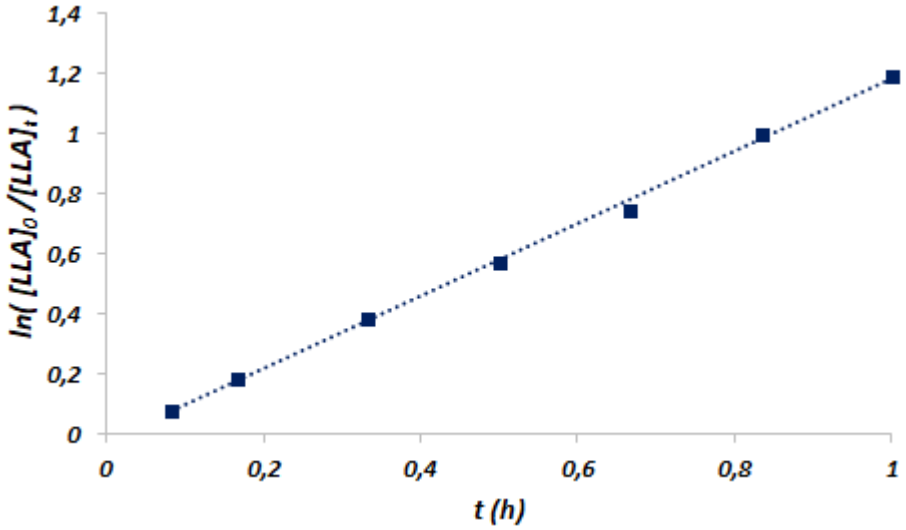

Figure 42: Pseudo-first order kinetic plots for ROP of L-LA.
Conditions: $[L\text{-}LA]_0$ = 1.4 M, $[L\text{-}LA]_0/[\mathbf{1}]_0$ = 100, T = 80 °C, and toluene as the solvent.

In *figure 43* the GPC analysis of the isolated polymer obtained using **1** are reported, it can be seen how the number-average molecular weights ($M_{n(expt)}$) increases linearly

with monomer conversion. The *Đs* are relatively narrow and constant during the polymerization process.

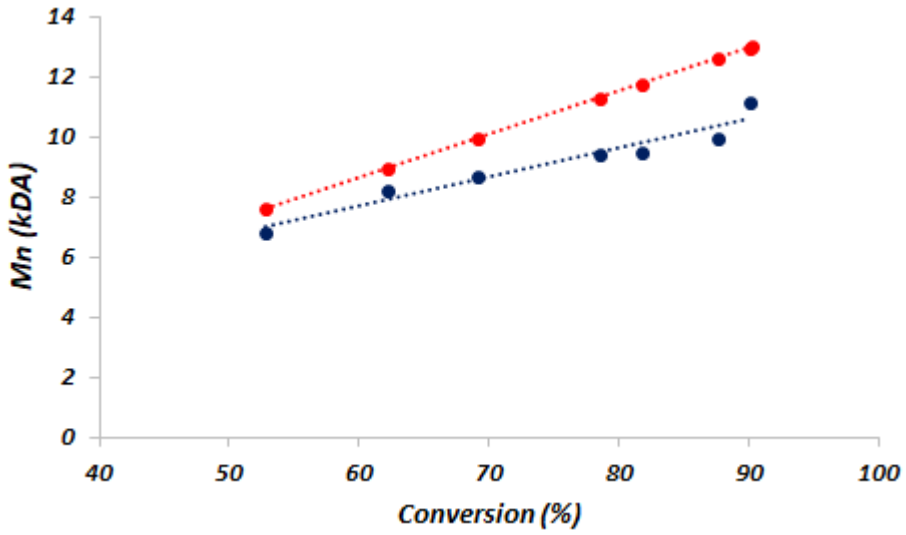

Figure 43: Plot of number-average molecular weights $M_{n(exp)}$(blue line) versus monomer conversion with theoretical $M_{n(theo}$(red line) using 1 as the catalyst.
Conditions: $[L\text{-}LA]_0$ = 1.4 M, $[L\text{-}LA]_0/[\mathbf{1}]_0$ = 100, T = 80 °C, and toluene as the solvent.

The $M_{n(exp)}$ resulted lower than the theoretical molecular weights ($M_{n(Theo)}$). This mismatch may be due to inter- and intramolecular transesterification processes that affect the polymerization process.

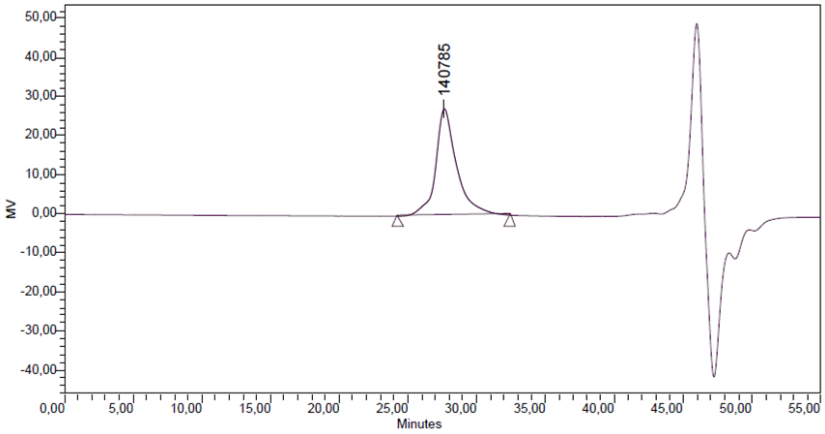

Figure 44: SEC of PLA obtained as in entry 5 table 2.

The polymers were analyzed by matrix-assisted laser desorption ionization time-of-flight (MALDI-TOF) Mass Spectrometry, which confirmed that the transesterification reactions are active during the polymerization (peaks in *figure 45* spaced by 72 Da).

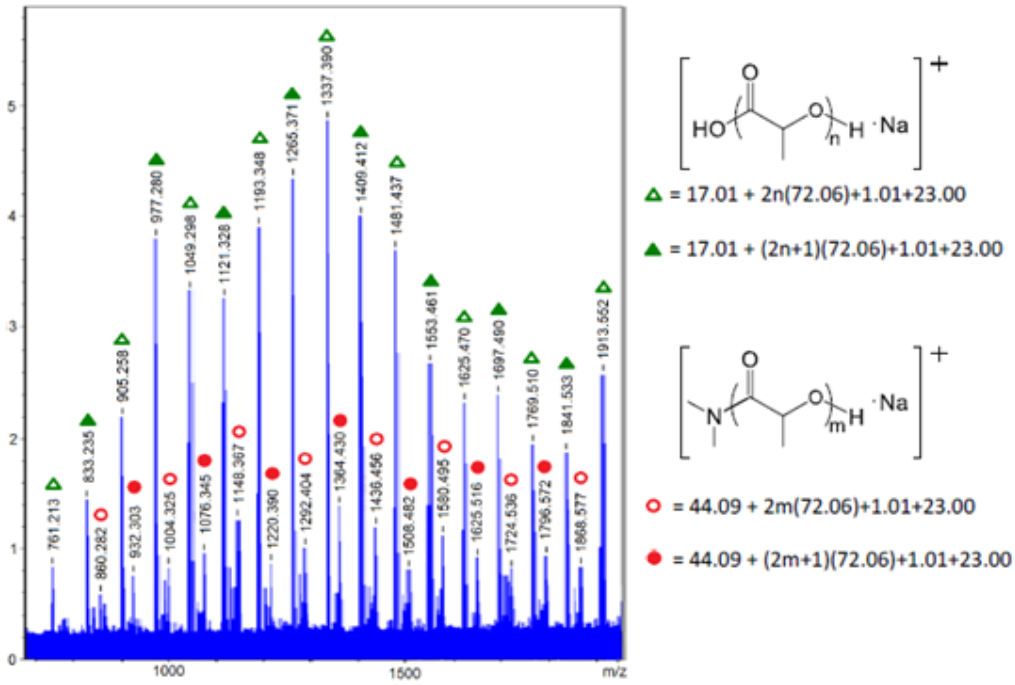

Figure 45: MALDI-TOF spectrum of PLA obtained with 1 as catalyst.

A polymerization run with a low molar ratio monomer/catalyst ([*L*-LA]/[**1**] = 10) was performed with the aim of deepening the initiation process. The NMR analysis of the isolated polymer showed the presence of two singlets at 2.95 and 3.03 ppm in the ^{1}H NMR spectra (*figure 46*), and two signals at 31.7 and 22.8 ppm in the ^{13}C NMR spectra (*figure 47*). These signals are attributable to two methyl groups of the *–C(=O)NMe$_2$* end group that originates from the nucleophilic attack of the amide *NMe$_2$* bound to the metal center to the carboxylic carbon of the monomer coordinated to the same metal center, according to the coordination-insertion mechanism.

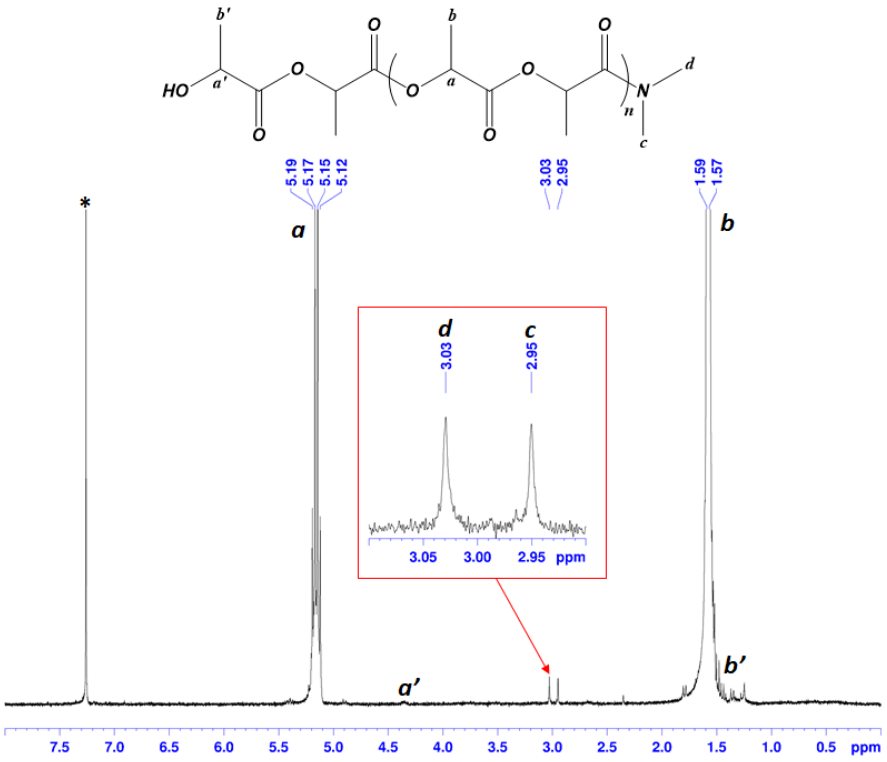

*Figure 46: ^{1}H NMR of oligomers of PLA obtained using 1 as catalyst (400.13 MHz, *$CDCl_3$, 25°C).*

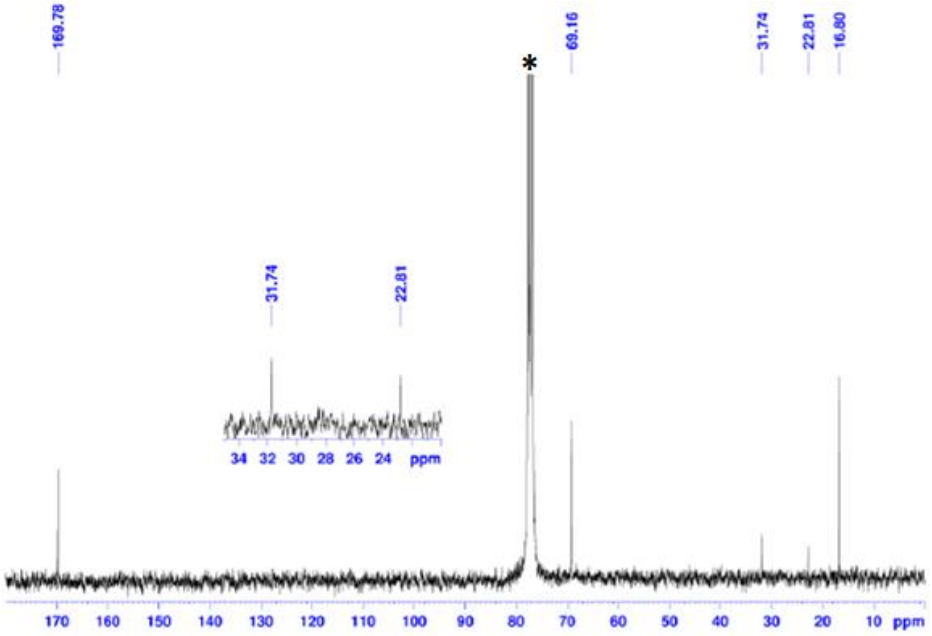

*Figure 47: ^{13}C NMR of oligomers of PLA obtained using 1 as catalyst (100.62 MHz, *$CDCl_3$, 25°C).*

To probe the robustness of the catalytic system, the amount of catalyst was reduced (entry 3, 4 and 5 in table 2). The catalyst still preserved a good activity using a [*L-LA*]/[cat] ratio of 1000, 2000 and 3000, reached a TOF of 59, 93 and 139 h^{-1}. The kinetic plot (*figure 48*) with these molar ratios confirmed that the polymerization

follows a first-order kinetic law with respect to the monomer concentration where the k_{app} decrease as the molar ratio increases (k_{app}^{1000} = 0.21 ± 0.01 h^{-1}, R^2_{1000}= 0.991; k_{app}^{2000} = 0.074 ± 0.009 h^{-1}, R^2_{2000}= 0.953; k_{app}^{3000} = 0.046 ± 0.006 h^{-1}, R^2_{3000}= 0.952). The $M_{n(exp)}$ increased with the [*L-LA*]/[cat] ratio but still remained lower that than $M_{n(Theo)}$ probably always due to transesterification reactions.

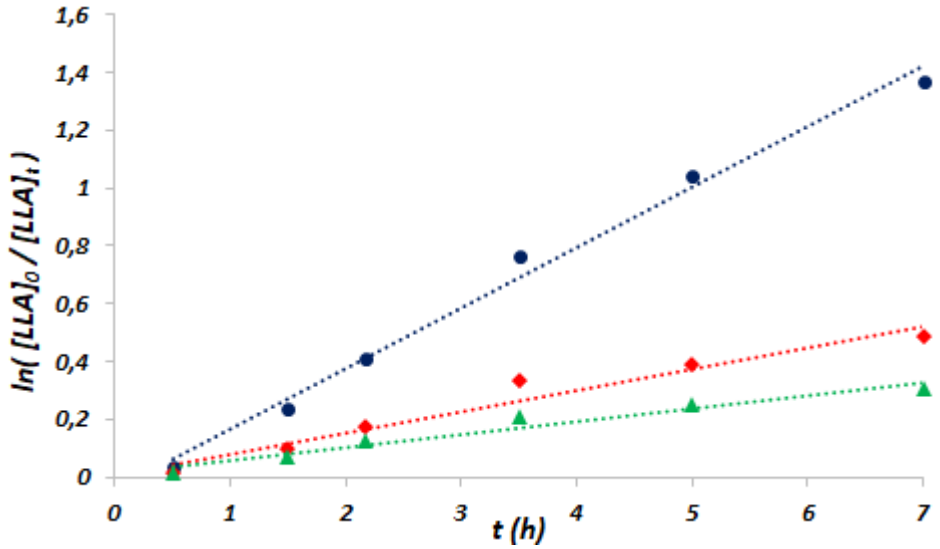

Figure 48: Pseudo-first order kinetic plots for ROP of L-LA with several [LLA]/[1] ratios (blue= 1000, red= 2000, green= 3000).
Conditions: $[L\text{-}LA]_0$ = 1.4 M, T = 80 °C, and toluene as the solvent.

With the aim of getting insight into the influence of substituents on the aniline nitrogen atoms, the complexes **2** and **3** were tested in the same conditions of **1** (entry 8 and 10 in table 2). The complex **2** with cyclohexyl substituents showed an activity in *ROP* of *L-LA* comparable to that observed for **1** (55% of monomer conversion in 1 hour) but it was less active with *rac-LA* (15% of monomer conversion in 2 hours). In 1 hour only 25% of *L-LA* was polymerized using the complex **3** featuring mesityl substituents. The plot $\ln([L\text{-}LA]_0/[L\text{-}LA]_t]$ versus time in *figure 41* show that the k_{app} for complex **3** is about four times lower than that found for **1** (k_{app}^{3} = 0.27 ± 0.01 h^{-1}), complex **2** have a k_{app} very similar to that of **1** (k_{app}^{2} = 0.90 ± 0.02 h^{-1}). From the experimental data it can be deduced that an increase of steric encumbrance around the metal center with cyclohexyl or mesityl group causes a lowering of the catalytic activity and a decrease in the propagation rate, probably the access to the catalytic site is more difficult for the monomer with **2** and **3** than **1**. However the transesterification reactions appear to be more significant going from **1** to **3**, as can be seen from the difference between the $M_{n(Theo)}$ and $Mn_{(exp)}$ (*figure 49* and *50*).

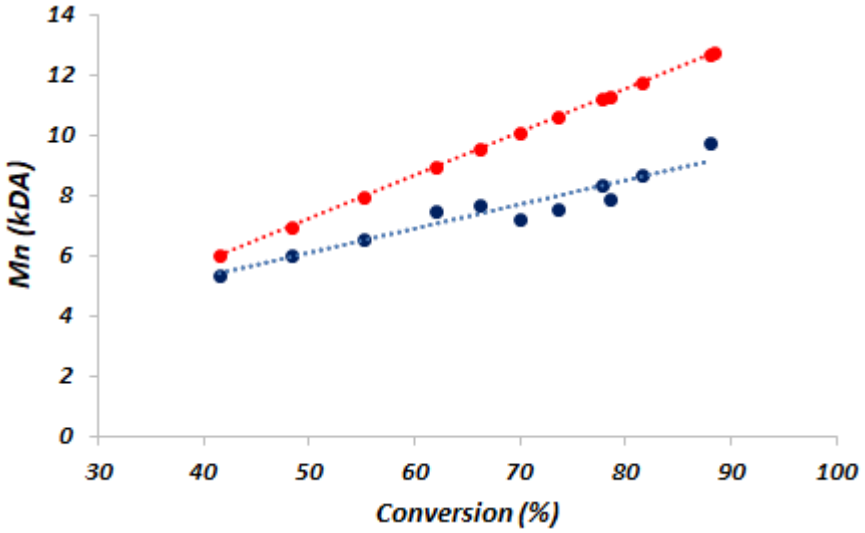

Figure 49: Plot of number-average molecular weights $M_{n(exp)}$(blue line) versus monomer conversion with theoretical $M_{n(theo}$(red line) using 2 as the catalyst.

Conditions: $[L\text{-}LA]_0$ = 1.4 M, $[L\text{-}LA]_0/[\mathbf{2}]_0$ = 100, T = 80 °C, and toluene as the solvent.

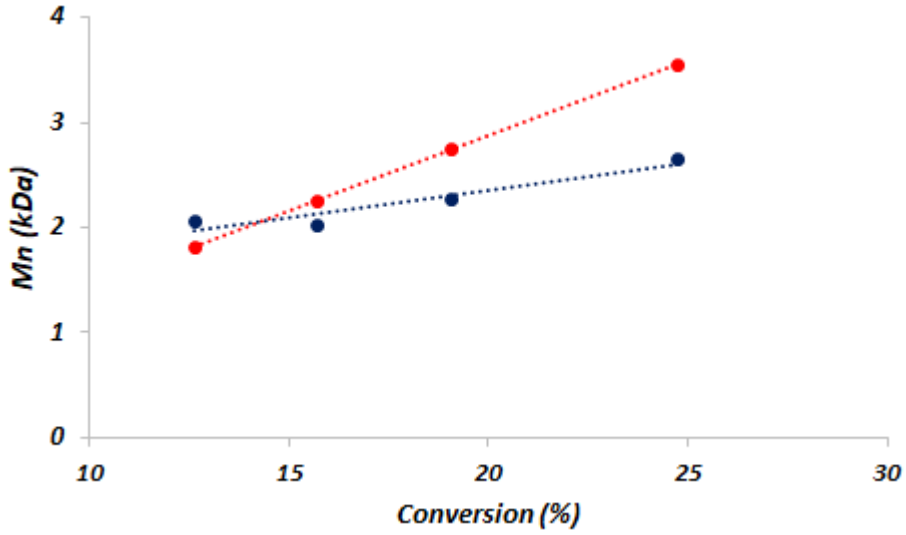

Figure 50: Plot of number-average molecular weights Mn(exp)(blue line) versus monomer conversion with theoretical Mn(theo(red line) using 3 as the catalyst.

Conditions: $[L\text{-}LA]_0$ = 1.4 M, $[L\text{-}LA]_0/[\mathbf{3}]_0$ = 100, T = 80 °C, and toluene as the solvent.

Changing the metal center from *Zr* to *Hf*, the catalytic activity of the complexes decreased, reached about 46% of *L-LA* polymerized in 1 hour (entry 12 and 14 table 2). The k_{app} of complex **4** was about half of that observed for **1** ($k_{app}^{\mathbf{4}}$ = 0.56 ± 0.01 h^{-1}). The $M_{n(exp)}$ obtained using **4** were very similar with those obtained with **1**, but still lower than $M_{n(Theo)}$ (*figure 51*).

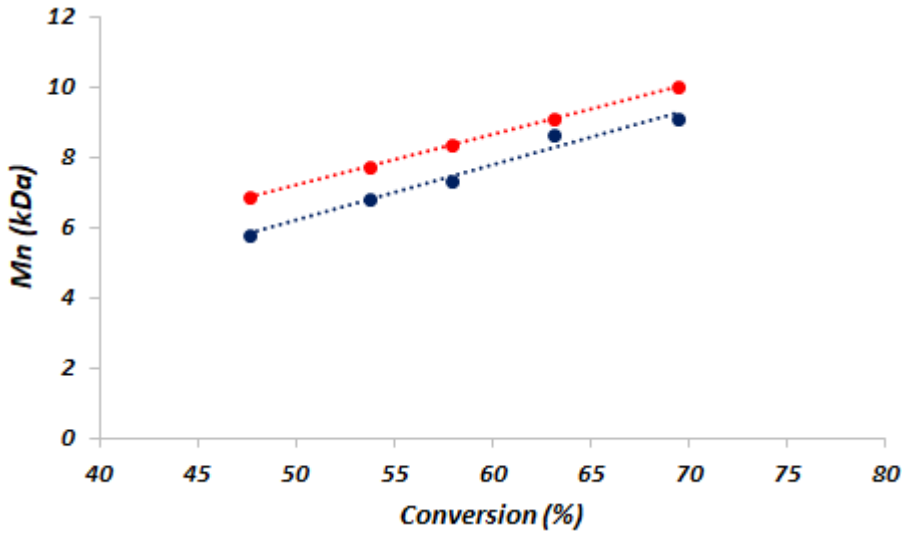

Figure 51: Plot of number-average molecular weights Mn(exp)(blue line) versus monomer conversion with theoretical Mn(theo(red line) using 4 as the catalyst.
Conditions: $[L\text{-}LA]_0$ = 1.4 M, $[L\text{-}LA]_0/[\mathbf{4}]_0$ = 100, T = 80 °C, and toluene as the solvent.

The activity trend of the complexes observed for *ROP* of *L-LA* was confirmed with the *rac-LA* (catalytic activity: **1**>**2**>**3**). However in the *ROP* of *rac-LA* the complexes appeared to be less active; in fact, the complex **1** reached 44 mol % conversion after 2 hours, quantitative conversion was reached in 16 hours (TOF of 6 h^{-1}; entry 7 in table 2) and the k_{app} was about one-third of that observed in *ROP* of *L-LA* (k_{app} = 0.31 ± 0.02 h^{-1}, R^2= 0.967). The inspection of the methine regions for the *poly-rac-LAs* obtained by **1** and **2** revealed that the microstructure is atactic. In the ^{1}H NMR spectrum of *poly-rac-LAs* obtained by **3**, the signal due to the mrm tetrad was the most intense, but it was not paired with a similar signal for the rmr tetrad (rmr:mrm = 1:3.7). The distribution of tetrads and the integration ratio of the peaks were inconsistent with either an atactic or an heterotactic microstructure. This may be a consequence of the redistribution of stereosequences because of the transesterification reactions that affect the polymerization process.

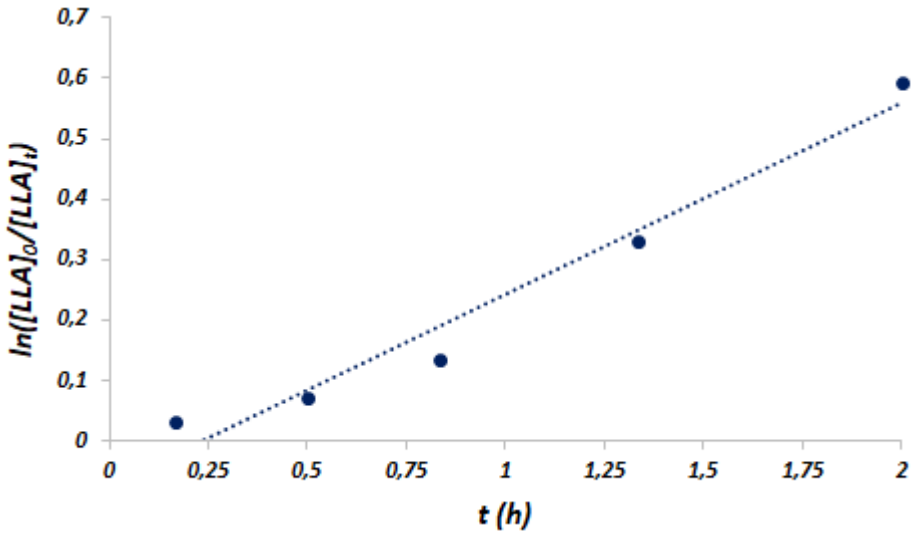

Figure 52: Pseudo-first order kinetic plots for ROP of rac-LA.
Conditions: $[rac\text{-}LA]_0$ = 1.4 M, $[rac\text{-}LA]_0/[\mathbf{1}]_0$ = 100, T = 80 °C, and toluene as the solvent.

With regard the **2** and **3**, the k_{app} values were very similar (k_{app}^2 = 0.12 ± 0.03 h^{-1}, k_{app}^3 = 0.11 ± 0.01 h^{-1}). $M_{n(exp)}$ grow linearly with the progress of the reaction and *Đ*s of the obtained polymer are in the range 1.12-1.17. However the $M_{n(exp)}$ have values that are about half of the $M_{n(Theo)}$.

The complex **1** was also tested in *ROP* of *ε-CL*, in toluene solution at 80°C with monomer/catalyst ratio of 100 (*figure 53*). The complex was able to convert 100 equivalents of monomer within 1 hour and showed a catalytic activity (TOF = 96 h^{-1}) comparable with *Zr/Hf-OSSO* complexes reported in literature. From kinetic study, the consumption of the *ε-CL* follows a first-order kinetic law (k_{app} = 0.069 ± 0.003 min^{-1}, R^2= 0.992).

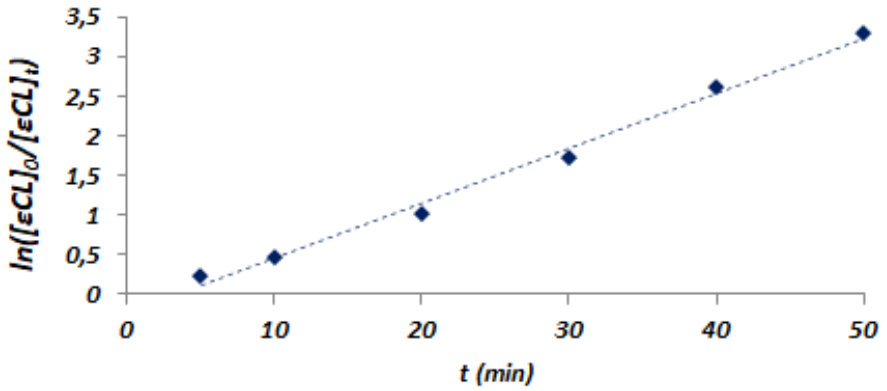

Figure 53: Pseudo-first order kinetic plots for ROP of ε-CL.
Conditions: $[\varepsilon\text{-}CL.]_0$ = 1.4 M, $[\varepsilon\text{-}CL.]_0/[\mathbf{1}]_0$ = 100, T = 80 °C, and toluene as the solvent.

The $M_{n(exp)}$ increase with progress of reaction, with *Đ*s values in the range 1.19-1.53. Also in this case, the $M_{n(exp)}$ are lower than $M_{n(Theo)}$. Subsequently the monomer/catalyst ratio was increased to 200 and 500 and the catalyst still preserved a good activity, reached TOF values of 192 and 376 h^{-1}.

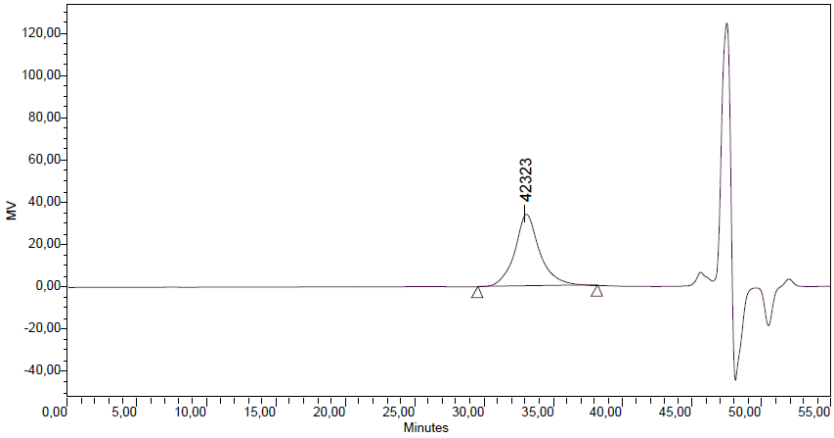

Figure 54: SEC of PCL. Conditions: [ε-CL]/[1] = 500, 2 ml of toluene, T = 80 °C, t = 1 h.

As well as made with *L-LA*, a polymerization run with a low molar ratio monomer/catalyst ([*ε-CL*]/[**1**]) was performed. In the ^{1}H NMR spectra (*figure 55*) of the isolated polymer coagulated in n-hexane, the resonances due to the terminal groups were clearly detectable. Two signals at 2.92 and 2.98 ppm are attributable to two methyl groups of the *–C(=O)NMe*$_2$ end group. The presence of these signals confirm that the *ROP* of cyclic esters with these new complexes follows a coordination-insertion mechanism.

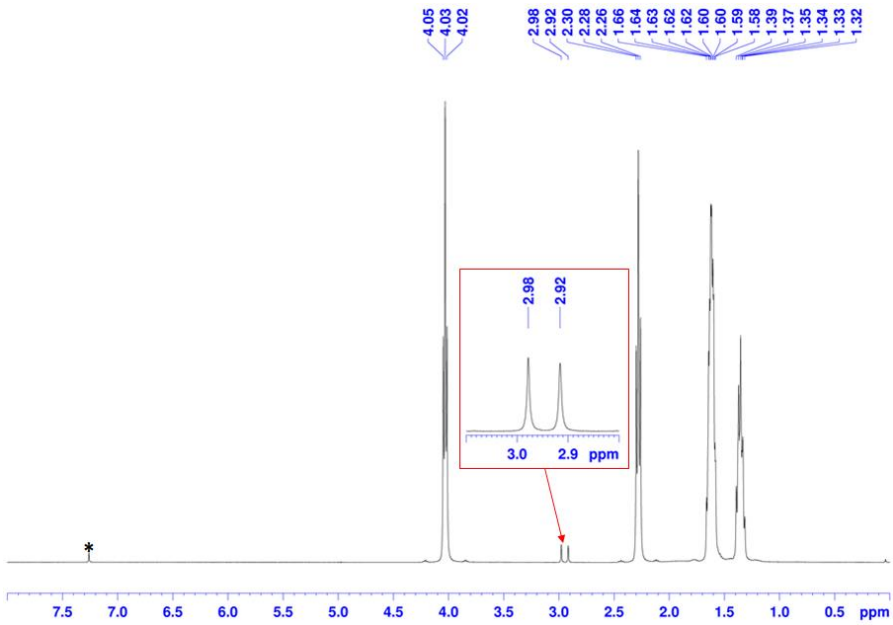

Figure 55: ^{1}H NMR of oligomers of PCL obtained using 1 as catalyst (400.13 MHz, *$CDCl_3$, 25°C).

2.4 Conclusions

In this chapter a series of new group *IV* metal complexes supported by a new class of tetradentate dianionic ligands was reported. The *Zr* and *Hf* complexes were obtained through a transamination reaction between the *NSSN*-ligands and $Zr(NMe_2)_4$ or $Hf(NMe_2)_4$ and characterized by ^{1}H and ^{13}C NMR spectroscopy. The NMR analysis revealed the presence in solution of the complexes as a single isomer with a C_2 symmetry. The X-ray diffraction analysis of the crystals obtained from cold hexane revealed that the complexes present a distorted octahedral coordination geometry around the metal center, adopting a pseudo-C_2-symmetrical configuration. The complexes are stable and rigid at different temperatures, as confirmed by NMR in the range 25-100 °C. All complexes were tested in *ROP* of cyclic esters. The most active complex was the zirconium complex with two isopropyl groups on the amide functions of the coordinate ligand. This complex is sterically less hindered and therefore allows an easier coordination of the monomer molecules at the catalytic sites. In fact, the substitution of the two isopropyl groups with other more bulky groups, such as the cyclohexyl or mesityl group, causes a decrease in the catalytic activity. *Zr-NSSN-ISO* showed a catalytic activity superior to those *Zr* complexes featuring *OSSO* ligands and comparable to that of the most active group *IV* complexes operating in a toluene solution. The replacement of the *Zr* atom with the *Hf* atom causes a decrease in the catalytic activity of the complexes, as already reported in literature. The inspections of the methine regions for the *poly-rac-LAs* obtained by this new metal complexes, showed that atactic *PLAs* are obtained. All complexes showed a good control over polymerization process leading to polymers with relatively narrow *Đ*s. However the $M_{n(exp)}$ obtained are lower than those expected cause of transesterification reactions that affect the polymerization process. The presence of the transesterification reactions was also confirmed by MALDI-TOF analysis. NMR analysis of the end groups of the polymer obtained from polymerization runs with a low monomer/catalyst ratio confirmed that the *ROP* of cyclic esters with these new metal complexes follows a coordination-insertion mechanism.

3 Monometallic *Al* complexes for *ROP* of cyclic esters

The *Al* complexes have been extensively investigated as catalysts for *ROP* of cyclic esters because they are colourless, earth abundant, inexpensive, biocompatible, and less toxic compared with many transition metals.

The ancillary ligands surrounding the aluminum center play a key role in determining the reactivity and selectivity of the catalyst. Over the past several decades, with the aim of developing new performing catalysts, *Al* complexes bearing ligands with a different combination of donor atoms have been reported.[66]

The most investigated complexes feature dianionic tetradentate *ONNO*-type ligands, such as salen, dialkoxy-diimino, salan, or salalen ligands as these complexes, above all, are able to afford *PLA* with a wide range of iso-/heterotactic structures.[67] Notable examples are reported in *figure 56*, it includes (a) the complexes reported by Spassky featuring chiral salen ligands that gave highly isotactic diblock *PLA* by an enantiomorphic-site control mechanism;[68] (b) the complexes reported by Nomura with achiral salen ligands that gave highly isotactic multiblock *PLA* by a chain-end control mechanism;[69] (c) the complexes reported by Gibson that gave *PLAs* of different tacticities depending on the phenolate substituents of the salan ligand;[70] (d) the

[66] P. Wang, X. Hao, J. Cheng, J. Chao, X. Chen, *Dalton Trans.*, ***2016***, *45, 9088-9096;* Y. –T. Huang, W. –C. Wang, C. –P. Hsu, W. –Y. Lu, W. –J. Chuang, M. Y. Chiang, Y. –C. Lai, H. –Y. Chen, *Polym. Chem.*, ***2016***, *7, 4367-4377;* N. Lu, Z. Jiang, H. Pei, W. Liu, Y. Li, Y. Dong, *Eur. J. Inorg. Chem.*, ***2017***, *1320-1327.*

[67] T. M. Ovitt, G. W. Coates, *J. Am. Chem. Soc.*, ***1996***, *121, 4072-4073;* Z. Zhong, P. J. Dijkstra, J. Feijen, *Angew. Chem., Int. Ed.*, ***2002***, *41, 4510-4513;* A. Alaaeddine, C. M. Thomas, T. Roisnel, J. –F. Carpentier, *Organometallics*, ***2009***, *28, 1469-1475;* P. McKeown, M. G. Davidson, G. Kociok-Kohn, M. D. Jones, *Chem. Commun.*, ***2016***, *52, 10431-10434;* S. Gesslbauer, H. Cheek, A. J. P. White, C. Romain, *Dalton Trans.*, ***2018***, *47, 10410-10414;* S. Gesslbauer, R. Savela, Y. Chen, A. J. P. White, C. Romain, *ACS Catal.*, ***2019***, *9, 7912-7920;* S. Gesslbauer, G. Hutchinson, A. J. P. White, J. Burés, C. Romain, *ACS Catal.*, ***2021***, *11, 4084-4093.*

[68] N. Spassky, M. Wisniewski, C. Pluta, A. Le Borgne, *Macromol. Chem. Phys.*, ***1996***, *197, 2627-2637.*

[69] N. Nomura, R. Ishii, M. Akakura, K. Aoi, *J. Am. Chem. Soc.*, ***2002***, *124, 5938-5939.*

[70] P. Hormnirun, E. L. Marshall, V. C. Gibson, A. J. P. White, D. J. Williams, *J. Am. Chem. Soc.*, ***2004***, *126, 2688-2689.*

complexes reported by Lamberti coordinated by salalen ligands that led to a gradient isotactic multiblock *PLA* through a combination of enantiomorphic-site and chain-end control mechanisms.[71]

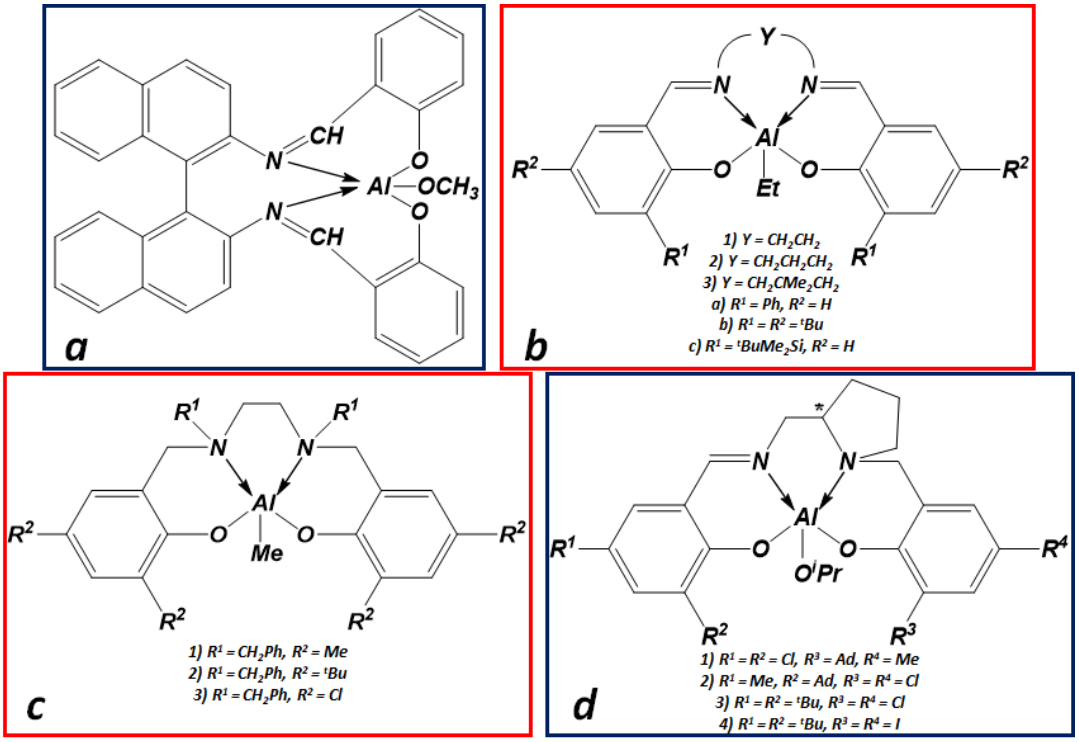

Figure 56: examples of ONNO-type Al complexes

Beyond these, a particular attention was paid to those ligands that combine an hard donor function (a phenolate or an amide function) with a soft neutral one (S- or P-donor atoms) as it was observed that this combination could modulate the acidity of the metal center with remarkable consequences on the catalytic performances. One of the first examples of *Al* complexes bearing ligands in which the anionic phenolate oxygen atoms are combined with neutral sulphur atoms are those reported by Okuda in 2005 (*figure 57*). He and his co-workers reported a series of *Al* alkyl complexes incorporating a dianionic *[OSSO]*-type ligand. The complexes, in presence of isopropanol, acted as catalyst for living *ROP* of *rac-LA*, achieving up to 93% of monomer conversion after 10 h, at 70 °C.[72]

[71] A. Pilone, K. Press, I. Goldberg, M. Kol, M. Mazzeo, M. Lamberti, *J. Am. Chem. Soc.*, ***2014**, 136, 8, 2940–2943.*

[72] H. Ma, G. Melillo, L. Oliva, T. P. Spaniol, U. Englert, J. Okuda, *Dalton Trans.*, ***2005**, 4, 721-727;* B. Lian, H. Ma, T. P. Spaniol, J. Okuda, *Dalton Trans.*, ***2009**, 41, 9033-9042.*

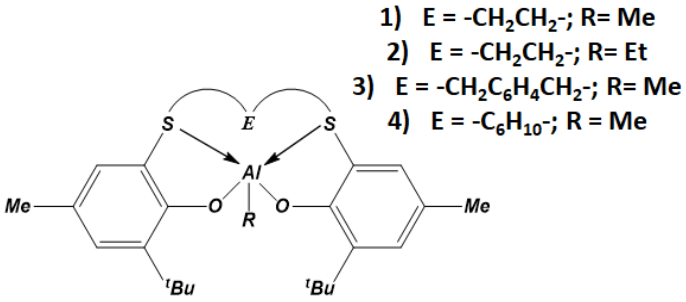

Figure 57: Al alkyl complexes supported by OSSO-type ligands.

Analogous complexes featuring bidentate *OS* ligands were reported by Lamberti et al.; these phenoxy-thioether *Al* complexes, in presence of methanol as cocatatalyst, were able to exert an effective control over the polymerization of *ε-CL* and *rac-/L-LA*. Moreover, it was observed that the substituent at the ortho-position of the aromatic ring (group *R* in *figure 58*) has an opposite effect on the catalytic activities of the two different cyclic esters.[73]

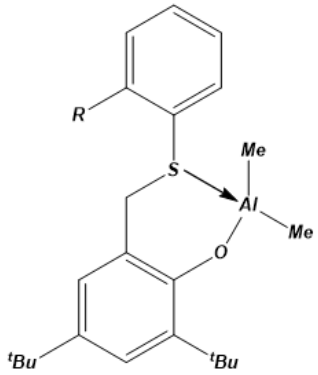

Complex	R
1	H
2	Br
3	CH_3
4	CF_3

Figure 58: phenoxy-thioether Al complexes.

As already stated in the previous chapters, this project is focused on the research for alternative coordination environment for the development of potentially active ring opening polymerization catalysts. The ligands described in the previous chapter feature a combination of hard and soft donor groups that, at the best of our knowledge, were never used for the development of *Al* catalyst for the *ROP* of cyclic esters. For these reason we decided to prepare *Al* complexes supported by this class of ligands, both bidentate *NS* and tetradentate *NSSN* ligands. In this chapter we report the synthesis and the characterization of monometallic tetracoordinate *Al* complexes supported by thioether-amine ligands and their use in the *ROP* of cyclic esters.

[73] M. Lamberti, I. D'Auria, M. Mazzeo, S. Milione, V. Bertolasi, D. Pappalardo, *Organometallics*, ***2012***, *31, 5551-5560.*

3.1 Synthesis and characterization of ligands

The mononucleating *NS* ligands prepared in this project contain an anionic nitrogen donor and neutral sulphur donor linked by a phenylene bridges. The aniline nitrogen atom bears an isopropyl group whereas the sulphur atom an alkyl group of different length, i.e. ethyl, isopropyl, n-hexyl or benzyl group. All ligands were prepared according to the following procedure: the 2-aminothiophenol was reacted with the opportune bromo-derivate in refluxing methanol to obtain an intermediate that was subsequently treated with acetone in presence of zinc and acetic acid according to *Scheme 3*.

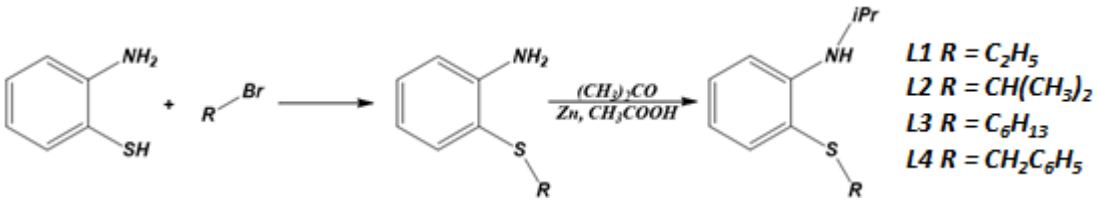

Scheme 3

The ligands were isolated as brown oils in good yields (58-80%) and were characterized by NMR and mass spectroscopy. The NMR signals were observed in the expected ranges for these compounds. In the ^{1}H NMR the methine proton of the isopropyl group was observed as a heptet in the range 3.5-4.0 ppm whereas the *NH* proton was observed as a singlet in the range 4.9-5.4 ppm.

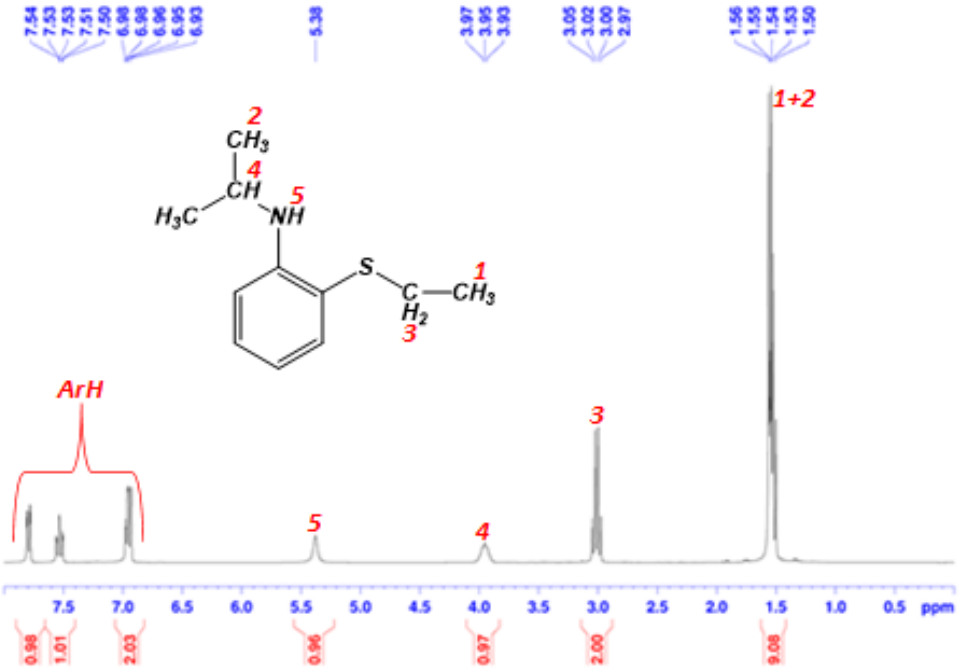

Figure 59: ^{1}H NMR of L1 ligand (400.13 MHz, *CD_2Cl_2, 25°C).

3.2 Synthesis and characterization of monometallic Al complexes (1-4)

The complexes **1-4** (*figure 60*) were synthesized by reaction the corresponding *NS*-type ligand with $AlMe_3$ in refluxing benzene (*Scheme 4*), in good yields (92-95%).

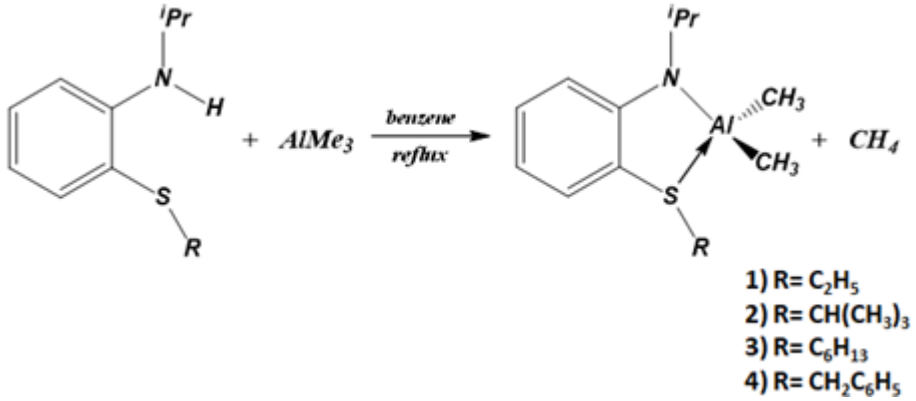

Scheme 4

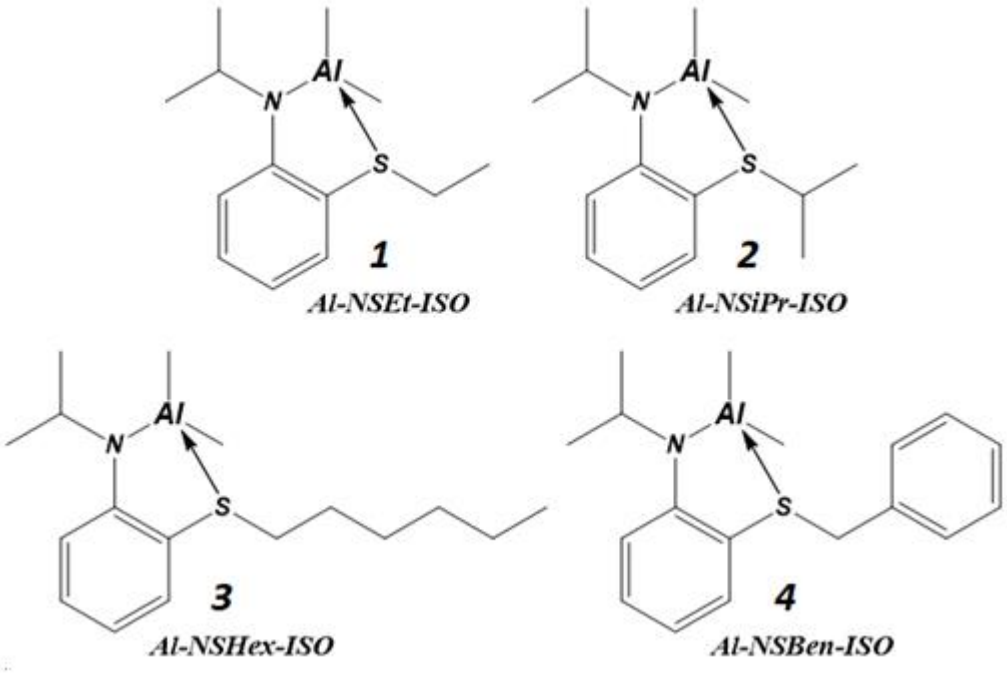

Figure 60: complexes 1-4

Each complex was characterized by ^{1}H and ^{13}C NMR spectroscopy and the $^{1}H/^{13}C$ attributions were done through HSQC experiments. In all cases, the ^{1}H NMR spectrum showed a signal at a chemical shift lower than 0 ppm, which was attributed to $–CH_3$ bound to the *Al* metal center and the disappearance of the signal related to the amine of the starting ligand which confirmed the complex formation.

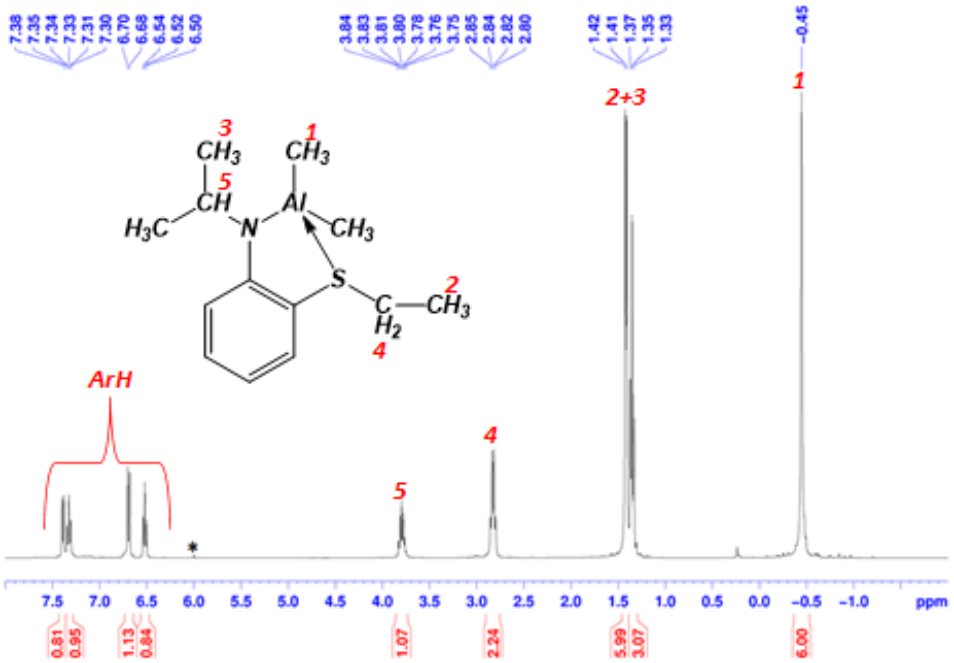

*Figure 61: ^{1}H NMR of complex 1 (400.13 MHz, *TCDE, 25°C).*

The NMR analysis of complex **1** performed at different temperatures, range 25-80 °C, showed no broadening or decomposition, indicating that the structure of the complex is stable at high temperatures. The NMR analysis of complex **1** performed in the range of temperature -60-25 °C, were carried out to explore the presence of fluxional process in solution. Going down in temperature, the NMR signals broadened and split into different sets of resonances, as can be seen in the *figure 64*.

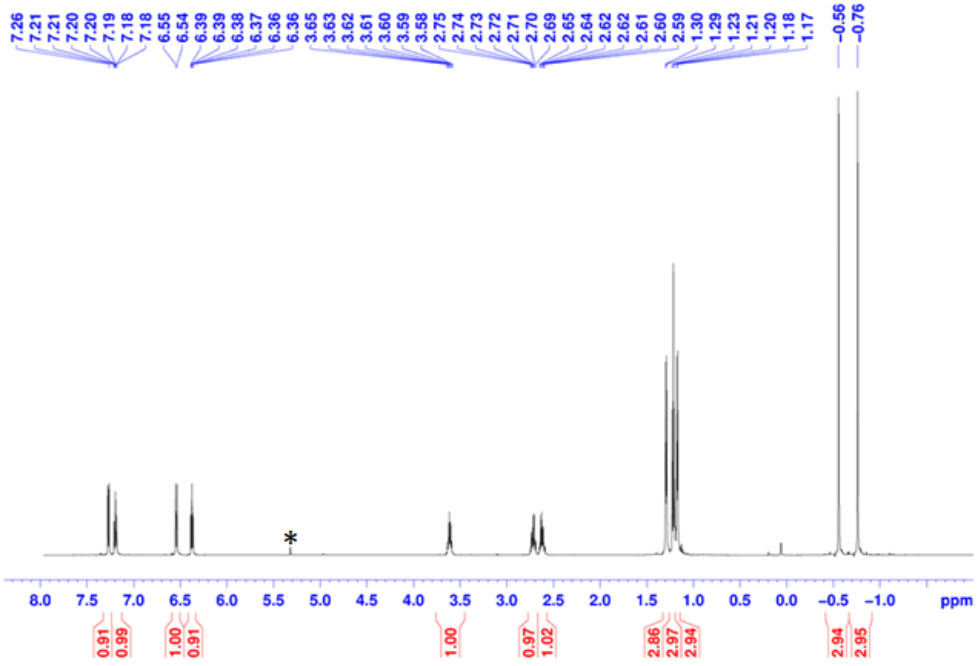

*Figure 62: ^{1}H NMR of complex 1 (400.13 MHz, *CD_2Cl_2, -60°C).*

In particular, the methyl of *Al–CH₃* group, which occurred as a single signal at -0.63 ppm at room temperature, appears as two singlets (-0.76 and -0.56 ppm) in a 1:1 intensity ratio, at -60 °C. Also the signals of *S-CH₂* group and *-CH₃* of the *N*-isopropyl group, were slitted into several signals (two multiplets at 2.62 and 2.72 ppm for the *S-CH₂* group; two doublets at 1.17 and 1.30 ppm for the methyls of the *NCH(CH₃)₂* group (see *figure 62*).

The pattern of the NMR signals observed at -60 °C is consistent with those expected for a C_1-symmetric structure. The coalescence of the signal is due to a rapid interconversion of the two enantiomers (*figure 63*) probably to a fast the inversion of the configuration at the sulphur atom.

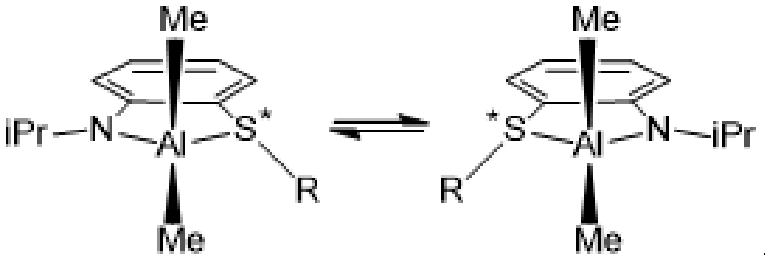

Figure 63: interconversion of two enantiomers of complex 1.

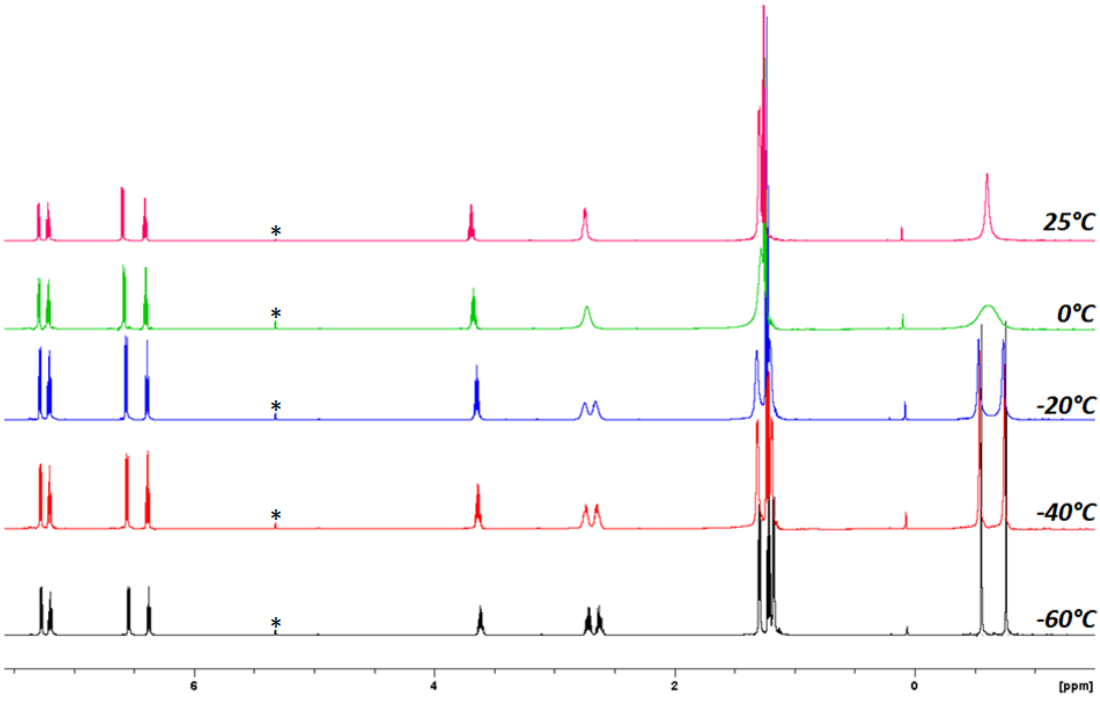

Figure 64: ^{1}H NMR of Al-NSEt-ISO complex (400.13 MHz, *CD_2Cl_2, variable temperature).

The nuclearity in solution of the complex **1** was verified through pulsed gradient spin-echo (PSGE) NMR spectroscopy. This method assesses translational motion of the

analyte in solution through determination of the diffusion coefficient (D_e) and comparing it with an internal standard. The D_e is a quantity inversely related to the molecular mass and for this reason, the PSGE method has been used to explore the aggregation properties of a series of organometallic molecules.[74] The D_e of complex **1** was determined by the 2D version of the PSGE experiment DOSY in a CH_2Cl_2 solution, using TMSS as internal standard. The molecular mass in solution (m) was estimated using the Graham's law of diffusion.

$$\boldsymbol{D = K(T/m)^{1/2}}$$

K: constant depends on geometric factors.

By assuming a constant temperature and that K is the same for both species in solution, the relative D_e of the complex (D_b) and TMSS (D_a) is given by:

$$\boldsymbol{Da/Db = (mb/ma)^{1/2}}$$

m_b: molecular mass of the complex;

m_a: molecular mass of the internal standard.

With this method is possible to calculate a molecular mass of an unknown species.

[74] J. Fielden, D. Long, A. M. Z. Slawin, P. Kogerler, L. Cronin, *Inorg. Chem.*, ***2007***, *46, 9090-9097*; G. Consiglio, S. Failla, P. Finocchiaro, I. P. Oliveri, R. Purello, S. Di Bella, *Inorg. Chem.*, ***2010***, *49, 5134-5142*; G. Consiglio, S. Failla, P. Finocchiaro, I. P. Oliveri, S. Di Bella, *Inorg. Chem.*, ***2012***, *51, 8409-8418.*

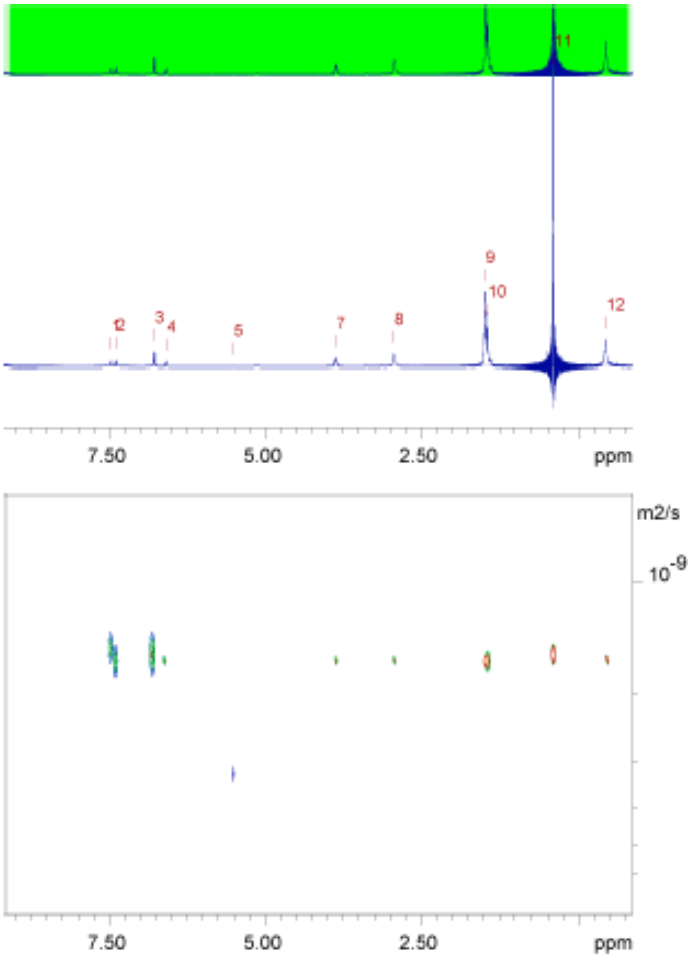

Figure 65: DOSY spectrum of Al-NSEt-ISO complex (400.13 MHz, $^{*}CD_2Cl_2$, 25°C).

The obtained D_e was converted into molecular mass to compare with the molecular masses of the monomeric and dimeric species. The results reported in table 3, support the structure of complex **1** as a monomeric species.

Table 3: ***Diffusion coefficient (D), estimated molecular mass (m) and molecular weight of monomeric (M_{mon}) and dimeric species (M_{dim}).***

$D_e^{Complex}$ ($x\ 10^{-9} m^2 s^{-1}$)	D_e^{TMSS} ($x\ 10^{-9} m^2 s^{-1}$)	$m_{calculated}$[a] (g/mol)	M_{mon} (g/mol)	M_{dim} (g/mol)
1.60	1.58	313	251	503

[a]Estimated using TMSS as internal standard and using CH_2Cl_2 as solvent.

DFT calculations were carried out on monometallic *Al* complexes to structurally characterize them, in addition to NMR analysis already performed. The *figure 68* shows the minimum energy structure of the **1**. In the figure it's possible to see that the *Al* atom adopts a distorted tetrahedral geometry, the nitrogen displays a trigonal planar geometry and the sulphur atom displays a trigonal pyramidal geometry. The *Al-S* bond

distances are between 2.446 and 2.453 Å. The use of topographic steric maps were used to observe the steric hindrance around the metal center. The catalytic site can be considered quite free since the ligand occupies a little area around the *Al* center (V_{bur}^{1}= 35.1%, V_{bur}^{2}= 36.2%, V_{bur}^{3}= 35.9%, V_{bur}^{4}= 34.4%).

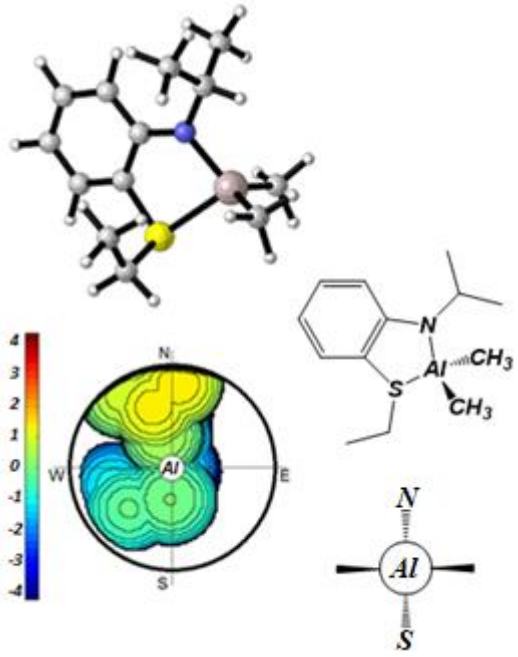

Figure 66: steric maps of Al-NSEt-ISO complex.

3.3 ROP of cyclic esters catalyzed by 1-4

The synthetized monometallic *Al* complexes were tested as catalysts in the *ROP* of several cyclic esters in toluene solution, in combination with isopropanol. The importance of an alcohol as co-initiator was confirmed by a polymerization test carried out in absence of ^{i}*PrOH*, complex **1** was found inactive. The complex **1** was found to be the most active among all the synthesized monometallic *Al* complexes, it was able to convert 82% of *L-LA* in 8 hours at 80 °C, its TOF was 10.2 $mol_{LA} \cdot mol_{Al}^{-1} \cdot h^{-1}$. Complexes **2 - 4** were less active, the TOF were 9.8, 9.2 and 8.7 $mol_{LA} \cdot mol_{Al}^{-1} \cdot h^{-1}$, respectively. Respect to the data reported in literature, the activities of **1-4** were higher respect to those of the related mono(phenoxy-imine)aluminum complexes under similar experimental conditions (TOF = 2–7 $mol_{LA} \cdot mol_{Al}^{-1} \cdot h^{-1}$).

Table 4: ROP of cyclic esters by 1-4

Entry	Complex	Monomer	[M]/[cat]	T (°C)	t (h)	Conv.[b] (%)	TOF (h^{-1})	$M_{n(theo)}$[c]
1	***1***	*L-LA*	100	80	8	82	10.2	6.0
2	***2***	*L-LA*	100	80	8	78	9.8	5.7
3	***3***	*L-LA*	100	80	8	73	9.2	5.3
4	***4***	*L-LA*	100	80	8	55	8.7	4.0
5	***1***	*rac-LA*	100	80	7	85	12.1	6.2
6	***1***	*L-LA*	100	100	4	92	22.9	6.7
7	***2***	*L-LA*	100	100	4	89	22.3	6.5
8	***3***	*L-LA*	100	100	4	90	22.6	6.6
9	***4***	*L-LA*	100	100	4	88	22.0	6.4
10	***1***	*ε-CL*	360	50	0.5	92	658.9	37.7
11[a]	***1***	*ε-CL*	500	25	4	77	96.6	22.1
12[a]	***1***	*ε-CL*	1000	25	18	53	29.4	30.3
13[a]	***1***	*ε-CL*	5000	25	18	0	0	-

All reaction were carried out in 2 mL of toluene and using 1-propanol as co-catalyst. Reaction conditions: 80°C, $[Cat]_0$= 14.0 mM, [Monomer]= 1.4 M, [Cocatalyst]/[cat]= 2; [a]2 ml of dichloromethane as solvent; [b]Molecular conversion determined by ^{1}H NMR spectroscopy ($CDCl_3$, 298 K); [c]Calculated molecular weight using $M_{n(theo)}$(kg/mol)=(((PM$_{Monomer}$ x [Mon]/[cocat] x conversion)/100) + PM$_{Cocat}$)/1000.

To get more information on *ROP* with these catalysts, the reactions were sampled by taking several aliquots of the product mixture at regular and scheduled intervals, the product mixture were analysed by ^{1}H NMR spectroscopy and GPC. In all cases it was observed that the polymerization starts instantaneously; it resulted first order with respect to the monomer concentration. In the figure below it's possible to see the linearity of the plot ln([*L-LA*]$_0$/[*L-LA*]$_t$] versus time. From the plots it's possible to see that the k_{app} of **1** is higher than those of the other *Al* complexes.

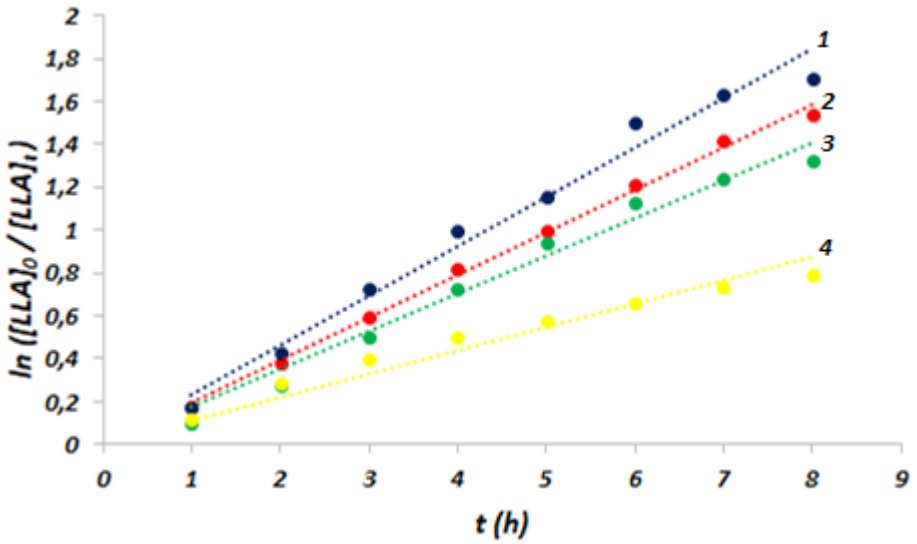

Figure 67: Pseudo-first order kinetic plots for ROP of L-LA by 1 (k_{app}= 0.23 ± 0.01 h^{-1}, R^2= 0.980, blue line), 2 (k_{app}= 0.20 ± 0.004 h^{-1}, R^2= 0.992, red line), 3 (k_{app}= 0.18 ± 0.01 h^{-1}, R^2= 0.980, green line), 4 (k_{app}= 0.11 ± 0.01 h^{-1}, R^2= 0.940, yellow line).

Conditions: [L-LA]$_0$ = 1.4 M, [L-LA]$_0$/[I]$_0$ = 100, [^{i}PrOH]$_0$/[I]$_0$ = 2, T = 80 °C, and toluene as the solvent.

To evaluate the effect of temperature on the polymerization reaction, kinetic experiments were carried out at 100 °C (entry 6, 7, 8, 9 in table 4). An increase of the polymerization activities was observed and almost quantitative conversions were obtained within 4 hours. Also at 100 °C the complex **1** still result the most complex active among the synthesized monometallic ones, reached a TOF of 23 $mol_{LA} \cdot mol_{Al}^{-1} \cdot h^{-1}$.

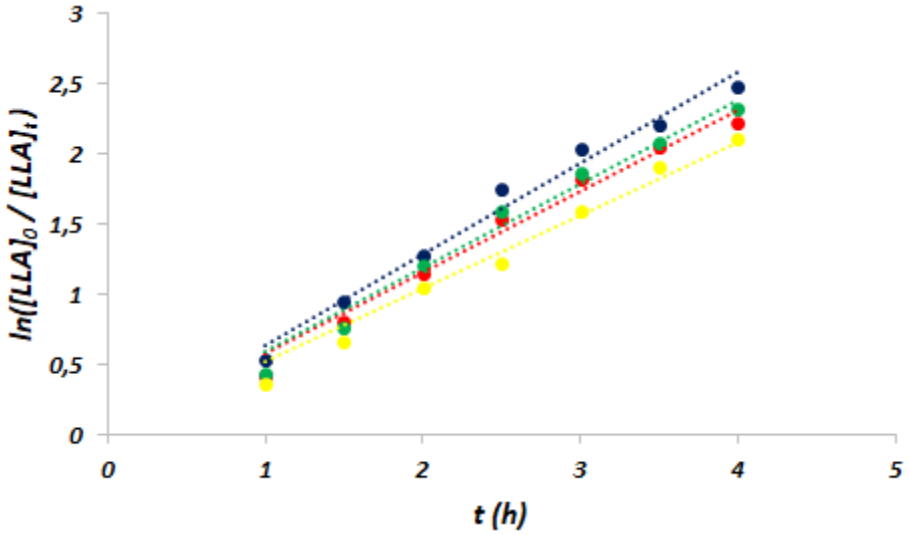

Figure 68: Pseudo-first order kinetic plots for ROP of L-LA by 1 (k_{app}= 0.64 ± 0.04 h^{-1}, R^2= 0.987, blue), 2 (k_{app}= 0.58 ± 0.04 h^{-1}, R^2= 0.980, red), 3 (k_{app}= 0.60 ± 0.04 h^{-1}, R^2= 0.978, green), 4 (k_{app}= 0.52 ± 0.02 h^{-1}, R^2= 0.980, yellow).

Conditions: $[L\text{-}LA]_0$ = 1.4 M, $[L\text{-}LA]_0/[I]_0$ = 100, $[^iPrOH]_0/[I]_0$ = 2, T = 100 °C, and 2 mL of toluene as the solvent.

To probe the robustness of the catalytic system, a series of kinetic tests at 100 °C were performed by reducing the amount of **1**.

Table 5: summary of the experiments for reaction order with respect 1.

Entry	[1] (mM)	[L-LA]/[1]	v_0 (Conv./h)[a]	k_1 (1/h)[b]	Conv. (%)[c]	TOF (h^{-1})
1	14.0	100	32.14	0.64 ± 0.03	92	23
2	4.7	300	27.62	0.53 ± 0.01	87	65
3	2.8	500	27.28	0.46 ± 0.01	83	104
4	2.0	700	25.66	0.43 ± 0.01	82	143

All reaction were carried out in 2 mL of toluene and using 1-propanol as co-catalyst. T = 100 °C, $[^iPrOH]_0/[\mathbf{1}]_0$ = 2. [a]Initial velocity obtained from plot of conversion vs time. [b]Kinetic constant obtained from pseudo-first order lot of ln[*L*-LA] vs time. [c]Molecular conversion determined by ^1H NMR spectroscopy ($CDCl_3$, 298 K) on sample after 4 hours.

The kinetic plots reported in *figure 69* show that the k_{app} decrease as the molar ratio increases and, from the log/log plot of the velocity (v_0) versus catalyst concentration (*figure 71*) and the log/log plot of the k_1 versus catalyst concentration (*figure 72*), a reaction order of one respect to the catalyst concentration was obtained.

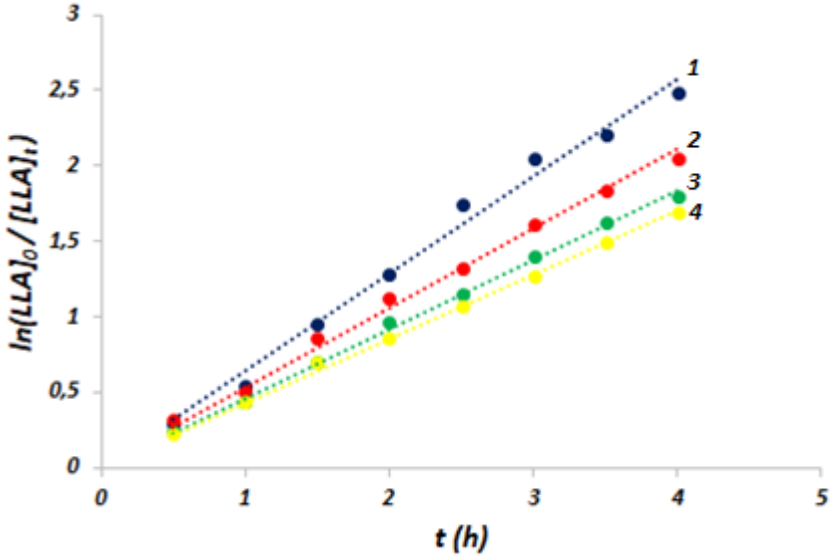

Figure 69: Pseudo-first order kinetic plots for experiments in Table 5. Entry 1 (blue line, R^2= 0.987), Entry 2 (red line, R^2= 0.994), Entry 3 (green line, R^2= 0.998), Entry 4 (yellow line, R^2= 0.998).

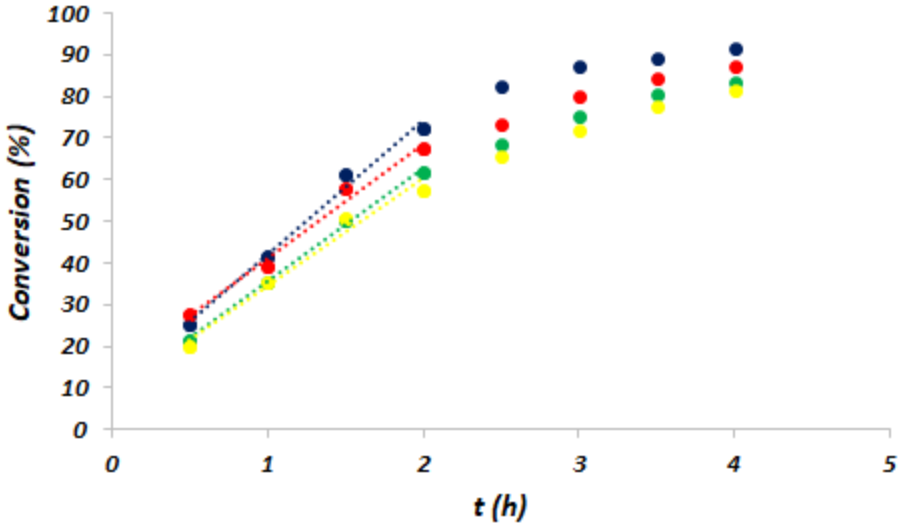

Figure 70: kinetic plots for experiments in Table 5. Plot of conversion vs time, for the determination of initial velocity v_0. Entry 1 (blue line, R^2= 0.988), Entry 2 (red line, R^2= 0.987), Entry 3 (green line, R^2= 0.997), Entry 4 (yellow line, R^2= 0.976).

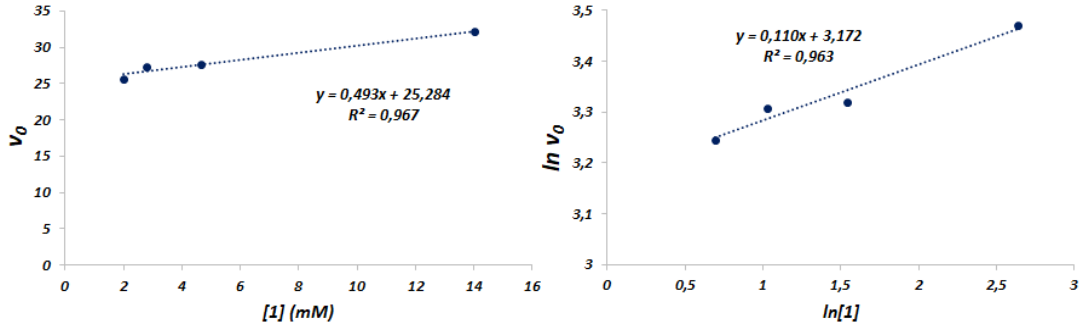

Figure 71: kinetic plots for experiments in Table 5. Plot of v_0 vs [1] and ln(v_0) vs ln([1]).

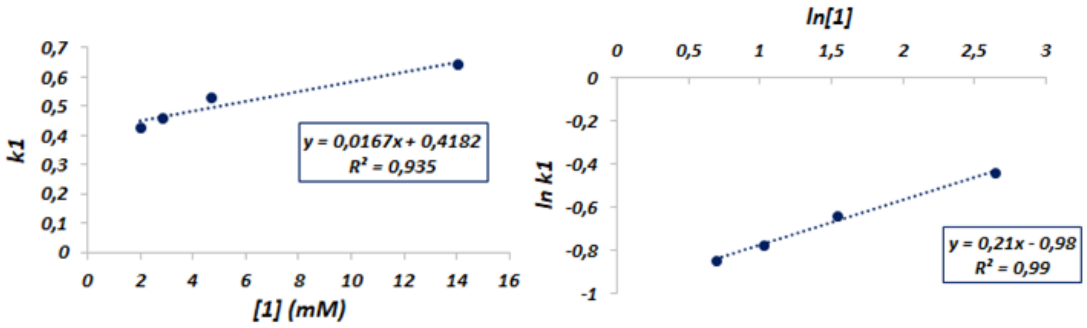

Figure 72: kinetic plots for experiments in Table 5. Plot of k_1 vs [1] and ln(k_1) vs ln([1]).

Subsequently, the complex **1** was tested in the *ROP* of *rac-LA*. Also in this case, the polymerization starts instantaneously, following a first order kinetic law with respect to the monomer concentration, reached a monomer conversion of 85% in seven hours with a k_{app} value similar to k_{app} for polymerization of *L-LA*, obtaining an atactic *PLA*.

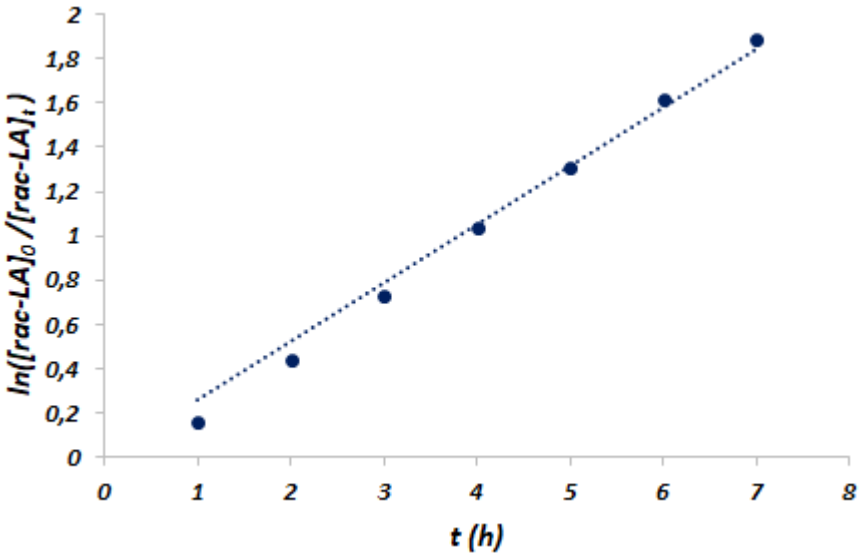

Figure 73: Pseudo-first order kinetic plots for ROP of rac-LA by 1 (k_{app}= 0.26 ± 0.002 h^{-1}, R^2= 0.989).
Conditions: $[rac\text{-}LA]_0$ = 1.4 M, $[L\text{-}LA]_0/[\mathbf{1}]_0$ = 100, $[^iPrOH]_0/[\mathbf{1}]_0$ = 2, T = 80 °C, and toluene as the solvent.

Complex **1** was also tested in *ROP* of *ε-CL*. Polymerization experiments were carried out in a toluene solution at 50 °C and in a dichloromethane at room temperature (entry 10, 11 and 12 in table 4). In these experimental conditions, complex 1 reached 92% of monomer conversion in 30 minutes (TOF= 658.9 $mol_{LA} \cdot mol_{Al}^{-1} \cdot h^{-1}$) and 77% in 4 hours at room temperature (TOF= 96.6 $mol_{LA} \cdot mol_{Al}^{-1} \cdot h^{-1}$).

A polymerization run with a low molar ratio monomer/catalyst ([*ε-CL*]/[**1**] = 25) was performed with the aim of deepening the initiation process. The NMR analysis of the isolated polymer obtained with complex **1** showed the presence of three signals at 1.18,

3.61 and 4.97 ppm in the ^{1}H NMR spectra (*figure 74*), and four signals at 24.77, 32.42, 62.65 and 67.55 ppm in the ^{13}C NMR spectra (*figure 75*). The signal at 3.61 ppm in the ^{1}H NMR spectra is attributable at -CH_2OH end group of the last monomeric unit, while the signals at 1.18 and 4.97 ppm originates from the nucleophilic attack of the $^{i}PrOH$ to the carboxylic carbon of the monomer coordinated to the metal center. The four signals in the ^{13}C NMR spectra are attributable: two to the last monomeric units and the other two to the ester bond formed by the $^{i}PrOH$ attack.[75] The same experiment, using the same reaction conditions, was repeated but using the *L-LA* as the monomer. The ^{1}H and ^{13}C spectra (*figure 76* and *77*) showed the presence of terminal group also in final *PLA*. This confirms that the reaction begins with the attack of the isopropoxy group on the carbonyl carbon of the monomer and ends with the hydrolysis of the *Al-O* bond between the growing polymer chain and the metal center.

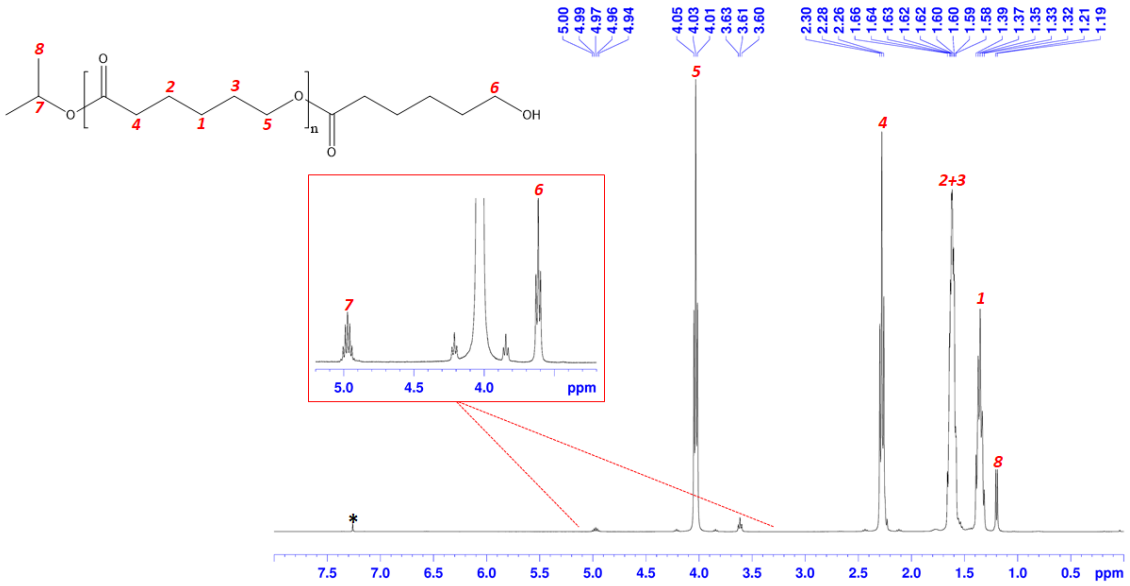

Figure 74: ^{1}H NMR of oligomers of PCL obtained using 1 as catalyst (400.13 MHz, *$CDCl_3$, 25°C).

[75] X. Zhou, L. Hong, *Colloid Polym. Sci.*, ***2013***, *291, 2155-2162;* M. Abdollahi, R. Bairami Habashi, M. Mohsen, *Ind. Crops Prod.*, ***2019***, *130, 547-557;* Q. Hu, S. Jie, P. Braunstein, B. –G. Li, *J. Organomet. Chem.*, ***2019***, *882, 1-9.*

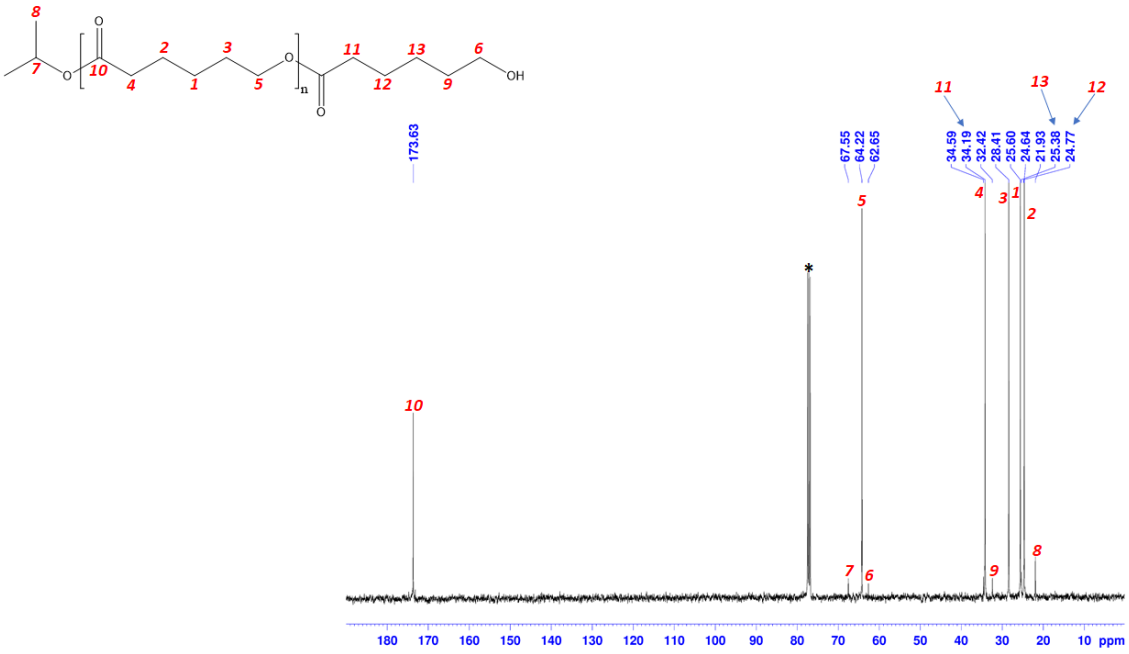

*Figure 75: ^{13}C NMR of oligomers of PCL obtained using 1 as catalyst (100.62 MHz, *$CDCl_3$, 25°C).*

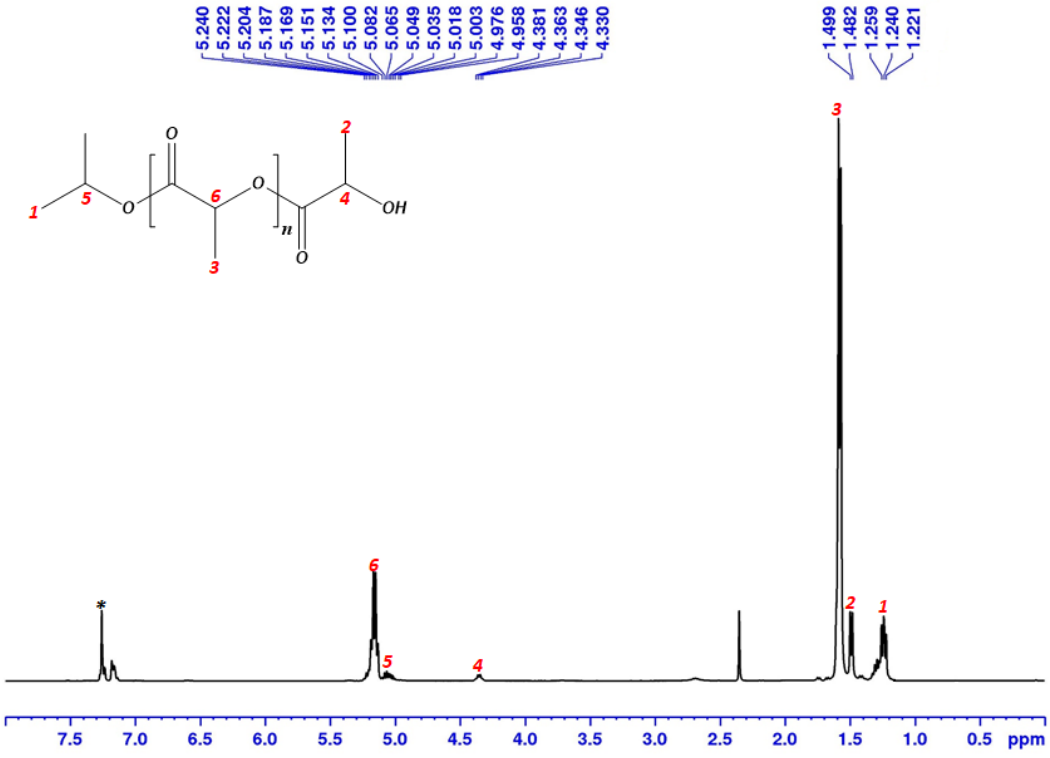

*Figure 76: ^{1}H NMR of oligomers of PLA obtained using 1 as catalyst (400.13 MHz, *$CDCl_3$, 25°C).*

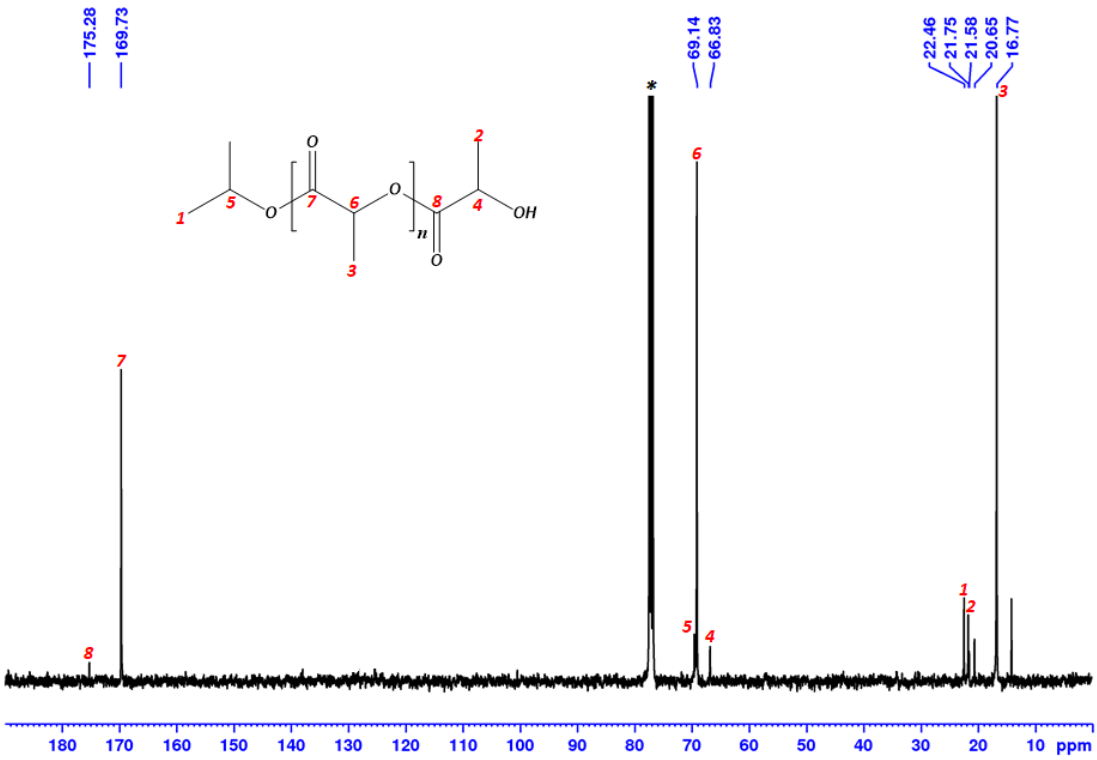

*Figure 77: ^{13}C NMR of oligomers of PLA obtained using 1 as catalyst (400.13 MHz, *$CDCl_3$, 25°C).*

3.4 Conclusions

A new series of *Al* metal complexes supported by bidentate mononucleating *NS* thioether-amine ligands have been developed. The *Al* complexes were obtained by reaction of the corresponding thioether-amine ligand with a single equivalent of $AlMe_3$, and characterized by ^{1}H and ^{13}C NMR spectroscopy. Among the monometallic complexes, the most active for the *ROP* of *L-LA* was **1**, with an ethyl group bonded to the sulphur atom. Probably the ethyl group causes a smaller steric hindrance than other groups of the other complexes, allowing an easier arrival at the metallic site of the cyclic esters to start the polymerization.

The temperature effect was investigated through kinetic tests. It was observed that by increasing the temperature from 80 to 100 °C, an increase in the polymerization rate and the catalytic activity of the catalysts occurs. In fact, almost quantitative conversions were achieved in 4 hours using the complexes at 100 °C, while using them at 80 °C, these conversions were not reached even after 8 hours.

The effect of the [*L-LA*]/[**1**] ratio on the polymerization was investigated through kinetic tests by reducing the amount of catalyst in the system progressively. The catalyst remained active, without a loss of activity (TOF = 143 $mol_{LA} \cdot mol_{Al}^{-1} \cdot h^{-1}$), even with [*L-LA*]/[**1**] ratio of 700, reached 82% of monomer conversion after 4 hours. **1** was also tested in the *ROP* of *ε-CL*. High conversions were obtained even using [*ε-CL*]/[**1**] ratio of 360 in a toluene solution at 50 °C, while using dichloromethane as solvent and decreasing temperature, the catalyst loses its catalytic activity.

NMR analysis on polymers with low molecular weight obtained by **1**, confirmed that the *ROP* stars with the attack of the co-initiator (isopropoxy group) on the carbonyl carbon of the monomer and ends with the hydrolysis of the *Al-O* bond between the growing polymer chain and the metal center.

4 Bimetallic *Al* complexes for *ROP* of cyclic esters

In the framework of the *ROP*, bimetallic complexes are considered as a class of catalysts with promising performances. In these species the two metallic centres are spatially close and can work in a concerted manner. In most cases, the cooperation has a positive influence on the catalytic performances and lead to an increase of the activities.

In the last few years a lot of bimetallic *Al* complexes were reported in literature, able to promote the *ROP* of several cyclic esters. Bimetallic *Al* five-coordinate complexes have been extensively investigated as catalyst for controlled and stereoselective *ROP* of *LA.*[76] The cooperation between several metal centers of a multinuclear *Al* complex based on a macrocyclic Schiff base ligand, was reported by Redshaw who proved that the multimetallic catalysts showed higher catalytic activity than monometallic analogue.[77] The cooperative effects on polymerization with a series of bimetallic *Al* complexes with bis-phenolato ligands has been proved by Yao (*figure 78*).[78]

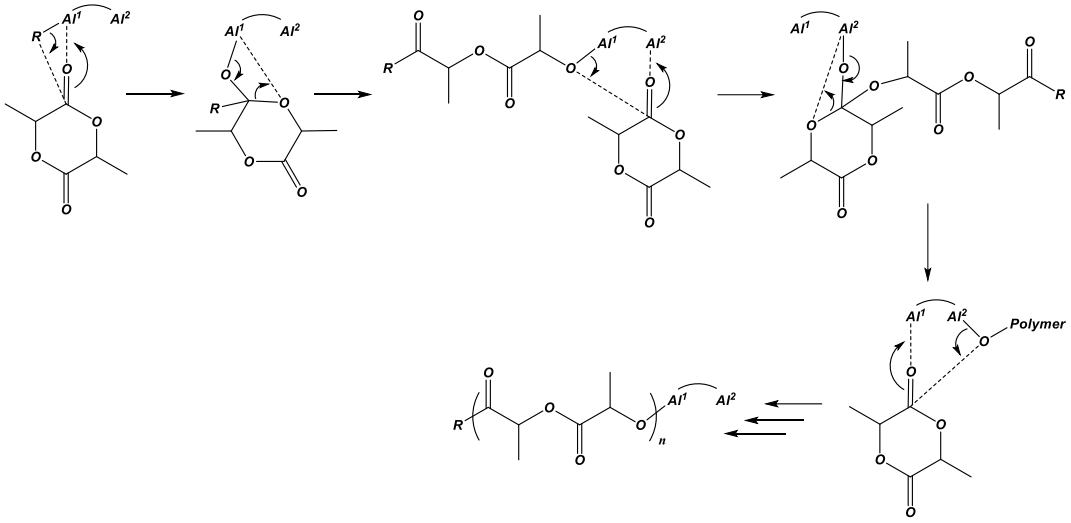

Figure 78: dual activation mechanism with bimetallic Al complex.

[76] J. Darensbourg, O. Karroonnirun, *Organometallics*, ***2010***, *29, 5627-5634;* H. –L. Hang, Y. Lin, J. –Y. Lin, K. Nomura, Y. S. Li, *Dalton Trans.*, ***2013***, *42, 12346-12353;* L. Li, B. Liu, D. Liu, C. Wu, S. Li, B. Liu, D. Cui, *Organometallics*, ***2014***, *33, 6474-6480;* Z. Sun, R. Duan, J. Yang, H. Zhang, S. Li, X. Pang, W. Chen, X. Chen, *RSC Adv.*, ***2016***, *6, 17531-17538.*

[77] T. Ouhadi, A. Hamitou, R. Jerome, Ph. Teyssie, *Macromolecules*, ***1976***, *9, 927-931;* A. Arbaoui, C. Redshaw, D. L. Hughes, *Chem. Commun.*, ***2008***, *39, 4717-4719.*

[78] W. Li, W. Wu, Y. Wang, Y. Yao, Y. Zhang, Q. Shen, *Dalton Trans.*, ***2011***, *40, 11378-11381.*

In the last few years a lot of bimetallic *Al* complexes have been extensively investigated as catalyst for *ROP* of cyclic esters in combination with an alcohol and reported in literature.[79] The importance of an alcohol for a good catalytic activity in these reactions is documented by several work. One of these concerns the bimetallic *Al* complexes supported by bridged anilido-aldimine ligands which resulted inactive in the *ROP* of *ε-CL* in absence of *BnOH*. For these catalysts was found that the highest catalytic activity can be obtained with an [*Al*]/[*BnOH*] molar ratio of 2, while an increase in *BnOH* causes not only a decrease in catalytic activity, but also in the Mn of the final polymer.[80]

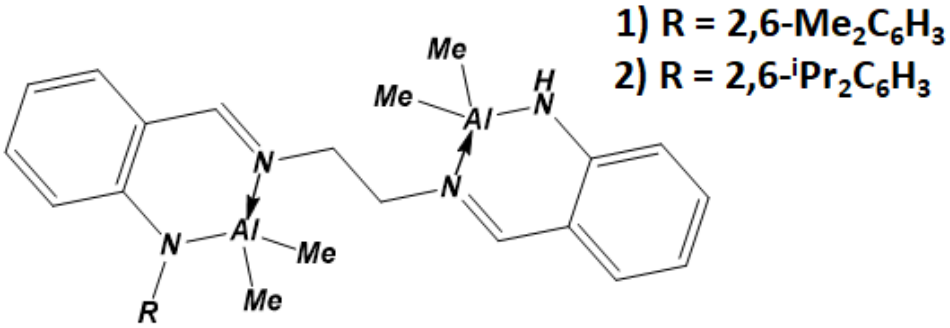

Figure 79: bimetallic Al complexes supported by bridged anilido-aldimine ligands.

Ma and Yao reported a series of dinuclear *Al* dialkyl complexes supported by bridge phenoxy-amine ligands in addition to the plausible dual activation mechanism of *ROP* with bimetallic *Al* complexes.[81]

[79] H. –L. Hang, Y. Lin, J. –Y. Lin, K. Nomura, Y. S. Li, *Dalton Trans.*, ***2013***, *42, 12346-12353;* L. Li, B. Liu, D. Liu, C. Wu, S. Li, B. Liu, D. Cui, *Organometallics*, ***2014***, *33, 6474-6480;* Z. Sun, R. Duan, J. Yang, H. Zhang, S. Li, X. Pang, W. Chen, X. Chen, *RSC Adv.*, ***2016***, *6, 17531-17538.*

[80] W. Yao, Y. Mu, A. Gao, W. Gao, L. Ye, *Dalton Trans.*, ***2008***, *3199–3206.*

[81] W. Li, W. Wu, Y. Wang, Y. Yao, Y. Zhang, Q. Shen, *Dalton Trans.*, ***2011***, *40, 11378-11381;* Y. Wang, H. Ma, *Chem. Commun.*, ***2012***, *48, 6729-6731;* Y. Wang, H. Ma, *J. Organomet. Chem.*, ***2013***, *731, 23-28;* X. –F. Yu, Z. –X. Wang, *Dalton Trans.*, ***2013***, *42, 3860-3868;* L. Chen, W. Li, D. Yuan, Y. Zhang, Q. Shen, Y. Yao, *Inorg. Chem.*, ***2015***, *54, 4699-4708.*

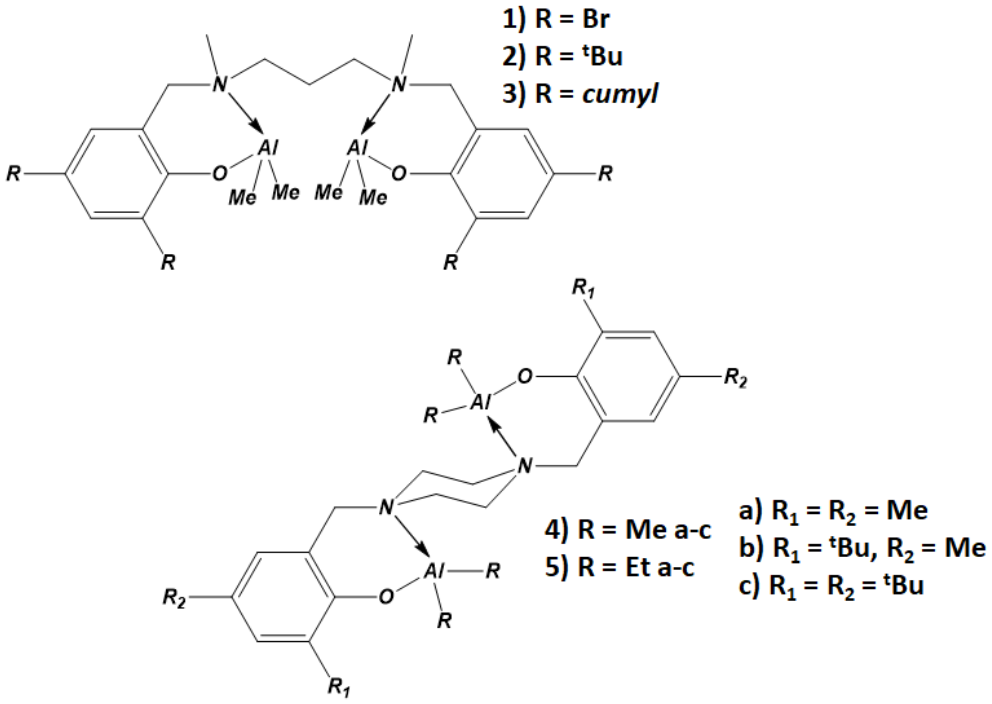

Figure 80: Al alkyl complexes supported by amine phenolate ligands and quinolinolato ligands.

Feijen, Coates and Nomura have reported various Schiff base complex systems based on five-coordinated *Al* atom.[82]

[82] N. Nomura, R. Ishii, M. Akakura, K. Aoi, *J. Am. Chem. Soc.*, ***2002***, *124, 5938-5939;* T. M. Ovitt, G. W. Coates, *J. Am. Chem. Soc.*, ***2002***, *124, 1316-1326;* Z. Y. Zhong, P. J. Dijkstra, J. Feijen, *J. Am. Chem. Soc.*, ***2003***, *125, 11291-11298;* Z. H. Tang, X. S. Chen, X. Pang, Y. K. Yang, X. F. Zhang, X. B. Jing, *Biomacromolecules*, ***2004***, *5, 965-970;* N. Nomura, R. Ishii, Y. Yamamoto, T. Kondo, *Chem. –Eur. J.*, ***2007***, *13, 4433-4451;* H. Du, X. Pang, H. Yu, X. Zhuang, X. Chen, D. Cui, X. Wang, X. Jing, *Macromolecules*, ***2007***, *40, 1904-1913;* X. Pang, H. Du, X. Chen, X. Wang, X. Jing, *Chem. –Eur. J.*, ***2008***, *14, 3126-3136; . W. Kleij, Chem. –Eur, J.*, ***2008***, *14, 10520-10529; S. J. Wezenberg, A. W. Kleij, Angew. Chem. Int. Ed.*, ***2008***, *47, 2354-2364;* D. J. Darensbourg, O. Karroonnirun, *Organometallics*, ***2010***, *29, 5627-5634;* P. J. Dijkstra, H. Z. Du, J. Feijen, *Polym. Chem.*, ***2011***, *2, 520-527;* X. Pang, R. Duan, X. Li, X. Chen, *Polym. Chem.*, ***2014***, *5, 3894-3900.*

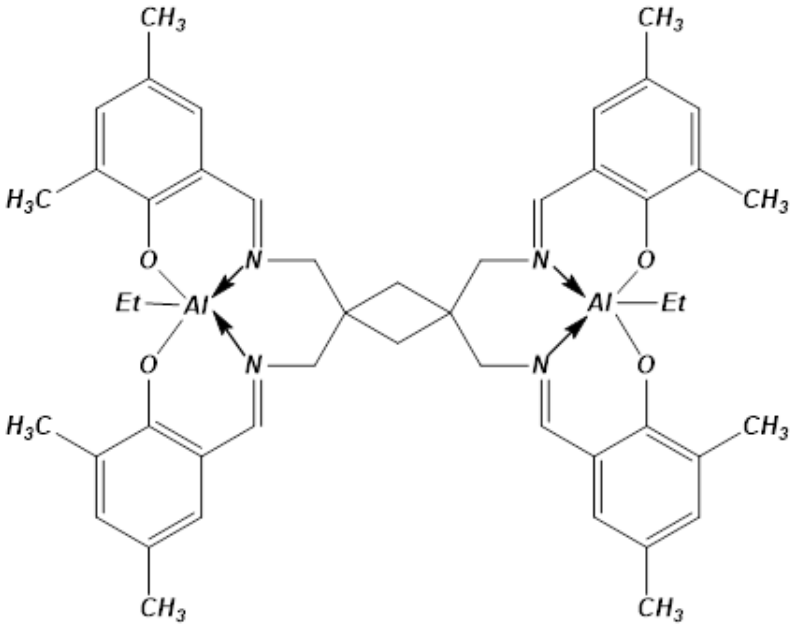

Figure 81: example of bimetallic Al five-coordinate complex.

Wang and Liu recently have reported a series of dinuclear *Al* complexes supported by bis-iminophenolate ligands that resulted very active in the *ROP* of *rac-LA*, obtaining high molecular weight polymers with narrow *Đs*.[83]

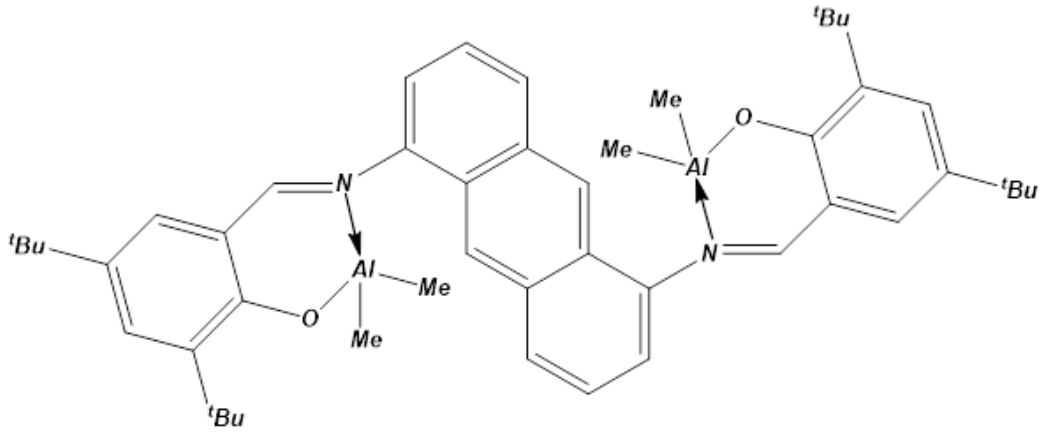

Figure 82: example of dinuclear Al complex supported by bis-iminophenolate ligand.

The influence of the distance between the *Al* centers has been explored by Mazzeo et al. with a set of dinuclear complexes. The complexes with longer alkyl bridges do not allow the cooperation between the reactive *Al* centers. For this reason the complexes with a longer bridge showed lower catalytic activity than that where the two metal centers are proximal. The results of Mazzeo's group confirmed, how other works in

[83] X. –F. Yu, Z. –X. Wang, *Dalton Trans.*, ***2013**, 42, 3860-3868;* T. Shi, Q. –D. Zheng, W. –W. Zuo, S. –Fu. Liu, Z. –B. Li, *Chin. J. Polym. Sci.*,***2018**, 36, 149-156.*

literature, that the cooperation between the metallic centres in a bi- or multinuclear species can be induced by an opportune ligand design. Specifically, higher activities were found for dinuclear *Al* complexes with a distance between the two metal centers in the range 5.3-6.6 Å.[84]

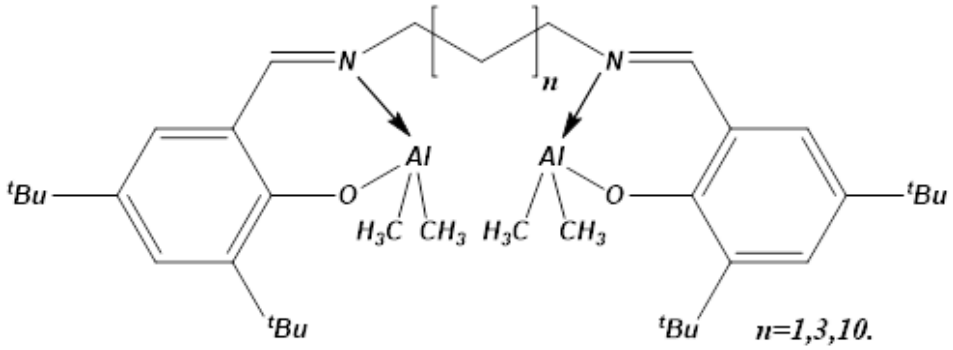

Figure 83: examples of bimetallic Al complexes studied by Mazzeo et al.

In this chapter we report the synthesis and the characterization of bimetallic tetracoordinate aluminum complexes supported by thioether-amine ligands and their use in the *ROP* of cyclic esters.

[84] F. Isnard, M. Lamberti, L. Lettieri, I. D'Auria, K. Press, R. Troiano, M. Mazzeo, *Dalton Trans.*, ***2016**, 45, 16001-16010;* F. Santulli, I. D'Auria, L. Boggioni, S. Losio, M. Proverbio, C. Costabile, M. Mazzeo, *Organometallics, **2020**, 39, 1213-1220.*

4.1 Synthesis and characterization of ligands

The binucleating *NSSN* ligands prepared in this project are reported in *Scheme 5*. The ligands **L1-3** consist of two N-isopropyl-aniline linked by a thioether-bridge of different lengths (i.e. -S(CH_2)$_n$S- with *n* = 2 (**L1**, *Scheme 5*), 3 (**L2**, *Scheme 5*) and 7 (**L3**, *Scheme 5*). These ligands were prepared to explore the effect of the separation between the two aluminum atoms in the corresponding complexes. Three additional ligands were also prepared **L4-6** (*Scheme 5*). Ligands **L4** and **L5** are structural variation of ligand **L1**: ligand **L4** features a cyclohexyl group linked to the nitrogen atom, instead of isopropyl group; ligand **L5** features a chlorine substituent on the aromatic ring, in para position respect to the sulphur atom. Ligand **L6** features a p-xylenyl bridges linking the two thioaniline moieties. These ligands were prepared following a procedure similar to that previously followed for the synthesis of the mononucleating bidentate ligands: the 2-aminothiophenol was reacted with the opportune di-bromo-derivate in refluxing methanol to obtain an intermediate that was subsequently alkylated to the nitrogen atoms according to *Scheme 5*.

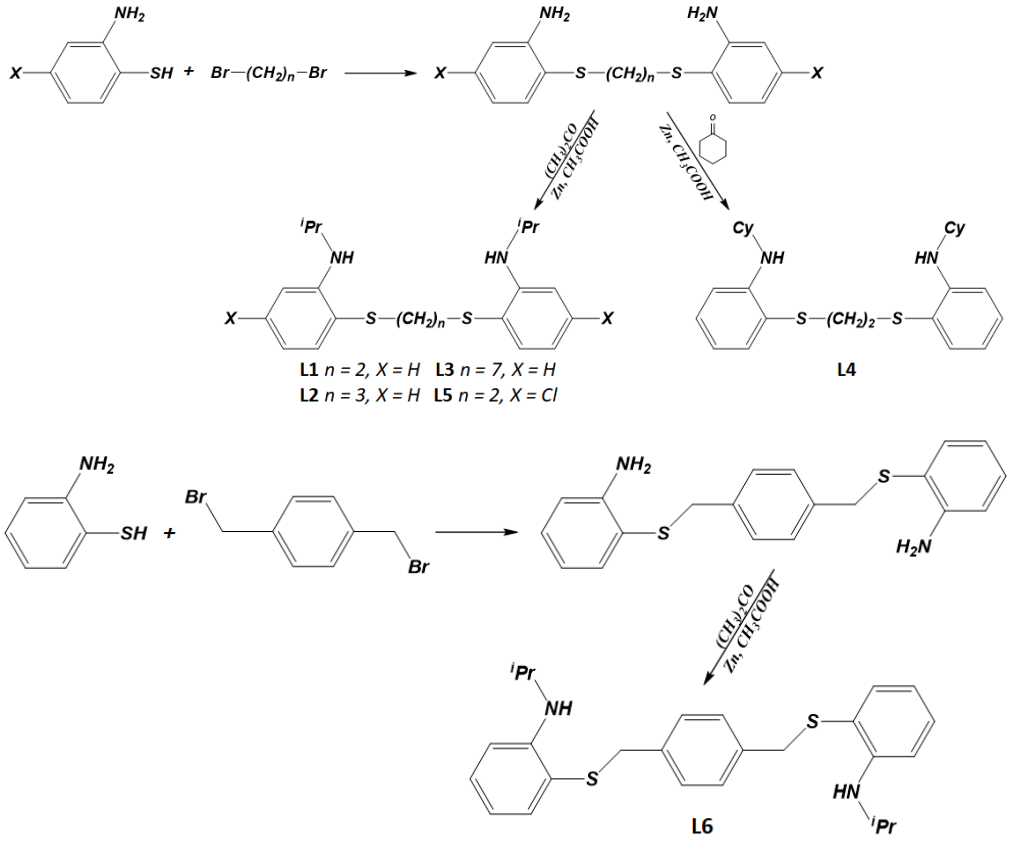

Scheme 5

All ligands were isolated in high yields (71-98%) after the opportune purification. The NMR signals were observed in the ranges expected for this class of compounds.

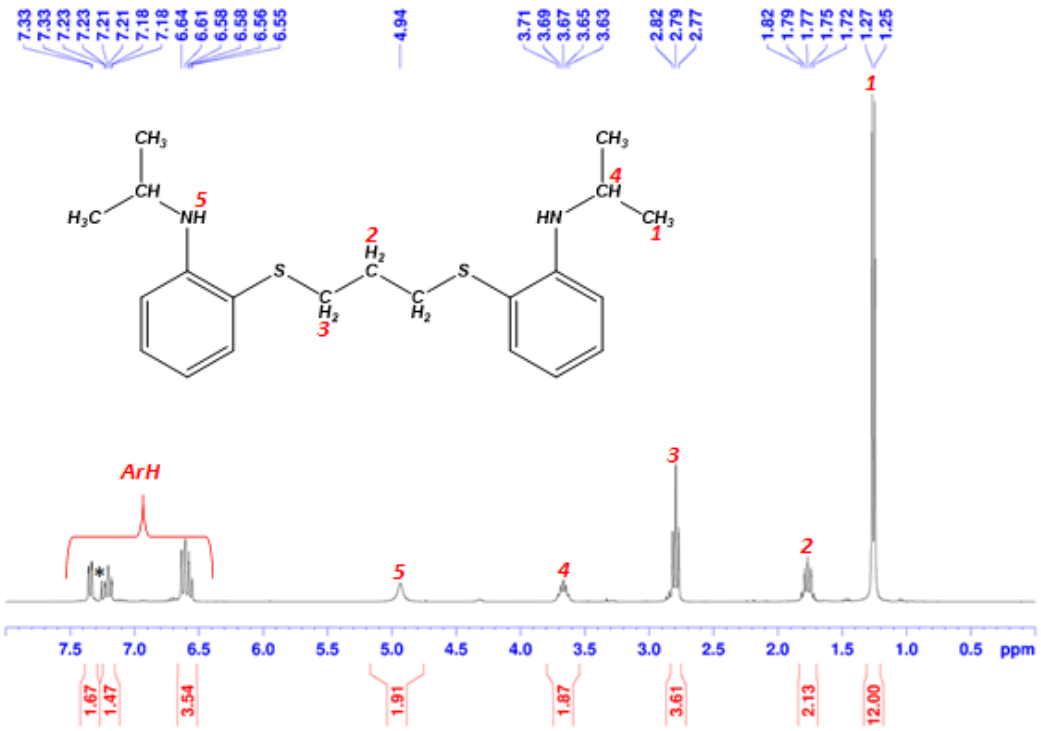

*Figure 84: ^{1}H NMR of NSSN-Pr-ISO ligand (400.13 MHz, *$CDCl_3$, 25°C).*

Recrystallization of the ligands in hexane afforded crystals suitable for X-Ray diffraction analysis. X-Ray structures are reported in *Crystallographic Data*. All ligands were full characterized by NMR spectroscopy. Ligand **L2** (*figure 85*) crystallizes in a triclinic unit cell according to the space group *P-1*. Torsional angles S1-C1-C2-C3 and C1-C2-C3-S2 both adopt a gauche conformation thus constraining the two aromatic rings to form an angle between their mean plane equal to 79.30(1)°. L10 molecule (monoclinic, P21/c) sits on a crystallographic inversion center. In this case, due to conditions imposed by the crystallographic elements, the molecule assumes a *trans* planar conformation, with the aromatic moieties pointing to opposite sides. Phenyl rings form an angle with the xylenyl group equal to 28.4 (1)°.

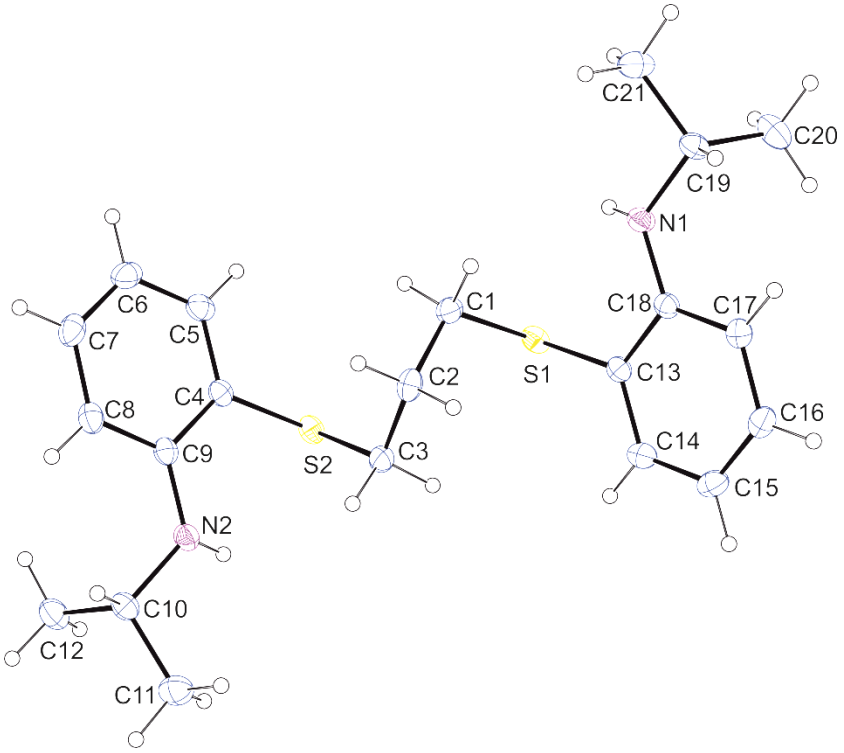

Figure 85: Ortep 3 view of NSSN-Pr-ISO ligand.

4.2 Synthesis and characterization of bimetallic Al complexes (1-6)

The complexes **1-6** (**1**= L1AlMe$_2$, **2**= L2AlMe$_2$, **3**= L3AlMe$_2$, **4**= L4AlMe$_2$, **5**= L5AlMe$_2$, **6**= L6AlMe$_2$) were synthesized by reaction OF the corresponding *NSSN*-type ligand with 2 *AlMe$_3$* in refluxing benzene (*Scheme 6*).

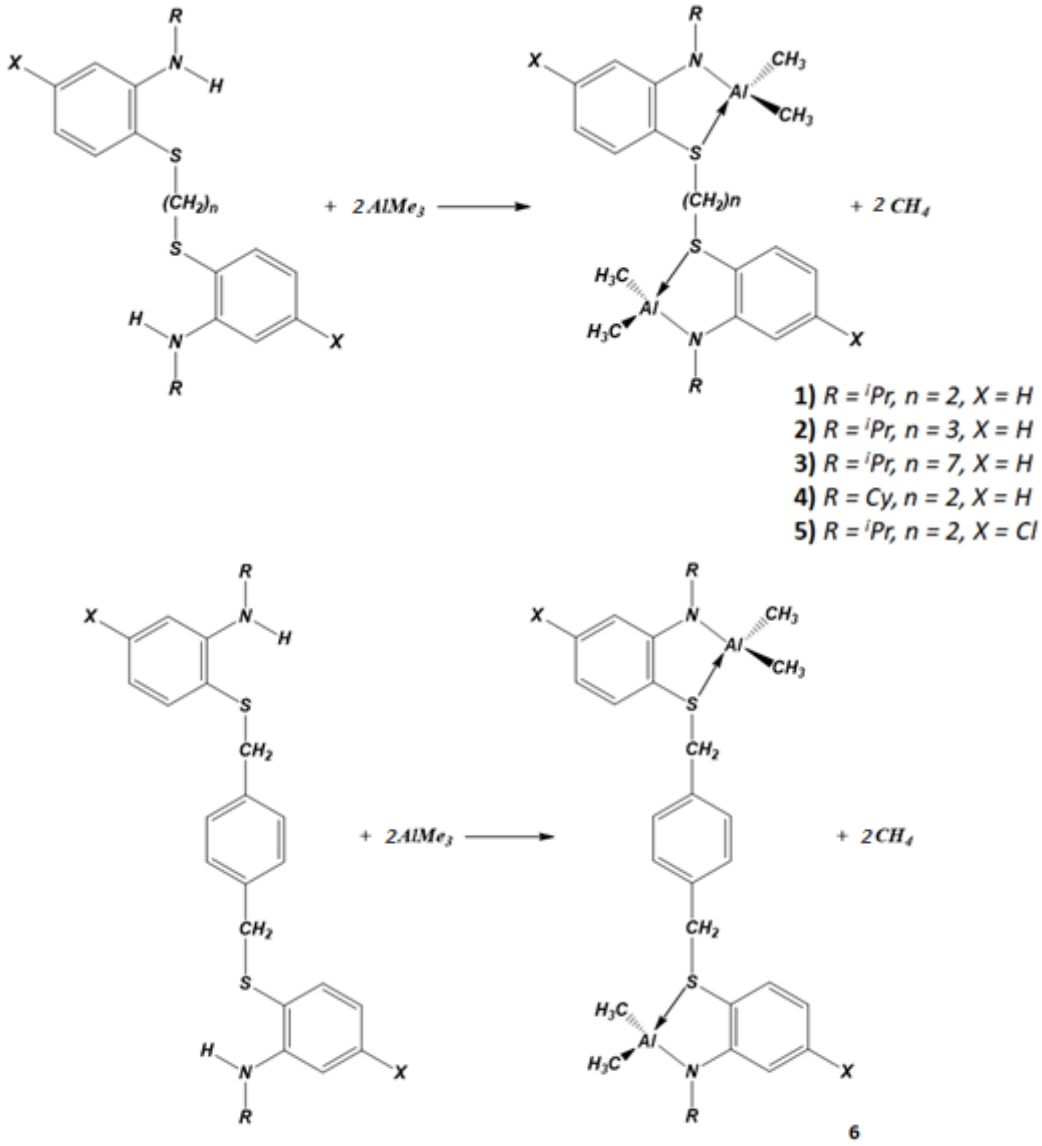

Scheme 6

The complexes **1-6** (*figure 86*) were obtained in good yields (76-87%). The products of the reactions were first characterized by NMR spectroscopy. All the signals in the ^{1}H and ^{13}C NMR spectra were consistent with the NMR pattern expected for the desired products. As an example, in the ^{1}H spectrum of **1** (*figure 87*), the *N-H* signal of the pre-ligand was absent and, at the same time, a resonances at -0.5 ppm,

attributable to the protons of the methyl groups bound to *Al*, was clearly observable. Moreover the signals of the ethylene bridge bound to the sulphur atoms were *high field* shifted respect to those of the free ligand suggesting the effective coordination of the sulphur to the metal center.

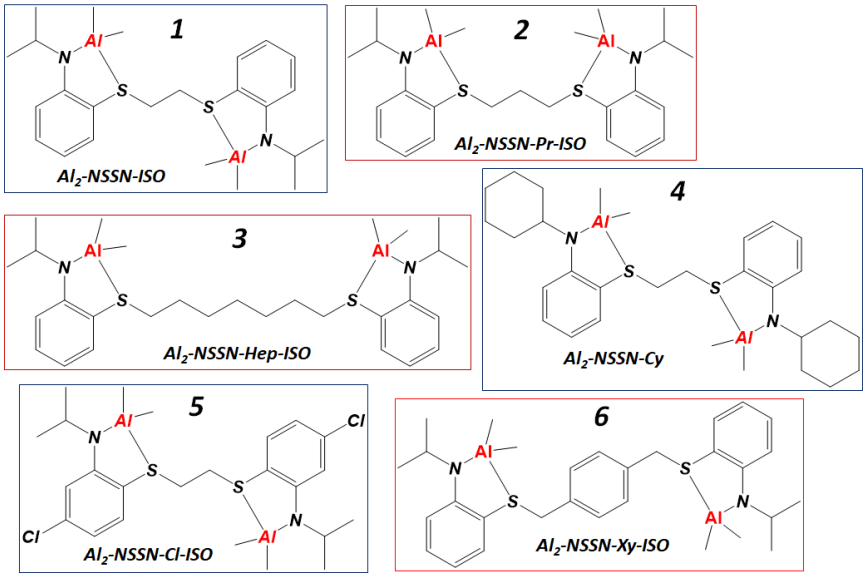

Figure 86: complexes 1-6

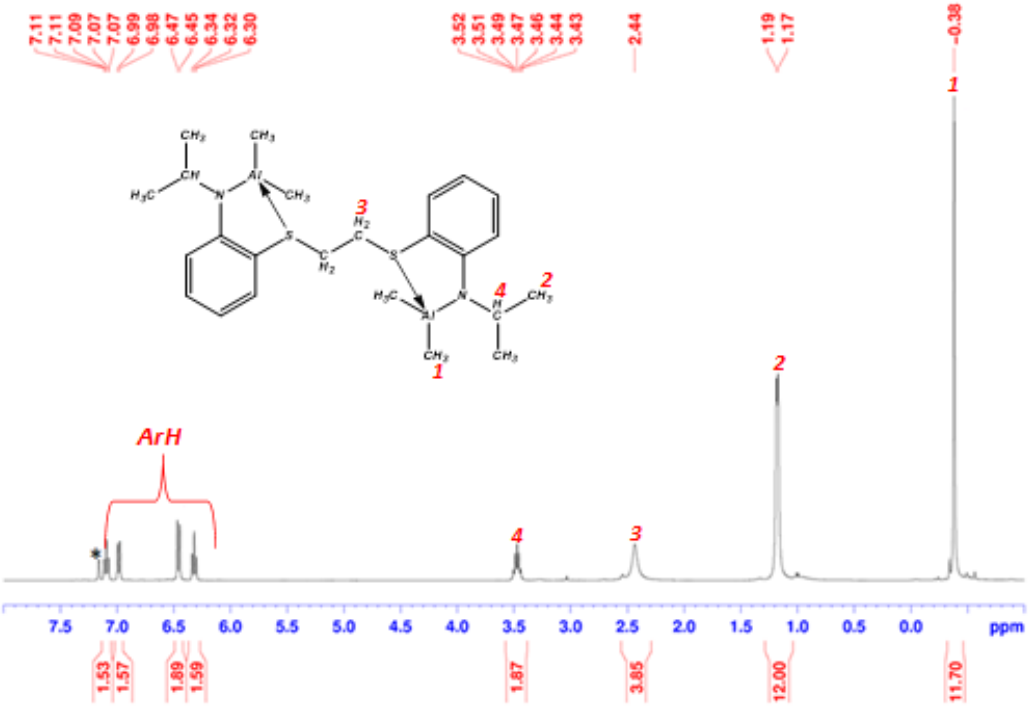

*Figure 87: ^{1}H NMR of complex 1 (400.13 MHz, *C_6D_6, 25°C).*

As already observed for the monometallic complexes, at room temperature the pattern of the signals for all the complexes **1-6** is consistent with those expected for highly

symmetric structures, i.e., the two methyl groups bound to the aluminum atom resonate as a singlet, the isopropyl group bound to the nitrogen atom displays the typical AX_6 spin pattern.

The NMR analysis of complex **6** performed at different temperatures, range 25-80 °C (*figure 88*), showed no broadening or coalescence of resonances.

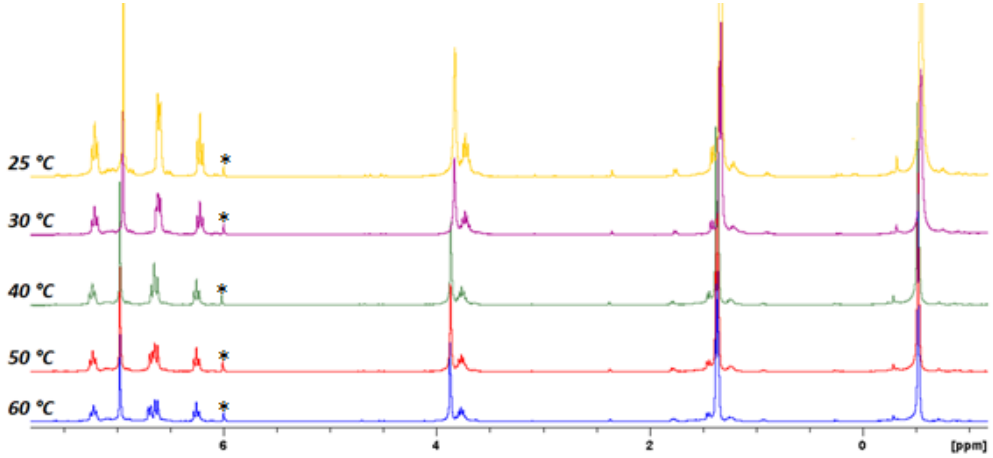

Figure 88: ^{1}H NMR of complex 6 (400.13 MHz, *TCDE, variable temperature).

Upon cooling a CD_2Cl_2 solution of **1** (*figure 89*), the NMR signals of the methyl and N-isopropyl groups resolved in an *AX* and AX_3X_3' spin pattern, respectively. The singlet at -0.69 ppm attributed to methyl groups bound to *Al* centers at 25 °C, as the temperature of the experiment begins to drop, they are split into several signals always below 0 ppm (between δ -0.83 and -0.64 ppm). This also applies to the other signals related to *S*-CH_2 bond and -CH_3 of the isopropyl group on amide functions.

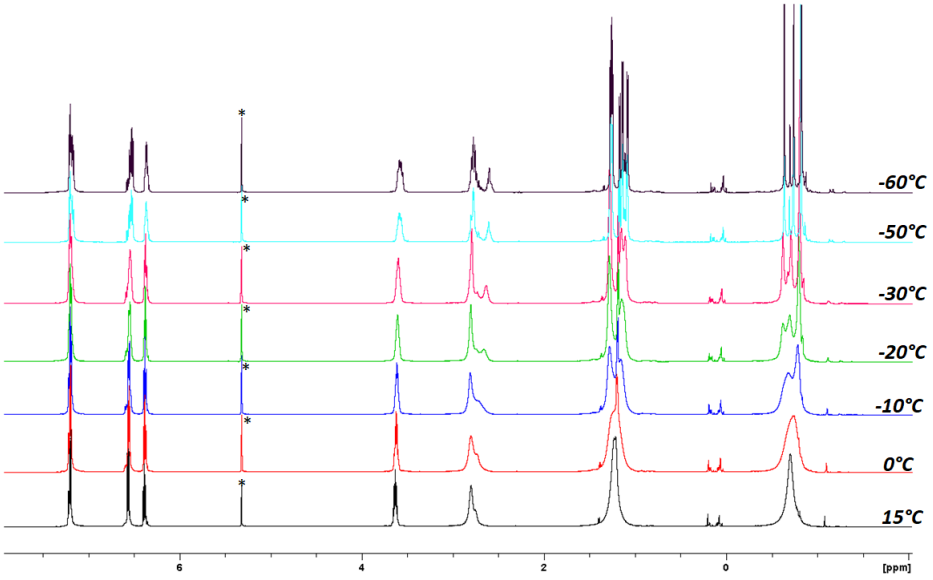

Figure 89: ^{1}H NMR of complex 1 (400.13 MHz, *CD_2Cl_2, variable temperature).

The crystal structures and the crystal data of the complexes are reported in *Crystallographic Data.* Complex **1** (*figure 90*) crystallizes according the P21/c monoclinic space group, while complex **4** crystallizes in the P-1 triclinic space group.

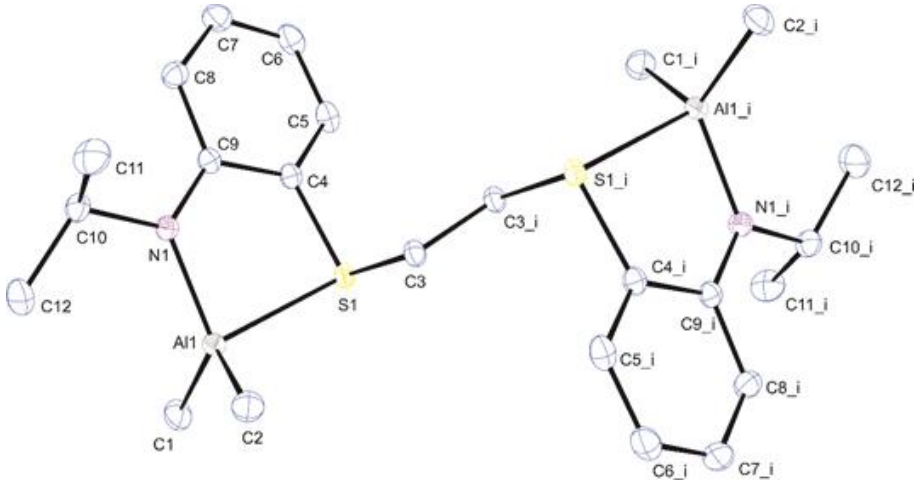

Figure 90: ORTEP 3 view of Al_2-NSSN-ISO complex.

Both molecules sit on a crystallographic inversion centre. Both bimetallic complexes are characterized by a distorted tetrahedral coordination of *Al* atoms, as shown by the rather wide *(CC)Al* or *(CN)Al* bite angles. Moreover, in both cases *Al*, *S* and *N* atoms are almost coplanar with the aromatic ring close to them. It can be easily noticed that there are notable similarities in the geometric parameters of the coordination environment within the two complexes. Moreover, it is worth pointing out that due to symmetry constraints, the two halves of the molecule lie in opposite directions in respect to the plane passing through the ethyl bridge and the S atoms. In particular, the plane containing the *Al* atom and the coordinated heteroatoms and the phenyl ring is almost perpendicular to the *S1-C1-C1_i-S1_i** mean plane (the angle between those mean planes is 80.27(4)° in complex **1** and 73.17(2)° in complex **2**). In complex **4**, cyclohexyl substituents show a chair conformation. The complex **2** crystallizes according the monoclinic P21/c space group and shows a distorted tetrahedral coordination around each metal centre. There are notable similarities in the geometric parameters of the coordination environment of complex **2**, in respect to **1** and **4** (see in *Crystallographic Data*). Moreover, the coordination environment of each metal is characterized by very similar geometrical parameters. It is worth noting that in the crystal structure of the ligand both *S1-C1-C2-C3* and *C1-C2-C3-S2* dihedral angles presented a nearly gauche conformation while in the complex **6** one of them assumes

a trans conformation, while the other is not significantly modified. For this reason in the complex, the angle between the mean planes of the aromatic rings is 71.7(1)°, and the angle between the coordination planes *Al1-N1-S1* and *Al2-N2-S2* is 70.87(6)°. The *Al-N* bond distances are consistent with other examples reported in the literature.[85] Also *Al-S* and *Al-C* distances are in agreement with those reported in the literature for analogous complexes.[86]

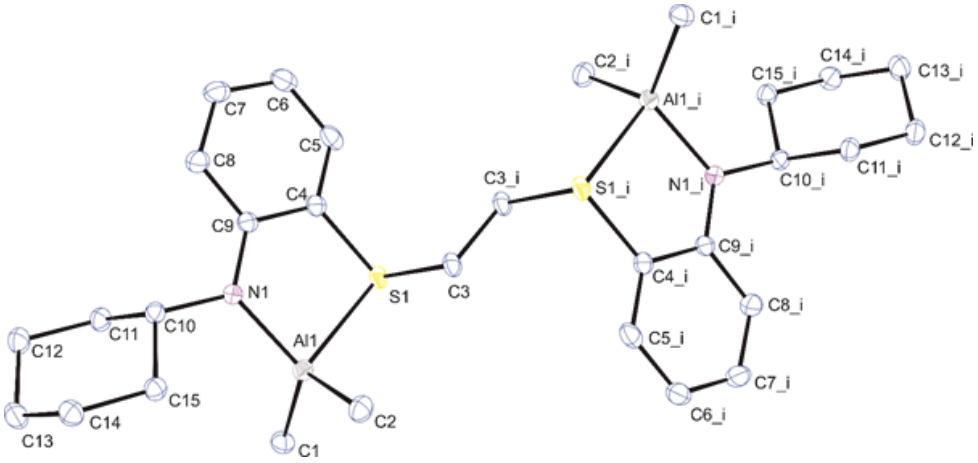

Figure 91: ORTEP 3 view of Al_2-NSSN-Cy complex.

[85] V. Ritleng, A. M. Oertel, M. J. Chetcuti, *Dalton Trans.*, ***2010***, *39, 8153-8160.*

[86] H. Ma, G. Melillo, L. Oliva, T. P. Spaniol, U. Englert, J. Okuda, *Dalton Trans.*, ***2005***, *4, 721-727;* D. Jim, X. Ma, Y. Liu, J. Peng, Z. Yang, *Appl. Organometal. Chem.*, ***2019***, *33, 4637-4647.*

4.3 ROP of cyclic esters catalyzed by 1-6

The synthetized bimetallic *Al* complexes were tested as catalysts in the *ROP* of several cyclic esters in toluene solution, in combination with isopropanol. The polymerization tests were carried out in the presence of isopropanol (two equivalents) in order to convert the alkyl complexes in the corresponding alkoxide derivatives that are considered more effective in the initiation step. All complexes were active and reached high monomer conversions within 8 hours. Complex **1** showed the highest activity. Respect to the data reported in literature, the activities of **1**-**4** were higher respect to those of the related mono(phenoxy-imine)aluminum complexes under similar experimental conditions. What emerged from the experimental results is that by increasing the bridge between the two sulphur atoms and connecting the two aromatic rings, a decrease in the catalytic activity of the catalyst is achieved.

Table 6: ROP of cyclic esters by 1-6

Entry	Complex	Monomer	[M]/[cat]	t (h)	Conv.[a] (%)	TOF (h^{-1})	$M_{n(theo)}$[b]	$M_{n(exp)}$[c]	$Đ$[c]
1	***1***	*L-LA*	200	24	42	3	-	-	-
2	***1***	*L-LA*	200	8	92	23	6.7	8.6	1.15
3	***1***	*L-LA*	500	24	91	19	16.5	12.8	1.24
4[d]	***1***	*L-LA*	1000	4	82	205	29.7	20.1	1.26
5	***2***	*L-LA*	200	8	89	22	6.5	8.2	1.17
6	***3***	*L-LA*	200	8	77	19	5.6	9.2	1.16
7	***4***	*L-LA*	200	8	91	23	6.5	8.0	1.16
8	***5***	*L-LA*	200	8	48	12	3.5	3.1	1.76
9	***6***	*L-LA*	200	8	83	21	6.1	5.7	1.60
10[e]	***1***	*ε-CL*	200	0.75	>99	267	5.8	11.3	1.19

All reaction were carried out in 2 mL of toluene and using 1-propanol as co-catalyst. Reaction conditions: 80°C, $[Cat]_0$= 7.0 mM, [Monomer]= 1.4 M, [Cocatalyst]/[cat]= 4; [a]Molecular conversion determined by ^1H NMR spectroscopy ($CDCl_3$, 298 K); [b]Calculated molecular weight using $M_{n(theo)}$(kg/mol)=(((PM$_{Monomer}$ x [Mon]/[cocat] x conversion)/100) + PM$_{Cocat}$)/1000; [c]Experimental molecular weight $M_{n(exp)}$(kg/mol) and $Đ$ determined by GPC using THF polystyrene standards and corrected using the factor 0.58 for PLA and 0.56 for PCL; [d]T = 100°C; [e]Reaction at room temperature in 2 ml of dichloromethane as solvent.

A kinetic study was performed with each catalyst to have more information about the catalytic activity of the complexes. Several aliquots of the product mixture were taken

at regular and scheduled intervals and analyzed by ^{1}H NMR spectroscopy to evaluate the monomer conversion. With all complexes, it was observed that the *ROP* of *L-LA* follows a first order kinetic law respect to the monomer concentration and, from the *figure 91*, it's possible to see that the k_{app} of **1** is bigger than those of the other bimetallic *Al* complexes.

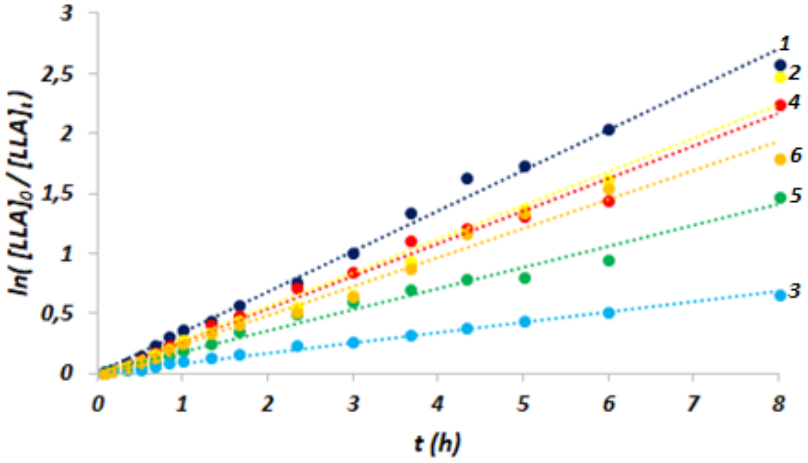

Figure 92: Pseudo-first order kinetic plots for ROP of L-LA by 1 (k_{app}= 0.34 ± 0.01 h^{-1}, R^2= 0.994, blue line), 4 (k_{app}= 0.27 ± 0.01 h^{-1}, R^2= 0.989, red line), 5 (k_{app}= 0.18 ± 0.01 h^{-1}, R^2= 0.983, green line), 2 (k_{app}= 0.28 ± 0.01 h^{-1}, R^2= 0.983, yellow line), 3 (k_{app}= 0.09 ± 0.002 h^{-1}, R^2= 0.994, light blue line), 6 (k_{app}= 0.24 ± 0.01 h^{-1}, R^2= 0.986, orange line).

Conditions: $[L\text{-}LA]_0$ = 1.4 M, $[L\text{-}LA]_0/[I]_0$ = 200, $[^{i}PrOH]_0/[I]_0$ = 4, T = 80 °C, and toluene as the solvent.

The GPC analysis of the isolated polymer obtained using **1**, revealed that the $M_{n(exp)}$ increases linearly with monomer conversion, leading to polymers with relatively narrow and constant *Đs* during the polymerization process (*figure 93*).

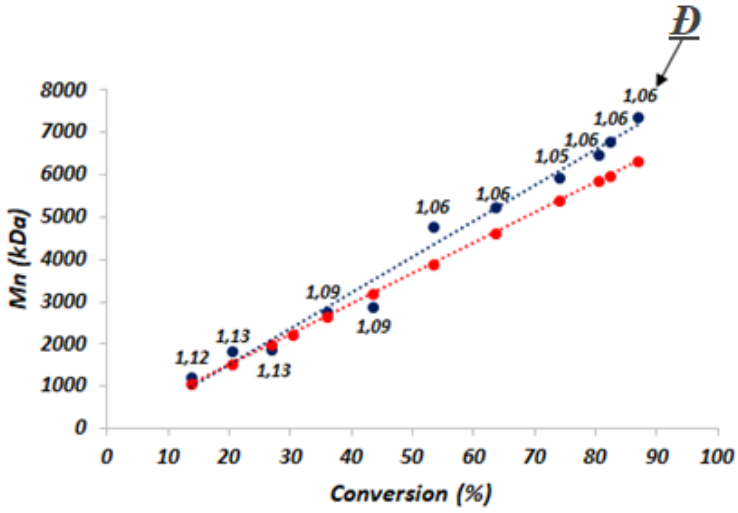

Figure 93: Plot of number-average molecular weights $M_{n(exp)}$(blue line) versus monomer conversion with theoretical $M_{n(theo)}$(red line) using 1 as the catalyst.

Conditions: $[L\text{-}LA]_0$ = 1.4 M, $[L\text{-}LA]_0/[\mathbf{1}]_0$ = 200, $[^{i}PrOH]_0/[\mathbf{1}]_0$ = 4, T = 80 °C, and toluene as the solvent.

The $M_{n(exp)}$ resulted were found to be very similar to the $M_{n(Theo)}$, a sign that the catalyst allows for good control over the polymerization process.

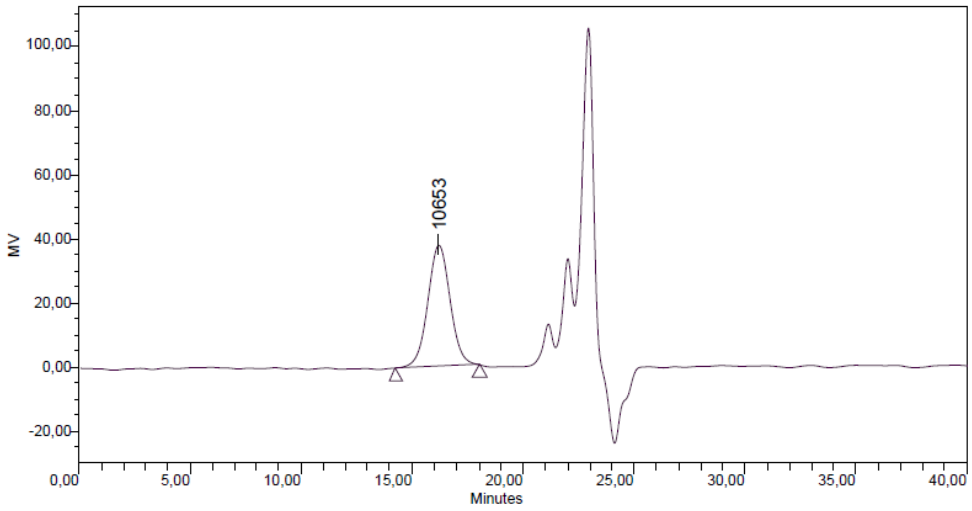

Figure 94: SEC of PLA obtained by 1 (conversion value: 74%).

The kinetic studies for **1** were repeated using a [*L-LA*]/[**1**] of 500. This ratio was obtained by decreasing the concentration of the catalyst (Entry 3 in table 6). The kinetic plots reported in *figure 95* show that the k_{app} decreases as the molar ratio increases.

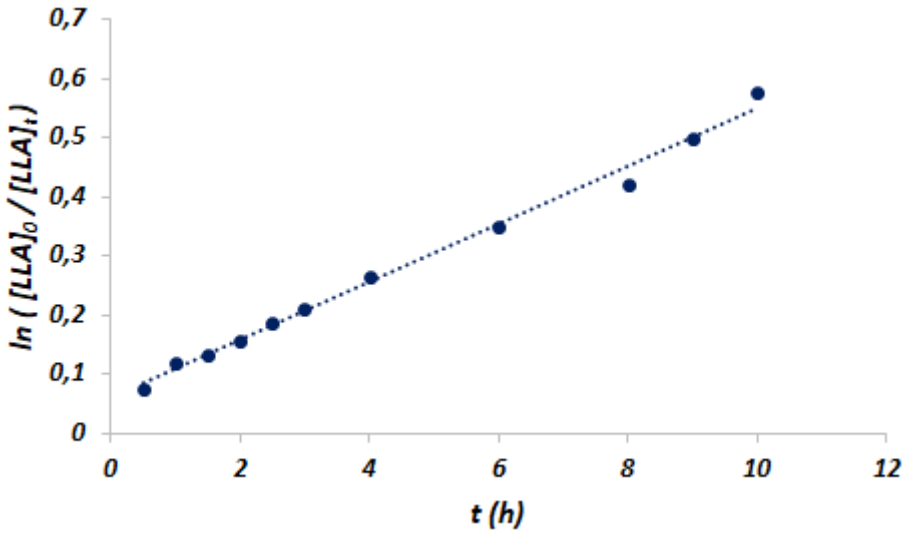

Figure 95: Pseudo-first order kinetic plots for ROP of L-LA by 1 (k_{app}= 0.05 ± 0.001 h^{-1}, R^2= 0.993).
Conditions: $[L\text{-}LA]_0$ = 1.4 M, $[L\text{-}LA]_0/[\mathbf{1}]_0$ = 500, $[^iPrOH]_0/[\mathbf{1}]_0$ = 4, T = 80 °C, and toluene as the solvent.

Also in this case the $M_{n(exp)}$ increases linearly with monomer conversion and the values were very similar to the $M_{n(Theo)}$, with *Đs* in the range 1.13-1.24 (*figure 96*).

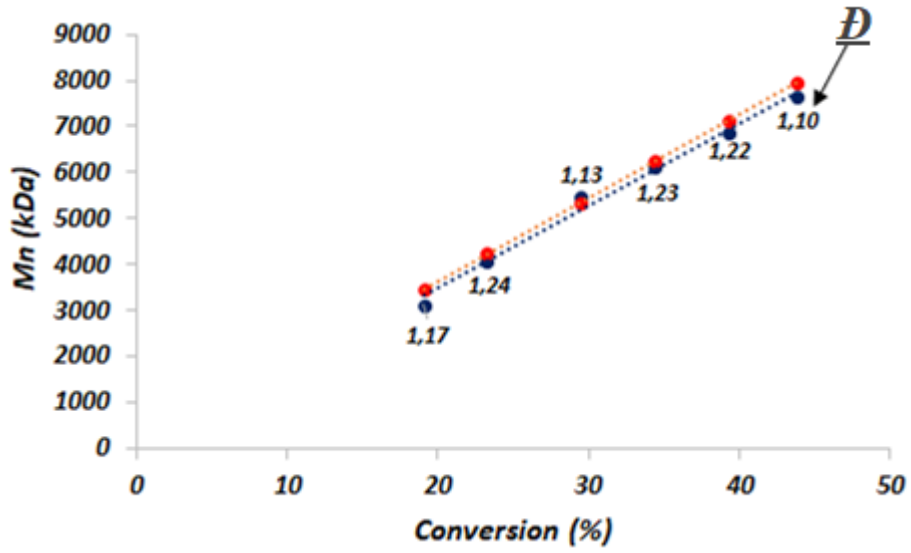

Figure 96: Plot of number-average molecular weights $M_{n(exp)}$(blue line) versus monomer conversion with theoretical $M_{n(theo)}$(red line) using 1 as the catalyst.
Conditions: $[L\text{-}LA]_0$ = 1.4 M, $[L\text{-}LA]_0/[\mathbf{1}]_0$ = 500, $[^iPrOH]_0/[\mathbf{1}]_0$ = 4, T = 80 °C, and toluene as the solvent.

With a monomer to catalyst ratio of 1000, the complex **1** still remained active but it was necessary to increase the polymerization temperature to 100 °C to complete the polymerization in a short reaction time (Entry 4 in table 6).

Kinetic experiments were conducted at different temperature (from 70 to 100 °C) with [*L-LA*]/[**1**] ratio fixed at 200 to determinate the activation energy (E_a) from the Arrhenius plot (*figure 98*). From kinetic studies, an E_a of 17.01 ± 0.05 kcal/mol was obtained.

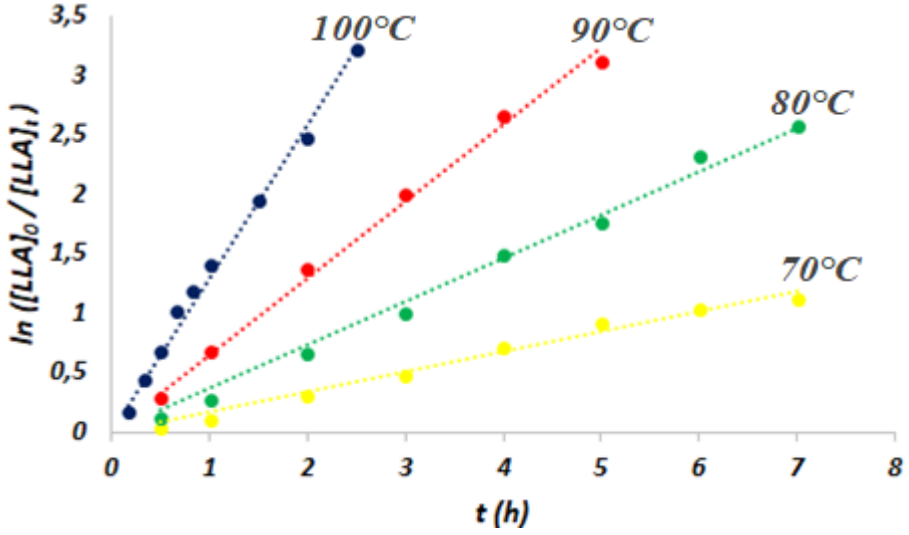

***Figure 97**: Pseudo-first order kinetic plots for ROP of L-LA by 1 at different temperatures: T= 100°C_blue line: k_{app}= 1.30 ± 0.04 h^{-1}, R^2= 0.992). T= 90°C_red line: k_{app}= 0.65 ± 0.02 h^{-1}, R^2= 0.995. T= 80°C_green line: k_{app}= 0.37 ± 0.01 h^{-1}, R^2= 0.992. T= 70°C_yellow line: k_{app}= 0.17 ± 0.01 h^{-1}, R^2= 0.984.*

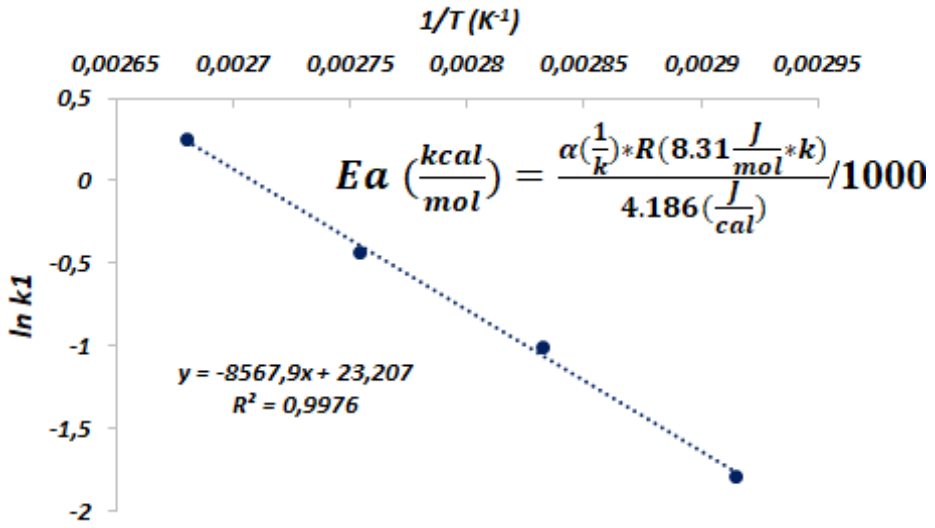

Figure 98: Plot of lnk_1 vs 1/T, in the range from 70 to 100 °C, for the determination of E_a.
Conditions: $[L\text{-}LA]_0$ = 1.4 M, $[L\text{-}LA]_0/[\mathbf{1}]_0$ = 200, $[^iPrOH]_0/[\mathbf{1}]_0$ = 4 and 2 mL of toluene as the solvent.

To get information on the polymerization process and on the end groups of the *PLA* chain, a polymer obtained with a low [monomer]/[catalyst] ratio ([*L-LA*]/[**1**] = 25), was prepared. From NMR analysis it can be seen that, in addition to the isotactic *PLA*, the isopropyl end groups are present. In the ^{1}H NMR spectra (*figure 99*), the methyl and the methine protons of the isopropyl group resonate at 1.24 and 5.04 ppm, respectively. The methyl and methine proton of the last monomeric unit resonate at 1.48 and 4.34 ppm. The signals at 20.63, 66.84 and 175.25 ppm in the ^{13}C NMR spectra (*figure 100*), are attributable at the last monomeric unit of the polymer, while the signals at 21.77 and 69.61 ppm, are associated with the terminal isopropyl group.

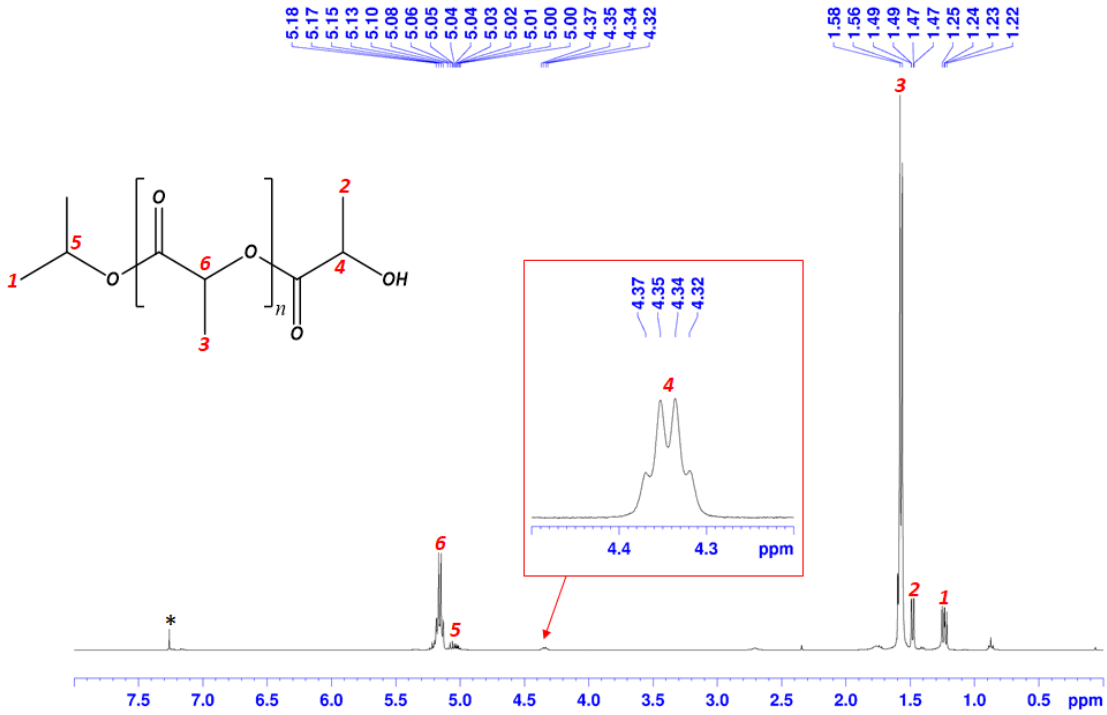

*Figure 99: ^{1}H NMR of oligomers of PLA obtained using 1 as catalyst (400.13 MHz, *$CDCl_3$, 25°C).*

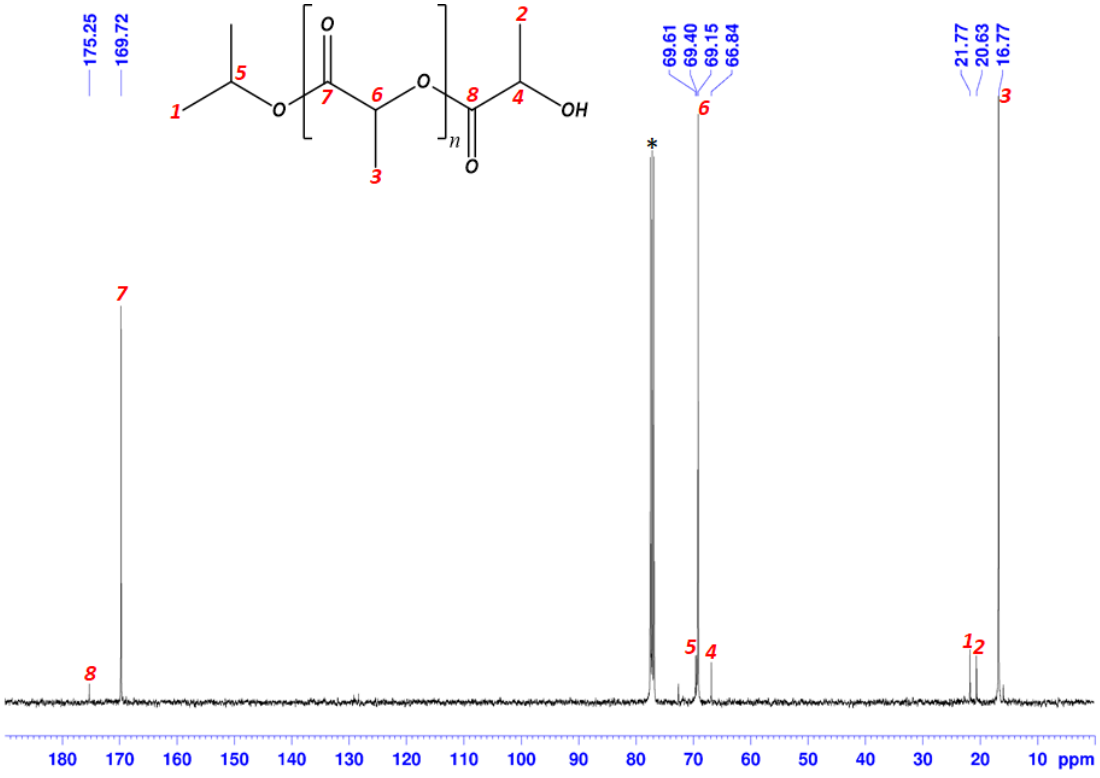

*Figure 100: ^{13}C NMR of oligomers of PLA obtained using 1 as catalyst (100.62 MHz, *$CDCl_3$, 25°C).*

4.4 Conclusions

A new series of bimetallic *Al* metal complexes supported by tetradentate thioether-amine *NSSN* ligands have been synthetized. The *Al* complexes were obtained by reaction of the corresponding thioether-amine ligands with two equivalents of $AlMe_3$, and characterized by ^{1}H and ^{13}C NMR spectroscopy. The NMR analysis confirmed that the bimetallic complexes are stable at different temperature in the range 25-60 °C. Complexes **1**-**6**, activated by isopropyl alcohol, are active in the *ROP* of *L-LA*, and the polymerizations follow a first-order kinetic law respect to the monomer concentration. The catalytic activities depend on the distance between the two metal centers; in fact by increasing the length of the bridge that connects the two aromatic rings, a loss of catalytic activity of the catalyst is observed, probably as a consequence of a non-possible cooperation between the two catalytic sites. Complex **1**, where the *Al* centers are more proximal, has been found to be the most active of the series. Furthermore, the ethyl groups on amide functions causes a smaller steric hindrance compared to the cyclohexyl group, thus facilitating the arrival at the catalytic sites of the monomer molecules. For this reason complex **1** shows better catalytic activity than **2**. The catalytic activity is also lowered by the introduction of two *Cl* atoms in meta positions respect amide function on aromatic rings.

An increase in the [*L-LA*]/[catalyst] ratio causes a slowdown in the polymerization rate but leads to polymers with a higher molecular weight. Complex **1** proved to be active even with [*L-LA*]/[**1**] ratio of 1000, it reaches 82% of monomer conversion after 4 hours (TOF = 205 h^{-1}).

An increase in the polymerization rate and the catalytic performance of the catalyst occurs increasing the temperature. It was possible to calculate the E_a of the polymerization process through a series of kinetic tests carried out at different temperatures.

Narrow *Đs* and a linear dependence between M_n and monomer conversion was observed, demonstrating that the complexes allow good control of polymerization.

5 *Al* complexes bearing tridentate ligands for *ROP* of cyclic esters

The pentacoordinate *Al* complexes with tridentate ligands represent another category of active complexes in the *ROP* of cyclic esters. However, the performances of these complexes have been scarcely investigated. Two representative examples are the following.

A series of aluminium complexes bearing *NNO*-tridentate ketiminate ligands have been reported by Lin (*figure 101*). The catalysts were active in *ROP* of *L-LA* in the presence of *BnOH* and one of these complexes promotes an "immortal" polymerization, giving polymers with expected M_n and narrow *Đs*.[87]

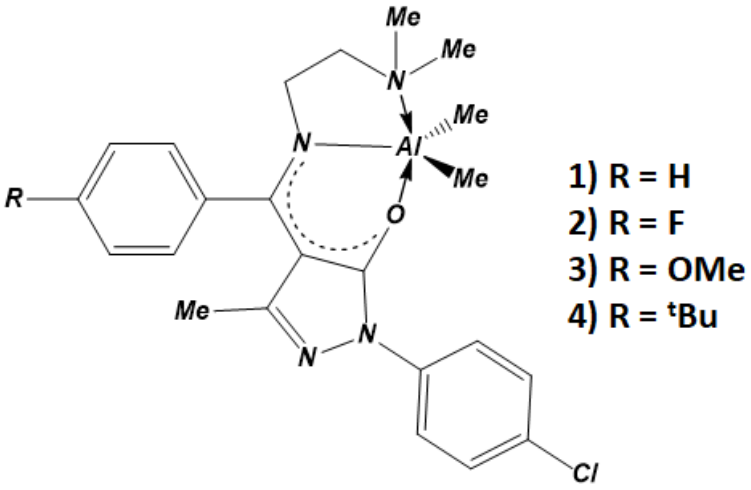

Figure 101: Al complexes bearing NNO-tridentate ketiminate ligands.

Mononuclear *Al* complexes bearing *NNN*-tridentate quinolinyl anilido-imine ligands have been synthetized, characterized and tested in *ROP* of *L-LA* by Mu and co-workers (*figure 102*). The catalysts, however, did not show high catalytic activities even if they allow to obtain polymers with narrow *Đs*.[88]

[87] H. –J. Chuang, Y. –C. Su, B.- -T. Ko, C. –C. Lin, *Inorg. Chem. Commun.*, ***2012***, *18, 38-42.*

[88] N. Yang, L. Xin, W. Gao, J. Zhang, X. Luo, X. Liu, Y. Mu, *Dalton Trans.*, ***2012***, *41, 11454-11463.*

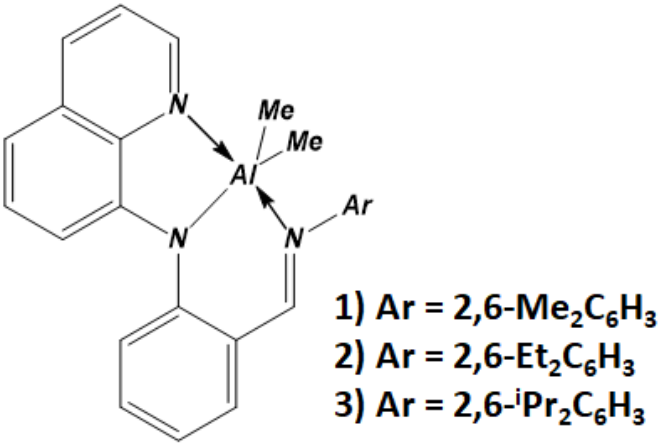

Figure 102: Al complexes bearing NNN-tridentate quinolinyl anilido-imine ligands.

As a part of our interest in the research for alternative coordination environment for potentially active *ROP* catalysts, we sought to modify the skeleton of the *NS* ligands in order to achieve a new class of ligands. In particular we thought to introduce an additional alcoholate function through an easy synthetic procedure and to obtain tridentate *NSO* ligands. At the best of our knowledge, this combination of donating functions were never explored for the development of *Al* catalyst. In this chapter we report the synthesis and the characterization of monometallic pentacoordinate *Al* complexes supported by *NSO* ligands and their use in the *ROP* of cyclic esters.

5.1 *Synthesis and characterization of Al complex bearing NSO-tridentate ligand*

The designed *NSO* ligand features a 2-propanol group bound to the sulphur atom. The synthesis was accomplished in two steps: a precursor of the ligand was obtained through the reaction of 2-aminothiophenol in a 1:1 ratio with propylene oxide in refluxing methanol in presence of NaOH. Then, the intermediate was alkylated at the nitrogen atom through a reductive amination of acetone using zinc/acetic acid according to *Scheme 7*.

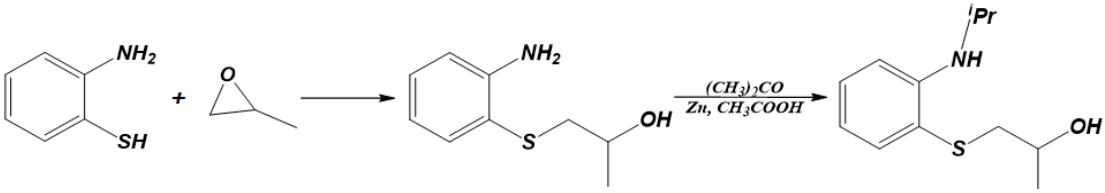

Scheme 7

The ligand was prepared in high yields and full characterized by ^{1}H NMR spectroscopy (*figure 103*). The NMR pattern of signals was consistent with the expected symmetry and the chemical shifts were observed in the typical ranges for this class of compounds.

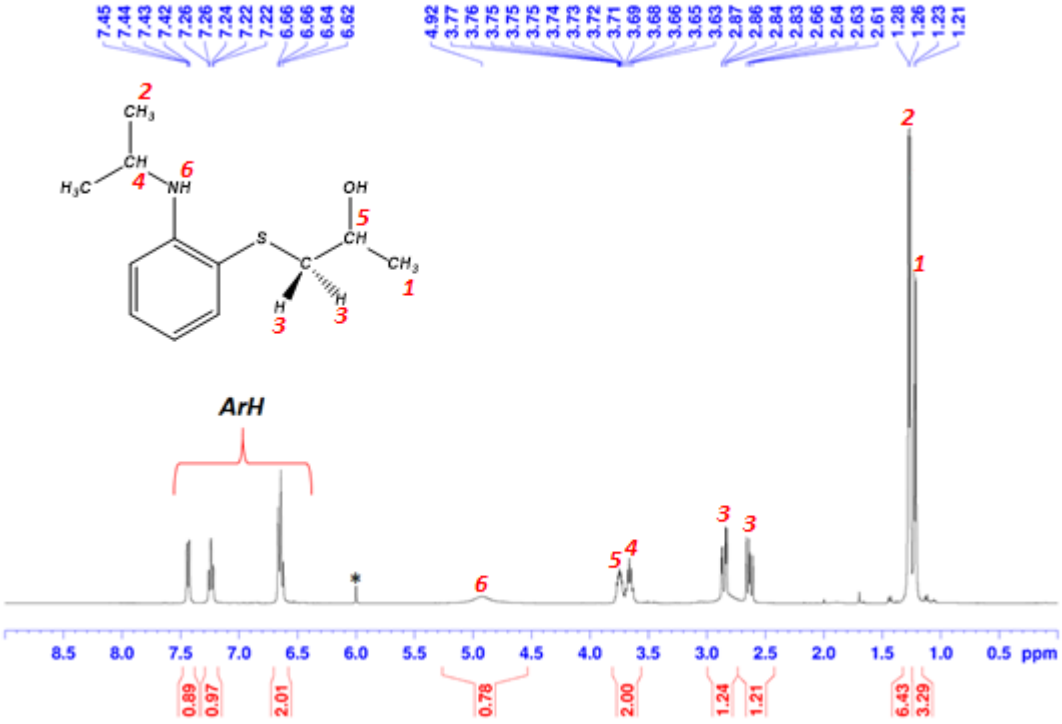

*Figure 103: ^{1}H NMR of NSO-ISO (400.13 MHz, *TCDE, 25°C).*

The complex was synthesized by reaction of the corresponding *NSO*-type ligand with *$AlMe_3$* in refluxing benzene (*scheme 8)*, in good yield (72%).

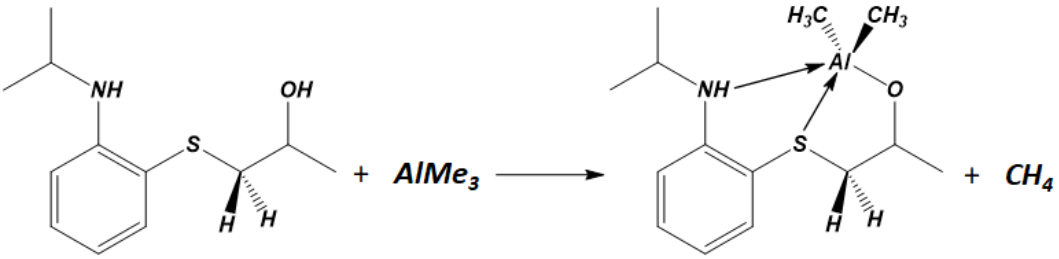

Scheme 8

In the ^{1}H NMR spectrum (*figure 104*) the *OH* signal of the ligand was absent, a sign that the ligand was actually deprotonated whereas the *NH* signal was still present, it appears as a doublet at 4.76 ppm. The integration ratio between the signals of the methyl bonded to aluminum and the methyl of the isopropyl group *NCH(CH₃)₂* was 1:1, this indicates that the ligand acts as monoanionic ligand. Respect to the pre-ligand, the resonances of the protons of the isopropyl group bound to nitrogen atom and of the alkyl groups bound to sulphur atom were shifted, this suggests the effective coordination of the sulphur and of the nitrogen atoms to the *Al* atom with the concomitant formation of a pentacoordinate mononuclear complex. The complex has no elements of symmetry, notwithstanding this, the two methyl groups bound to the aluminum atom appear equivalent and this suggests the presence of fast exchange involving the complex.

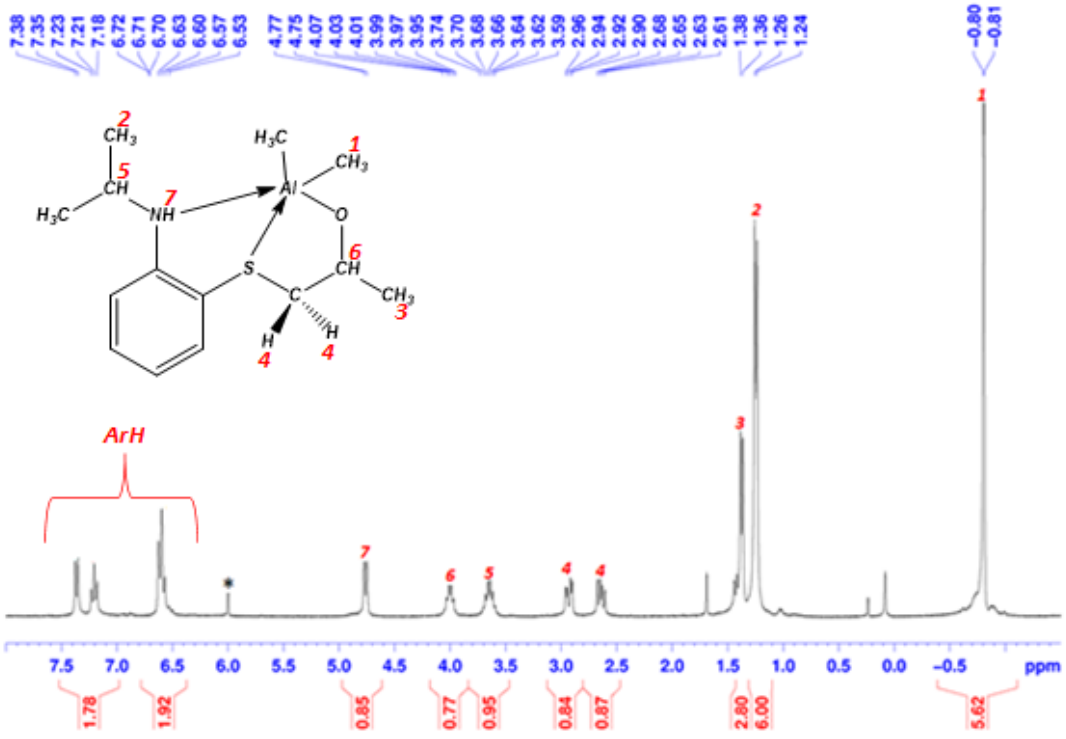

*Figure 104: ^{1}H NMR of Al-NSO-ISO complex (400.13 MHz, *TCDE, 25°C).*

In order to check the thermal stability of the complex, VT NMR analysis in the range 25-80 °C was performed (*figure 104*). No sign of variation or decomposition was observed, this indicates that the structure is stable in solution at high temperature.

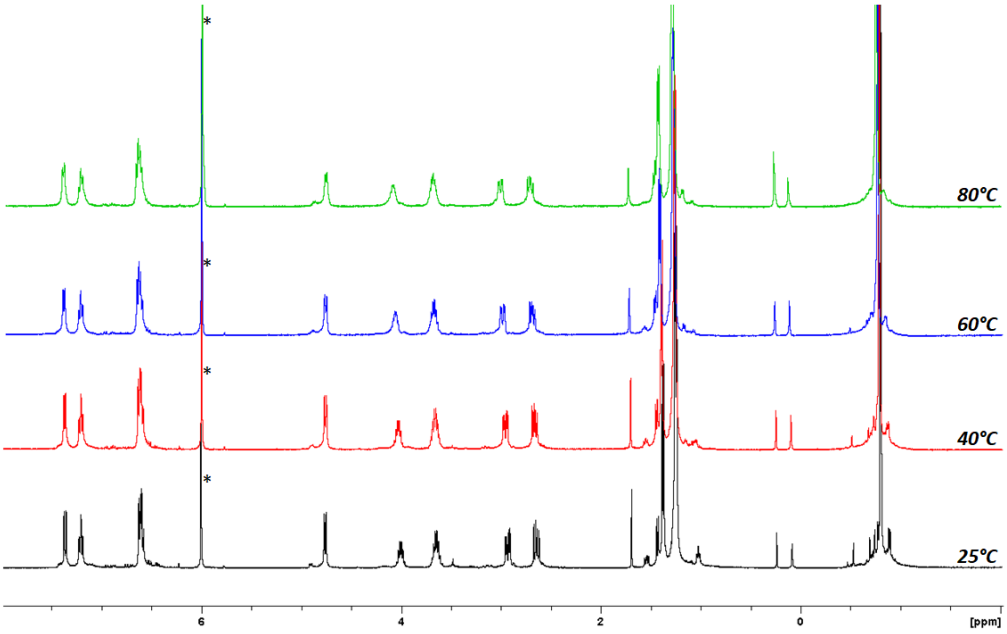

Figure 105: ^{1}H NMR of Al-NSO-ISO complex (400.13 MHz, *TCDE, variable temperature).

5.2 ROP of cyclic esters by Al-NSO-ISO

Al-NSO-ISO complex was tested as catalyst in the *ROP* of several cyclic esters in toluene solution, in combination with ^{i}*PrOH*. The importance of an alcohol as co-initiator was confirmed by a polymerization, where the complex was found to be inactive in absence of ^{i}*PrOH*. The most significant results are shown in table 7 where it can be seen how the complex is able to promote the polymerization of various cyclic esters and proceeded very efficiently with very high activity (TOF up to 12766 $mol_{CL} \cdot mol_{Al}^{-1} \cdot h^{-1}$ for *ε-CL* and 501 $mol_{LA} \cdot mol_{Al}^{-1} \cdot h^{-1}$ for *rac-LA*). To probe the robustness of the catalytic system in *ROP* of *rac-LA*, a polymerization run was performed by reducing the amount of the catalyst (entry 6 in table 7). The catalyst remained active (TOF = 49 $mol_{LA} \cdot mol_{Al}^{-1} \cdot h^{-1}$), even with [*L-LA*]/[**1**] ratio of 1000, reached 79% of monomer conversion after 16 hours. The complex has also proved active in the *ROP* of *β*-butyrolactone. However, higher temperatures are required to reach conversions above 50% in a short time (entry 8 in table 7).

Table 7: ROP of cyclic esters by Al-NSO-ISO.

Entry	Monomer	[M]/[Cat]	t (min)	Conv.[a] (%)	TOF (h^{-1})	$M_{n(theo)}$[b]
1	*ε-CL*	1000	5	77	9254	44.1
2	*ε-CL*	2000	10	78	9389	89.4
3	*ε-CL*	4000	10	53	12766	121.5
4	*ε-CL*	4000	40	81	4878	185.7
5	*rac-LA*	500	240	79	198	28.5
6	*rac-LA*	1000	960	79	49	56.8
7[d]	*rac-LA*	500	60	50	501	18.1
8[d]	*β-BL*	100	240	61	15	2.7
9	*β-BL*	100	240	24	6	1.1

All reaction were carried out in 2 mL of toluene and using 1-propanol as co-catalyst. Reaction conditions: 80°C, $[Cat]_0$= 14.0 mM, [Monomer]= 1.4 M, [Cocatalyst]/[cat]= 2; [a]Molecular conversion determined by ^{1}H NMR spectroscopy ($CDCl_3$, 298 K); [b]Calculated molecular weight using $M_{n(theo)}$(kg/mol)=(((PM$_{Monomer}$ x [Mon]/[cocat] x conversion)/100) + PM$_{Cocat}$)/1000.

Different kinetic tests were carried out with three monomers by taking different aliquots of the product mixture at regular and scheduled time intervals and analysing them by ^{1}H NMR spectroscopy. In all cases it was observed that the polymerization

follows a first order kinetic law with respect to the monomer concentration. In the figure below it's possible to see the linearity of the plot $\ln([Mon]_0/[Mon]_t]$ versus time using the *Al-NSO-ISO* (*figure 106*).

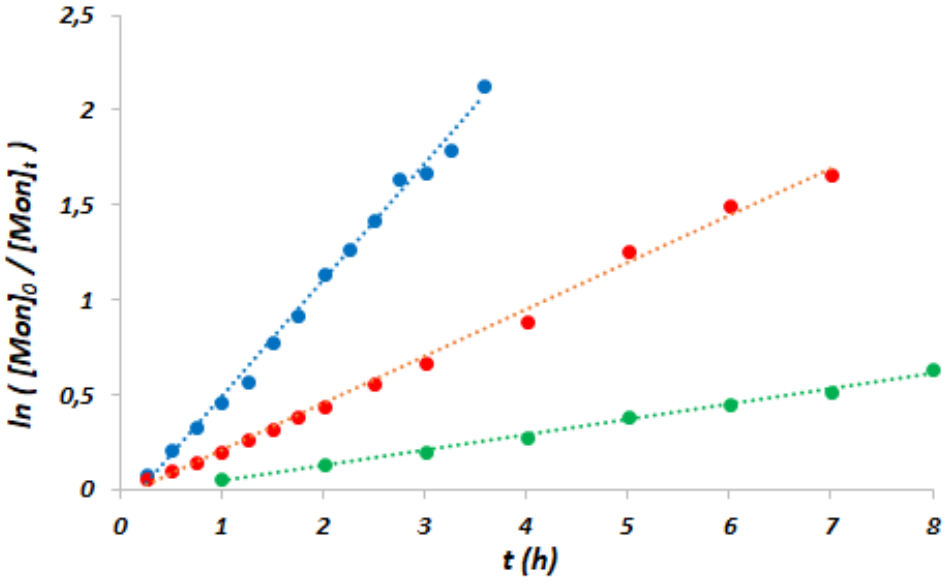

Figure 106: Pseudo-first order kinetic plots for ROP with several monomers by Al-NSO-ISO: blue line - rac-LA (k_{app}= 0.613 ± 0.013 h^{-1}, R^2= 0.995); red line – L-LA (k_{app}= 0.247 ± 0.004 h^{-1}, R^2= 0.996); green line – ϐ BL (k_{app}= 0.081 ± 0.002 h^{-1}, R^2= 0.996).

*Conditions: $[Monomer]_0$ = 1.4 M, $[Monomer]_0/[$**Al-NSO-ISO**$]_0$ = 100, $[^iPrOH]_0/[$**Al-NSO-ISO**$]_0$ = 2, T = 80 °C, and toluene as the solvent.*

Kinetic experiments were conducted at different temperature (from 70 to 100 °C) with [*rac-LA*]/[***Al-NSO-ISO***] ratio fixed at 100 to determinate the activation energy (E_a) from the Arrhenius plot (*figure 108*). From kinetic studies, an E_a of 17.90 ± 0.03 kcal/mol was obtained. The inspection of the methine regions for the *PLA* obtained by this new complex revealed that the microstructure is atactic.

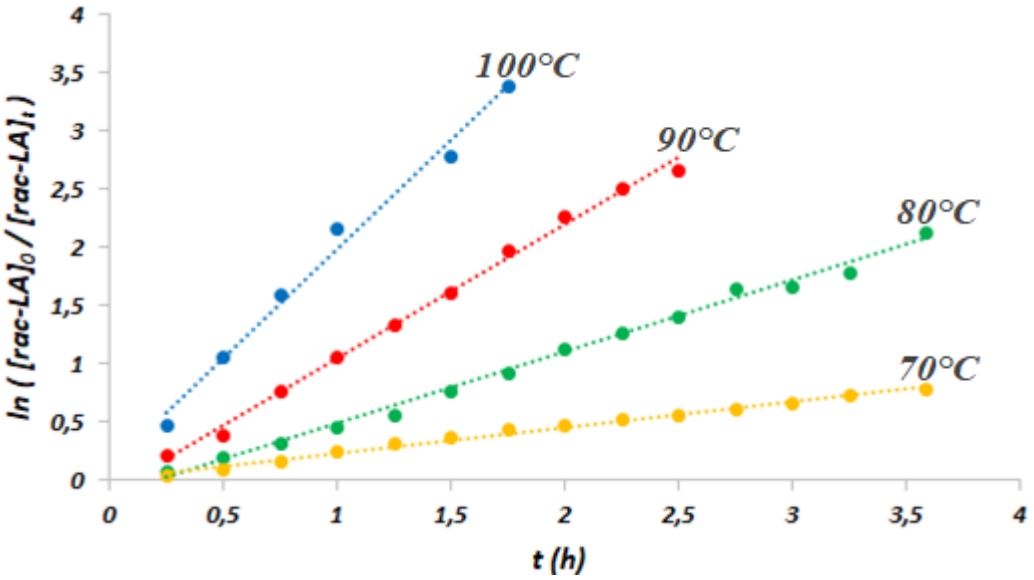

Figure 107: Pseudo-first order kinetic plots for ROP of rac-LA by Al-NSO-ISO at different temperatures: T= 100°C_blue line: k_{app}= 1.865 ± 0.099 h^{-1}, R^2= 0.989). T= 90°C_red line: k_{app}= 1.147 ± 0.026 h^{-1}, R^2= 0.996. T= 80°C_green line: k_{app}= 0.613 ± 0.013 h^{-1}, R^2= 0.995. T= 70°C_yellow line: k_{app}= 0.222 ± 0.006 h^{-1}, R^2= 0.992.

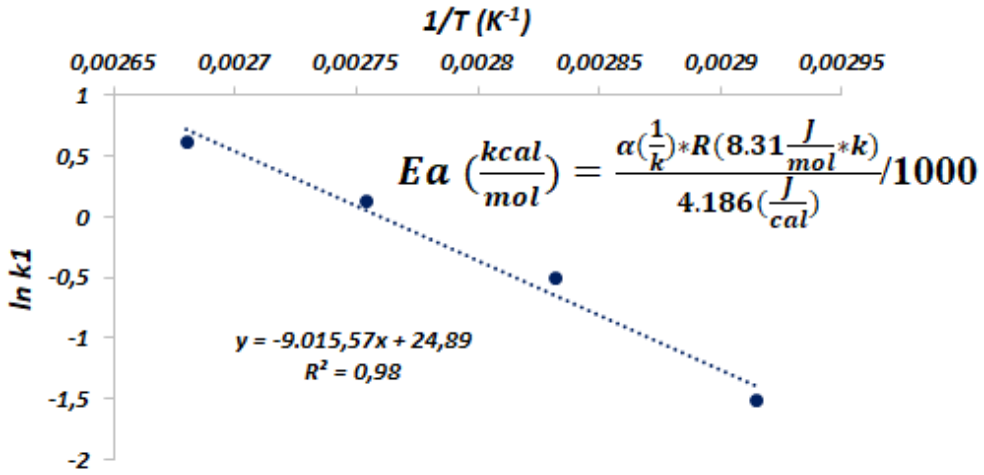

Figure 108: Plot of $\ln k_1$ vs 1/T, in the range from 70 to 100 °C, for the determination of E_a.
*Conditions: $[rac\text{-}LA]_0$ = 1.4 M, $[rac\text{-}LA]_0/[$**Al-NSO-ISO**$]_0$ = 100, $[^iPrOH]_0/[$**Al-NSO-ISO**$]_0$ = 2 and 2 mL of toluene as the solvent.*

The complex was also tested in melt polymerizations of *rac*- and *L-LA*, adding only isopropanol, and in a polymerization of *ε-CL* without using solvent. The complex showed good activities at 190 °C, converting 560 and 520 equivalent of *rac-LA* and *L-LA* respectively in 5 minutes ($TOF_{rac\text{-}LA}$ = 563 $mol_{LA} \cdot mol_{Al}^{-1} \cdot h^{-1}$; $TOF_{L\text{-}LA}$ = 522 $mol_{LA} \cdot mol_{Al}^{-1} \cdot h^{-1}$). At 100 °C, the complex converted 3255 equivalents of *ε-CL*, reaching a TOF value equal to 39058 $mol_{CL} \cdot mol_{Al}^{-1} \cdot h^{-1}$.

A polymerization run with a low molar ratio monomer/catalyst ([*ε-CL*]/[***Al-NSO-ISO***] = 25) was performed to confirm that the reaction begin with the attack of the alcohol

to the monomer and ends with the hydrolysis of the *Al-O* bond between the growing polymer chain and the metal center. The ^{1}H and ^{13}C NMR analysis of the isolated polymer (*figure 109* and *110*) shows signals very similar to those observed in the previous chapter, the presence of an isopropyl group (proton 7 and 8) and the existence of the carbon of isopropyl at 22.04 and 69.97 ppm at the end of the polymer chain.

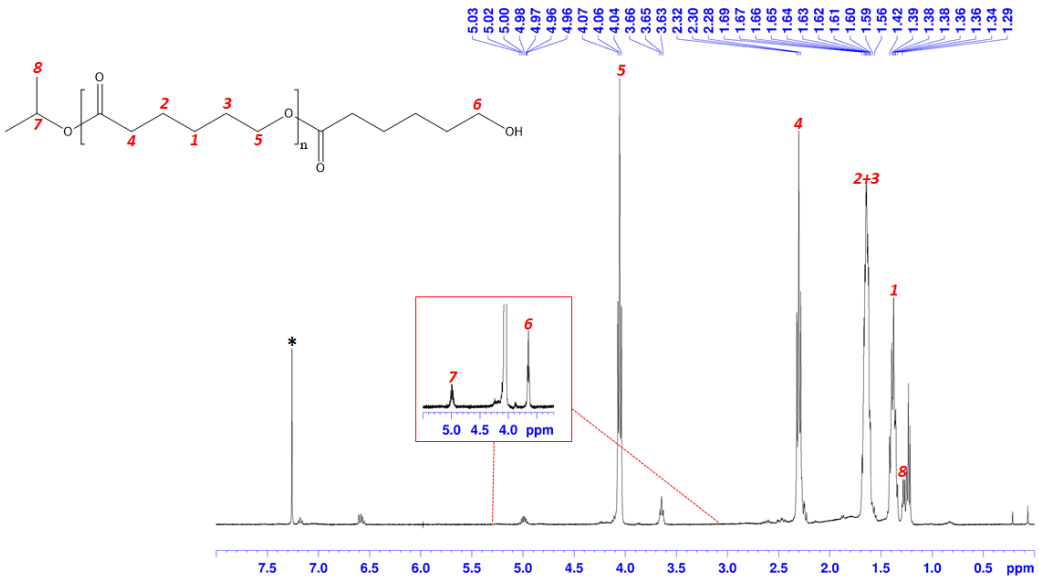

Figure 109: ^{1}H NMR of oligomers of PCL obtained using Al-NSO-ISO as catalyst (400.13 MHz, *$CDCl_3$, 25°C).

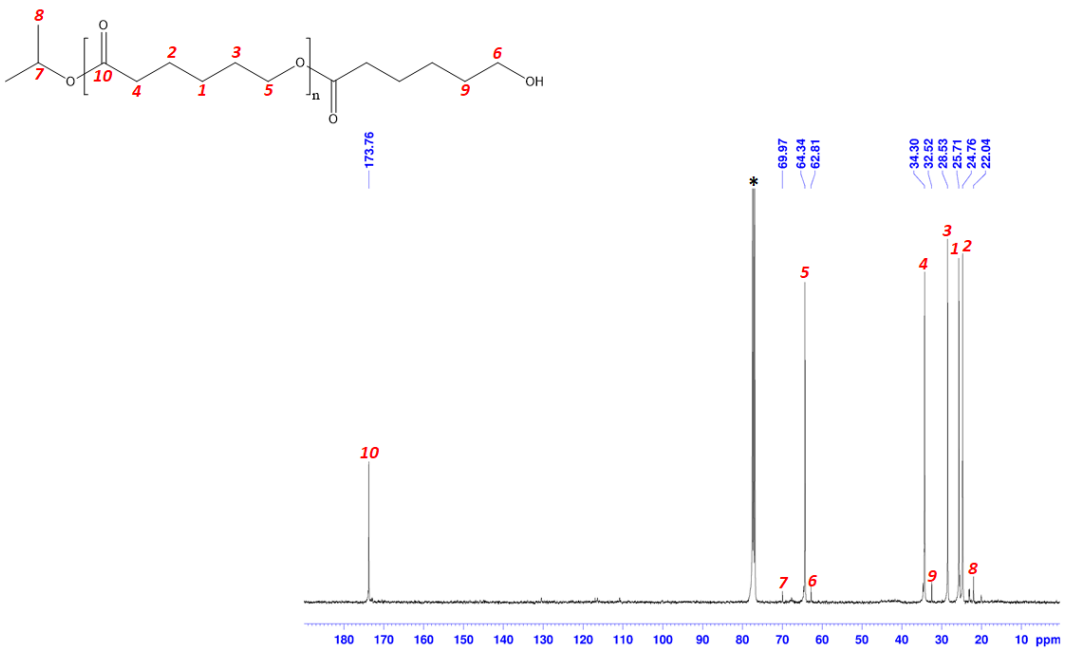

Figure 110: ^{13}C NMR of oligomers of PCL obtained using Al-NSO-ISO as catalyst (400.13 MHz, *$CDCl_3$, 25°C).

5.3 Conclusions

A new pentacoordinate *Al* complex has been developed and characterized by ^{1}H and ^{13}C NMR spectroscopy. The variable temperature NMR analysis, confirmed that it stable at different temperature in the range 25-80 °C.

The complex is inactive in absence of *^{i}PrOH* in pure toluene in *ROP* of cyclic esters.

The *PLA* obtained by *rac*-LA polymerization with this new *Al* complex, showed an atactic microstructure from the distribution of tetrads and the integration ratio of the peaks.

The catalytic system showed a relatively high activity toward *ε-CL*, reached TOF values even higher than 10000 h^{-1}. The catalyst has also been shown to be active in the polymerization of *β-BL* even if temperatures higher than 80 °C are necessary to have conversions above 50% within a few hours. The temperature effect on polymerization process was investigated in a temperature range between 70 and 100 °C and the E_a was calculated. An increase in the polymerization rate and the catalytic activity of the complex occurs passing from 70 to 100 °C. The catalyst resulted very active in melt polymerization of *LA* and in *ROP* of *ε-CL* without solvent. The test with a low monomer/catalyst ratio revealed by NMR analysis and the corresponding signals, the insertion of the alcohol during the polymerization reaction.

6 Experimental part: synthesis and characterization of ligands used in the research project.

6.1 Synthesis and characterization of 1,2-bis(aminophenylthio)ethane

1,2-bis(aminophenylthio)ethane [NSSN] was synthesized following a procedure reported in literature (*figure 111*). 1,2-dibromoethane (7.3 g, 39 mmol) was added dropwise to a refluxing solution of 2-aminothiophenol (9.8 g, 78 mmol) and sodium hydroxide (3.1 g, 78 mmol) in methanol (100 mL). The refluxing reaction mixture was stirred for 18 h.

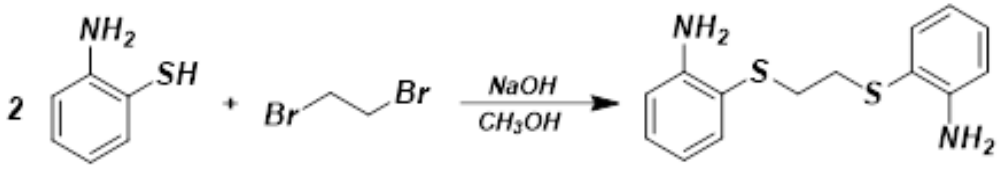

Figure 111: synthesis of NSSN.

On completion of reaction, the solvent was removed in vacuo and the reaction mixture was cooled to room temperature. Water (50 mL) was added and the reaction mixture was extracted with diethyl ether (4x 50 mL). The organic layers was dried with anhydrous Na_2SO_4, filtered and evaporated to dryness in vacuo to get a yellow solid product (10.7 g, yield = 99 %).

^{1}H NMR (400.13 MHz, $CDCl_3$, 25 °C) δ ppm. 6.64-7.31 (m, 8H, ArH), 4.35 (s, 4H, 2x NH_2), 2.86 (s, 4H, 2x S-CH_2). ^{13}C NMR (100.62 MHz, $CDCl_3$, 25 °C) δ ppm. 34.61, 115.16, 116.86, 118.71, 130.15, 136.30, 148.68.

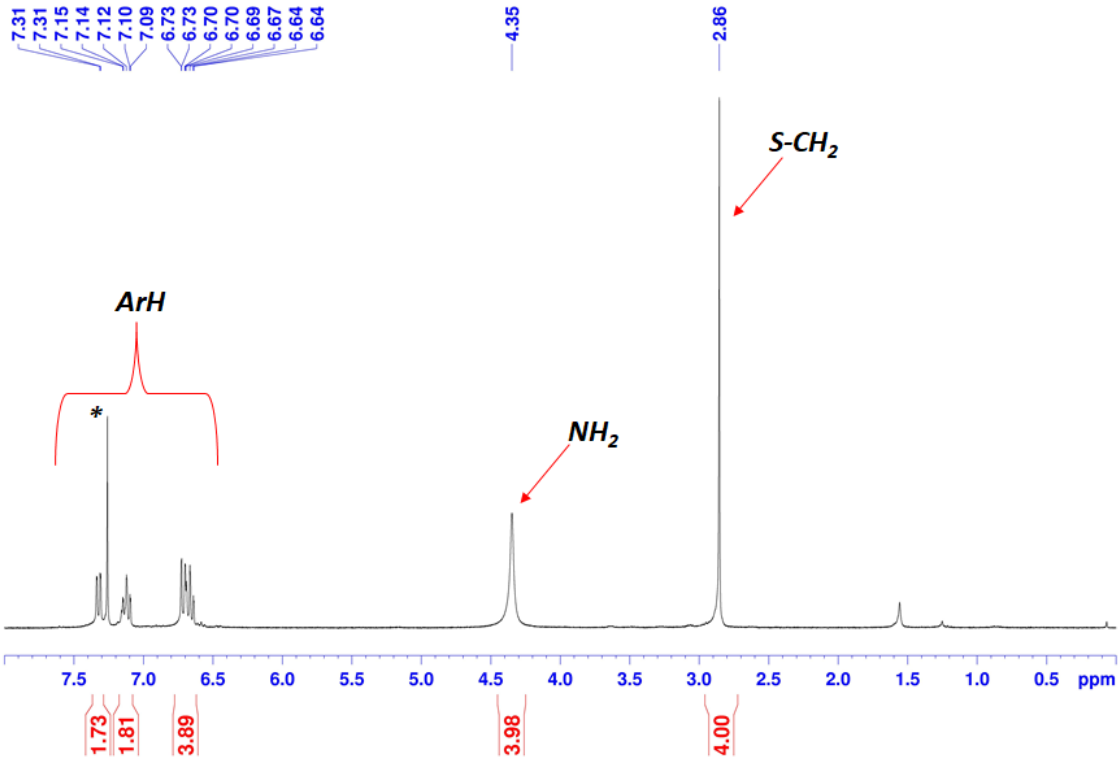

*Figure 112: ^{1}H NMR of NSSN (400.13 MHz, *$CDCl_3$, 25°C).*

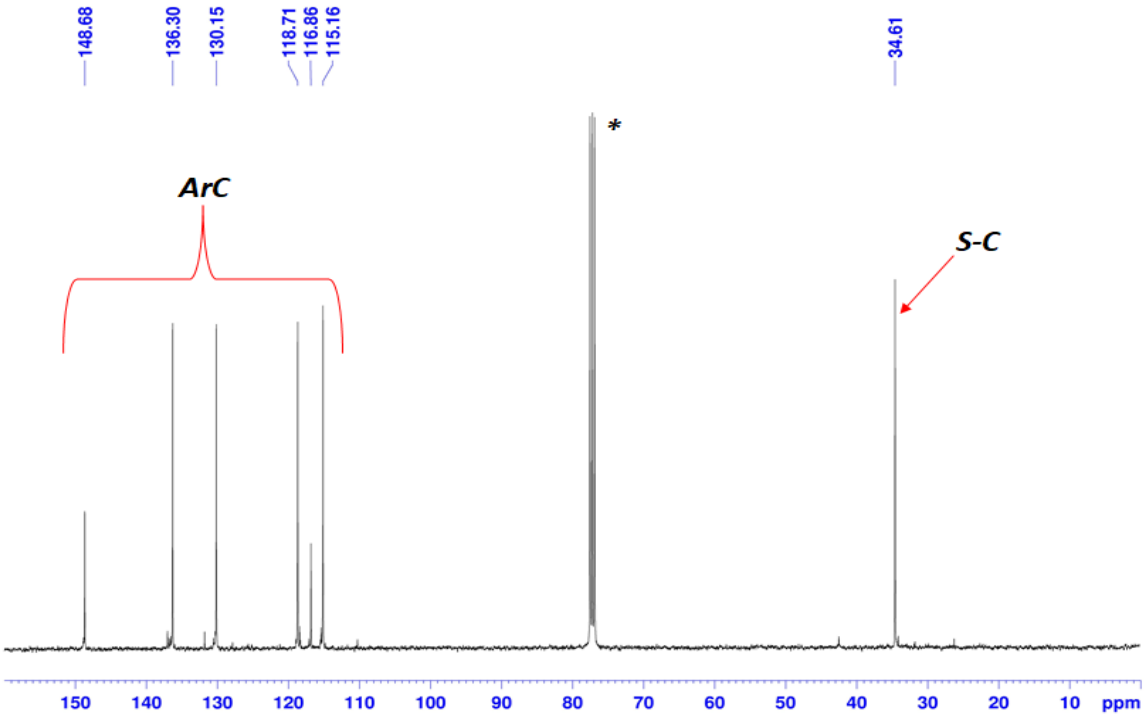

*Figure 113: ^{13}C NMR of NSSN (100.62 MHz, *$CDCl_3$, 25°C).*

6.2 Synthesis and characterization of 2,2'-(ethane-1,2-diylbis(sulfanediyl))bis(N-isopropylaniline)

2,2'-(ethane-1,2-diylbis(sulfanediyl))bis(N-isopropylaniline) [NSSN-ISO] was synthesized through a condensation reaction between acetone and *NSSN* (*figure 114*). The reaction was carried in a zinc/acetic acid mixture to obtain the reduction of imine formed from condensation reaction. To a 250 mL round-bottom one-necked flask equipped with a condenser and charged with a teflon-sealed stir bar were added *NSSN* (5.79 g, 21 mmol), zinc (13.73 g, 0.21 mol), acetic acid (60 mL) and acetone (12,20 g, 0.21 mol). The mixture was stirring to room temperature for 48 h.

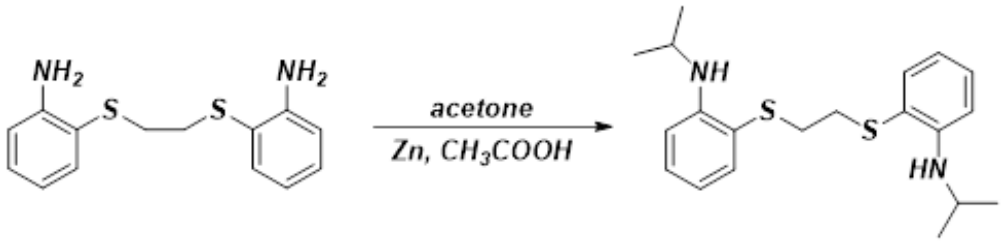

Figure 114: synthesis of NSSN-ISO ligand.

After it was cooled to room temperature, the mixture was quenched in a mixture of NH_3 30% aqueous solution (150 mL), diethyl ether (200 mL) and ice. The organic layers was dried with anhydrous $MgSO_4$, filtered and evaporated to dryness in vacuo to get a yellow solid product (7,7 g, yield = 98 %).

^{1}H NMR (400.13 MHz, CD_2Cl_2, 25 °C) δ ppm. 6.54-7.33 (m, 8H, ArH), 4.94 (s, 2H, 2x NH), 3.63-3.67 (q, 2H, 2x CH), 2.77 (s, 4H, 2x S-CH_2), 1.23 (d, J = 6.38 Hz, 12H, 4x CH_3). ^{13}C NMR (100.62 MHz, CD_2Cl_2, 25 °C) δ ppm. 22.57, 34.51, 43.91, 110.56, 115.93, 115.97, 130.22, 136.52, 148.65.

A *NSSN-ISO* solution (1 mg/mL in CH_2Cl_2) was analyzed by MALDI spectroscopy using hydroxybenzoic acid as matrix and the result was reported in *figure 118. HRMS* (MALDI). Calcd for $C_{20}H_{29}N_2S_2$ ($[M + H]^+$: m/z 361.1772. Found: m/z 361.1785.

Crystallization of *NSSN-ISO* from hexane afforded crystals suitable for X-ray analysis. Single crystal structure was reported in *Crystallographic Data (figure 276).*

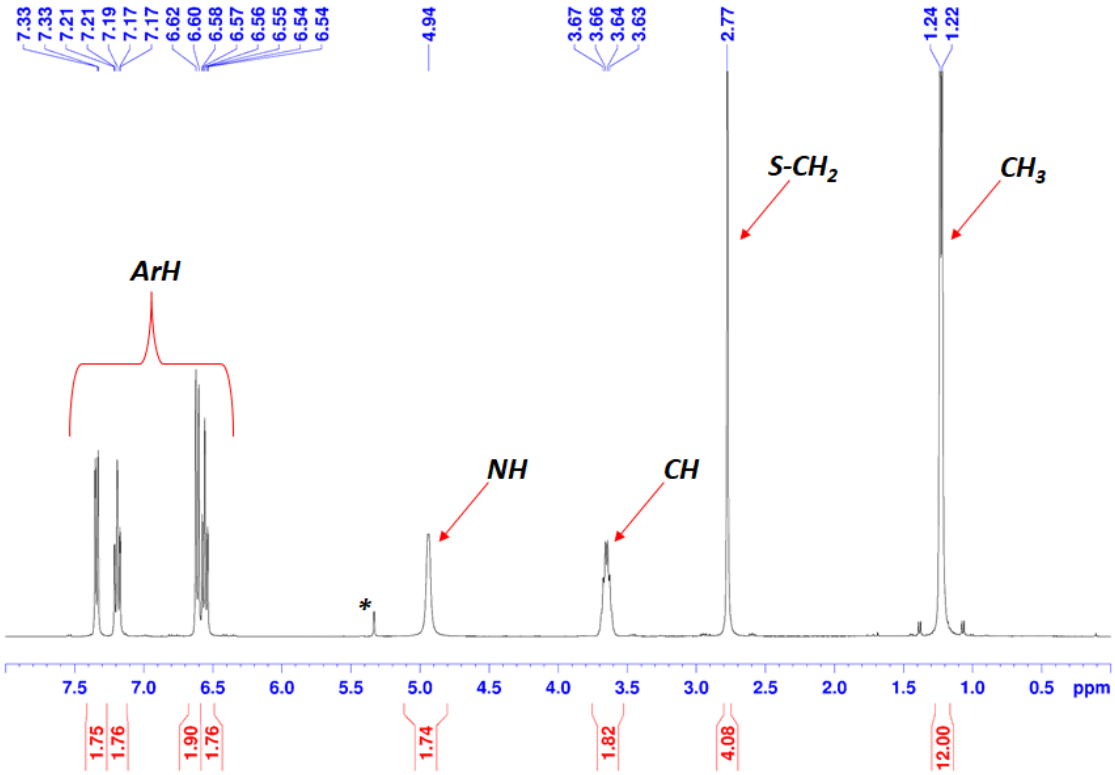

*Figure 115: ^{1}H NMR of NSSN-ISO ligand (400.13 MHz, *CD_2Cl_2, 25°C).*

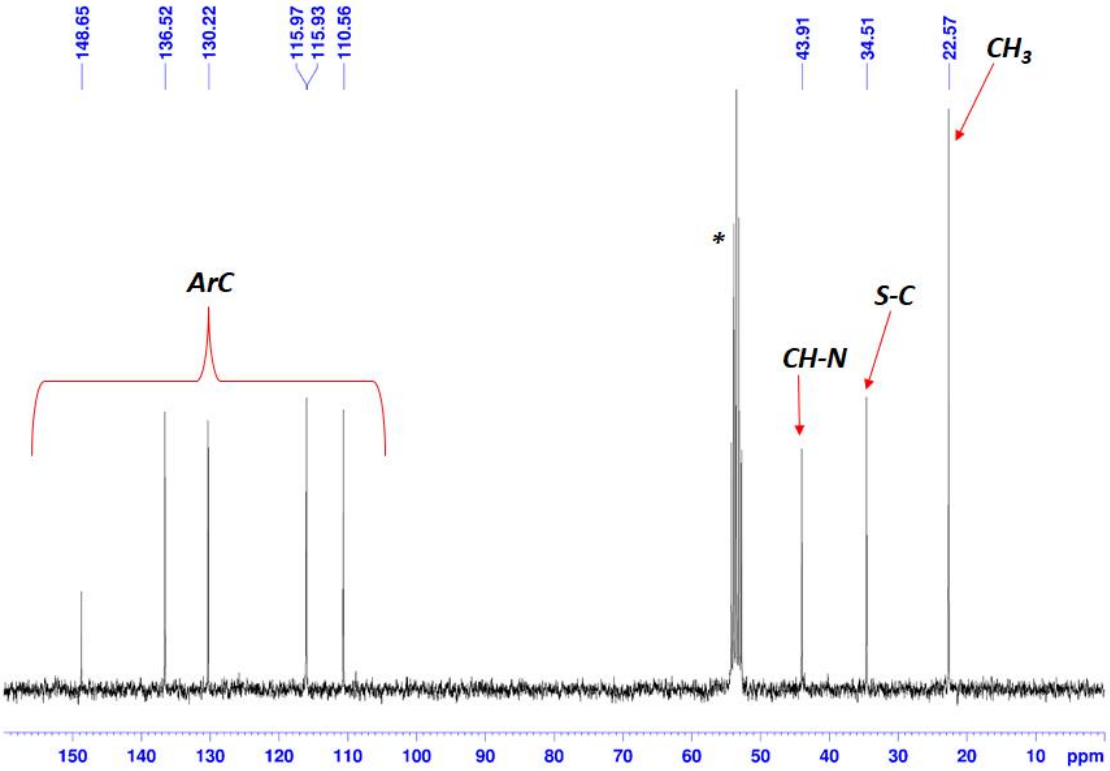

*Figure 116: ^{13}C NMR of NSSN-ISO ligand (100.62 MHz, *CD_2Cl_2, 25°C).*

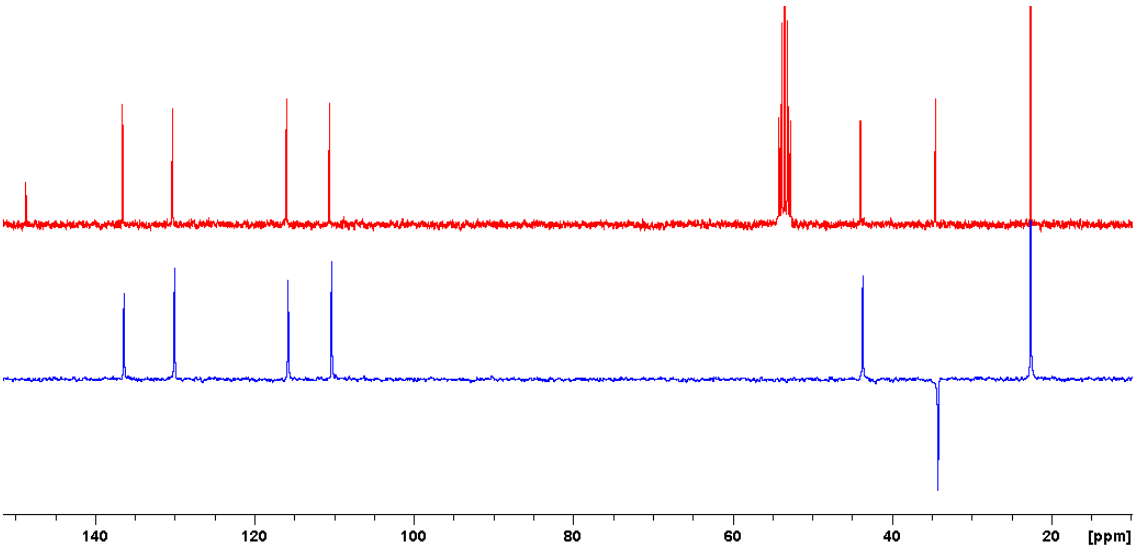

*Figure 117: DEPT 135 of NSSN-ISO ligand (100.62 MHz, *CD_2Cl_2, 25°C).*

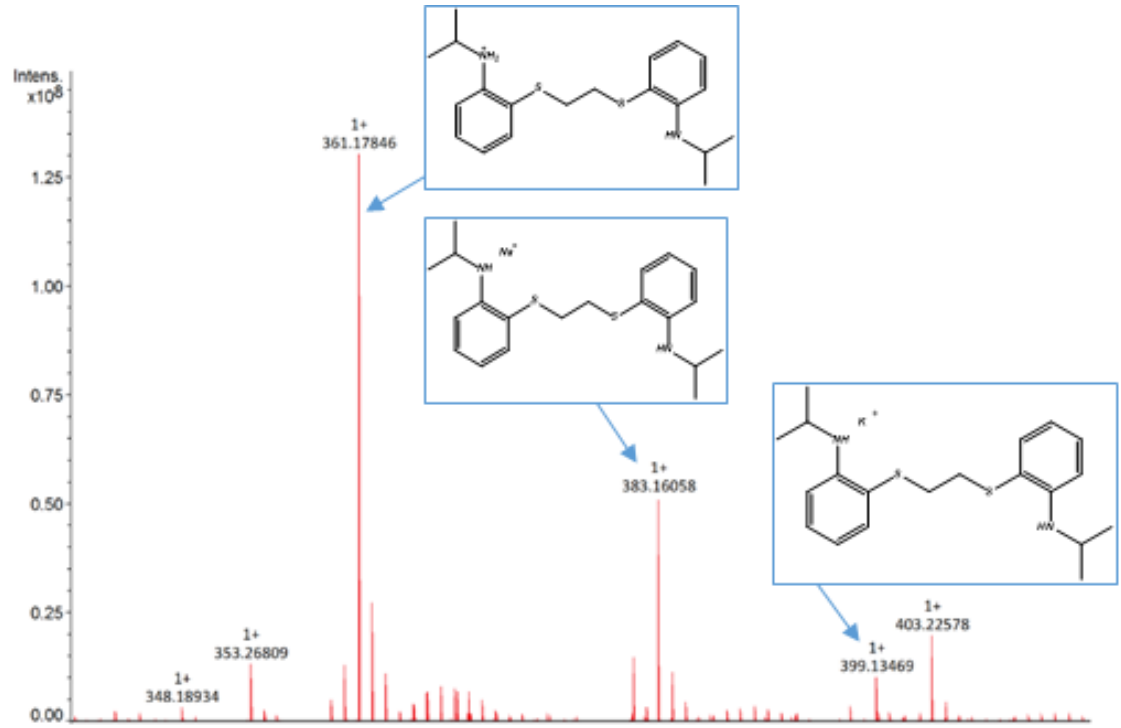

Figure 118: Maldi-MS spectrum of NSSN-ISO ligand.

6.3 Synthesis and characterization of 2,2'-(ethane-1,2-diylbis(sulfanediyl))bis(N-cyclohexylaniline)

2,2'-(ethane-1,2-diylbis(sulfanediyl))bis(N-cyclohexylaniline) [NSSN-CY] was synthesized with a similar procedure reported for *NSSN-ISO* but replacing acetone with cyclohexanone (*figure 119*).[89]

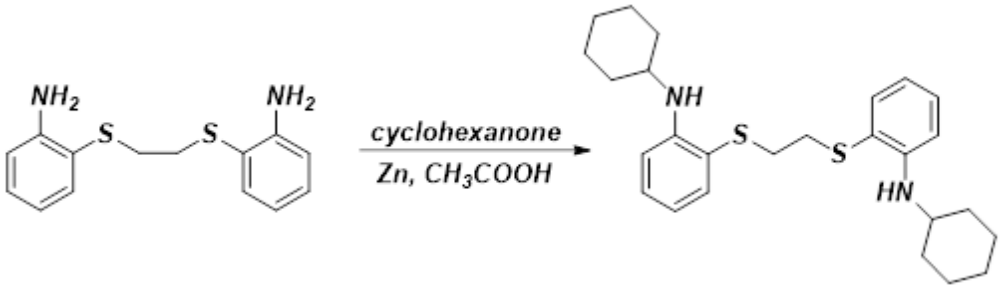

Figure 119: synthesis of NSSN-CY ligand.

To a 250 mL round-bottom one-necked flask equipped with a condenser and charged with a teflon-sealed stir bar were added *NSSN* (6.67 g, 24 mmol), zinc (15.8 g, 0.24 mol), acetic acid (100 mL) and cyclohexanone (9.48 g, 48 mmol). The mixture was heated to 65 °C for 48 h. After it was cooled to room temperature, the mixture was quenched with NH_3 30% aqueous solution (200 mL) and diethyl ether (300 mL). The organic layers dried with anhydrous $MgSO_4$ and whitish solid product is obtained on removal of solvent (10.3 g, yield = 97 %).

^{1}H NMR (400.13 MHz, $CDCl_3$, 25 °C) δ ppm. 6.52-7.35 (m, 8H, ArH), 5.01 (s, 2H, 2x NH), 3.27-3.30 (m, 2H, 2x CH), 2.77 (s, 4H, 2x S-CH_2), 1.21-2.02 (m, 20H, cyclohexyl). ^{13}C NMR (100.62 MHz, $CDCl_3$, 25 °C) δ ppm. 25.08, 26.10, 33.35, 34.83, 51.48, 110.75, 110.76, 116.18, 130.50, 136.96, 148.72.

A *NSSN-CY* solution (1 µg/mL in CH_2Cl_2) was analyzed by electrospray spectroscopy and the result was reported in *figure 123*. *HRMS* (ESI). Calcd for $C_{26}H_{37}N_2S_2$ ($[M + H]^+$: m/z 441.2393. Found: m/z 441.2392.

Crystallization of *NSSN-CY* from diethyl ether afforded crystals suitable for X-ray analysis. Single crystal structure was reported in *Crystallographic Data (figure 277).*

[89] F. Hild, L. Brelot, S. Dagorne, *Organometallics, **2011**, 30, 5457-5462.*

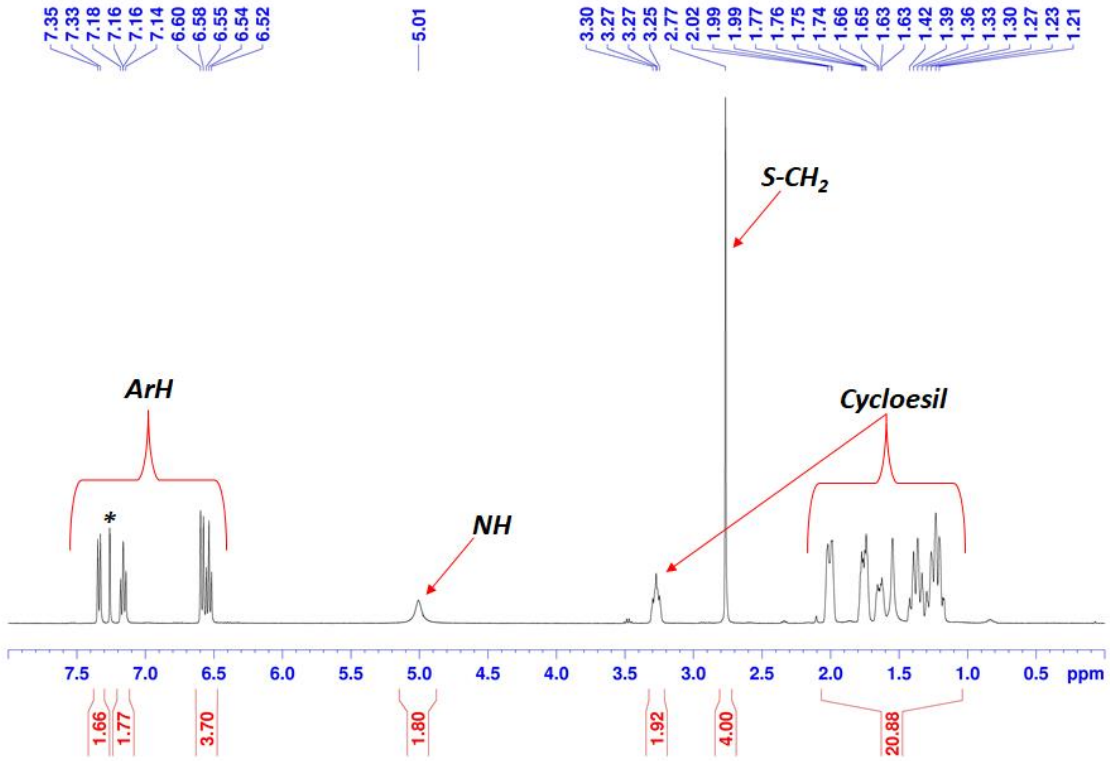

*Figure 120: ^{1}H NMR of NSSN-CY ligand (400.13 MHz, *$CDCl_3$, 25°C).*

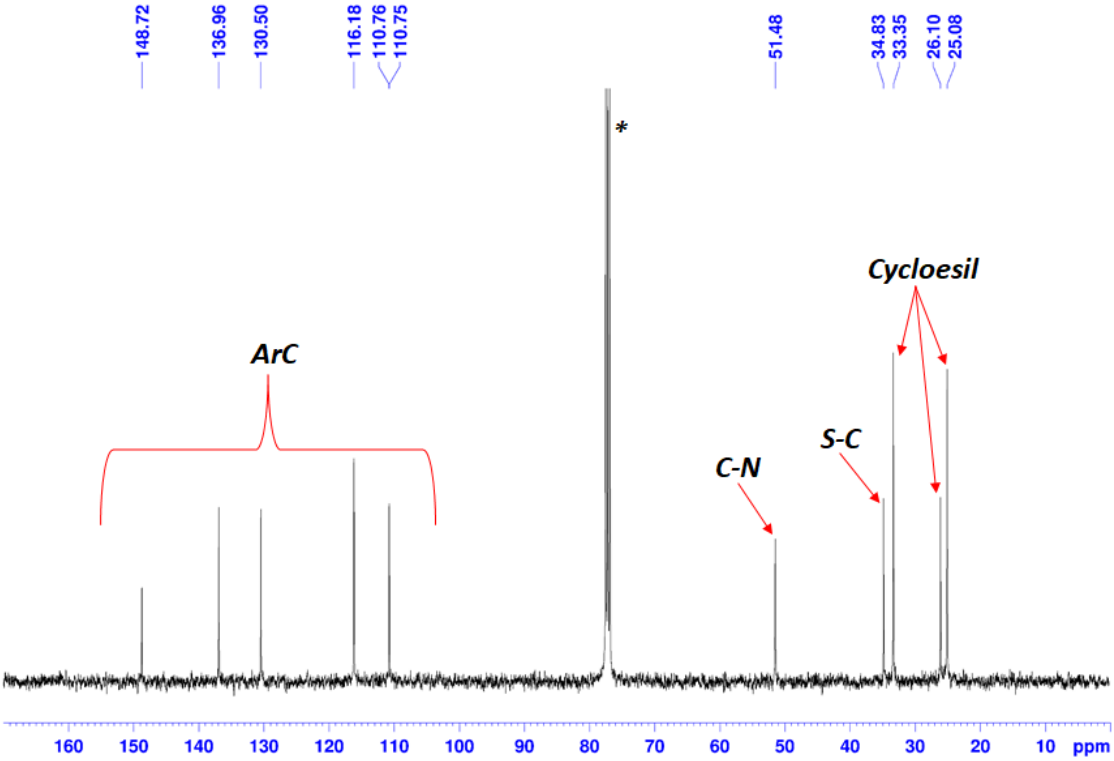

*Figure 121: ^{13}C NMR of NSSN-CY ligand (100.62 MHz, *$CDCl_3$, 25°C).*

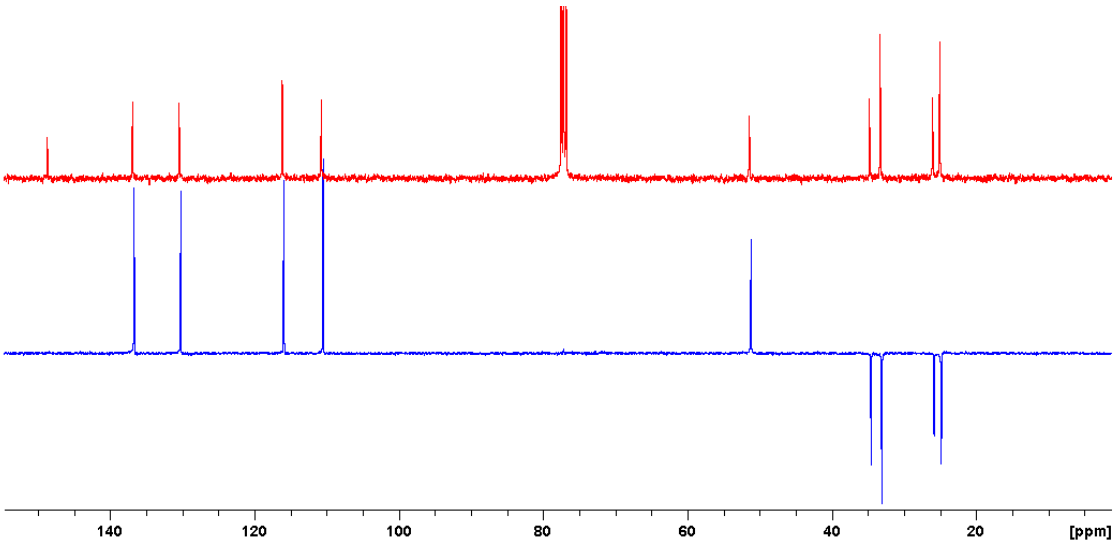

*Figure 122: DEPT 135 of NSSN-CY ligand (100.62 MHz, *$CDCl_3$, 25°C).*

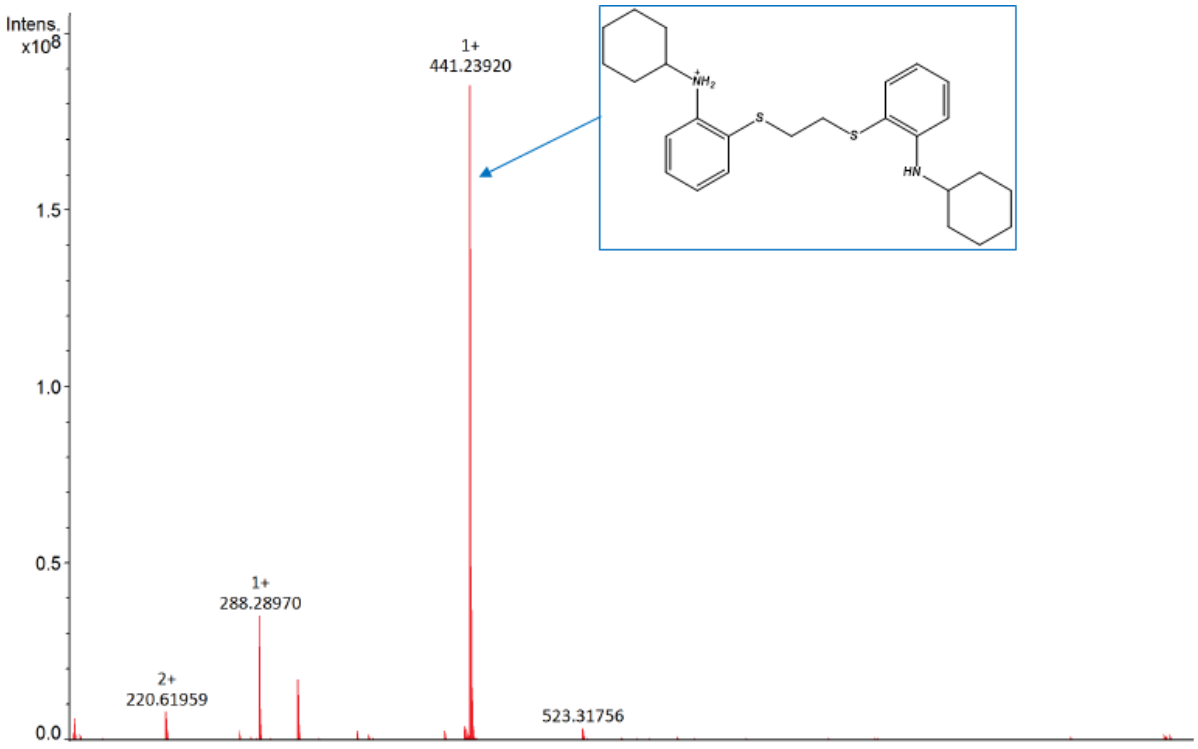

Figure 123: ESI-MS spectrum of NSSN-CY ligand.

6.4 Synthesis and characterization of N,N'-((ethane-1,2-diylbis(sulfadeniyl))bis(2,1-phenylene))bis(2,4,6-trimethylaniline)

N,N'-((ethane-1,2-diylbis(sulfadeniyl))bis(2,1-phenylene))bis(2,4,6-trimethylaniline) [NSSN-MESY] was synthesized using a coupling reaction developed by Buchwald (*figure 124*).[90]

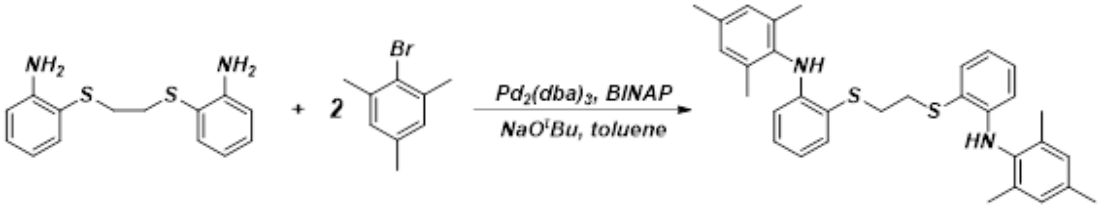

Figure 124: synthesis of NSSN-MESY ligand.

A Schlenk flask was charged with *NSSN* (0.6 g, 2.2 mmol), mesityl bromide (0.8 g, 4.0 mmol), tris(dibenzylideneacetone)dipalladium(0) (0.078 g, 0.085 mmol), *rac*-2,2'-bis(diphenylphosphino)-1,1'-binaphthyl (0.13 g, 0.21 mmol), sodium *tert*-butoxide (0.63 g, 6.56 mmol) and toluene (15 mL). The reaction mixture was stirred and heated to 110 °C under a stream of N_2 for 72 hours. After it was cooled to room temperature, the mixture was quenched with saturated NH_4Cl aqueous solution and extracted with methylene chloride. The organic layers dried with anhydrous $MgSO_4$ and concentrated to dryness under reduce pressure to afford a brown oil. The product was purified via flash column chromatography (SiO_2, 230-400 mesh, *n*-hexane/CH_2Cl_2, 4/1, as eluent) to give a white solid (0.5 g, yield = 45 %).

^{1}H NMR (400.13 MHz, CD_2Cl_2, 25 °C) δ ppm. 6.03-7.39 (m, 12H, ArH), 6.41 (s, 4H, 2x NH), 3.01 (s, 4H, 2x S-CH_2), 2.29 (s, 6H, *p*-CH_3), 2.06 (s, 12H, *o*-CH_3). ^{13}C NMR (100.62 MHz, CD_2Cl_2, 25 °C) δ ppm. 18.31, 21.06, 34.79, 111.35, 116.23, 117.67, 129.50, 130.61, 135.53, 136.25, 136.62, 136.79, 148.29.

A *NSSN-MESY* solution (1 mg/mL in CH_2Cl_2) was analyzed by MALDI spectroscopy using hydroxybenzoic acid as matrix and the result was reported in *figure 127*. *HRMS* (MALDI). Calcd for $C_{32}H_{36}N_2S_2$ ($[M]^+$: m/z 512.2320. Found: m/z 512.2311.

[90] J. P. Wolfe, S. Wagaw, S. L. Buchwald, *J. Am. Chem. Soc.*, ***1996***, *118, 7215-7216;* J. P. Wolfe, S. Wagaw, J. F. Marcoux, S. L. Buchwald, *Acc. Chem. Res.*, ***1998***, *31, 805-818.*

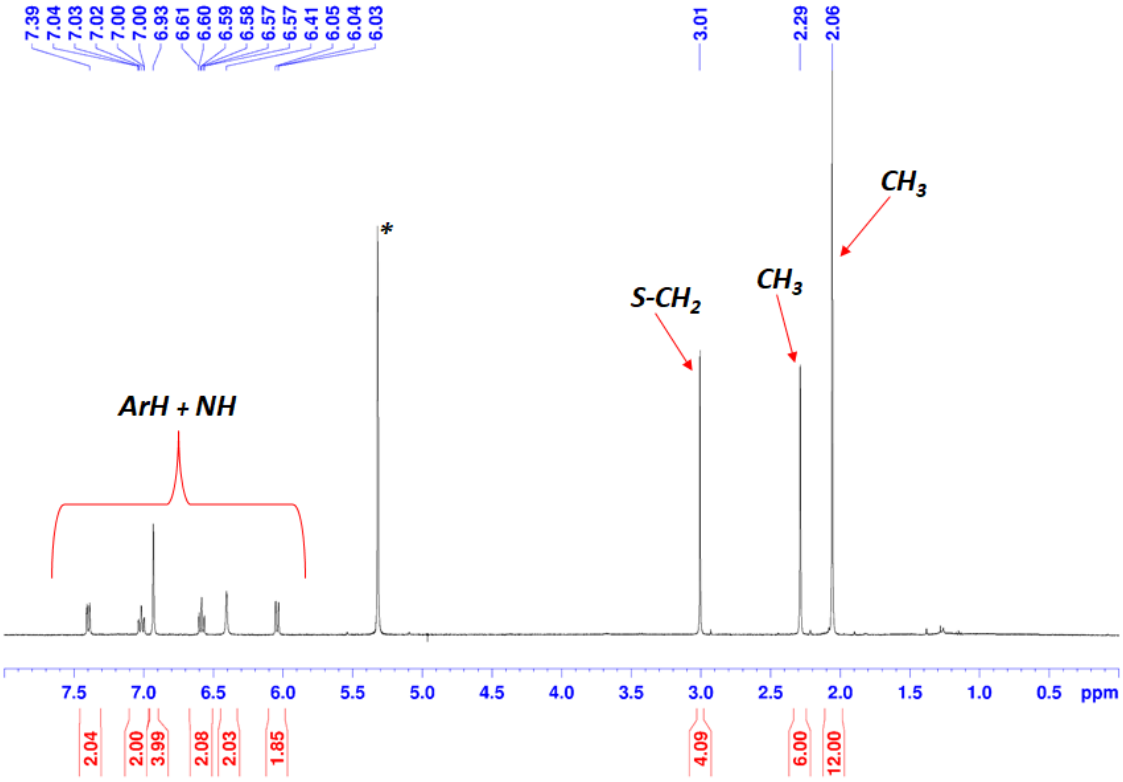

*Figure 125: ^{1}H NMR of NSSN-MESY ligand (400.13 MHz, *CD_2Cl_2, 25°C).*

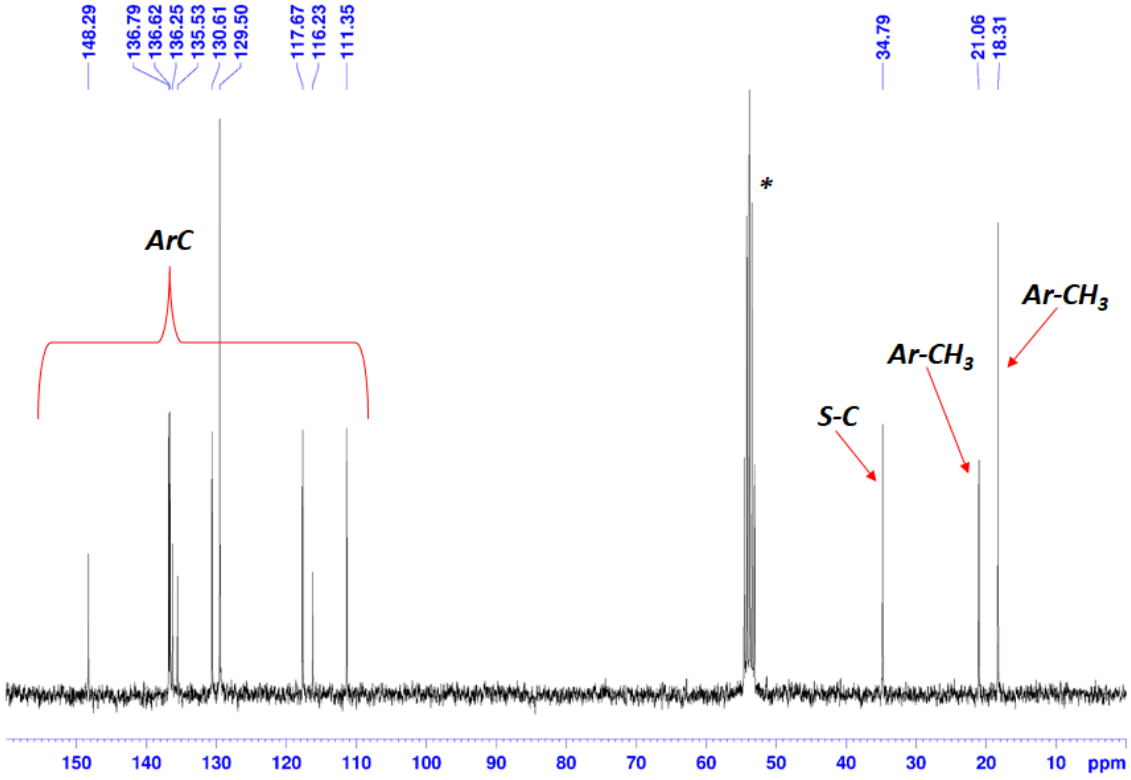

*Figure 126: ^{13}C NMR of NSSN-MESY ligand (100.62 MHz, *CD_2Cl_2, 25°C).*

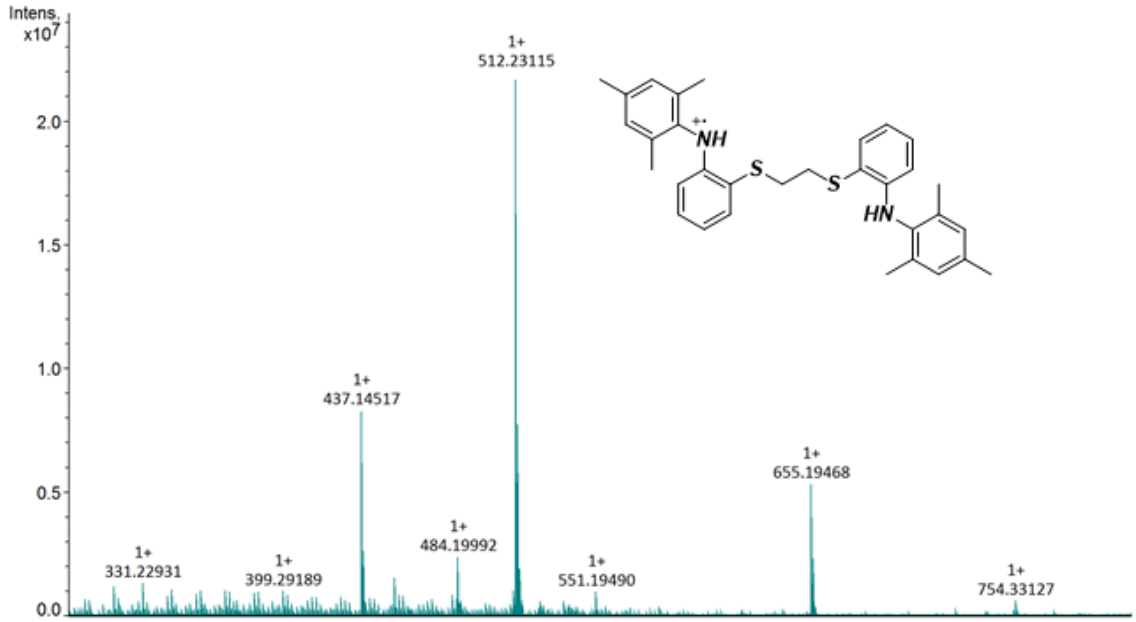

Figure 127: Maldi-MS spectrum of NSSN-MESY ligand.

6.5 Synthesis and characterization of 6,6'-(ethane-1,2-diylbis(sulfanediyl))bis(3-chloroaniline)

6,6'-(ethane-1,2-diylbis(sulfanediyl))bis(3-chloroaniline) [NSSN-Cl] was synthesized with a similar procedure reported for *NSSN* but replacing 2-aminothiophenol with 2-amino-4-chlorobenzenethiol (*figure 128*). 1,2-Dibromoethane (5.98 g, 32 mmol) was added dropwise to a refluxing solution of 2-amino-4-chlorobenzenethiol (10.17 g, 64 mmol) and sodium hydroxide (2.56 g, 64 mmol) in methanol (200mL). The refluxing reaction mixture was stirred for 7 h.

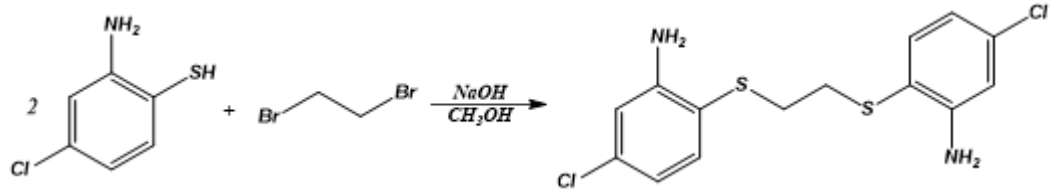

Figure 128: synthesis of NSSN-Cl.

Upon completion of the reaction, the solvent was removed in vacuo and the reaction mixture was cooled to room temperature. Water (70 mL) was added and the reaction mixture was extracted with diethyl ether (3x50 mL). The organic layer was dried with anhydrous $MgSO_4$ and evaporated to dryness in vacuo to get a white solid product (10.36 g, yield = 94%).

^{1}H NMR (400.13 MHz, CD_2Cl_2, 25 °C): δ 6.60−7.24 (m, 6H, ArH), 4.48 (s, 4H, NH_2), 2.80 (s, 4H, S−CH_2). ^{13}C NMR (100.62 MHz, CD_2Cl_2, 25 °C): δ 34.31, 114.23, 114.82, 118.07, 135.49, 137.22, 149.69.

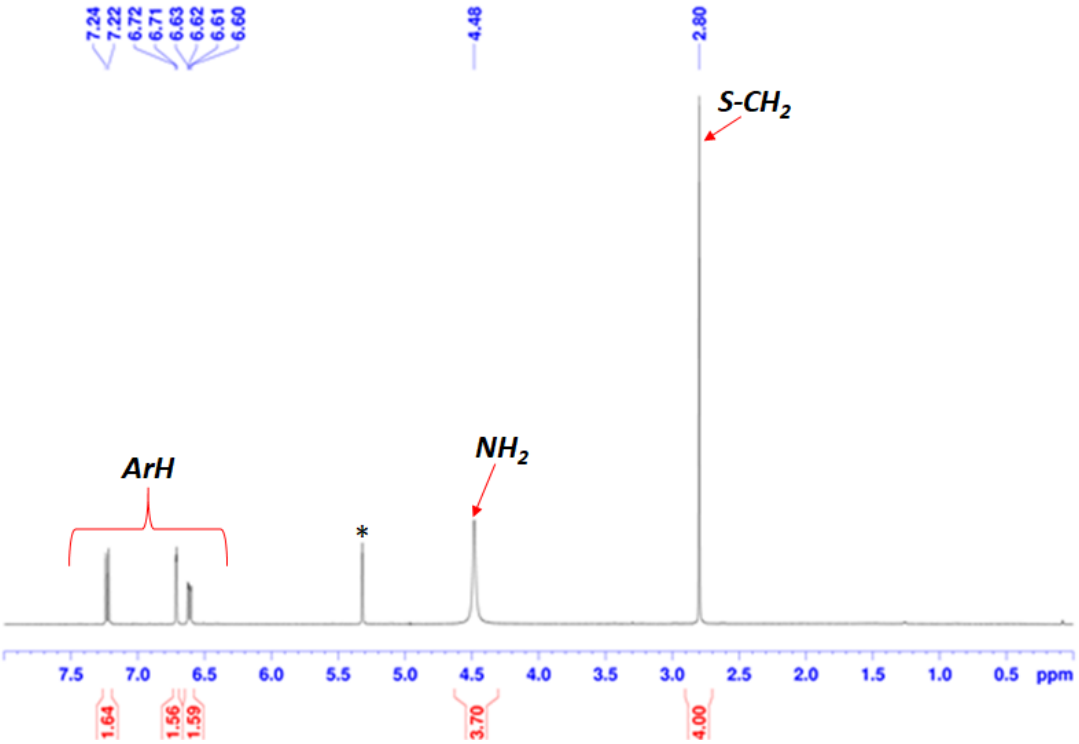

*Figure 129: ^{1}H NMR of NSSN-Cl (400.13 MHz, *CD_2Cl_2, 25°C).*

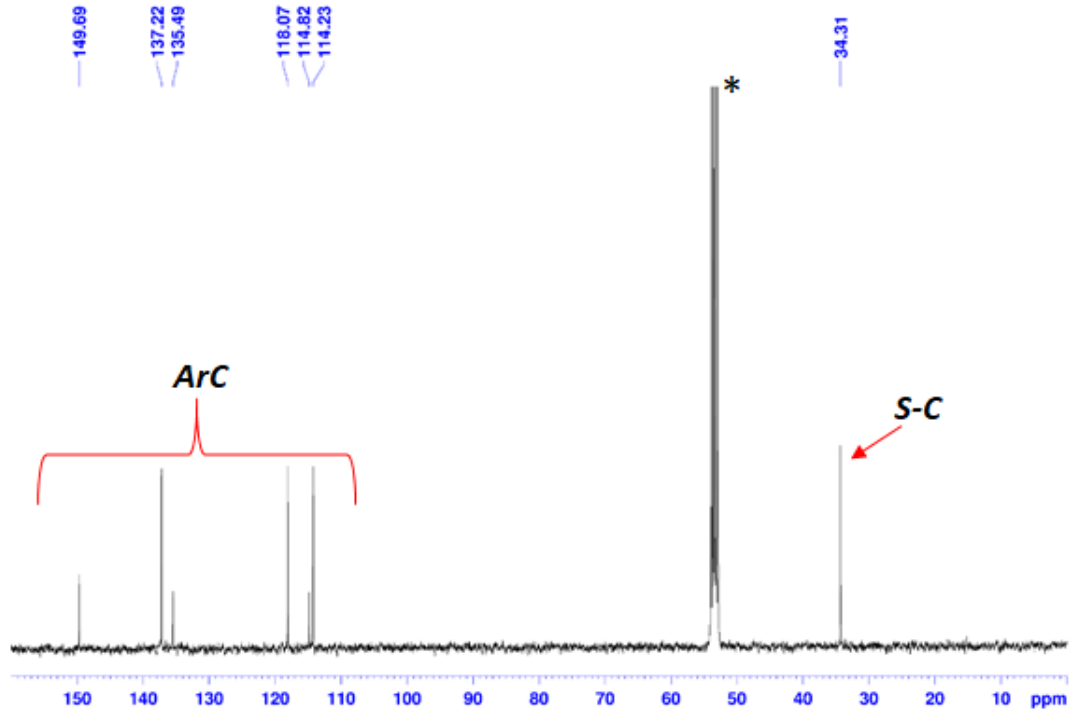

*Figure 130: ^{13}C NMR of NSSN-Cl (100.62 MHz, *CD_2Cl_2, 25°C).*

6.6 *Synthesis and characterization of 6,6'-(ethane-1,2-diylbis(sulfanediyl))bis(3-chloro-N-isopropylaniline)*

6,6'-(ethane-1,2-diylbis(sulfanediyl))bis(3-chloro-N-isopropylaniline) [NSSN-Cl-ISO] was synthesized with a similar procedure reported for *NSSN-ISO* (*figure 131*). *[NSSN-Cl]* (7.59 g, 22 mmol), zinc (14.38 g, 0.22 mol), acetic acid (100 mL), and acetone (12.78 g, 0.22 mol) were added to a 250 mL round-bottom one necked flask equipped with a condenser and a Teflon-sealed stirbar.

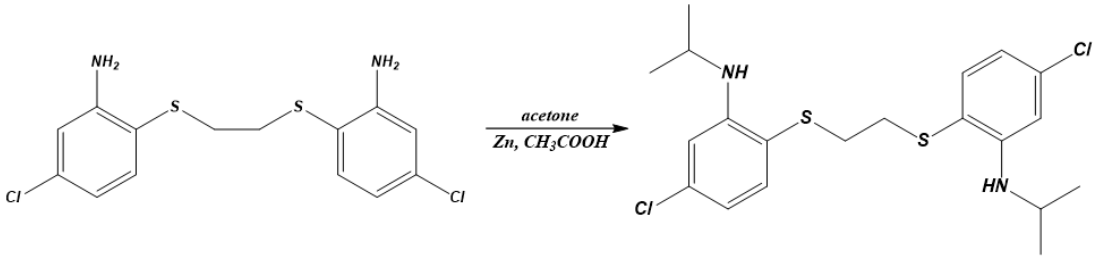

Figure 131: synthesis of NSSN-Cl-ISO ligand.

The mixture was heated to room temperature for 24 h. After it was cooled to room temperature, the mixture was quenched with a 30% NH_3 aqueous solution (150 mL) and dichloromethane (200 mL). The organic layer was dried with anhydrous $MgSO_4$, and a white oil product was obtained upon removal of the solvent. The oil was dissolved in hexane and placed in the freezer. The product is crystallized from hexane as a white solid (8.32 g, yield = 88%).

^{1}H NMR (400.13 MHz, CD_2Cl_2, 25 °C): δ 6.48-7.24 (m, 6H, ArH), 4.98 (s, 2H, NH), 3.56 (m, 2H, N-CH), 2.68 (s, 4H, S-CH_2), 1.19 (d, J = 6.31 Hz, 12H, CH_3).^{13}C NMR (100.62 MHz, CD_2Cl_2, 25 °C): δ 22.37, 34.20, 43.97, 110.16, 114.16, 115.62, 136.22, 137.58, 149.38.

A *NSSN-Cl-ISO* solution (1 mg/mL in CH_2Cl_2) was analyzed by MALDI spectroscopy using hydroxybenzoic acid as matrix and the result was reported in *figure 135*. *HRMS* (MALDI). Calcd for $C_{20}H_{27}Cl_2N_2S_2$ ($[M + H]^+$: m/z 429.0987. Found: m/z 429.1005.

Crystallization of *NSSN-Cl-ISO* from hexane afforded crystals suitable for X-ray analysis. Single crystal structure was reported in *Crystallographic Data (figure 280).*

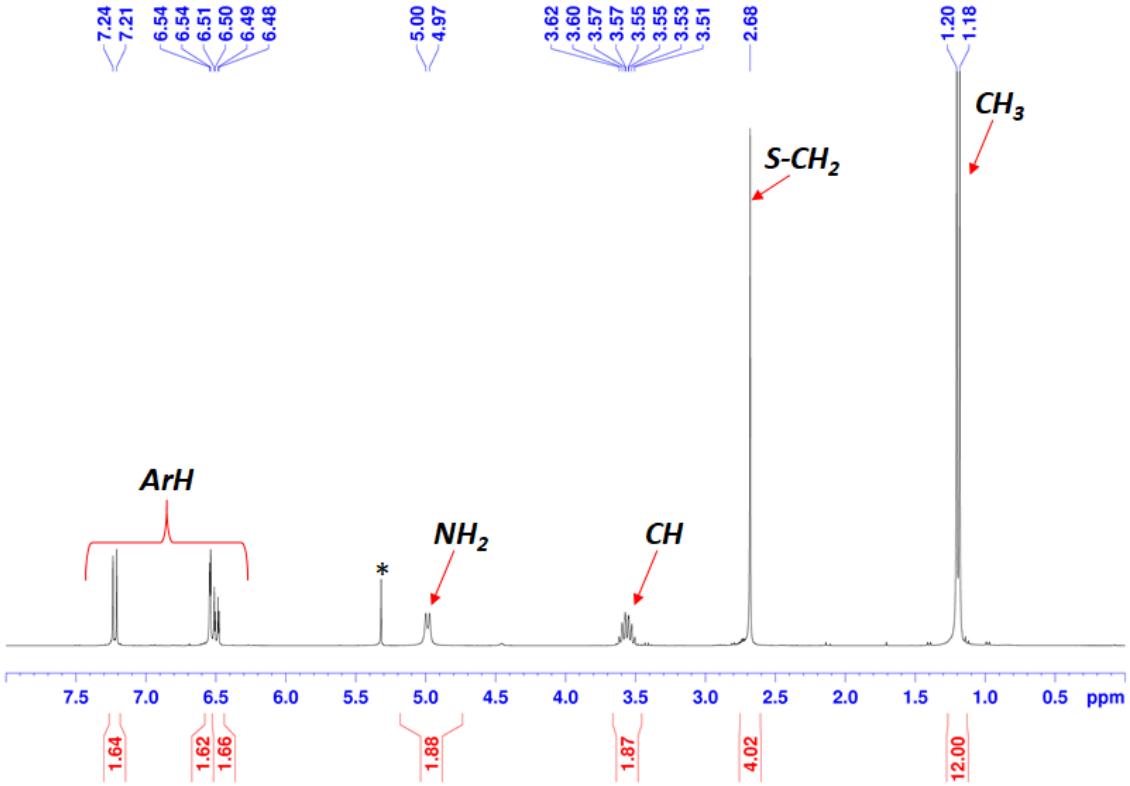

*Figure 132: ^{1}H NMR of NSSN-Cl-ISO ligand (400.13 MHz, *CD_2Cl_2, 25°C).*

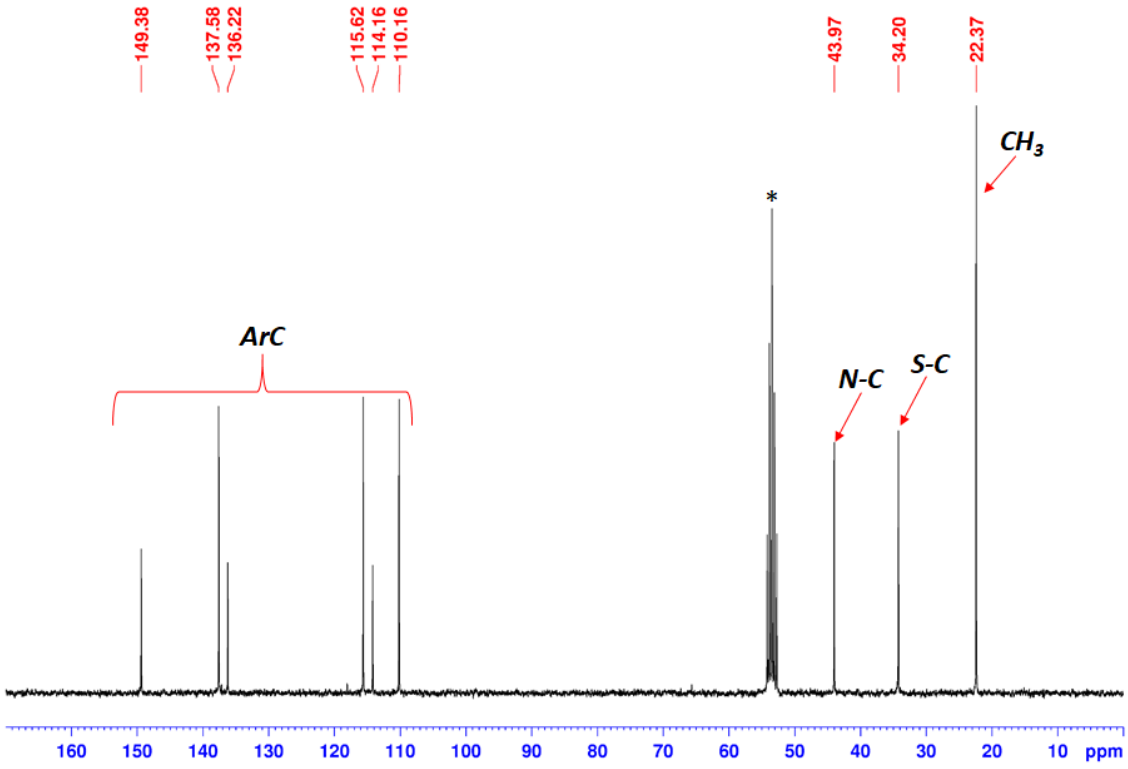

*Figure 133: ^{13}C NMR of NSSN-Cl-ISO ligand (100.62 MHz, *CD_2Cl_2, 25°C).*

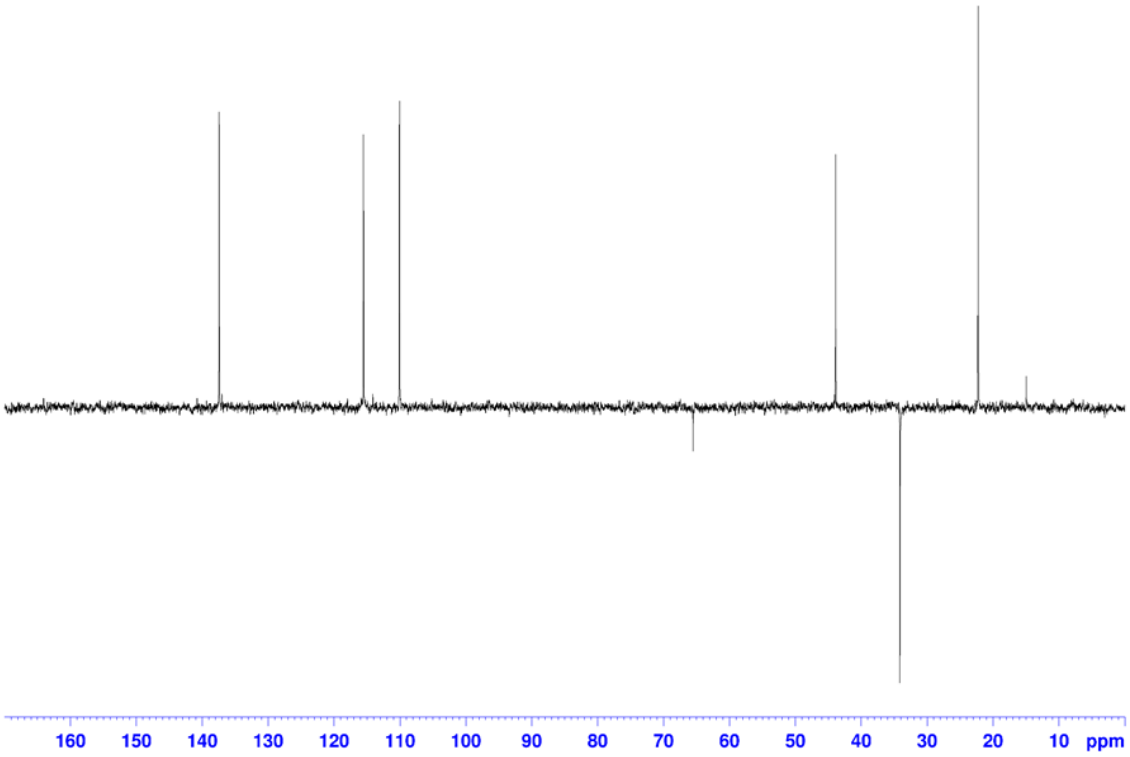

*Figure 134: DEPT 135 of NSSN-Cl-ISO (100.62 MHz, *CD_2Cl_2, 25°C).*

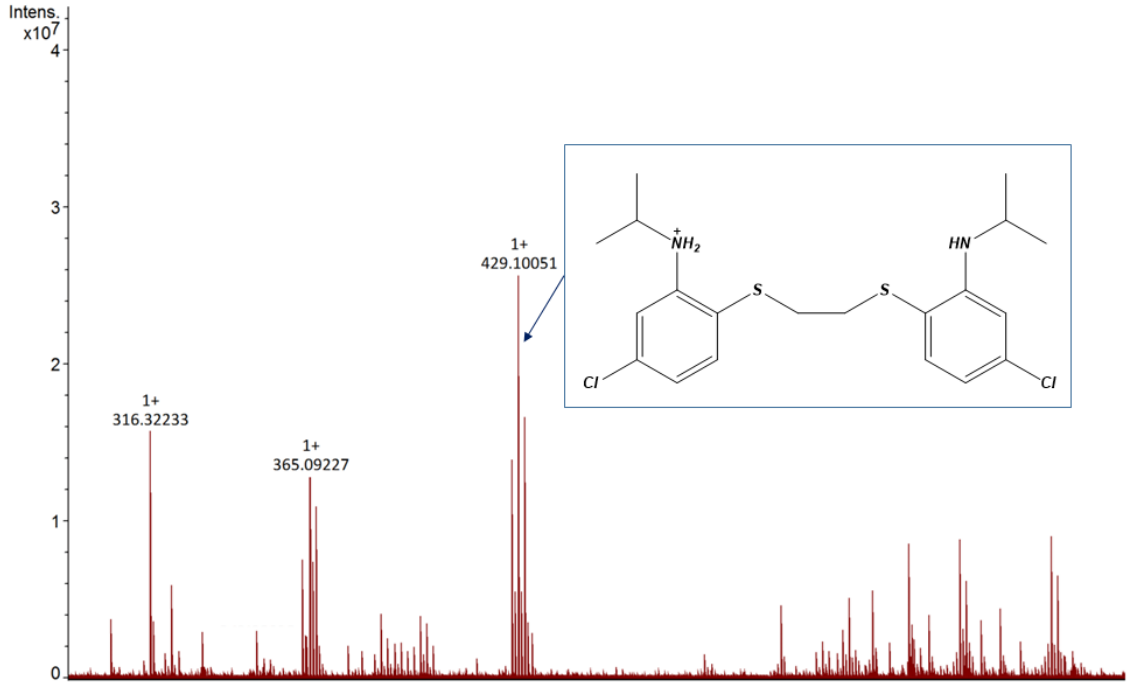

Figure 135: Maldi-MS spectrum of NSSN-Cl-ISO ligand.

6.7 Synthesis and characterization of 2,2'-(propane-1,3-diylbis(sulfanediyl))dianiline

2,2'-(propane-1,3-diylbis(sulfanediyl))dianiline [NSSN-Pr] was synthesized with a similar procedure reported for *NSSN* but replacing 1,2-dibromoethane with 1,3-dibromopropane (*figure 136*). 1,3-dibromopropane (11.51 g, 57 mmol) was added dropwise to a refluxing solution of 2-aminothiophenol (14.27 g, 0.114 mol) and sodium hydroxide (4.56 g, 0.114 mol) in methanol (250 mL). The refluxing reaction mixture was stirred for 4 h.

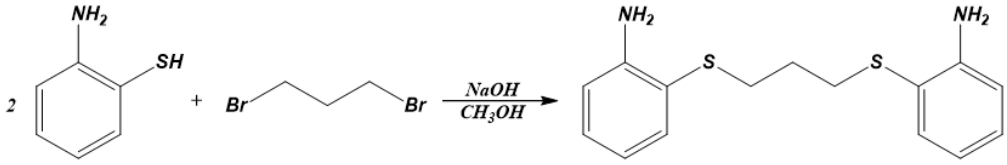

Figure 136: synthesis of NSSN-Pr.

Upon completion of the reaction, the solvent was removed in vacuo and the reaction mixture was cooled to room temperature. Water (70 mL) was added and the reaction mixture was extracted with dichloromethane (3x50 mL). The organic layer was dried with anhydrous $MgSO_4$ and evaporated to dryness in vacuo to get a yellow solid product (15.21 g, yield = 92%).

^{1}H NMR (400.13 MHz, $CDCl_3$, 25 °C): δ 6.65−7.14 (m, 8H, ArH), 4.24 (s, 4H, NH_2), 2.82 (t, 4H, S−CH_2), 1.79 (q, 2H, CH_2). ^{13}C NMR (100.62 MHz, $CDCl_3$, 25 °C): δ 29.16, 33.39, 114.96, 117.41, 118.54, 129.82, 136.12, 148.39.

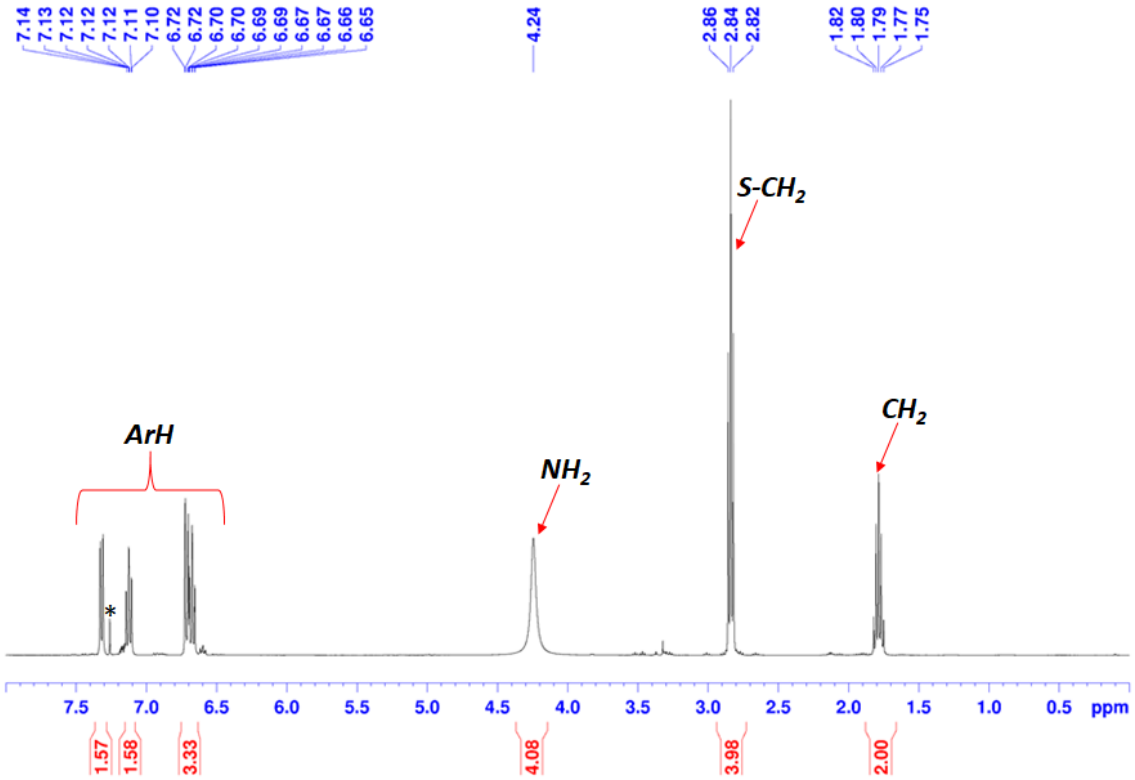

*Figure 137: ^{1}H NMR of NSSN-Pr (400.13 MHz, *$CDCl_3$, 25°C).*

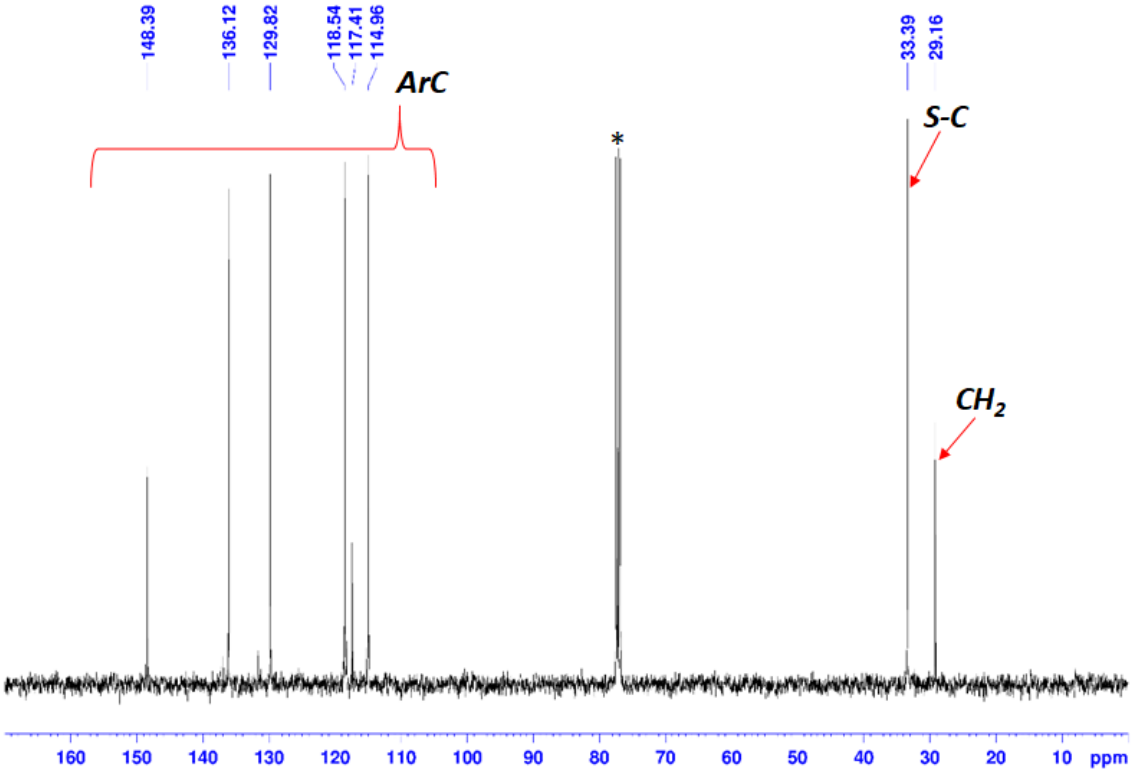

*Figure 138: ^{13}C NMR of NSSN-Pr (100.62 MHz, *$CDCl_3$, 25°C).*

6.8 Synthesis and characterization of 2,2'-(propane-1,3-diylbis(sulfanediyl))bis(N-isopropylaniline)

2,2'-(propane-1,3-diylbis(sulfanediyl))bis(N-isopropylaniline) [NSSN-Pr-ISO] was synthesized with a similar procedure reported for *NSSN-ISO* (*figure 139*). *[NSSN-Pr]* (15.21 g, 52 mmol), zinc (34 g, 0.52 mol), acetic acid (150 mL), and acetone (30.20 g, 0.52 mol) were added to a 250 mL round-bottom one necked flask equipped with a condenser and a Teflon-sealed stirbar. The mixture was heated to room temperature for 24 h.

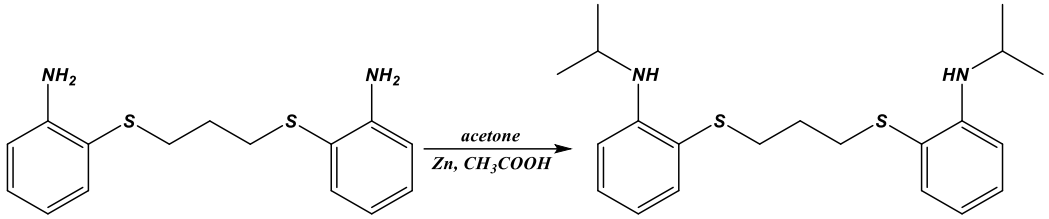

Figure 139: synthesis of NSSN-Pr-ISO ligand.

After it was cooled to room temperature, the mixture was quenched with a 30% NH_3 aqueous solution (200 mL) and dichloromethane (200 mL). The organic layer was dried with anhydrous $MgSO_4$, and an orange oil product was obtained upon removal of the solvent. The oil was dissolved in pentane and placed in the freezer. The product is crystallized from pentane as an orange solid (14.22 g, yield = 73%).

^{1}H NMR (400.13 MHz, $CDCl_3$, 25 °C): δ 6.55-7.33 (m, 8H, ArH), 4.94 (s, 2H, NH), 3.67 (m, 2H, N-CH), 2.79 (t, 4H, S-CH_2), 1.77 (q, 2H, CH_2), 1.26 (d, J = 6.29 Hz, 12H, CH_3). ^{13}C NMR (100.62 MHz, $CDCl_3$, 25 °C): δ 23.04, 29.01, 33.48, 44.07, 110.66, 116.18, 116.80, 130.20, 136.63, 148.48.

A *NSSN-Pr-ISO* solution (1 mg/mL in CH_2Cl_2) was analyzed by MALDI spectroscopy using hydroxybenzoic acid as matrix and the result was reported in *figure 143*. *HRMS* (MALDI). Calcd for $C_{21}H_{31}N_2S_2$ ($[M + H]^+$: m/z 375.1923. Found: m/z 375.1944.

Crystallization of *NSSN-Pr-ISO* from hexane afforded crystals suitable for X-ray analysis. Single crystal structure was reported in *Crystallographic Data (figure 278).*

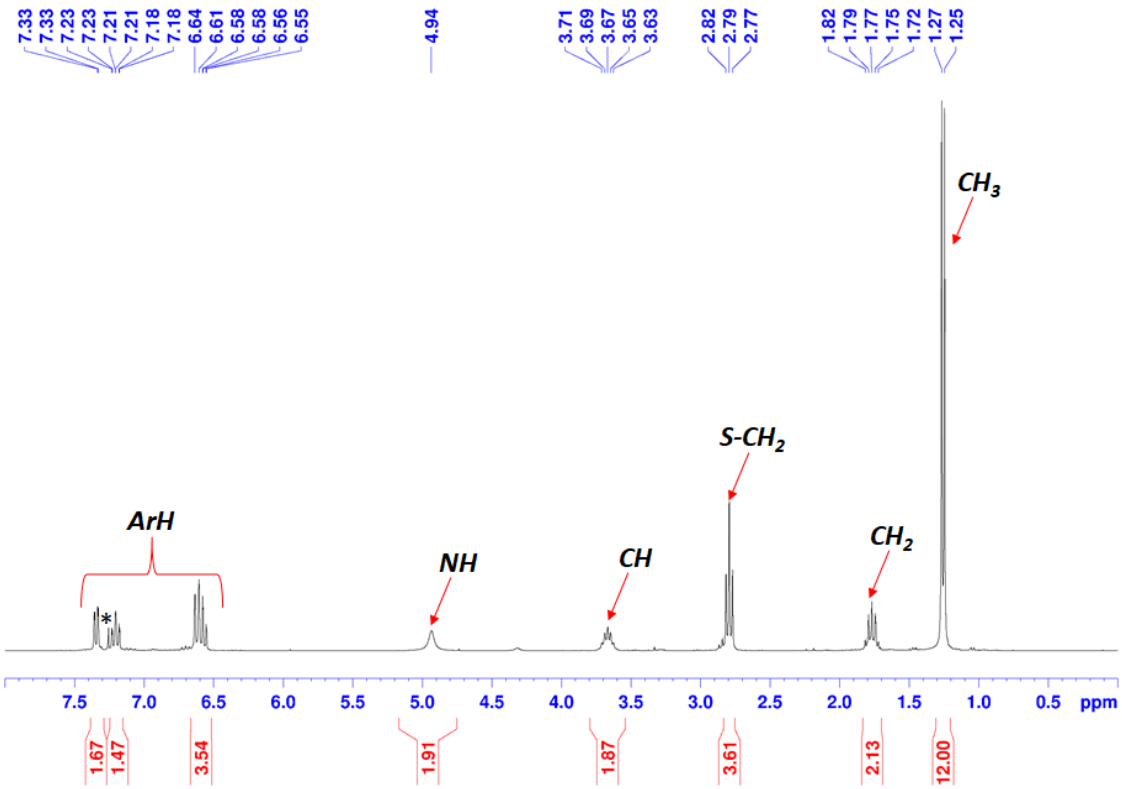

*Figure 140: ^{1}H NMR of NSSN-Pr-ISO ligand (400.13 MHz, *$CDCl_3$, 25°C).*

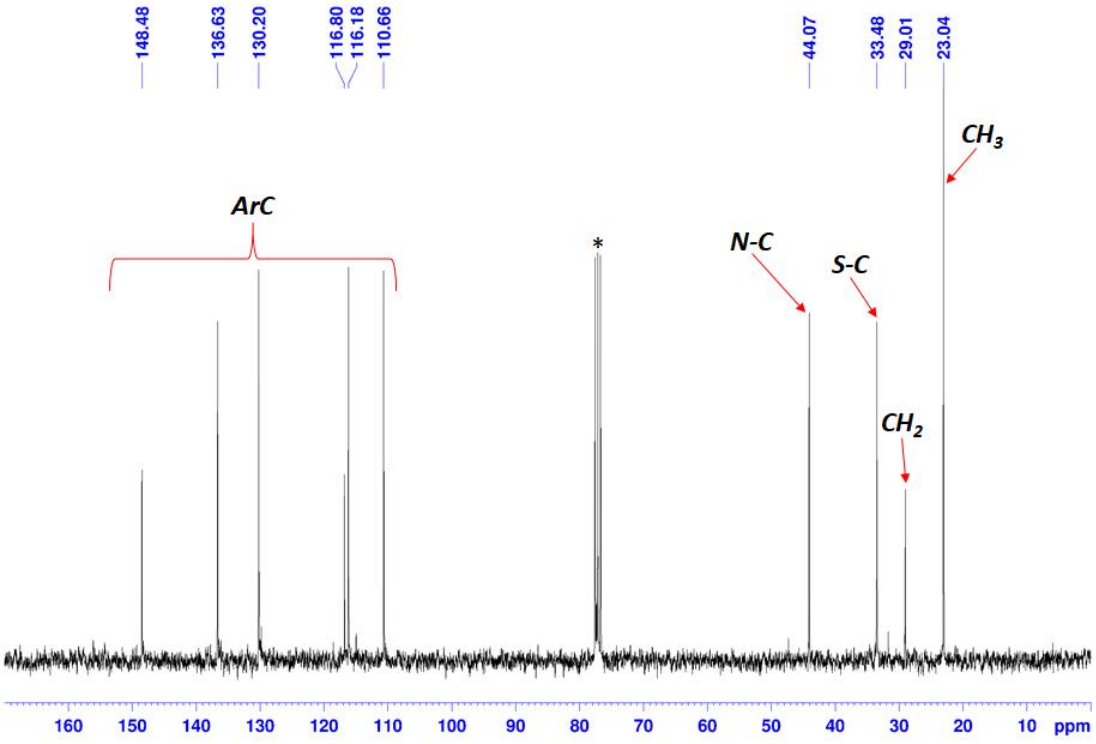

*Figure 141: ^{13}C NMR of NSSN-Pr-ISO ligand (100.62 MHz, *$CDCl_3$, 25°C).*

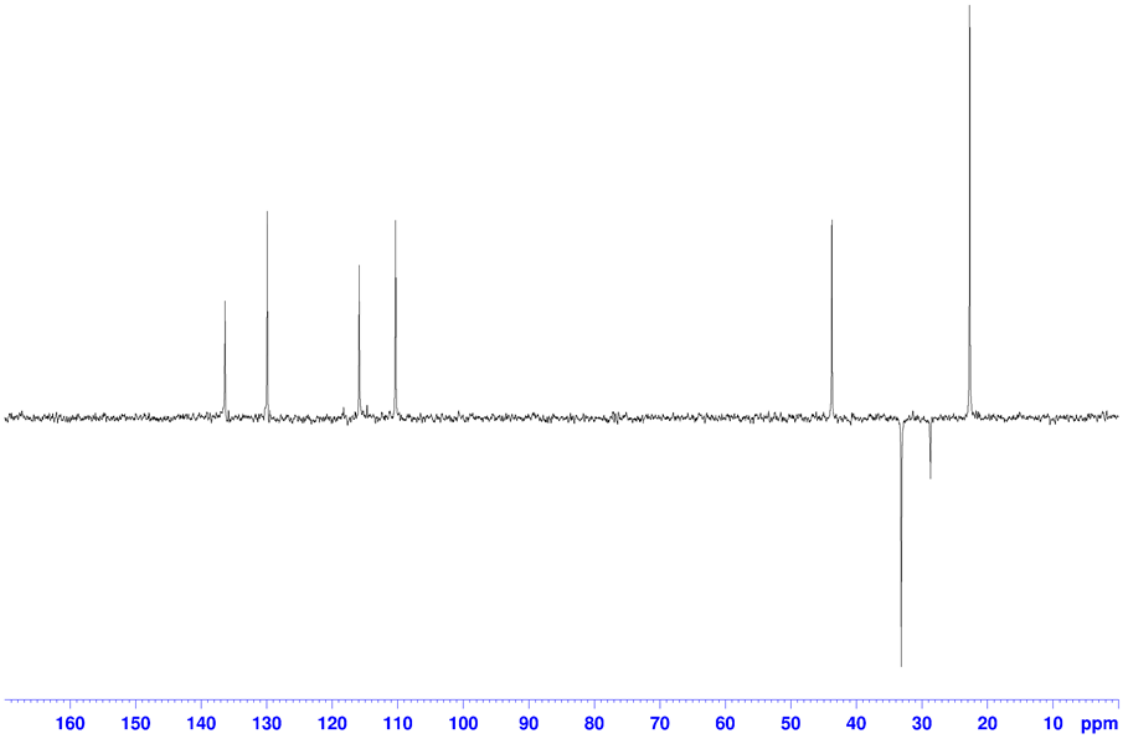

*Figure 142: DEPT 135 NMR of NSSN-Pr-ISO ligand (100.62 MHz, *$CDCl_3$, 25°C).*

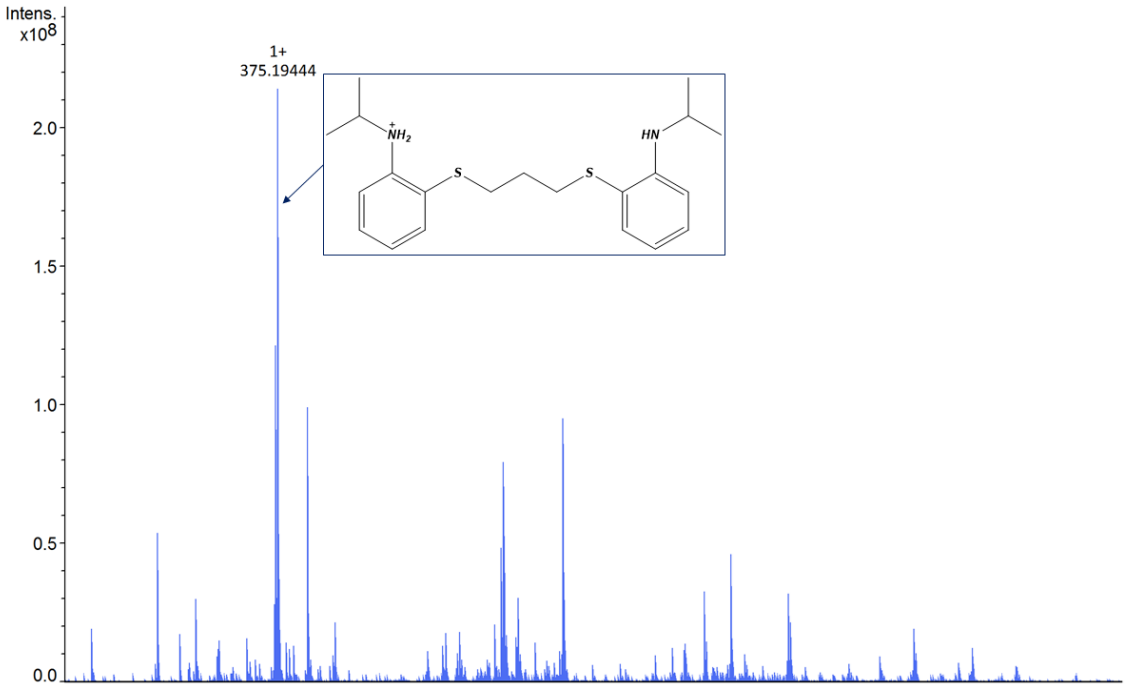

Figure 143: Maldi-MS spectrum of NSSN-Pr-ISO ligand.

6.9 Synthesis and characterization of 2,2'-(heptane-1,7-diylbis(sulfanediyl))dianiline

2,2'-(heptane-1,7-diylbis(sulfanediyl))dianiline [NSSN-Hep] was synthesized with a similar procedure reported for *NSSN* but replacing 1,2-dibromoethane with 1,7-dibromoheptane (*figure 144*). 1,7-dibromoheptane (5.32 g, 21 mmol) was added dropwise to a refluxing solution of 2-aminothiophenol (5.26 g, 42 mmol) and sodium hydroxide (1.68 g, 42 mmol) in ethanol (150 mL). The refluxing reaction mixture was stirred for 7 h.

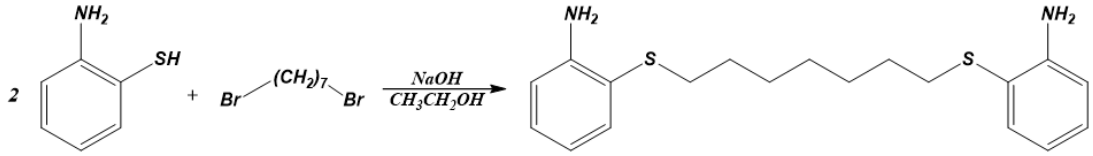

Figure 144: synthesis of NSSN-Hep.

Upon completion of the reaction, the solvent was removed in vacuo and the reaction mixture was cooled to room temperature. Water (70 mL) was added and the reaction mixture was extracted with diethyl ether (3x50 mL). The organic layer was dried with anhydrous $MgSO_4$ and evaporated to dryness in vacuo to get a yellow oil, which corresponds, to the desired product (6.32 g, yield = 87%).

^{1}H NMR (400.13 MHz, CD_2Cl_2, 25 °C): δ 6.52−7.00 (m, 8H, ArH), 4.27 (s, 4H, NH_2), 2.60 (t, 4H, S−CH_2), 1.14-1.47 (m, 10H, CH_2). ^{13}C NMR (100.62 MHz, CD_2Cl_2, 25 °C): δ 28.82, 29.00, 29.85, 34.98, 114.98, 118.39, 118.44, 129.63, 135.72, 148.64.

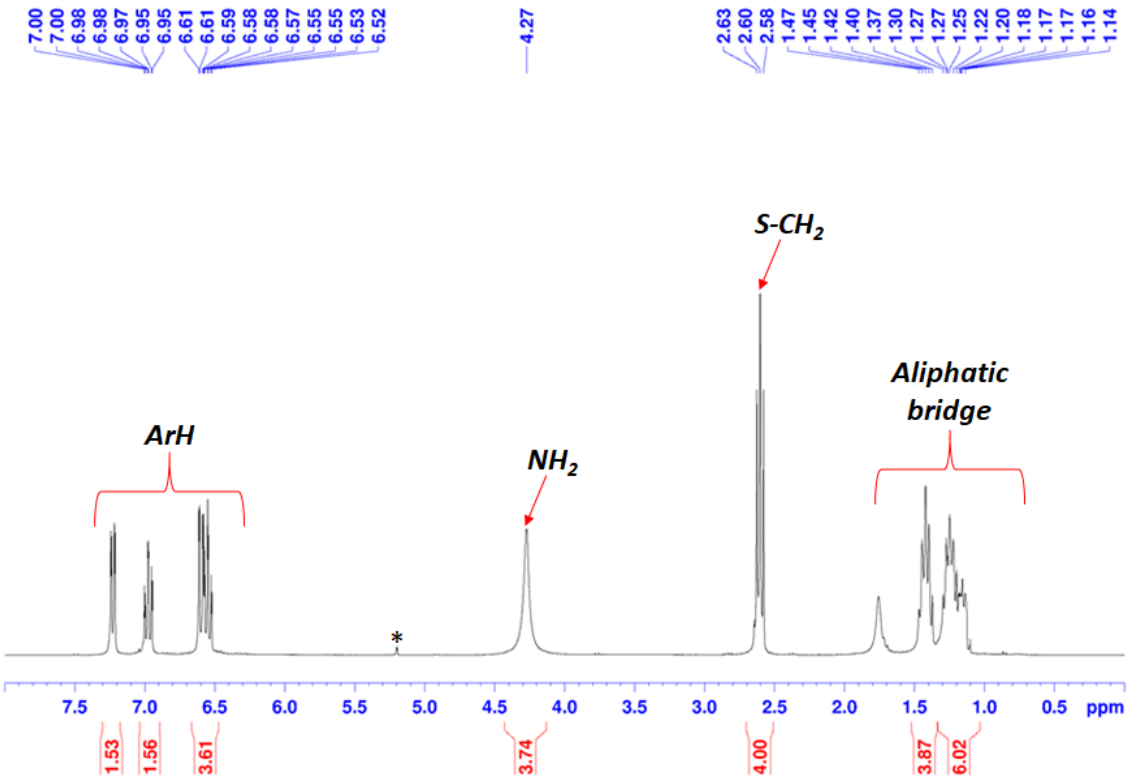

*Figure 145: ^{1}H NMR of NSSN-Hep (400.13 MHz, *CD_2Cl_2, 25°C).*

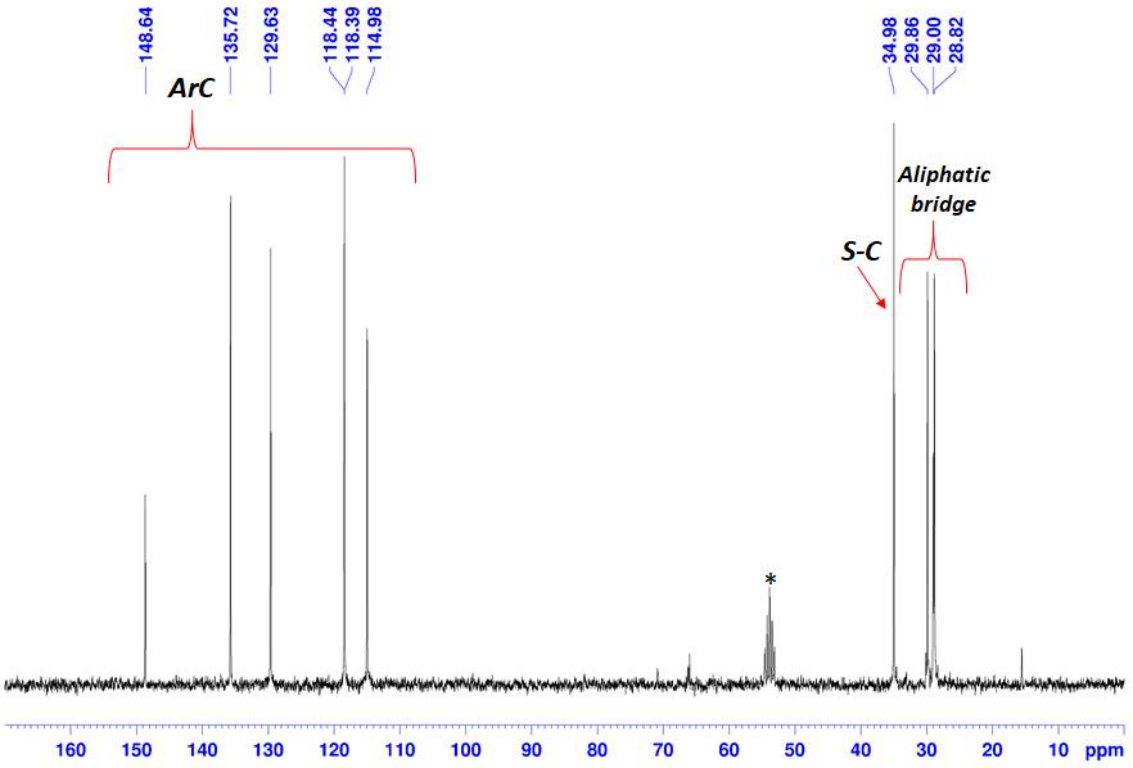

*Figure 146: ^{13}C NMR of NSSN-Hep (100.62 MHz, *CD_2Cl_2, 25°C).*

6.10 Synthesis and characterization of 2,2'-(heptane-1,7-diylbis(sulfanediyl))bis(N-isopropylaniline)

2,2'-(heptane-1,7-diylbis(sulfanediyl))bis(N-isopropylaniline) [NSSN-Hep-ISO] was synthesized with a similar procedure reported for *NSSN-ISO* (*figure 147*). *[NSSN-Hep]* (6.32 g, 18 mmol), zinc (11.78 g, 0.18 mol), acetic acid (100 mL), and acetone (10.45, 0.18 mol) were added to a 250 mL round-bottom onenecked flask equipped with a condenser and a Teflon-sealed stirbar. The mixture was heated to room temperature for 24 h.

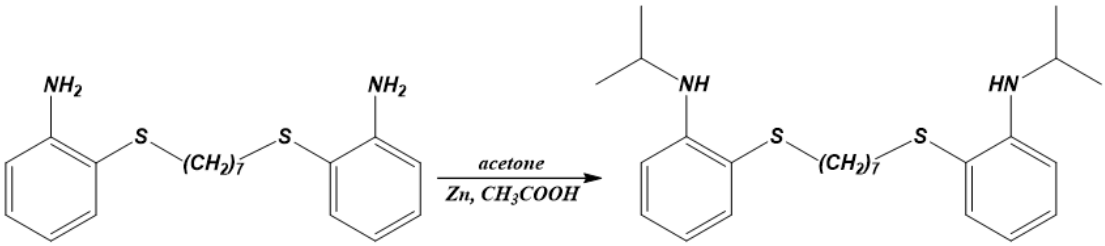

Figure 147: synthesis of NSSN-Hep-ISO ligand.

After it was cooled to room temperature, the mixture was quenched with a 30% NH_3 aqueous solution (150 mL) and dichloromethane (200 mL). The organic layer was dried with anhydrous $MgSO_4$, and an orange solid product was obtained upon removal of the solvent (5.02 g, yield = 65%).

^{1}H NMR (400.13 MHz, CD_2Cl_2, 25 °C): δ 6.59-7.41 (m, 8H, ArH), 4.91 (s, 2H, NH), 3.70 (m, 2H, N-CH), 2.71 (t, 4H, S-CH_2), 1.20-1.61 (m, 22H, CH_2+CH_3). ^{13}C NMR (100.62 MHz, CD_2Cl_2, 25 °C): δ 23.15, 28.96, 29.15, 29.99, 35.51, 44.44, 110.92, 116.41, 118.41, 130.18, 136.51, 148.85.

A *NSSN-Hep-ISO* solution (1 mg/mL in CH_2Cl_2) was analyzed by MALDI spectroscopy using hydroxybenzoic acid as matrix and the result was reported in *figure 151*. *HRMS* (MALDI). Calcd for $C_{25}H_{39}N_2S_2$ ($[M + H]^+$: m/z 431.2549. Found: m/z 430.2506.

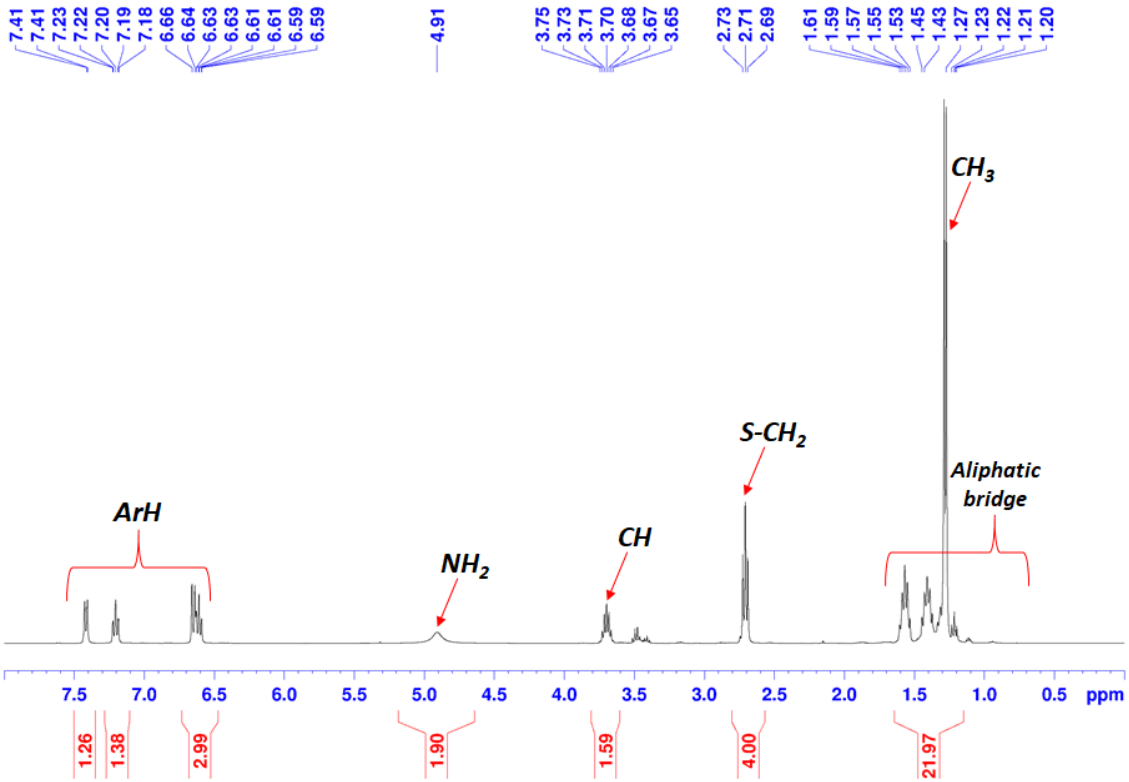

*Figure 148: ^{1}H NMR of NSSN-Hep-ISO ligand (400.13 MHz, *CD_2Cl_2, 25°C).*

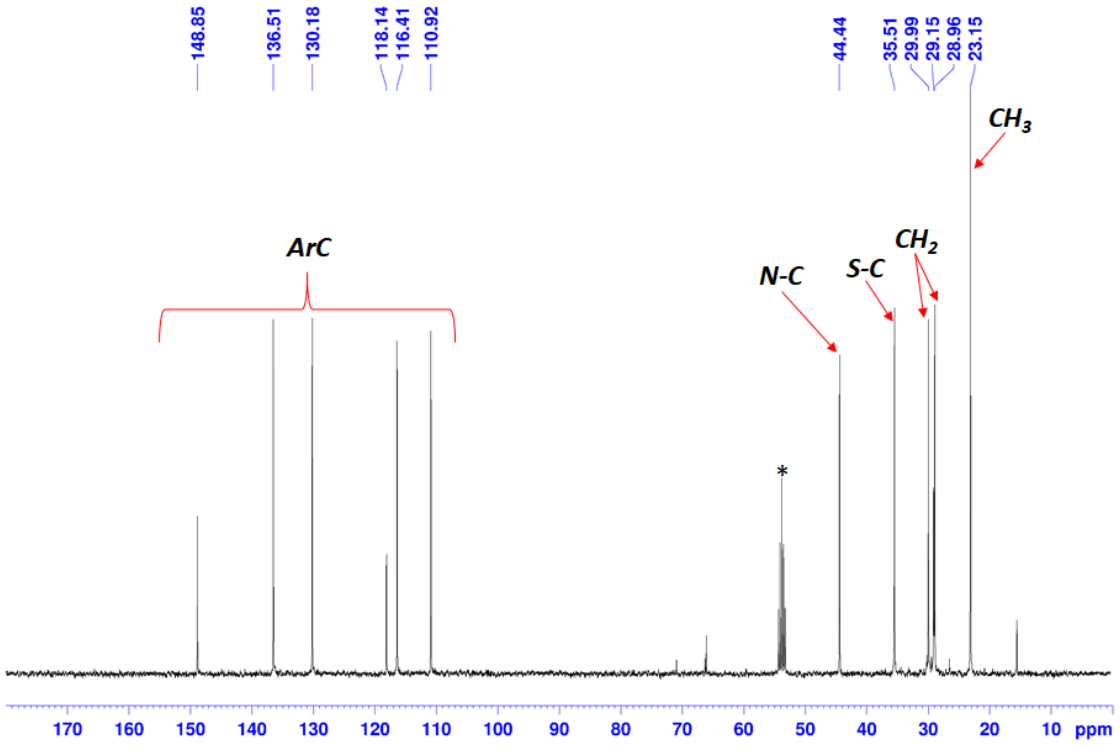

*Figure 149: ^{13}C NMR of NSSN-Hep-ISO ligand (100.62 MHz, *CD_2Cl_2, 25°C).*

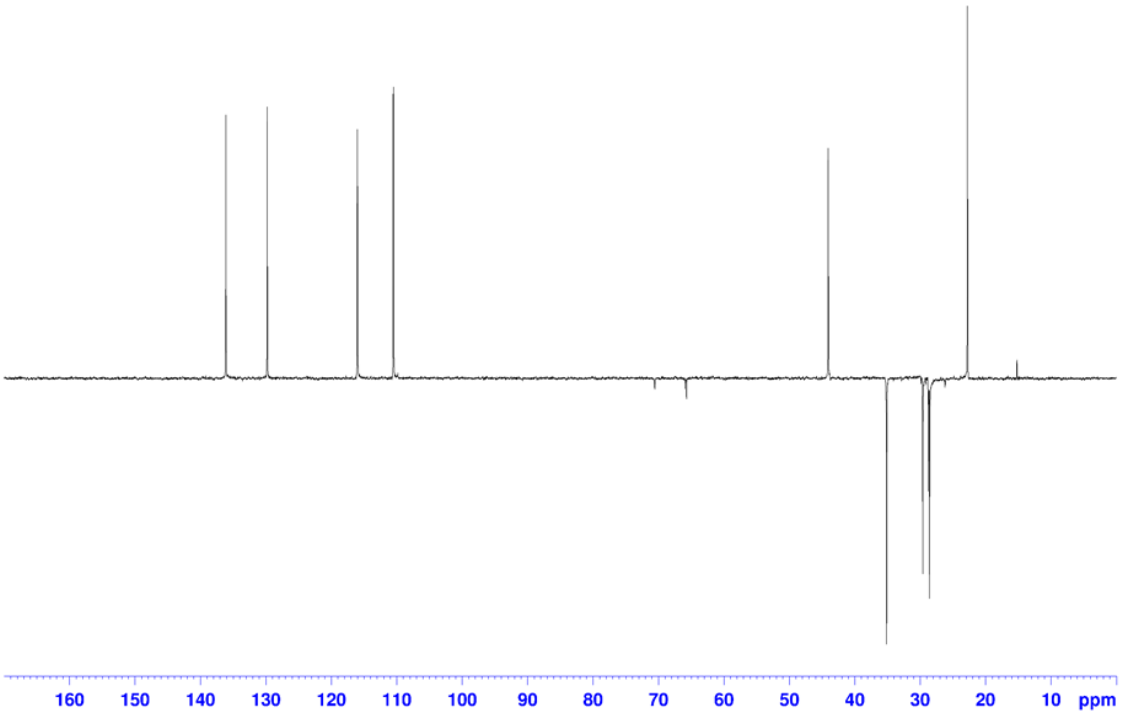

*Figure 150: DEPT 135 NMR of NSSN-Hep-ISO ligand (100.62 MHz, *CD_2Cl_2, 25°C).*

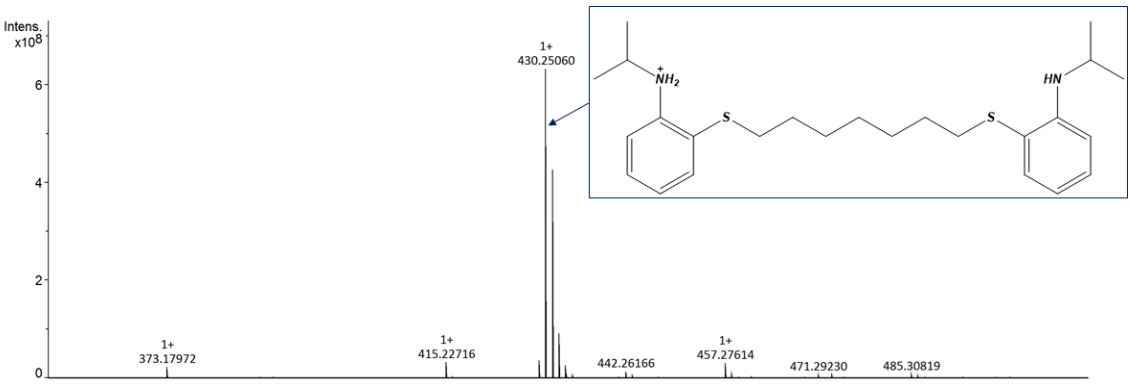

Figure 151: Maldi-MS spectrum of NSSN-Hep-ISO ligand.

6.11 Synthesis and characterization of 2,2'-((1,4-phenylenebis(methylene))bis(sulfanediyl))dianiline

A solution of α,α'-Dibromo-p-xylene (10.43 g, 40 mmol) in tetrahydrofuran (100 mL) was added dropwise to a refluxing solution of 2-aminothiophenol (10.01 g, 80 mmol) and sodium hydroxide (3.2 g, 80 mmol) in ethanol (250 mL) (*figure 152*). The refluxing reaction mixture was stirred for 1 h.

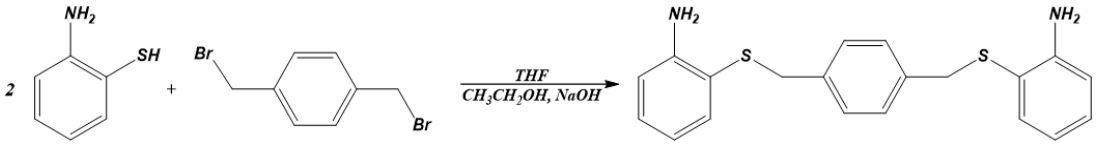

Figure 152: synthesis of NSSN-Xy.

Upon completion of the reaction, the solvent was removed in vacuo and the reaction mixture was cooled to room temperature. Water (70 mL) was added and the reaction mixture was extracted with dichloromethane (3x50 mL). The organic layer was dried with anhydrous $MgSO_4$ and evaporated to dryness in vacuo to get a white solid product (10.81 g, yield = 78%).

^{1}H NMR (400.13 MHz, CD_2Cl_2, 25 °C): δ 6.58-7.12 (m, 12H, ArH), 4.25 (s, 4H, NH_2), 3.86 (s, 4H, S-CH_2). ^{13}C NMR (100.62 MHz, CD_2Cl_2, 25 °C): δ 39.42, 115.06, 117.42, 118.49, 129.14, 130.29, 136.61, 137.59. 149.17.

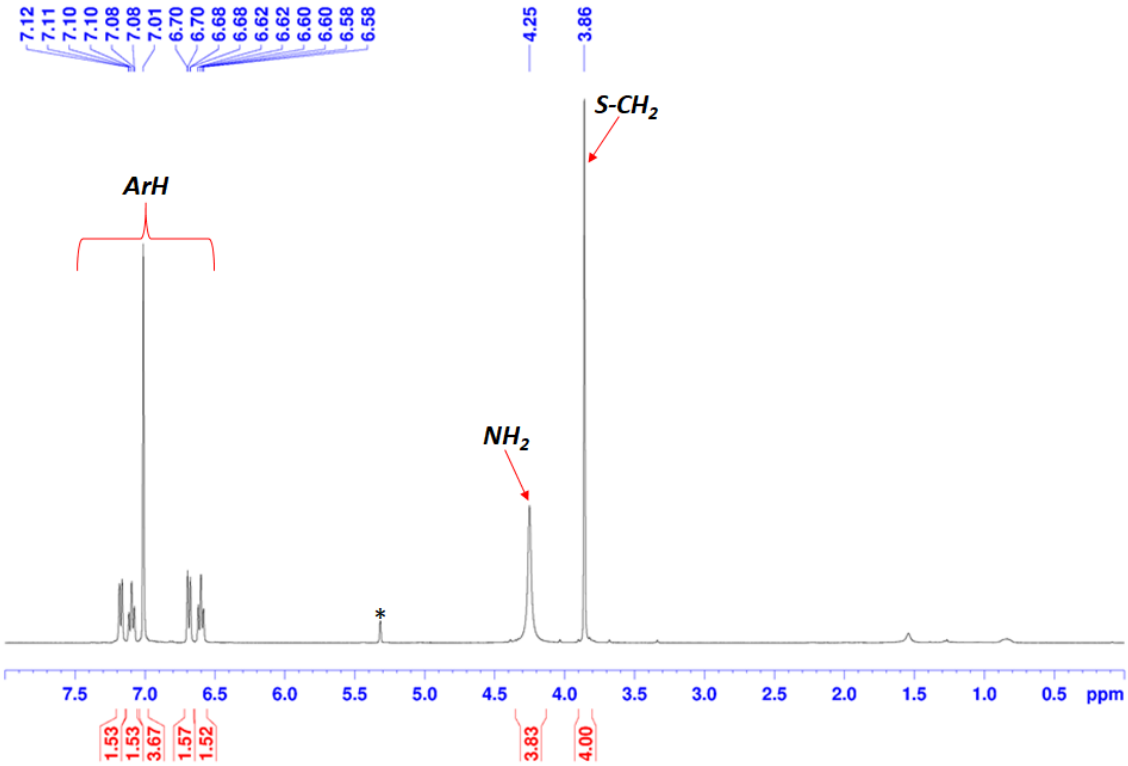

*Figure 153: ^{1}H NMR of NSSN-Xy (400.13 MHz, *CD_2Cl_2, 25°C).*

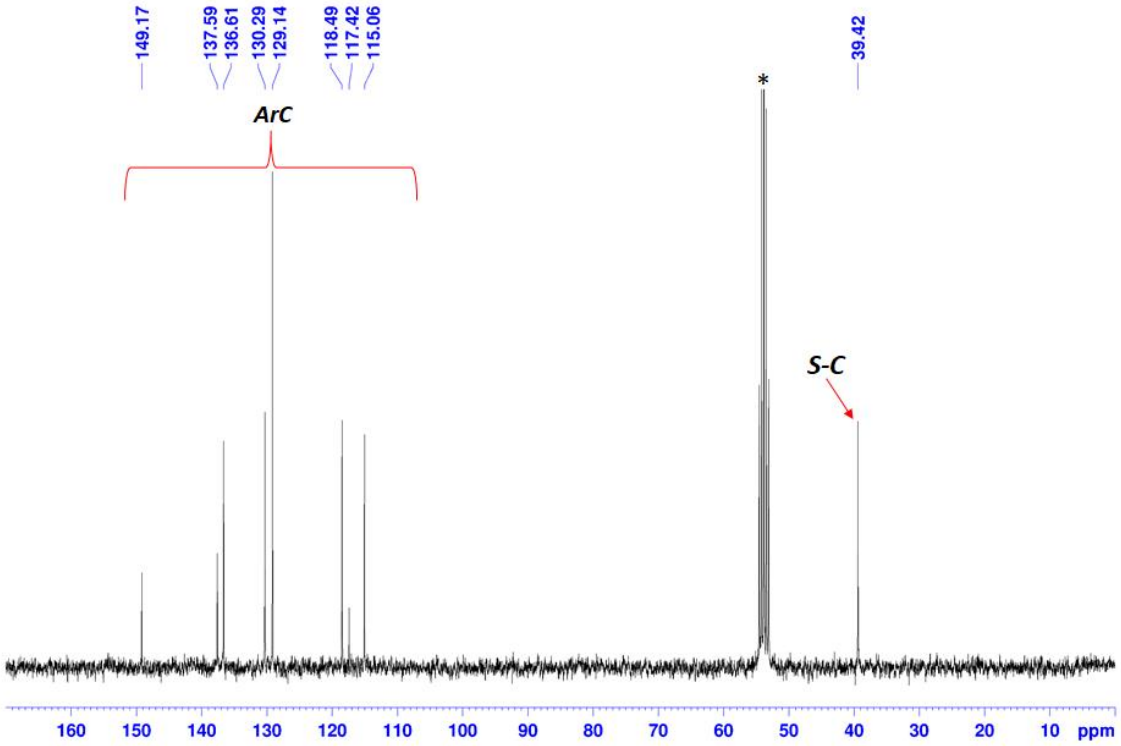

*Figure 154: ^{13}C NMR of NSSN-Xy (100.62 MHz, *CD_2Cl_2, 25°C).*

6.12 Synthesis and characterization of 2,2'-((1,4-phenylenebis(methylene))bis(sulfanediyl))bis(N-isopropylaniline)

2,2'-((1,4-phenylenebis(methylene)bis(sulfanediyl))bis(N-isopropylaniline) [NSSN-Xy-ISO] was synthesized with a similar procedure reported for *NSSN-ISO* (*figure 155*). *[NSSN-Xy]* (7.32 g, 21 mmol), zinc (13.58 g, 0.21 mol), acetic acid (100 mL), and acetone (12.20 g, 0.21 mol) were added to a 250 mL round-bottom one necked flask equipped with a condenser and a Teflon-sealed stirbar. The mixture was heated to room temperature for 24 h.

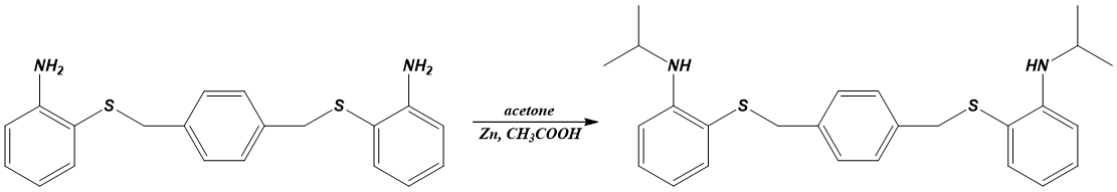

Figure 155: synthesis of NSSN-Xy-ISO ligand.

After it was cooled to room temperature, the mixture was quenched with a 30% NH_3 aqueous solution (150 mL) and dichloromethane (200 mL). The organic layer was dried with anhydrous $MgSO_4$, and a brown solid product was obtained upon removal of the solvent (6.51 g, yield = 71%).

^{1}H NMR (400.13 MHz, CD_2Cl_2, 25 °C): δ 6.48-7.21 (m, 12H, ArH), 4.88 (s, 2H, NH), 3.81 (s, 4H, S-CH_2), 3.60 (m, 2H, N-CH), 1.18 (d, J = 6.25 Hz, 12H, CH_3). ^{13}C NMR (100.62 MHz, CD_2Cl_2, 25 °C): 22.99, 39.69, 44.27, 110.83, 116.23, 117.15, 129.17, 130.64, 137.03, 137.63, 148.94.

A *NSSN-Xy-ISO* solution (1 µg/mL in CH_2Cl_2) was analyzed by electrospray spectroscopy and the result was reported in *figure 159*. *HRMS* (ESI). Calcd for $C_{26}H_{33}N_2S_2$ ($[M + H]^+$: m/z 437.2080. Found: m/z 437.2080.

Crystallization of *NSSN-Xy-ISO* from pentane afforded crystals suitable for X-ray analysis. Single crystal structure was reported in *Crystallographic Data (figure 279).*

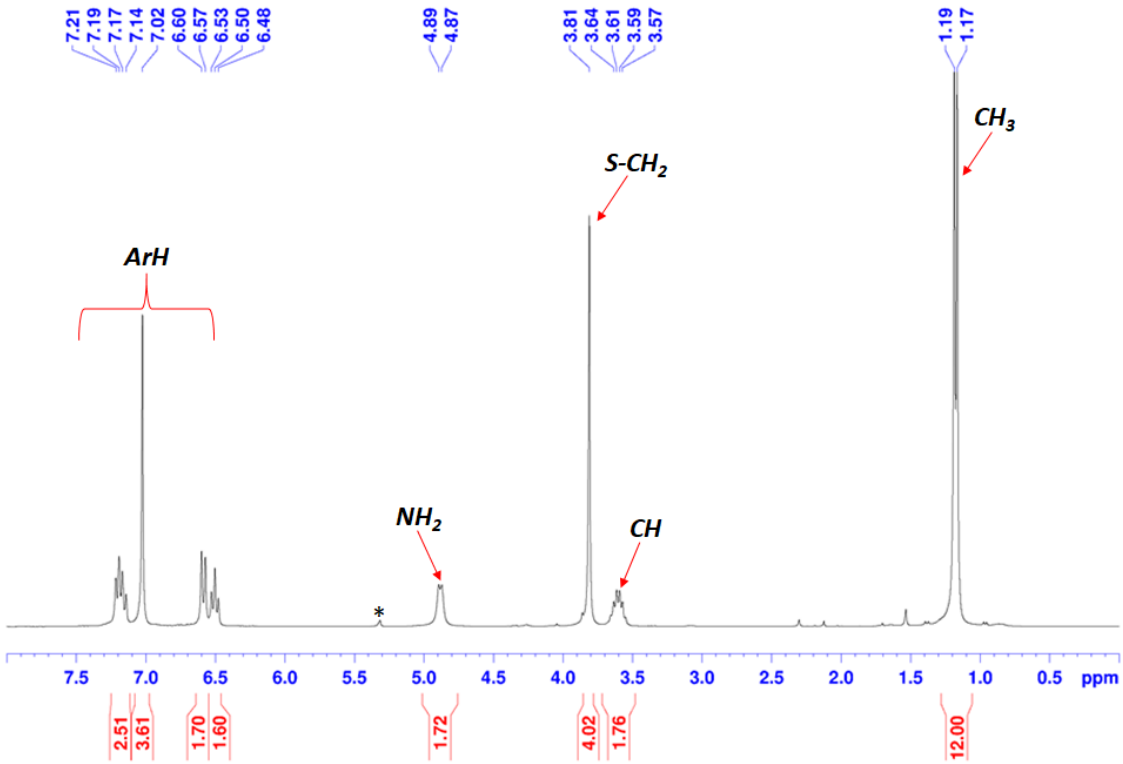

*Figure 156: ^{1}H NMR of NSSN-Xy-ISO ligand (400.13 MHz, *CD_2Cl_2, 25°C).*

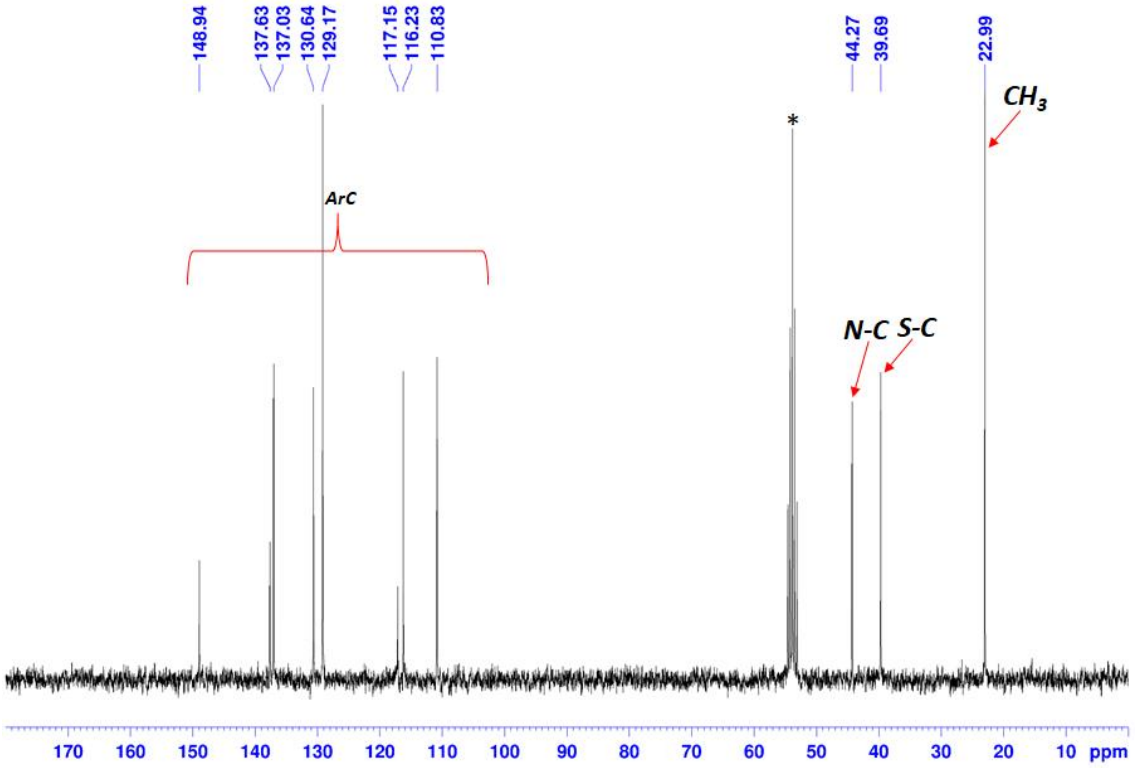

*Figure 157: ^{13}C NMR of NSSN-Xy-ISO ligand (100.62 MHz, *CD_2Cl_2, 25°C).*

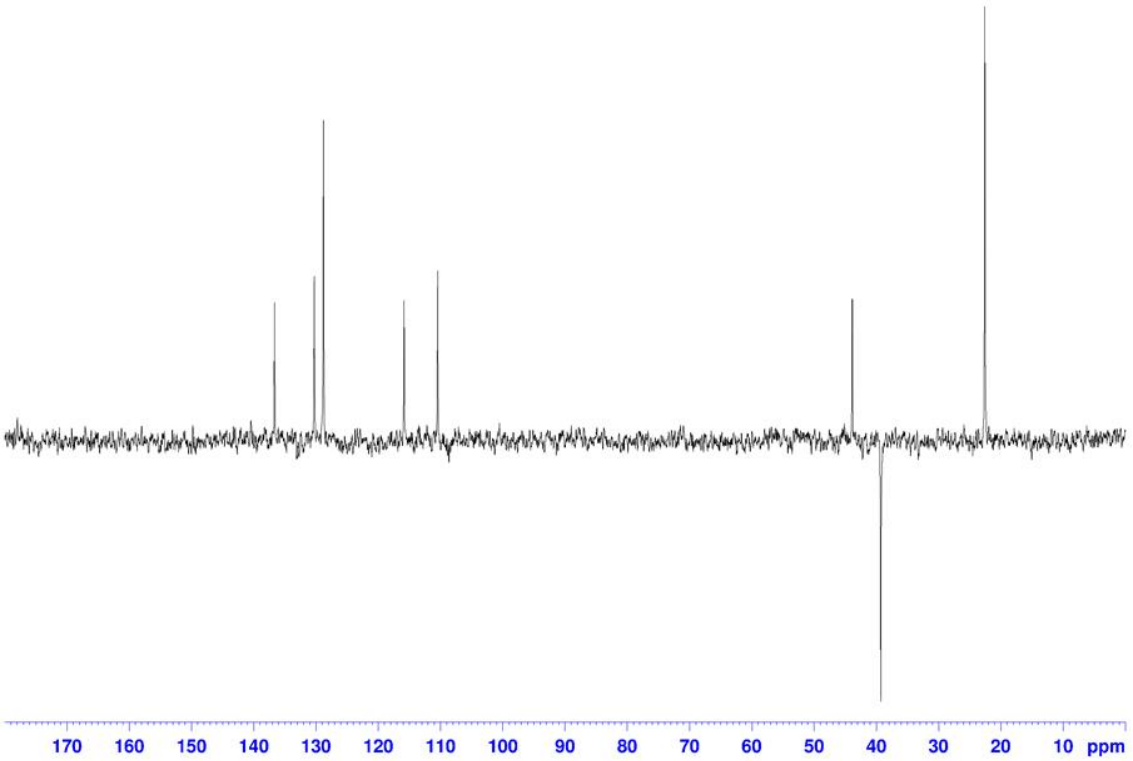

*Figure 158: DEPT 135 NMR of NSSN-Xy-ISO ligand (100.62 MHz, *CD_2Cl_2, 25°C).*

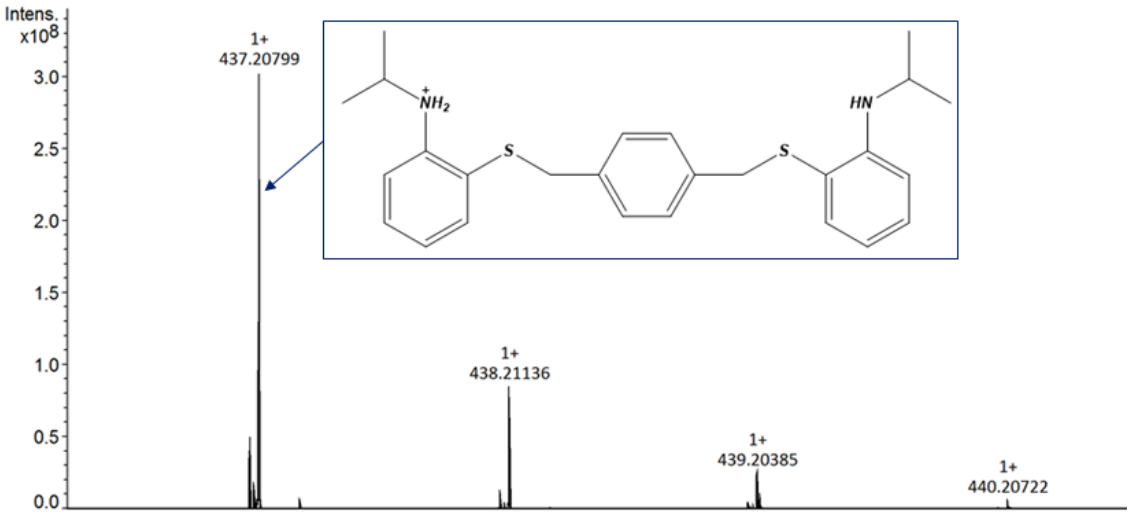

Figure 159: ESI-MS spectrum of NSSN-Xy-ISO ligand.

6.13 Synthesis and characterization of 2-(ethyltio)aniline

2-(ethyltio)aniline [NSEt] was was synthesized with a similar procedure reported for *NSSN* but replacing 1,2-dibromoethane with bromoethane (*figure 160*). Bromoethane (10.24 g, 94 mmol) was added dropwise to a refluxing solution of 2-aminothiophenol (10.72 g, 86 mmol) and sodium hydroxide (3.77 g, 94 mmol) in ethanol (150 mL). The refluxing reaction mixture was stirred for 1 h.

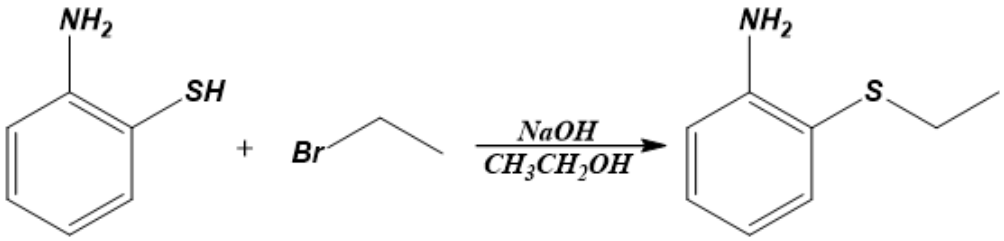

Figure 160: synthesis of NSEt.

Upon completion of the reaction, the solvent was removed in vacuo and the reaction mixture was cooled to room temperature. Water (60 mL) was added and the reaction mixture was extracted with diethyl ether (3x60 mL). The organic layer was dried with anhydrous $MgSO_4$ and evaporated to dryness in vacuo to get a yellow oil product (10.96 g, yield = 83%).

^{1}H NMR (400.13 MHz, CD_2Cl_2, 25 °C): δ 6.66-7.37 (m, 4H, ArH), 4.38 (s, 2H, NH_2), 2.76 (q, 2H, S-CH_2), 1.21 (t, 3H, CH_3). ^{13}C NMR (100.62 MHz, CD_2Cl_2, 25 °C): δ 15.06, 29.11, 114.97, 117.99, 118.45, 129.79, 136.01, 148.84.

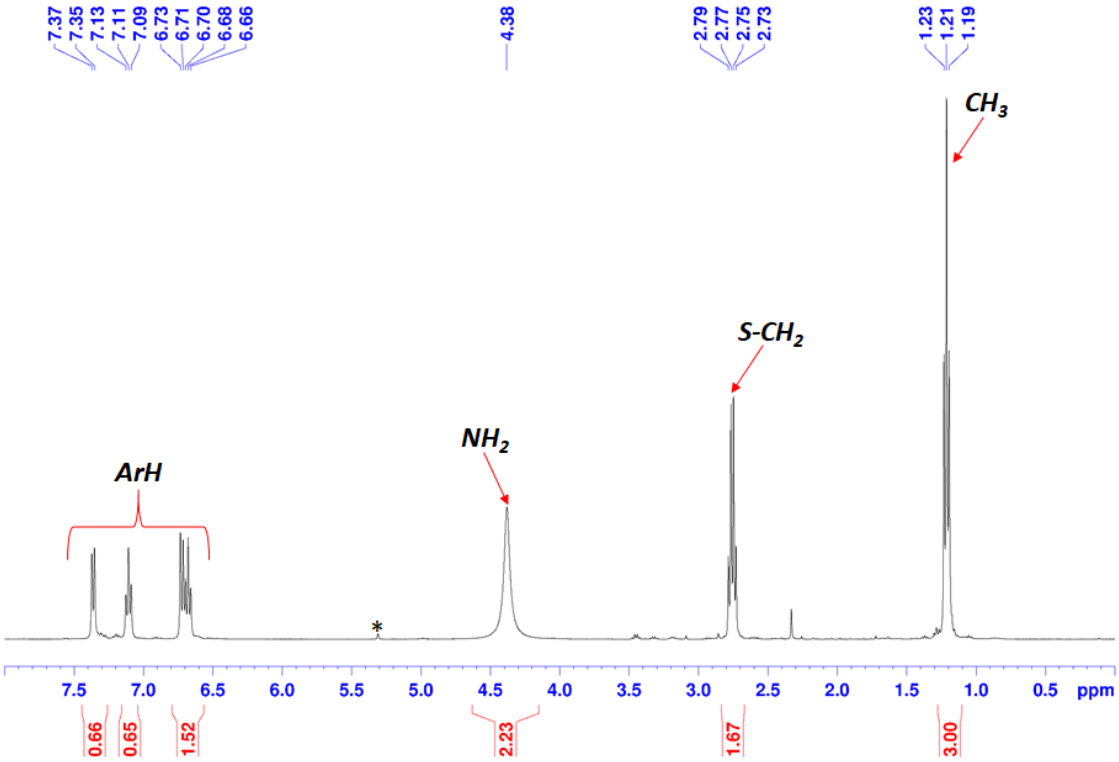

*Figure 161: ^{1}H NMR of NSEt (400.13 MHz, *CD_2Cl_2, 25°C).*

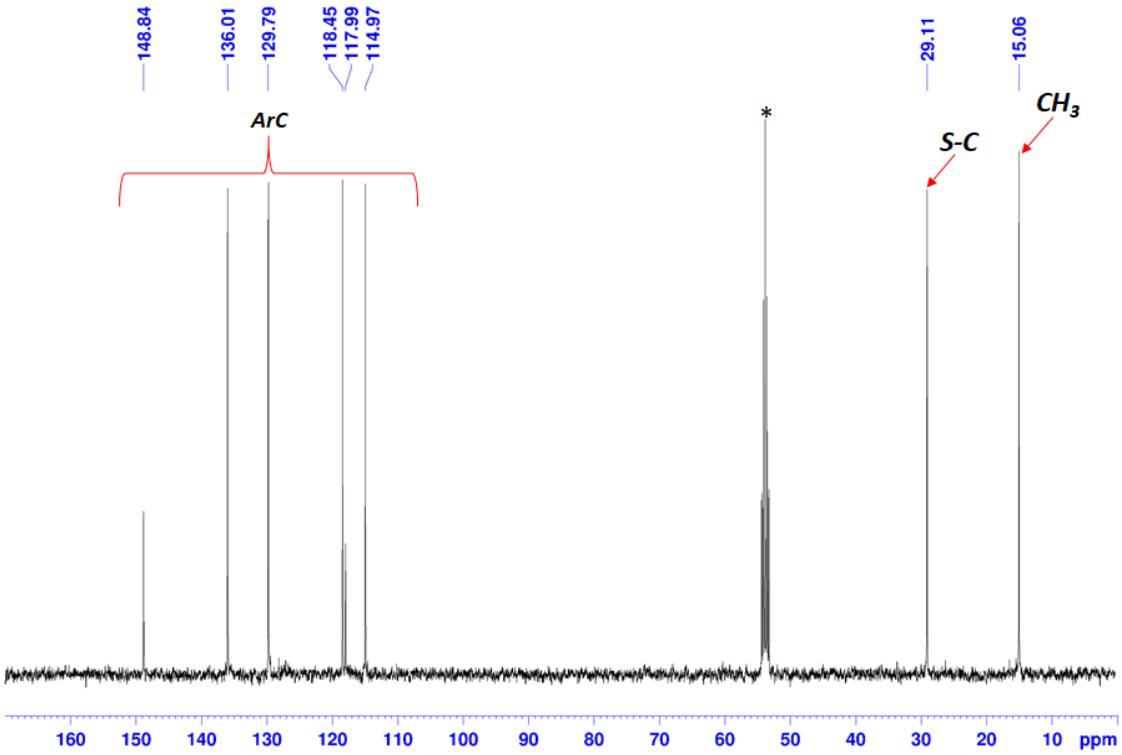

*Figure 162: ^{13}C NMR of NSEt (100.62 MHz, *CD_2Cl_2, 25°C).*

6.14 Synthesis and characterization of 2-(ethyltio)-N-isopropylaniline

2-(ethyltio)-N-isopropylaniline [NSEt-ISO] was synthesized with a similar procedure reported for *NSSN-ISO* (*figure 163*). *[NSEt]* (10.96 g, 72 mmol), zinc (23 g, 0.36 mol), acetic acid (200 mL), and acetone (12.54 g, 0.22 mol) were added to a 250 mL round-bottom one necked flask equipped with a condenser and a Teflon-sealed stirbar. The mixture was stirred to room temperature for 24 h.

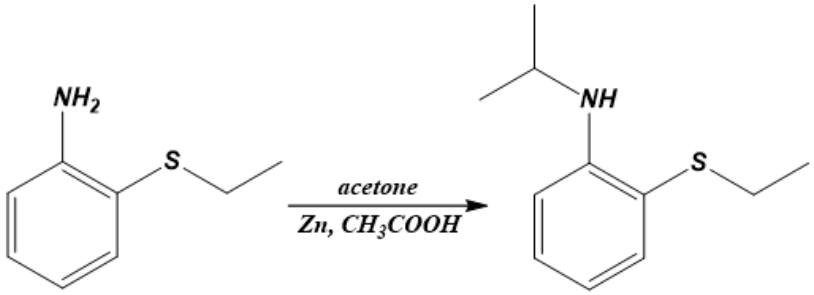

Figure 163: synthesis of NSEt-ISO ligand.

After it was cooled to room temperature, the mixture was quenched with a 30% NH_3 aqueous solution (300 mL) and diethyl ether (300 mL). The organic layer was dried with anhydrous $MgSO_4$, and a brown oil product was obtained upon removal of the solvent (8.1 g, yield = 58%).

^{1}H NMR (400.13 MHz, CD_2Cl_2, 25 °C): δ 6.93-7.54 (m, 4H, ArH), 5.38 (s, 1H, NH), 3.95 (m, 1H, N-CH), 3.01 (q, 2H, S-CH_2), 1.50-1.56 (m, 9H, CH_3). ^{13}C NMR (100.62 MHz, CD_2Cl_2, 25 °C): δ 15.53, 23.43, 29.57, 44.49, 111.13, 116.69, 117.81, 130.57, 137.04, 149.15.

An *NSEt-ISO* solution (1 µg/mL in CH_2Cl_2) was analyzed by electrospray spectroscopy and the result was reported in *figure 167*. *HRMS* (ESI). Calcd for $C_{11}H_{18}NS$ ($[M + H]^+$: m/z 196.1154. Found: m/z 196.1156.

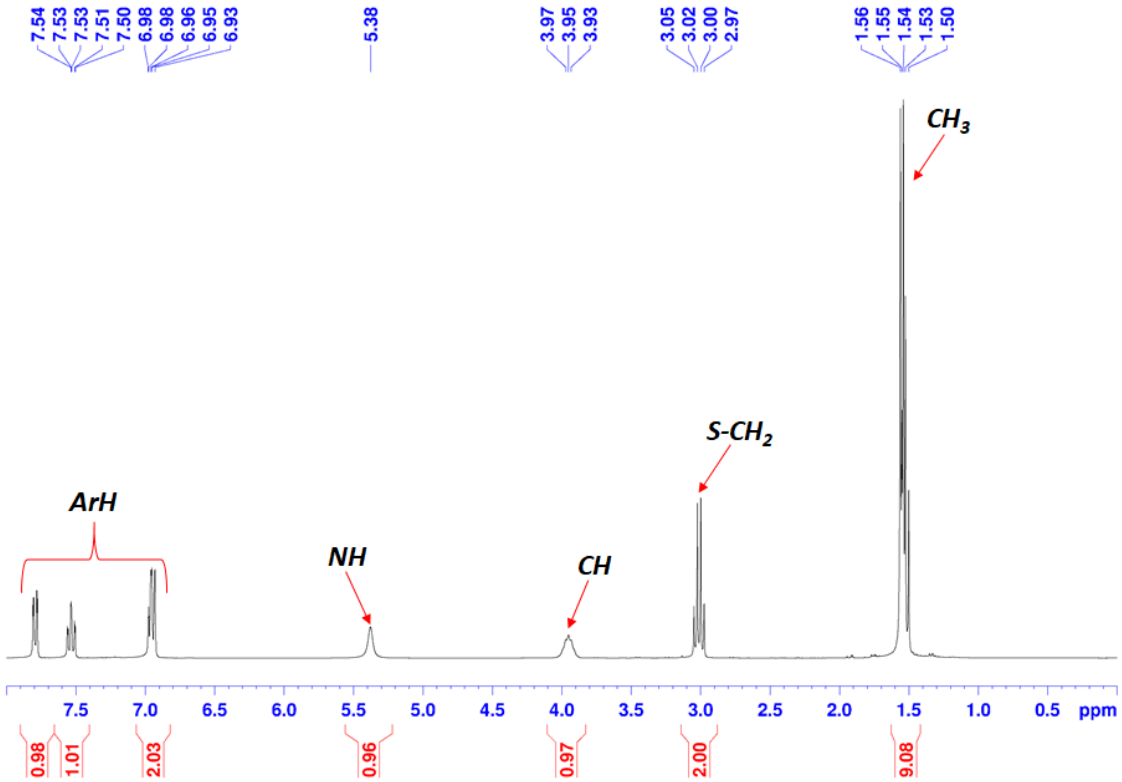

*Figure 164: ^{1}H NMR of NSEt-ISO ligand (400.13 MHz, *CD_2Cl_2, 25°C).*

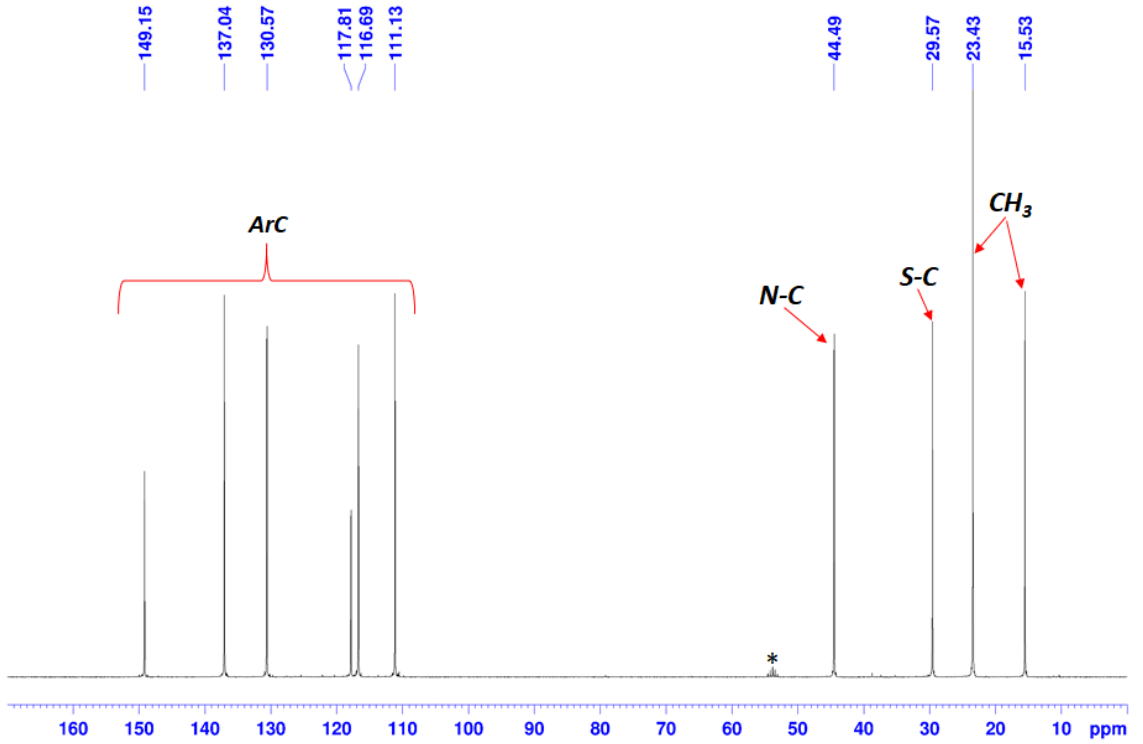

*Figure 165: ^{13}C NMR of NSEt-ISO ligand (100.62 MHz, *CD_2Cl_2, 25°C).*

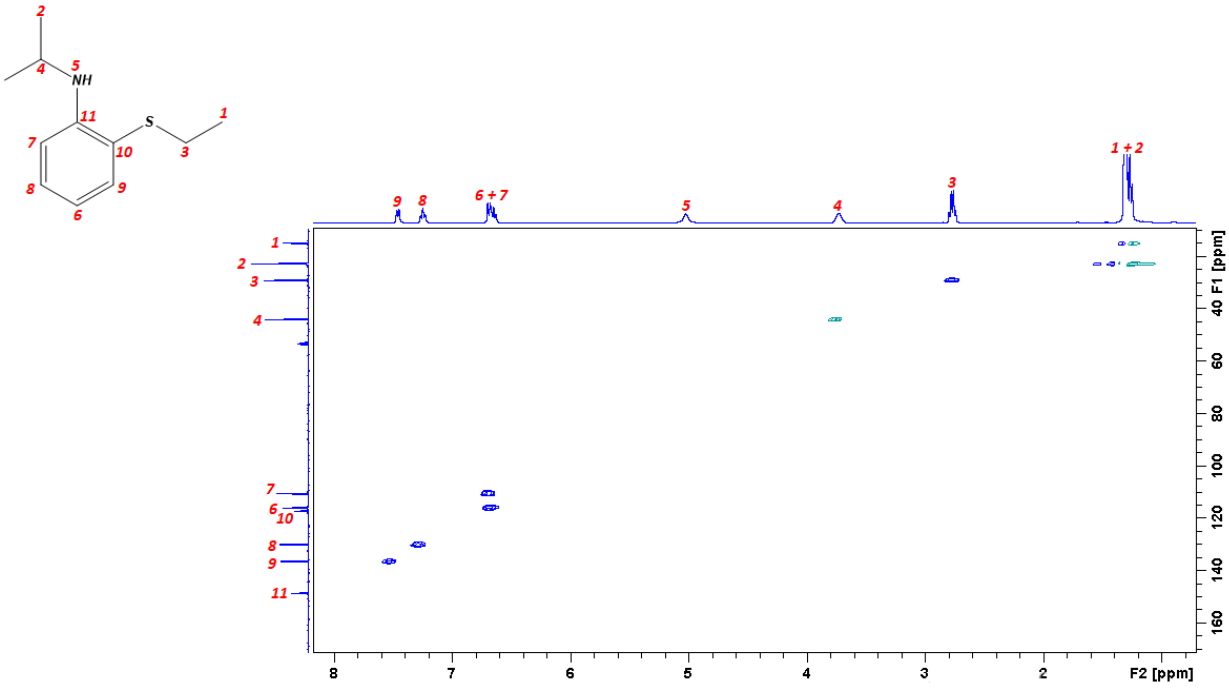

*Figure 166: $^{1}H - ^{13}C$ HSQC spectrum NMR of NSEt-ISO ligand (400.13/100.62 MHz, *CD_2Cl_2, 25°C).*

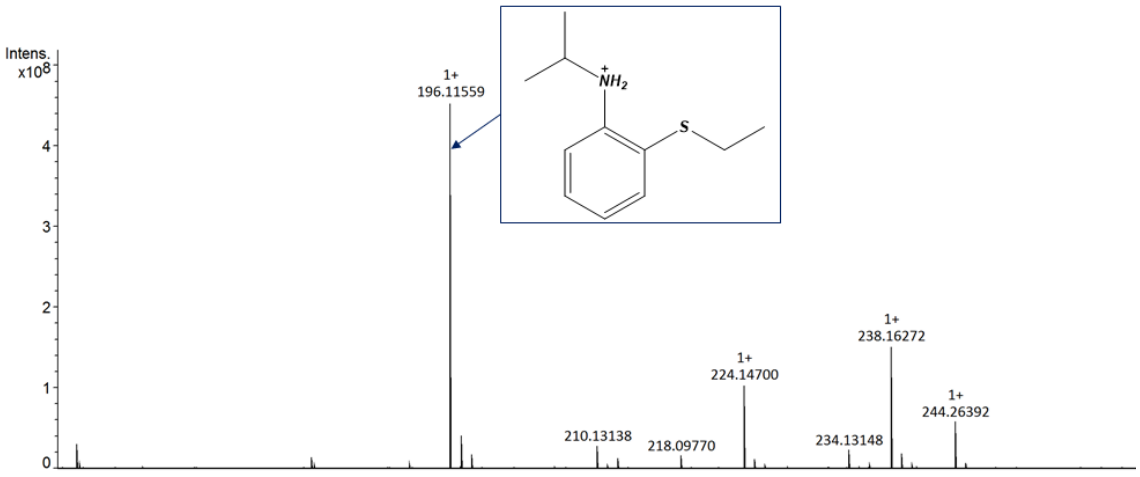

Figure 167: ESI-MS spectrum of NSEt-ISO ligand.

6.15 Synthesis and characterization of 2-(isopropylthio)aniline

2-(isopropyltio)aniline [NSiPr] was was synthesized with a similar procedure reported for *NSSN* but replacing 1,2-dibromoethane with 2-bromopropane (*figure 168*). 2-bromopropane (6.06 g, 49 mmol) was added dropwise to a refluxing solution of 2-aminothiophenol (5.61 g, 45 mmol) and sodium hydroxide (1.97 g, 50 mmol) in ethanol (150 mL). The refluxing reaction mixture was stirred for 1 h.

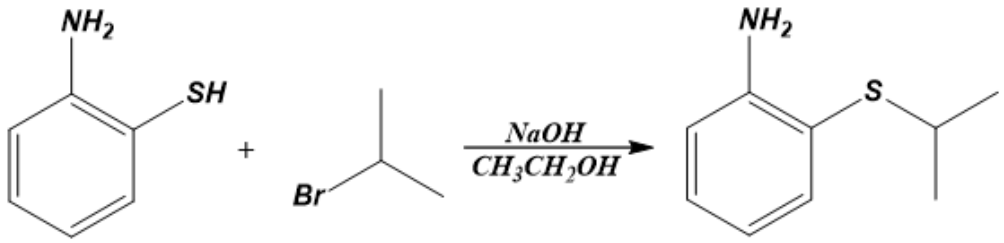

Figure 168: synthesis of NSiPr.

Upon completion of the reaction, the solvent was removed in vacuo and the reaction mixture was cooled to room temperature. Water (60 mL) was added and the reaction mixture was extracted with diethyl ether (3x60 mL). The organic layer was dried with anhydrous $MgSO_4$ and evaporated to dryness in vacuo to get a brown oil product (6.05 g, yield = 80%).

^{1}H NMR (400.13 MHz, CD_2Cl_2, 25 °C): δ 6.74-7.23 (m, 4H, ArH), 4.51 (s, 2H, NH_2), 3.29 (m, 1H, S-CH), 1.33 (d, J = 6.72 Hz, 6H, CH_3). ^{13}C NMR (100.62 MHz, CD_2Cl_2, 25 °C): δ 23.51, 38.95, 115.01, 117.44, 118.30, 130.25, 137.48, 149.59.

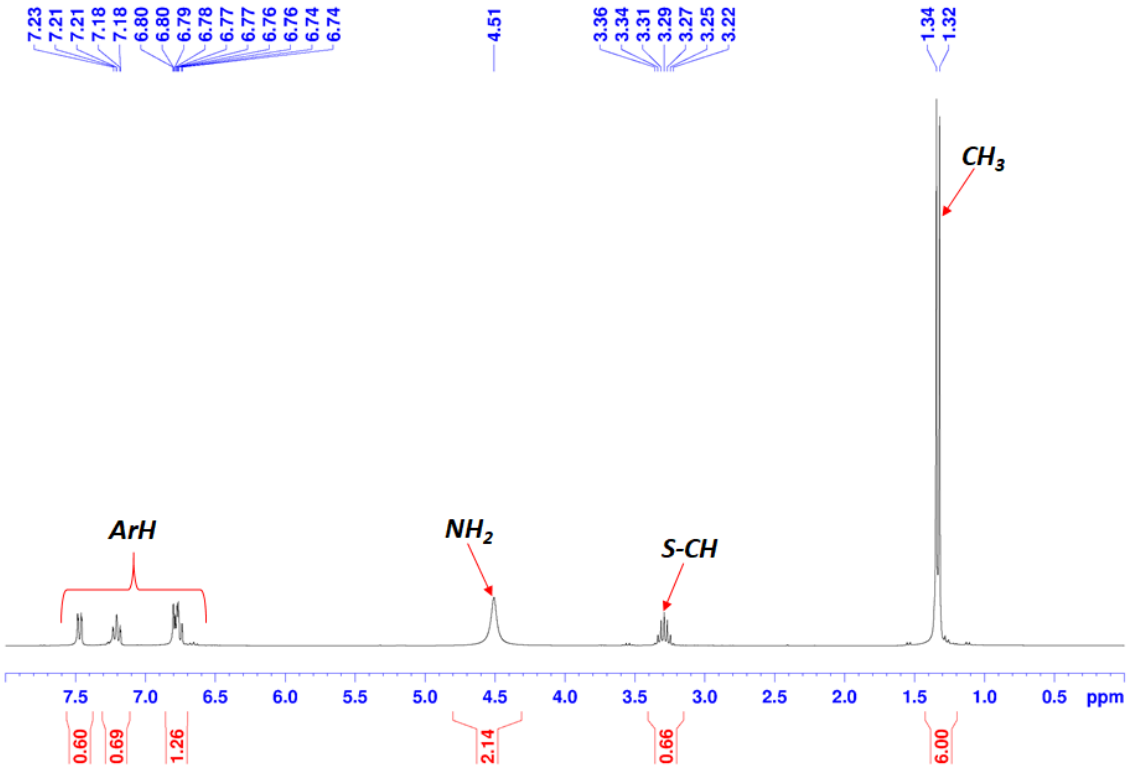

*Figure 169: ^{1}H NMR of NSiPr (400.13 MHz, *CD_2Cl_2, 25°C).*

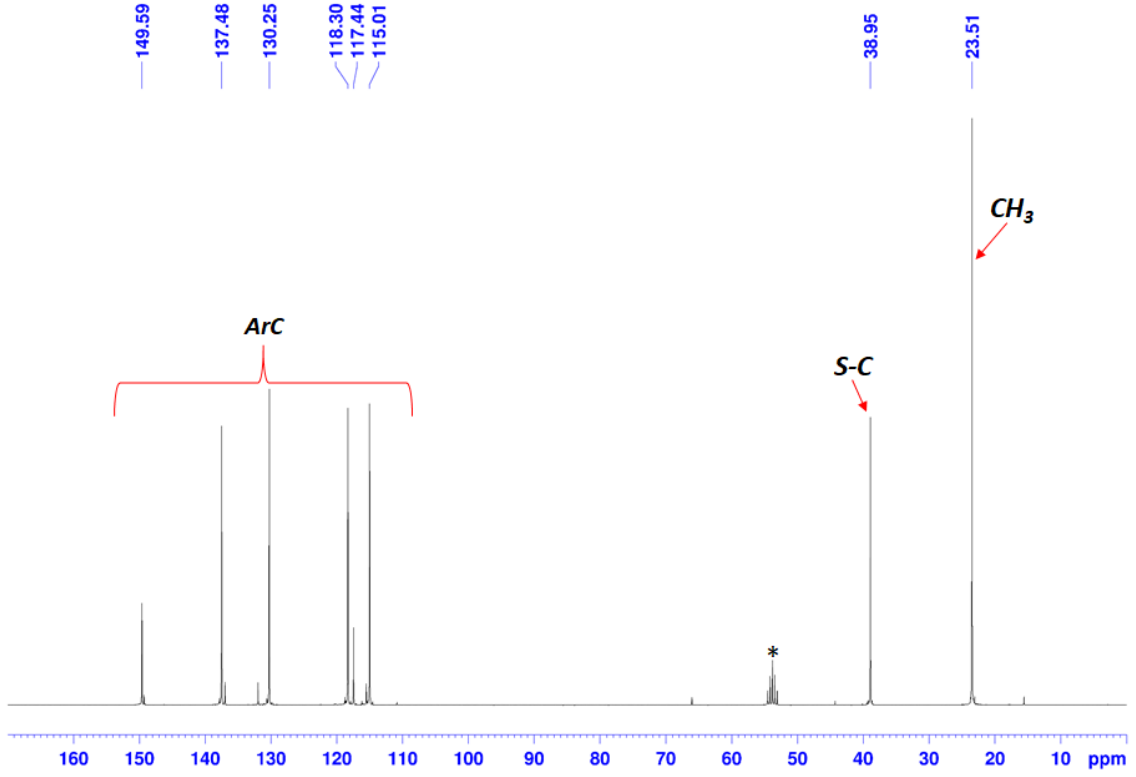

*Figure 170: ^{13}C NMR of NSiPr (100.62 MHz, *CD_2Cl_2, 25°C).*

6.16 Synthesis and characterization of N-isopropyl-2-(isopropylthio)aniline

N-isopropyl-2-(isopropylthio)aniline [NSiPr-ISO] was synthesized with a similar procedure reported for *NSSN-ISO* (*figure 171*). *[NSiPr]* (6.05 g, 36 mmol), zinc (11.83 g, 0.18 mol), acetic acid (200 mL), and acetone (10.51 g, 0.18 mol) were added to a 250 mL round-bottom one necked flask equipped with a condenser and a Teflon-sealed stirbar. The mixture was stirred to room temperature for 24 h.

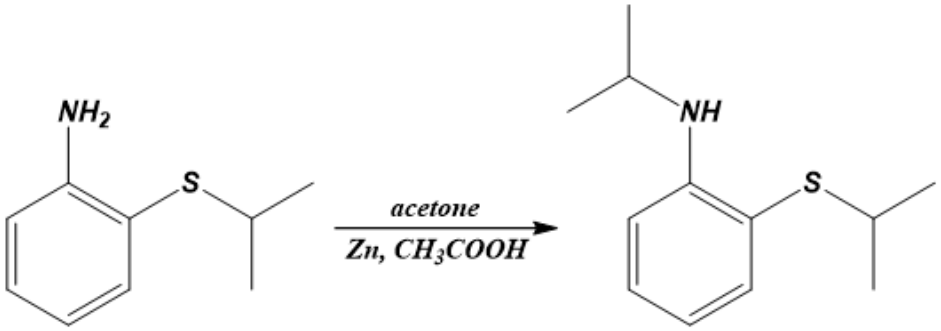

Figure 171: synthesis of NSiPr-ISO ligand.

After it was cooled to room temperature, the mixture was quenched with a 30% NH_3 aqueous solution (300 mL) and dichloromethane (300 mL). The organic layer was dried with anhydrous $MgSO_4$, and a brown oil product was obtained upon removal of the solvent (4.87 g, yield = 64%).

^{1}H NMR (400.13 MHz, CD_2Cl_2, 25 °C): δ 6.58-7.42 (m, 4H, ArH), 5.08 (s, 1H, NH), 3.69 (m, 1H, N-CH), 3.15 (m, 1H, S-CH), 1.27 (m, 12H, CH_3). ^{13}C NMR (100.62 MHz, CD_2Cl_2, 25 °C): δ 23.16, 23.59, 39.43, 44.42, 110.87, 116.19, 117.22, 130.66, 137.93, 149.67.

An *NSiPr-ISO* solution (1 µg/mL in CH_2Cl_2) was analyzed by electrospray spectroscopy and the result was reported in *figure 175*. *HRMS* (MALDI). Calcd for $C_{12}H_{20}NS$ ($[M + H]^+$: m/z 210.1311. Found: m/z 210.1322.

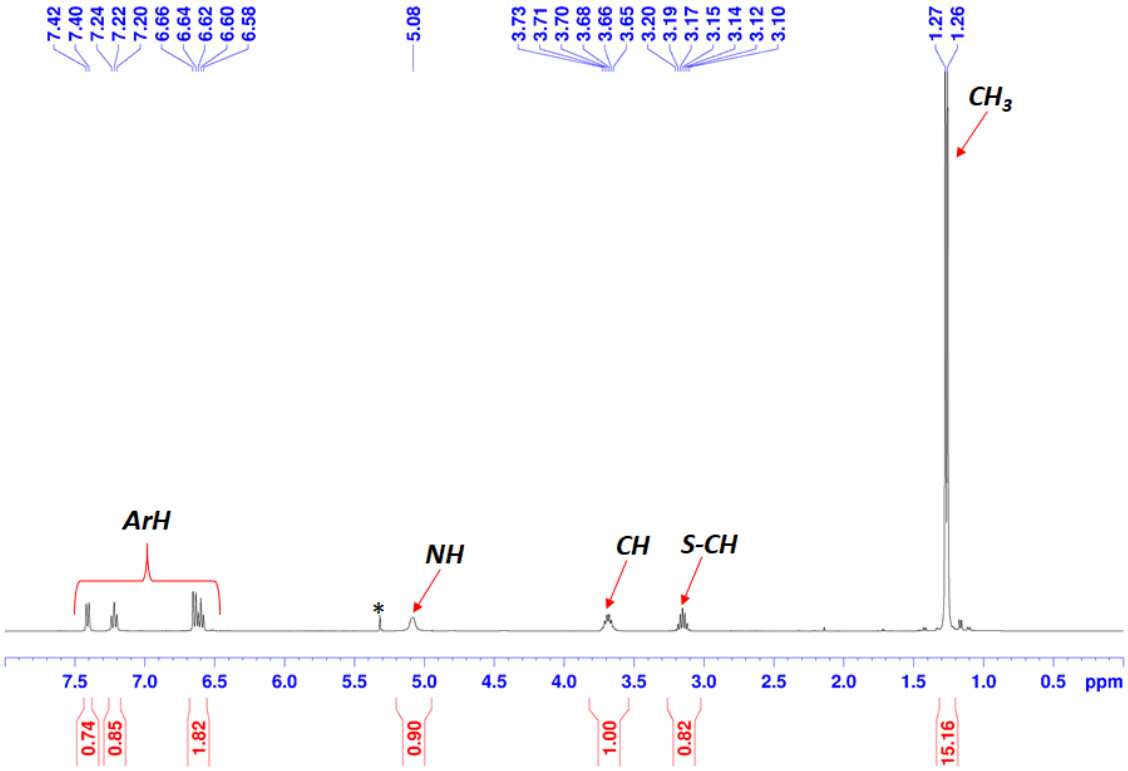

*Figure 172: ^{1}H NMR of NSiPr-ISO ligand (400.13 MHz, *CD_2Cl_2, 25°C).*

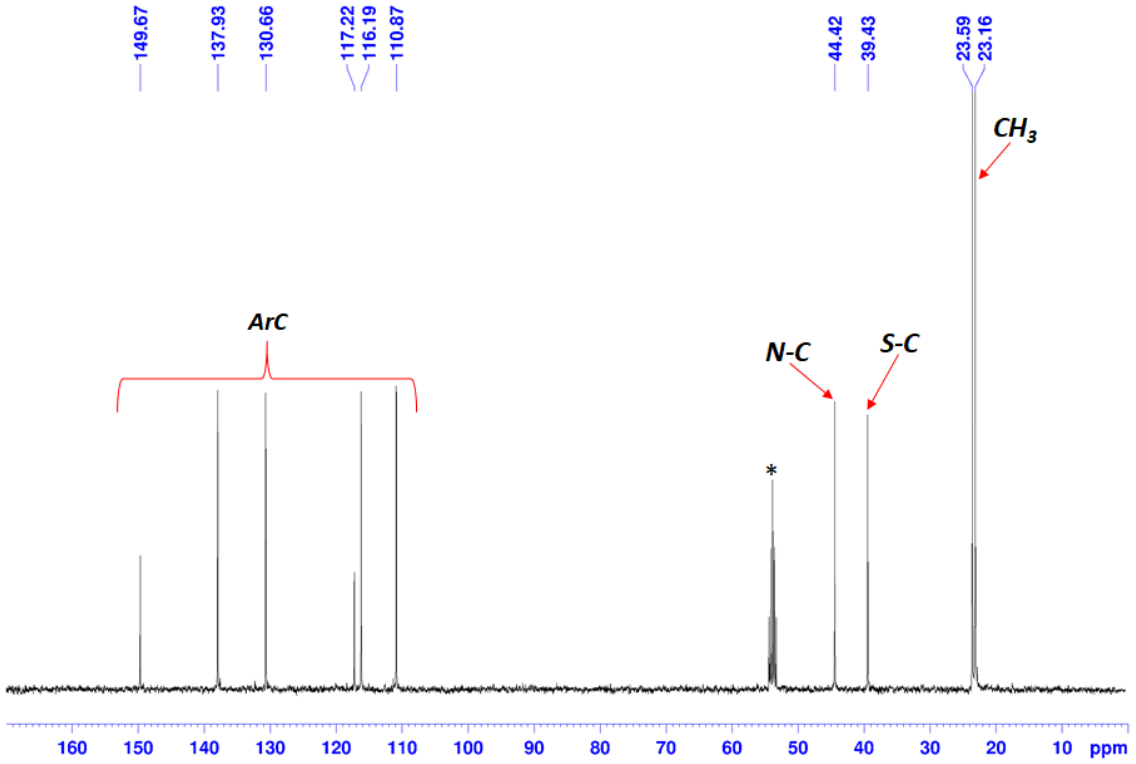

*Figure 173: ^{13}C NMR of NSiPr-ISO ligand (100.62 MHz, *CD_2Cl_2, 25°C).*

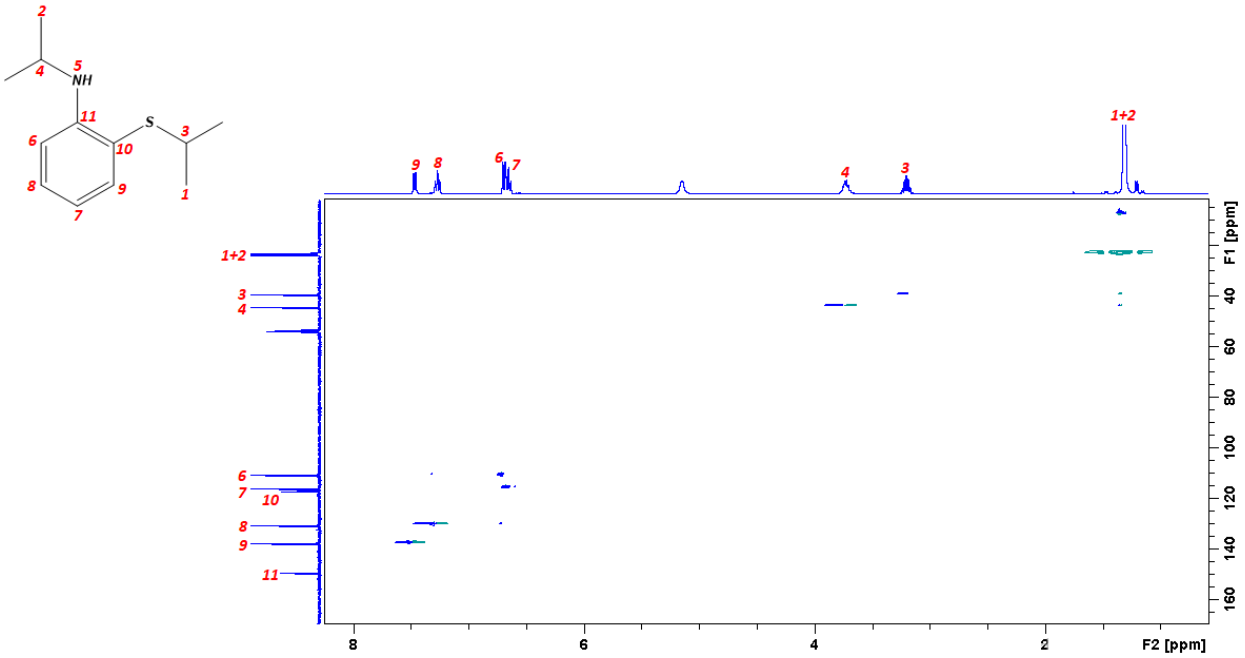

*Figure 174: ^{1}H – ^{13}C HSQC spectrum HSQC of NSiPr-ISO ligand (400.13/100.62 MHz, *CD_2Cl_2, 25°C).*

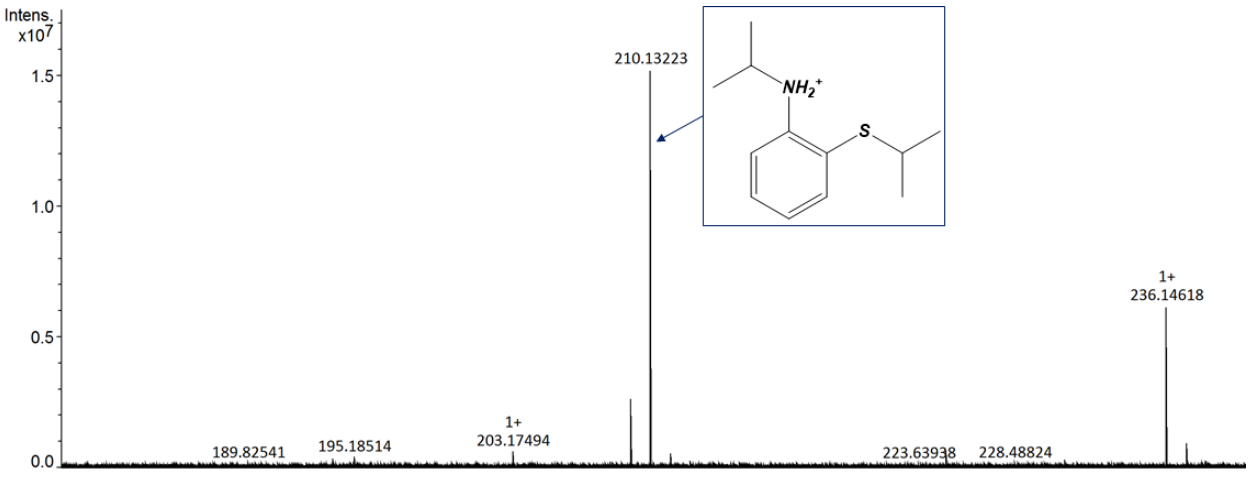

Figure 175: Maldi-MS spectrum of NSiPr-ISO ligand.

6.17 Synthesis and characterization of 2-(hexylthio)aniline

2-(hexylthio)aniline [NSHex] was synthesized with a similar procedure reported for *NSSN* but replacing 1,2-dibromoethane with 1-chlorohexane (*figure 176*). 1-chlorohexane (11.08 g, 92 mmol) was added dropwise to a refluxing solution of 2-aminothiophenol (10.25 g, 82 mmol) and sodium hydroxide (3.60 g, 90 mmol) in ethanol (150 mL). The refluxing reaction mixture was stirred for 1 h.

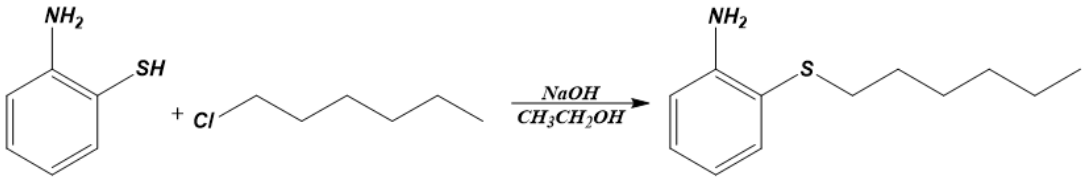

Figure 176: synthesis of NSHex.

Upon completion of the reaction, the solvent was removed in vacuo and the reaction mixture was cooled to room temperature. Water (60 mL) was added and the reaction mixture was extracted with diethyl ether (3x60 mL). The organic layer was dried with anhydrous $MgSO_4$ and evaporated to dryness in vacuo to get a brown oil product (15.43 g, yield = 90%).

^{1}H NMR (400.13 MHz, CD_2Cl_2, 25 °C): δ 6.70-7.17 (m, 4H, ArH), 4.43 (s, 2H, NH_2), 2.79 (t, 2H, S-CH_2), 0.93-1.67 (m, 11H, CH_2+CH_3). ^{13}C NMR (100.62 MHz, CD_2Cl_2, 25 °C): δ 14.31, 23.03, 28.83, 30.07, 31.86, 35.17, 115.02, 118.52, 118.55, 129.71, 135.84, 148.74.

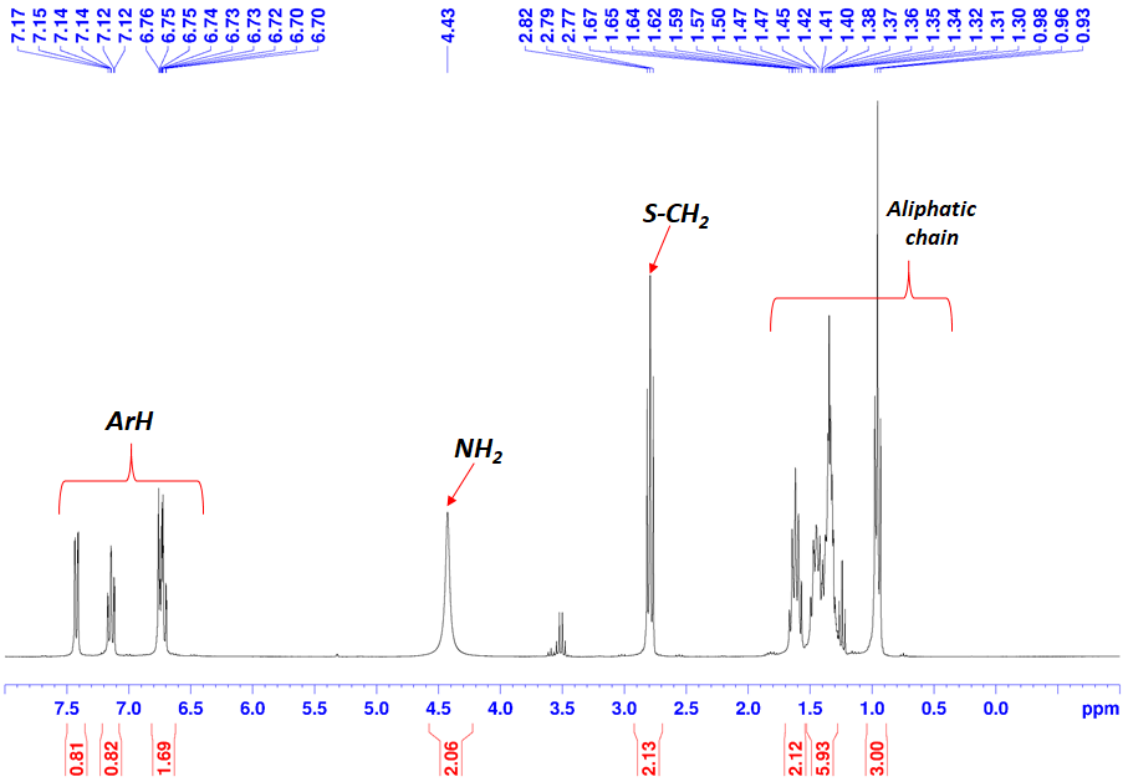

*Figure 177: ^{1}H NMR of NSHex (400.13 MHz, *CD_2Cl_2, 25°C).*

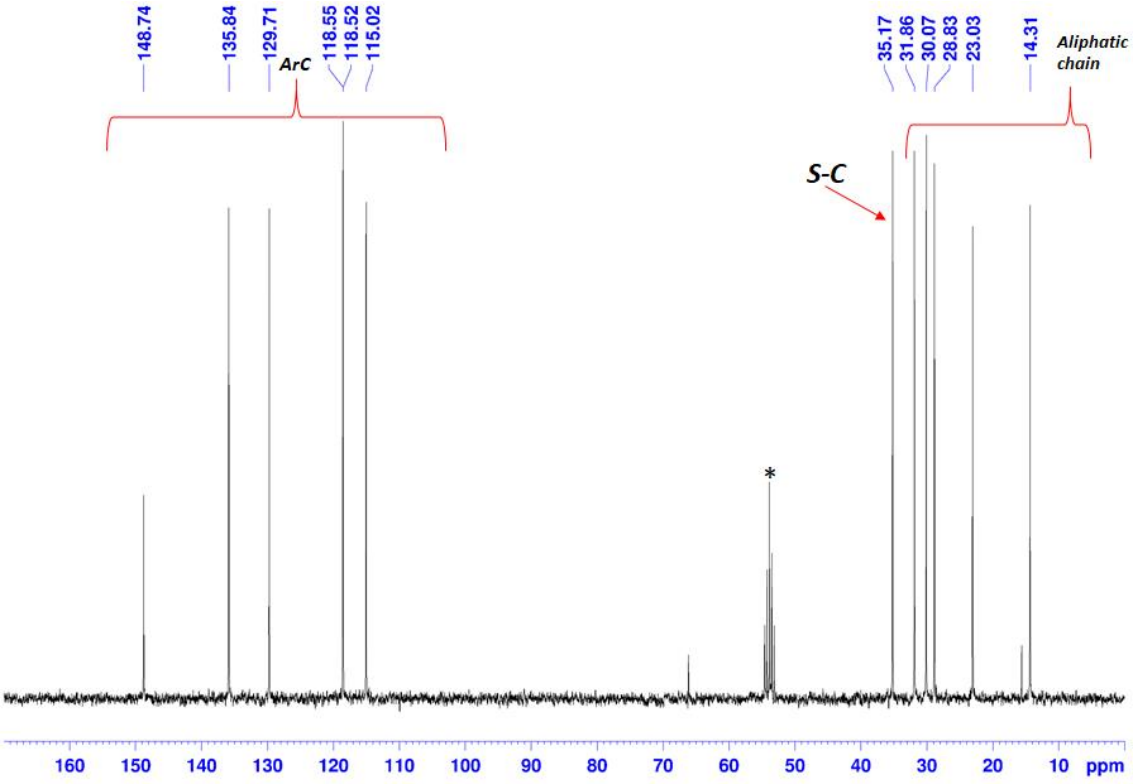

*Figure 178: ^{13}C NMR of NSHex (100.62 MHz, *CD_2Cl_2, 25°C).*

6.18 Synthesis and characterization of 2-(hexylthio)-N-isopropylaniline

2-(hexylthio)-N-isopropylaniline [NSHex-ISO] was synthesized with a similar procedure reported for *NSSN-ISO* (*figure 179*). *[NSHex]* (15.43 g, 74 mmol), zinc (24.19 g, 0.37 mol), acetic acid (200 mL), and acetone (21.49 g, 0.37 mol) were added to a 250 mL round-bottom one necked flask equipped with a condenser and a Teflon-sealed stirbar. The mixture was heated to room temperature for 24 h.

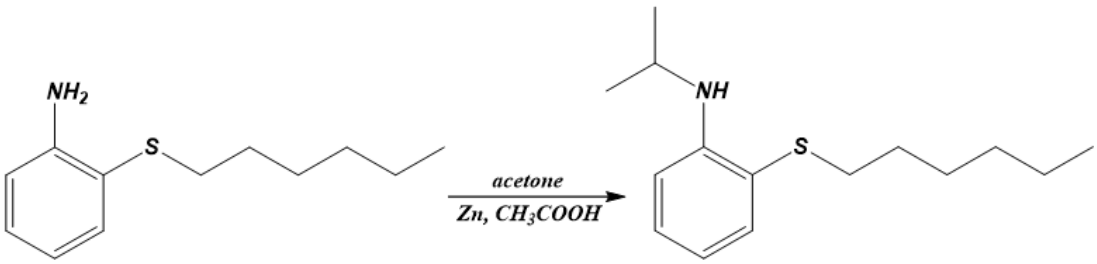

Figure 179: synthesis of NSHex-ISO ligand.

After it was cooled to room temperature, the mixture was quenched with a 30% NH_3 aqueous solution (300 mL) and dichloromethane (300 mL). The organic layer was dried with anhydrous $MgSO_4$, and a brown oil product was obtained upon removal of the solvent (11.64 g, yield = 63%).

^{1}H NMR (400.13 MHz, CD_2Cl_2, 25 °C): δ 6.52-7.36 (m, 4H, ArH), 4.92 (s, 1H, NH), 3.65 (m, 1H, N-CH), 2.66 (t, 2H, S-CH_2), 0.86 (t, 3H, CH_3), 1.21-1.56 (m, 14H, CH_2+CH_3). ^{13}C NMR (100.62 MHz, CD_2Cl_2, 25 °C): δ 14.29, 23.04, 23.10, 28.81, 30.04, 31.86, 35.61, 44.39, 110.84, 116.33, 118.12, 130.16, 136.52, 148.88.

An *NSHex-ISO* solution (1 mg/mL in CH_2Cl_2) was analyzed by maldi spectroscopy and the result was reported in *Figure X*. *HRMS* (MALDI). Calcd for $C_{15}H_{26}NS$ ([M + H]$^+$: m/z 252.1780. Found: m/z 251.1696.

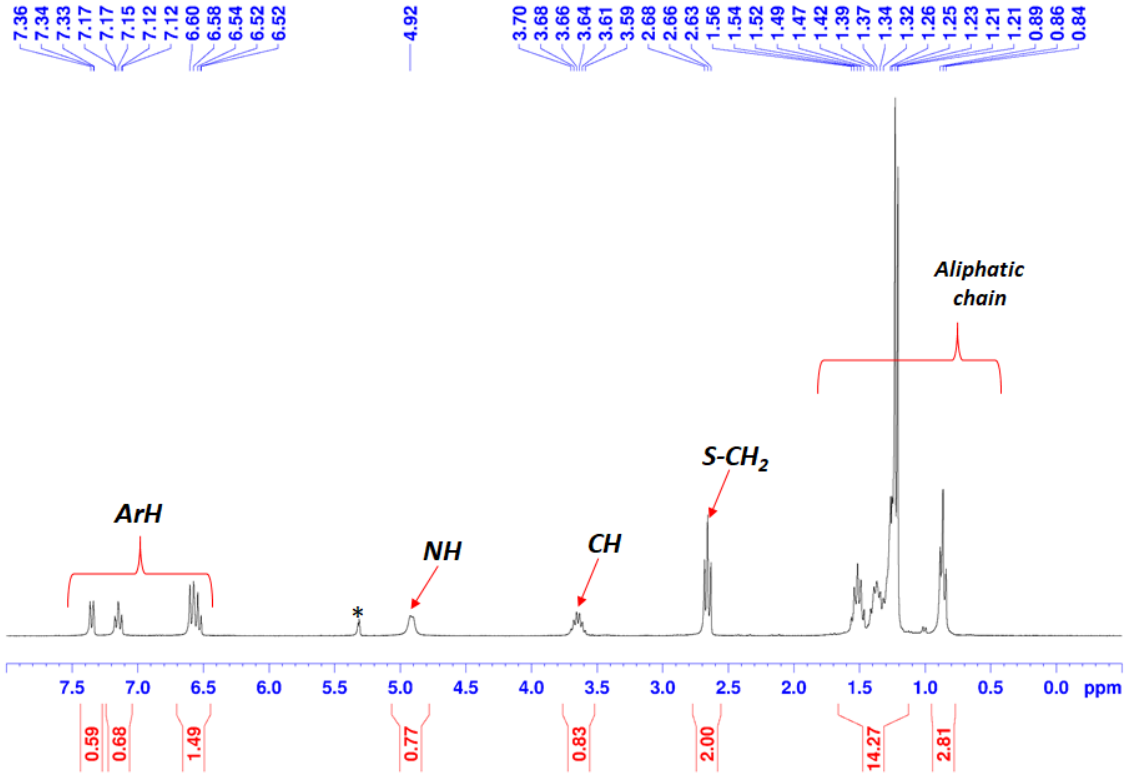

*Figure 180: ^{1}H NMR of NSHex-ISO ligand (400.13 MHz, *CD_2Cl_2, 25°C).*

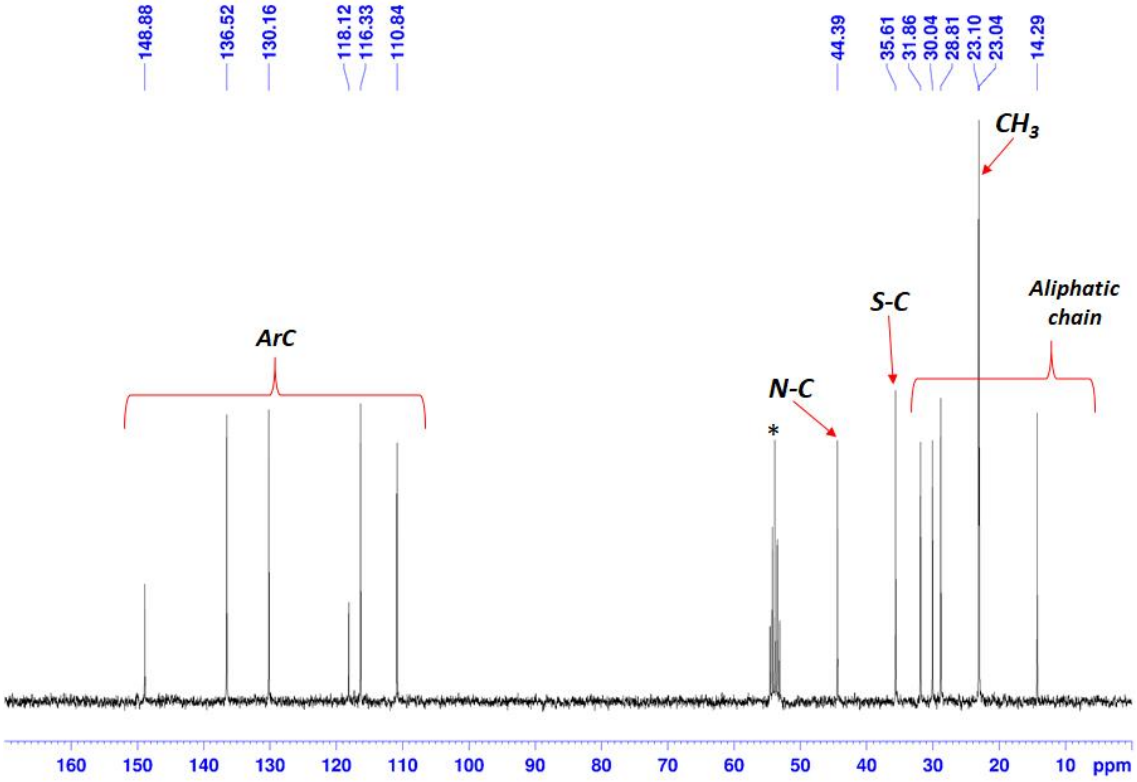

*Figure 181: ^{13}C NMR of NSHex-ISO ligand (100.62 MHz, *CD_2Cl_2, 25°C).*

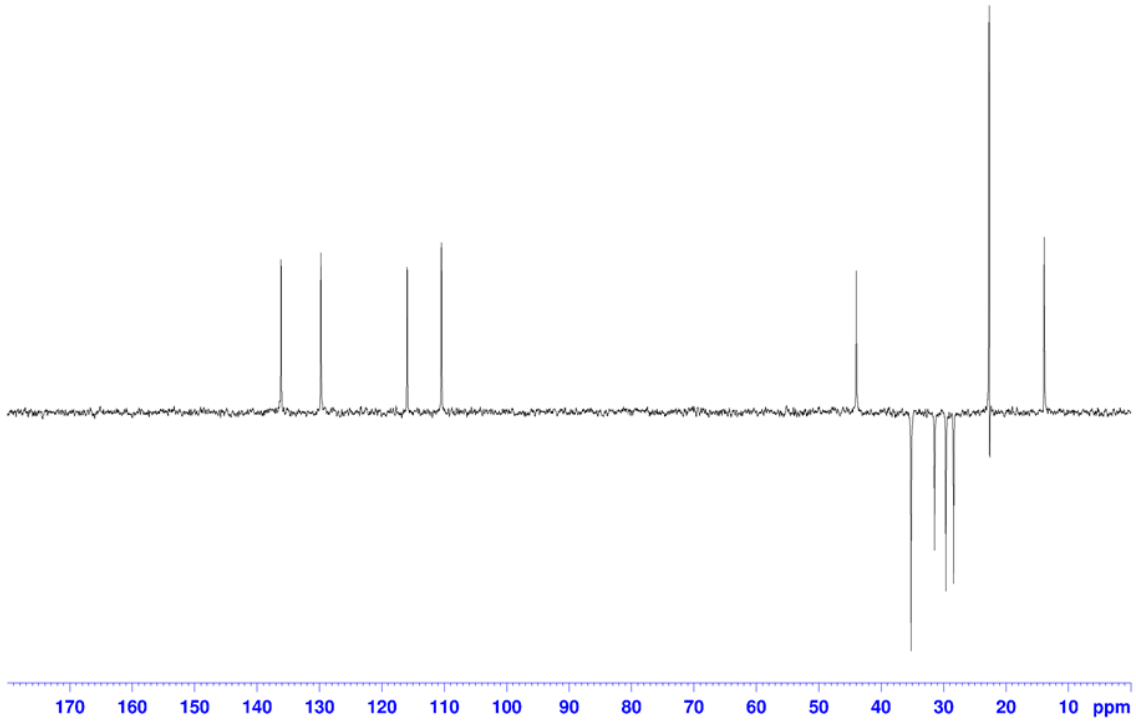

*Figure 182: DEPT 135 NMR of NSHex-ISO ligand (100.62 MHz, *CD_2Cl_2, 25°C).*

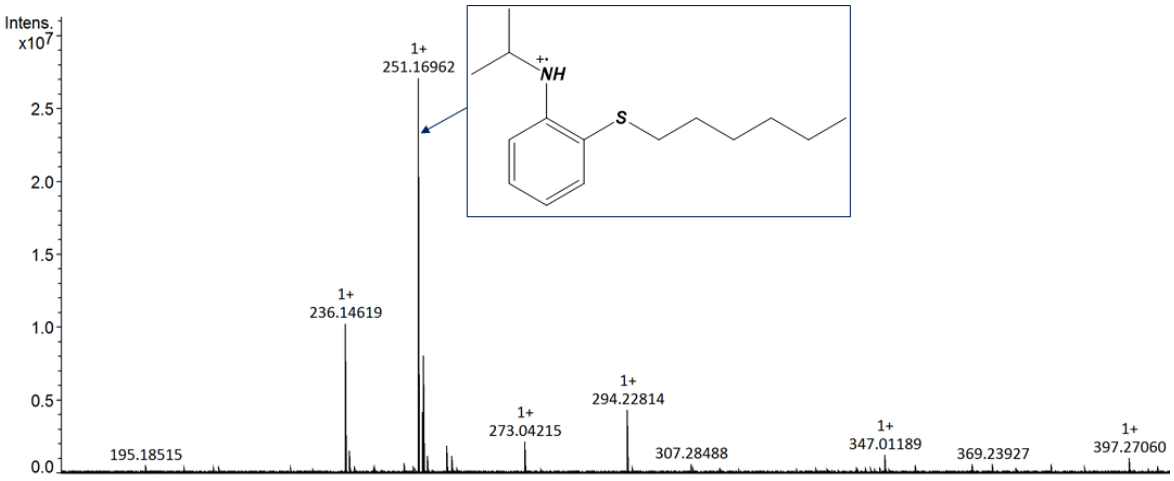

Figure 183: Maldi-MS spectrum of NSHex-ISO ligand.

6.19 Synthesis and characterization of 2-(benzylthio)aniline

2-(benzylthio)aniline [NSBen] was synthesized with a similar procedure reported for *NSSN* but replacing 1,2-dibromoethane with (bromomethyl)benzene. (Bromomethyl)benzene (10.55 g, 91 mmol) was added dropwise to a refluxing solution of 2-aminothiophenol (11.40 g, 91 mmol) and sodium hydroxide (4.00 g, 0.1 mol) in ethanol (150 mL) (*figure 184*). The refluxing reaction mixture was stirred for 1 h.

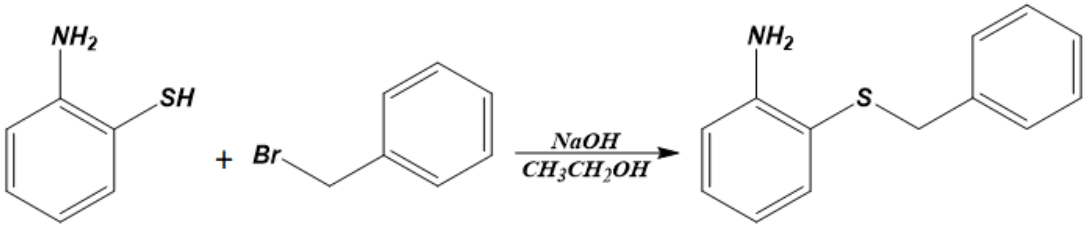

Figure 184: synthesis of NSBen.

Upon completion of the reaction, the solvent was removed in vacuo and the reaction mixture was cooled to room temperature. Water (60 mL) was added and the reaction mixture was extracted with diethyl ether (3x60 mL). The organic layer was dried with anhydrous $MgSO_4$ and evaporated to dryness in vacuo to get a dark red oil product (17.59 g, yield = 90%).

^{1}H NMR (400.13 MHz, CD_2Cl_2, 25 °C): δ 6.61-7.25 (m, 7H, ArH), 4.32 (s, 2H, NH_2), 3.94 (s, 2H, S-CH_2). ^{13}C NMR (100.62 MHz, CD_2Cl_2, 25 °C): δ 39.70, 115.06, 117.58, 118.49, 127.32, 128.66, 129.20, 130.28, 136.56, 138.80, 149.08.

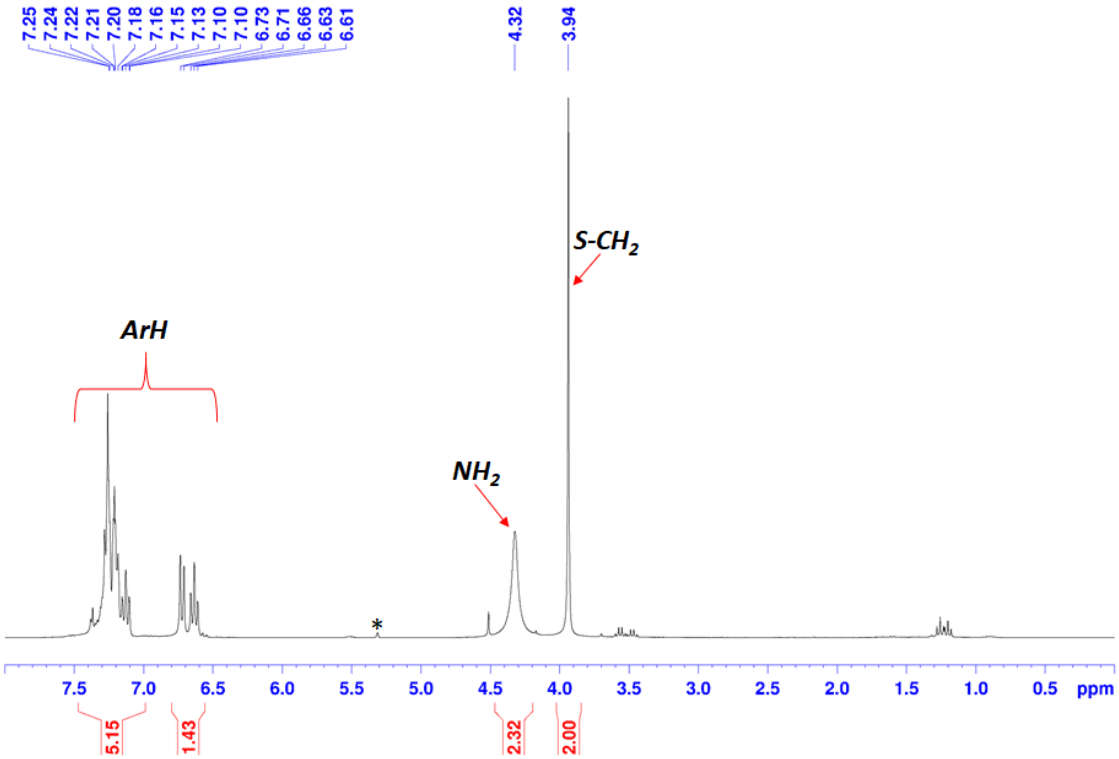

*Figure 185: ^{1}H NMR of NSBen (400.13 MHz, *CD_2Cl_2, 25°C).*

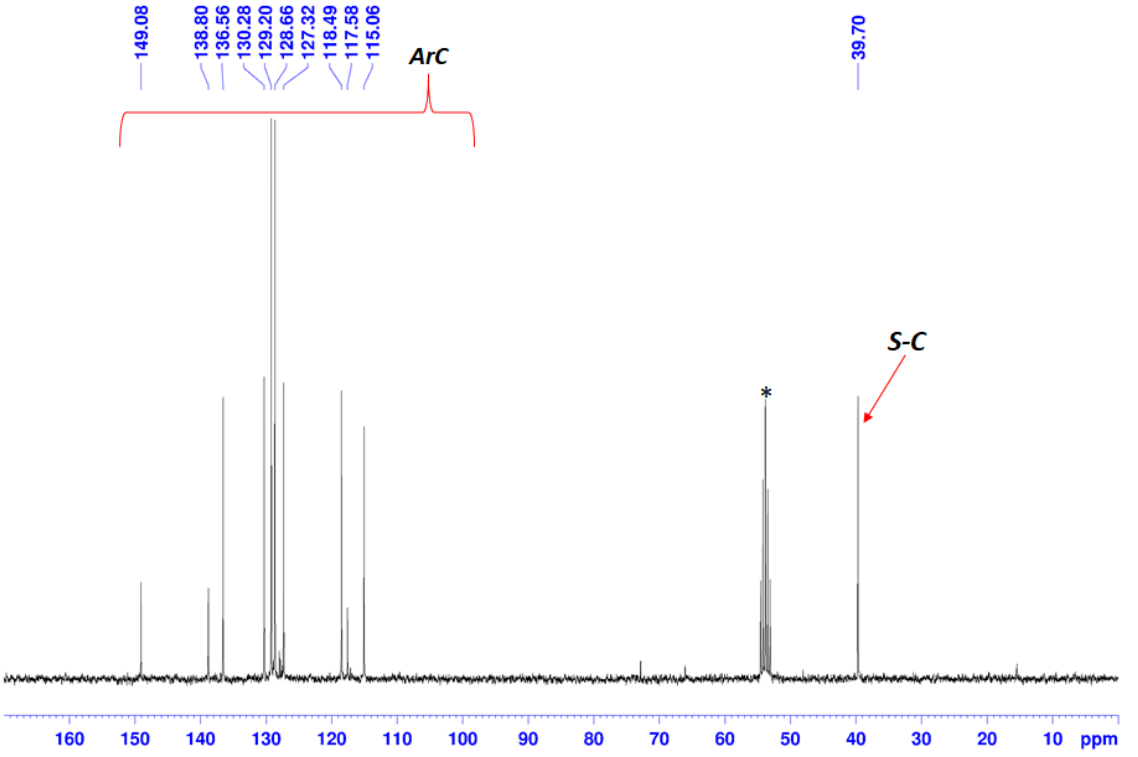

*Figure 186: ^{13}C NMR of NSBen (100.62 MHz, *CD_2Cl_2, 25°C).*

6.20 Synthesis and characterization of 2-(benzylthio)-N-isopropylaniline

2-(benzylthio)-N-isopropylaniline [NSBen-ISO] was synthesized with a similar procedure reported for *NSSN-ISO* (*figure 187*). *[NSBen]* (17.59 g, 82 mmol), zinc (26.81 g, 0.41 mol), acetic acid (200 mL), and acetone (14.29 g, 0.25 mol) were added to a 250 mL round-bottom one necked flask equipped with a condenser and a Teflon-sealed stirbar. The mixture was stirred to room temperature for 24 h.

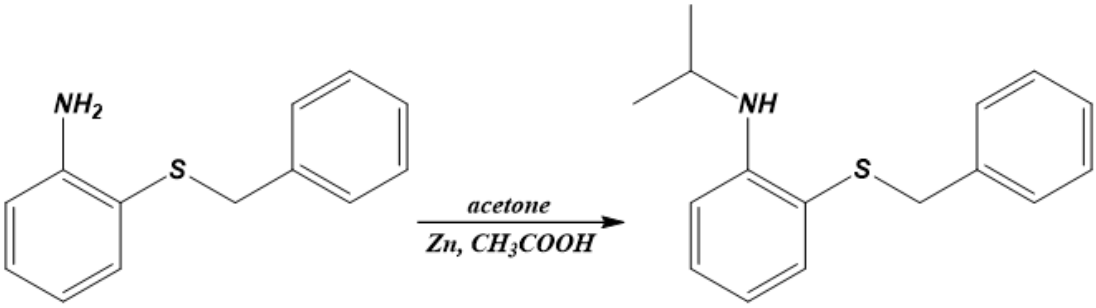

Figure 187: synthesis of NSBen-ISO ligand.

After it was cooled to room temperature, the mixture was quenched with a 30% NH_3 aqueous solution (300 mL) and diethyl ether (300 mL). The organic layer was dried with anhydrous $MgSO_4$, and a brown oil product was obtained upon removal of the solvent (15.6 g, yield = 74%).

^{1}H NMR (400.13 MHz, CD_2Cl_2, 25 °C): δ 1.21 (d, J = 6.36 Hz, 6H, CH_3), 3.63 (m, 1H, N-CH), 3.90 (s, 2H, S-CH_2), 4.94 (s, 1H, NH), 6.54-7.27 (m, 7H, ArH). ^{13}C NMR (100.62 MHz, CD_2Cl_2, 25 °C): δ 22.98, 40.15, 44.25, 110.83, 116.27, 117.17, 127.33, 128.70, 129.19, 130.68, 137.12, 139.00, 149.05.

An *NSBen-ISO* solution (1 µg/mL in CH_2Cl_2) was analyzed by electrospray spectroscopy and the result was reported in *figure 191*. *HRMS* (ESI). Calcd for $C_{11}H_{18}NS$ ($[M + H]^+$: m/z 258.1311. Found: m/z 257.1244.

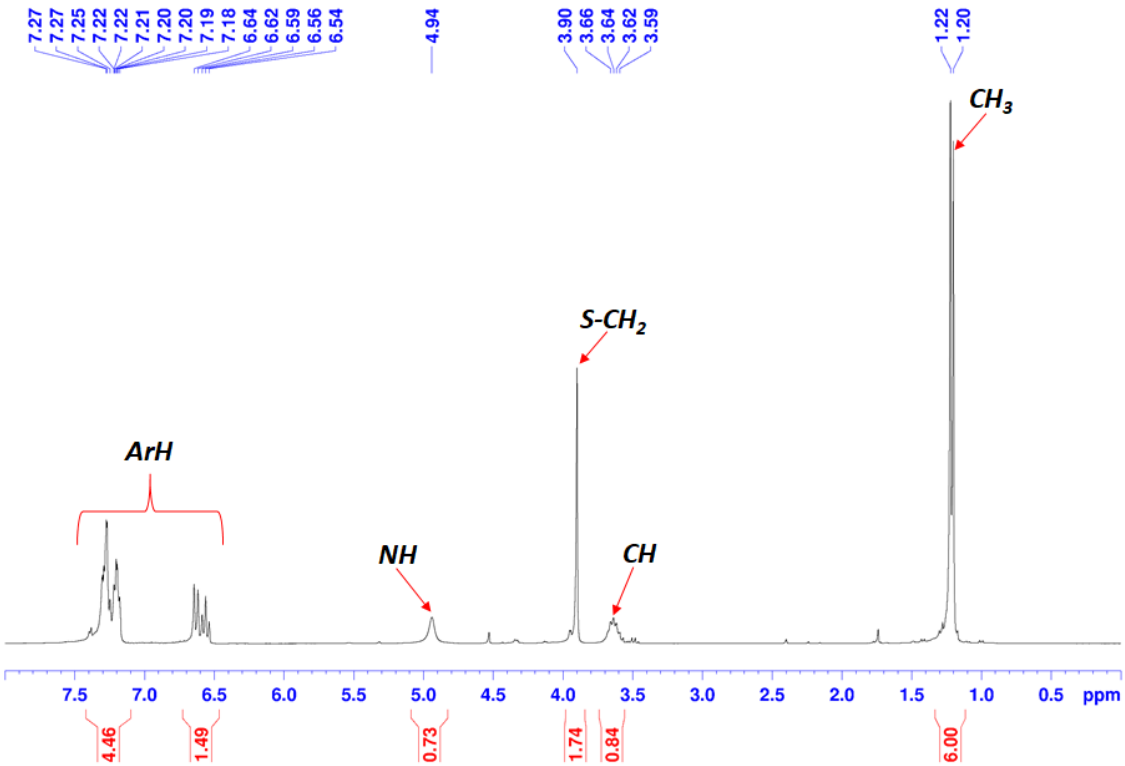

*Figure 188: ^{1}H NMR of NSBen-ISO ligand (400.13 MHz, *CD_2Cl_2, 25°C).*

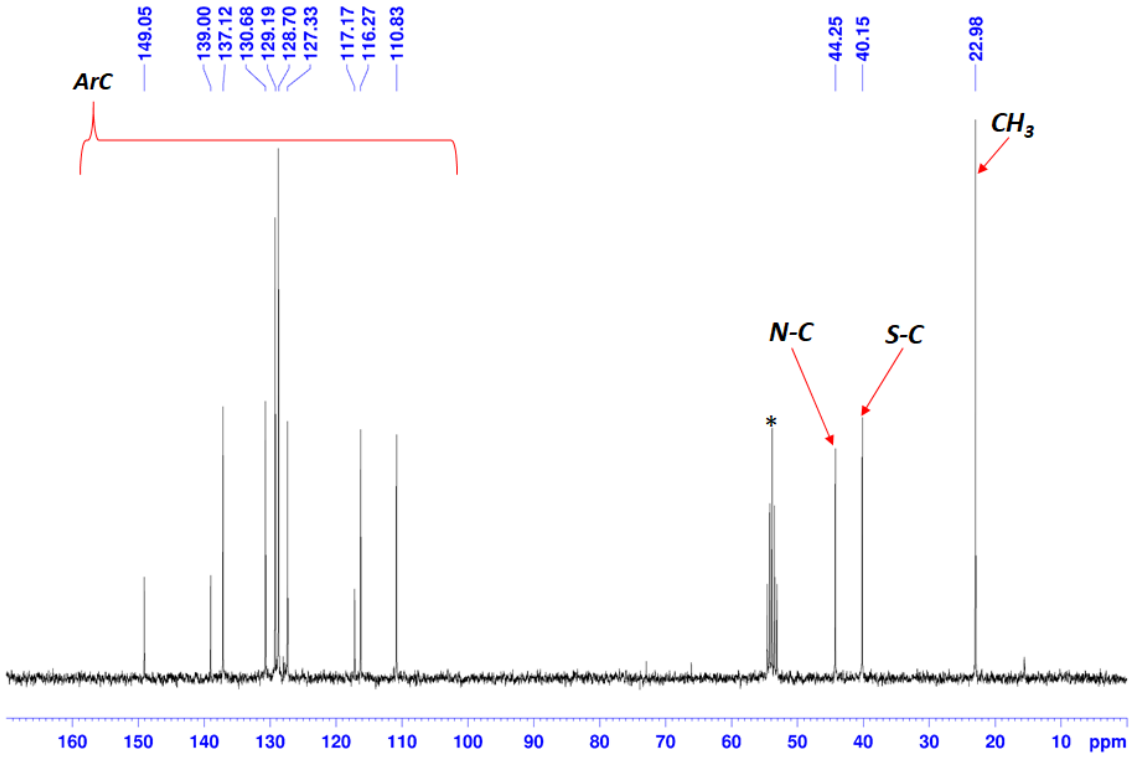

*Figure 189: ^{13}C NMR of NSBen-ISO ligand (100.62 MHz, *CD_2Cl_2, 25°C).*

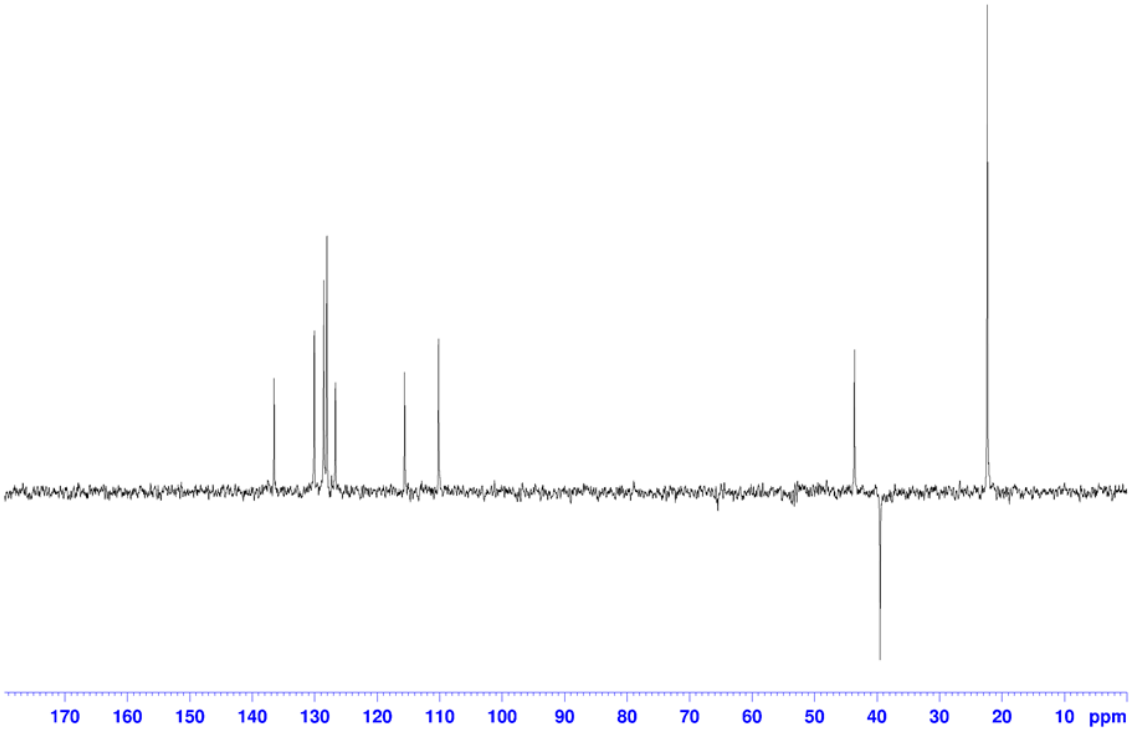

*Figure 190: DEPT 135 NMR of NSBen-ISO ligand (100.62 MHz, *CD_2Cl_2, 25°C).*

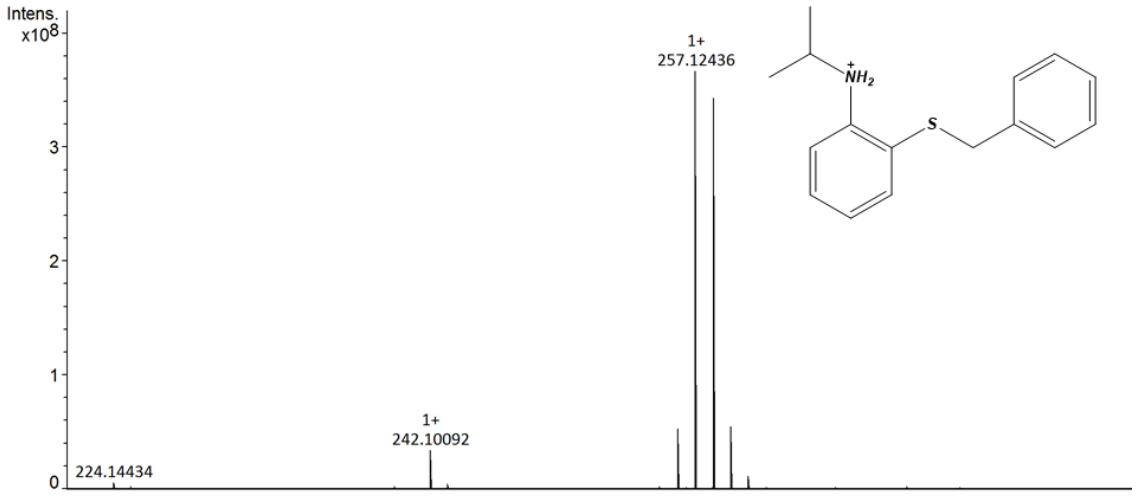

Figure 191: ESI-MS spectrum of NSBen-ISO.

6.21 Synthesis and characterization of 1-((2-aminophenyl)thio)propan-2-ol

Propylene oxide (4.0 g, 68 mmol) was added dropwise to a refluxing solution of of 2-aminothiophenol (8.6 g, 68 mmol) and sodium hydroxide (2.7 g, 68 mmol) in methanol (250 mL) (*figure 192*). The refluxing reaction mixture was stirred for 2 h.

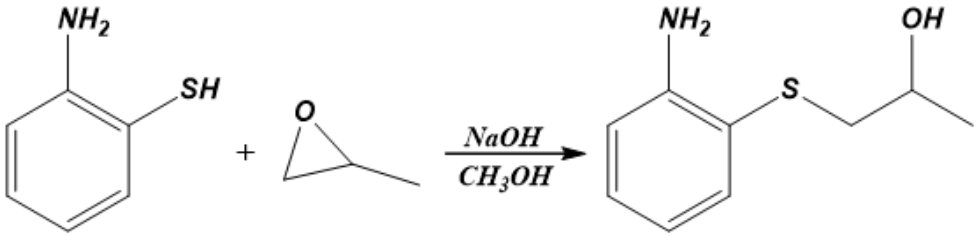

Figure 192: synthesis of NSO.

After 2 h, the solvent was removed in vacuo and the reaction mixture was cooled to room temperature. Water (50 mL) was added and the reaction mixture was extracted with diethyl ether (4x 50 mL). The organic layers was dried with anhydrous $MgSO_4$, filtered and evaporated to dryness in vacuo to get a brown oil (9.9 g, yield = 79 %).

^{1}H NMR (400.13 MHz, CD_2Cl_2, 25 °C): δ 6.67-7.40 (m, 4H, ArH), 4.43 (s, 2H, NH_2), 3.72 (m, 1H, O-CH), 2.60-2.92 (m, 2H, S-CH_2), 1.17 (d, J = 6.20 Hz, 3H, CH_3). ^{13}C NMR (100.62 MHz, CD_2Cl_2, 25 °C): δ 22.10, 44.73, 66.32, 115.49, 117.70, 119.09, 130.36, 136.51, 148.91.

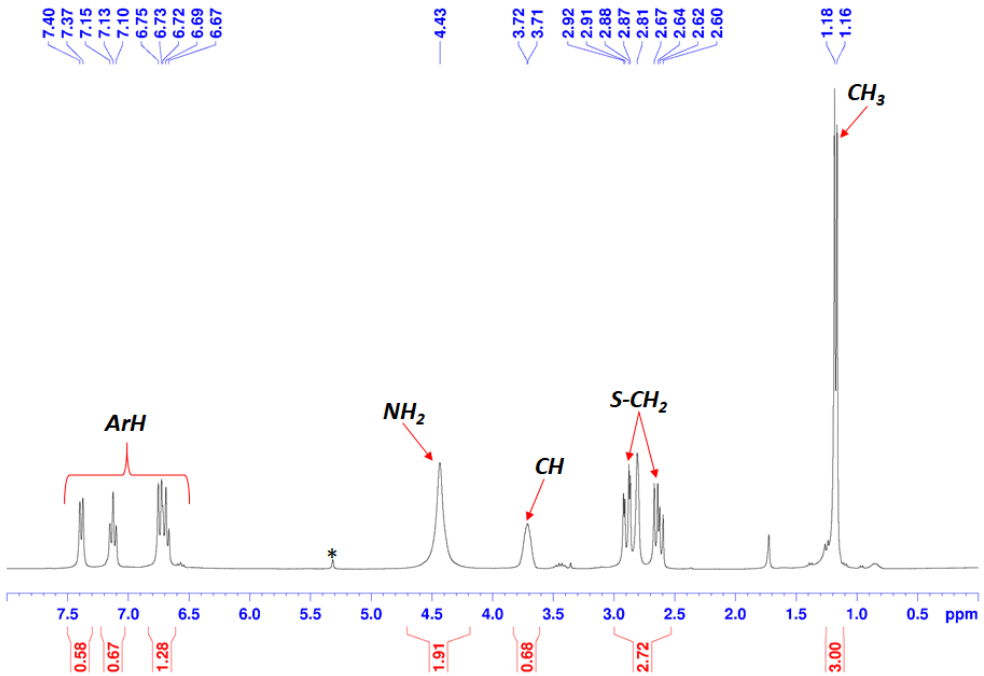

Figure 193: ^{1}H NMR of NSO (400.13 MHz, *CD_2Cl_2, 25°C).

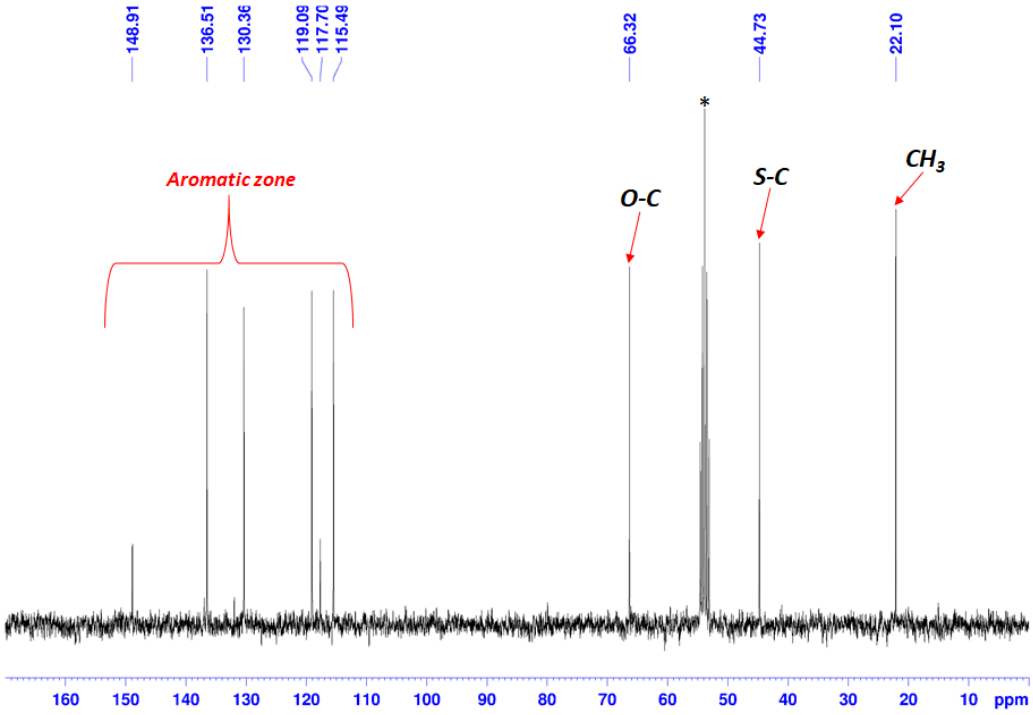

*Figure 194: ^{13}C NMR of NSO (100.62 MHz, *CD_2Cl_2, 25°C).*

6.22 Synthesis and characterization of 1-((2-(isopropylamino)phenyl)thio)propan-2-ol

1-((2-(isopropylamino)phenyl)thio)propan-2-ol [NSO-ISO] was synthesized with a similar procedure reported for *NSSN-ISO* (*figure 195*). *[NSO]* (9.8 g, 53 mmol), zinc (34.82 g, 0.53 mol), acetic acid (250 mL), and acetone (30.90 g, 0.53 mol) were added to a 500 mL round-bottom one necked flask equipped with a condenser and a Teflon-sealed stirbar. The mixture was stirred to room temperature for 24 h.

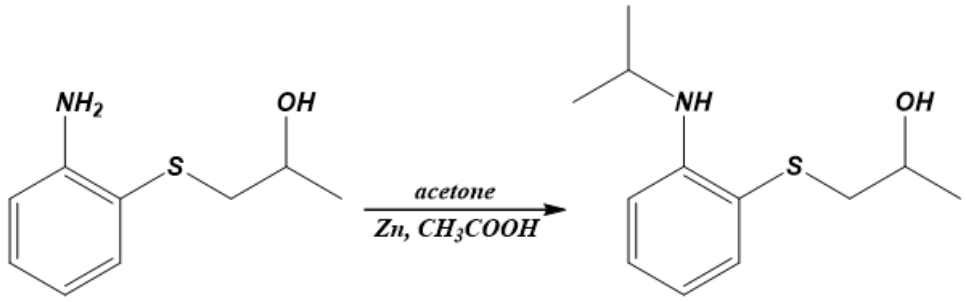

Figure 195: synthesis of NSBen-ISO ligand.

After it was cooled to room temperature, the mixture was quenched with a 30% NH_3 aqueous solution (350 mL) and dichloromethane (300 mL). The organic layer was dried with anhydrous $MgSO_4$, and a yellow oil product was obtained upon removal of the solvent (11.2 g, yield = 83%).

^{1}H NMR (400.13 MHz, TCDE, 25 °C): δ 6.62-7.45 (m, 4H, ArH), 4.92 (s, 1H, NH), 3.63-3.77 (m, 2H, O-CH+N-CH), 2.61-2.87 (m, 2H, S-CH_2), 1.27 (d, J = 6.27 Hz, 3H, CH_3), 1.22 (d, J = 6.10 Hz, 3H, CH_3). ^{13}C NMR (100.62 MHz, TCDE, 25 °C): δ 21.84, 22.74, 22.83, 43.89, 44.22, 65.96, 110.98, 116.56, 116.61, 130.38, 136.48, 148.20.

An *NSO-ISO* solution (1 mg/mL in CH_2Cl_2) was analyzed by MALDI spectroscopy and the result was reported in *figure 200*. *HRMS* (MALDI). Calcd for $C_{12}H_{20}NOS$ ([M + H]$^+$: m/z 226.1260. Found: m/z 226.1270.

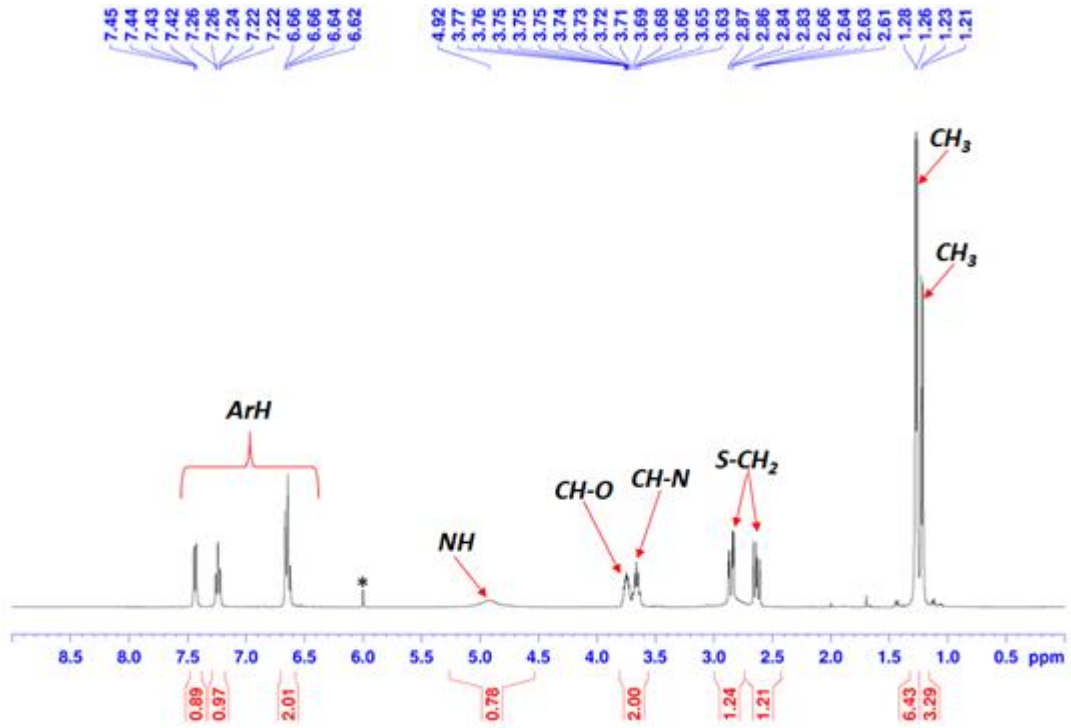

*Figure 196: ^{1}H NMR of NSO-ISO (400.13 MHz, *TCDE, 25°C).*

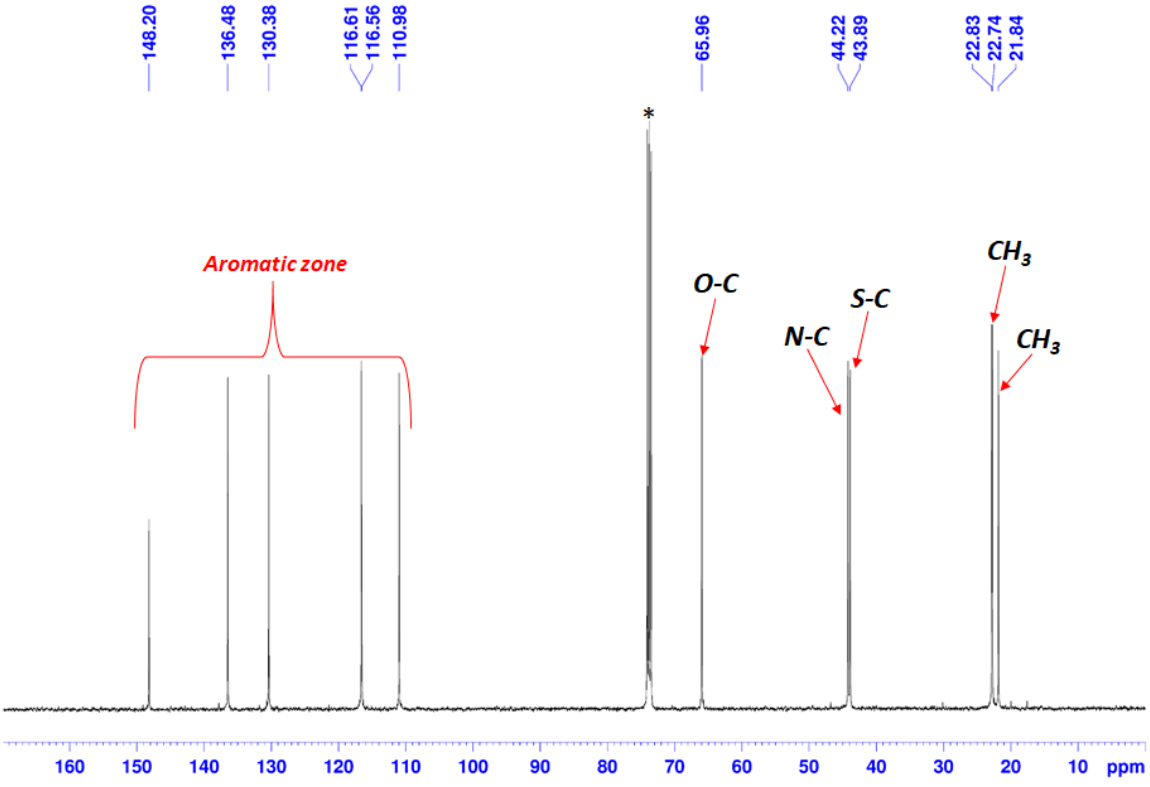

*Figure 197: ^{13}C NMR of NSO-ISO (100.62 MHz, *TCDE, 25°C).*

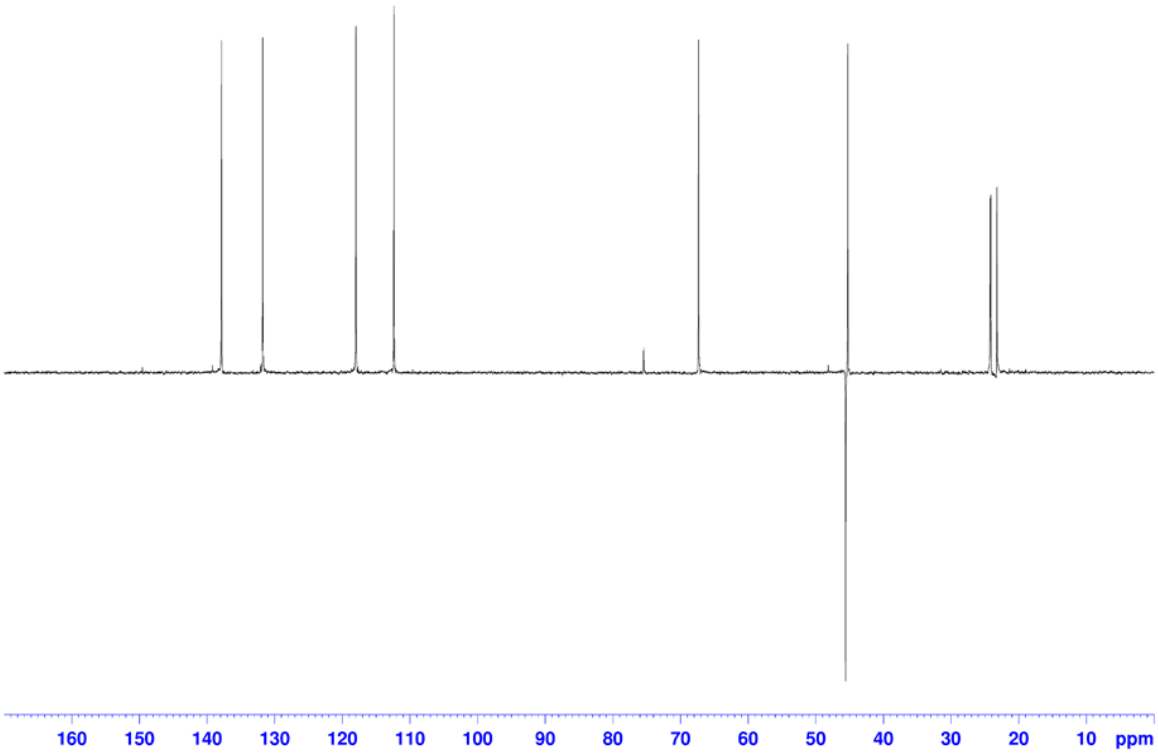

*Figure 198: DEPT 135 NMR of NSO-ISO ligand (100.62 MHz, *TCDE, 25°C).*

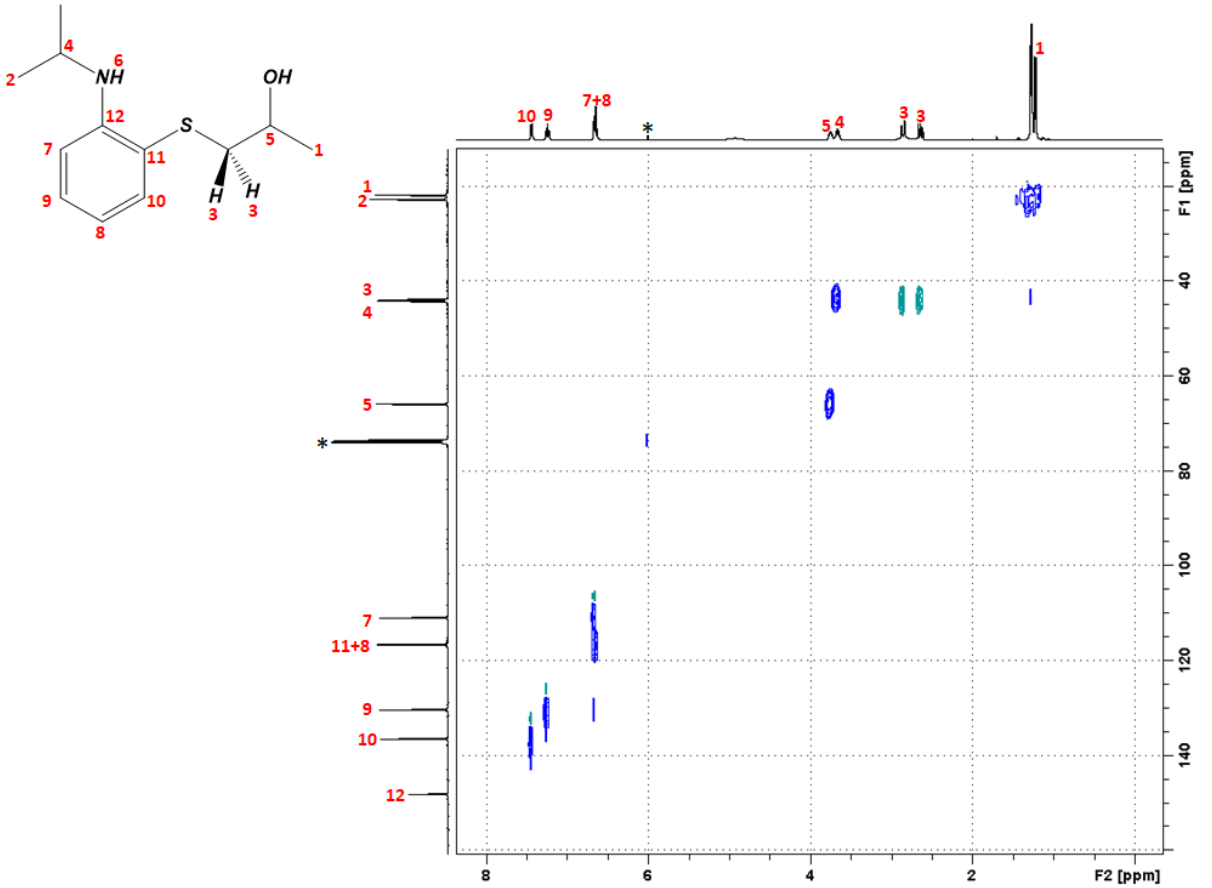

*Figure 199: ^{1}H – ^{13}C HSQC spectrum HSQC of NSO-ISO ligand (400.13/100.62 MHz, *TCDE, 25°C).*

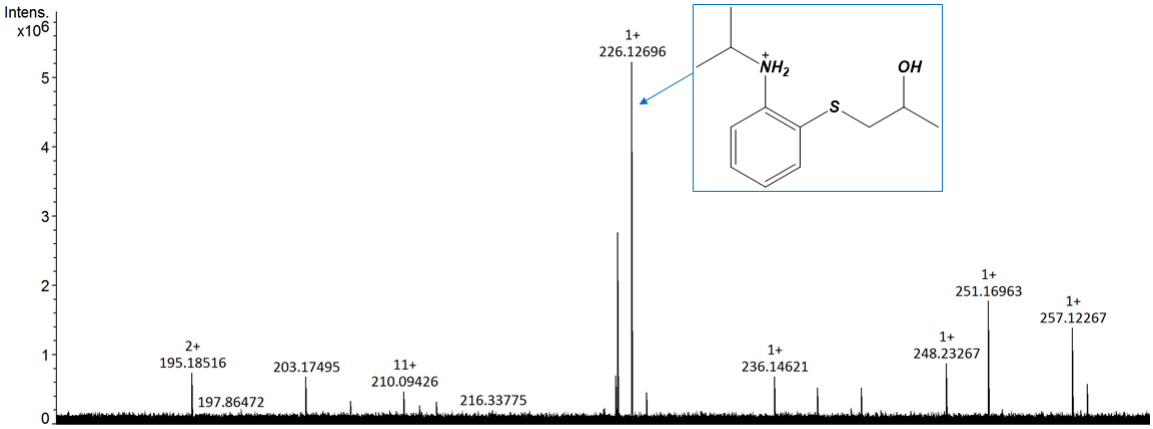

Figure 200: Maldi-MS spectrum of NSO-ISO ligand.

7 Experimental part: synthesis and characterization of group IV metal complexes in the research project.

7.1 Synthesis and characterization of Zr-NSSN-ISO complex

The corresponding *Zr-NSSN-ISO* complex was synthesized by reaction of *NSSN-ISO* proligand with homoleptic metal precursor $Zr(NMe_2)_4$ in toluene as shown in *figure 201*.[91]

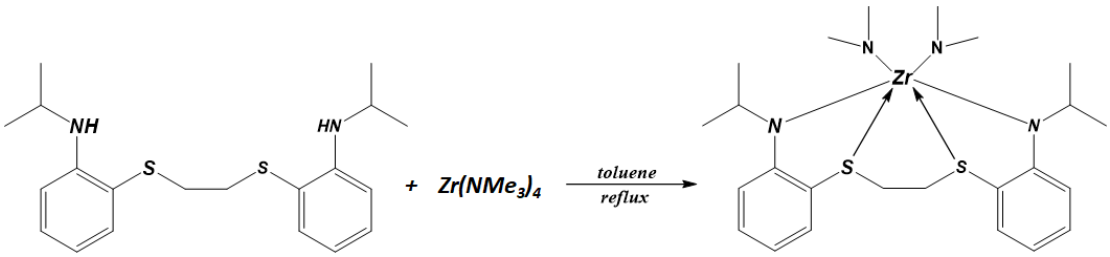

Figure 201: synthesis of Zr-NSSN-ISO complex.

To a 250 mL round-bottom one-necked flask equipped with a condenser and charged with a teflon-sealed stir bar were added *NSSN-ISO* (0.53 g, 1.5 mmol), $Zr(NMe_2)_4$ (0.40 g, 1.5 mmol) and toluene (30 mL). The mixture was stirring to reflux for 24 h. After it was cooled to room temperature, the solvent and volatile components was removed in vacuo. The solid product was washed with dry pentane (5 mL), filtered and dried under reduced pressure to give the product as an orange solid (0.68 g, yield = 85 %).

^{1}H NMR (400.13 MHz, $CDCl_3$, 25 °C) δ ppm. 7.19 (dd, J_1=7.49 Hz, J_2=1.39 Hz, 2H, ArH), 7.10 (m, 2H, ArH), 6.73 (m, 2H, ArH), 6.40 (m, 2H, ArH), 4.17 (m, 2H, 2x CH), 3.12 (d, J=10.27 Hz, 2H, 1x S-CH_2), 2.90 (s, 12H, 2x N(CH_3)$_2$), 2.70 (d, J=10.22 Hz, 2H, 1x S-CH_2), 1.45 (d, J=6.68 Hz, 12H, 4x CH_3). ^{13}C NMR (100.62 MHz, $CDCl_3$, 25 °C) δ ppm. 161.03, 135.33, 130.73, 115.55, 114.48, 114.26, 48.26, 44.51, 39.67, 22.23, 21.81. The attribution of aromatic H and C signals was possible by HSQC experiment.

The complex is insoluble in cold hexane. The crystals for X-ray diffraction analysis was obtained dissolving 20 mg of complex into a vial with hot hexane. The vial was cooled to room temperature. After a few days some crystals are formed into vial and

[91] P. Mehrkhodavandi, R. R. Schrock, P. J. Bonitatebus, *Organometallics*, ***2002***, *21, 5785-5798.*

they are analyzed by X-ray diffraction analysis. The single crystal structure was reported in Cristallographic Data (*figure 281)*.

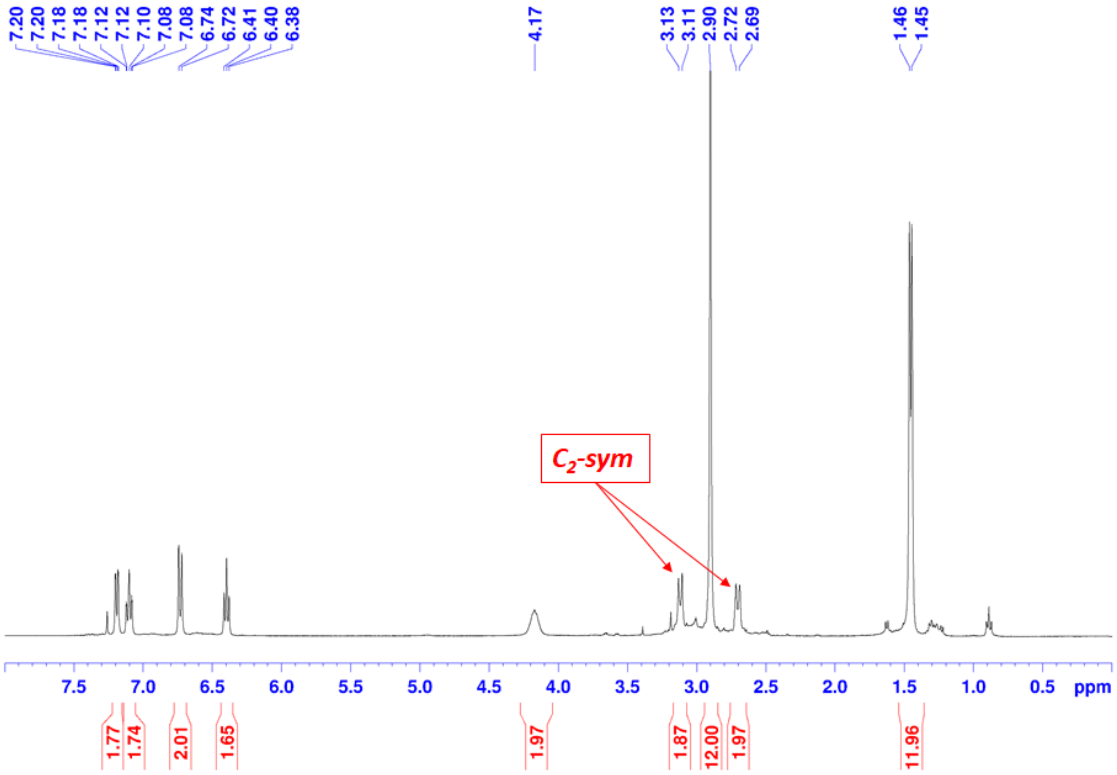

*Figure 202: ^{1}H NMR of Zr-NSSN-ISO complex (400.13 MHz, *$CDCl_3$, 25°C).*

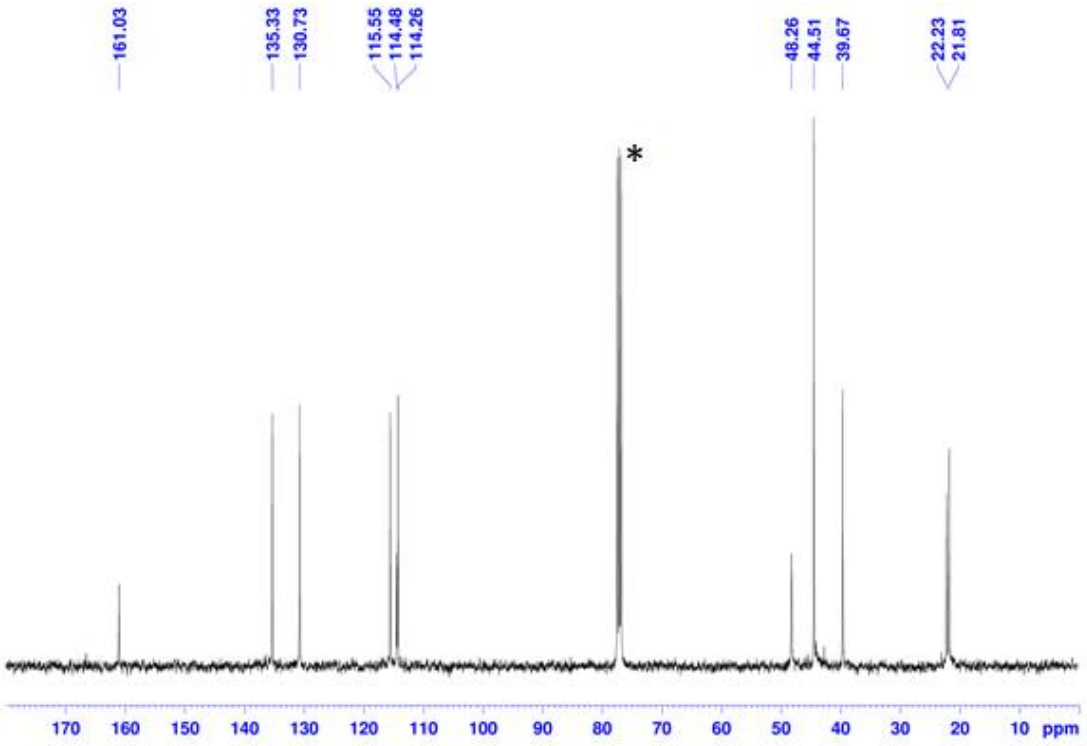

*Figure 203: ^{13}C NMR of Zr-NSSN-ISO complex (100.62 MHz, *$CDCl_3$, 25°C).*

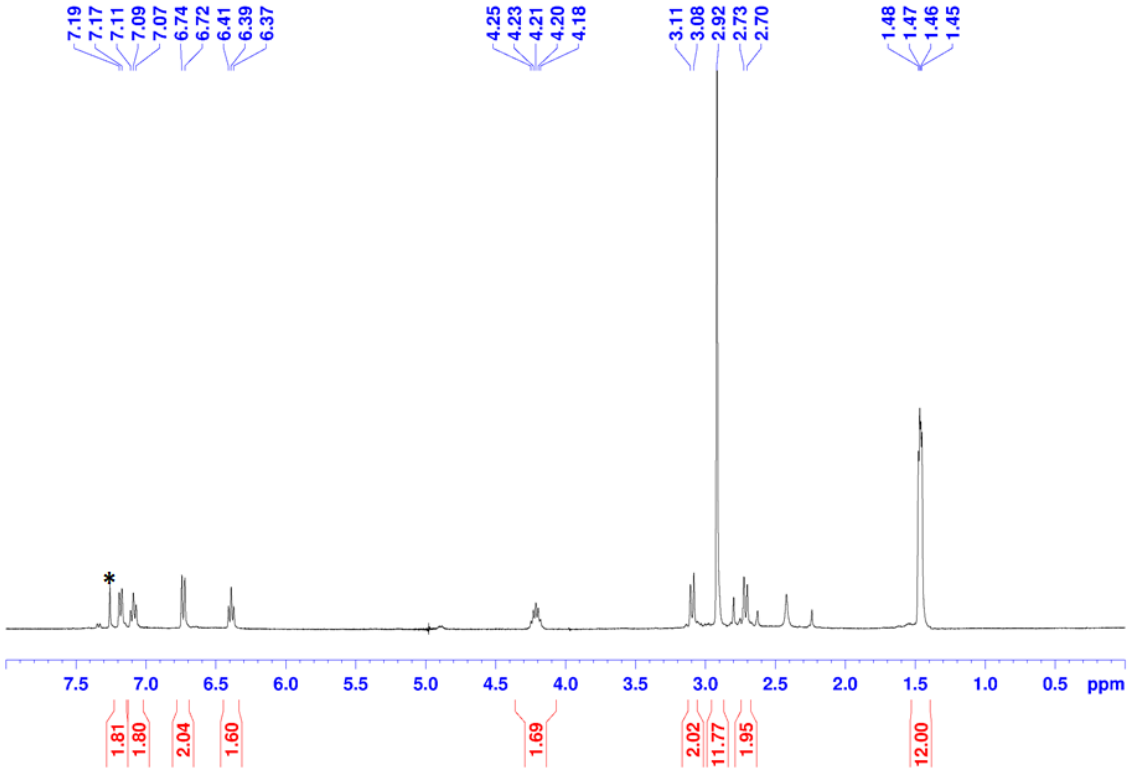

*Figure 204: ^{1}H NMR of Zr-NSSN-ISO complex (400.13 MHz, *$CDCl_3$, 60°C).*

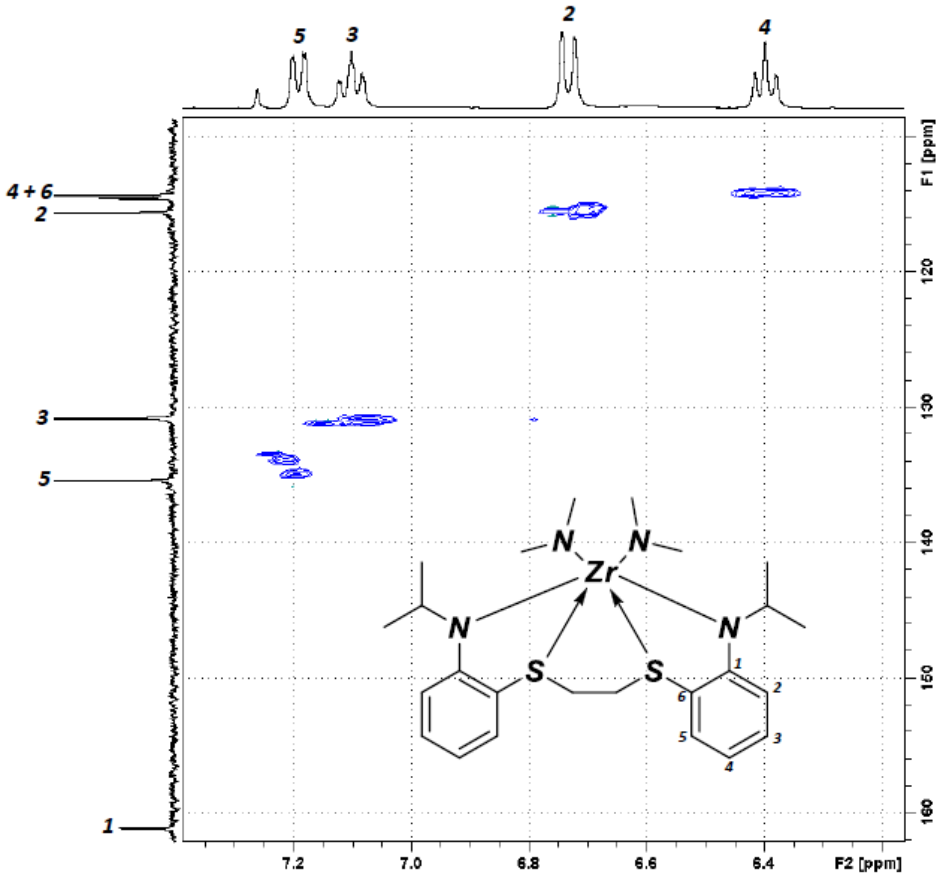

Figure 205: ^{1}H – ^{13}C HSQC spectrum of Zr-NSSN-ISO (aromatic zone) complex (400.13/100.62 MHz, $CDCl_3$, 25°C).

7.2 Synthesis and characterization of Zr-NSSN-CY complex

The corresponding *Zr-NSSN-CY* complex was synthesized by reaction of *NSSN-CY* proligand with homoleptic metal precursor $Zr(NMe_2)_4$ in toluene as shown in *figure 206.*

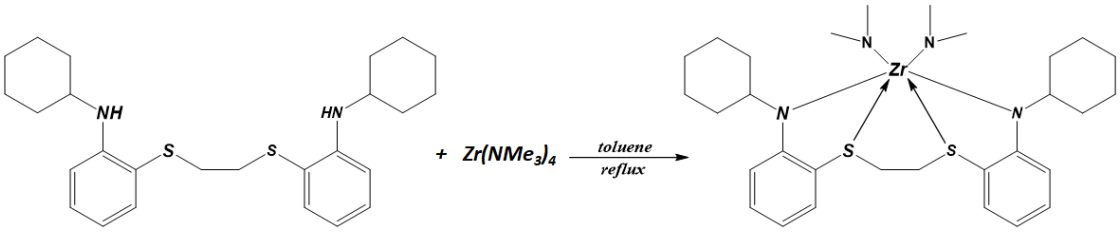

Figure 206: synthesis of Zr-NSSN-CY complex.

The synthesis process is similar to what described in paragraph 7.1.

NSSN-CY (0.70 g, 1.6 mmol), $Zr(NMe_2)_4$ (0.42 g, 1.6 mmol) and toluene (50 mL).

The solid product was washed with dry pentane (5 mL), filtered and dried under reduced pressure to give the product as an orange solid (0.72 g, yield = 73 %).

^{1}H NMR (400.13 MHz, $CDCl_3$, 55 °C) δ ppm. 7.15 (m, 2H, ArH), 7.07 (m, 2H, ArH), 6.82 (m, 2H, ArH), 6.37 (m, 2H, ArH), 3.61 (m, 2H, 2x CH), 3.11 (d, J = 0.18 Hz, 2H, 1x S-CH_2), 2.93 (s, 12H, 2x N(CH_3)$_2$), 2.70 (d, J = 9.43 Hz, 2H, 1x S-CH_2), 2.24-1.17 (m, 22H, 2xCyclohexyl).^{13}C NMR (100.62 MHz, $CDCl_3$, 55 °C) δ ppm. 161.69, 135.28, 130.82, 115.31, 114.09, 114.03, 58.74, 44.78, 39.99, 32.01, 31.48, 27.06, 26.40.

The complex is insoluble in cold hexane. The crystals for X-ray diffraction analysis was obtained dissolving 20 mg of complex into a vial with hot hexane. The vial was cooled to room temperature. After a few days some crystals are formed into vial and they are analyzed by X-ray diffraction analysis. The single crystal structure was reported in *figure 282.*

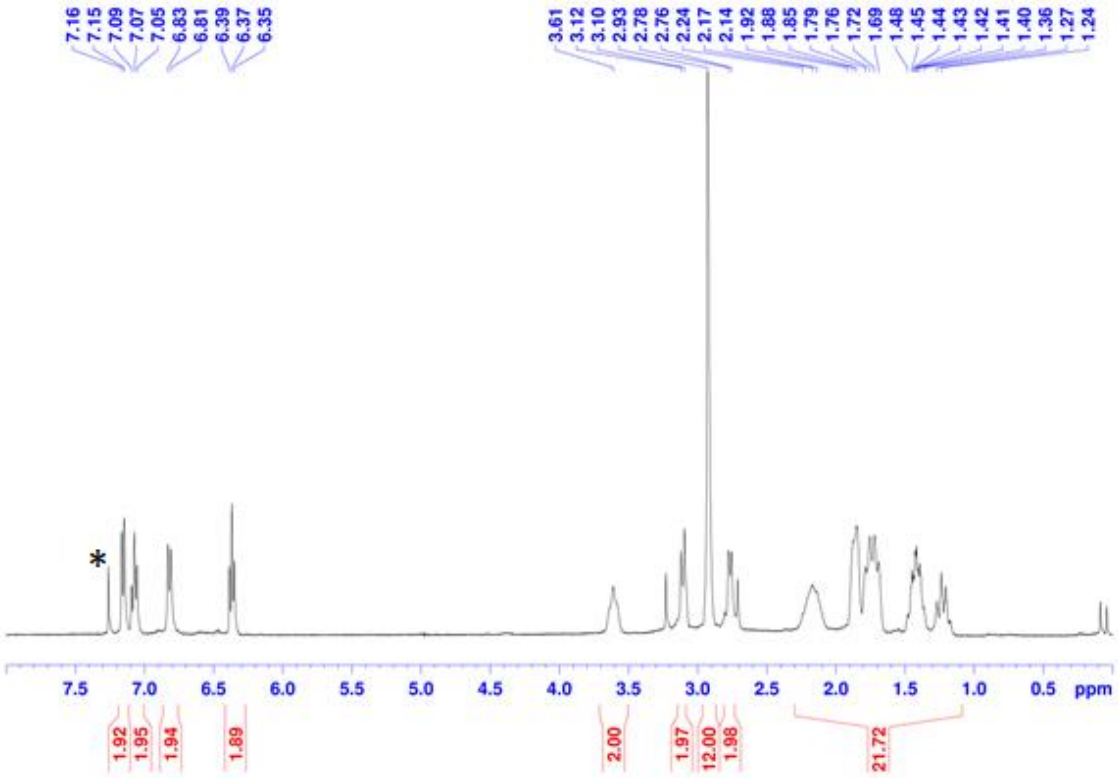

*Figure 207: ^{1}H NMR of Zr-NSSN-CY complex (400.13 MHz, *$CDCl_3$, 25°C).*

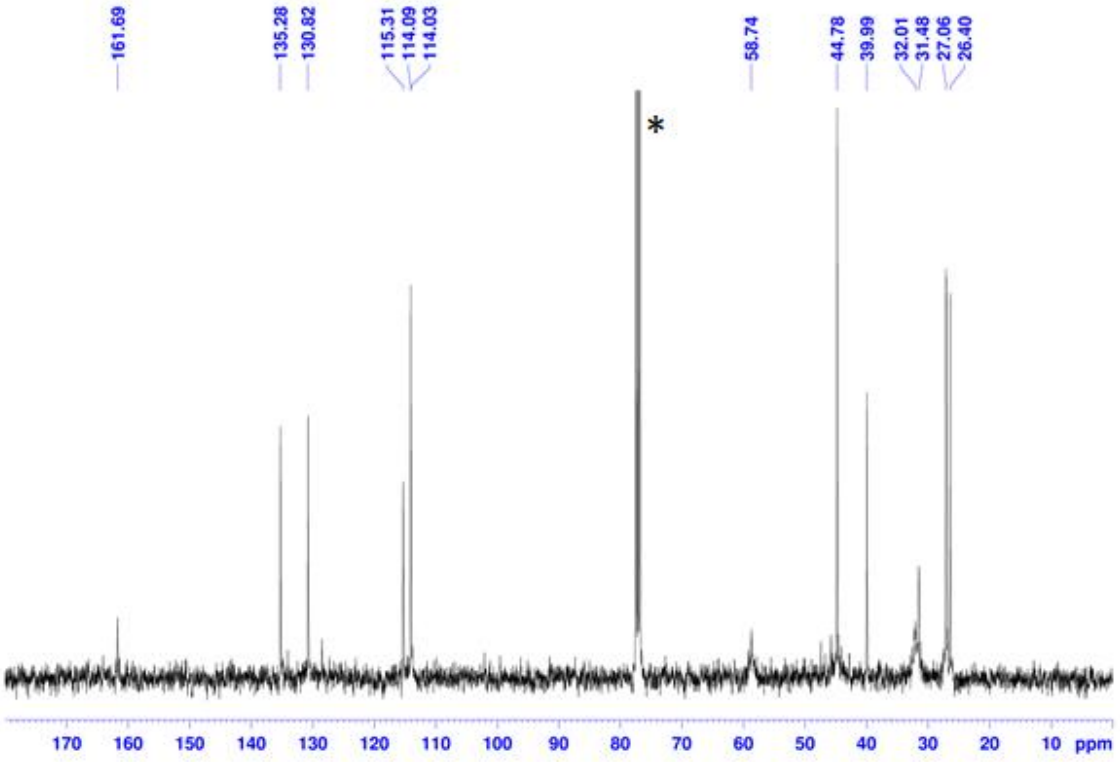

*Figure 208: ^{13}C NMR of Zr-NSSN-CY complex (100.62 MHz, *$CDCl_3$, 25°C).*

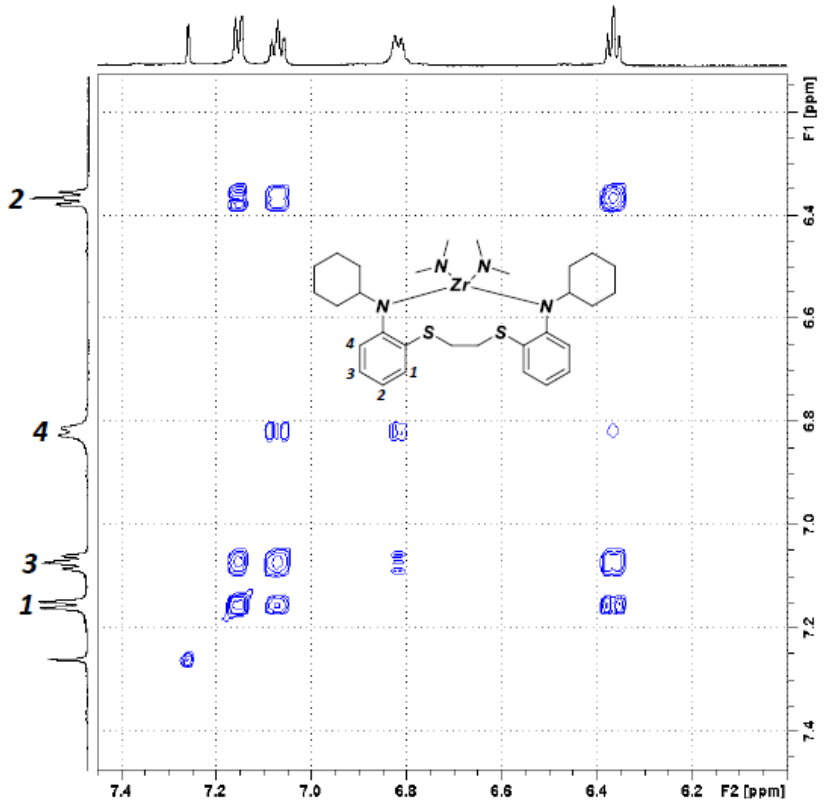

Figure 209: $^{1}H - {}^{1}H$ COSY spectrum of Zr-NSSN-CY (aromatic zone) complex (400.13/400.13 MHz, $CDCl_3$, 25°C).

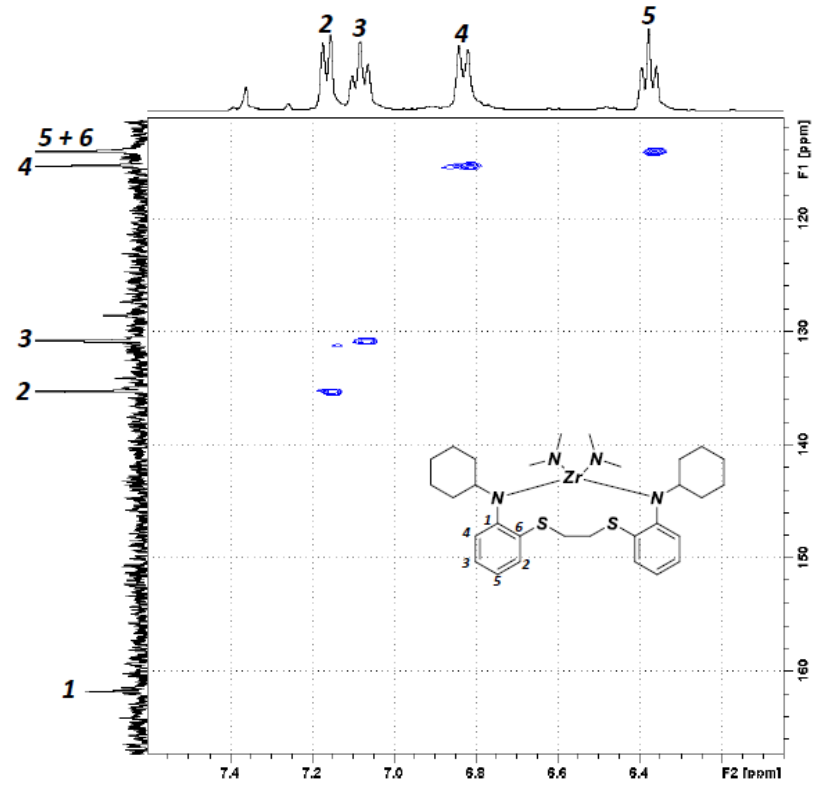

Figure 210: $^{1}H - {}^{13}C$ HSQC spectrum of Zr-NSSN-CY (aromatic zone) complex (400.13/100.62 MHz, $CDCl_3$, 25°C).

7.3 Synthesis and characterization of Zr-NSSN-MESY complex

The corresponding *Zr-NSSN-MESY* complex was synthesized by reaction of *NSSN-MESY* proligand with homoleptic metal precursor *$Zr(NMe_2)_4$* in toluene as shown in *figure 211*.

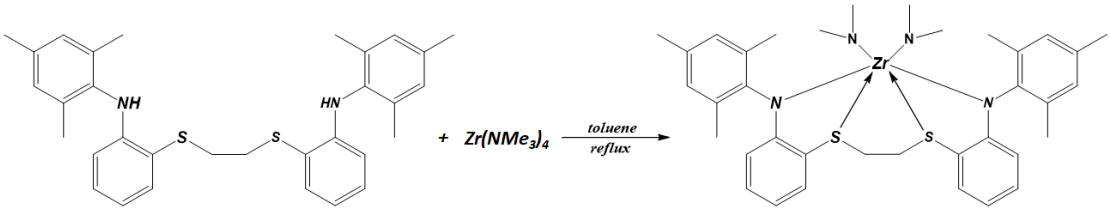

Figure 211: synthesis of Zr-NSSN-MESY complex.

The synthesis process is similar to what described in paragraph 7.1.

NSSN-MESY (0.52 g, 1.0 mmol), $Zr(NMe_2)_4$ (0.27 g, 1.0 mmol) and toluene (30 mL).

The final product was washed with dry pentane (10 mL), filtered and dried under reduced pressure to give the product as an brown solid (0.41 g, yield = 60 %).

^{1}H NMR (400.13 MHz, $CDCl_3$, 55 °C) δ ppm. 7.25 (m, 2H, ArH), 6.92 (m, 6H, ArH), 6.45 (m, 2H, ArH), 5.72 (m, 2H, ArH), 3.25 (d, J = 9.82 Hz, 2H, 1x S-CH_2), 3.04 (d, J = 9.90 Hz, 2H, 1x S-CH_2), 2.30 (s, 12H, 2x N(CH_3)$_2$), 2.26 (s, 6H, CH_3Ar), 2.18 (s, 6H, CH_3Ar), 2.00 (s, 6H, CH_3Ar). ^{13}C NMR (100.62 MHz, $CDCl_3$, 55 °C) δ ppm. 161.15, 145.90, 135.73, 135.48, 134.34, 132.85, 131.84, 129.71, 129.48, 115.18, 113.70, 111.51, 39.44, 20.90, 19.80, 18.21.

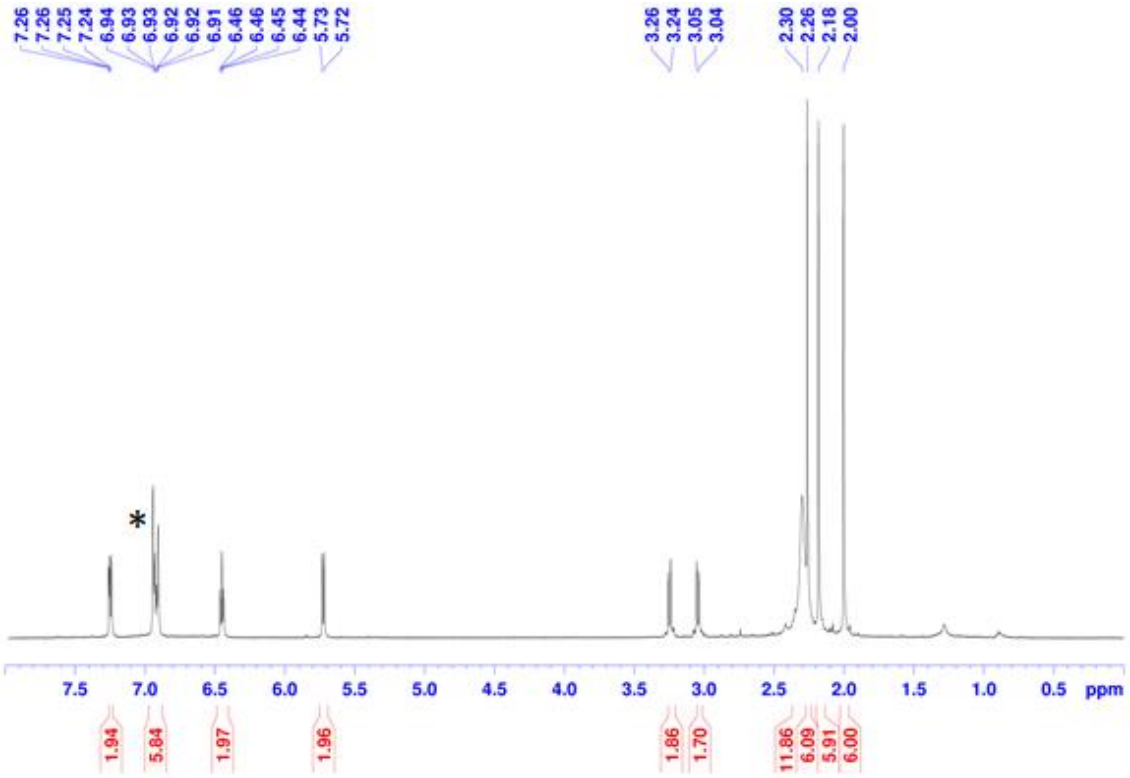

*Figure 212: ^{1}H NMR of Zr-NSSN-MESY complex (400.13 MHz, *$CDCl_3$, 55°C).*

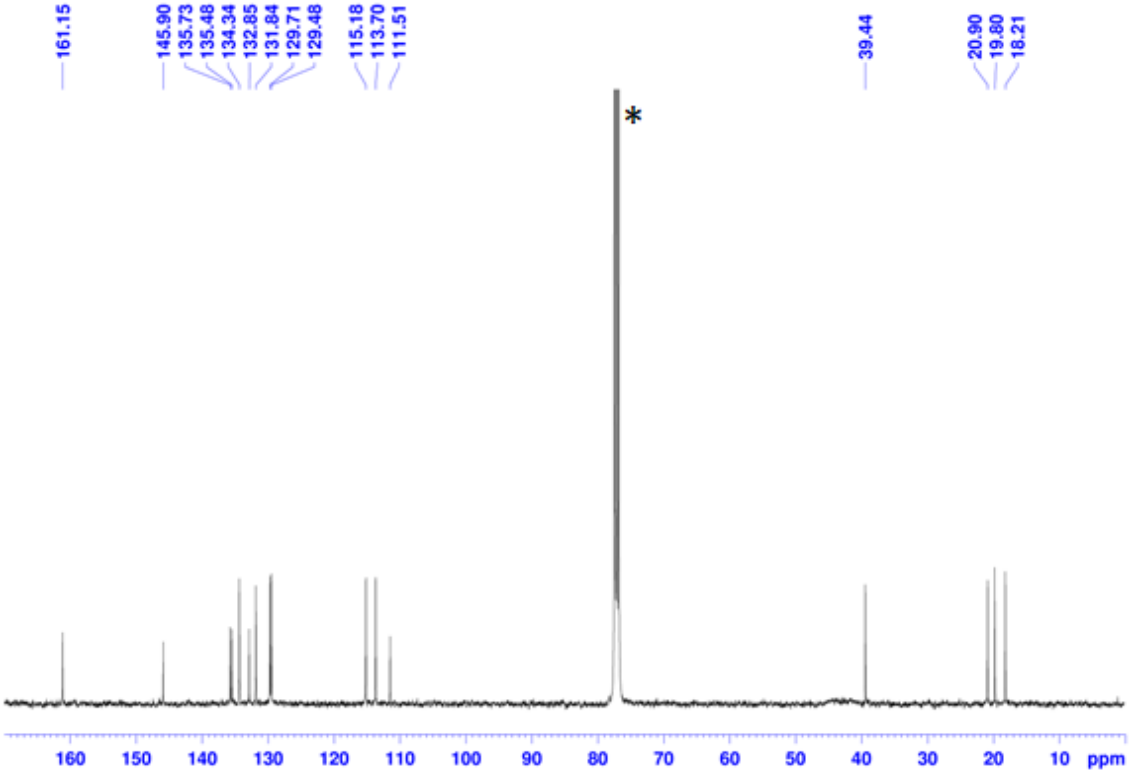

*Figure 213: ^{13}C NMR of Zr-NSSN-MESY complex (100.62 MHz, *$CDCl_3$, 55°C).*

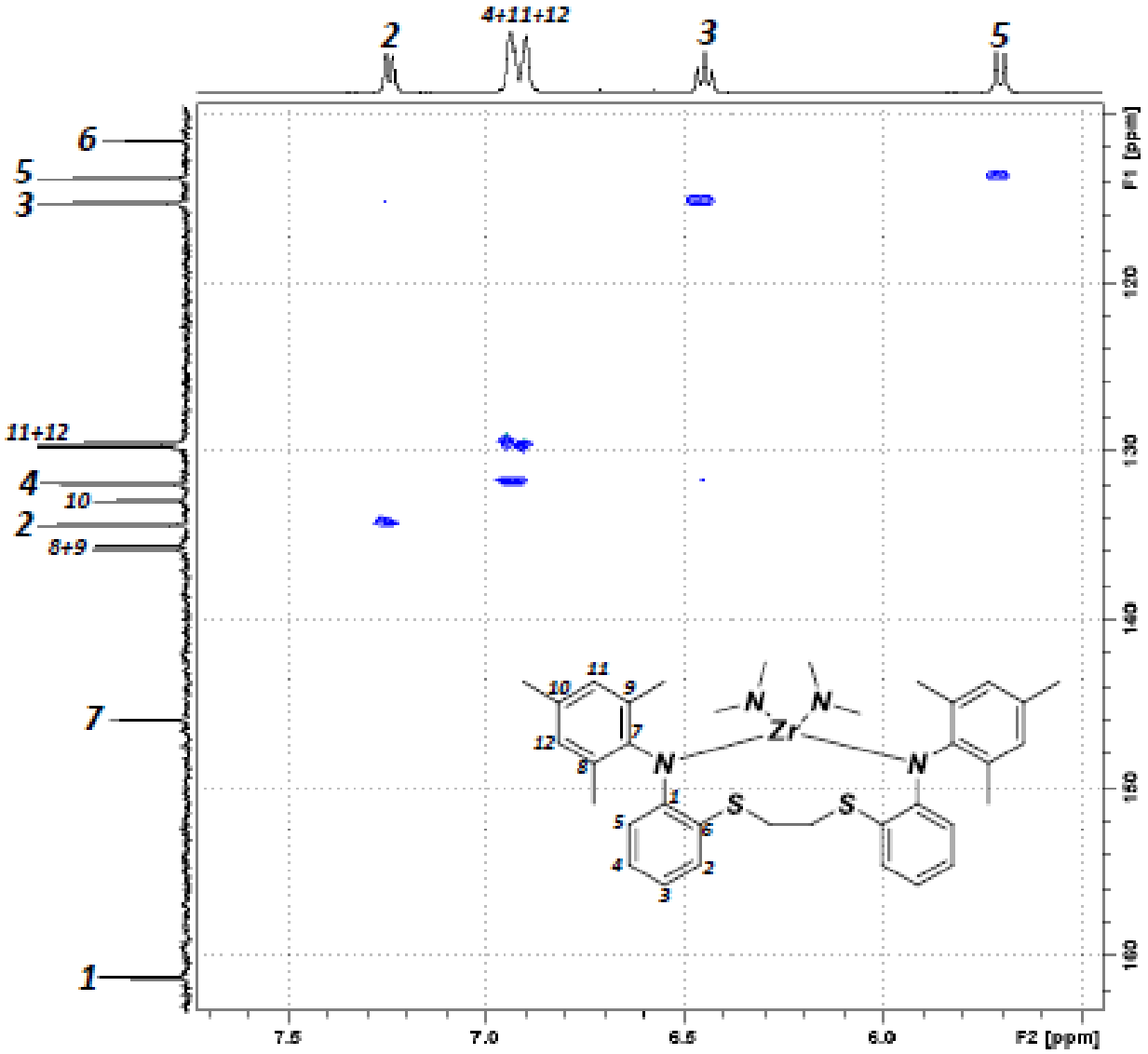

Figure 214: $^{1}H - ^{13}C$ HSQC spectrum of Zr-NSSN-MESY (aromatic zone) complex (400.13/100.62 MHz, $CDCl_3$, 25°C).

7.4 Synthesis and characterization of Hf-NSSN-ISO complex

The corresponding *Hf-NSSN-ISO* complex was synthesized by reaction of *NSSN-ISO* proligand with homoleptic metal precursor $Hf(NMe_2)_4$ in toluene as shown in *figure 215.*

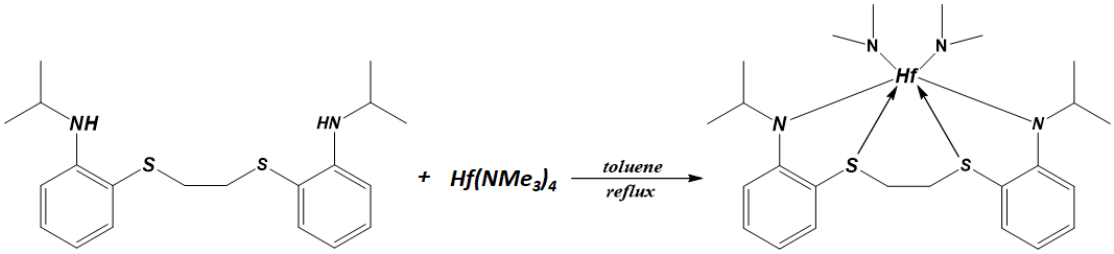

Figure 215: synthesis of Hf-NSSN-ISO complex.

To a 250 mL round-bottom one-necked flask equipped with a condenser and charged with a teflon-sealed stir bar were added *NSSN-ISO* (1.09 g, 3.0 mmol), $Hf(NMe_2)_4$ (1.07 g, 3.0 mmol) and toluene (30 mL). The mixture was stirring to reflux for 24 h. After it was cooled to room temperature, the solvent and volatile components was removed in vacuo at 35 °C. The solid product was washed with dry pentane (10 mL), filtered and dried under reduced pressure to give the product as an yellow solid (1.01 g, yield = 54 %).

^{1}H NMR (400.13 MHz, $CDCl_3$, 55 °C) δ ppm. 7.18 (m, 2H, ArH), 7.10 (m, 2H, ArH), 6.76 (m, 2H, ArH), 6.39 (m, 2H, ArH), 4.25 (m, 2H, 2x CH), 3.17 (d, J = 9.88 Hz, 2H, 1x S-CH_2), 2.96 (s, 12H, 2x N(CH_3)$_2$), 2.71 (d, J = 9.87 Hz, 2H, 1x S-CH_2), 1.47 (m, 12H, 4x CH_3). ^{13}C NMR (100.62 MHz, $CDCl_3$, 55 °C) δ ppm. 161.84, 135.31, 130.64, 116.57, 114.09, 113.72, 47.85, 43.95, 39.64, 22.03, 21.32.

The complex is insoluble in cold hexane. The crystals for X-ray diffraction analysis was obtained dissolving 20 mg of complex into a vial with hot hexane. The vial was cooled to room temperature. After a few days some crystals are formed into vial and they are analyzed by X-ray diffraction analysis. The single crystal structure was reported in *figure 281.*

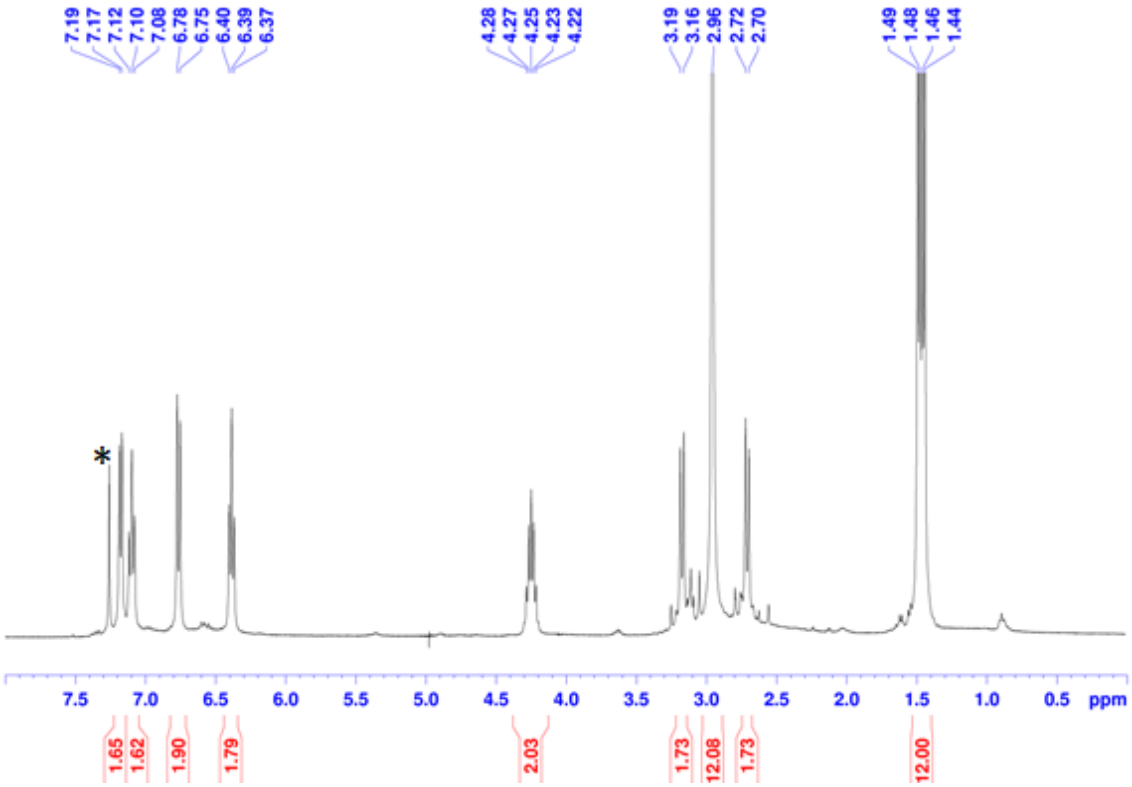

*Figure 216: ^{1}H NMR of Hf-NSSN-ISO complex (400.13 MHz, *$CDCl_3$, 55°C).*

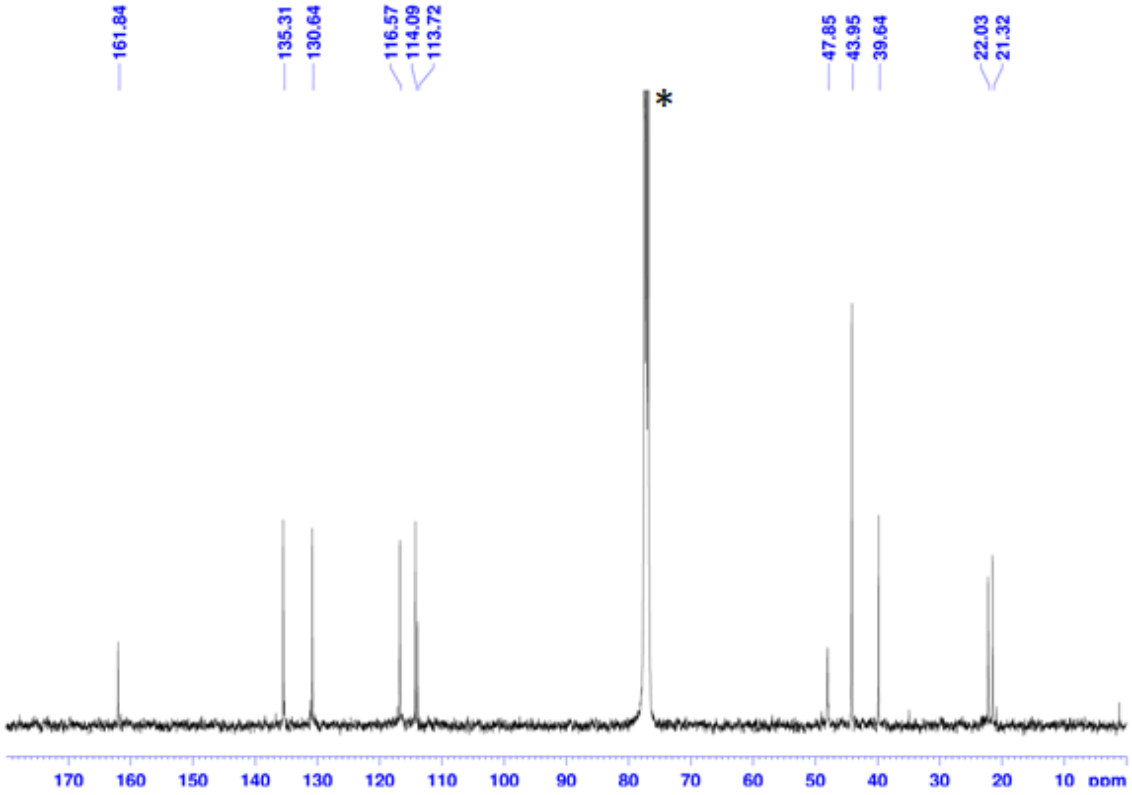

*Figure 217: ^{13}C NMR of Hf-NSSN-ISO complex (100.62 MHz, *$CDCl_3$, 55°C).*

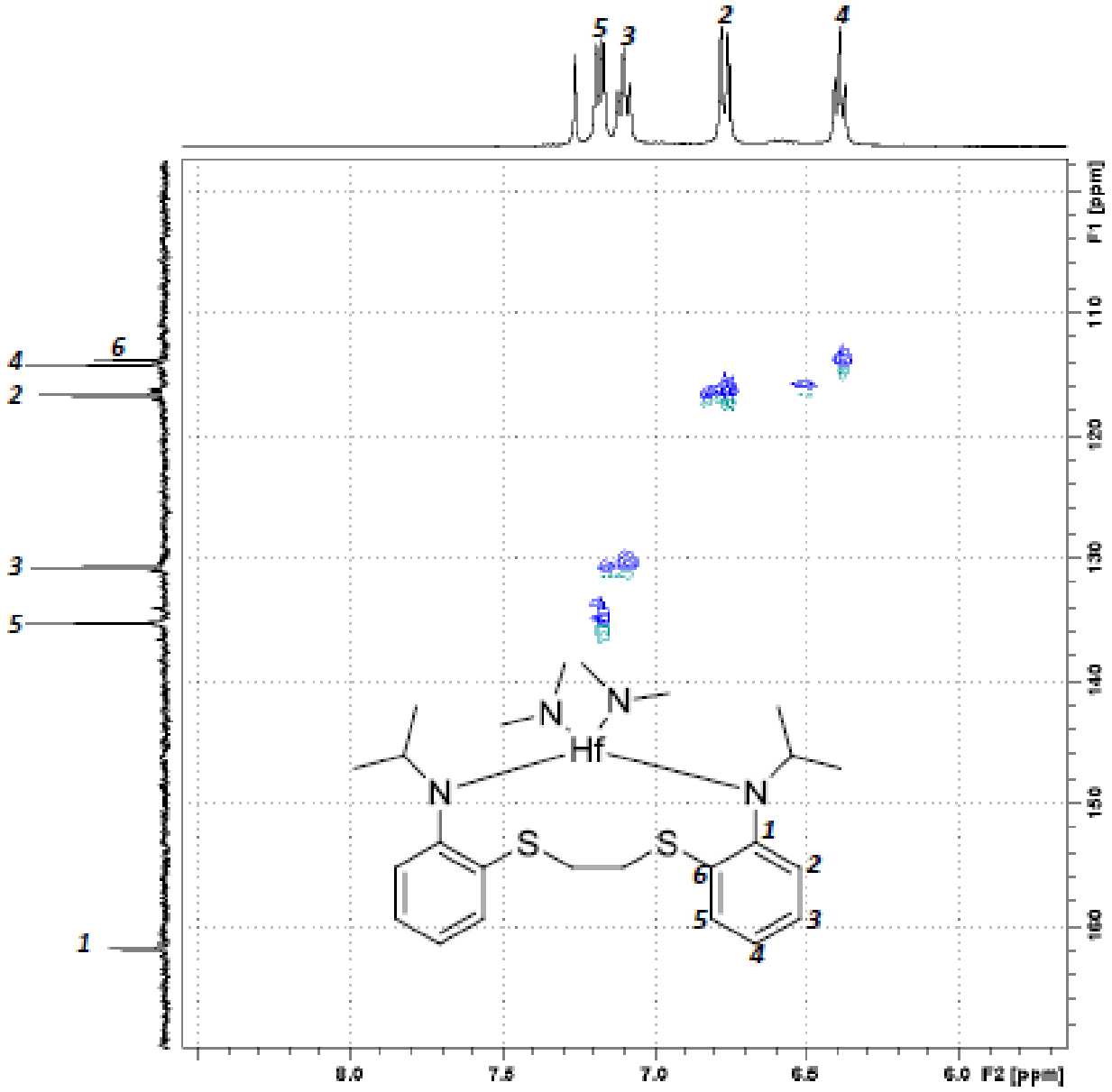

Figure 218: ^{1}H – ^{13}C HSQC spectrum of Hf-NSSN-ISO (aromatic zone) complex (400.13/100.62 MHz, $CDCl_3$, 55°C).

7.5 Synthesis and characterization of Hf-NSSN-CY complex

The corresponding *Hf-NSSN-CY* complex was synthesized by reaction of *NSSN-CY* proligand with homoleptic metal precursor *$Hf(NMe_2)_4$* in toluene as shown in *figure 219.*

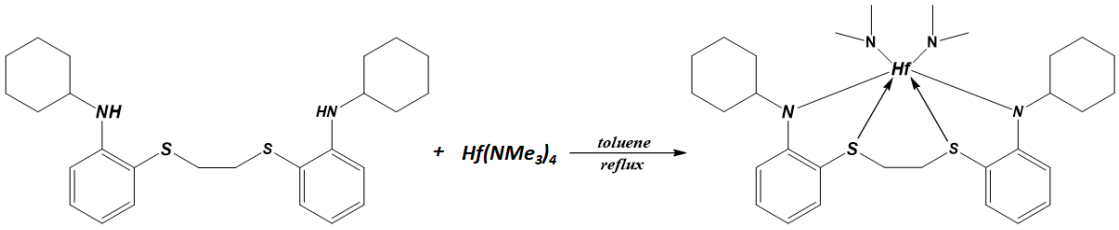

Figure 219: synthesis of Hf-NSSN-CY complex.

The synthesis process is similar to what described in paragraph 7.4.

NSSN-CY (1.02 g, 2.3 mmol), *$Hf(NMe_2)_4$* (0.82 g, 2.3 mmol) and toluene (60 mL). The solid product was washed with dry hexane (10 mL), filtered and dried under reduced pressure to give the product as an yellow solid (1.35 g, yield = 83 %).

^{1}H NMR (400.13 MHz, $CDCl_3$, 55 °C) δ ppm. 7.15 (m, 2H, ArH), 7.08 (m, 2H, ArH), 6.87 (m, 2H, ArH), 6.37 (m, 2H, ArH), 3.68 (m, 2H, 2x CH), 3.18 (d, J = 9.96 Hz, 2H, 1x S-CH_2), 2.98 (s, 12H, 2x N(CH_3)$_2$), 2.76 (d, J = 9.40 Hz, 2H, 1x S-CH_2), 2.22-2.18 (m, 22H, 2xCyclohexyl). ^{13}C NMR (100.62 MHz, $CDCl_3$, 55 °C) δ ppm. 162.67, 135.40, 130.85, 116.54, 114.14, 113.52, 58.48, 44.41, 40.07, 31.80, 31.15, 27.09, 27.01, 26.38.

The complex is insoluble in cold hexane. The crystals for X-ray diffraction analysis was obtained dissolving 20 mg of complex into a vial with hot hexane. The vial was cooled to room temperature. After a few days some crystals are formed into vial and they are analyzed by X-ray diffraction analysis. The single crystal structure was reported in *figure 282.*

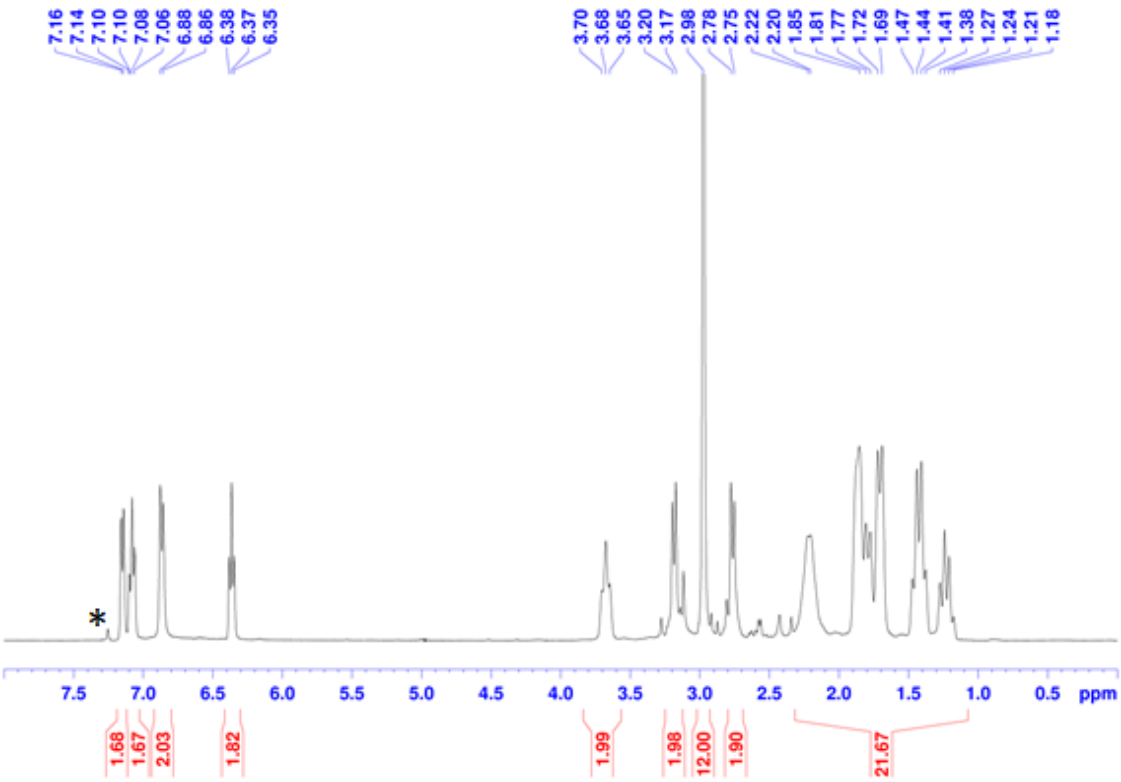

*Figure 220: ^{1}H NMR of Hf-NSSN-CY complex (400.13 MHz, *$CDCl_3$, 55°C).*

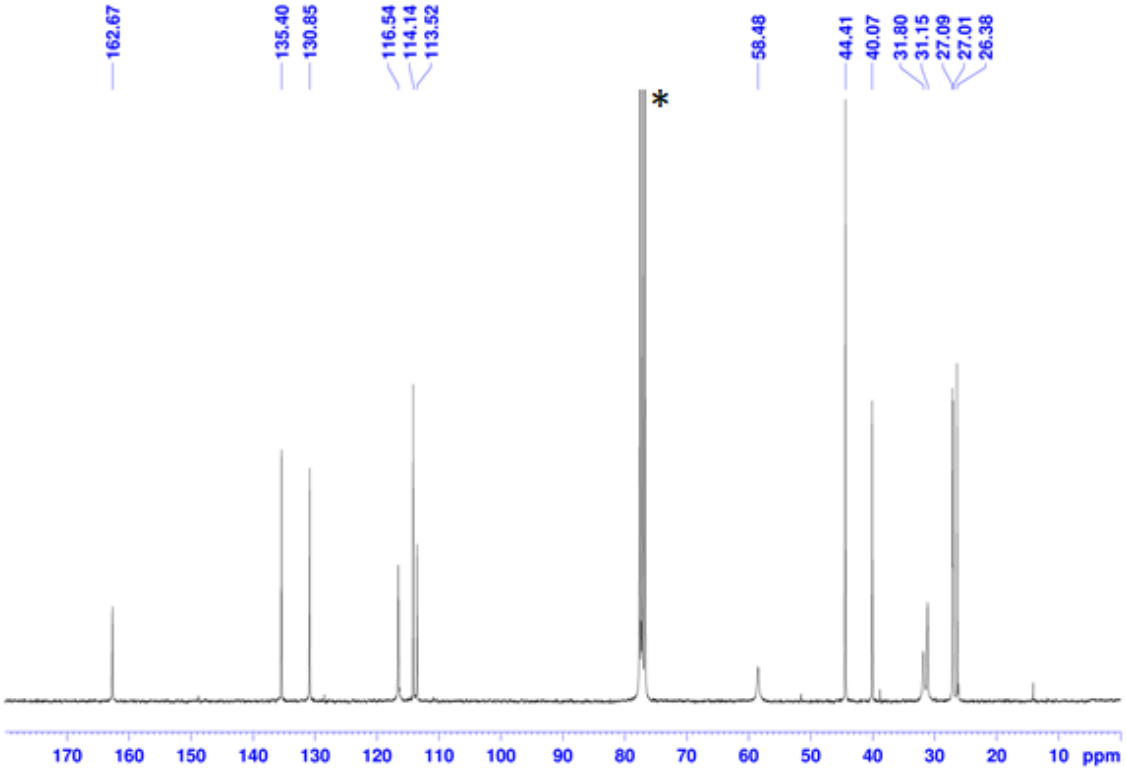

*Figure 221: ^{13}C NMR of Hf-NSSN-CY complex (100.62 MHz, *$CDCl_3$, 55°C).*

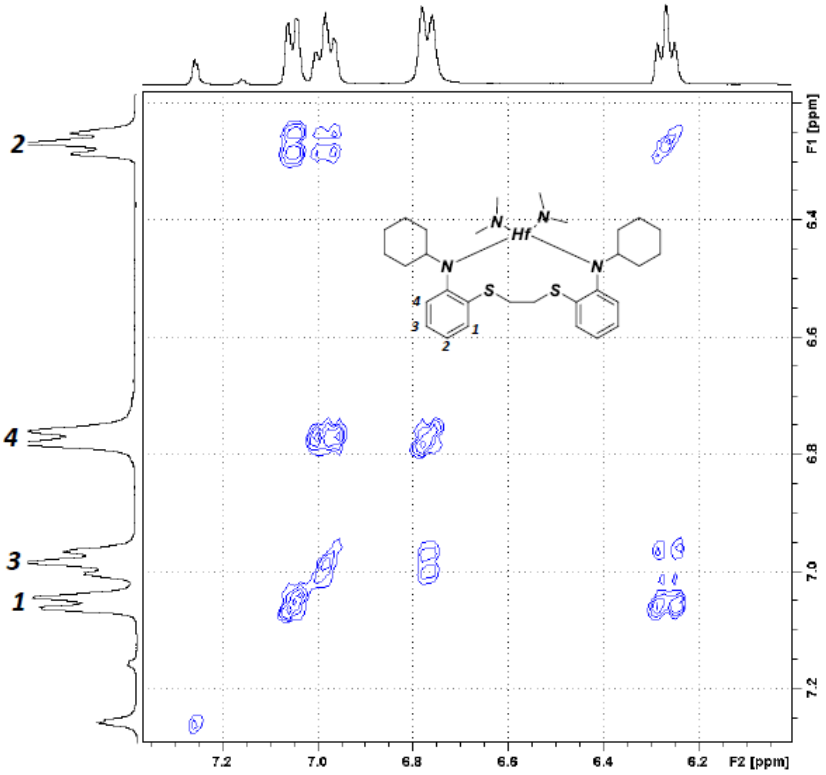

Figure 222: $^{1}H - {}^{1}H$ COSY spectrum of Hf-NSSN-CY (aromatic zone) complex (400.13/400.13 MHz, $CDCl_3$, 55°C).

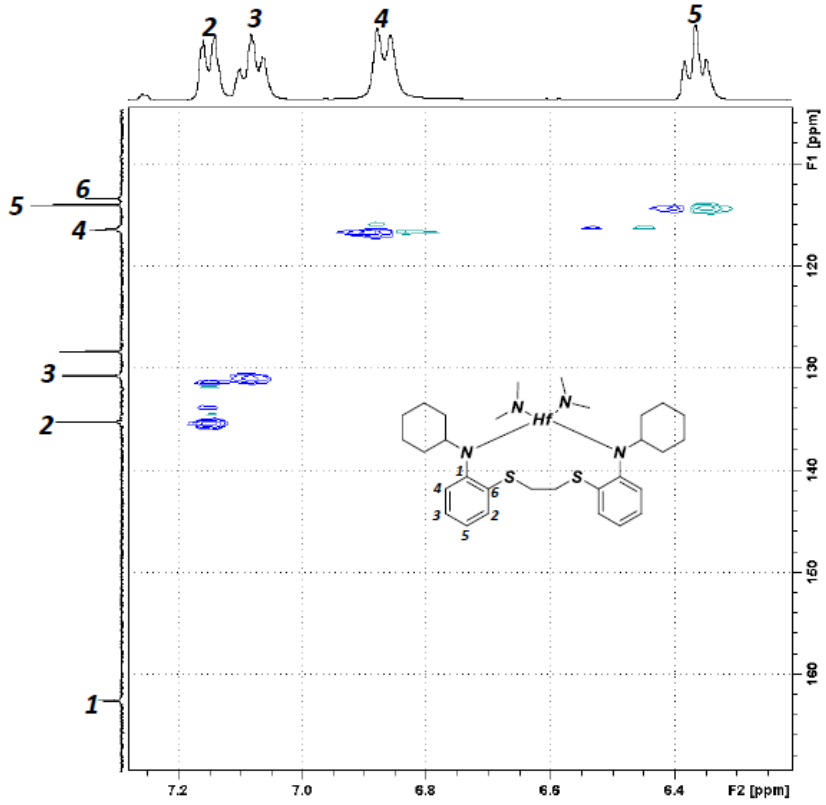

Figure 223: $^{1}H - {}^{13}C$ HSQC spectrum of Hf-NSSN-CY (aromatic zone) complex (400.13/100.62 MHz, $CDCl_3$, 55°C).

8 Experimental part: synthesis and characterization Bi- and Monometallic Al complexes in the research project.

8.1 Synthesis and characterization of Al_2-NSSN-ISO complex

The corresponding *Al_2-NSSN-ISO* complex was synthesized by reaction of *NSSN-ISO* proligand with *Al_2Me_6* in benzene as shown in *figure 224.*

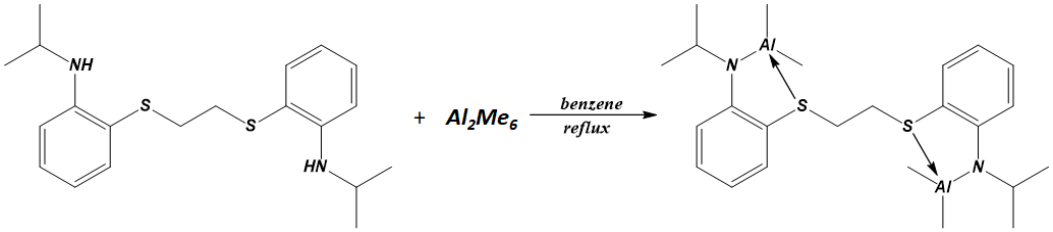

Figure 224: synthesis of Al_2-NSSN-ISO complex.

A solution of *Al_2Me_6* (0.25 g, 1.72 mmol) in benzene (10 mL) was added to a solution of *[NSSN-ISO]* (0.62 g, 1.72 mmol) in benzene (10 mL). The resulting grey solution was refluxed for 16 h, after which the volatiles were removed under vacuum. The solid product was washed with pentane (10 mL) to give *Al_2-NSSN-ISO* as white solid (0.62 g, yield = 76%). Suitable crystals for X-ray diffraction analysis were obtained by cooling a hexane solution at -20 °C overnight. The single crystal structure was reported in Cristallographic Data (*figure 283).*

^{1}H NMR (400.13 MHz, C_6D_6, 25 °C): δ -0.38 (s, 12H, Al-CH_3), 1.18 (d, J = 5.80 Hz, 12H, CH_3), 2.44 (s, 4H, S-CH_2), 3.47 (m, 2H, N-CH), 6.32 (t, J = 7.25 Hz, 2H, ArH), 6.46 (m, J = 8.55 Hz, 2H, ArH), 6.98 (dd, J_1 = 7.56 Hz, J_2 = 1.10, 2H, ArH), 7.09 (t, J = 7.81 Hz, 2H, ArH). ^{1}H NMR (400.13 MHz, CD_2Cl_2, 25 °C): δ -0.69 (s, 12H, Al-CH_3), 1.24 (d, 12H, CH_3), 2.81 (s, 4H, S-CH_2), 3.65 (m, 2H, N-CH), 6.38 (t, J = 7.22 Hz, 2H, ArH), 6.41 (m, J = 8.49 Hz, 2H, ArH), 7.21 (m, J = 7.43 Hz, 4H, ArH). ^{13}C NMR (100.62 MHz, C_6D_6, 25 °C): δ -8.40, 23.12, 34.13, 45.81, 108.79, 112.86, 113.71, 133.29, 135.84, 155.86.

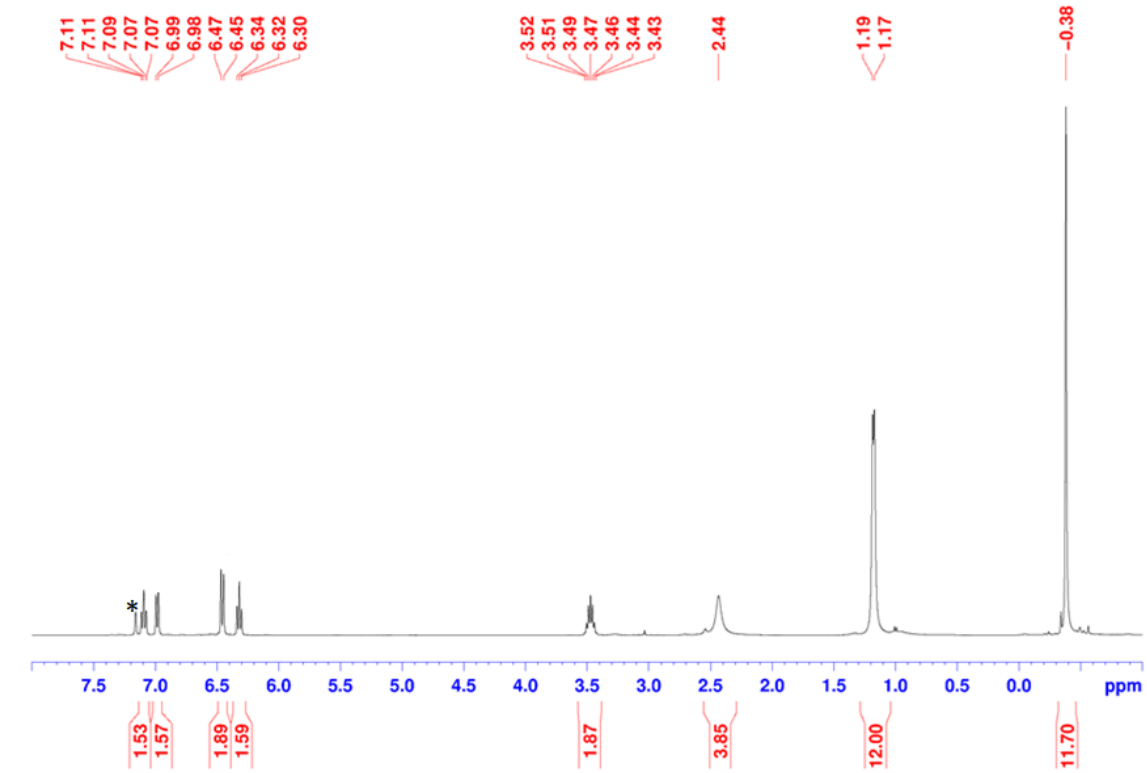

*Figure 225: ^{1}H NMR of Al_2-NSSN-ISO complex (400.13 MHz, *C_6D_6, 25°C).*

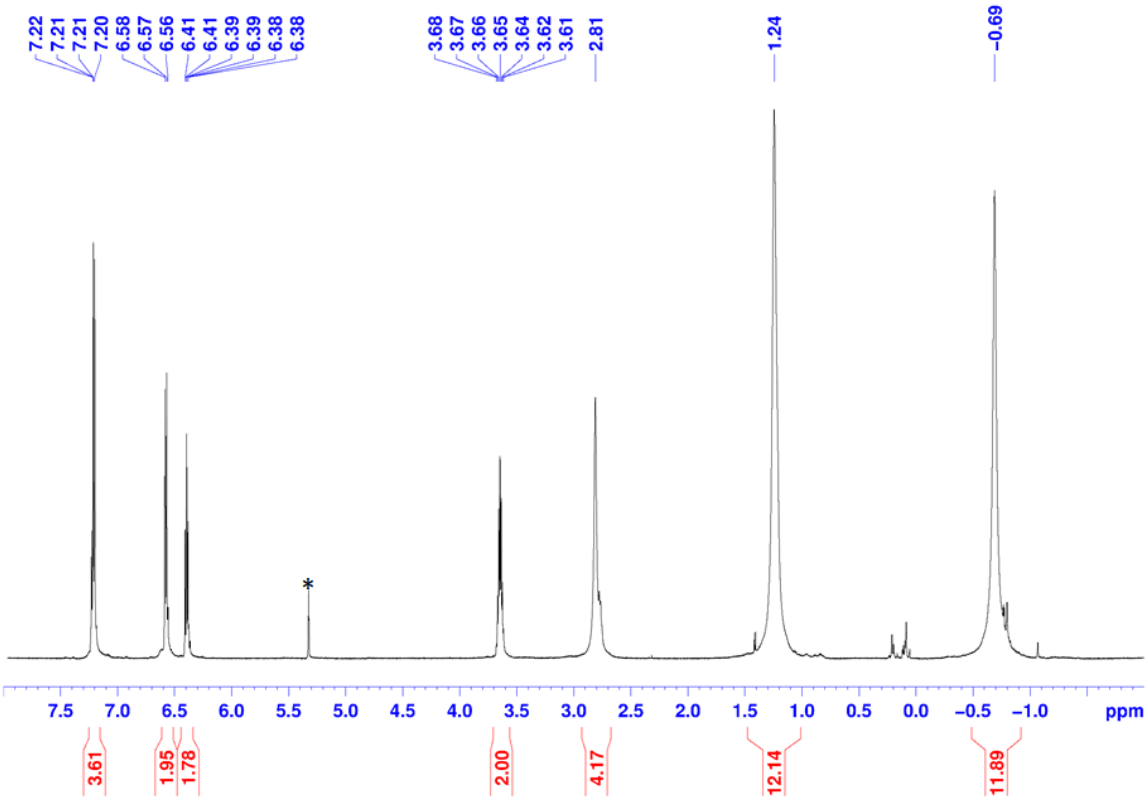

*Figure 226: ^{1}H NMR of Al_2-NSSN-ISO complex (400.13 MHz, *CD_2Cl_2, 25°C).*

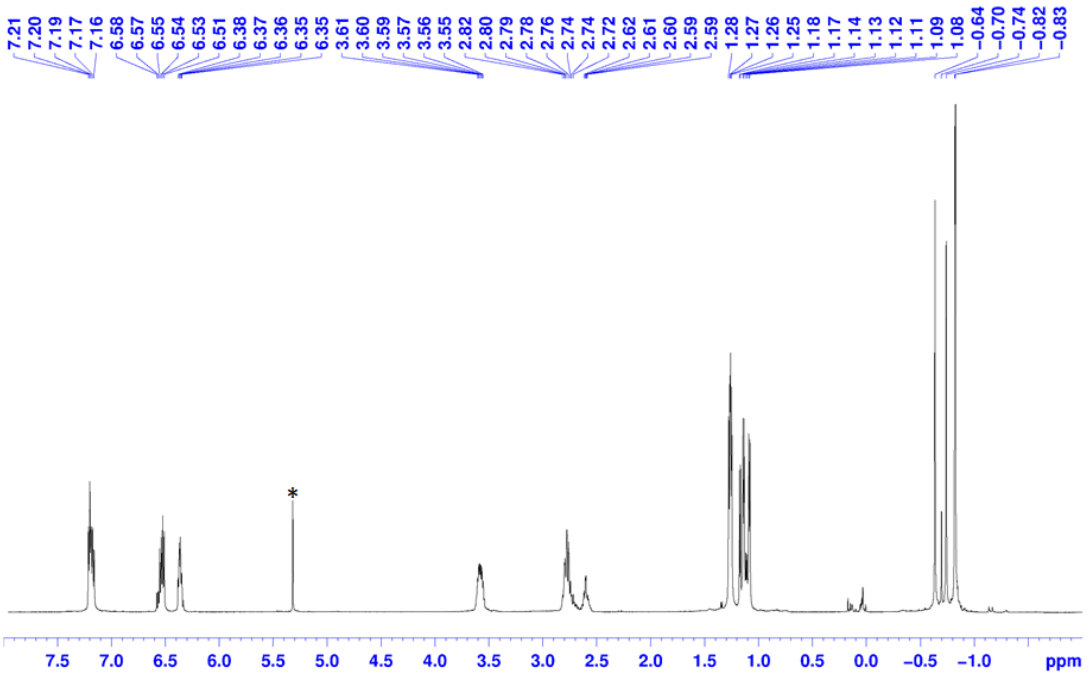

*Figure 227: ^{1}H NMR of Al_2-NSSN-ISO complex (400.13 MHz, *CD_2Cl_2, -60°C).*

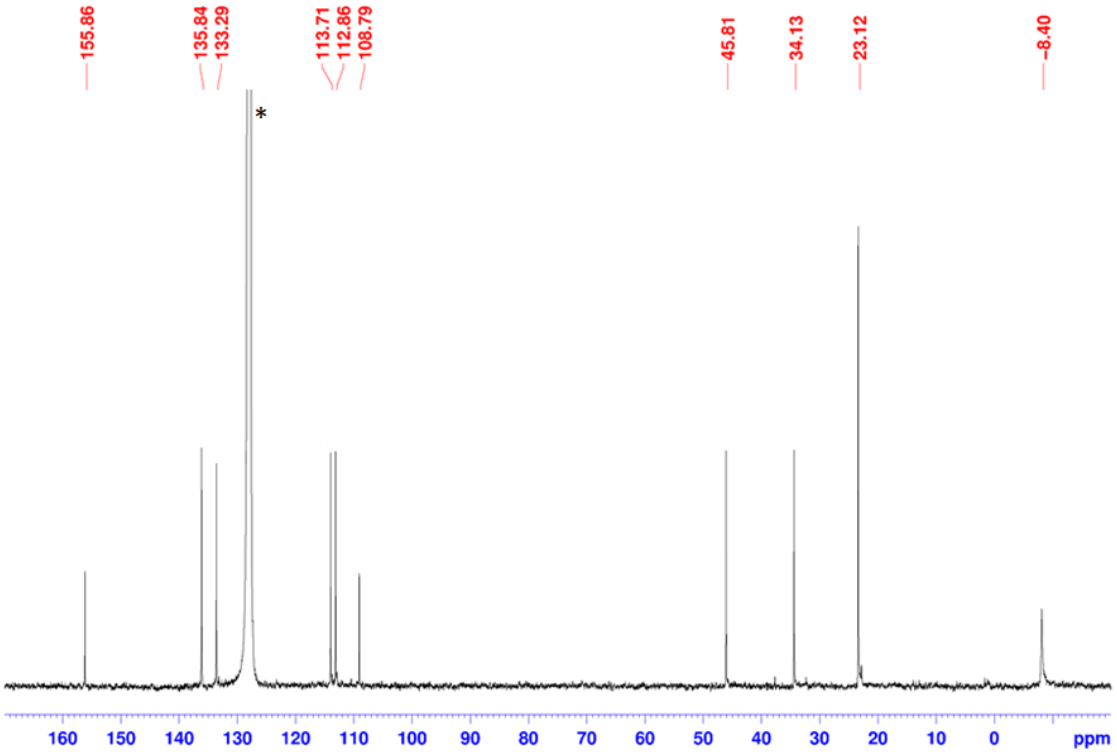

*Figure 228: ^{13}C NMR of Al_2-NSSN-ISO complex (100.62 MHz, *C_6D_6, 25°C).*

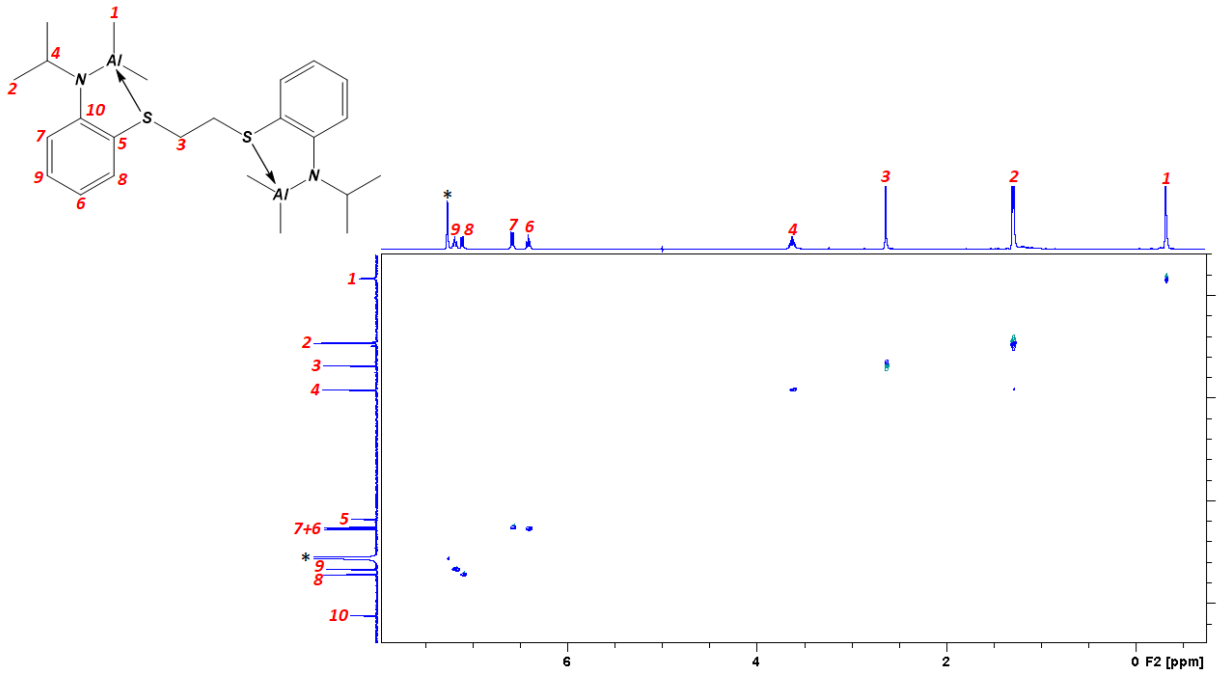

Figure 229: ^{1}H – ^{13}C HSQC spectrum of Al_2-NSSN-ISO complex (400.13/100.62 MHz, *C_6D_6, 25°C).

8.2 Synthesis and characterization of Al_2-NSSN-Cy complex

The corresponding *Al_2-NSSN-CY* complex was synthesized by reaction of *NSSN-Cy* proligand with *Al_2Me_6* in benzene as shown in *figure 230.*

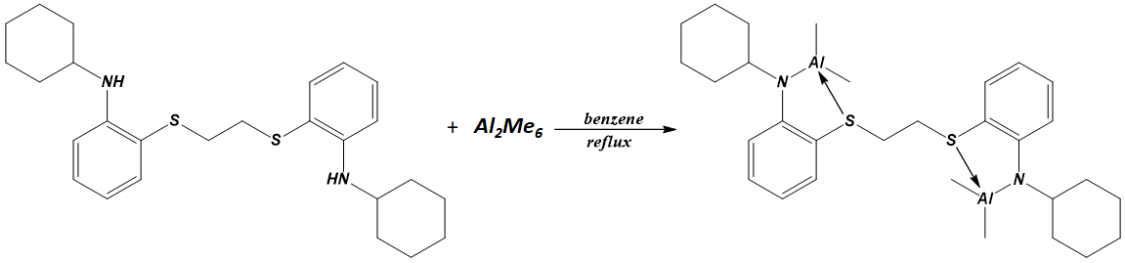

Figure 230: synthesis of Al_2-NSSN-Cy complex.

The synthesis process is similar to what described in paragraph 8.1.

Al_2Me_6 (0.19 g, 1.29 mmol) in benzene (8 mL) and a solution of [*NSSN-Cy*] (0.57 g, 1.29 mmol) in benzene (10 mL). The solid product was washed with dry hexane (10 mL), filtered and dried under reduced pressure to give the product as an yellow solid (1.35 g, yield = 83 %). Suitable crystals for X-ray diffraction analysis were obtained by cooling a hexane solution at -20 °C overnight. The single crystal structure was reported in Cristallographic Data (*figure 284).*

^{1}H NMR (400.13 MHz, C_6D_6, 25 °C) δ -0.39 (s, 12H, Al-CH_3), 1.07-2.11 (m, 20H, Cy), 2.58 (s, 4H, S-CH_2), 3.20 (m, 2H, CH), 6.32 (t, J = 7.27 Hz, 2H, ArH), 6.56 (m, J = 8.51 Hz, 2H, ArH), 7.04 (m, J = 7.77 Hz, 2H, ArH), 7.09 (t, J = 7.38 Hz, 2H, ArH). ^{13}C NMR (100.62 MHz, C_6D_6, 25 °C): δ -7.95, 26.27, 26.37, 34.40, 34.55, 55.22, 109.04, 113.07, 113.98, 133.51, 136.21, 156.06.

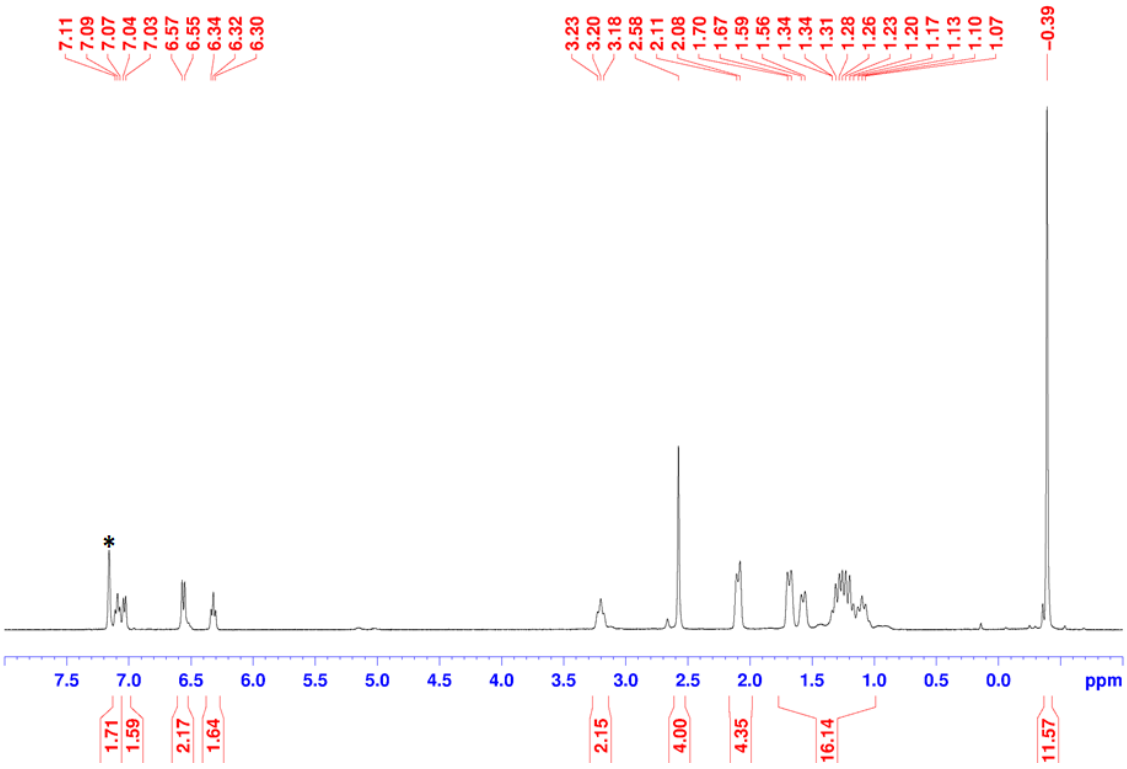

*Figure 231: ^{1}H NMR of Al_2-NSSN-Cy complex (400.13 MHz, *C_6D_6, 25°C).*

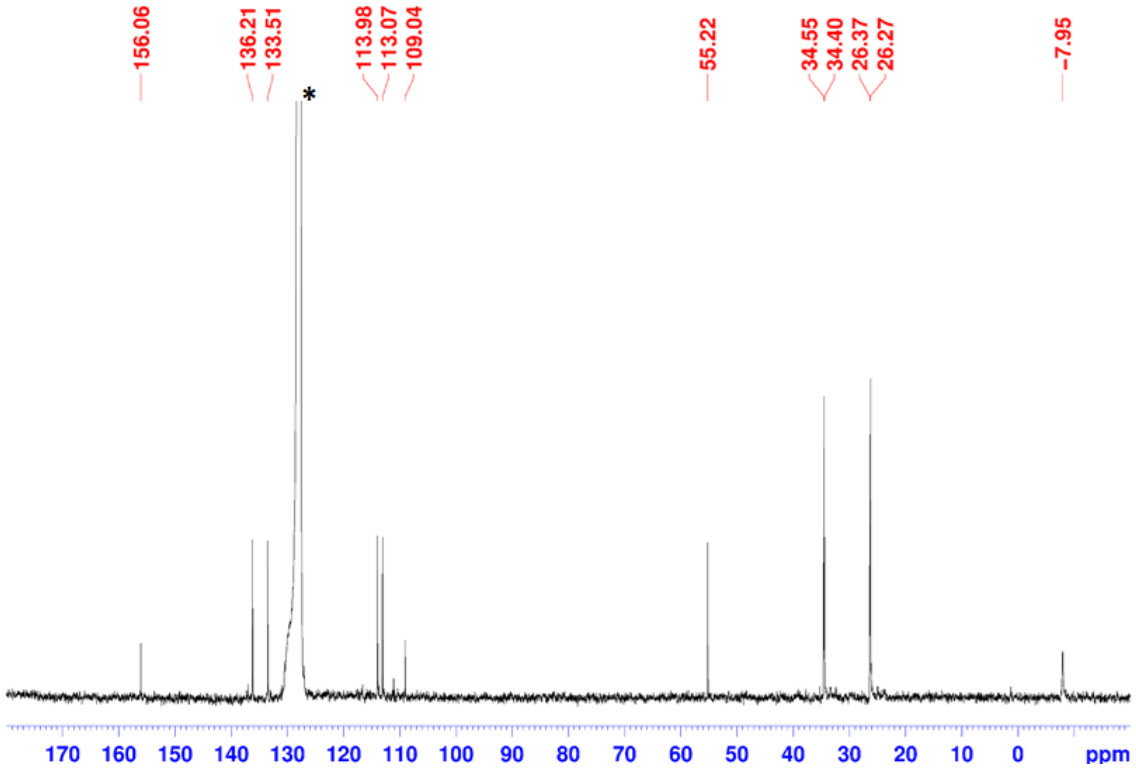

*Figure 232: ^{13}C NMR of Al_2-NSSN-Cy complex (100.62 MHz, *C_6D_6, 25°C).*

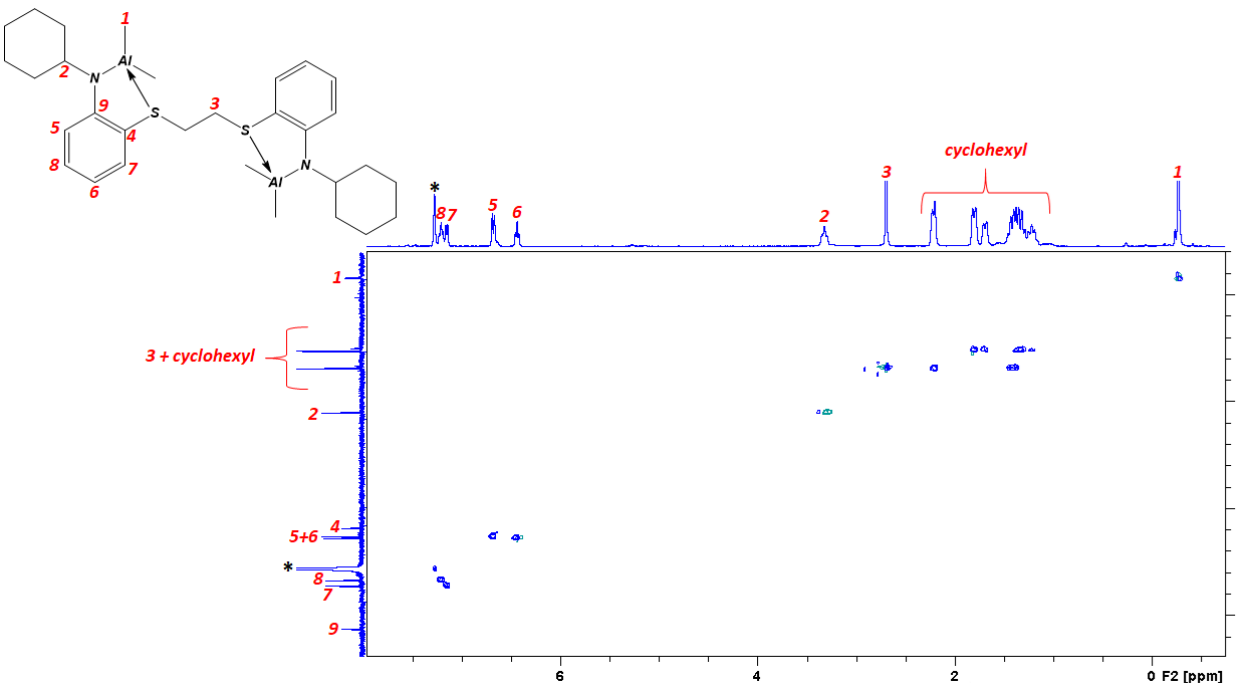

*Figure 233: $^{1}H - ^{13}C$ HSQC spectrum of Al_2-NSSN-Cy complex (400.13/100.62 MHz, *C_6D_6, 25°C).*

8.3 Synthesis and characterization of Al_2-NSSN-Cl-ISO complex

The corresponding *Al_2-NSSN-Cl-ISO* complex was synthesized by reaction of *NSSN-Cl-ISO* proligand with *Al_2Me_6* in benzene as shown in *figure 234.*

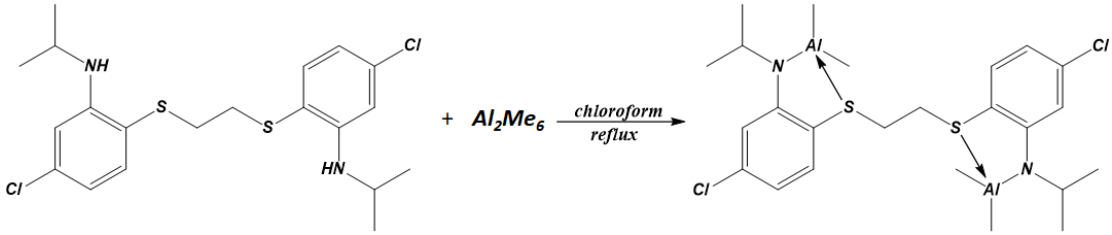

Figure 234: synthesis of Al_2-NSSN-Cl-ISO complex.

A solution of *Al_2Me_6* (0.19 g, 1.30 mmol) in chloroform (10 mL) was added to a solution of [*NSSN-ISO-Cl*] (0.56 g, 1.30 mmol) in chloroform (10 mL). The resulting grey solution was refluxed for 16 h, after which the volatiles were removed under vacuum. The solid product was washed with hexane (2 x 10 mL) to give *Al_2-NSSN-Cl-ISO* as white solid (0.57 g, yield = 81%).

^{1}H NMR (400.13 MHz, C_6D_6, 25 °C) δ -0.37 (s, 12H, Al-CH_3), 1.24 (d, J = 6.54 Hz, 12H, CH_3), 1.48 (q, 2H, CH_2), 2.21 (t, 4H, S-CH_2), 3.57 (m, 2H, N-CH), 6.34 (m, J = 7.50 Hz, 2H, ArH), 6.52 (m, J = 8.48 Hz, 2H, ArH), 6.96 (dd, J_1 = 7.61 Hz, J_2 = 1.33 Hz, 2H, ArH), 7.13 (t, J = 7.77 Hz, 2H, ArH). ^{13}C NMR (100.62 MHz, C_6D_6, 60 °C): δ -7.90, 23.45, 25.25, 36.07, 46.13, 110.33, 112.99, 113.89, 133.31, 136.15, 156.00.

Suitable crystals for X-ray diffraction analysis were obtained by cooling a pentane solution at -20 °C overnight.

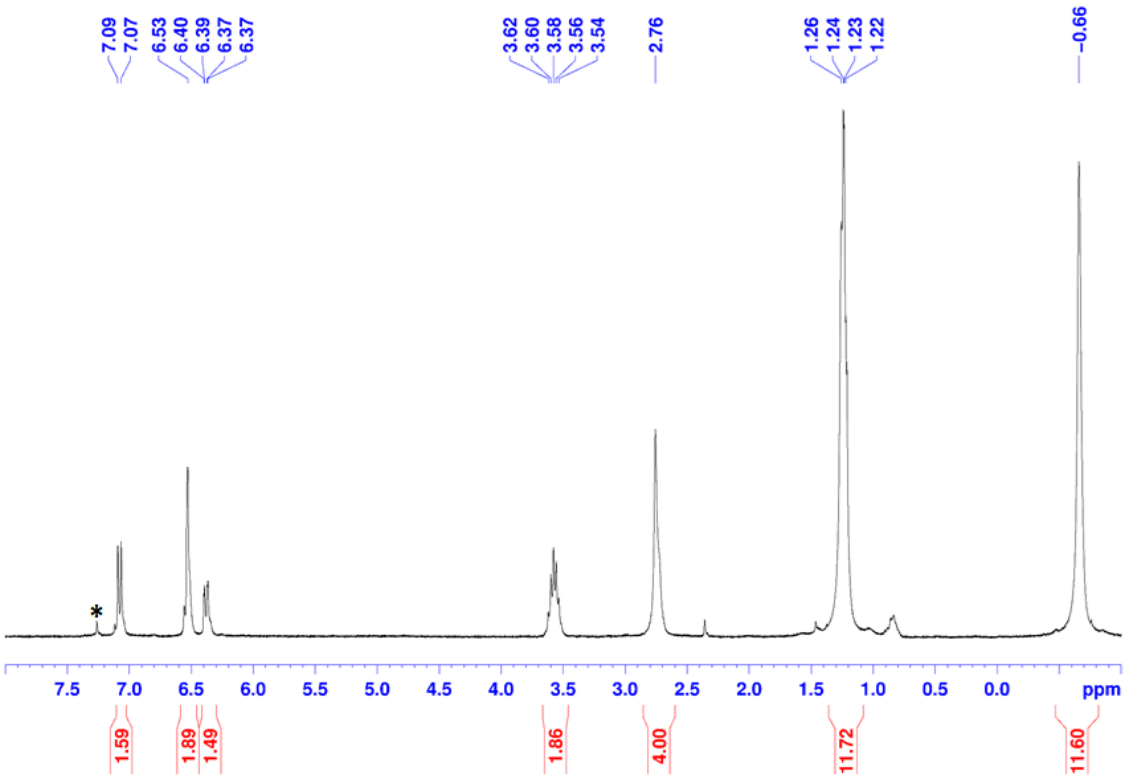

*Figure 235: ^{1}H NMR of Al_2-NSSN-Cl-ISO complex (400.13 MHz, *$CDCl_3$, 25°C).*

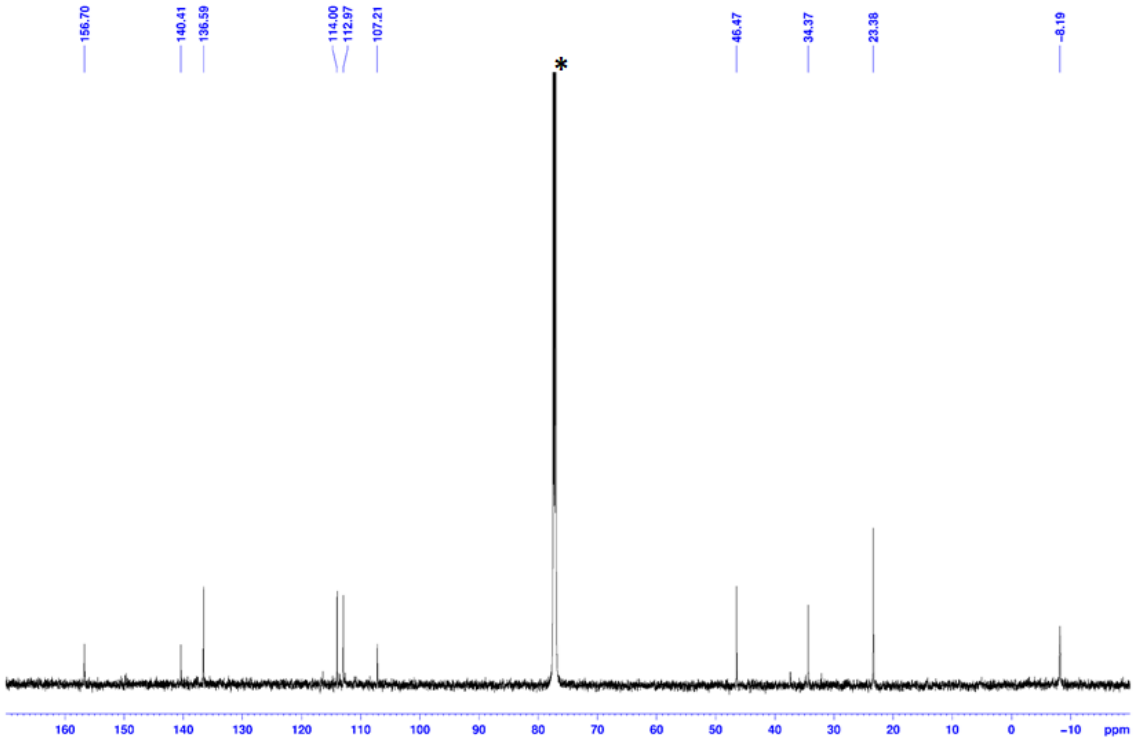

*Figure 236: ^{13}C NMR of Al_2-NSSN-Cl-ISO complex (100.62 MHz, *$CDCl_3$, 25°C).*

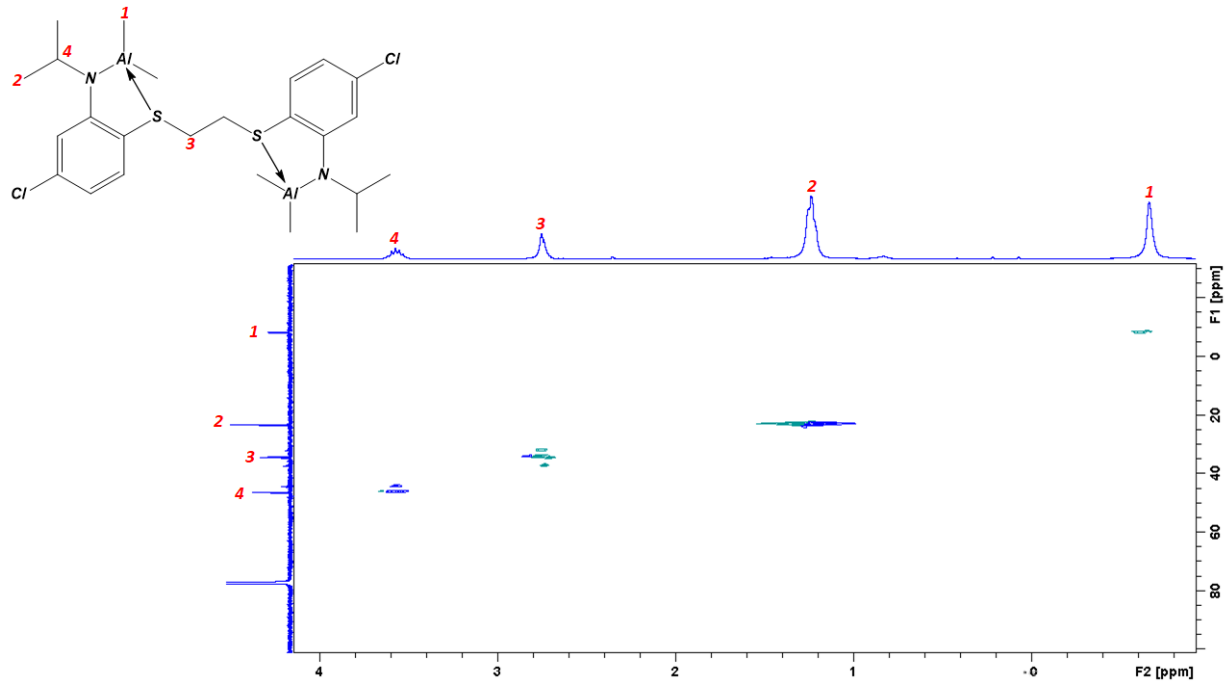

*Figure 237: ^{1}H – ^{13}C HSQC spectrum of Al_2-NSSN-Cl-ISO complex (aliphatic zone – 400.13/100.62 MHz, *$CDCl_3$, 25°C).*

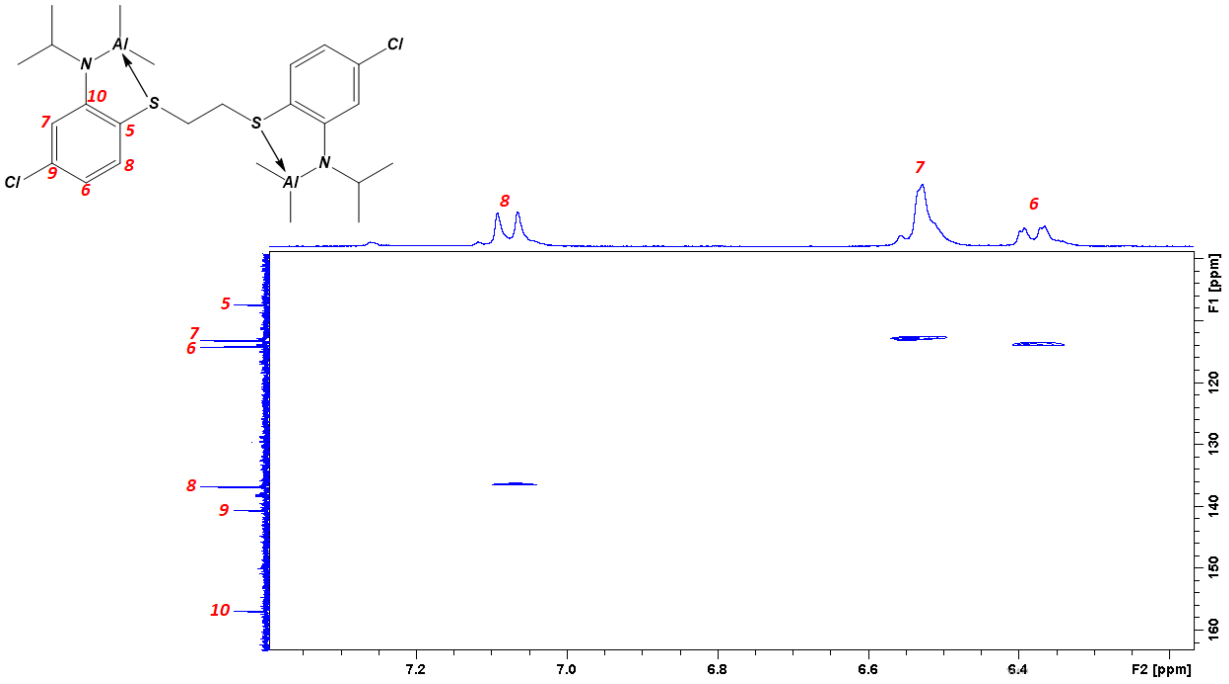

*Figure 238: ^{1}H – ^{13}C HSQC spectrum of Al_2-NSSN-Cl-ISO complex (aromatic zone – 400.13/100.62 MHz, *$CDCl_3$, 25°C).*

8.4 Synthesis and characterization of Al_2-NSSN-Pr-ISO complex

The corresponding *Al_2-NSSN-Pr-ISO* complex was synthesized by reaction of *NSSN-Pr-ISO* proligand with *Al_2Me_6* in benzene as shown in *figure 239.*

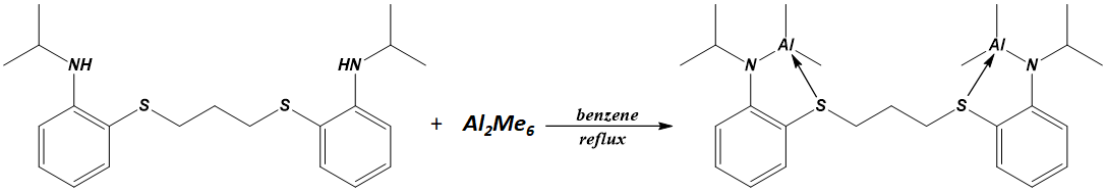

Figure 239: synthesis of Al_2-NSSN-Pr-ISO complex.

The synthesis process is similar to what described in paragraph 8.1.

Al_2Me_6 (0.18 g, 1.25 mmol) in benzene (8 mL) and a solution of [*NSSN-Pr-ISO*] (0.47 g, 1.25 mmol) in benzene (10 mL). The solid product was washed with dry hexane (10 mL), filtered and dried under reduced pressure to give the product as an yellow solid (0.53 g, yield = 87 %). Suitable crystals for X-ray diffraction analysis were obtained by cooling a hexane solution at -20 °C overnight. The single crystal structure was reported in Cristallographic Data (*figure 285).*

^{1}H NMR (400.13 MHz, C_6D_6, 25 °C): δ -0.37 (s, 12H, Al-CH_3), 1.24 (d, J = 6.54 Hz, 12H, CH_3), 1.48 (q, 2H, CH_2), 2.21 (t, 4H, S-CH_2), 3.57 (m, 2H, N-CH), 6.34 (m, J = 7.50 Hz, 2H, ArH), 6.52 (m, J = 8.48 Hz, 2H, ArH), 6.96 (dd, J_1 = 7.61 Hz, J_2 = 1.33 Hz, 2H, ArH), 7.13 (t, J = 7.77 Hz, 2H, ArH). ^{13}C NMR (100.62 MHz, C_6D_6, 25 °C): δ -7.90, 23.45, 25.25, 36.07, 46.13, 110.33, 112.99, 113.89, 133.31, 136.15, 156.00.

Suitable crystals for X-ray diffraction analysis were obtained by cooling a hexane solution at -20 °C overnight.

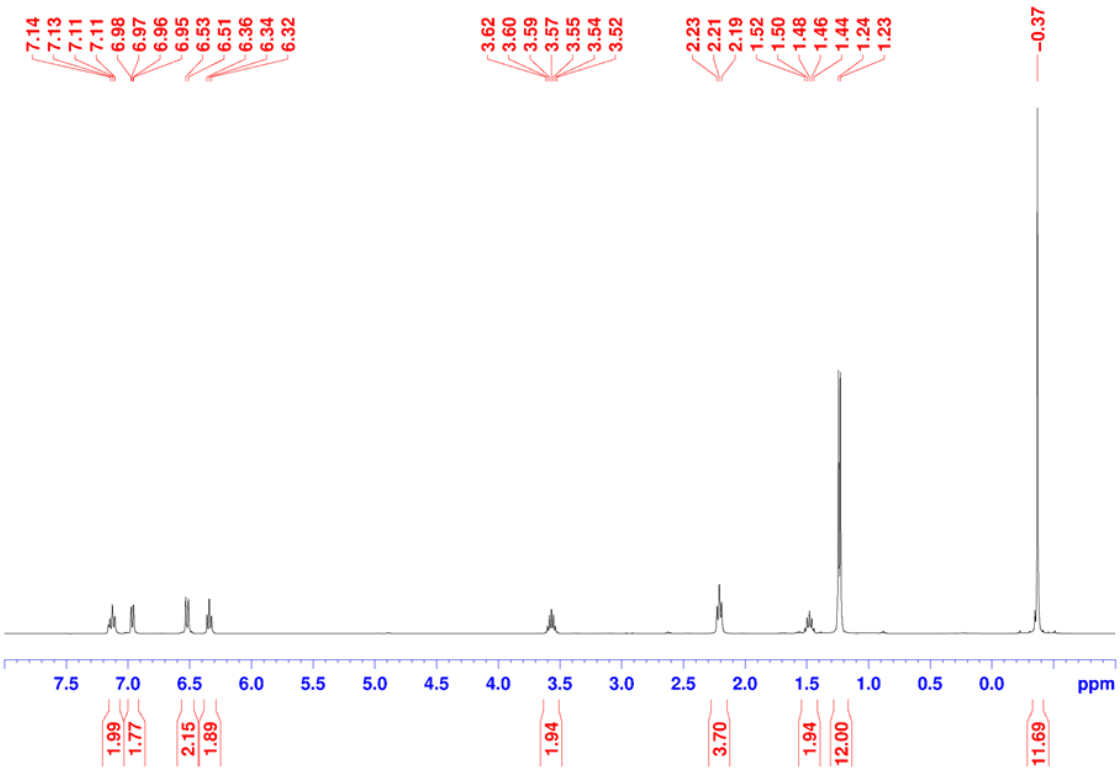

*Figure 240: ^{1}H NMR of Al_2-NSSN-Pr-ISO complex (400.13 MHz, *C_6D_6, 25°C).*

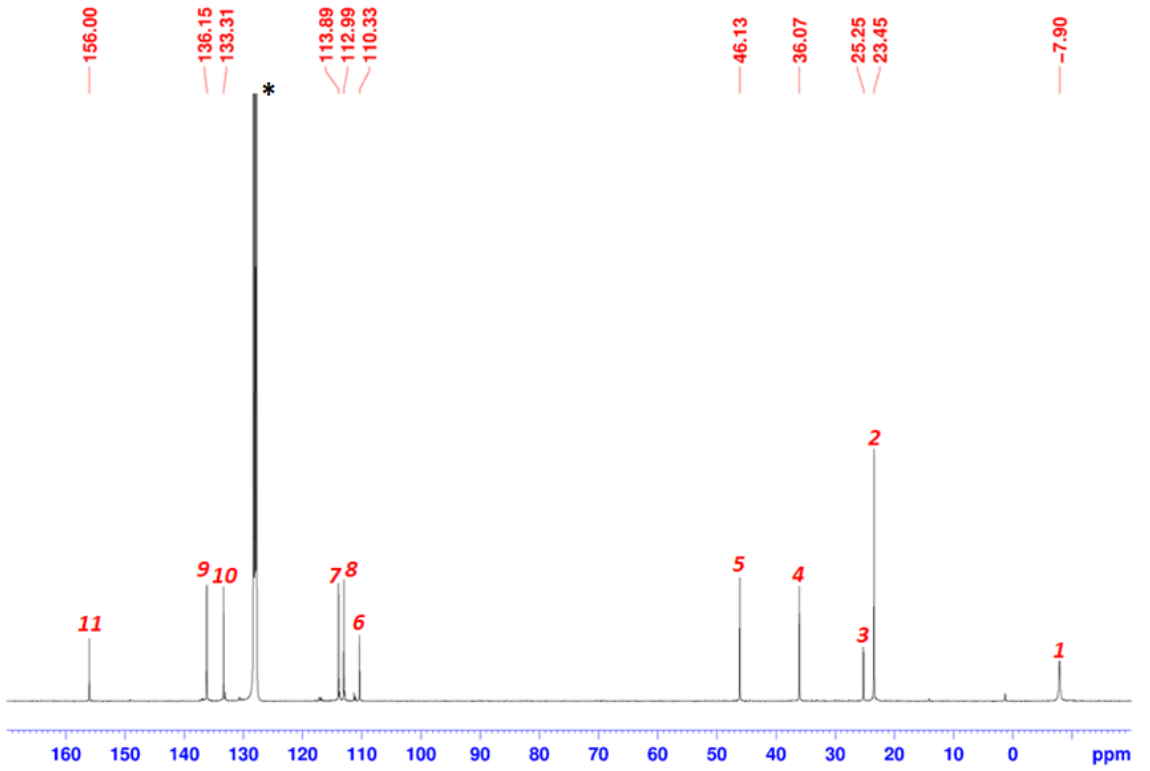

*Figure 241: ^{13}C NMR of Al_2-NSSN-Pr-ISO complex (100.62 MHz, *C_6D_6, 25°C).*

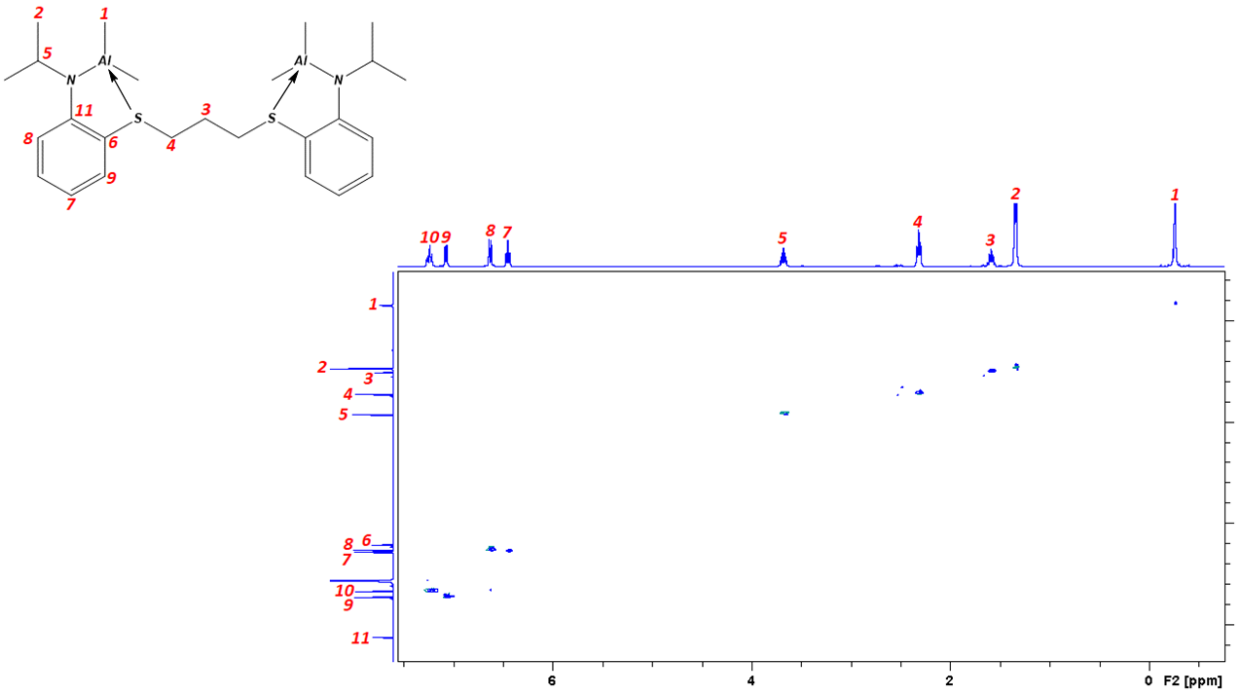

Figure 242: $^{1}H - ^{13}C$ HSQC spectrum of Al_2-NSSN-Pr-ISO complex (400.13/100.62 MHz, $*C_6D_6$, 25°C).

8.5 Synthesis and characterization of Al_2-NSSN-Hep-ISO complex

The corresponding *Al_2-NSSN-Hep-ISO* complex was synthesized by reaction of *NSSN-Hep-ISO* proligand with *Al_2Me_6* in benzene as shown in *figure 243*.

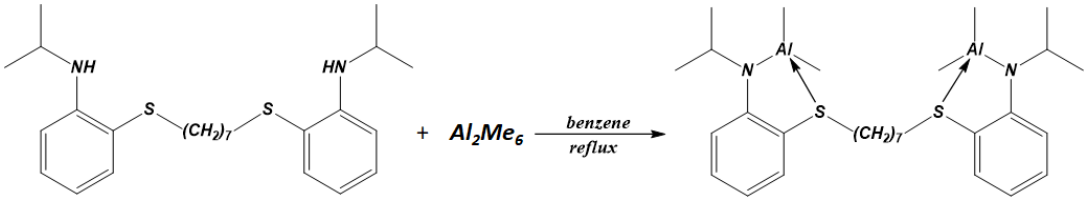

Figure 243: synthesis of Al_2-NSSN-Pr-ISO complex.

The synthesis process is similar to what described in paragraph 8.1.

Al_2Me_6 (0.25 g, 1.76 mmol) in benzene (8 mL) and a solution of [*NSSN-Hep-ISO*] (0.76 g, 1.76 mmol) in benzene (10 mL). The solid product was washed with dry hexane (10 mL), filtered and dried under reduced pressure to give the product as an yellow solid (0.80 g, yield = 84 %).

^{1}H NMR (400.13 MHz, C_6D_6, 25 °C): δ -0.33 (s, 12H, Al-CH_3), 0.74-1.23 (m, 22H, CH_2+CH_3), 2.32 (t, 4H, S-CH_2), 3.56 (m, 2H, N-CH), 6.35 (t, J = 7.48 Hz, 2H, ArH), 6.50 (m, J = 8.46 Hz, 2H, ArH), 7.08-7.13 (m, 4H, ArH). ^{13}C NMR (100.62 MHz, C_6D_6, 25 °C): δ -7.60, 23.52, 27.36, 28.23, 28.49, 38.39, 46.17, 111.51, 112.91, 113.68, 133.10, 135.99, 156.06.

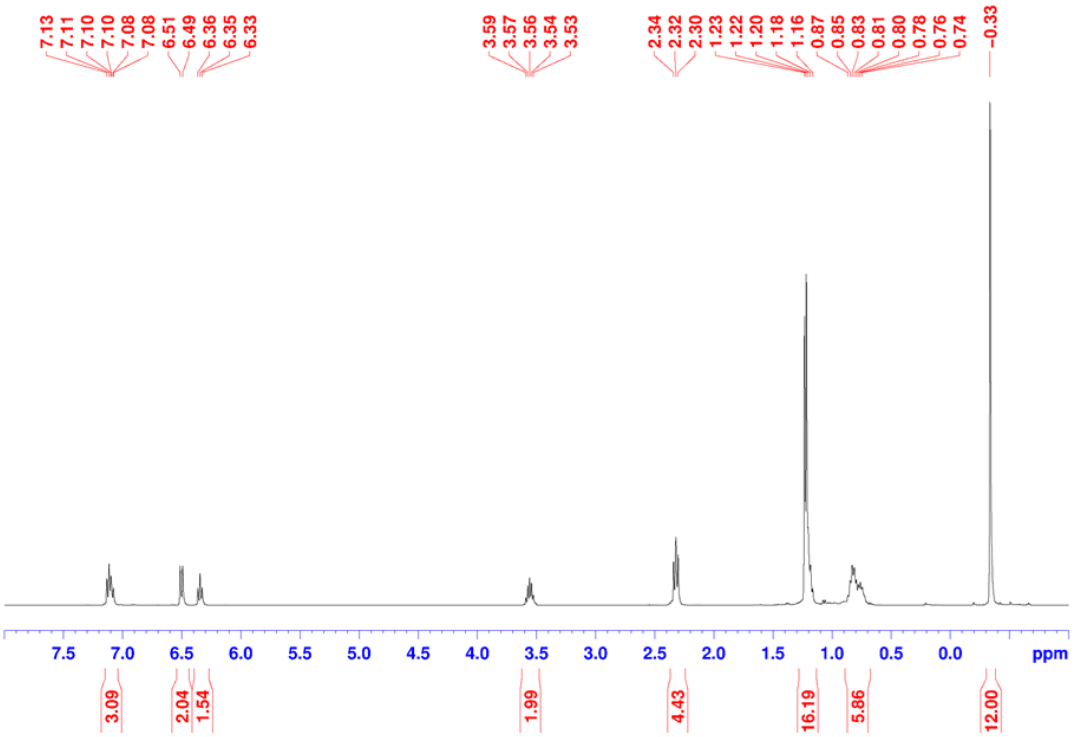

*Figure 244: ^{1}H NMR of Al_2-NSSN-Hep-ISO complex (400.13 MHz, *C_6D_6, 25°C).*

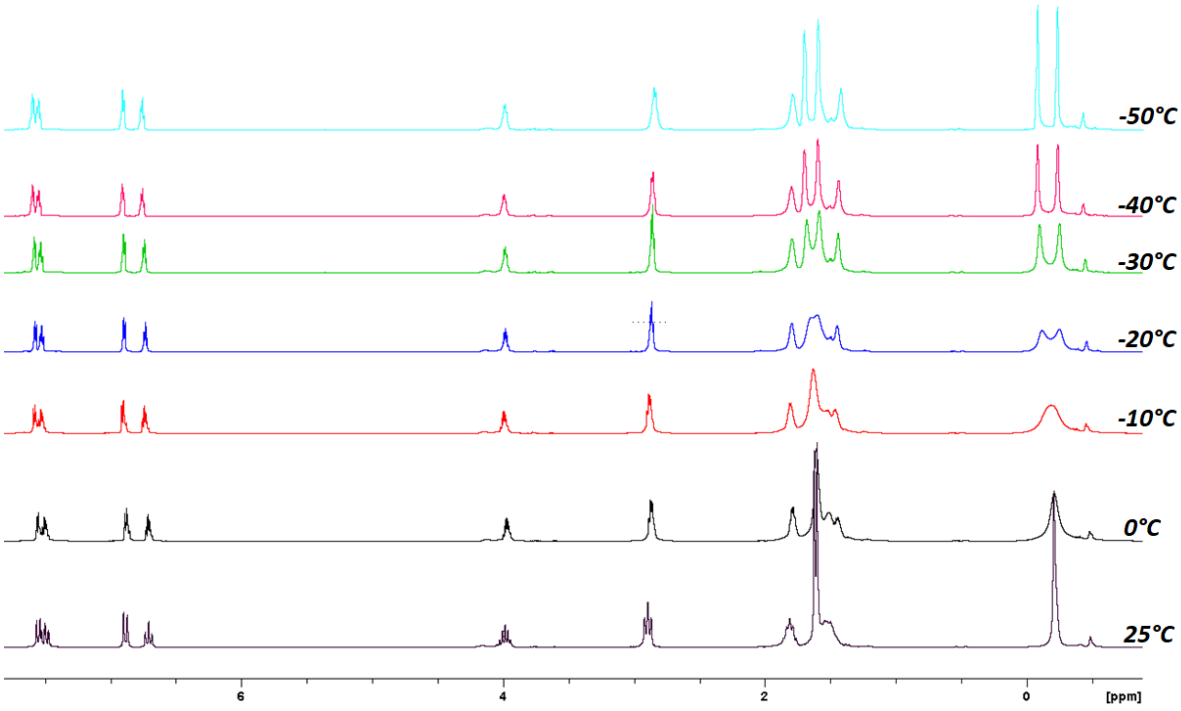

*Figure 245: ^{1}H NMR of Al_2-NSSN-Hep-ISO (400.13 MHz, *CD_2Cl_2, variable temperature).*

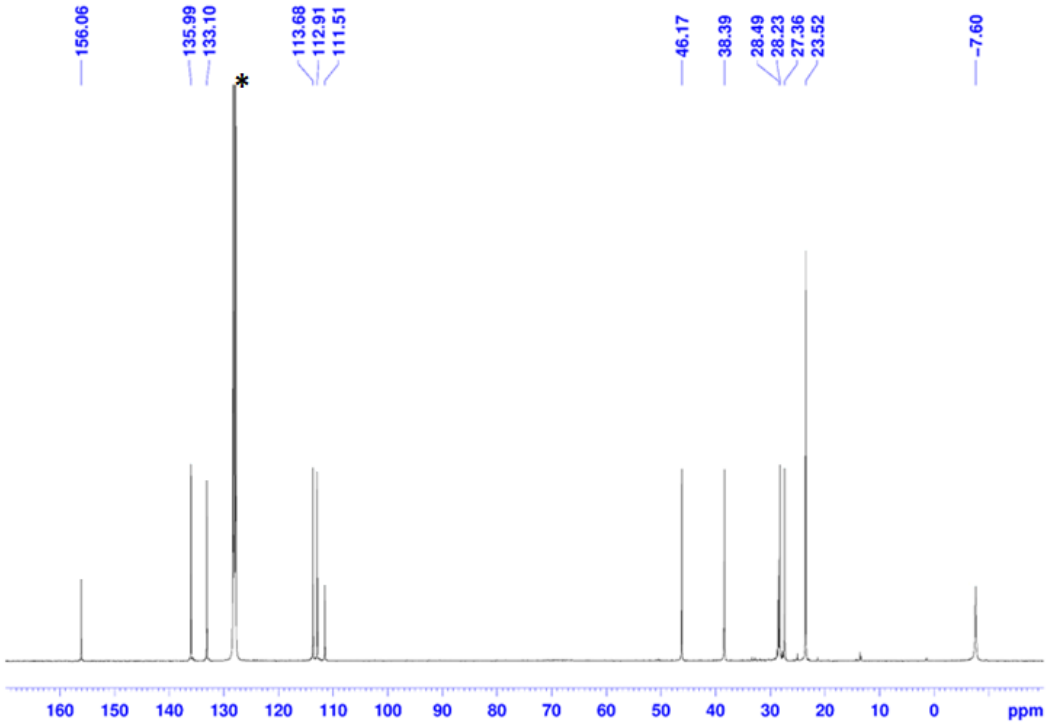

*Figure 246: ^{13}C NMR of Al_2-NSSN-Hep-ISO complex (100.62 MHz, *C_6D_6, 25°C).*

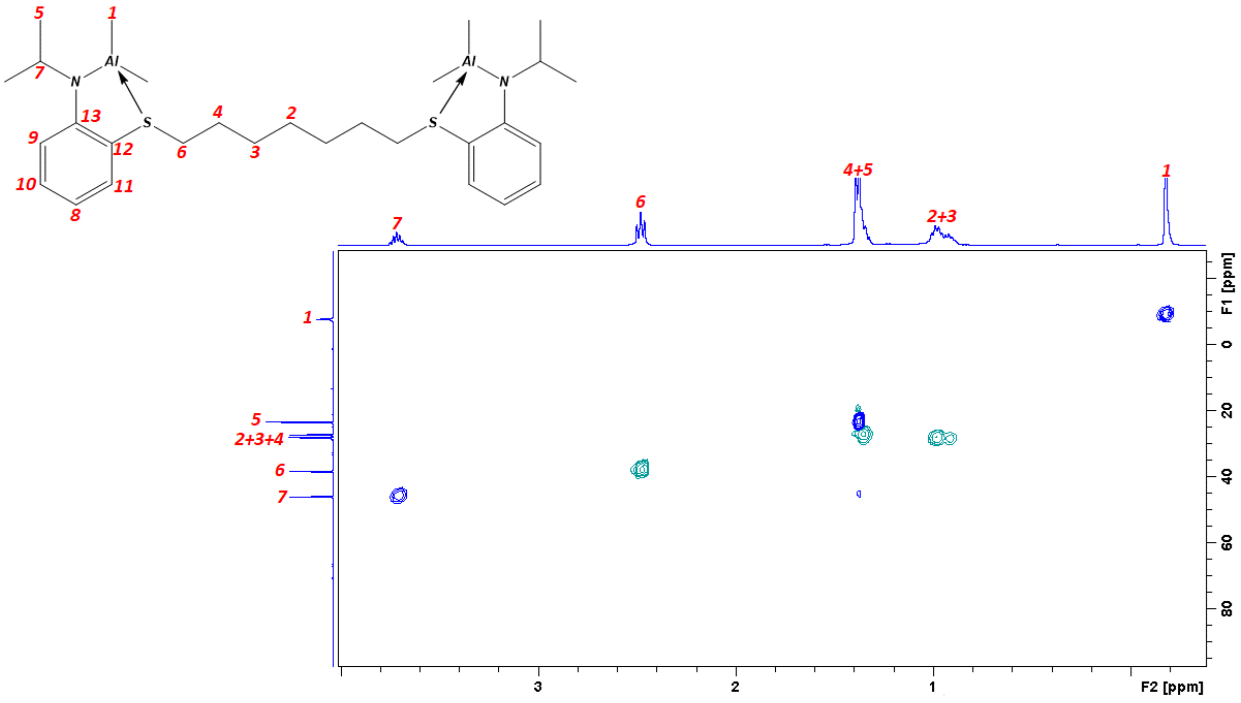

*Figure 247: ^1H – ^{13}C HSQC spectrum of Al_2-NSSN-Hep-ISO complex (aliphatic zone – 400.13/100.62 MHz, *C_6D_6, 25°C).*

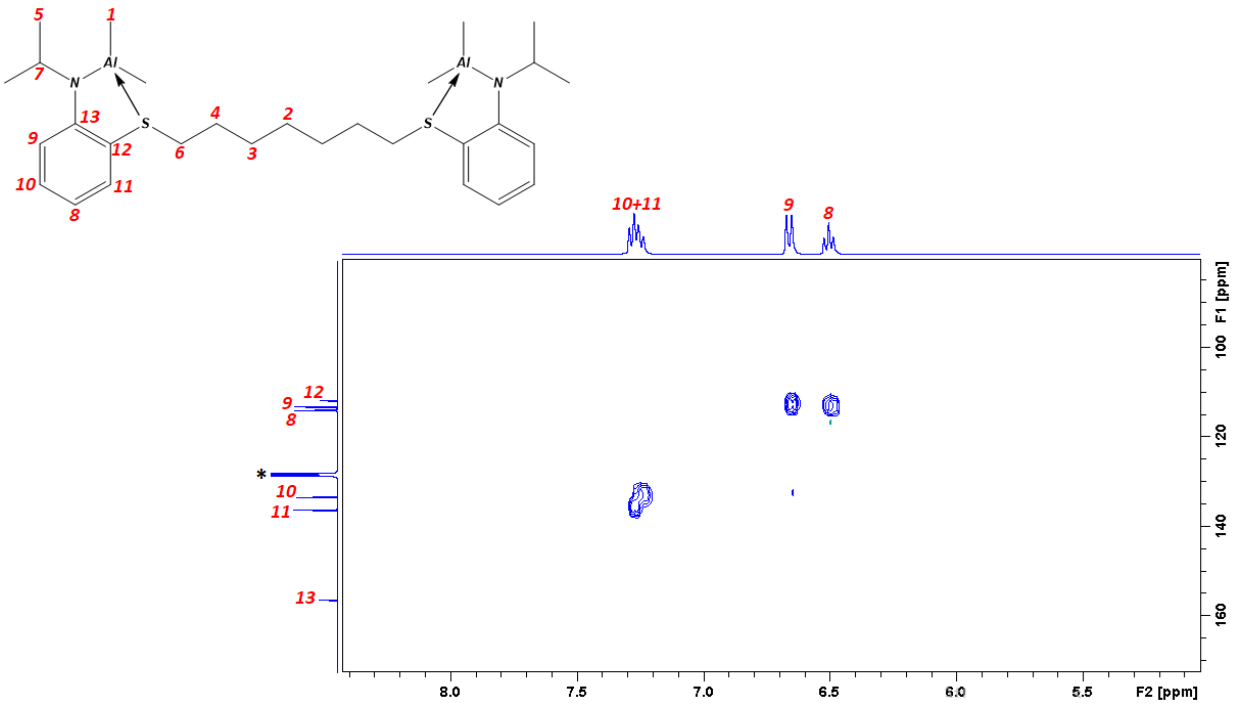

Figure 248: ^{1}H – ^{13}C HSQC spectrum of Al_2-NSSN-Hep-ISO complex (aromatic zone – 400.13/100.62 MHz, *C_6D_6, 25°C).

8.6 *Synthesis and characterization of Al_2-NSSN-Xy-ISO complex*

The corresponding *Al_2-NSSN-Xy-ISO* complex was synthesized by reaction of *NSSN-Xy-ISO* proligand with *Al_2Me_6* in benzene as shown in *figure 249*.

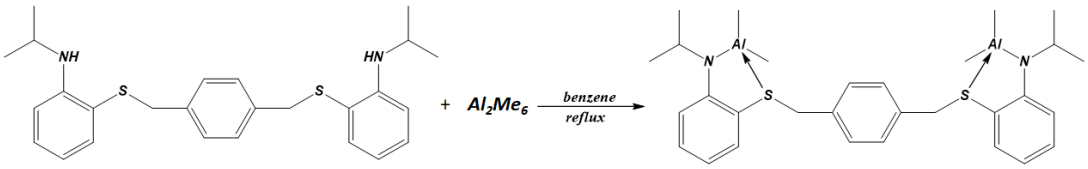

Figure 249: synthesis of Al_2-NSSN-Xy-ISO complex.

The synthesis process is similar to what described in paragraph 8.1.

Al_2Me_6 (0.27 g, 1.90 mmol) in benzene (10 mL) and a solution of [*NSSN-Xy-ISO*] (0.83 g, 1.90 mmol) in benzene (20 mL). The solid product was washed with dry hexane (10 mL), filtered and dried under reduced pressure to give the product as an orange solid (0.85 g, yield = 81 %).

^{1}H NMR (400.13 MHz, TCDE, 60 °C): δ -0.53 (s, 12H, Al-CH_3), 1.36 (d, 12H, CH_3), 3.76 (m, 2H, N-CH), 3.86 (s, 4H, S-CH_2), 6.24 (t, J = 7.23 Hz, 2H, ArH), 6.62 (m, J = 8.65 Hz, 2H, ArH), 6.67 (m, J = 7.70 Hz, 2H, ArH), 6.96 (s, 4H, ArH), 7.21 (t, J = 7.65 Hz, 2H, ArH). ^{13}C NMR (100.62 MHz, TCDE, 60 °C): δ -8.16, 23.21, 42.13, 45.61, 109.93, 111.93, 112.65, 129.79, 132.71, 133.96, 136.03, 155.21.

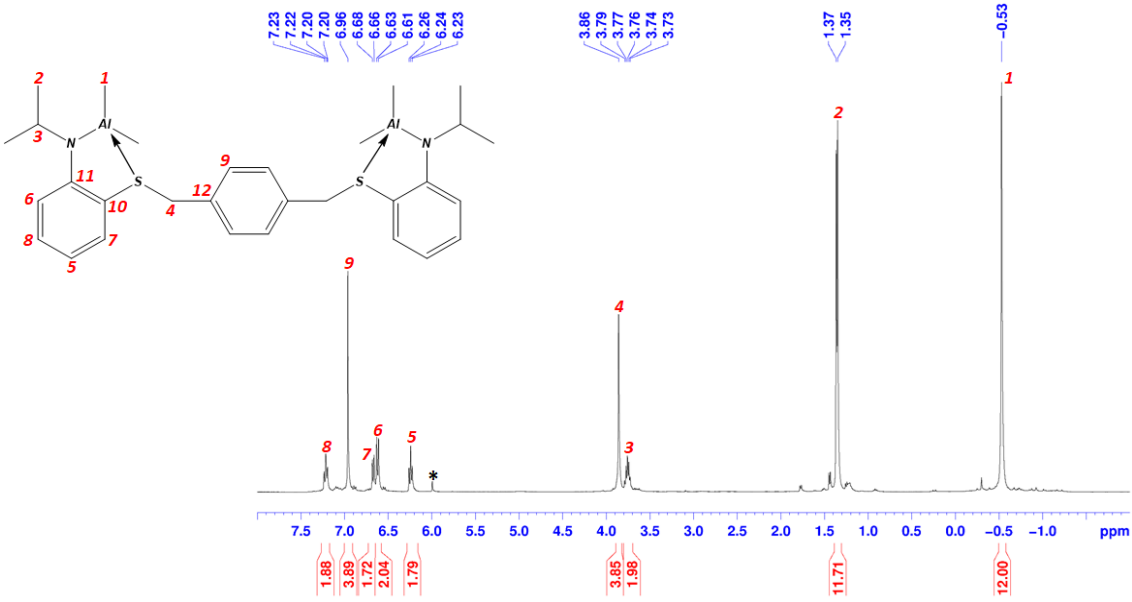

*Figure 250: ^{1}H NMR of Al_2-NSSN-Xy-ISO complex (400.13 MHz, *TCDE, 60°C).*

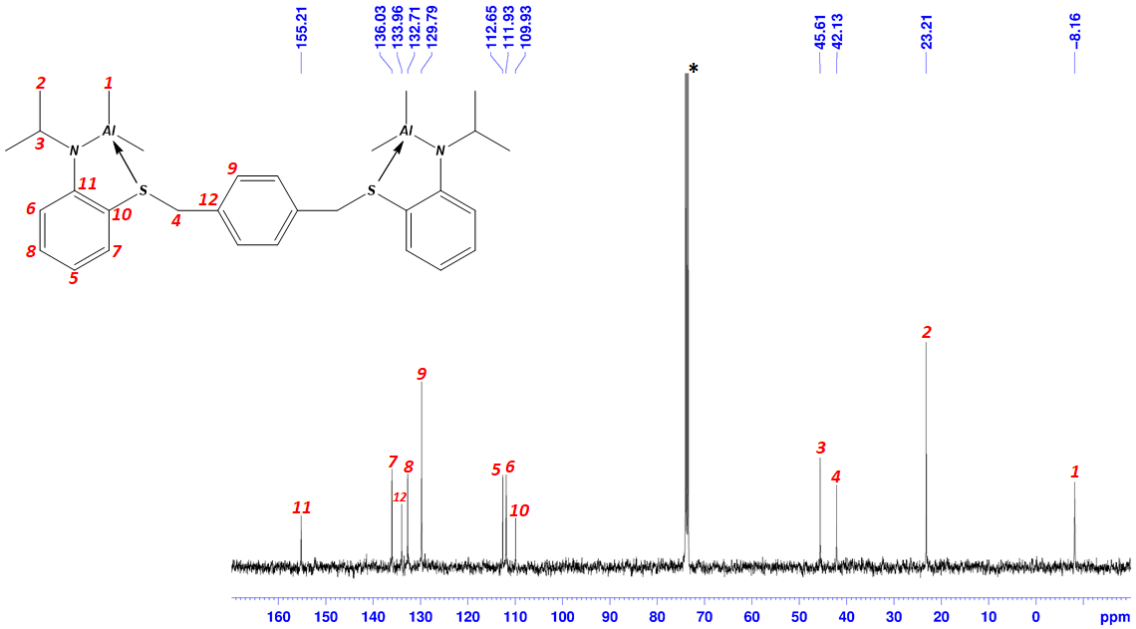

Figure 251: ^{13}C NMR of Al_2-NSSN-Xy-ISO complex (100.62 MHz, *TCDE, 60°C).

8.7 Synthesis and characterization of Al-NSEt-ISO

The corresponding *Al-NSEt-ISO* complex was synthesized by reaction of *NSEt-ISO* proligand with Al_2Me_6 in benzene as shown in *figure 252.*

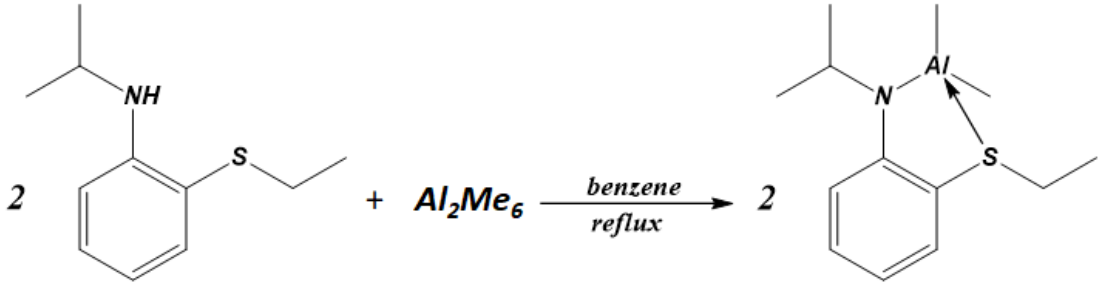

Figure 252: synthesis of Al-NSEt-ISO complex.

A solution of $AlMe_3$ (0.32 g, 2.26 mmol) in benzene (2 mL) was added to a solution of 2-(ethylthio)-N-isopropylaniline [*NSEt_ISO*] (0.83 g, 4.26 mmol) in benzene (3 mL). The resulting brown solution was refluxed for 16 h, after which the volatiles were removed under vacuum. The brown oil product was recovered in a vial (0.99 g, yield = 93%).

^{1}H NMR (400.13 MHz, TCDE, 25 °C): δ -0.45 (s, 6H, Al-CH_3), 1.35 (t, 3H, CH_3), 1.42 (d, J = 6.36 Hz, 6H, CH_3), 2.83 (q, 2H, S-CH_2), 3.80 (m, 1H, N-CH), 6.52 (t, J = 7.12 Hz, 1H, ArH), 6.69 (m, J = 7.61 Hz, 1H, ArH), 7.32 (t, J = 7.72 Hz, 1H, ArH), 7.36 (m, J = 7.56 Hz, 1H, ArH).

^{1}H NMR (400.13 MHz, C_6D_6, 25 °C): δ -0.21 (s, 6H, Al-CH_3), 0.85 (t, 3H, CH_3), 1.35 (d, J = 6.34 Hz, 6H, CH_3), 2.28 (q, 2H, S-CH_2), 3.66 (m, 1H, N-CH), 6.48 (t, J = 7.09 Hz, 1H, ArH), 6.62 (m, J = 7.60 Hz, 1H, ArH), 7.20 (m, J = 7.68 Hz, 1H, ArH), 7.24 (m, J = 7.54 Hz, 1H, ArH). ^{13}C NMR (100.62 MHz, C_6D_6, 25 °C): δ -7.46, 12.37, 23.44, 32.56, 48.04, 110.94, 112.68, 113.49, 133.07, 136.22, 155.95.

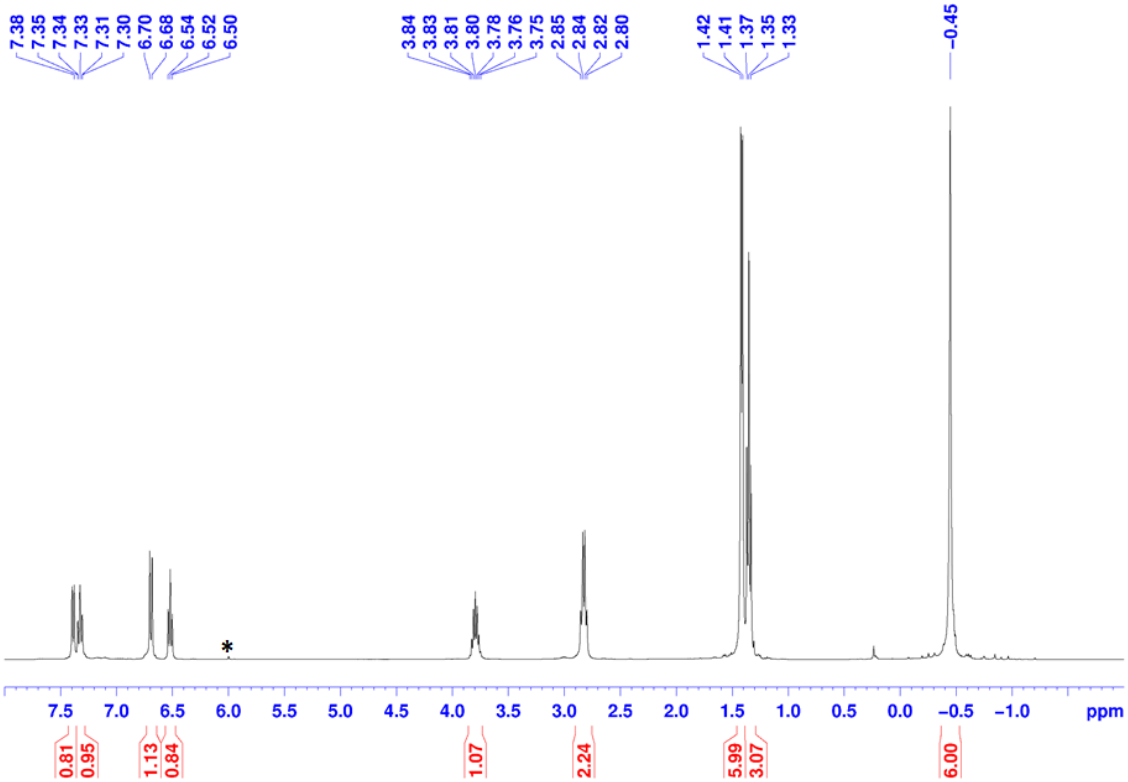

*Figure 253: ^{1}H NMR of Al-NSEt-ISO complex (400.13 MHz, *TCDE, 25°C).*

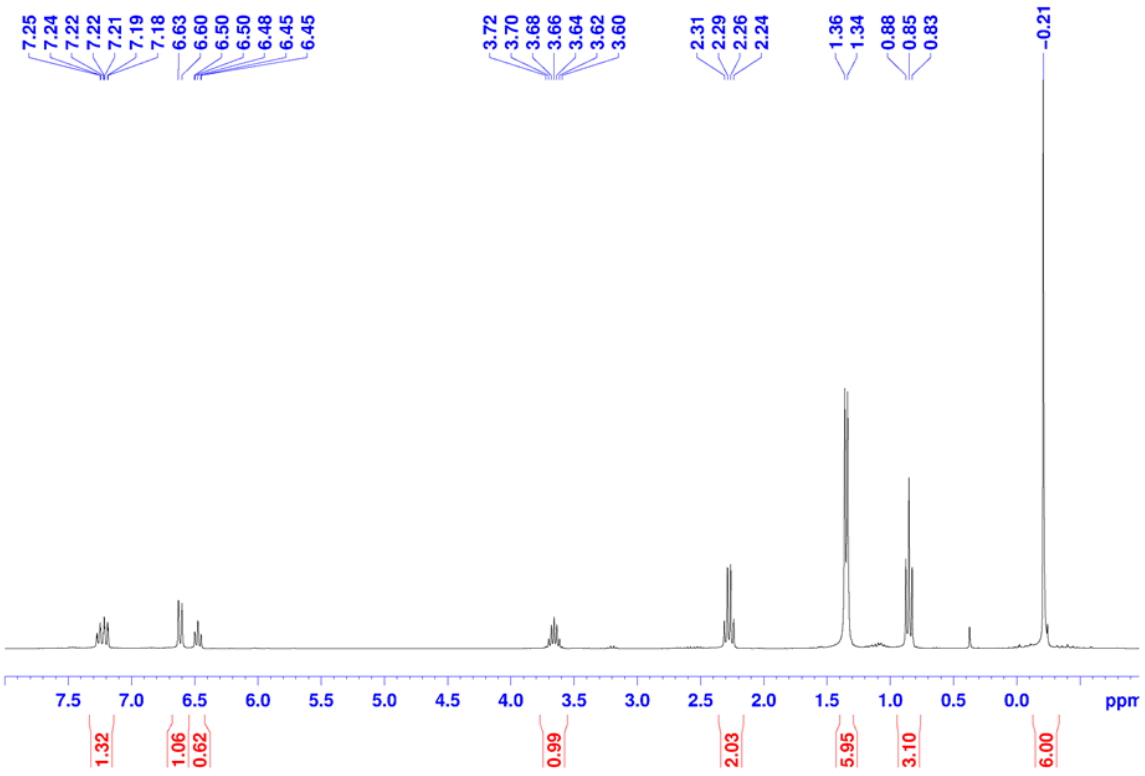

*Figure 254: ^{1}H NMR of Al-NSEt-ISO complex (400.13 MHz, *C_6D_6, 25°C).*

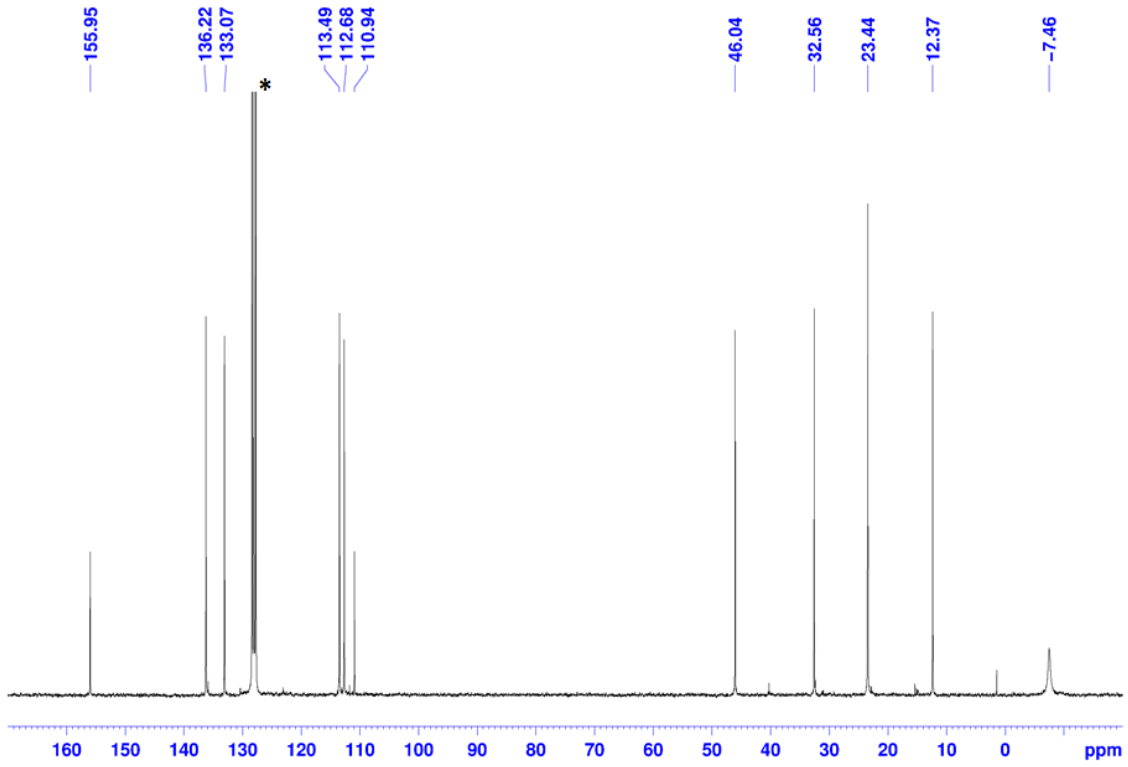

*Figure 255: ^{13}C NMR of Al-NSEt-ISO complex (100.62 MHz, *C_6D_6, 25°C).*

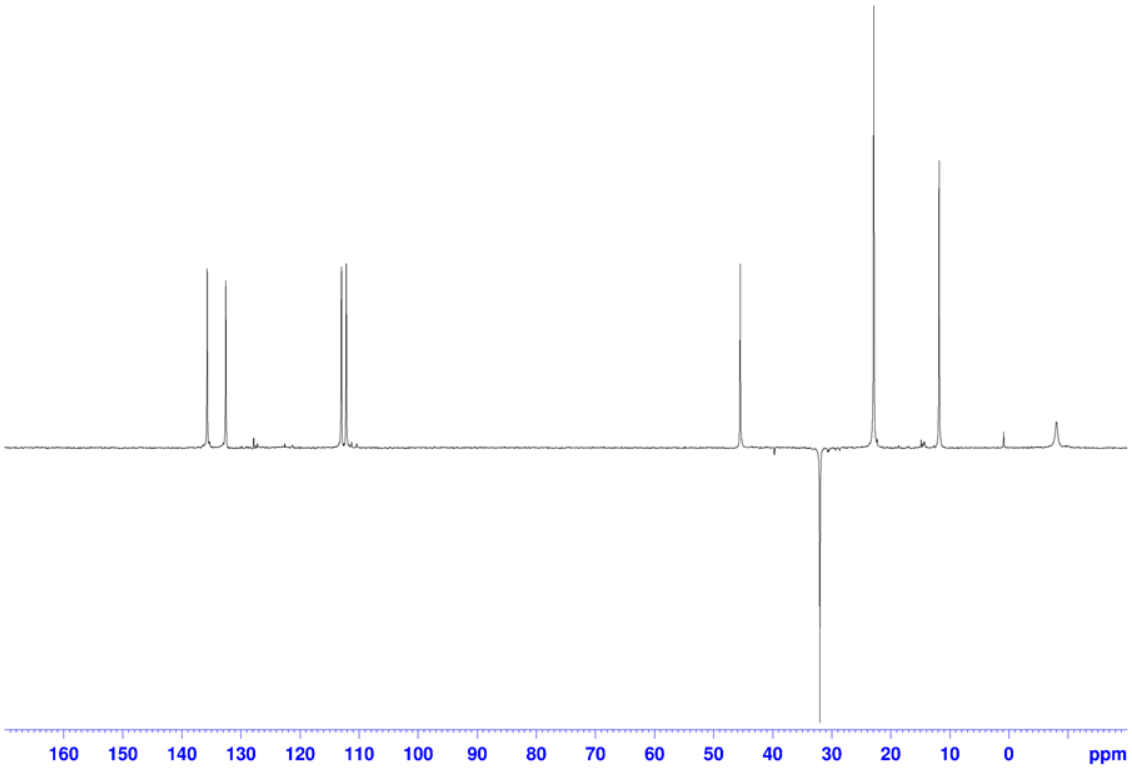

*Figure 256: DEPT 135 NMR of Al-NSEt-ISO complex (100.62 MHz, *C_6D_6, 25°C).*

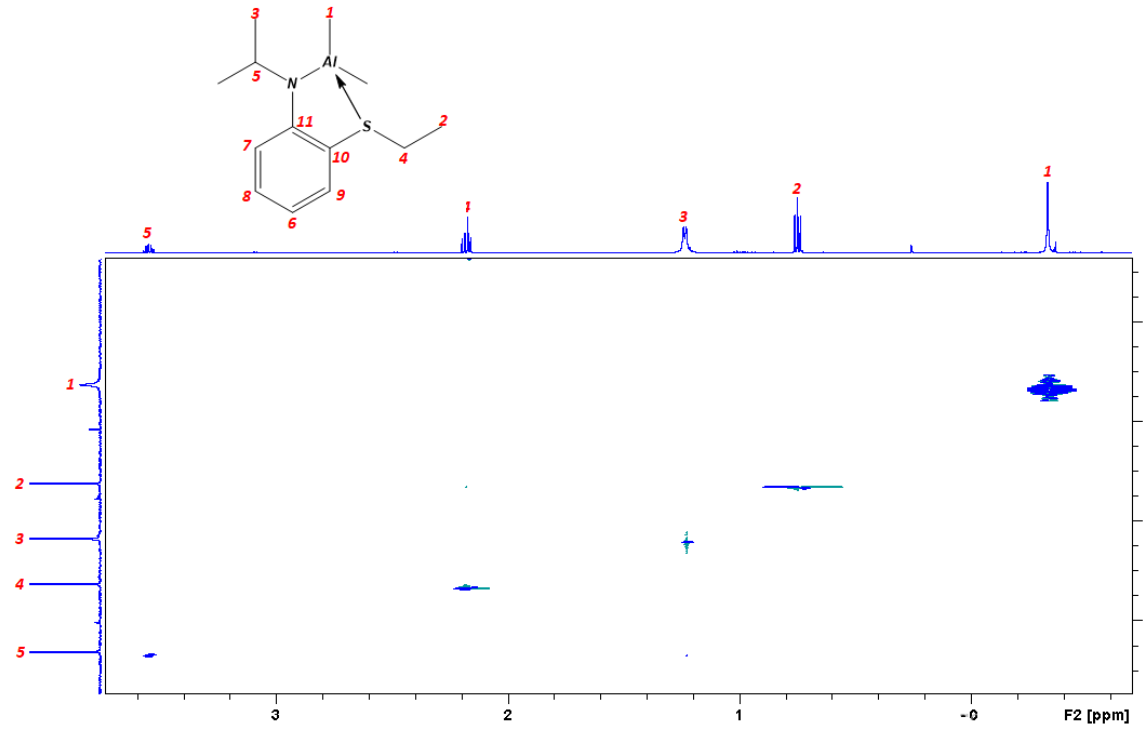

*Figure 257: $^{1}H - ^{13}C$ HSQC spectrum of Al-NSEt-ISO complex (aliphatic zone – 400.13/100.62 MHz, *C_6D_6, 25°C).*

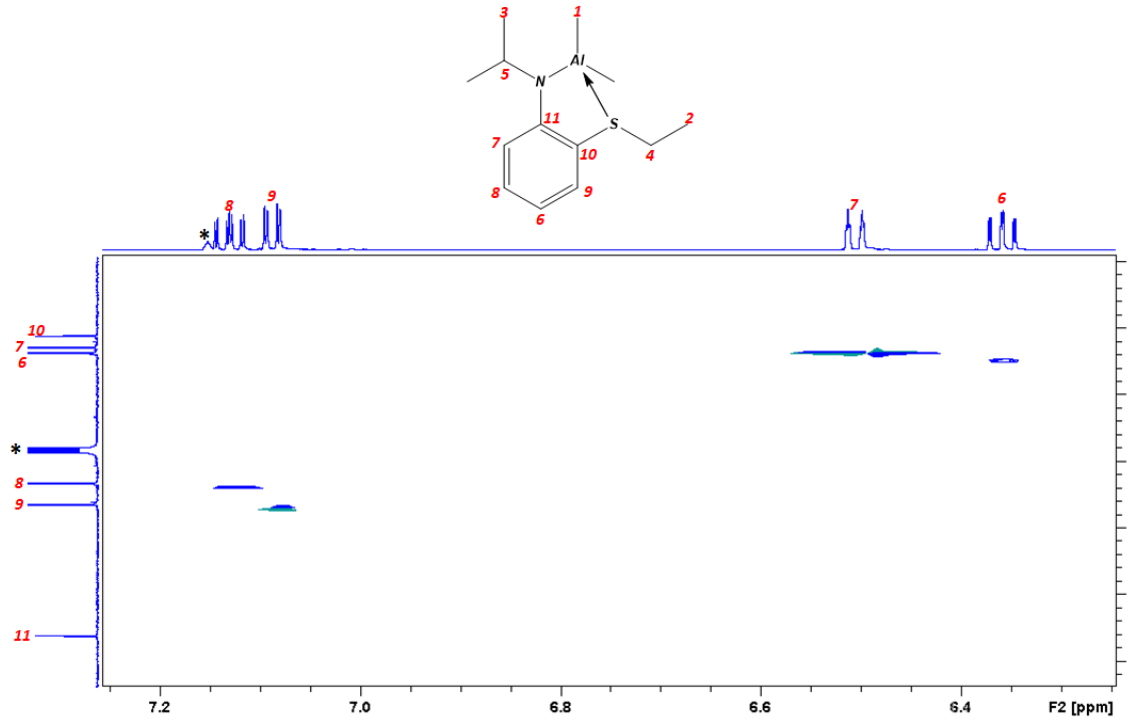

*Figure 258: $^{1}H - ^{13}C$ HSQC spectrum of Al-NSEt-ISO complex (aromatic zone – 400.13/100.62 MHz, *C_6D_6, 25°C).*

8.8 Synthesis and characterization of Al-NSiPr-ISO

The corresponding *Al-NSiPr-ISO* complex was synthesized by reaction of *NSiPr-ISO* proligand with Al_2Me_6 in benzene as shown in *figure 259.*

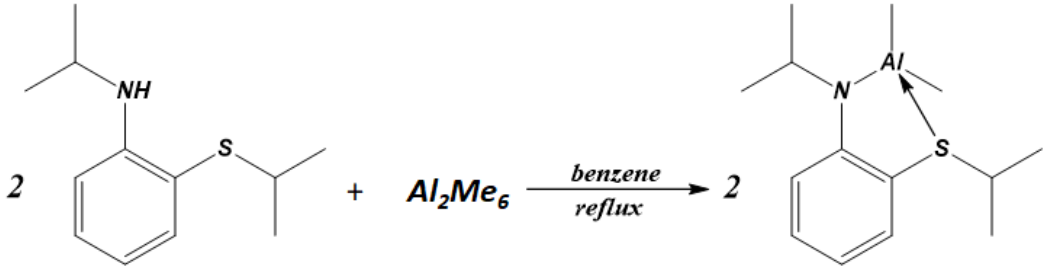

Figure 259: synthesis of Al-NSiPr-ISO complex.

The synthesis process is similar to what described in paragraph 8.7.

Al_2Me_6 (0.24 g, 1.66 mmol) in benzene (2 mL) and a solution of [*NSiPr-ISO*] (0.66 g, 3.33 mmol) in benzene (3 mL). The resulting brown solution was refluxed for 16 h, after which the volatiles were removed under vacuum. The brown oil product was recovered in a vial (0.84 g, yield = 95%).

^{1}H NMR (400.13 MHz, C_6D_6, 25 °C): δ -0.30 (s, 6H, Al-CH_3), 0.81 (d, J = 6.65 Hz, 6H, CH_3), 1.20 (d, J = 6.24 Hz, 6H, CH_3), 2.83 (m, 1H, S-CH_2), 3.53 (m, 1H, N-CH), 6.33 (m, J = 7.46 Hz, 1H, ArH), 6.49 (m, J = 8.57 Hz, 1H, ArH), 7.07 (m, J_1 = 7.62 Hz, J_2 = 1.16 Hz, 1H, ArH), 7.12 (t, J = 7.60 Hz, 1H, ArH). ^{13}C NMR (100.62 MHz, C_6D_6, 25 °C): δ -6.98, 20.90, 23.41, 42.09, 46.03, 109.67, 112.56, 113.43, 133.17, 136.85, 156.80.

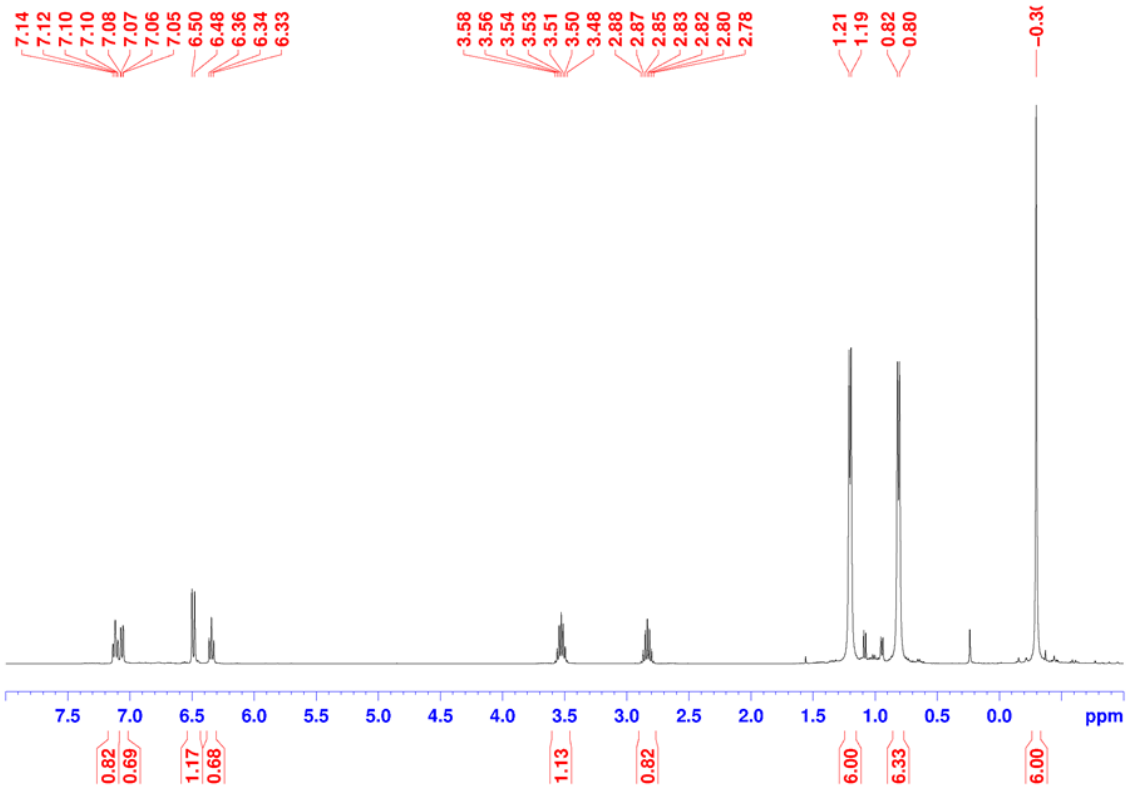

*Figure 260: ^{1}H NMR of Al-NSiPr-ISO complex (400.13 MHz, *C_6D_6, 25°C).*

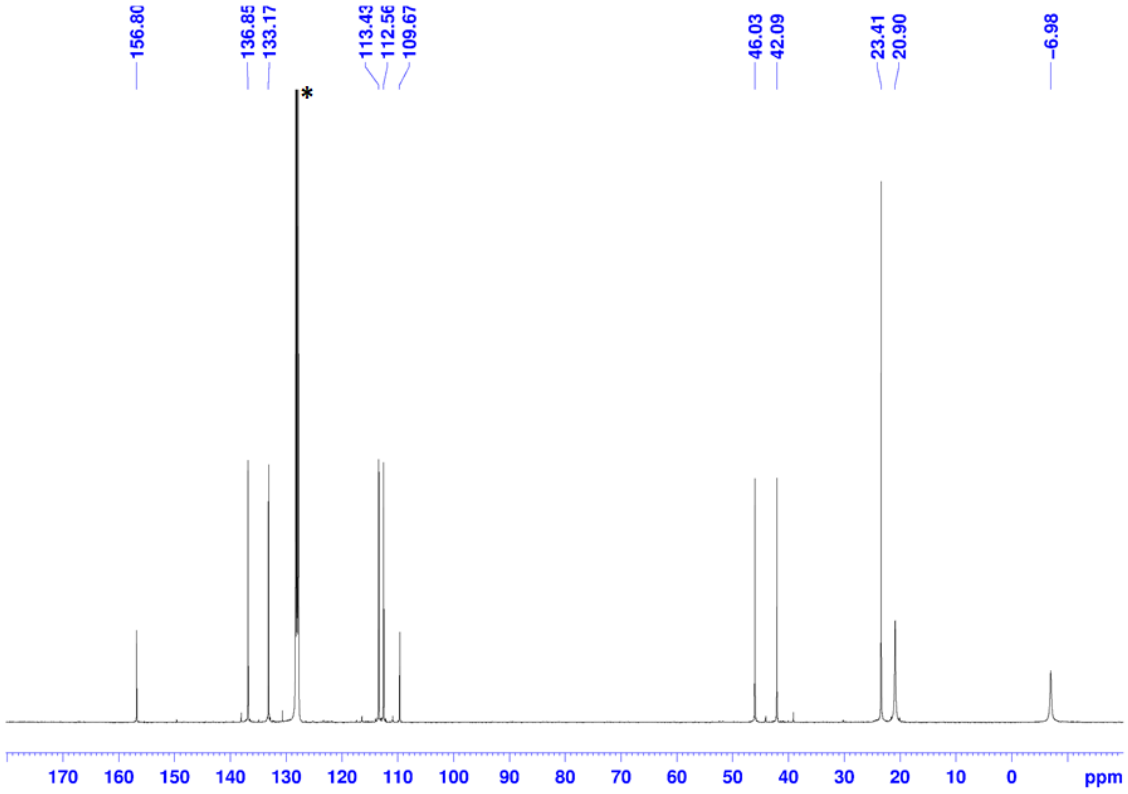

*Figure 261: ^{13}C NMR of Al-NSiPr-ISO complex (100.62 MHz, *C_6D_6, 25°C).*

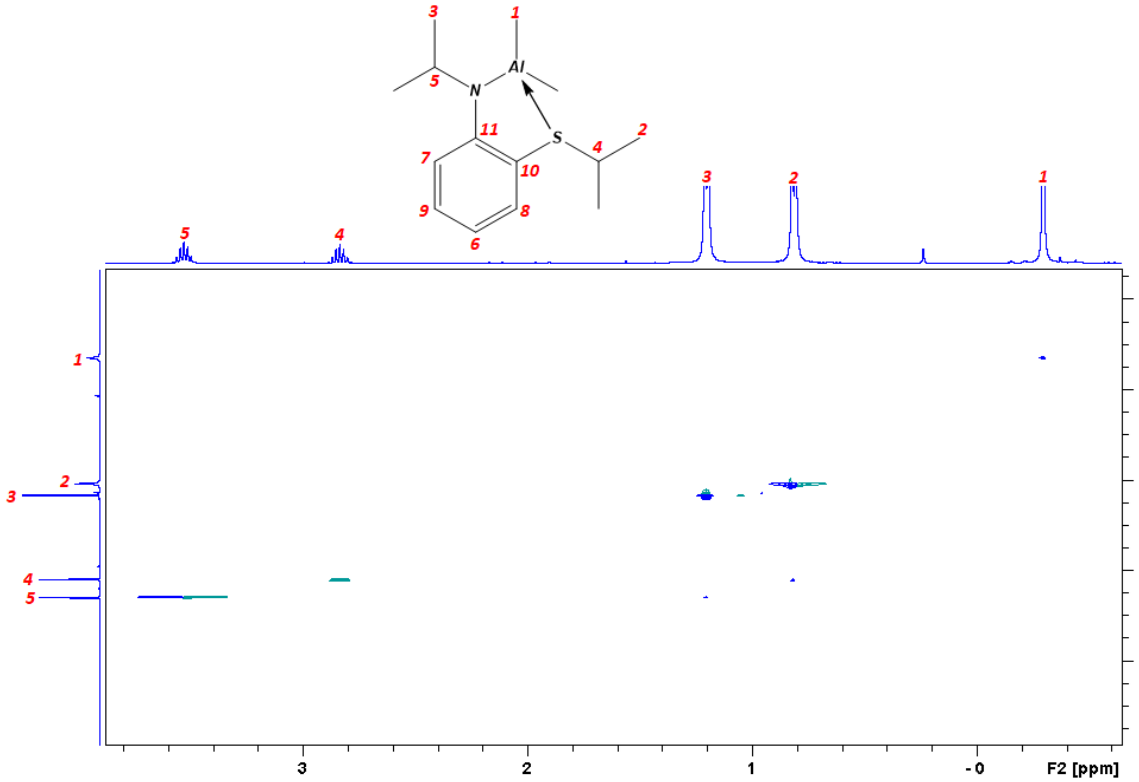

*Figure 262: $^{1}H - ^{13}C$ HSQC spectrum of Al-NSiPr-ISO complex (aliphatic zone – 400.13/100.62 MHz, *C_6D_6, 25°C).*

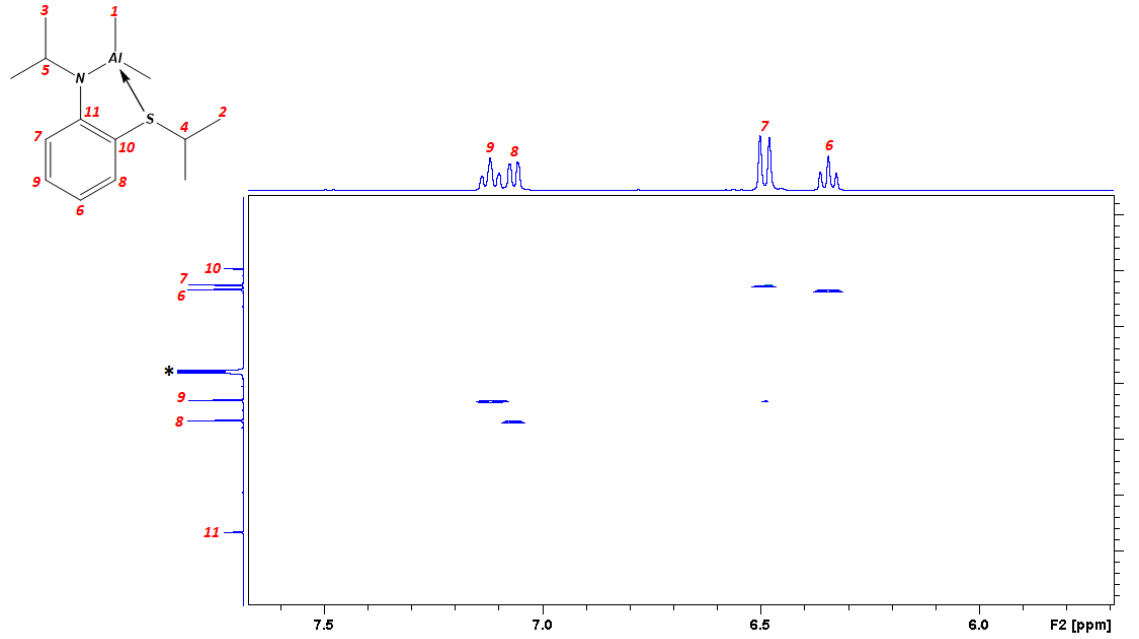

*Figure 263: $^{1}H - ^{13}C$ HSQC spectrum of Al-NSiPr-ISO complex (aromatic zone – 400.13/100.62 MHz, *C_6D_6, 25°C).*

8.9 *Synthesis and characterization of Al-NSHex-ISO*

The corresponding *Al-NSHex-ISO* complex was synthesized by reaction of *NSHex-ISO* proligand with Al_2Me_6 in benzene as shown in *figure 264.*

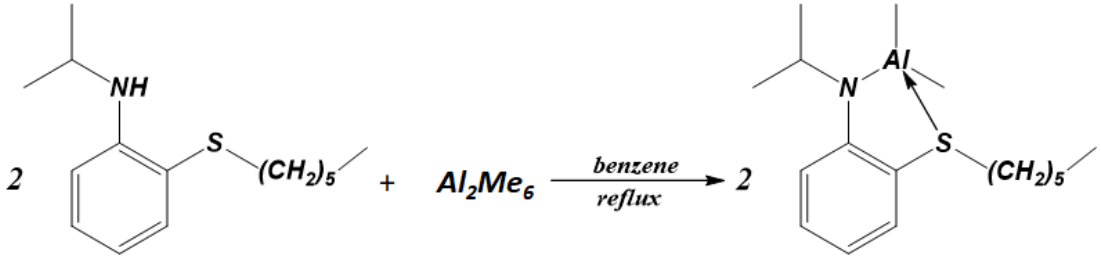

Figure 264: synthesis of Al-NSEx-ISO complex.

The synthesis process is similar to what described in paragraph 8.7.

Al_2Me_6 (0.32 g, 2.28 mmol) in benzene (2 mL) and a solution of [*NSHex-ISO*] (1.07 g, 4.27 mmol) in benzene (3 mL). The resulting yellow solution was refluxed for 16 h, after which the volatiles were removed under vacuum. The brown oil product was recovered in a vial (0.99 g, yield = 92%).

^{1}H NMR (400.13 MHz, C_6D_6, 25 °C): δ -0.38 (s, 6H, Al-CH_3), 0.76 (t, 3H, CH_3), 0.95-1.30 (m, 14H, CH_3+CH_2), 2.32 (t, 2H, S-CH_2), 3.55 (m, 1H, N-CH), 6.34 (t, J_1 = 7.39 Hz, J_2 = 1.02 Hz, 1H, ArH), 6.48 (m, J = 8.45 Hz, 1H, ArH), 7.07-7.11 (m, 2H, ArH). ^{13}C NMR (100.62 MHz, C_6D_6, 25 °C): δ -7.42, 14.26, 22.83, 23.51, 27.51, 28.31, 31.54, 38.51, 46.10, 111.47, 112.72, 113.55, 133.01, 136.08, 155.90.

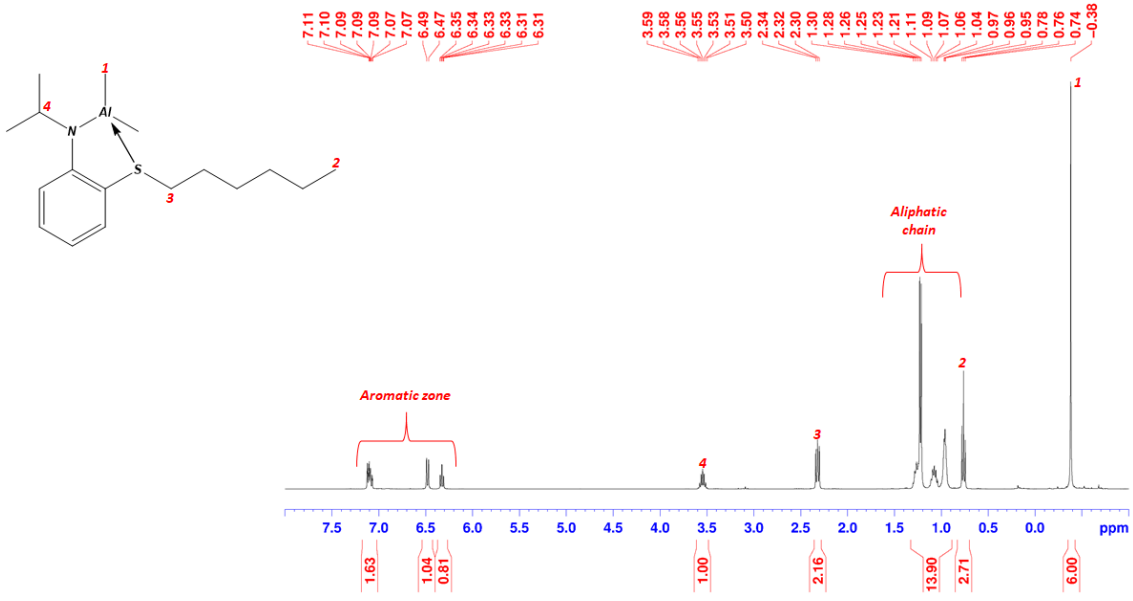

Figure 265: ^{1}H NMR of Al-NSHex-ISO complex (400.13 MHz, *C_6D_6, 25°C).

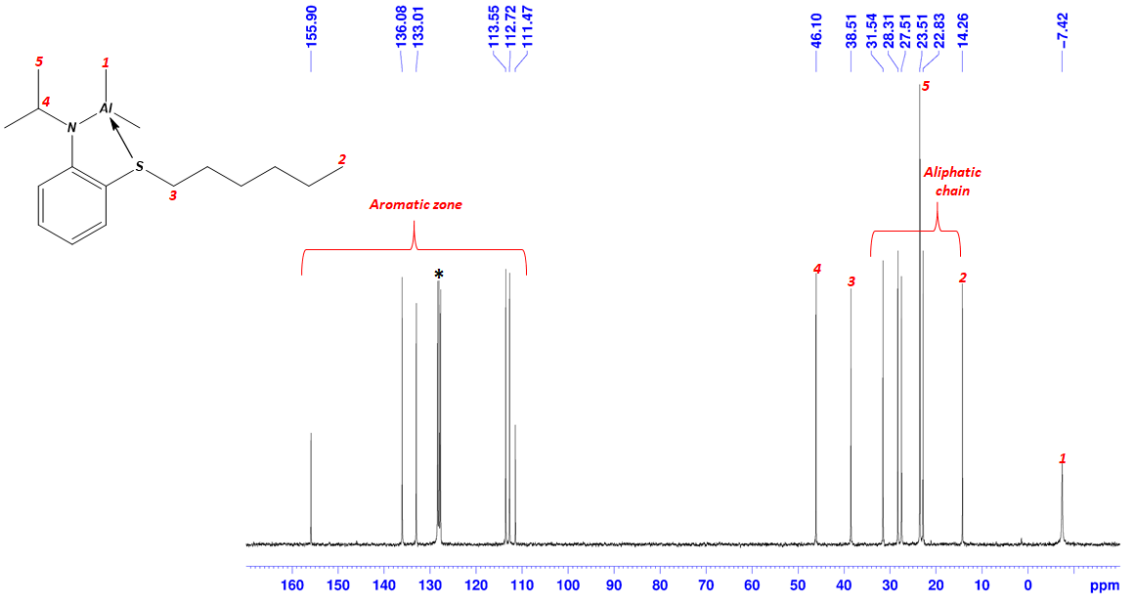

*Figure 266: ^{13}C NMR of Al-NSHex-ISO complex (100.62 MHz, *C_6D_6, 25°C).*

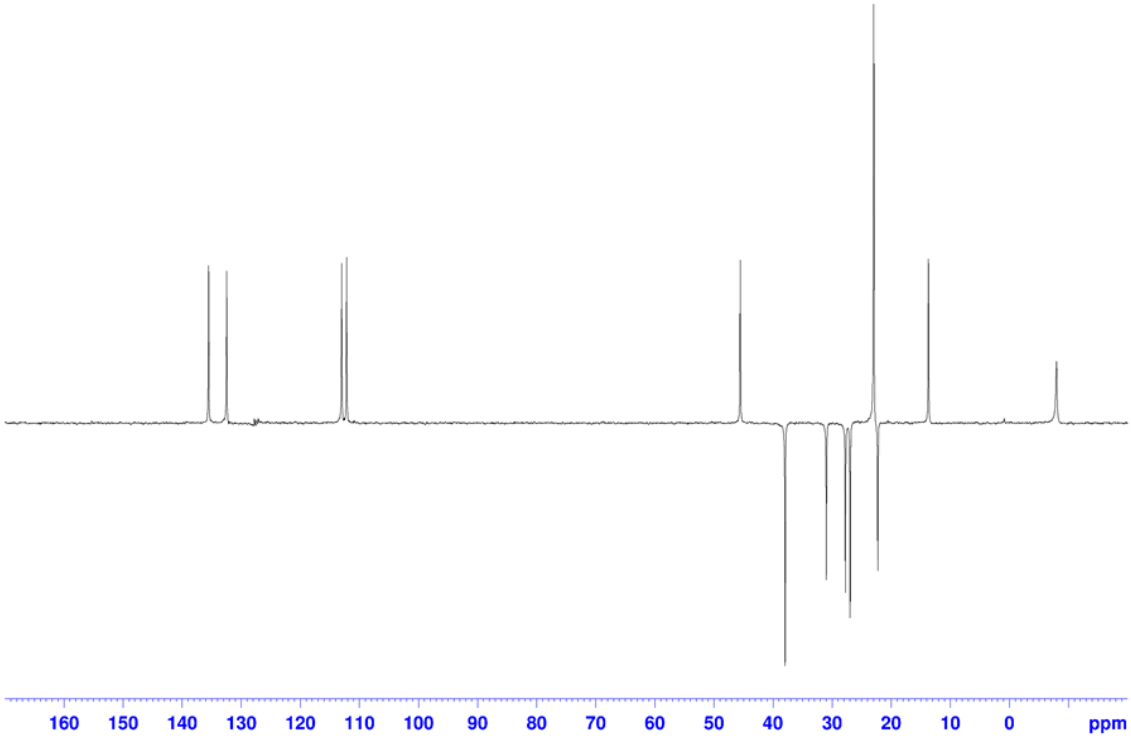

*Figure 267: DEPT 135 of Al-NSHex-ISO complex (100.62 MHz, *C_6D_6, 25°C).*

8.10 Synthesis and characterization of Al-NSBen-ISO

The corresponding *Al-NSBen-ISO* complex was synthesized by reaction of *NSBen-ISO* proligand with Al_2Me_6 in benzene as shown in *figure 268.*

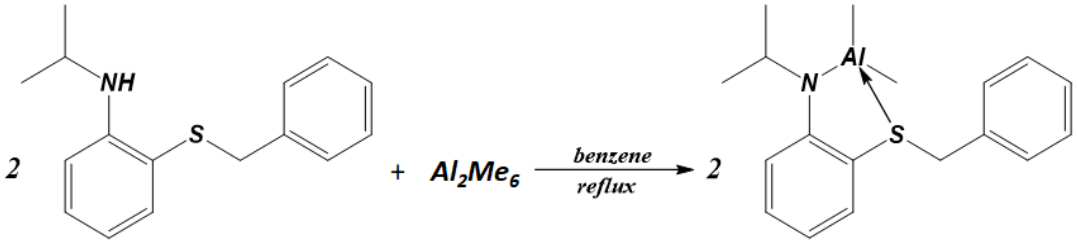

Figure 268: synthesis of Al-NSBen-ISO complex.

The synthesis process is similar to what described in paragraph 8.7.

Al_2Me_6 (0.31 g, 2.15 mmol) in benzene (2 mL) and a solution of [*NSBen-ISO*] (1.05 g, 4.09 mmol) in benzene (3 mL). The resulting brown solution was refluxed for 16 h, after which the volatiles were removed under vacuum. The brown oil product was recovered in a vial (0.99 g, yield = 92%).

^{1}H NMR (400.13 MHz, C_6D_6, 25 °C): δ -0.27 (s, 6H, Al-CH_3), 1.31 (d, J = 6.58 Hz, 6H, CH_3), 3.59 (s, 2H, S-CH_2), 3.66 (m, 1H, N-CH), 6.15-7.14 (m, 9H, ArH). ^{13}C NMR (100.62 MHz, C_6D_6, 25 °C): δ -7.69, 23.60, 42.89, 46.17, 110.74, 112.60, 113.48, 128.20, 128.66, 130.06, 133.22, 134.54, 136.69, 155.97.

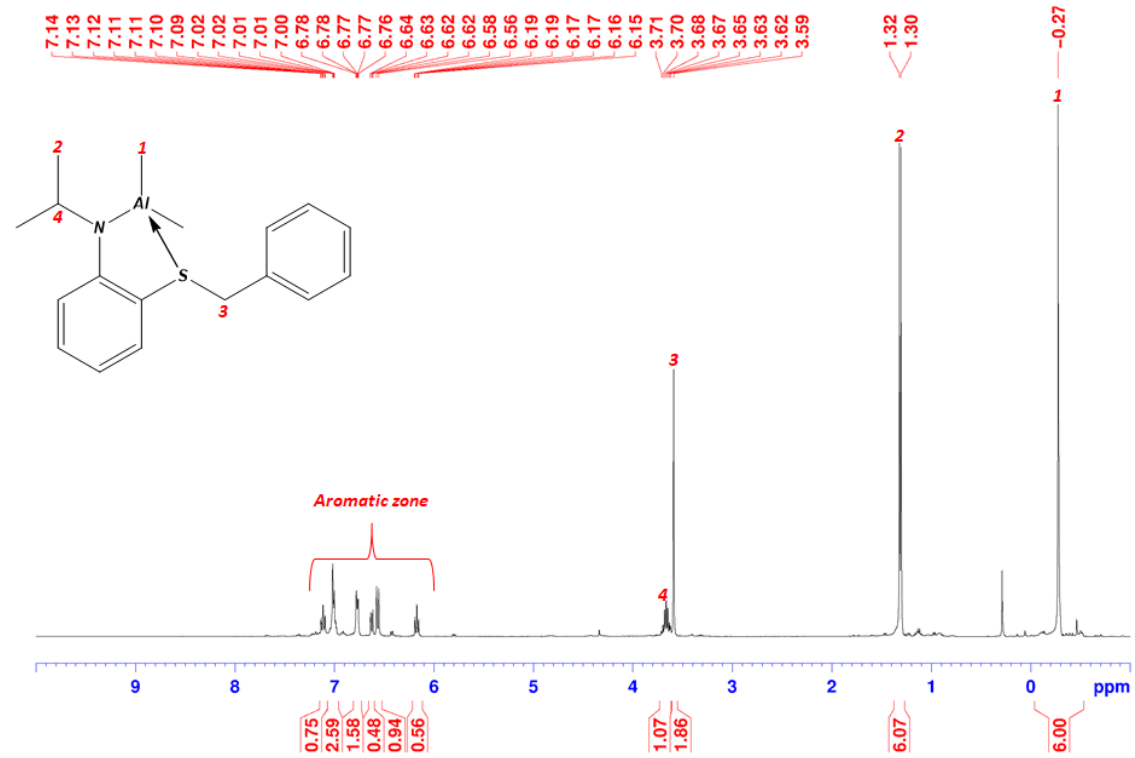

*Figure 269: ^{1}H NMR of Al-NSBen-ISO complex (400.13 MHz, *C_6D_6, 25°C).*

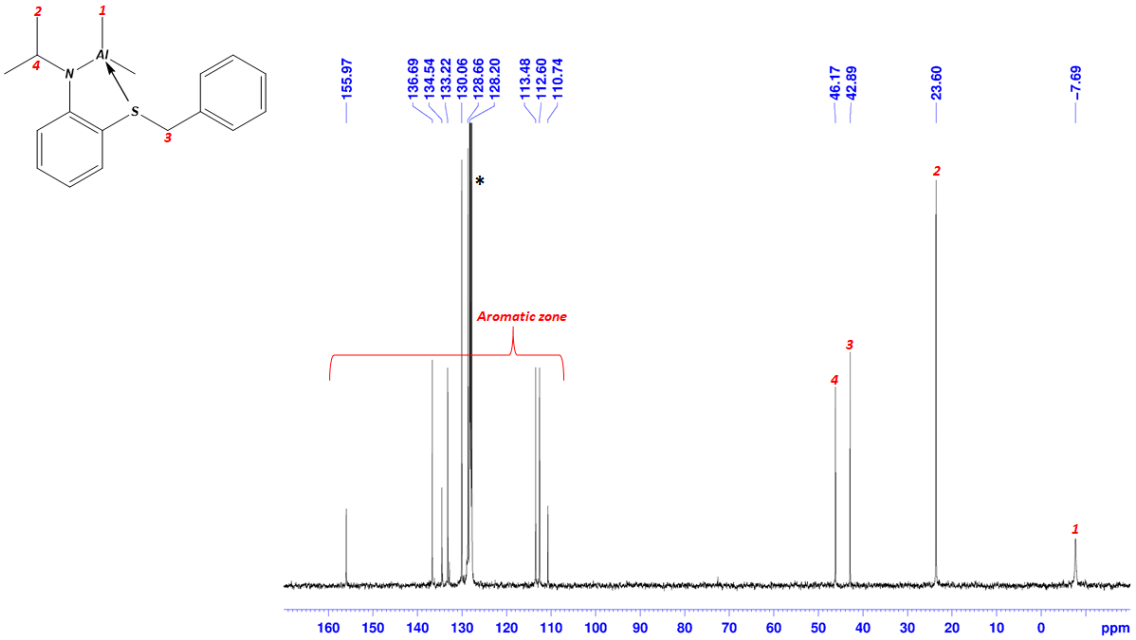

*Figure 270: ^{13}C NMR of Al-NSBen-ISO complex (100.62 MHz, *C_6D_6, 25°C).*

8.11 Synthesis and characterization of Al-NSO-ISO

The corresponding *Al-NSO-ISO* complex was synthesized by reaction of *NSO-ISO* proligand with Al_2Me_6 in benzene as shown in *figure 271*.

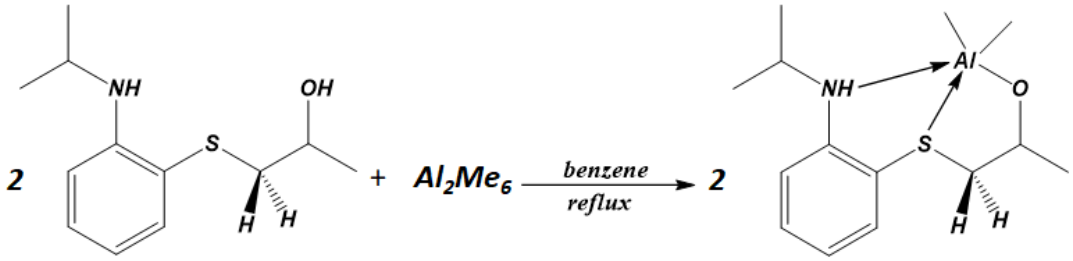

Figure 271: synthesis of Al-NSO-ISO complex.

The synthesis process is similar to what described in paragraph 8.7.

Al_2Me_6 (0.25 g, 1.73 mmol) in benzene (2 mL) and a solution of [*NSO-ISO*] (0.78 g, 3.46 mmol) in benzene (3 mL). The resulting brown solution was refluxed for 16 h, after which the volatiles were removed under vacuum. The brown oil product was recovered in a vial (0.70 g, yield = 72%).

^{1}H NMR (400.13 MHz, TCDE, 25 °C): δ -0.81 (d, J = 1.56 Hz, 6H, Al-CH_3), 1.25 (d, J = 6.17 Hz, 6H, CH_3), 1.37 (d, J = 6.00 Hz, 3H, CH_3), 2.64 (m, J_1 = 13.01 Hz, J_2 = 7.49 Hz, 1H, S-CH), 2.93 (m, J_1 = 12.91 Hz, J_2 = 4.73 Hz, 1H, S-CH), 3.66 (m, 1H, N-CH), 4.00 (m, 1H, O-CH), 4.76 (d, J = 7.97 Hz, 1H, NH), 6.64 (m, J = 8.80 Hz, 2H, ArH), 7.21 (m, J = 7.80 Hz, 1H, ArH), 7.36 (m, J = 7.59 Hz, 1H, ArH). ^{13}C NMR (100.62 MHz, TCDE, 25 °C): δ -8.62, 22.20, 22.80, 22.85, 42.52, 43.87, 69.73, 110.72, 116.22, 116.29, 130.19, 135.62, 147.89.

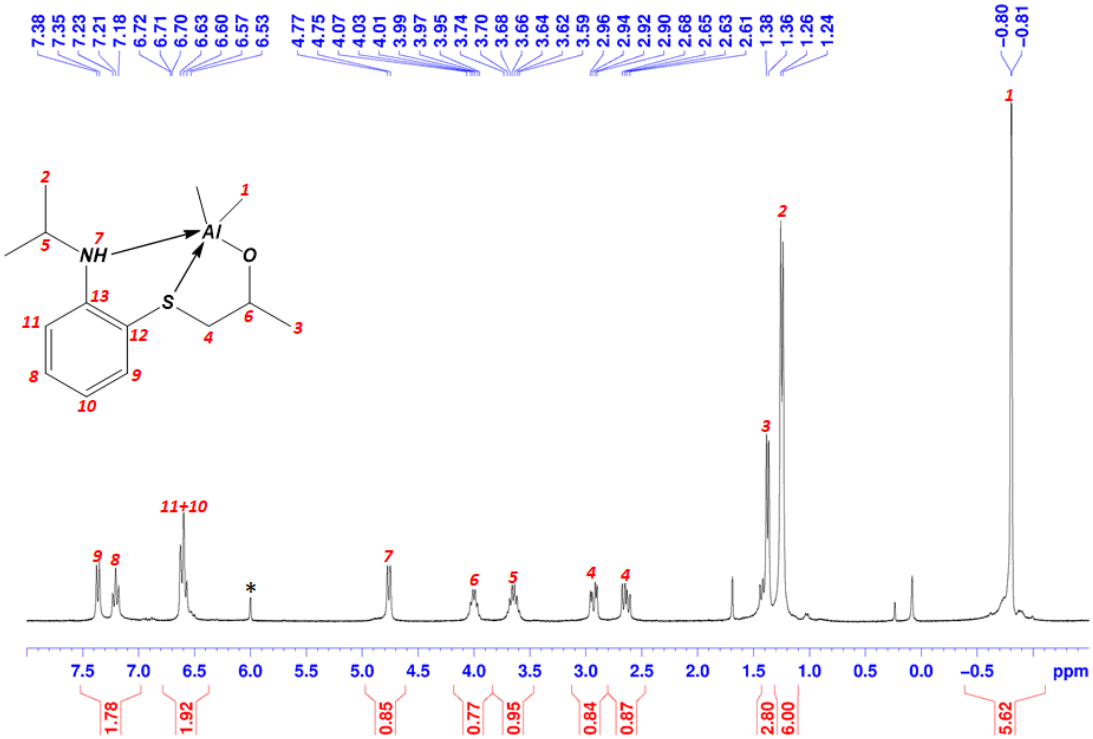

*Figure 272: ^{1}H NMR of Al-NSO-ISO complex (400.13 MHz, *TCDE, 25°C).*

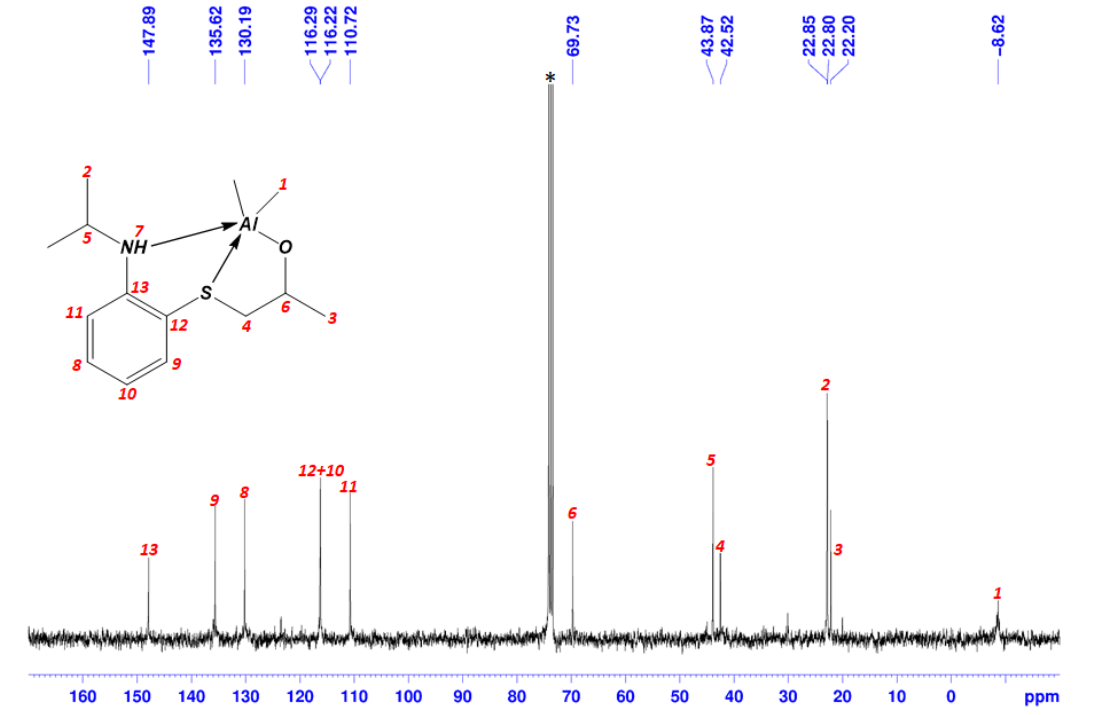

*Figure 273: ^{13}C NMR of Al-NSO-ISO complex (400.13 MHz, *TCDE, 25°C).*

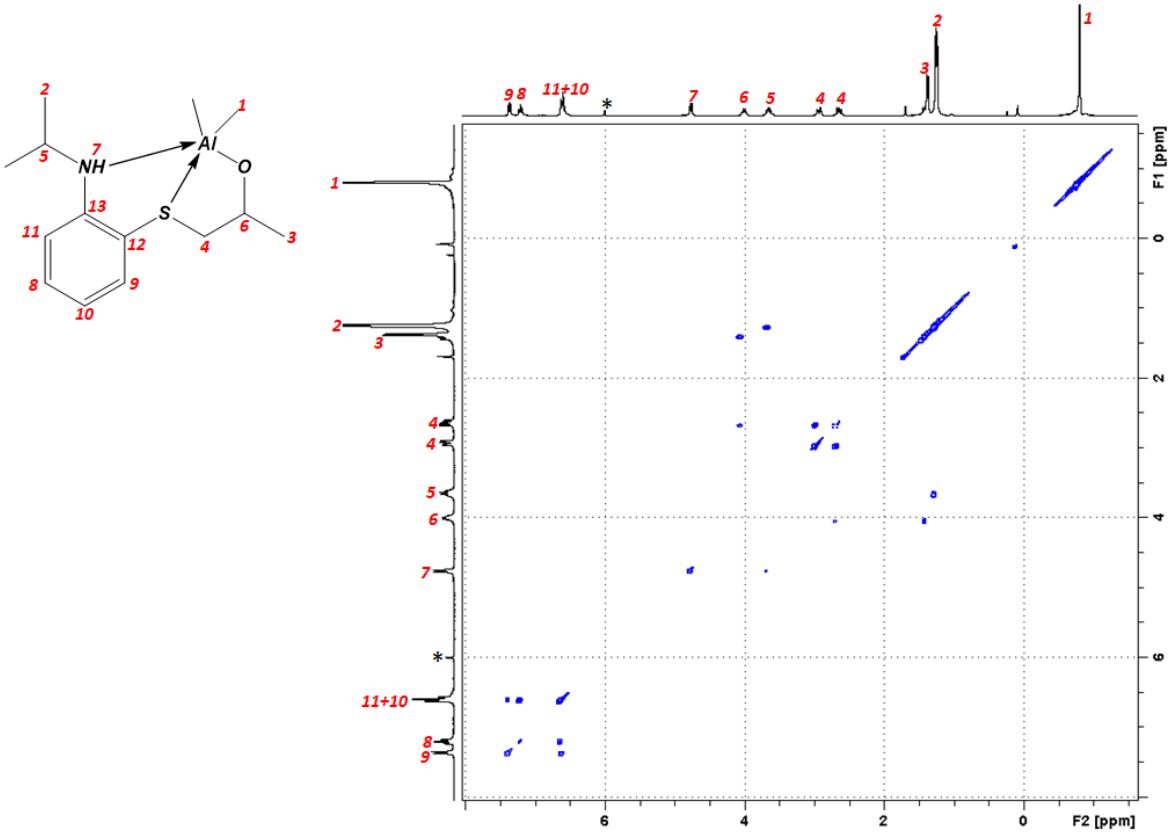

*Figure 274: $^{1}H - {}^{1}H$ COSY spectrum of Al-NSO-ISO complex (400.13/400.13 MHz, *TCDE, 25°C).*

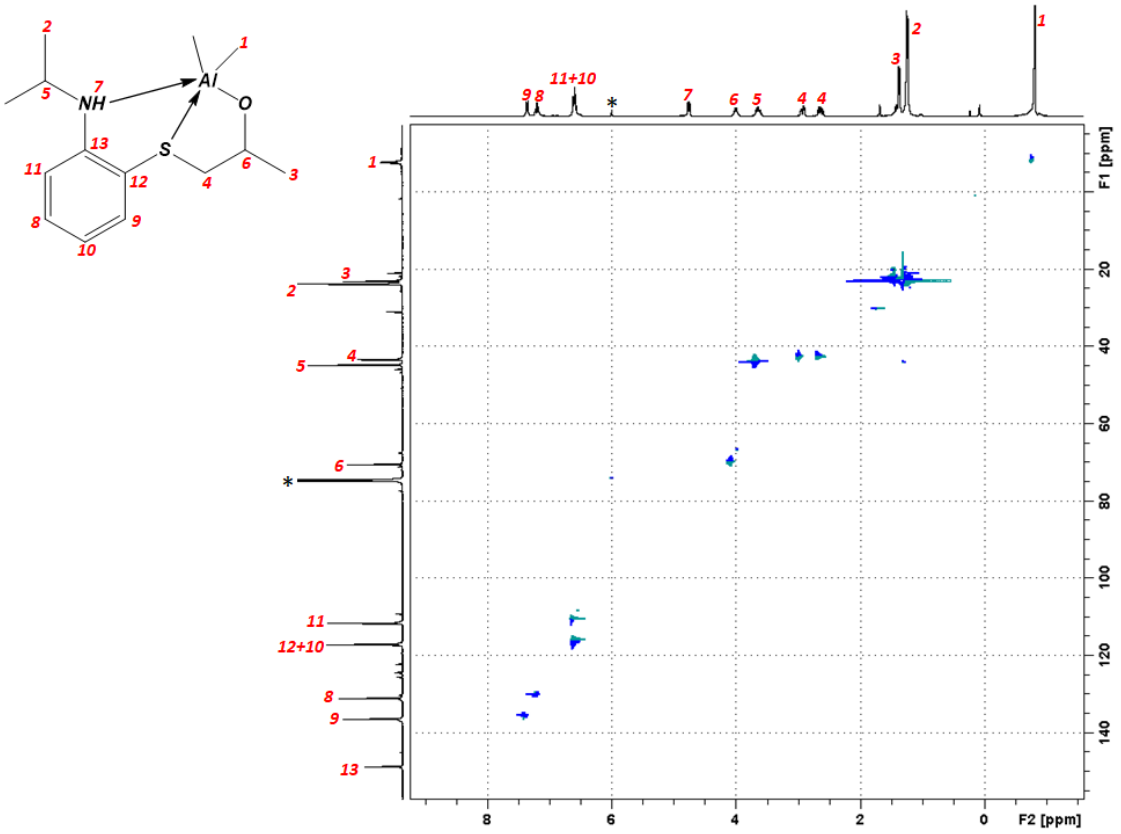

*Figure 275: $^{1}H - {}^{13}C$ HSQC spectrum of Al-NSO-ISO complex (400.13/100.62 MHz, *TCDE, 25°C).*

9 Crystallographic Data

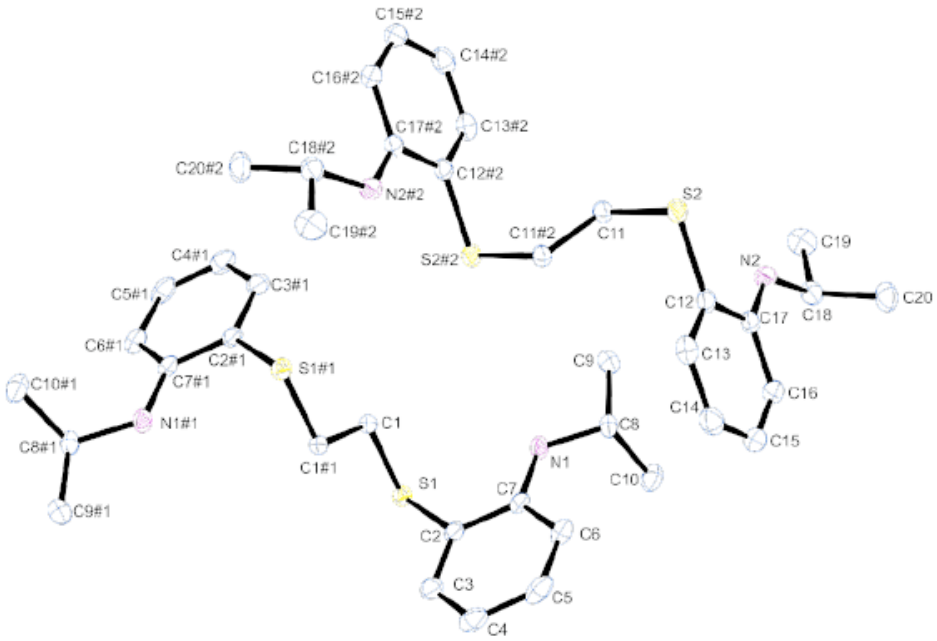

Figure 276: Ortep 3 view of NSSN-ISO molecule. Symmetry transformations used to generate equivalent atoms: #1:-x+1, -y+2, -z; #2: -x+2, -y+1, -z. Thermal ellipsoids are shown at the 30% probability level.

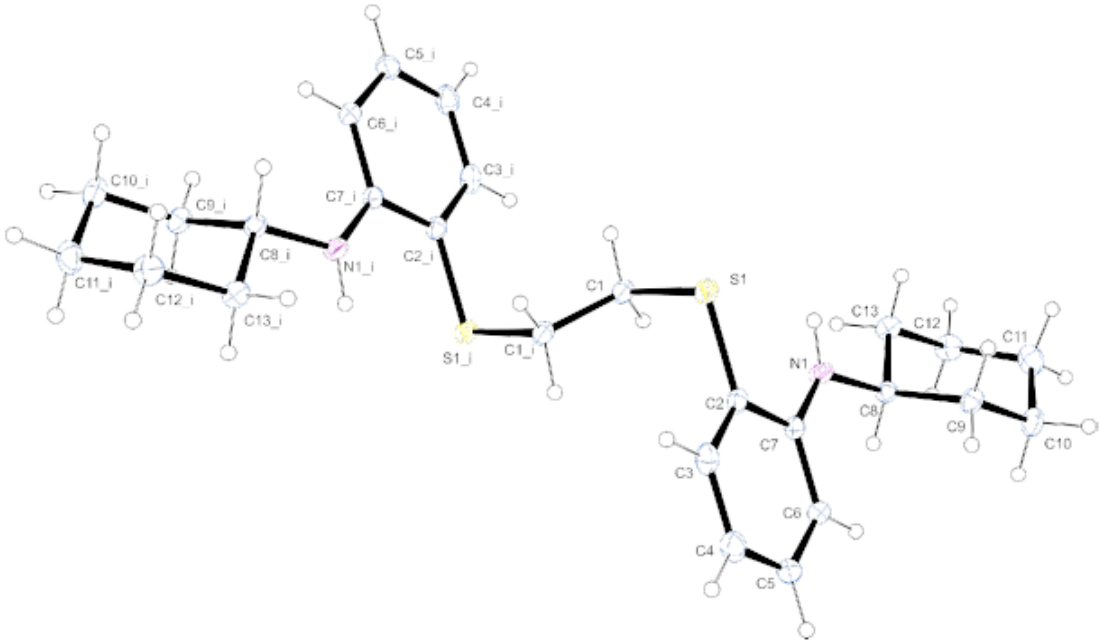

Figure 277: Ortep 3 view of NSSN-Cy molecule. Symmetry transformations used to generate equivalent atoms: #1: -x+2, -y, -z+1. Thermal ellipsoids are shown at the 30% probability level.

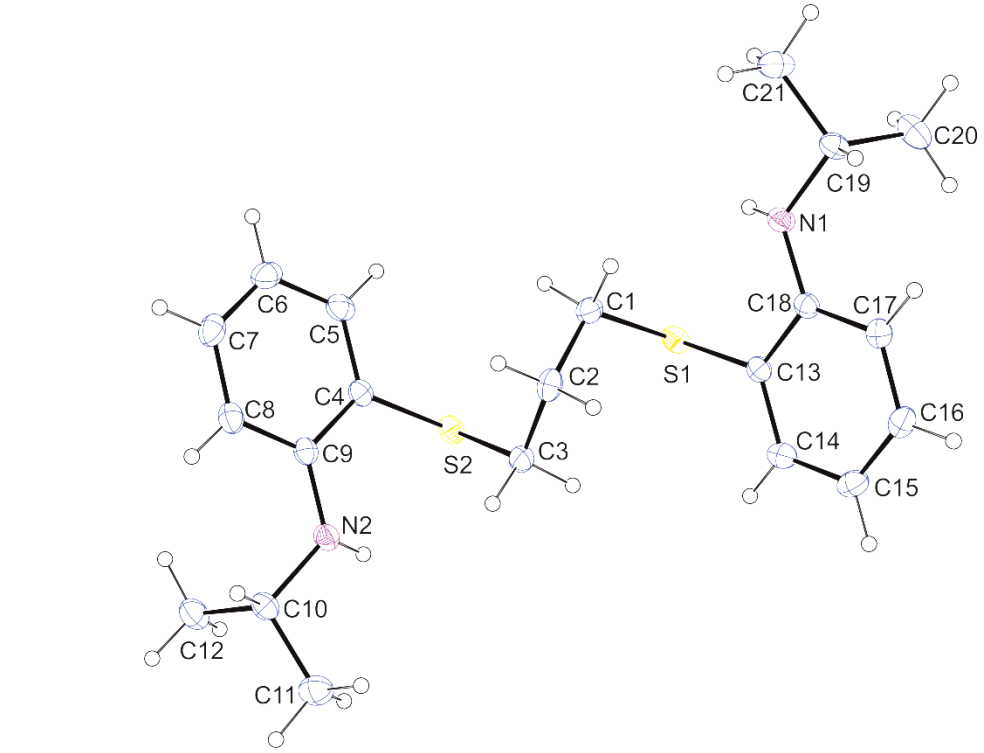

Figure 278: Ortep 3 view of NSSN-Pr-ISO molecule. Symmetry transformations used to generate equivalent atoms: #1: -x, -y+2, -z. Thermal ellipsoids are shown at the 30% probability level.

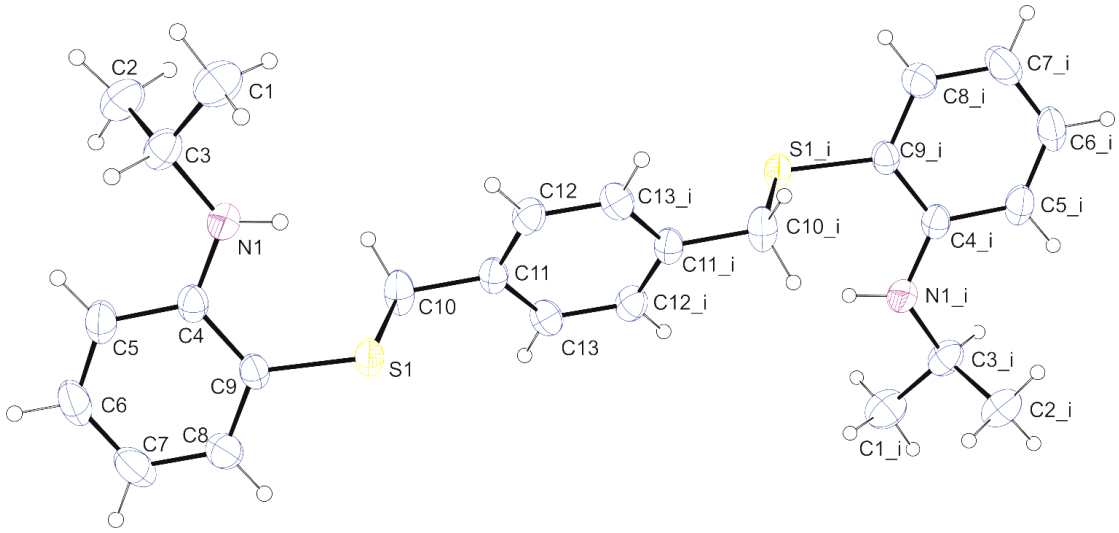

Figure 279: Ortep 3 view of NSSN-Xy-ISO molecule. Symmetry transformations used to generate equivalent atoms: #1: -x, -y+2, -z. Thermal ellipsoids are shown at the 30% probability level.

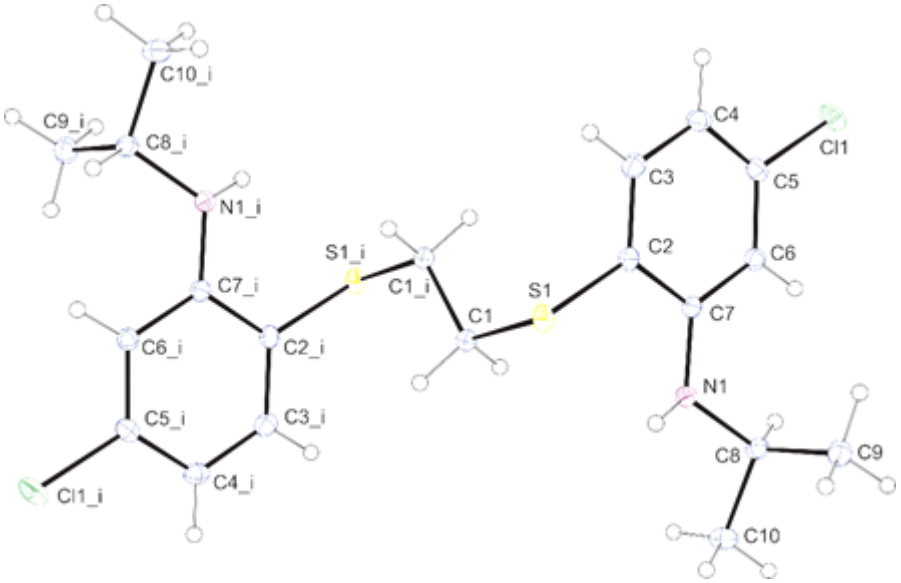

Figure 280: Ortep 3 view of NSSN-Xy-ISO molecule. Symmetry transformations used to generate equivalent atoms: #1: -x, -y+1, -z+1. Thermal ellipsoids are shown at the 30% probability level.

Table 8: Crystallographic Data of NSSN-ISO, NSSN-Cy, NSSN-Pr-ISO, NSSN-Xy-ISO and NSSN-Cl-ISO.

	NSSN-ISO	**NSSN-Cy**	**NSSN-Pr-ISO**	**NSSN-Xy-ISO**	**NSSN-Cl-ISO**
Chemical formula	$C_{20}H_{28}N_2S_2$	$C_{26}H_{36}N_2S_2$	$C_{21}H_{30}N_2S_2$	$C_{26}H_{32}N_2S_2$	$C_{20}H_{26}Cl_2N_2S_2$
Crystal size (mm)	0.400 x 0.300 x 0.300	0.300 x 0.300 x 0.200	0.500 x 0.400 x 0.400	0.500 x 0.500 x 0.500	0.600 x 0.600 x 0600
Crystal habitus, colour	Prism, white	Prism, white	Prism, yellow	Prism, white	Prism, white
Formula weight	360.56	440.69	374.59	436.65	429.45
Temperature (K)	173	173	173	173	173
λ (Å)	0.71073	0.71073	0.71073	0.71073	0.71073
Crystal system	Triclinic	Monoclinic	Triclinic	Monoclinic	Monoclinic
Space group	P -1	P 21/c	P -1	P 21/c	P 21/c
a (Å)	8.8830(19)	9.413(3)	9.2650(17)	8.164(1)	12.729(3)
b (Å)	9.2850(18)	9.7870(9)	9.513(2)	7.803(1)	8.974(1)
c (Å)	12.6030(10)	14.001(4)	12.849(3)	20.066(1)	9.290(1)
α (Å)	80.127(14)	90	74.886(14)	90	90
β (Å)	77.956(14)	114.692(17)	79.894(13)	110.71(1)	104.27(1)
γ (Å)	82.623(15)	90	75.813(17)	90	90
Volume ($Å^3$)	996.93(3)	1171.9(5)	1052.4(4)	1195.7(1)	1028.5(2)
Z	2	2	2	2	2
D_{calcd} $(g \cdot cm^3)$	1.201	1.249	1.182	1.213	1.387
μ (mm^{-1})	0.271	0.243	0.259	0.238	0.526
F (000)	388	476	404	468	468
Theta range (°)	3.089 to 27.499	3.063 to 27.498	3.097 to 27.496	3.395 to 27.503	3.205 to 27.520
Reflections collected	12413	6654	23174	7019	8701
Unique observed reflections	4509 [R(int) = 0.0264]	2657 [R(int) = 0.0195]	4787 [R(int) = 0.0279]	2704 [R(int) = 0.0258]	2338 [R(int) = 0.0221]
Data/parameters	4509/217	2657/136	4787/232	2704/139	2338/121
$R1^{[a]}$, $wR2^{[b]}[I>2\sigma(I)]$	R1 = 0.0356, wR2 = 0.0799	R1 = 0.0316, wR2 = 0.0868	R1 = 0.0316, wR2 = 0.0915	R1 = 0.0400, wR2 = 0.1186	R1 = 0.0257, wR2 = 0.0777
$R1^{[a]}$, $wR2^{[b]}$*(all data)*	R1 = 0.0468, wR2 = 0.0849	R1 = 0.0371, wR2 = 0.0928	R1 = 0.0391, wR2 = 0.1027	R1 = 0.0543, wR2 = 0.1342	R1 = 0.0304, wR2 = 0.0841
Largest diff. peak and hole $(e \cdot Å^{-3})$	0.231 and -0.226	0.268 and -0.0195	0.331 and -0.242	0.290 and -0.199	0.298 and -0.266

[a] $R_1 = \Sigma||Fo|-|Fc|/\Sigma|Fo|$; [b] $wR_2 = [\Sigma w(Fo^2-Fc^2)^2/\Sigma w(Fo^2)^2]^{1/2}$

Table 9: Selected bond lengths [Å] and angles (°) of NSSN-ISO ligand.

C(12)-S(2)-C(11)	102.55(7)
C(1)#1-C(1)-S(1)	111.85(13)
C(11)#2-C(11)-S(2)	112.75(15)
N(1)-C(7)-C(6)	122.15(14)
N(1)-C(7)-C(2)	120.29(13)
C(6)-C(7)-C(2)	117.48(14)
C(7)-N(1)-C(8)	123.27(12)
C(13)-C(12)-C(17)	120.25(15)
C(13)-C(12)-S(2)	119.23(12)
C(17)-C(12)-S(2)	120.46(12)
N(2)-C(17)-C(16)	122.40(14)
N(2)-C(17)-C(12)	120.38(14)
C(16)-C(17)-C(12)	117.18(15)
C(17)-N(2)-C(18)	123.51(13)
C(3)-C(2)-C(7)	120.63(14)
C(3)-C(2)-S(1)	119.67(12)
C(7)-C(2)-S(1)	119.70(11)
N(1)-C(8)-C(9)	108.35(12)
N(1)-C(8)-C(10)	112.87(13)
C(9)-C(8)-C(10)	110.59(13)
C(15)-C(16)-C(17)	121.43(16)
C(4)-C(3)-C(2)	120.71(16)
N(2)-C(18)-C(19)	108.30(14)
N(2)-C(18)-C(20)	113.03(14)
C(19)-C(18)-C(20)	111.21(15)
C(14)-C(13)-C(12)	121.10(16)
C(5)-C(6)-C(7)	120.74(16)
C(6)-C(5)-C(4)	121.43(16)
C(5)-C(4)-C(3)	118.98(16)
C(15)-C(14)-C(13)	118.96(17)
C(16)-C(15)-C(14)	121.08(17)

Symmetry transformations used to generate equivalent atoms: #1 –x+1, -y+2, -z; #2 –x+2, -y+1, -z.

Table 10: Selected bond lengths [Å] and angles (°) of NSSN-Cy ligand.

S(1)-C(2)	1.7650(13)
S(1)-C(1)	1.8195(14)
N(1)-C(7)	1.3707(15)
N(1)-C(8)	1.4546(15)
N(1)-H(15)	0.8799
C(2)-C(3)	1.3860(17)
C(2)-C(7)	1.4119(16)
C(9)-C(10)	1.5200(17)

C(9)-C(8)	1.5286(17)
C(3)-C(4)	1.382(2)
C(7)-C(6)	1.4002(17)
C(6)-C(5)	1.3764(18)
C(13)-C(8)	1.5179(17)
C(13)-C(12)	1.5214(18)
C(1)-C(1)#1	1.507(2)
C(10)-C(11)	1.516(2)
C(5)-C(4)	1.379(2)
C(12)-C(11)	1.523(2)
C(2)-S(1)-C(1)	101.76(6)
C(7)-N(1)-C(8)	123.13(10)
C(7)-N(1)-H(15)	116.0
C(8)-N(1)-H(15)	115.2
C(3)-C(2)-C(7)	120.23(11)
C(3)-C(2)-S(1)	119.63(10)
C(7)-C(2)-S(1)	120.06(9)
C(10)-C(9)-C(8)	110.36(10)
C(4)-C(3)-C(2)	121.16(12)
N(1)-C(7)-C(6)	122.13(11)
N(1)-C(7)-C(2)	120.26(11)
C(6)-C(7)-C(2)	117.60(11)
C(5)-C(6)-C(7)	120.97(12)
C(8)-C(13)-C(12)	110.92(10)
C(1)#1-C(1)-S(1)	112.61(12)
N(1)-C(8)-C(13)	109.04(10)
N(1)-C(8)-C(9)	113.88(10)
C(13)-C(8)-C(9)	109.53(10)
C(11)-C(10)-C(9)	111.02(11)
C(6)-C(5)-C(4)	121.23(13)
C(13)-C(12)-C(11)	111.61(11)
C(5)-C(4)-C(3)	118.80(12)
C(10)-C(11)-C(12)	111.58(11)

Symmetry transformations used to generate equivalent atoms: #1 –x+2, -y, -z+1.

Table 11: Selected bond lengths [Å] and angles (°) of NSSN-Pr-ISO ligand.

S(1)-C(13)	1.7702(14)
S(1)-C(1)	1.8189(15)
S(2)-C(4)	1.7680(14)
S(2)-C(3)	1.8185(15)
N(1)-C(18)	1.3745(17)
N(1)-C(19)	1.4567(17)
N(1)-H(22)	0.9093
N(2)-C(9)	1.3732(18)
N(2)-C(10)	1.4600(17)

N(2)-H(23)	0.8969
C(13)-C(14)	1.3891(19)
C(13)-C(18)	1.4136(18)
C(1)-C(2)	1.516(2)
C(1)-H(1A)	0.9900
C(1)-H(1B)	0.9900
C(4)-C(5)	1.389(2)
C(4)-C(9)	1.4171(18)
C(14)-C(15)	1.384(2)
C(14)-H(14)	0.9500
C(9)-C(8)	1.4018(19)
C(18)-C(17)	1.4012(19)
C(19)-C(21)	1.515(2)
C(19)-C(20)	1.521(2)
C(19)-H(19)	1.0000
C(2)-C(3)	1.513(2)
C(2)-H(2A)	0.9900
C(2)-H(2B)	0.9900
C(17)-C(16)	1.379(2)
C(17)-H(17)	0.9500
C(3)-H(3A)	0.9900
C(3)-H(3B)	0.9900
C(8)-C(7)	1.379(2)
C(8)-H(8)	0.9500
C(16)-C(15)	1.381(2)
C(16)-H(16)	0.9500
C(5)-H(5)	1.381(2)
C(12)-C(10)	1.524(2)
C(12)-H(12A)	0.9800
C(12)-H(12B)	0.9800
C(12)-H(12C)	0.9800
C(6)-C(7)	1.381(2)
C(6)-H(6)	0.9500
C(15)-H(15)	0.9500
C(7)-H(7)	0.9500
C(21)-H(21A)	0.9800
C(21)-H(21B)	0.9800
C(21)-H(21C)	0.9800
C(10)-C(11)	1.513(2)
C(10)-H(10)	1.0000
C(11)-H(11A)	0.9800
C(11)-H(11B)	0.9800
C(11)-H(11C)	0.9800
C(20)-H(20A)	0.9800
C(20)-H(20B)	0.9800
C(20)-H(20C)	0.9800

C(13)-S(1)-C(1)	102.51(6)
C(4)-S(2)-C(3)	101.57(6)
C(18)-N(1)-C(19)	123.33(11)
C(18)-N(1)-H(22)	115.4
C(19)-N(1)-H(22)	113.3
C(9)-N(2)-C(10)	123.55(11)
C(9)-N(2)-H(23)	116.7
C(10)-N(2)-H(23)	111.6
C(14)-C(13)-C(18)	120.10(12)
C(14)-C(13)-S(1)	119.29(10)
C(18)-C(13)-S(1)	120.54(10)
C(2)-C(1)-S(1)	114.72(10)
C(2)-C(1)-H(1A)	108.6
S(1)-C(1)-H(1A)	108.6
C(2)-C(1)-H(1B)	108.6
S(1)-C(1)-H(1B)	108.6
H(1A)-C(1)-H(1B)	107.6
C(5)-C(4)-C(9)	120.16(13)
C(5)-C(4)-S(2)	119.57(11)
C(9)-C(4)-S(2)	120.24(10)
C(15)-C(14)-C(13)	121.16(13)
C(15)-C(14)-H(14)	119.4
C(13)-C(14)-H(14)	119.4
N(2)-C(9)-C(8)	122.47(12)
N(2)-C(9)-C(4)	119.67(12)
C(8)-C(9)-C(4)	117.84(13)
N(1)-C(18)-C(17)	122.30(12)
N(1)-C(18)-C(13)	119.90(12)
C(17)-C(18)-C(13)	117.73(12)
N(1)-C(19)-C(21)	107.88(12)
N(1)-C(19)-C(20)	112.68(12)
C(21)-C(19)-C(20)	111.53(14)
N(1)-C(19)-H(19)	108.2
C(21)-C(19)-H(19)	108.2
C(20)-C(19)-H(19)	108.2
C(3)-C(2)-C(1)	115.23(12)
C(3)-C(2)-H(2A)	108.5
C(1)-C(2)-H(2A)	108.5
C(3)-C(2)-H(2B)	108.5
C(1)-C(2)-H(2B)	108.5
H(2A)-C(2)-H(2B)	107.5
C(16)-C(17)-C(18)	121.00(13)
C(16)-C(17)-H(17)	119.5
C(18)-C(17)-H(17)	119.5
C(2)-C(3)-S(2)	115.12(10)
C(2)-C(3)-H(3A)	108.5

S(2)-C(3)-H(3A)	108.5
C(2)-C(3)-H(3B)	108.5
S(2)-C(3)-H(3B)	108.5
H(3A)-C(3)-H(3B)	107.5
C(7)-C(8)-C(9)	120.63(14)
C(7)-C(8)-H(8)	119.7
C(9)-C(8)-H(8)	119.7
C(17)-C(16)-C(15)	121.11(13)
C(17)-C(16)-H(16)	119.4
C(15)-C(16)-H(16)	119.4
C(6)-C(5)-C(4)	120.88(14)
C(6)-C(5)-H(5)	119.6
C(A)-C(5)-H(5)	119.6
C(10)-C(12)-H(12A)	109.5
C(10)-C(12)-H(12B)	109.5
H(12A)-C(12)-H(12B)	109.5
C(10)-C(12)-H(12C)	109.5
H(12A)-C(12)-H(12C)	109.5
H(12B)-C(12)-H(12C)	109.5
C(5)-C(6)-C(7)	119.17(14)
C(5)-C(6)-H(6)	120.4
C(7)-C(6)-H(6)	120.4
C(16)-C(15)-C(14)	118.90(13)
C(16)-C(15)-H(15)	120.6
C(14)-C(15)-H(15)	120.6
C(8)-C(7)-C(6)	121.26(14)
C(8)-C(7)-H(7)	119.4
C(6)-C(7)-H(7)	119.4
C(19)-C(21)-H(21A)	109.5
C(19)-C(21)-H(21B)	109.5
H(21A)-C(21)-H(21B)	109.5
C(19)-C(21)-H(21C)	109.5
H(21A)-C(21)-H(21C)	109.5
H(21B)-C(21)-H(21C)	109.5
N(2)-C(10)-C(11)	107.77(12)
N(2)-C(10)-C(12)	112.53(12)
C(11)-C(10)-C(12)	111.52(13)
N(2)-C(10)-H(10)	108.3
C(11)-C(10)-H(10)	108.3
C(12)-C(10)-H(10)	108.3
C(10)-C(11)-H(11A)	109.5
C(10)-C(11)-H(11B)	109.5
H(11A)-C(11)-H(11B)	109.5
C(10)-C(11)-H(11C)	109.5
H(11A)-C(11)-H(11C)	109.5
H(11B)-C(11)-H(11C)	109.5

C(19)-C(20)-H(20A)	109.5
C(19)-C(20)-H(20B)	109.5
H(20A)-C(20)-H(20B)	109.5
C(19)-C(20)-H(20C)	109.5
H(20A)-C(20)-H(20C)	109.5
H(20B)-C(20)-H(20C)	109.5

Symmetry transformations used to generate equivalent atoms: #1 –x, -y+2, -z.

Table 12: Selected bond lengths [Å] and angles (°) of NSSN-Xy-ISO ligand.

S(1)-C(9)	1.7665(16)
S(1)-C(10)	1.8129(19)
C(9)-C(8)	1.383(3)
C(9)-C(4)	1.411(3)
C(4)-N(1)	1.374(2)
C(4)-C(5)	1.402(2)
C(11)-C(13)	1.377(3)
C(11)-C(12)	1.382(3)
C(11)-C(10)	1.503(2)
C(13)-C(12) #1	1.381(3)
C(13)-H(13)	0.9300
C(12)-H(12)	0.9300
N(1)-C(3)	1.464(2)
N(1)-H(14)	0.8812
C(3)-C(1)	1.513(3)
C(3)-C(2)	1.521(3)
C(3)-H(3)	0.9800
C(10)-H(10A)	0.9700
C(10)-H(10B)	0.9700
C(8)-C(7)	1.384(3)
C(8)-H(8)	0.9300
C(5)-C(6)	1.364(3)
C(5)-H(5)	0.9300
C(7)-C(6)	1.367(4)
C(7)-H(7)	0.9300
C(6)-H(6)	0.9300
C(2)-H(2A)	0.9600
C(2)-H(2B)	0.9600
C(2)-H(2C)	0.9600
C(1)-H(1A)	0.9600
C(1)-H(1B)	0.9600
C(1)-H(1C)	0.9600
C(9)-S(1)-C(10)	103.01(8)
C(8)-C(9)-C(4)	120.11(16)
C(8)-C(9)-S(1)	118.70(14)
C(4)-C(9)-S(1)	121.05(13)

N(1)-C(4)-C(5)	122.51(17)
N(1)-C(4)-C(9)	119.70(15)
C(5)-C4)-C(9)	117.79(17)
C(13)-C(11)-C(12)	118.27(16)
C(13)-C(11)-C(10)	121.23(17)
C(12)-C(11)-C(10)	120.47(17)
C(11)-C(13)-C(12)#1	120.71(17)
C(11)-C(13)-H(13)	119.6
C(12)#1-C(13)-H(13)	119.6
C(13)#1-C(12)-C(11)	121.02(17)
C(13)#1-C(12)-H(12)	119.5
C(11)-C(12)-H(12)	119.5
C(4)-N(1)-C(3)	123.04(16)
C(4)-N(1)-H(14)	114.3
C(3)-N(1)-H(14)	116.9
N(1)-C(3)-C(1)	108.72(17)
N(1)-C(3)-C(2)	110.62(17)
C(1)-C(3)-C(2)	111.38(19)
N(1)-C(3)-H(3)	108.7
C(1)-C(3)-H(3)	108.7
C(2)-C(3)-H(3)	108.7
C(11)-C(10)-S(1)	107.92(12)
C(11)-C(10)-H(10A)	110.1
S(1)-C(10)-H(10A)	110.1
C(11)-C(10)-H(10B)	110.1
S(1)-C(10)-H(10B)	110.1
H(10A)-C(10)-H(10B)	108.4
C(9)-C(8)-C(7)	120.7(2)
C(9)-C(8)-H(8)	119.6
C(7)-C(8)-H(8)	119.6
C(6)-C(5)-C(4)	120.5(2)
C(6)-C(5)-H(5)	119.8
C(4)-C(5)-H(5)	119.8
C(6)-C(7)-C(8)	119.0(2)
C(6)-C(7)-H(7)	120.5
C(8)-C(7)-H(7)	120.5
C(5)-C(6)-C(7)	121.95(19)
C(5)-C(6)-H(6)	119.0
C(7)-C(6)-H(6)	119.0
C(3)-C(2)-H(2A)	109.5
C(3)-C(2)-H(2B)	109.5
H(2A)-C(2)-H(2B)	109.5
C(3)-C(2)-H(2C)	109.5
H(2A)-C(2)-H(2C)	109.5
H(2B)-C(2)-H(2C)	109.5
C(3)-C(1)-H(1A)	109.5

C(3)-C(1)-H(1B)	109.5
H(1A)-C(1)-H(1B)	109.5
C(3)-C(1)-H(1C)	109.5
H(1A)-C(1)-H(1C)	109.5
H(1B)-C(1)-H(1C)	109.5

Symmetry transformations used to generate equivalent atoms: #1 –x, -y+2, -z.

Table 13: Selected bond lengths [Å] and angles (°) of NSSN-Cl-ISO ligand.

S(1)-C(2)	1.7702(13)
S(1)-C(1)	1.8178(14)
Cl(1)-C(5)	1.7341(13)
N(1)-C(7)	1.3754(16)
N(1)-C(8)	1.4599816)
N(1)-H(14)	0.8900
C(1)-C(1)#1	1.512(2)
C(1)-H(1A)	0.9900
C(1)-H(1B)	0.9900
C(2)-C(3)	1.3895(19)
C(2)-C(7)	1.4141(18)
C(3)-C(4)	1.385(2)
C(3)-H(3)	0.9500
C(5)-C(6)	1.3839(18)
C(6)-C(7)	1.4031(18)
C(6)-H(6)	0.9500
C(8)-C(10)	1.5211(19)
C(8)-C(9)	1.521(2)
C(8)-H(8)	1.0000
C(9)-C(9A)	0.9800
C(9)-H(9B)	0.9800
C(9)-H(9C)	0.9800
C(10)-H(10A)	0.9800
C(10)-H(10B)	0.9800
C(10)-H(10C)	0.9800
C(2)-S(1)-C(1)	101.22(6)
C(7)-N(1)-C(8)	122.45(11)
C(7)-N(1)-H(14)	113.2
C(8)-N(1)-H(14)	113.3
C(1)#1-C(1)-S(1)	112.03(12)
C(1)#1-C(1)-H(1A)	109.2
S(1)-C(1)-H(1A)	109.2
C(1)#1-C(1)-H(1B)	109.2
S(1)-C(1)-H(1A)	109.2
C(1)#1-C(1)-H(1B)	109.2
S(1)-C(1)-H(1B)	109.2
H(1A)-C(1)-H(1B)	107.9

C(3)-C(2)-C(7)	120.38(12)
C(3)-C(2)-S(1)	119.81(10)
C(7)-C(2)-S(1)	119.78(10)
C(4)-C(3)-C(2)	121.58(12)
C(4)-C(3)-H(3)	119.2
C(2)-C(3)-H(3)	119.2
C(5)-C(4)-C(3)	117.61(12)
C(5)-C(4)-H(4)	121.2
C(3)-C(4)-H(4)	121.2
C(4)-C(5)-C(6)	122.66(12)
C(4)-C(5)-Cl(1)	119.13(10)
C(6)-C(5)-Cl(1)	118.21(11)
C(5)-C(6)-C(7)	119.91(12)
C(5)-C(6)-H(6)	120.0
C(7)-C(6)-H(6)	120.0
N(1)-C(7)-C(6)	121.81(11)
N(1)-C(7)-C(2)	120.29(12)
C(6)-C(7)-C(2)	117.85(12)
N(1)-C(8)-C(10)	108.62(11)
N(1)-C(8)-C(9)	112.28(11)
C(10)-C(8)-C(9)	111.02(11)
N(1)-C(8)-H(8)	108.3
C(10)-C(8)-H(8)	108.3
C(9)-C(8)-H(8)	108.3
C(8)-C(9)-H(9A)	109.5
C(8)-C(9)-H(9B)	109.5
H(9A)-C(9)-H(9B)	109.5
C(8)-C(9)-H(9C)	109.5
H(9A)-C(9)-H(9C)	109.5
H(9B)-C(9)-H(9C)	109.5
C(8)-C(10)-H(10A)	109.5
C(8)-C(10)-H(10B)	109.5
H(10A)-C(10)-H(10B)	109.5
C(8)-C(10)-H(10C)	109.5
H(10A)-C(10)-H(10C)	109.5
H(10B)-C(10)-H(10C)	109.5

Symmetry transformations used to generate equivalent atoms: #1 –x, -y+1, -z+1.

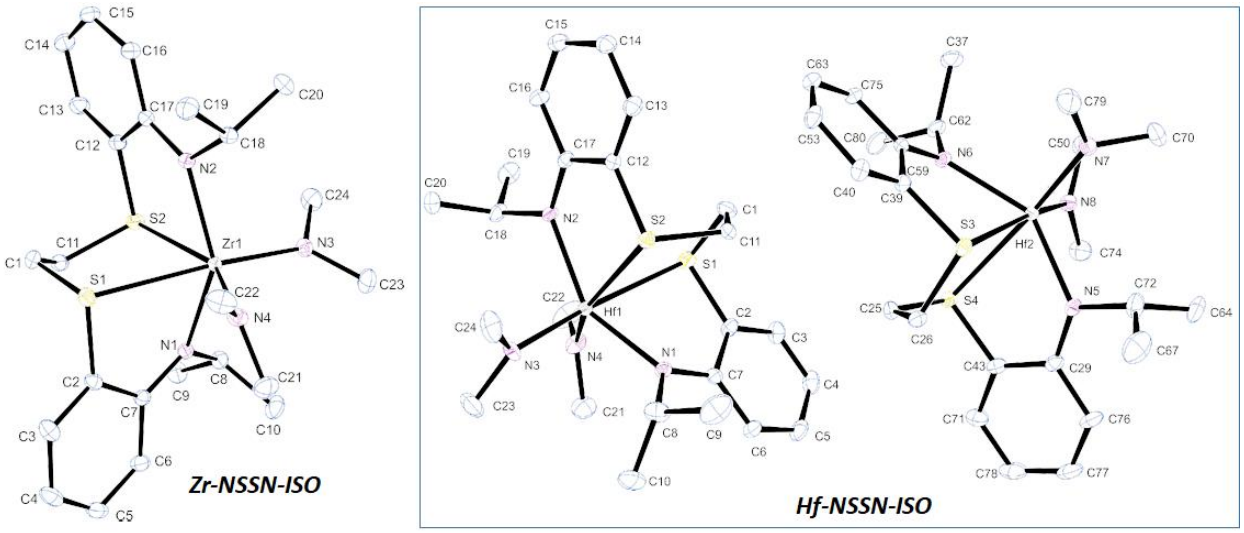

Figure 281: Ortep 3 view of Zr-NSSN-ISO and Hf-NSSN-ISO. Thermal ellipsoids are shown at the 30% probability level.

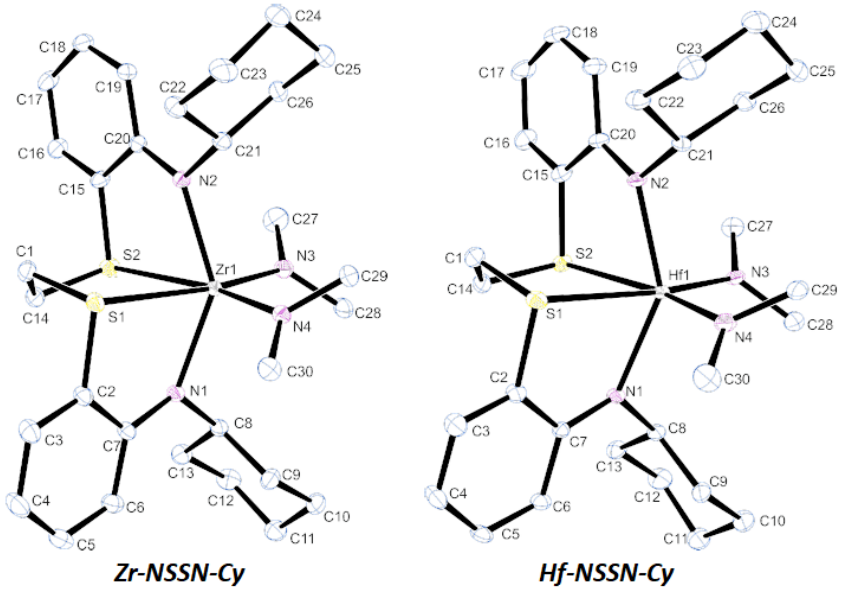

Figure 282: Ortep 3 view of Zr-NSSN-Cy and Hf-NSSN-Cy. Thermal ellipsoids are shown at the 30% probability level.

Table 14: Crystallographic Data of Zr-NSSN-ISO and Hf-NSSN-ISO.

	Zr-NSSN-ISO	**Hf-NSSN-ISO**
Chemical formula	$C_{24}H_{38}N_4S_2Zr$	$C_{24}H_{38}N_4S_2Hf$
Crystal size (mm)	0.400 x 0.300 x 0.200	0.300 x 0.300 x 0.200
Crystal habitus, colour	Prism, yellow	Prism, yellow
Formula weight	537.92	625.19
Temperature (K)	173 (2)	173 (2)
λ (Å)	0.71073	0.71073
Crystal system	Triclinic	Monoclinic
Space group	P -1	P 21/c
a (Å)	9.0020(6)	26.175
b (Å)	11.8900(18)	11.574
c (Å)	12.4210(13)	17.575
α (Å)	83.688(12)	90
β (Å)	82.115(9)	97.71
γ (Å)	80.344(10)	90
Volume (Å^3)	1293.1(3)	5276.1
Z	2	8
D_{calcd} $(g \cdot cm^3)$	1.382	1.574
μ (mm^{-1})	0.605	4.131
F (000)	564	2512
Theta range (°)	3.034 to 27.496	3.046 to 27.534
Reflections collected	15970	31262
Unique observed reflections	587 [R(int) = 0.0208]	11327 [R(int) = 0.0369]
Data/parameters	5873/281	11237/575
R1[a], wR2[b][I>2σ(I)]	R1 = 0.0212, wR2 = 0.0517	R1 = 0.0414, wR2 = 0.0979
R1[a], wR2[b](all data)	R1 = 0.0277, wR2 = 0.0560	R1 = 0.0599, wR2 = 0.1065
Largest diff. peak and hole ($e \cdot$ Å^{-3})	0.364 and -0.278	1.584 and -2.642

[a] $R_1 = \Sigma||Fo|-|Fc|/\Sigma|Fo|$; [b] $wR_2 = [\Sigma w(Fo^2-Fc^2)^2/\Sigma w(Fo^2)^2]^{1/2}$

Table 15: Crystallographic Data of Zr-NSSN-Cy and Hf-NSSN-Cy.

	Zr-NSSN-Cy	**Hf-NSSN-Cy**
Chemical formula	$C_{30}H_{46}N_4S_2Zr$	$C_{30}H_{46}N_4S_2Hf$
Crystal size (mm)	0.400 x 0.200 x 0.200	0.200 x 0.200 x 0.100
Crystal habitus, colour	Prism, yellow	Prism, yellow
Formula weight	618.05	705.32
Temperature (K)	173 (2)	173 (2)
λ (Å)	0.71073	0.71073
Crystal system	Orthorombic	Orthorombic
Space group	P b c a	P b c a
a (Å)	14.045(4)	14.094(5)
b (Å)	16.0520(16)	16.049(5)
c (Å)	26.701(12)	26.653(9)
α (Å)	90	90
β (Å)	90	90
γ (Å)	90	90
Volume (Å^3)	6020(3)	6029(4)
Z	8	8
D_{calcd} $(g \cdot cm^3)$	1.364	1.554
μ (mm^{-1})	0.530	3.625
F (000)	2608	2864
Theta range (°)	3.021 to 27.514	3.019 to 27.516
Reflections collected	35192	23630
Unique observed reflections	6900 [R(int) = 0.0417]	6872 [R(int) = 0.0369]
Data/parameters	6900/338	6872/338
R1[a], wR2[b][I>2σ(I)]	R1 = 0.0359, wR2 = 0.0802	R1 = 0.0350, wR2 = 0.0784
R1[a], wR2[b](all data)	R1 = 0.0506, wR2 = 0.0863	R1 = 0.0560, wR2 = 0.0880
Largest diff. peak and hole $(e \cdot Å^{-3})$	0.716 and -0.593	1.440 and -3.040

[a] $R_1 = \Sigma||Fo|-|Fc|/\Sigma|Fo|$; [b] $wR_2 = [\Sigma w(Fo^2-Fc^2)^2/\Sigma w(Fo^2)^2]^{1/2}$

Table 16: Selected bond lenghts [Å] and angles (°) of Zr,Hf-NSSN-ISO and Zr,Hf-NSSN-Cy.

M = Zr, Hf	*Zr-NSSN-ISO*	*Zr-NSSN-Cy*[a]	*Hf-NSSN-ISO*	*Hf-NSSN-Cy*
M1-S1	2.7382(5)	2.724(1)[2.728(1)]	2.780(1)	2.753(1)
M1-S2	2.8113(5)	2.778(1)[2.758(1)]	2.779(1)	2.754(1)
M1-N4	2.057(1)	2.030(5)[2.025(5)]	2.061(2)	2.041(4)
M1-N3	2.059(1)	2.041(5)[2.047(5)]	2.055(2)	2.045(3)
M1-N2	2.154(1)	2.147(4)[2.173(4)]	2.194(2)	2.177(3)
M1-N1	2.212(1)	2.168(4)[2.179(4)]	2.187(2)	2.180(3)
N3-M1-S1	173.02(4)	172.59(15)[170.7(1)]	168.94(6)	168.97(10)
N4-M1-S2	155.05(4)	156.87(16)[169.93(14)]	167.89(6)	169.53(11)
N3-M1-N2	97.90(5)	97.88(18)[107.00(19)]	94.26(8)	94.11(13)
N4-M1-N3	103.73(5)	103.9(2)[97.7(2)]	99.77(8)	98.99(14)
N3-M1-N1	98.90(5)	98.86(18)[96.64(18)]	110.01(7)	108.15(13)
N3-M1-S2	100.03(4)	98.82(16)[92.37(16)]	92.03(6)	91.18(10)
S-C-C-S	60.57(15)	59.9(5)[62.9(5)]	65.2(2)	65.6(4)

[a]*Zr-NSSN-Cy* complex crystallizes as a racemic mixture in the unit cell.

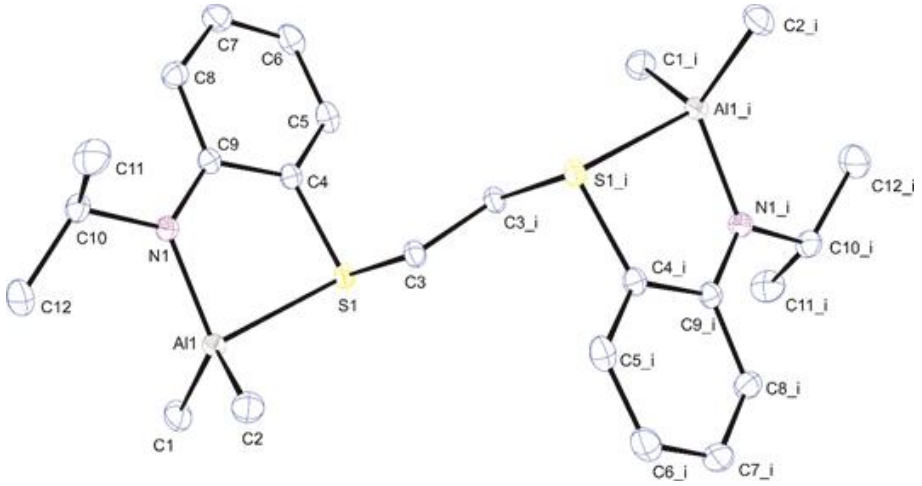

Figure 283: Ortep 3 view of Al_2-NSSN-ISO. Thermal ellipsoids are shown at the 30% probability level.

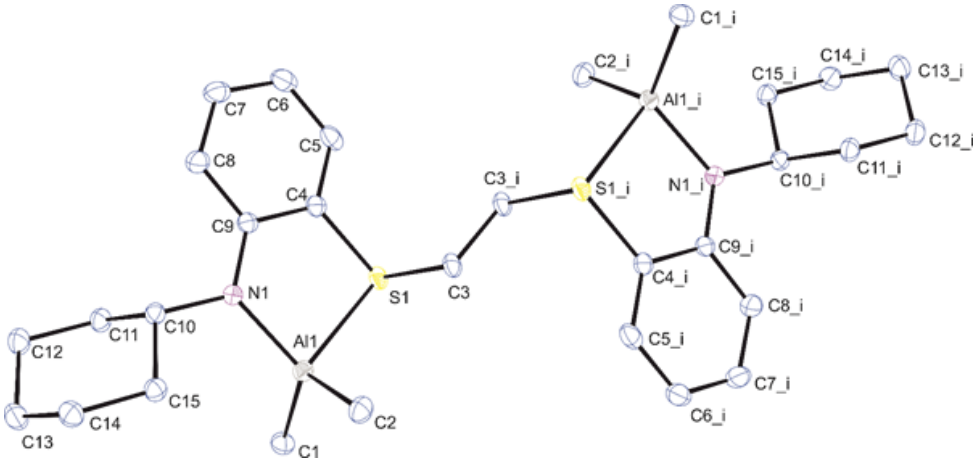

Figure 284: Ortep 3 view of Al_2-NSSN-Cy. Thermal ellipsoids are shown at the 30% probability level.

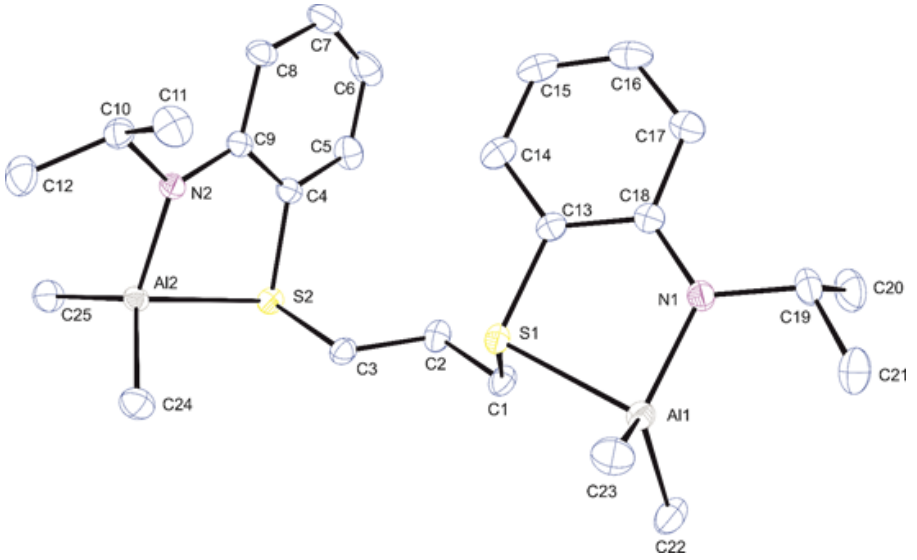

Figure 285: Ortep 3 view of Al_2-NSSN-Pr-ISO. Thermal ellipsoids are shown at the 30% probability level.

Table 17: Crystallographic Data of Al_2-NSSN-ISO, Al_2-NSSN-Cy and Al_2-NSSN-Pr-ISO.

	Al_2-NSSN-ISO	**Al_2-NSSN-Cy**	**Al_2-NSSN-Pr-ISO**
Chemical formula	$C_{24}H_{38}N_2S_2Al_2$	$C_{30}H_{46}N_2S_2Al_2$	$C_{25}H_{40}N_2S_2Al_2$
Crystal size (mm)	0.400 x 0.300 x 0.200	0.400 x 0.200 x 0.200	0.400 x 0.300 x 0.200
Crystal habitus, colour	Prism, brown	Prism, brown	Prism, white
Formula weight	472.64	552.76	486.67
Temperature (K)	173 (2)	173 (2)	173 (2)
λ (Å)	0.71073	0.71073	0.71073
Crystal system	Monoclinic	Triclinic	Monoclinic
Space group	P 21/c	P -1	P 21/c
a (Å)	10.0670(7)	8.643(3)	13.858(1)
b (Å)	11.4490(16)	9.059(2)	15.645(4)
c (Å)	12.776(2)	11.111(4)	14.197(1)
α (Å)	90	90	90
β (Å)	115.188(13)	95.387(18)	114.36(2)
γ (Å)	90	90	90
Volume (Å^3)	1332.5(3)	748.8(4)	2803.9(1)
Z	2	2	2
D_{calcd} $(g \cdot cm^3)$	1.178	1.226	1.153
μ (mm^{-1})	0.279	0.258	0.267
F (000)	508	297	1048
Theta range (°)	3.273 to 27.504	3.246 to 27.496	3.043 to 27.512
Reflections collected	14108	10695	24044
Unique observed reflections	3037 [R(int) = 0.0403]	3423 [R(int) = 0.0404]	6357 [R(int) = 0.0440]
Data/parameters	3037/140	3423/165	6357/288
$R1^{[a]}$, $wR2^{[b]}$[I>2σ(I)]	R1 = 0.0368, wR2 = 0.0920	R1 = 0.0439, wR2 = 0.1237	R1 = 0.0487, wR2 = 0.1369
$R1^{[a]}$, $wR2^{[b]}$(all data)	R1 = 0.0552, wR2 = 0.1047	R1 = 0.0594, wR2 = 0.1406	R1 = 0.0825, wR2 = 0.1681
Largest diff. peak and hole ($e \cdot$ Å^{-3})	0.391 and -0.362	0.370 and -0.363	0.353 and -0.303

[a] $R_1 = \Sigma||Fo|-|Fc|/\Sigma|Fo|$; [b] $wR_2 = [\Sigma w(Fo^2-Fc^2)^2/\Sigma w(Fo^2)^2]^{1/2}$

Table 18: Selected bond lengths [Å] and angles (°) of Al_2-NSSN-ISO.

S(1)-C(4)	1.7713(19)
S(1)-C(3)	1.8301(18)
S(1)-Al(1)	2.4311(8)
Al(1)-N(1)	1.8669(16)
Al(1)-C(2)	1.949(2)
Al(1)-C(1)	1.958(2)
N(1)-C(9)	1.370(2)
N(1)-C(10)	1.472(2)
C(1)-H(1A)	0.9800

C(1)-H(1B)	0.9800
C(1)-H(1C)	0.9800
C(2)-H(2A)	0.9800
C(2)-H(2B)	0.9800
C(2)-H(2C)	0.9800
C(10)-C(11)	1.509(3)
C(10)-C(12)	1.520(3)
C(10)-H(10)	1.0000
C(12)-H(12A)	0.9800
C(12)-H(12B)	0.9800
C(12)-H(12C)	0.9800
C(11)-H(11A)	0.9800
C(11)-H(11B)	0.9800
C(11)-H(11C)	0.9800
C(9)-C(8)	1.415(3)
C(9)-C(4)	1.418(3)
C(8)-C(7)	1.381(3)
C(8)-H(8)	0.9500
C(7)-C(6)	1.382(3)
C(7)-H(7)	0.9500
C(6)-C(5)	1.378(3)
C(6)-H(6)	0.9500
C(5)-C(4)	1.395(3)
C(5)-H(5)	0.9500
C(3)-C(3)#1	1.510(3)
C(3)-H(3A)	0.9900
C(3)-H(3B)	0.900
C(4)-S(1)-C(3)	101.39(8)
C(4)-S(1)-Al(1)	92.27(6)
C(3)-S(1)-Al(1)	100.60(6)
N(1)-Al(1)-C(2)	118.27(9)
N(1)-Al(1)-C(1)	115.80(9)
C(2)-Al(1)-C(1)	119.21(10)
N(1)-Al(1)-S(1)	86.35(5)
C(2)-Al(1)-S(1)	101.21(7)
C(1)-Al(1)-S(1)	107.90(7)
C(9)-N(1)-C(10)	118.02(15)
C(9)-N(1)-Al(1)	120.85(12)
C(10)-N(1)-Al(1)	121.09(12)
Al(1)-C(1)-H(1A)	109.5
Al(1)-C(1)-H(1B)	109.5
H(1A)-C(1)-H(1B)	109.5
Al(1)-C(1)-H(1C)	109.5
H(1A)-C(1)-H(1C)	109.5
H(1B)-C(1)-H(1C)	109.5
Al(1)-C(2)-H(2A)	109.5

Al(1)-C(2)-H(2B)	109.5
H(2A)-C(2)-H(2B)	109.5
Al(1)-C(2)-H(2C)	109.5
H(2A)-C(2)-H(2C)	109.5
H(2B)-C(2)-H(2C)	109.5
N(1)-C(10)-C(11)	110.36(16)
N(1)-C(10)-C(12)	110.18(16)
C(11)-C(10)-C(12)	111.06(18)
N(1)-C(10)-H(10)	108.4
C(11)-C(10)-H(10)	108.4
C(12)-C(10)-H(10)	108.4
C(10)-C(12)-H(12A)	109.5
C(10)-C(12)-H(12B)	109.5
H(12A)-C(12)-H(12B)	109.5
C(10)-C(12)-H(12C)	109.5
H(12A)-C(12)-H(12C)	109.5
H(12B)-C(12)-H(12C)	109.5
C(10)-C(11)-H(11A)	109.5
C(10)-C(11)-H(11B)	109.5
H(11A)-C(11)-H(11B)	109.5
C(10)-C(11)-H(11C)	109.5
H(11A)-C(11)-H(11C)	109.5
H(11B)-C(11)-H(11C)	109.5
N(1)-C(9)-C(8)	124.73(16)
N(1)-C(9)-C(4)	120.03(16)
C(8)-C(9)-C(4)	115.23(16)
C(7)-C(8)-C(9)	121.52(19)
C(7)-C(8)-H(8)	119.2
C(9)-C(8)-H(8)	119.2
C(8)-C(7)-C(6)	121.73(19)
C(8)-C(7)-H(7)	119.1
C(6)-C(7)-H(7)	119.1
C(5)-C(6)-C(7)	118.69(18)
C(5)-C(6)-H(6)	120.7
C(7)-C(6)-H(6)	120.7
C(6)-C(5)-C(4)	120.30(19)
C(6)-C(5)-H(5)	119.9
C(4)-C(5)-H(5)	119.9
C(5)-C(4)-C(9)	122.26(17)
C(5)-C(4)-S(1)	119.57(15)
C(9)-C(4)-S(1)	118.16(13)
C(3)#1-C(3)-S(1)	110.79(17)
C(3)#1-C(3)-H(3A)	109.5
S(1)-C(3)-H(3A)	109.5
C(3)#1-C(3)-H(3B)	109.5
S(1)-C(3)-H(3B)	109.5

H(3A)-C(3)-H(3B)	108.1

Symmetry transformations used to generate equivalent atoms: #1 -x+1,-y+1,-z+1.

Table 19: Selected bond lengths [Å] and angles (°) of Al_2-NSSN-Cy.

S(1)-C(4)	1.776(2)
S(1)-C(3)	1.825(2)
S(1)-Al(1)	2.4292(11)
Al(1)-N(1)	1.8639(19)
Al(1)-C(1)	1.951(2)
Al(1)-C(2)	1.967(2)
N(1)-C(9)	1.371(3)
N(1)-C(10)	1.465(3)
C(9)-C(8)	1.411(3)
C(9)-C(4)	1.421(3)
C(4)-C(5)	1.380(3)
C(3)-C(3)#1	1.504(4)
C(3)-H(3A)	0.9900
C(3)-H(3B)	0.9900
C(5)-C(6)	1.382(4)
C(5)-H(5)	0.9500
C(10)-C(15)	1.520(3)
C(10)-C(11)	1.531(3)
C(10)-H(10)	1.0000
C(15)-C(14)	1.523(3)
C(15)-H(15A)	0.9900
C(15)-H(15B)	0.9900
C(8)-C(7)	1.377(3)
C(8)-H(8)	0.9500
C(11)-C(12)	1.526(3)
C(11)-H(11A)	0.9900
C(11)-H(11B)	0.9900
C(13)-C(12)	1.516(3)
C(13)-C(14)	1.525(3)
C(13)-H(13A)	0.9900
C(13)-H(13B)	0.9900
C(1)-H(1A)	0.9800
C(1)-H(1B)	0.9800
C(1)-H(1C)	0.9800
C(12)-H(12A)	0.9900
C(12)-H(12B)	0.9900
C(6)-C(7)	1.385(4)
C(6)-H(6)	0.9500
C(2)-H(2A)	0.9800
C(2)-H(2B)	0.9800
C(2)-H(2C)	0.9800

C(14)-H(14A)	0.9900
C(14)-H(14B)	0.9900
C(7)-H(7)	0.9500
C(4)-S(1)-C(3)	103.83(10)
C(4)-S(1)-Al(1)	93.46(8)
C(3)-S(1)-Al(1)	99.37(8)
N(1)-Al(1)-C(1)	118.41(10)
N(1)-Al(1)-C(2)	117.44(10)
C(1)-Al(1)-C(2)	115.18(11)
N(1)-Al(1)-S(1)	86.29(6)
C(1)-Al(1)-S(1)	106.79(8)
C(2)-Al(1)-S(1)	106.99(8)
C(9)-N(1)-C(10)	118.38(17)
C(9)-N(1)-Al(1)	122.12(14)
C(10)-N(1)-Al(1)	119.34(14)
N(1)-C(9)-C(8)	124.7(2)
N(1)-C(9)-C(4)	120.07(19)
C(8)-C(9)-C(4)	115.20(19)
C(5)-C(4)-C(9)	122.4(2)
C(5)-C(4)-S(1)	119.57(18)
C(9)-C(4)-S(1)	117.90(16)
C(3)#1-C(3)-S(1)	110.7(2)
C(3)#1-C(3)-H(3A)	109.5
S(1)-C(3)-H(3A)	109.5
C(3)#1-C(3)-H(3B)	109.5
S(1)-C(3)-H(3B)	109.5
H(3A)-C(3)-H(3B)	108.1
C(4)-C(5)-C(6)	120.6(2)
C(4)-C(5)-H(5)	119.7
C(6)-C(5)-H(5)	119.7
N(1)-C(10)-C(15)	109.80(17)
N(1)-C(10)-C(11)	112.27(17)
C(15)-C(10)-C(11)	109.95(17)
N(1)-C(10)-H(10)	108.2
C(15)-C(10)-H(10)	108.2
C(11)-C(10)-H(10)	108.2
C(10)-C(15)-C(14)	111.76(18)
C(10)-C(15)-H(15A)	109.3
C(14)-C(15)-H(15A)	109.3
C(10)-C(15)-H(15B)	109.3
C(14)-C(15)-H(15B)	109.3
H(15A)-C(15)-H(15B)	107.9
C(7)-C(8)-C(9)	121.7(2)
C(7)-C(8)-H(8)	119.1
C(9)-C(8)-H(8)	119.1
C(12)-C(11)-C(10)	111.04(19)

C(12)-C(11)-H(11A)	109.4
C(10)-C(11)-H(11A)	109.4
C(12)-C(11)-H(11B)	109.4
C(10)-C(11)-H(11B)	109.4
H(11A)-C(11)-H(11B)	108.0
C(12)-C(13)-C(14)	111.2(2)
C(12)-C(13)-H(13A)	109.4
C(14)-C(13)-H(13A)	109.4
C(12)-C(13)-H(13B)	109.4
C(14)-C(13)-H(13B)	109.4
H(13A)-C(13)-H(13B)	108.0
Al(1)-C(1)-H(1A)	109.5
Al(1)-C(1)-H(1B)	109.5
H(1A)-C(1)-H(1B)	109.5
Al(1)-C(1)-H(1C)	109.5
H(1A)-C(1)-H(1C)	109.5
H(1B)-C(1)-H(1C)	109.5
C(13)-C(12)-C(11)	111.49(19)
C(13)-C(12)-H(12A)	109.3
C(11)-C(12)-H(12A)	109.3
C(13)-C(12)-H(12B)	109.3
C(11)-C(12)-H(12B)	109.3
H(12A)-C(12)-H(12B)	108.0
C(5)-C(6)-C(7)	118.3(2)
C(5)-C(6)-H(6)	120.8
C(7)-C(6)-H(6)	120.8
Al(1)-C(2)-H(2A)	109.5
Al(1)-C(2)-H(2B)	109.5
H(2A)-C(2)-H(2B)	109.5
Al(1)-C(2)-H(2C)	109.5
H(2A)-C(2)-H(2C)	109.5
H(2B)-C(2)-H(2C)	109.5
C(15)-C(14)-C(13)	111.25(19)
C(15)-C(14)-H(14A)	109.4
C(13)-C(14)-H(14A)	109.4
C(15)-C(14)-H(14B)	109.4
C(13)-C(14)-H(14B)	109.4
H(14A)-C(14)-H(14B)	108.0
C(8)-C(7)-C(6)	121.7(2)
C(8)-C(7)-H(7)	119.2
C(6)-C(7)-H(7)	119.2

Symmetry transformations used to generate equivalent atoms: #1 -x,-y,-z.

Table 20: Selected bond lengths [Å] and angles (°) of Al_2-NSSN-Pr-ISO.

S(1)-C(13)	1.774(3)	1.774(3)
S(1)-C(1)	1.832(3)	1.832(3)
S(1)-Al(1)	2.4184(10)	2.4184(10)
S(2)-C(4)	1.770(3)	1.770(3)
S(2)-C(3)	1.824(3)	1.824(3)
S(2)-Al(2)	2.4165(10)	2.4165(10)
Al(1)-N(1)	1.866(2)	1.866(2)
Al(1)-C(23)	1.943(3)	1.943(3)
Al(1)-C(22)	1.953(3)	1.953(3)
Al(2)-N(2)	1.869(2)	1.869(2)
Al(2)-C(25)	1.944(3)	1.944(3)
Al(2)-C(24)	1.966(3)	1.966(3)
N(2)-C(9)	1.365(3)	1.365(3)
N(2)-C(10)	1.469(3)	1.469(3)
N(1)-C(18)	1.369(4)	1.369(4)
N(1)-C(19)	1.468(3)	1.468(3)
C(9)-C(8)	1.414(4)	1.414(4)
C(9)-C(4)	1.414(4)	1.414(4)
C(18)-C(17)	1.415(4)	1.415(4)
C(18)-C(13)	1.416(4)	1.416(4)
C(4)-C(5)	1.386(4)	1.386(4)
C(13)-C(14)	1.387(4)	1.387(4)
C(1)-C(2)	1.513(4)	1.513(4)
C(1)-H(1A)	0.9900	0.9900
C(1)-H(1B)	0.9900	0.9900
C(3)-C(2)	1.514(4)	1.514(4)
C(3)-H(3A)	0.9900	0.9900
C(3)-H(3B)	0.9900	0.9900
C(8)-C(7)	1.378(5)	1.378(5)
C(8)-H(8)	0.9500	0.9500
C(14)-C(15)	1.376(5)	1.376(5)
C(14)-H(14)	0.9500	0.9500
C(24)-H(24A)	0.9800	0.9800
C(24)-H(24B)	0.9800	0.9800
C(24)-H(24C)	0.9800	0.9800
C(10)-C(12)	1.511(4)	1.511(4)
C(10)-C(11)	1.515(4)	1.515(4)
C(10)-H(10)	1.0000	1.0000
C(17)-C(16)	1.381(5)	1.381(5)
C(17)-H(17)	0.9500	0.9500
C(2)-H(2A)	0.9900	0.9900
C(2)-H(2B)	0.9900	0.9900
C(19)-C(21)	1.514(5)	1.514(5)
C(19)-C(20)	1.520(4)	1.520(4)
C(19)-H(19)	1.0000	1.0000

C(25)-H(25A)	0.9800	0.9800
C(25)-H(25B)	0.9800	0.9800
C(25)-H(25C)	0.9800	0.9800
C(23)-H(23A)	0.9800	0.9800
C(23)-H(23B)	0.9800	0.9800
C(23)-H(23C)	0.9800	0.9800
C(22)-H(22A)	0.9800	0.9800
C(22)-H(22B)	0.9800	0.9800
C(22)-H(22C)	0.9800	0.9800
C(12)-H(12A)	0.9800	0.9800
C(12)-H(12B)	0.9800	0.9800
C(12)-H(12C)	0.9800	0.9800
C(15)-C(16)	1.369(5)	1.369(5)
C(15)-H(15)	0.9500	0.9500
C(6)-C(7)	1.371(5)	1.371(5)
C(6)-C(5)	1.378(5)	1.378(5)
C(6)-H(6)	0.9500	0.9500
C(16)-H(16)	0.9500	0.9500
C(7)-H(7)	0.9500	0.9500
C(5)-H(5)	0.9500	0.9500
C(11)-H(11A)	0.9800	0.9800
C(11)-H(11B)	0.9800	0.9800
C(11)-H(11C)	0.9800	0.9800
C(21)-H(21A)	0.9800	0.9800
C(21)-H(21B)	0.9800	0.9800
C(21)-H(21C)	0.9800	0.9800
C(20)-H(20A)	0.9800	0.9800
C(20)-H(20B)	0.9800	0.9800
C(20)-H(20C)	0.9800	0.9800
C(13)-S(1)-C(1)	103.12(13)	103.12(13)
C(13)-S(1)-Al(1)	93.28(9)	93.28(9)
C(1)-S(1)-Al(1)	101.24(9)	101.24(9)
C(4)-S(2)-C(3)	101.49(12)	101.49(12)
C(4)-S(2)-Al(2)	92.15(9)	92.15(9)
C(3)-S(2)-Al(2)	98.45(10)	98.45(10)
N(1)-Al(1)-C(23)	116.43(13)	116.43(13)
N(1)-Al(1)-C(22)	116.81(14)	116.81(14)
C(23)-Al(1)-C(22)	118.18(15)	118.18(15)
N(1)-Al(1)-S(1)	86.56(8)	86.56(8)
C(23)-Al(1)-S(1)	105.79(11)	105.79(11)
C(22)-Al(1)-S(1)	106.44(10)	106.44(10)
N(2)-Al(2)-C(25)	115.48(13)	115.48(13)
N(2)-Al(2)-C(24)	117.21(12)	117.21(12)
C(25)-Al(2)-C(24)	118.75(14)	118.75(14)
N(2)-Al(2)-S(2)	86.42(7)	86.42(7)
C(25)-Al(2)-S(2)	104.99(11)	104.99(11)

C(24)-Al(2)-S(2)	107.21(10)	107.21(10)
C(9)-N(2)-C(10)	118.0(2)	118.0(2)
C(9)-N(2)-Al(2)	120.09(17)	120.09(17)
C(10)-N(2)-Al(2)	121.30(18)	121.30(18)
C(18)-N(1)-C(19)	118.6(2)	118.6(2)
C(18)-N(1)-Al(1)	121.55(18)	121.55(18)
C(19)-N(1)-Al(1)	119.83(19)	119.83(19)
N(2)-C(9)-C(8)	125.2(3)	125.2(3)
N(2)-C(9)-C(4)	120.0(2)	120.0(2)
C(8)-C(9)-C(4)	114.8(3)	114.8(3)
N(1)-C(18)-C(17)	124.9(3)	124.9(3)
N(1)-C(18)-C(13)	120.2(2)	120.2(2)
C(17)-C(18)-C(13)	114.9(3)	114.9(3)
C(5)-C(4)-C(9)	122.7(3)	122.7(3)
C(5)-C(4)-S(2)	119.0(2)	119.0(2)
C(9)-C(4)-S(2)	118.3(2)	118.3(2)
C(14)-C(13)-C(18)	122.9(3)	122.9(3)
C(14)-C(13)-S(1)	119.0(2)	119.0(2)
C(18)-C(13)-S(1)	118.1(2)	118.1(2)
C(2)-C(1)-S(1)	113.23(18)	113.23(18)
C(2)-C(1)-H(1A)	108.9	108.9
S(1)-C(1)-H(1A)	108.9	108.9
C(2)-C(1)-H(1B)	108.9	108.9
S(1)-C(1)-H(1B)	108.9	108.9
H(1A)-C(1)-H(1B)	107.7	107.7
C(2)-C(3)-S(2)	112.9(2)	112.9(2)
C(2)-C(3)-H(3A)	109.0	109.0
S(2)-C(3)-H(3A)	109.0	109.0
C(2)-C(3)-H(3B)	109.0	109.0
S(2)-C(3)-H(3B)	109.0	109.0
H(3A)-C(3)-H(3B)	107.8	107.8
C(7)-C(8)-C(9)	121.8(3)	121.8(3)
C(7)-C(8)-H(8)	119.1	119.1
C(9)-C(8)-H(8)	119.1	119.1
C(15)-C(14)-C(13)	120.1(3)	120.1(3)
C(15)-C(14)-H(14)	119.9	119.9

Symmetry transformations used to generate equivalent atoms: #1 -x,-y,-z.

10 General Information

10.1 Materials and methods

Laboratory glassware such as vials, NMR tubes and flasks for reactions were dried overnight at 120 °C in the oven. All preparations and subsequent manipulation of air- and/or water-sensitive compounds were carried out under a dry nitrogen or argon atmosphere using a Braun single station drybox or standard Sclenk techniques. All solvents (hexane, pentane and toluene), purchased by Sigma Aldrich, were appropriately dried over $CaCl_2$ and after purified by distillation from sodium under a nitrogen atmosphere. The ligands used for the synthesis of complexes were anhydrificated in vacuum with P_2O_5 before use. *L*- and *rac*-lactide were purified by crystallization from dry toluene and stored in vacuum under P_2O_5. Liquid monomers (ε-caprolactone and β-butyrolactone) were dried with CaH_2 and distilled under reduce pressure. Isopropyl alcohol were distilled over magnesium turnings. Deuterated solvents (C_6D_6, $CDCl_3$, CD_2Cl_2, TCDE and toluene-d_8) were purchased from Cambridge Isotope Laboratories, Inc., degassed and dried with 4 Å molecular sieves prior to use. All other chemicals were commercially available and used as received unless otherwise stated.

10.2 Instruments and Measurements

The NMR spectra were recorded on Bruker Advance 400 and 600 MHz spectrometer at 25 °C. Chemical shift (**d**) are listed as parts per million and coupling constants (**J**) in hertz. ^{1}H NMR spectra are referenced using the residual solvent peak at **d** 7.16 for C_6D_6, **d** 7.26 for $CDCl_3$, **d** 5.32 for CD_2Cl_2, **d** 6.00 for TCDE and **d** 2.08, 6.97, 7.01, 7.09 for toluene-d_8. ^{13}C NMR spectra are referenced using the residual solvent peak at **d** 128.06 for C_6D_6, **d** 77.16 for $CDCl_3$, **d** 53.84 for CD_2Cl_2, **d** 73.78 for TCDE and **d** 20.43, 125.13, 127.96, 128.87, 137.48 for toluene-d_8. Variable-temperature ^{1}H NMR experiments were performed in J. Young NMR tube using TCDE, toluene-d_8 and CH_2Cl_2 as solvents at Bruker Avance 400 or 600 spectrometer.

The M_n and M_w of polyesters were estimated by gel permeation chromatography (GPC) at 30 °C, using THF as solvent, flow rate of eluent 1 mL/min, and polystyrene standards as reference. M_n was corrected using the factor of 0.58 for *PLA*, 0.56 for

PCL and 0.54 for *PHB*, according to the literature.[92] The measurement were performed on a Waters 1525 binary system equipped with a Waters 2414 RI detector using four Styragel columns (range 1000-1000000 Å). Every value was the average of two independent measurements.

The polyesters samples were analysed also by thermal analysis (DSC) using TA Instruments DSC Q2000 under a N_2 flow with a heating and cooling rate of 10 °C/min in the range -40 to 200 °C.

The mass spectra were registered by Bruker solariX XR Fourier transform ion cyclotron resonance mass spectrometer, using 2,5-dihydroxybenzoic acid (DHB) as matrix for MALDI. The laser power was 15% and the acquisition was in positive mode. In a general procedure of MALDI-TOF MS sample preparation a 1 mg of substance or polymer was dissolved in 1.0 mL of CH_2Cl_2. 4 µL of this solution was mixed to 45 µL of solution of DHB 40 mM in CH_2Cl_2. The final solution was deposed on the MALDI target for the acquisition.

Data collection of single crystals was performed in flowing N_2 at 173 °K on a Bruker-Nonius kappaCCD diffractometer equipped with an Oxford Cryostream apparatus (MoKα radiation, CCD rotation images, thick slices, φ scans + ω scans to fill the asymmetric unit). Semiempirical absorbtion corrections (multi-scan SADABS)[93] were applied. The structure was solved by direct methods (SIR 97 package)[94] and refined by the full matrix least-squares method (SHELXL program of SHELXL-2018/3)[95] on F^2 against all independent measured reflections, using anisotropic thermal parameters for all non-hydrogen atoms. H atoms were placed in calculated positions with Ueq equal to those of the carrier atom and refined by the riding method. Only the N-H atoms of the ligands molecules (*Pr*, ethyl and xylenyl) were found in difference Fourier

[92] T. Biela, A. Duda, S. Penczek, *Macromol. Symp.*, ***2002***, *183, 1-10.*

[93] G. M. Sheldrick, SADABS, Program for empirical absorption correction, University of Göttingen, Germany, ***1996***.

[94] A. Altomare, M. C. Burla, M. Camalli, G. L. Cascarano, C. Giacovazzo, A. Guagliardi, A. G. G. Moliterni, G. Polidori, R. Spagna, *J. Appl. Cryst.*, ***1999***, *32, 115-119.*

[95] G. M. Sheldrick, Crystal structure refinement with *SHELXL.Acta Crystallogr. Sect. C Struct. Chem.*, ***2015***, *71, 3–8.*

maps and their coordinates were refined without restraints. The figures were generated using the ORTEP-3 program.[96]

DFT calculations were performed with the program suite Gaussian 09.[97] All geometries were optimized without constraints at the BP86 lelevel, i.e., employing the exchange and correlation functionals of Becke and Perdew, respectively.[98] For *Zr* complexes the basis set employed was LANL2DZ with associated effective-core potentials for *Zr* atom and 6-31G(d) for all other atoms.[99] Stationary point geometries were characterized as local minima on the potential energy surfaces. The absence of an imaginary frequency verified that structures were true minima at their respective levels of theory. The structures of the transition states were located by applying Schlegel's synchronous-transit-guided quasi-Newton (QST2) method, as implemented in Gaussian 09. The transition states were verified with frequency calculations to ensure that they were first-order saddle points with only one negative eigenvalue.

---

[96] L. J. Farrugia, WinGXandORTEP for Windows: *An update. J. Appl. Crystallogr.*, ***2012***, *45*, *849–854*.

[97] M. J. Frisch, G. W. Trucks, H. B. Schlegel, G. E. Scuseria, M. A. Robb, J. R. Cheeseman, G. Scalmani, V. Barone, B. Mennucci, G. A. Petersson, H. Nakatsuji, M. Caricato, X. Li, H. P. Hratchian, A. F. Izmaylov, J. Bloino, G. Zheng, J. L. Sonnenberg, M. Hada, M. Ehara, K. Toyota, R. Fukuda, J. Hasegawa, M. Ishida, T. Nakajima, Y. Honda, O. Kitao, H. Nakai, T. Vreven, Junio J.. A. Montgomery, J. E. Peralta, F. Ogliaro, M. Bearpark, J. J. Heyd, E. Brothers, K. N. Kudin, V. N. Staroverov, R. Kobayashi, J. Normand, K. Raghavachari, A. Rendell, J. C. Burant, S. S. Iyengar, J. Tomasi, M. Cossi, N. Rega, J. M. Millam, M. Klene, J. E. Knox, J. B. Cross, V. Bakken, C. Adamo, J. Jaramillo, R. Gomperts, R. E. Stratmann, O. Yazyev, A. J. Austin, R. Cammi, C. Pomelli, J. W. Ochterski, R. L. Martin, K. Morokuma, V. G. Zakrzewski, G. A. Voth, P. Salvador, J. J. Dannenberg, S. Dapprich, A. D. Daniels, O. Farkas, J. B. Foresman, J. V. Ortiz, J. Cioslowski, *Fox, D. J. Gaussian 09, revision A.02; Gaussian, Inc.: Wallingford, CT,* ***2009***.

[98] A. D. Becke, *Phys. Rev. A: At., Mol., Opt. Phys.*, ***1998***, *38*, *3098-3100;* J. P. Perdew, *Phys. Rev. B: Condens. Matter Mater. Phys.*, ***1986***, *33*, *8822-8824;* J. P. Perdew, *Phys. Rev. B: Condens. Matter Mater. Phys.*, ***1986***, *34*, *7406-7406.*

[99] P. J. Hay, W. R. Wadt, *J. Chem. Phys.*, ***1985***, *82*, *270-283.*

10.3 Typical procedure for cyclic ester polymerization

In a typical polymerization, prepared in a Braun Labmaster glovebox, a Schlenk flask (10 cm^3) was charged sequentially with monomer (ε-caprolactone, β-butyrolactone, *L*- or *rac*-lactide), catalyst, and possible cocatalyst, and solvent. The mixture was thermostated at the required temperature and, at specified time intervals, a small amount of the reaction mixture was sampled by a pipet and quenched in wet $CDCl_3$ to evaluate the yields by ^1H NMR spectroscopy. The conversion was determinate by integration of the monomer versus polymer methine resonances. The polymerization was stopped quenching with n-hexane. The obtained polymer was recovered by filtration, dried in vacuum at 40 °C for 24 h and characterized by using NMR spectroscopy and SEC.

Investigation about the non-zero intercepts in the kinetic plot of *LA*: in a Braun Labmaster glovebox was prepared two Schlenk flask of 10 cm^3. The first flask was charged with lactide (0.404 g, 2.80 mol) and dry toluene (1.0 mL). The second flask was instead charged with catalyst (28.0 μmol) and dry toluene (1.0 mL). Both mixtures were thermostated at 80 °C and the catalyst solution was added to the other as soon as the lactide dissolved in the solvent. The conversion at specified time intervals was evaluated by ^1H NMR spectroscopy as previously explained. The polymerization was stopped quenching with n-hexane e the final polymer was treated and characterized as previously mentioned.

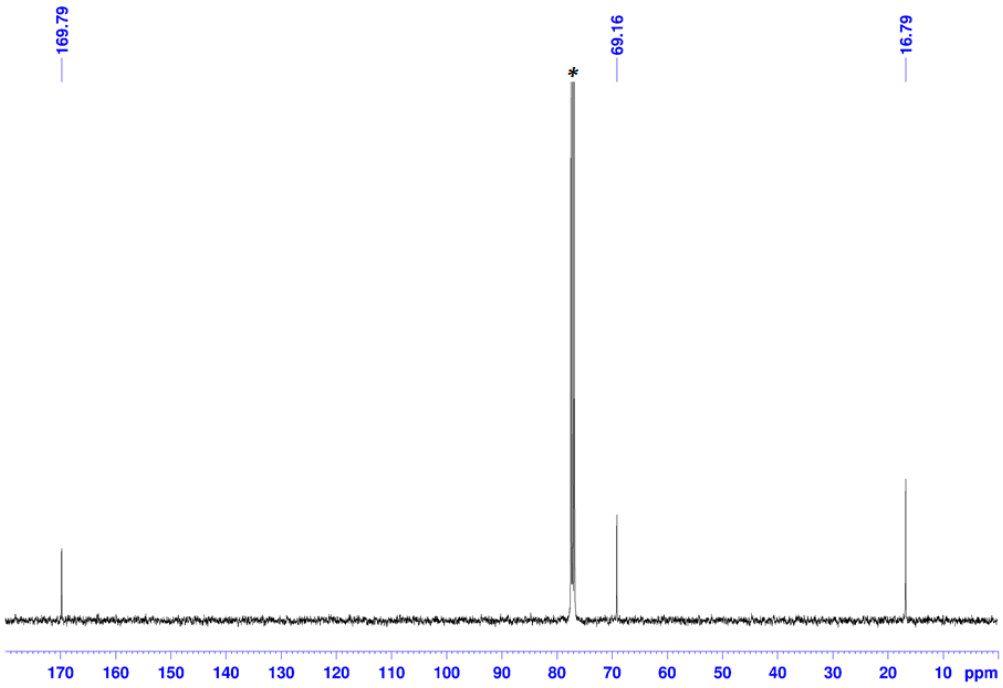

*Figure 286: ^{13}C NMR of PLA (entry 1, table 2 – 400.13 MHz, *$CDCl_3$, 25°C).*

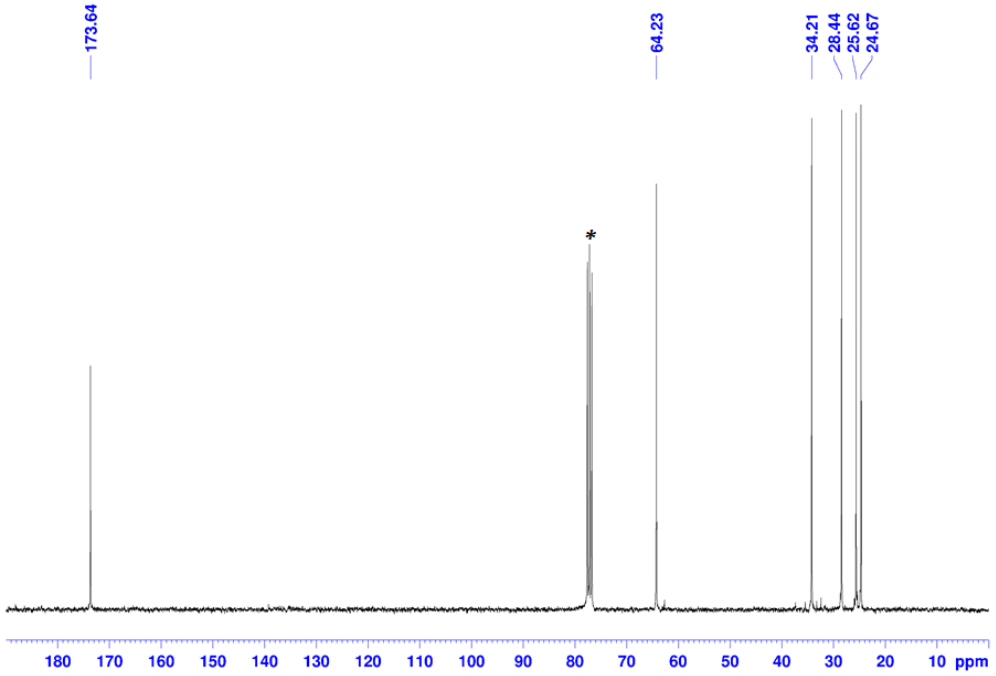

*Figure 287: ^{13}C NMR of PCL obtained by Zr-NSSN-ISO (100.62 MHz, *$CDCl_3$, 25°C).*

Conditions: $[\varepsilon\text{-CL}]_0$ = 1.4 M, [ε-CL]/[catalyst], T = 80 °C, and toluene as the solvent.

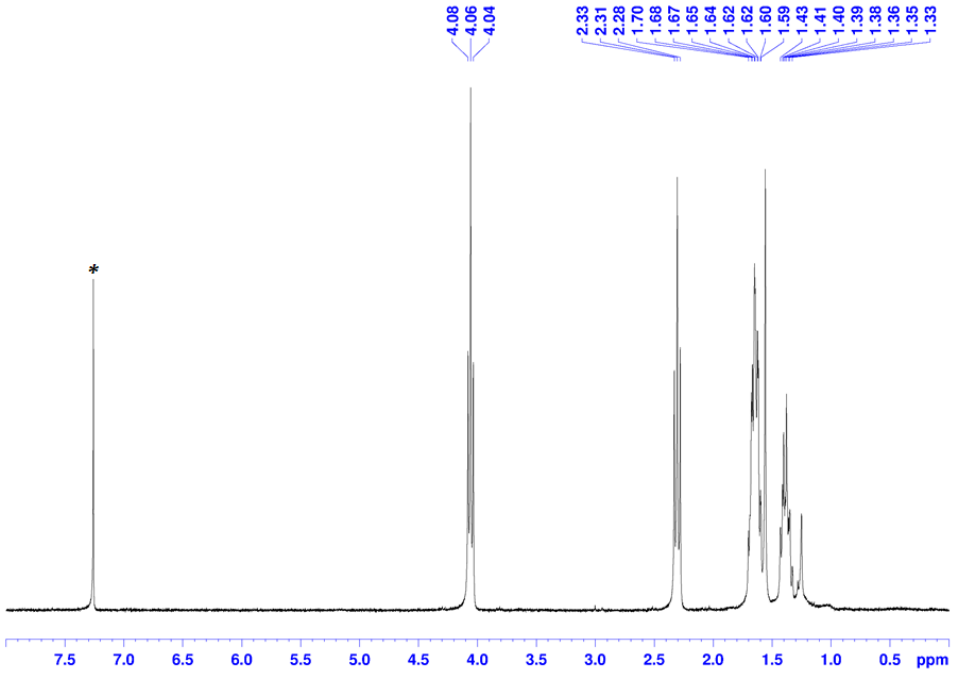

*Figure 288: ^{1}H NMR of PCL (entry 10, table 4 – 400.13 MHz, *$CDCl_3$, 25°C).*

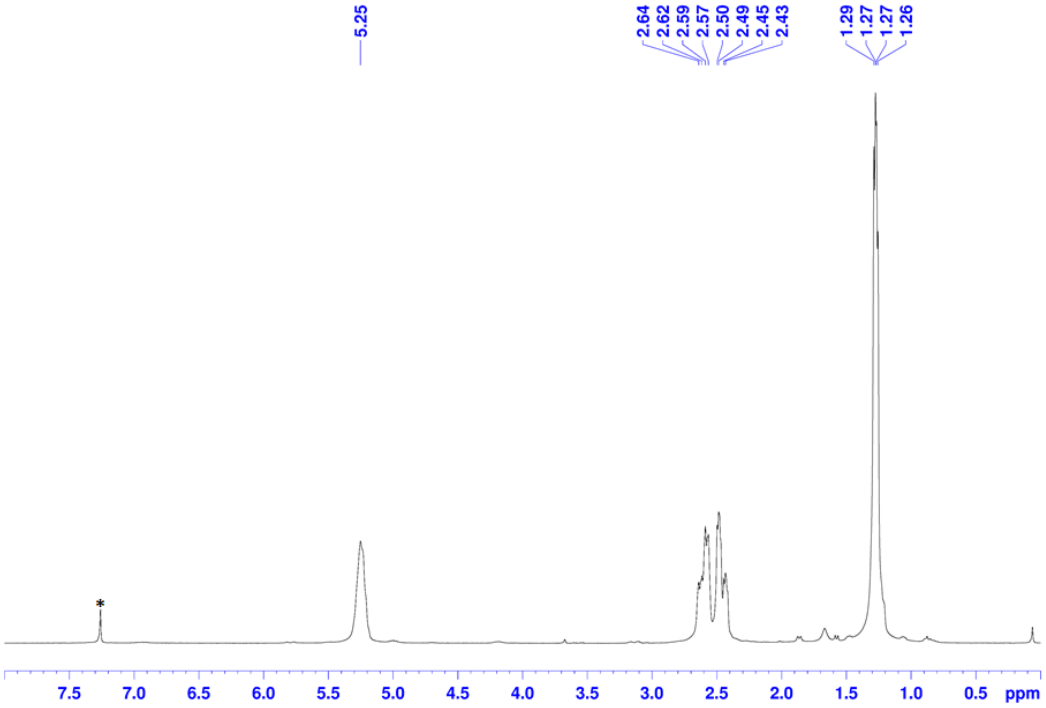

*Figure 289: ^{1}H NMR of PBL (entry 8, table 7 - 400.13 MHz, *$CDCl_3$, 25°C).*

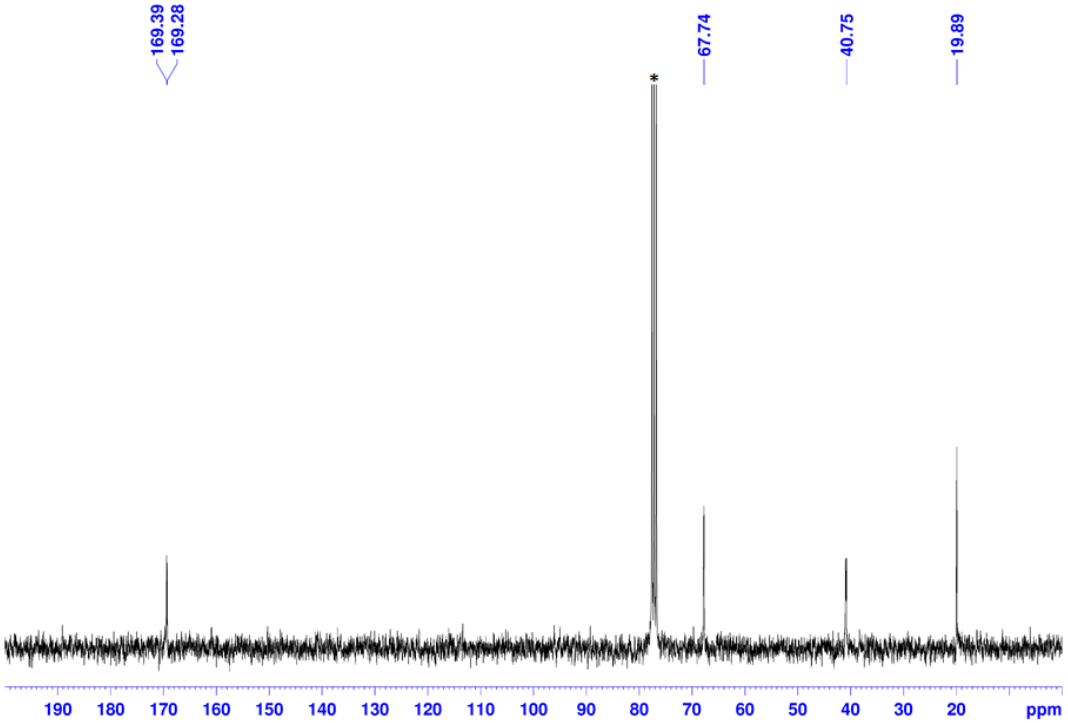

*Figure 290: ^{13}C NMR of PBL (entry 8, table 7 - 100.62 MHz, *$CDCl_3$, 25°C).*

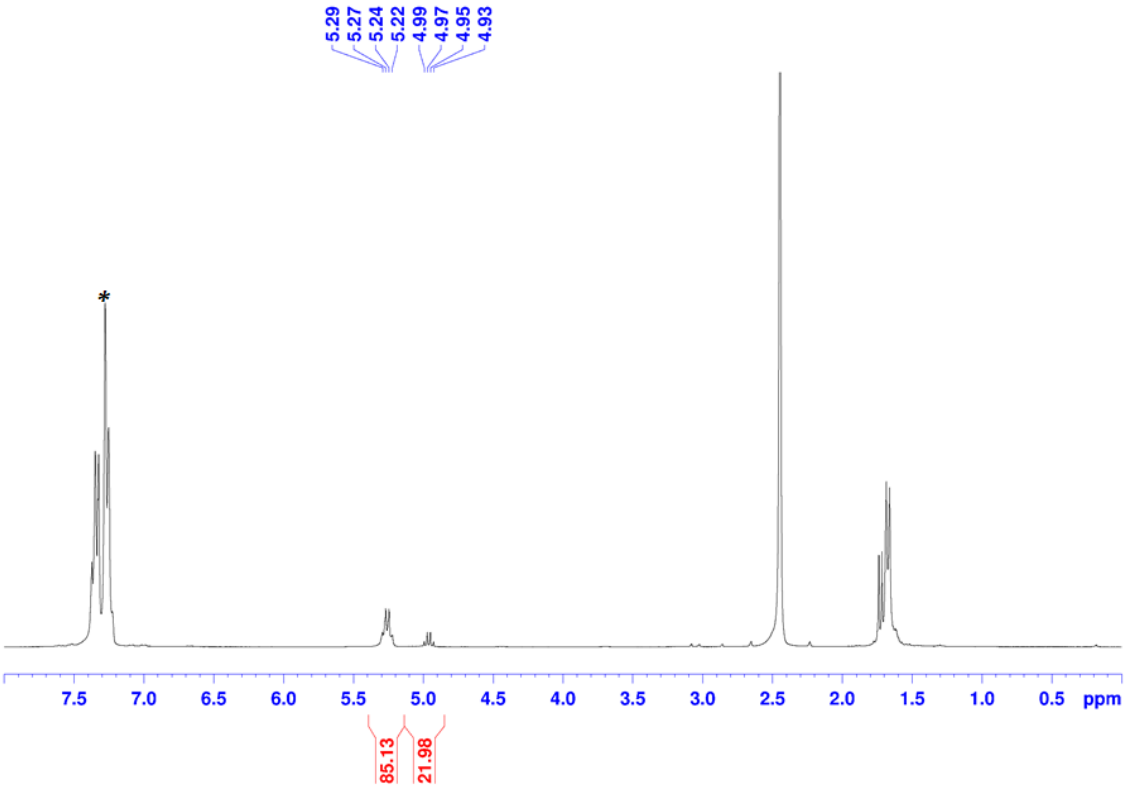

*Figure 291: ^{1}H NMR spectrum of an aliquot from a PLA formation reaction, used for monomer conversion determination (400.13 MHz, *$CDCl_3$, 25°C).*

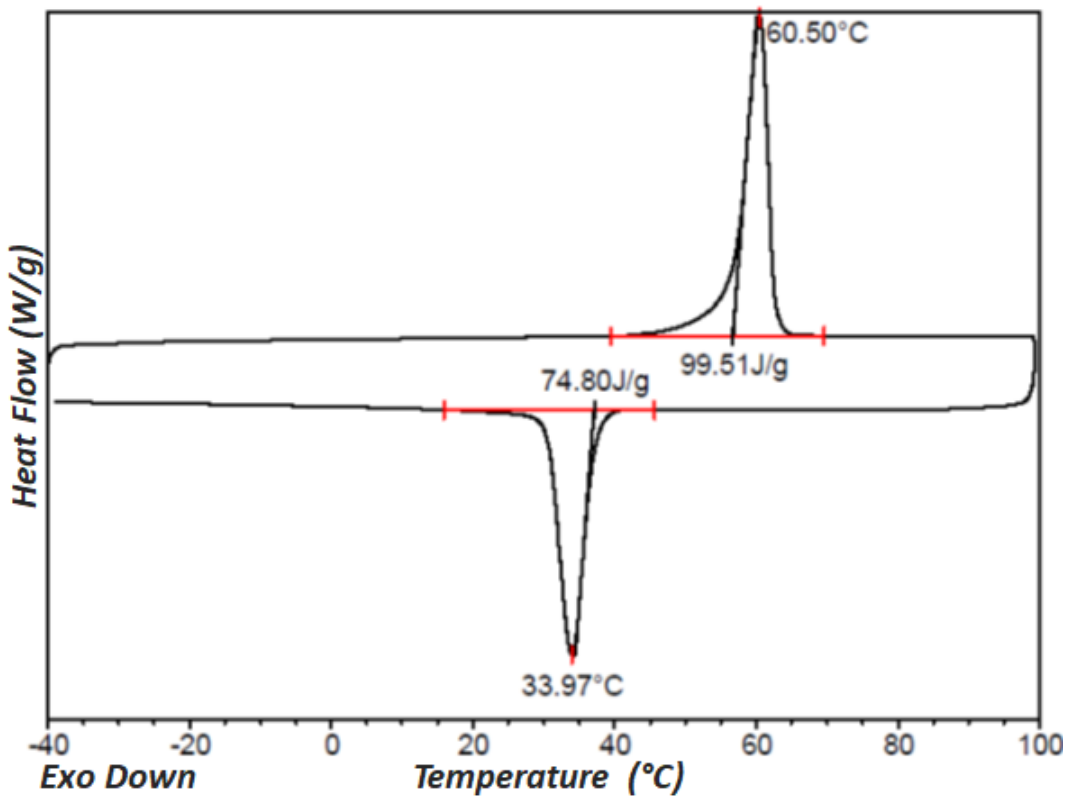

Figure 292: DSC thermogram of PCL sample obtained as in entry 10, table 4.

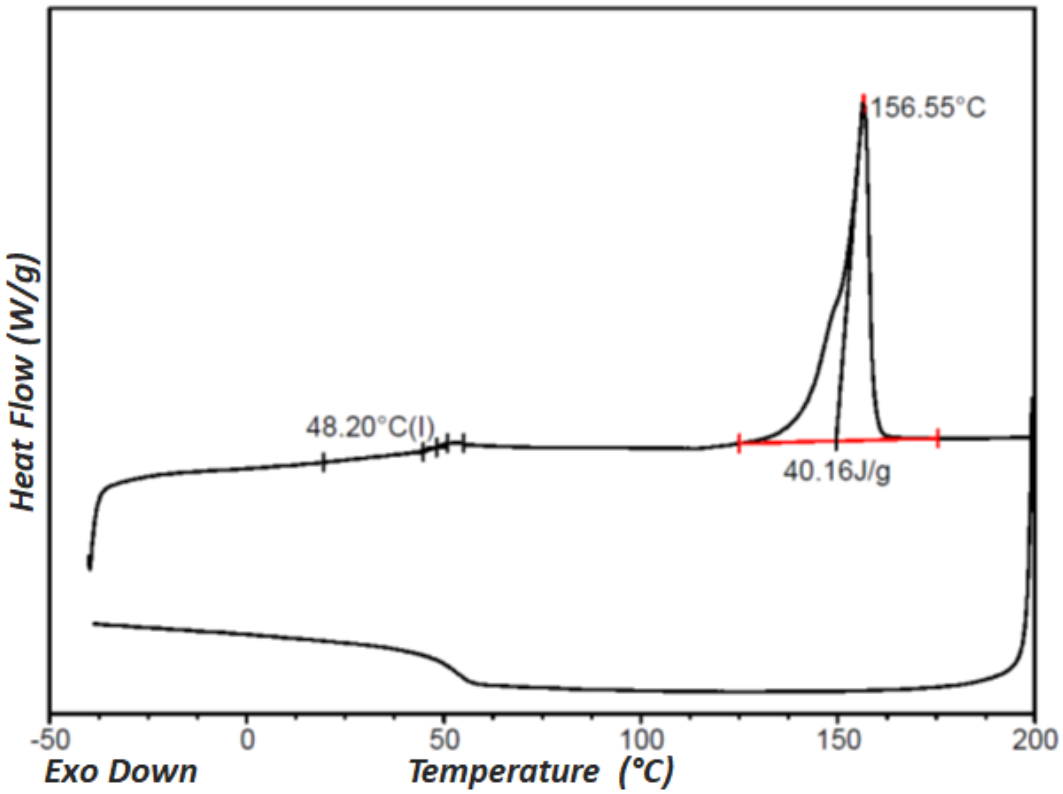

Figure 293: DSC thermogram of PLA sample obtained as in entry 1, Table 2.

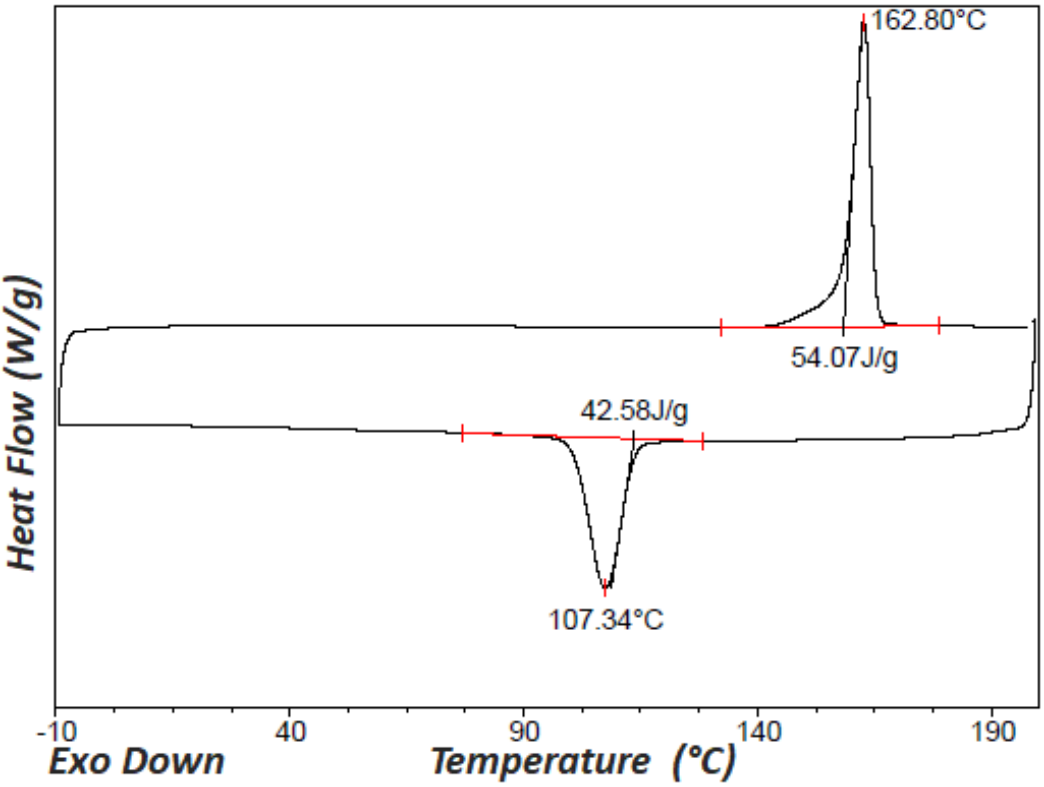

Figure 294: DSC thermogram of PLA sample obtained as in entry 3, table 6.

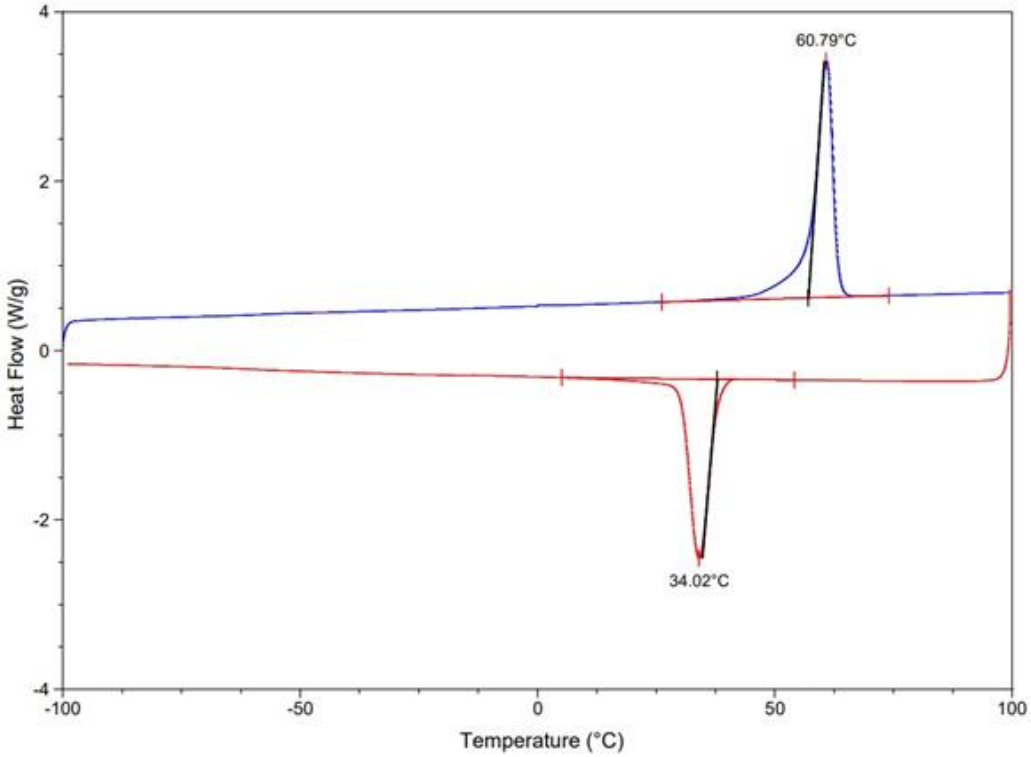

Figure 295: DSC thermogram of PCL sample obtained as in entry 10, table 6.

THANKS

-Prof. Stefano Milione: per avermi supportato e guidato in questo fantastico percorso. Per avermi indirizzato sempre correttamente verso il raggiungimento di un obiettivo, non lasciandomi girovagare a vuoto.

-Prof. Carmine Capacchione e Prof. Alfonso Grassi: per tutti i consigli che mi avete dato ogni volta che chiedevo un consiglio, non solo in ambito scientifico. Non servono parole per dirvi quanto sia grande la mia stima per voi, prima come uomini e poi come chimici.

-Prof. Giuseppina Roviello: parte della mia tesi è anche merito vostro. Ringraziarvi mi sembra davvero il minimo. Ho sperato di poterlo fare personalmente ma purtroppo questa pandemia ci ha tolto non poche possibilità di incontrarci. GRAZIE!

-Irene e Antonella: parte del lavoro contenuto in questa tesi è anche merito vostro per questo mi sembra più che dovuto dirvi GRAZIE. Grazie per aver sopportato il mio caratteraccio e credetemi quando vi dico che ho sempre cercato di trasmettervi la mia esperienza in laboratorio nel miglior modo possibile.

-Patrizia Oliva: ci fosse stata una volta in cui mi avessi detto "No Salvatore non ti posso aiutare". Grazie per tutto il supporto che mi hai dato e per le risate condivise che mi hanno aiutato a render più leggere parecchie giornate.

-Tutti i ragazzi che sono passati e che resteranno nel Lab1 ed Altri per i momenti condivisi insieme: Yuri, Fatemeh, Antonella, Francesco, Veronica, Vito, David, Francesca, Irene, Daniele, Natalia, Antonio, Peppino, Ginevia, Marco, Lorenzo, Rocco, Francesca, Giusy, ecc.

-Denise: per tutto il supporto che mi hai sempre dato quando ci sono stati quei momenti NO in cui dicevo "Non ce la posso fare!" e per la notizia più bella che mi hai dato proprio quando stavo per concludere questo percorso.

-La mia famiglia: non mi piace scrivervi qualcosa, ma potete benissimo immaginare la vostra importanza per me.

Con te non servono parole per dirti quanto importante sei stata e sarai sempre per me. Per questo ti dico solo:

"Sim, é verdade! Tudo vem mas nem sempre tudo passa como você falou!".